Landsat-4 Science Characterization Early Results

Volume IV—Applications

NASA

Landsat-4 Science Characterization Early Results

Volume IV—Applications

John L. Barker, *Editor*
NASA Goddard Space Flight Center
Greenbelt, Maryland

Proceedings of the Landsat-4 Science Characterization
Early Results Symposium, February 22-24, 1983
held at NASA Goddard Space Flight Center
Greenbelt, Maryland

Page intentionally left blank

LANDSAT-4 SCIENCE CHARACTERIZATION EARLY RESULTS

CONTENTS

Volume I: MULTISPECTRAL SCANNER

CONTENTS (Continued)

CONTENTS (Continued)

CONTENTS (Continued)

CONTENTS (Continued)

Volume IV: APPLICATIONS

CONTENTS (Continued)

CONTENTS (Continued)

CONTENTS (Continued)

OVERVIEW OF TM "APPLICATIONS" RESEARCH REPORTS

Darrel L. Williams
NASA/Goddard Space Flight Center

Volumes I, II and III of the Early Results Symposium proceedings provide detailed information regarding the evaluation of Landsat-4 MSS and TM sensor performance and data quality. In general, both sensors were found to be operating satisfactorily, and fully processed data products generated from MSS and TM raw data are of good and excellent quality, respectively (see Alford, Barker).

The excellent quality of the very first TM data products was a boon for those researchers who were primarily interested in evaluating TM data from an "applications" perspective. In other words, the excellent quality of the data allowed these researchers to proceed directly with applications analyses, without spending a significant amount of time applying various corrections to the data. The early results derived from the applications-oriented assessment of TM data are presented in this volume (i.e., Volume IV).

A total of twenty-four papers are contained in Volume IV. They cover a full range of research activities, which have been summarized in Table IV.1 under the following headings: discipline specific applications; comparison of results obtained from TM versus MSS data; evaluation of sensor performance and data quality; and presentation/utilization of new data processing, analysis or display techniques. By reviewing Table IV.1, each reader can quickly locate those papers which contain information of greatest personal interest. It should be noted that this summary table was produced by me after reading all of the papers provided to me as "applications-oriented." Individual researchers may feel that I have improperly characterized the thrust of their work, or that their work does not belong in the "applications" volume at all. To those individuals, I apologize. In the remainder of this overview, I would like to briefly summarize what I feel were some of the key and/or unexpected results presented in these papers.

Generation of TM Products for General Use

Although many applications users may not want to be bothered with assessing data quality or applying corrections to the data, they should be somewhat familiar with the data processing procedures that take place in generating a fully processed CCT product from the raw TM data. Barker, et al. (1983), do an excellent job of "presenting some of the features and characteristics of various digital image products used to produce the generally available final digital image product, the CCT-PT" (see Vol. II). The CCT-PT (i.e., fully processed digital image data) was the standard product type analyzed by the investigators reporting in the volume. Therefore, I encourage everyone to read this particular report in order to become familiar with the characteristics of this data.

Sensor and Data Quality Evaluation

Detailed summaries of the results obtained by assessing MSS and TM sensor performance and data quality are presented in Volumes I, II, and III. However, several of the reports in this volume also address data quality (see Table IV.1). Most of these reports briefly discuss the coherent noise problems associated with all Landsat-4 MSS data and some TM data. Three investigators conducted more in-depth assessments of data quality. MacDonald, et al. (1983), assessed TM band-to-band registration accuracy, geometric fidelity, and modulation transfer function (MTF). They found that: (a) TM band-to-band registration for the bands within the primary focal plane was better than specified, but that band-to-band registration of bands in the primary focal plane with bands in the "cooled" focal plane did not meet specifications (note: this misregistration was due to a software problem which has been corrected; see Vol. III); (b) geometric performance of TM data, without ground control correction, exceeded their expectations (i.e., less than 1/10 pixel rms under an affine transformation to a 7-1/2 minute U.S.G.S. map); and (c) the MTF for TM band 5 agreed with prelaunch specifications when the effects of cubic convolution resampling and the atmosphere were removed. Bizzell and Prior (1983) also evaluated various aspects of TM data quality. They discuss their findings relative to the expected improvements to be gained with TM data "both relative to the MSS and on its own merit." They concluded that "the TM sensor and associated ground processing are performing equal to the high expectations and within advertised specifications" and that "the overall TM system ... shows much promise for benefits in future analysis activities."

Price (1983) took a totally different approach in assessing data quality. He presents a very interesting assessment based on a comparison of the information content, or entropy, of simultaneously acquired TM and MSS data for a number of sub-image areas within a representative agricultural scene. He found that "the information content of all bands of MSS and TM is considerably below the potential capability of the sensor/transmitter system. This results from the bunching of data in a moderately narrow Gaussian distribution about a mean value in the lower half of the dynamic range of each instrument." However, Price went on to conclude that in general "the results are more encouraging than expected," "the new channels (i.e., TM5 and TM7) have greater values of H (i.e., information content) than the visible bands," and that "these new channels provide not just a marginal improvement, but a substantial gain in information."

TM Versus MSS Comparisons/Discipline Specific Applications

The Thematic Mapper is a second-generation electromechanical scanner with numerous upgrades over the familiar MSS's. Of particular interest to the user community were the improved spatial resolution, increased radiometric sensitivity, refined locations and widths of the green, red, and near-infrared spectral bands, and new spectral bands in the blue, middle infrared, and thermal infrared regions. Although pre-launch simulation studies indicated that TM data would provide significant enhancements over MSS data for various applications, a key question which needed to be addressed following the launch of Landsat-4 was, "Would the spectral, spatial, and radiometric improvements incorporated into the design of the TM sensor result in improved capability to

extract useful information from real TM data, as compared to the MSS?" Key results of investigator efforts to answer this question are summarized in this section.

The Landsat-4 spacecraft configuration permits the simultaneous operation of both the MSS and TM sensor systems. This capability significantly reduces the number of variables which must be addressed when making comparisons of the advantages or disadvantages of one sensor configuration versus the other (i.e., both sensors are looking through the same atmosphere at the same ground cover conditions). Therefore, if simultaneously acquired data are analyzed in a consistent manner, any differences in the results obtained should be (primarily) a function of sensor characteristics.

Numerous Landsat Image Data Quality Assessment (LIDQA) investigators utilized simultaneously acquired TM and MSS data to compare the advantages and disadvantages of the new instrument vis-a-vis the old. The primary means of comparing data from the two sensors involved the classification of each data set into general land cover/land use categories (or other discipline specific categories), followed by comparisons of the results obtained. It should be noted that although the overall approach to comparing the sensor data was common, the rigor of the actual analyses varied over the entire range from strictly qualitative to quantitative and/or theoretical. To the best of my knowledge, none of the investigators found MSS to be better than TM data for their particular application, a few found no significant advantage in having TM data over MSS, but a vast majority found TM data to be significantly better than MSS data for their particular application. In general, the LIDQA investigators concluded that, of the three key sensor parameters (i.e., spectral, spatial, and radiometric resolution), the TM's improved spectral resolution was the parameter of greatest significance, particularly the availability of the two middle infrared bands. However, nearly an equal number of investigators felt that the TM's improved spatial resolution was the most significant factor that the TM sensor design has to offer. Assessments of the contribution of improved radiometric resolution (i.e., signal-to-noise and quantization) were virtually non-existent.

Williams, et al. (1983), presents a statistical technique which can be utilized to isolate and quantitatively assess the impact of key sensor parameter on classification accuracy. Utilizing this technique in conjunction with November 2, 1982 Landsat-4 TM data of the Washington, D.C. area, they concluded that the TM's improved spectral and radiometric capabilities each had a significant, positive impact on classification accuracy as compared to the MSS. They also found that the TM's improved spatial resolution had no significant impact, either positive or negative, on classification accuracy. They felt that the lack of a significant, positive impact was primarily a function of the inability of standard per-point classifiers to take advantage of the significant amount of additional information contained in finer spatial resolution data. Indeed, the advantages of finer spatial resolution data can be readily verified by simple photointerpretative comparisons of simultaneously acquired TM and MSS data. Several investigators concluded that photointerpretation of TM imagery could be used to update land use maps (at scales up to 1:24,000), or to replace high altitude aircraft photography for certain applications. For example, Quattrochi (1983), stated that "In many

situations, it may in fact be advantageous to bypass digital classification of the data and employ interpretation methodologies to derive the required information." He went on to say that "... a town the size of Union City (i.e., Tennessee, pop. approximately 15,000, with about eight square miles within its city limits) could barely be discriminated through photointerpretation, let alone be digitally classified as an urban area, from MSS data. Yet, with the TM, it is possible to classify components of the city and visually locate and discriminate individual buildings."

Significant advantages associated with the TM's spectral resolution, particularly the capability to make measurements in four distinct regions within the electromagnetic spectrum (i.e., visible, near IR, middle IR, and thermal IR), were reported for every major discipline area. The biggest contribution of "new information" is coming from the two middle IR bands (i.e., TM band 5 (1.55-1.75 μm) and TM band 7 (2.08-2.35 μm)). For example, DeGloria and Colwell (1983), reported the ability to separate sugar beets from alfalfa using TM band 5, whereas no significant difference in the spectral response from these two crops was apparent in the visible and near IR bands. Quattrochi (1983), compared agricultural crop classification accuracy derived from a three-data, multitemporal MSS data set with a single-data TM scene, and found that the single-data TM results were 17% better than those for the multitemporal MSS. Not only were the TM results significantly better, but one TM acquisition replaced what could only be achieved with multitemporal MSS data. MacDonald, et al. (1983), performed a classification of soybeans using TM data, both with and without the middle IR bands. They found that there was a 25% improvement in soybean classification accuracy when the middle IR bands were utilized. They also found that the classification accuracy for sorghum was significantly enhanced by using the thermal band data. Bizzell and Prior (1983), analyzed TM data primarily from an agricultural applications point-of-view and found that: (a) the best three bands for the separability of classes always included at least one band from the visible, near IR, and middle IR region, and (b) if no middle IR band was used in classification the overall performance was significantly degraded. Sadowski, et al. (1983), stated that the middle IR bands may be especially useful because of: (a) the large range of variability in digital values found for five separate land cover classes, and (b) low correlations with other spectral bands for vegetated land cover and water. They also stated that low correlations between the blue band (TM band 1) and other spectral bands suggest its utility for studying variations within areas of water as well as vegetated land areas.

Dozier (1983), confirmed the utility of the middle IR bands, particularly TM band 5, for discriminating snow and clouds. For geology applications, Abrams, et al. (1983), reported that color composites produced from real TM data confirmed earlier results derived using aircraft simulated TM data; namely that the 2.08-2.35 μm band was useful for discriminating areas of hydrothermal alteration. As reported earlier, Price (1983), also found the middle IR bands to contain a substantial amount of information. He also cautions data users against routinely using the thermal IR data in conjunction with the reflective band data because " ... the physical processes accounting for radiance values in the thermal IR are quite different from those in the visible and near IR."

In summary, TM data were found to be significantly better than MSS data for discipline specific applications by a vast majority of the investigators. Spectral and spatial resolution improvements were the key factors most often acknowledged. Photointerpretation of TM imagery was conducted by numerous investigators to realize the full benefit of the finer spatial resolution data. (Note: Sadowski, et al. (1983), conducted image interpretation tests to determine which TM band color composite combinations were most preferred by interpreters.) The significance of the availability of spectral information from the middle IR region was repeatedly substantiated. The reader is cautioned that the analysis of TM data with techniques developed during the past decade using MSS data will not always lead to significantly better results than one could obtain with MSS data. The combined effect of more spectral bands and finer spatial resolution can lead to greater within class variability that results in greater spectral class overlap or confusion. However, this effect may be offset somewhat by the fact that the finer spatial resolution results in a greater percentage of "field center (i.e., pure) pixels" and a smaller percentage of "border or mixed pixels." The development of new or improved digital classification techniques to take advantage of the vast amount of information contained in TM data are needed.

New Processing, Analysis, or Display Techniques

As described, the TM's improved sensor parameters have significantly increased the amount of information contained in the data, and numerous investigators have looked at various ways to strip out this information to place it in a readily digestible format. Most of the reports in this volume describe new display techniques which involve transformation from red, green, and blue color space into hue, saturation, and intensity space. Haydn (1983), discusses this type of approach in detail.

It should be noted that numerous investigators used principal components analysis techniques to transform the data in an attempt to reduce data dimensionality, etc. This technique has been widely used for the past several years with MSS data, particularly multitemporal data. Therefore, I did not consider it to be "new."

Summary

Applications-oriented users of TM data have every reason to be excited about the possibility of opening up new horizons using TM data. The data appear to be of excellent quality, and the investigations conducted to date, although preliminary, substantiate the findings of earlier research conducted with simulated TM data. This volume contains several excellent articles which could serve as an aid to those who are planning to analyze TM data in the future. The reader is encouraged to read all of the articles in this volume, but if time does not permit, please refer to the summary table (i.e., Table IV.1) to select those articles which address topics of greatest personal interest.

TABLE IV.1

SUMMARY OF KEY TOPICS DISCUSSED IN THE PAPERS CONTAINED IN VOLUME IV

Investigators	Discipline Specific Applications	Comparisons of TM vs. MSS Data	Sensor/Data Quality Evaluation	New Processing, Analysis, or Display Techniques
Brumfield, et al.	Land cover/land use (surface mine mapping)			
Goodenough, et al.	Land cover/land use		X	
Jackson, et al.	Land cover/land use		X	
Markham	Land cover/land use	X		
Middleton, et al.	Land cover/land use	X		
Sadowski, et al.	Land cover/land use	X		X
Toll	Land cover/land use	X		
Williams, et al.	Land cover/land use	X		X
Bizzell and Prior	Agriculture, land cover/land use	X	X	
DeGloria and Colwell	Agriculture	X	X	
MacDonald, et al.	Agriculture	X	X	
Price	Agriculture	X	X	X
Quattrochi	Agriculture, forest, urban/suburban	X		
Thompson, et al.	Agriculture (soil)			
Abrams, et al.	Geology	X	X	X
Everett, et al.	Geology			X
Hayden	Geology			X
Short	Geology			
Gervin, et al.	Hydrology, land cover/land use	X		
Ackleson and Klemas	Wetlands mapping (submerged plant communities)			
Hardisky and Klemas	Wetlands mapping (live biomass estimation)	X		
Dozier	Snow mapping		X	
Schiebe, et al.	Water quality	X		

IMPACT OF THEMATIC MAPPER SENSOR CHARACTERISTICS ON CLASSIFICATION ACCURACY

Darrel L. Williams
James R. Irons
Brian L. Markham
Ross F. Nelson
David L. Toll

NASA/Goddard Space Flight Center

Richard S. Latty

University of Maryland

Mark L. Stauffer

Computer Science Corporation

Introduction

The second decade of land remote sensing from space was inaugurated on July 16, 1982 with the successful launch of Landsat-4. Landsat-4 carries two remote sensing devices in orbit: the familiar Multispectral Scanner (MSS) and a new sensor, the Thematic Mapper (TM), which was designed to provide an improved source of data to the remote sensing community. Relative to the MSS, the TM offers finer spatial resolution, new and more optimally placed spectral bands, and improved radiometric sensitivity quantized over eight bits rather than six bits (Table 1). These enhancements in sensor capability were expected to significantly improve data quality and information content, and thereby increase the utility of the data for earth resources observations. Therefore, during the first year of the Landsat-4 mission, the substantiation and quantification of the quality and utility of the data acquired by the TM sensor was a primary goal of the Landsat-4 Project Science Office.

One method commonly used to assess the relative utility of data acquired by different remote sensing devices is to compare classification accuracies. Numerous studies using data collected by aircraftmounted Thematic Mapper simulators (TMS) were conducted prior to the launch of Landsat-4 to quantify the overall improvement in classification accuracy expected from TM data relative to MSS data.[1] However, few of these studies attempted to identify the impact or contribution of individual sensor parameters (e.g., spectral, spatial, and radiometric resolution) on classification accuracy. The effect of altering individual sensor attributes can be anticipated qualitatively. For example, the addition of spectral bands can enable the discrimination of previously inseparable categories by providing data from portions of the spectrum where category reflectivities become disparate. Similarly, improved radiometric resolution and increased signal-to-noise ratios may facilitate category discrimination by enhancing between-category boundaries. In contrast, the refinement of spatial resolution can have offsetting effects on classification accuracy.[2] Finer resolution tends to decrease the proportion of mixed pixels and, thus, enhances classification accuracy.[3,4] Classification is hindered, however, by an increase of within-category spectral heterogeneity at finer resolutions.[5,6,7,8]

The Thematic Mapper represents the results of an ambitious research and development effort in which all of these major improvements in remote sensing capability were simultaneously integrated into one system. Classification results obtained from TM data are indicative of the interactions of all the sensor attributes operating simultaneously, and thus, complicated a more quantitative evaluation of the effects attributable to each individual sensor improvement.The capability to derive such quantitative information, however, would significantly benefit scientists and engineers in defining sensor parameter requirements and in designing new sensors for future remote sensing missions.

With this in mind, a group of discipline scientists within the Earth Resources Branch at NASA's Goddard Space Flight Center in Greenbelt, Maryland, developed and conducted an experiment to quantify the effect of each TM sensor parameter on classification accuracy. This paper discusses the experimental design and summarizes the results obtained using TM data acquired over the Washington, D.C. area on November 2, 1982.

Study Site/Data Description

Accurate, detailed ground reference information was an important component of the study. To facilitate the collection and field verification of the ground reference data, an area near Goddard was selected as the general study area. This area is bounded on the west by Washington, D.C., on the north by Baltimore, Maryland, on the east by the Cheasapeake Bay, and on the south by northern Charles County, Maryland (Figure 1). Stereo, color infrared aerial photography at a scale of 1:40,000 was collected over this area on July 13, 1982, just prior to the launch of Landsat-4.

The area is characterized by a diversity of urban, suburban, and rural land cover types. The western portion of the area contains numerous residential developments associated with suburban Washington, D.C. The entire area includes intensive urban fringe development, suburban multifamily and single family residential tracts, and low density single family developments. Numerous commercial support services such as shopping centers, industrial complexes, gravel quarries and airports are also scattered throughout the study area. The area lacks heavy industry, but does include the Fort Meade and Andrews Air Force Base military complexes. In addition, the region includes areas of agriculture and forest cover. The agricultural areas are primarily small, scattered fields. Principal crops are corn, soybeans, and tobacco, with areas of pasture and grassland. The study site includes the USDA/Beltsville Agricultural Research Center. In terms of areal extent, forest is the predominant cover type, and consists primarily of mixed deciduous forest, mixed hardwood-conifer and isolated conifer stands. The area also includes lowland vegetation communities associated with the Chesapeake Bay estuaries.

Although Landsat-4 was launched on July 16, 1982, cloud-free, seven-band TM imagery of the entire study area was not acquired until November 2, 1982. TM and MSS imagery were collected simultaneously, and both data sets were of excellent quality (e.g., no cloud cover, minimal haze, spacecraft and sensors operating normally, etc.). However, the November data set was far from optimal for general category discrimination as deciduous trees were in fall coloration, most agricultural crops had senesced and many fields had been harvested. In addition, total scene illumination was reduced because of low sun angle conditions, and therefore, the full dynamic range and quantization capabilities of the TM and MSS sensors were not utilized. Nevertheless, a decision was made to proceed with the analyses because: (1) it afforded the first opportunity to test the experimental design/methodology with real TM data; (2) a quantitative assessment of the attributes of TM sensor parameters relative to MSS was desired as soon as possible; and (3) a ground reference data base for an alternative area could not be created in a timely, cost-effective manner.

Procedures

The Experimental Design

The first step in the work presented here was to design an experiment which could isolate the effect of the increased spectral, spatial and radiometric resolution capabilities of the TM sensor on classification performance. Ideally,

the capability to assess the impact of each factor (i.e., sensor parameter) individually, and in all possible combinations, was desired. The work of Sigman and Craig[9] with TMS data suggested a promising methodology based on a multifactor analysis of variance (ANOVA) approach. The multifactor ANOVA approach permits one to simultaneously investigate the effects and interactions of two or more factors, and is therefore more efficient than the traditional experimental approach of manipulating only one factor at a time while keeping all other conditions constant.[10] Thus, this approach was adopted for application to actual TM data, because it permits the evaluation of the effect of three factors (i.e., spectral, spatial, and radiometric resolution) on classification accuracy, where each factor has two levels (i.e., TM and MSS). This is referred to as a three factor, fixed-effects ANOVA design and requires the analysis of eight treatments. For this study, each treatment consisted of a distinct digital image data set possessing the following characteristics:

A 30 meters/8 bits/6 bands (actual TM data)
B 80 meters/8 bits/6 bands
C 30 meters/6 bits/6 bands
D 80 meters/6 bits/6 bands
E 30 meters/8 bits/3 bands
F 80 meters/8 bits/3 bands
G 30 meters/6 bits/3 bands
H 80 meters/6 bits/3 bands (simulated MSS from TM)

(NOTE: Items underlined are those factors which have changed relative to treatment A, where treatment A consists of actual TM data.)

Data sets for each of the eight treatments were created by degrading TM data (Treatment A) to approximate MSS characteristics for each factor (e.g., TM data are spatially degraded to approximate the coarser MSS spatial resolution).* These data sets were then classified in a consistent manner. The multifactor ANOVA design enabled the statistical testing of the significance of differences in accuracy between treatments. Thus, the testing resulted in a quantitative assessment of the effect of each sensor improvement, individually and in combination with other improvements, on classification performance.

Data Preparation and Analysis

Several major activities were involved in preparing and analyzing the data. These included: interpretation of the aerial photography and digitization of the results to create a digital ground reference data set; extraction of the TM data corresponding to the study sites; preprocessing of the TM data to simulate MSS spectral bands, spatial resolution, and radiometric characteristics as required by the ANOVA design; selection of training and test pixels for each cover type; clustering and classification of the data; and an assessment of the accuracies obtained for each data set.

Photointerpretation and Digitization. As previously mentioned, color IR aerial photography at a scale of 1:40,000 was acquired on July 13, 1982, just prior to the scheduled launch of Landsat-4. Nine frames were randomly selected for detailed analysis. Prior to photointerpretation, a decision was made to minimize the effects of distortions typically found toward the edges of aerial photographs by working with a sub-frame area designated by plus-or-minus 50 mm from the principal point of the 241 mm (nine inch) format photography. The resultant 100 mm square area represents roughly the center 20% of an entire frame and

*(NOTE: The assessments were made relative to MSS sensor characteristics, since the MSS is the currently accepted "operational" instrument with which the remote sensing community is most familiar.)

encompasses an area of approximately 1,600 hectares. These 1:40,000 scale sub-frame areas were then photographically enlarged by a factor of four to attain a nominal scale of 1:10,000 and paper prints were produced. Clear acetate film was laid on top of each photograph so that the photointerpretation results could be drafted directly onto the film overlay. A minimum mapping unit criterion of 15 m (i.e., one-half the instantaneous-field-of-view of the TM) was used to differentiate distinct land cover categories. However, in the case of agricultural fields, the minimum mapping unit was utilized only to separate one field from another; no attempt was made to delineate within-field variability. Using this approach, seventeen Level II/III land cover/land use categories (Table 2) were identified, outlined and labeled. It should be noted that the land cover/land use categories are not always mutually exclusive because of the inability to strictly adhere to the 15 meter minimum mapping unit criterion in areas of high spatial variability, such as residential subdivisions. For instance, land use rather than land cover categories were used in situations where the land cover components of the categories (e.g., the roofs, lawns, trees, and concrete/asphalt areas of a residential neighborhood) occupied areas with spatial dimensions approximately equal to or smaller than the 15 m minimum mapping unit. The photointerpretation and labeling results were verified and/or updated by field visits and enumeration during the last week in October, just prior to the TM data acquisition.

To reduce analyst bias and provide for accurate, efficient processing of the data, the labeled polygons on the acetate film were digitized and geometrically registered to the TM data. The TM digital imagery served as the cartographic reference to avoid unnecessary resampling of the TM data. The registration was accomplished by matching control points in the TM data and the photography. The control points were marked on the acetate overlays and were incorporated in the digitizing process. All digitizing and registration processing was accomplished by a contract vendor (Chicago Aerial Survey*) with comprehensive software and hardware for automated digitization. Briefly, each overlay was placed on a drum scanner with a resolution of 40 lines per millimeter. The scanner generated a digital representation of the polygons in a raster format. Each digitized line was thinned to a width of one raster element. The raster format data were converted to vector format data, and then, using the ground control points, registered to the TM digital image data. This approach avoided the inaccuracies inherent in the manual digitization of the polygons with a hand-held cursor and digitization table.

After creating the vector format data, each digitized polygon was labeled with the appropriate land cover/land use category at an interactive editing station. These thematic data sets were transformed back into two files of raster data for each interpreted photograph. One raster file contained cells representing surface areas of 28.5m-by-28.5m.** This file could then be digitally overlayed onto the four data sets having TM spatial resolution characteristics (i.e., Treatments A, C, E, and G). The other file contained 57m-by-57m cells which could be directly overlayed onto the spatially degraded data sets (i.e., Treatments B, D, F, and H). These registered, digital, thematic data sets in raster format thus served as the ground reference information.

---

*Company names are given for descriptive purposes only and do not imply endorsement by NASA.

**(NOTE: Although the spatial resolution (IFOV) of Thematic Mapper is 30m, pixels in the standard P-tape output product are resampled to a dimension of 28.5m-by-28.5m. This is done so that the data can be easily registered to the 57m-by-57m MSS P-tape data by simple integer replication.)

Extraction and Preprocessing of TM Data. The TM data corresponding to the nine randomly selected study sites were extracted from the original P-format data tapes to facilitate subsequent processing (Figure 2). Each extracted segment of TM data was 256-by-256 pixels in size and contained all six bands of 30m resolution data. The thermal IR data, which are collected at a ground resolution of 120m, were omitted from this study due to the significant difference in spatial resolution.

The ANOVA design required the original TM data to be degraded spectrally, spatially, and radiometrically to simulate MSS specifications for each of these sensor parameters. However, the precise simulation of MSS radiometry, spectral bands, and spatial resolution from TM data is not possible due to inherent differences in spectral band cutoffs, radiometric response, acrosstrack scanning strategies, etc. Therefore, certain compromises or simplifying assumptions had to be made in degrading TM data to simulate MSS characteristics, and the procedures which were used are described below:

(i) Spectral Simulation - The spectral simulation of MSS was achieved by using only TM bands 2, 3, and 4, which was the best approximation available for the MSS complement of bands. TM band 2 (0.52 - 0.60 μm) closely approximates MSS band 1 (0.50 - 0.60 μm) and TM band 3 (0.63 - 0.69 μm) closely approximates MSS band 2 (0.60 - 0.70 μm). TM band 4 (0.76 0.90 μm) includes portions of MSS band 3 (0.70 - 0.80 μm) and MSS band 4 (0.80 - 1.10 μm). For vegetated targets, which constitute a majority of the cover types in the study area, TM band 4 can be considered a good approximation of MSS band 4, as both cover major portions of the 0.74 1.10 μm region in which reflectance is related to biomass.[11] MSS band 3 includes a spectral region of transition between low vegetation reflectivity due to chlorophyll absorption (ending at approximately 0.71 μm) and a region of high vegetation reflectivity (beginning at approximately 0.75 μm) and, for this reason, is not optimal for vegetation discrimination. Therefore, the inability to simulate MSS band 3 was not considered critical.

(ii) Radiometric Simulation - The radiometric analysis consisted of a comparison of quantization levels. The MSS simulation was achieved by mapping the 0-to-255 potential bins for the TM data into 0-to-63 bins for MSS data (i.e., each TM datum was divided by four and rounded to the nearest integer). In taking this approach, the simplifying assumption was made that the dynamic range and signal-to-noise ratios of both sensor systems are comparable for the similar spectral bands. Neither assumptions were precisely correct. Therefore, this approach simply addresses the issue of six bit versus eight bit quantization, rather than TM radiometric sensitivity versus MSS radiometric sensitivity.

(iii) Spatial Simulation - The simulation of MSS spatial resolution was achieved by computing the simple arithmetic average over a three-by-three pixel window of the TM data. The window was moved across the image two columns at a time to simulate the 57m along-scan MSS sampling rate relative to the MSS 80m IFOV. After moving across an image, the averaging window was incremented two lines to approximate the geometric resampling of MSS data to reduce the 80 m nominal pixel dimension in the along-track to 57 m. Thus, the 57m-by-57m pixel format of the standard MSS P-tape product distributed by EROS was simulated.

An assessment of how well the above procedures actually simulated MSS sensor performance was possible because Landsat-4 MSS data were acquired simultaneously with the TM data during the November 2, 1982 overpass. By comparing results obtained from data set H (i.e., simulated MSS data from TM)

with results obtained by analyzing real MSS data (which was simultaneously obtained), the validity of the procedures used to degrade TM data to simulate MSS characteristics could be assessed. For example, if the simulation procedures were perfect, one would expect no difference in the classification accuracies obtained from either data set. Thus, for the sole purpose of assessing the appropriateness of the above simulation procedures, a ninth data set, referred to as treatment I, and consisting of real MSS data, was appended to the eight-block ANOVA design. The results obtained by comparing treatment H (simulated MSS) with treatment I (real MSS) will be presented in the results and discussion section of this paper.

Selection of Training and Test Pixels. Training and test pixels for each of the 17 land cover/land use categories were needed from each of the eight data set treatments in the ANOVA experimental design. The samples obtained from a given data set were used for clustering, classification, and tabulation of classification accuracy results for that particular treatment. To facilitate statistical testing and to treat each class as equally important, regardless of the frequency of class occurrence in the study area, an equal number of training and test pixels were needed for all land cover/land use categories.

The selection of sample pixels was automated using the digitized ground reference data previously described. Software was written to randomly select an equal number of pixels from each land cover/land use class in the ground reference data; 550 pixels per class were chosen for the 57m data, and 2200 pixels for the 28.5 m data. The size of the sample was limited by the actual number of pixels in the smallest ground reference class (i.e., soybeans was the smallest class; it contained 571 pixels at the 57m resolution, and 2244 pixels at the 28.5m resolution).

Two sets of random samples were generated in this manner for each treatment in the ANOVA design. Two replicates were produced for each sample set by training and testing on different sections of the sample. Hence, for a given treatment, two sample sets with two replicates per set resulted in a total of four replicates. For a given replicate, 400 of the 550 randomly selected 57m pixels in each class were to be used in clustering to produce training statistics. The remaining 150 pixels were classified according to the training statistics for all classes and these results were used to test the accuracy of the classification. A similar ratio of training (1600 of 2200) to test (600 of 2200) pixels were utilized for the 28.5m data sets.

Clustering and Classification of the Sampled Data. Training statistics for the sampled data described above were derived using the ISOCLS clustering algorithm.[12] Clustering was performed separately on each set of training pixels for each land use/land cover class from each treatment. The ISOCLS program parameters were set such that the program behaved as an iterative, point migration clustering algorithm where the initial cluster means tend to migrate towards the centroids of the natural spectral groupings with each iteration. The program parameters were adjusted so that the program acted in a consistent manner for all eight treatments. No editing of the resulting training statistics was performed (i.e., no merging or deleting of spectral classes). The intent was to prevent the incorporation of analyst bias into classification results. Although the lack of editing limited classification accuracies, the consistent application of the clustering procedure permitted a more valid comparison of classification accuracies between treatments.

In all, 544 different clustering procedures were performed (eight ANOVA treatments, four replicates per treatment, 17 cover classes per replicate) resulting in 32 different sets of training statistics (eight treatments, four replicates).Each sample of test pixels was then classified using the appropriate set of training statistics and a per-pixel Gaussian maximum likelihood classifier. Classification accuracy figures were derived from the test pixel results.

Contingency matrices were generated to display the number of test pixels correctly classified, along with errors of omission and commission. The sum of the diagonal values (i.e., the number of correctly classified test pixels in each cover class) in each matrix divided by the total number of test pixels provided an overall classification accuracy value. Since the classification procedure was repeated four times per data treatment, the four accuracy values per treatment were used to conduct the three-factor ANOVA. The analysis was performed using the SAS ANOVA procedure.[13] This procedure allowed the analysis of both individual factor effects and factor interactions.

Results and Discussion

The overall classification accuracies obtained for the eight treatments in the ANOVA design are summarized in Table 3. For each treatment, the mean and standard deviation of the four replicates described in the clustering and classification section are shown. The overall accuracy values range from a high of 37.9% (Treatment B; 80 meter/8 bits/6 bands) to a low of 25.7% (Treatment G; 30 meter/6 bits/3 bands), for a maximum range in accuracies of 12.2%. The average accuracy for all treatments was 31%.

These extremely low accuracy figures were of concern. A careful review of all aspects of the experimental design and data processing revealed no improper applications of the selected data analysis procedures. Keeping in mind that the goal of the experiment was to conduct a rigorous, statistical assessment of differences in classification accuracy due to data characteristics, and not to maximize classification accuracy, the low accuracy values are attributable to the following factors: (1) the experimental design itself was a key factor since it was laid out so as to minimize or eliminate analyst bias so that differences in classification accuracies were solely attributable to data characteristics and not to analyst skill; (2) 17 detailed Level II/III land cover/land use classes were delineated and a majority of the classes represented "vegetative" cover conditions which were spectrally quite similar to one another due to the time of year of data acquisition; and (3) the selection of sample pixels for training and testing was totally guided by the digitized ground reference data; therefore, "border" pixels as well as "field center" pixels were selected and any minor inaccuracies in the registration of the reference data to the TM data could have resulted in contaminated sample data (i.e., samples for a given category could have come from different cover types causing "mixed" training statistics).

As further substantiation of the validity of the methodology and results, the impacts of (1) allowing analyst interaction to edit training statistics

prior to classification, and (2) simply decreasing the number of land cover/land use categories were briefly investigated. In the first test, treatment A (i.e., real TM data) was re-analyzed using standard methodology where the analyst is allowed to interact with the computer to edit training statistics. No new training sites were chosen and 17 land cover/land use classes were maintained. Classification accuracy rose from 36.7% to 62%. In the second test, the 17 Level II/III categories were aggregated into five Level I/II categories (i.e., water, crops, pasture and grass, forest, and urban), and classification accuracy by treatment, as well as average accuracy over all treatments, was calculated. As in the original case, no analyst interaction during training or classification was permitted. The accuracy values for the five class case ranged from 59.5% to 71.7%, with an average value of 65.7%, as compared to respective values of 25.7%, 37.9% and 31% for the 17 class case. The classification accuracy values obtained in both of these additional tests certainly seemed reasonable given the ground rules of the experimental design and the time of year that the data were collected.

As previously mentioned, the validity or appropriateness of the techniques used to degrade TM data to simulate MSS characteristics were also evaluated. In this instance, real MSS data (Bands 1, 2, and 4) acquired during the November 2, 1982 overpass were registered (and resampled) to the simulated data sets, and were subjected to the same analysis procedures as the simulated MSS data. The actual MSS data yielded a classification accuracy of 20.5%, as compared to 26.7% for the simulated MSS data (see Table 3). This 6.2% difference in accuracy was in the expected direction (i.e., simulated MSS was better) and was considered to be a result of the following facts: (1) the real MSS data were subjected to an additional registration and resampling process in comparison to the simulated data sets, and this may have slightly degraded the real MSS data; (2) known limitations in the degradation process itself, e.g., the inability to adequately treat signal-to-noise, resulting in the fact that degraded TM data is still superior to MSS in signal-to-noise; and (3) the quality of Landat-4 MSS data has been degraded somewhat by coherent noise in the system[14] and this is believed to have an impact on attainable classification accuracies in comparison to degraded TM data. Thus, the compromises or simplifying assumptions that were made in degrading TM data to simulate MSS characteristics were appropriate. A direct comparison of real TM data with real MSS data (i.e., Treatment A versus Treatment I in Table 3) indicates a 16.2% improvement in favor of TM, as compared to the 10% improvement indicated by using simulated MSS data. It should be noted that Treatment I is not a true component of the ANOVA design, and, therefore, it will not be included in the remaining discussion.

Following the tabulation of classification accuracies, the statistical testing of the significance of the differences in accuracies among treatments was conducted. The results are summarized in Tables 4, 5, 6 and 7. To reiterate, the factors being evaluated in the fixed-effects ANOVA design were: spatial resolution (30 m versus 80 m), number of spectral bands (six versus three), and quantization level (eight bit versus six bit). The two levels of each factor reflect TM and MSS sensor characteristics.

Table 4 presents the analysis of variance results. Significant effects (at a 0.05 probability of Type I error; $\alpha=0.05$) were determined using the F-test. Starting at the bottom of the table with the interaction terms, we see that the three-way interaction term was not significant; however, the two-way interaction effects are all significant, particularly the spectral*radiometric interaction. This spectral* radiometric interaction shows up primarily as a

larger increase in classification accuracy when going from three bands to six bands at eight bit quantization relative to six bit quantization (i.e., 7.1% to 7.7% versus 3.3% to 5.5%) (see Table 5).

Since the significance of the interaction terms makes the interpretation of the main effects in the model less clear, the individual treatment means were pairwise compared.[10] Differences in classification accuracies between treatments which differed in only one factor were analyzed using the Tukey procedure for multiple comparisons (i.e., test the hypothesis that differences between treatment mean accuracies are significantly different from zero at Tukey $\alpha=0.05$). The increase from three to six spectral bands increased classification accuracy 3% to 8% depending on the levels of the other factors, and all differences were significant (Table 5). The increase in quantization from six bits to eight bits also increased classification accuracy over the range from 3% to 8%, and all differences were significantly greater than zero (Table 6). However, the increase in spatial resolution from 80 m to 30 m had mixed effects on classification accuracy within the range of plus-or-minus 2%, and none of the differences in accuracy were significant (Table 7).

These results strongly suggest that quantization level improvements and the addition of new spectral bands in the visible and middle IR regions (both afforded by the TM sensor design) will result in improved capabilities to accurately delineate land cover categories using a per-point Gaussian maximum likelihood classifier. On the other hand, results indicate that the increase in spatial resolution to 30 m does not significantly enhance classification accuracy. This result may appear surprising, because side-by-side visual comparisons of simultaneously acquired TM and MSS imagery indicate that the TM data contains much more spatial detail. In fact, properly enhanced TM subimages can be easily confused with high altitude aerial photography. The "insignificance" of the improved spatial resolution can be related to the fact that the experiment was structured around the use of a maximum likelihood, per-point classifier which performs the class assignments solely on the basis of the spectral characteristics of the pixel; it does not integrate any information on texture, tone or the spatial characteristics of the neighboring pixels. Another factor which may affect the measure of spatial resolution importance is the level of detail associated with the ground reference categories. For example, within-field variations not apparent in MSS data are now obvious in TM data, and the ground reference data did not identify these types of variations. These variations often represent actual physical properties of the target, and grouping the data into broad categories may not take full advantage of the information available in the TM data. These factors may bias the result in favor of the MSS and not fully represent the spatial improvements of the TM which are obvious in side-by-side visual comparisons of TM and MSS imagery. In view of these results, emphasis should be placed on developing a thorough understanding of the characteristics of fine spatial resolution data, as well as algorithms which take better advantage of these characteristics for information extraction. The remote sensing communities' perception of processing, analysis, and application of remotely sensed data, previously structured around the properties and characteristics of MSS data, will need to change. This may include the redefinition of categories and category characteristics, as broad land cover classes may not be appropriate for use with fine resolution data. Without further understanding of fine resolution data, digital analysis capabilities will benefit more from new sensors with enhanced radiometric sensitivities and additional, well-placed spectral bands than from new sensors with finer spatial resolution.

Summary

A fixed effect, three factor (two levels per factor) analysis of variance experiment was conducted to quantitatively assess the significance of the improved spectral, spatial and radiometric resolution capabilities of the Landsat-4 Thematic Mapper sensor relative to the familiar MSS sensor. TM data acquired over the Washington, D.C. area on November 2, 1982 were utilized. The original TM data were progressively degraded in spectral, spatial and radiometric characteristics to simulate the MSS, and classification accuracies were derived in a consistent manner for all eight treatments in the ANOVA design. Statistical testing of the significance of differences in classification accuracies between treatments indicated that the increased number of spectral bands and the improved quantization capabilities afforded by the TM sensor design would lead to significant improvements in classification accuracies attainable relative to MSS. In contrast, however, the improved spatial resolution provided by the TM sensor did not enhance classification accuracy. This latter result was felt to be more a function of the type of classification algorithms available today (i.e., perpoint decision criterion), rather than a definitive statement on the benefits (or lack thereof) associated with finer spatial resolution data. This can be substantiated by simple photointerpretation of simultaneously acquired TM and MSS imagery. Thus, improvements in the understanding and analyses of fine spatial resolution data should be developed prior to, or in concert with, the development of new remote sensing devices having even finer spatial resolution than the TM. In lieu of such developments, emphasis should be placed on increasing the number of spectral bands and improving radiometric sensitivity and quantization.

Acknowledgments

References

1. Irons, J.R. 1982. Summary of Research Addressing the Potential Utility of Thematic Mapper Data for Renewable Resource Applications. NASA Technical Memorandum 83965.

2. Markham, B.L. and J.R.G. Townshend. 1981. Land Cover Classification Accuracy as a Function of Sensor Spatial Resolution. Proceedings of the Fifteenth International Symposium on Remote Sensing of Environment. Ann Arbor, MI.

3. Morgenstern, J.P., R.F. Nalepka, and J.D. Erickson. 1981. Investigation of Thematic Mapper Spatial, Radiometric, and Spectral Resolution. Proc. of the 11th International Symp. on Remote Sensing of the Environment, 1977, pp. 693-701.

4. Pitts, D.E. and Gautam Badhwar. 1980. Field Size, Length, and Width Distributions Based on LACIE Ground Truth Data. Remote Sensing of Environment, Vol. 10, 1980. pp. 201-213.

5. Kan, E.P.F. and D.A. Ball. 1974. Data Resolution Versus Forestry Classification. JSC-90578. 22 p.

6. Landgrebe, D.A., L. Beihl and W. Simmons. 1977. An Empirical Study of Scanner System Parameters. IEEE Transactions on Geoscience Electronics, Vol. GE-15, No. 3, July 1977, pp. 120-130. LARS #110976.

7. Sadowski, F.G., W.A. Malila, J.E. Sarno, and R.F. Nalepka. 1977. The Influence of Multispectral Scanner Spatial Resolution on Forest Feature Classification. Proc. of the 11th International Symp. of Remote Sensing of Environ., 1977, pp. 1279-1288.
8. Latty, R.S. and R.M. Hoffer. 1981. ComputerBased Classification Accuracy Due to Data Spatial Resolution Using Per-Point Versus Per-Field Classification Techniques. Proc. of the Machine Processing of Remotely Sensed Data Symposium, 1981, pp. 384-393.

9. Sigman, R. and M. Craig, 1981. Potential Utility of Thematic Mapper Data in Estimating Crop Areas. Proc. of Fifteenth International Symposium on Remote Sensing of Environment. Ann Arbor, MI.

10. Neter, J. and W. Wasserman. 1974. Applied Linear Statistical Models, Richard D. Irwin, Inc. Homeward, IL. 842 p.

11. Tucker, C.J. 1978. A Comparison of Satellite Sensor Bands for Vegetation Monitoring, Photogrammetric Engineering and Remote Sensing, 44(11): 1369-1380.

12. Minter, R.T. 1972. Computer Program Documentation for ISOCLS, Iterative Self-Organizing Clustering Program. Program C094. Prepared for NASA/JSC under contract NAS 9-12200 by Lockheed Electronics Company, Inc. Houston, TX.

13. Barr, A.J., J.H. Goodnight, J.P. Sall, and J.T. Helwig. 1976. A User's Guide to SAS 76. SAS Institute Inc. Raleigh, NC.

14. Alford, W.L. 1983. Landsat-4 Multispectral Scanner Performance Evaluation Summary, Vol. 1 of the Landsat-4 Scientific Characterization Early Results Symposium, NASA/Goddard Space Flight Center, Greenbelt, MD

Table 1. Comparison of Landsat-4 TM and MSS Sensor Capabilities

Band Designation	Thematic Mapper (TM)		Multispectral Scanner Subsystem (MSS)	
	Bandpass (Micrometers)	Radiometric Sensitivity (NEΔρ)	Bandpass (Micrometers)	Radiometric Sensitivity (NEΔρ)
Spectral Band 1	0.45 - 0.52	0.8%	0.5 - 0.6	0.57%
Spectral Band 2	0.52 - 0.60	0.5%	0.6 - 0.7	0.57%
Spectral Band 3	0.63 - 0.69	0.5%	0.7 - 0.8	0.65%
Spectral Band 4	0.76 - 0.90	0.5%	0.8 - 1.1	0.70%
Spectral Band 5	1.55 - 1.75	1.0%		
Spectral Band 6	10.40 -12.50	0.5° Kelvin (NEΔT)		
Spectral Band 7	2.08 - 2.35	2.4%		
Ground IFOV		30 meters (Bands 1-5, 7) 120 meters (Band 6)	82 meters (Bands 1-4)	
Data Rate		85 megabits/sec	15 megabits/sec	
Quantization Levels		256	64	

Table 2. Summary of the Seventeen Land Cover/Land Use Categories Delineated in the Ground Reference Data

Land Cover Categories:

1. water
2. agriculture - miscellaneous crops
3. corn - standing
4. corn - stubble
5. shrubland
6. grassland/pasture
7. soybeans
8. bare soil - plowed fields
9. bare soil - cleared land
10. hardwood forest, >70% of the forest canopy, 50-100% canopy closure
11. hardwood forest, >70% of the forest component, 10-50% canopy closure
12. conifer forest, >70% of the forest component, 10-100% canopy closure
13. mixed-wood forest, 10-100% canopy closure
14. asphalt

Land Use Categories:

15. residential - single family dwelling
16. residential - multifamily dwelling
17. industrial/commercial

Table 3. Overall Classification Accuracy as a Function of Sensor/Data Characteristics and the Number of Land Cover Classes Being Delineated.

| Treatment | Characteristics | Case I[†] | | | Case II[#] |
		Mean	S.D.	Change Relative to Treatment "A"	
A	30 meter/8 bit/6 bands	36.7(62)*	0.73	N.A	71.7
B	80 meter/8 bit/6 bands	37.9	1.13	+1.2	71.5
C	30 meter/6 bit/6 bands	31.2	1.27	-5.5	68.4
D	80 meter/6 bit/6 bands	29.9	1.05	-6.8	63.0
E	30 meter/8 bit/3 bands	29.0	0.39	-7.7	65.1
F	80 meter/8 bit/3 bands	30.9	1.50	-5.8	64.4
G	30 meter/6 bit/3 bands	25.7	0.57	-11.0	59.5
H	80 meter/6 bit/3 bands	26.7	0.98	-10.0	62.2
I	Real MSS - Band 1, 2, 4	20.6	0.37	-16.2	54.9

(NOTE: Items underlined are those factors changing relative to A, i.e., Actual TM Data)

* Accuracy obtained when analyst interaction was permitted to edit training statistics.
† Case I Accuracies based upon use of 17 detailed land cover/land use classes.
# Case II Accuracies based upon use of 5 aggregated land cover classes.

IV-21

Table 4. Analysis of Variance Results

Factor	DF	Sum of Squares	F Value	α level at which significant
Spatial	1	3.645	3.54	0.0719
Spectral	1	276.125	268.52	<0.0001
Radiometric	1	219.451	213.40	<0.0001
Spatial*Spectral	1	4.061	3.95	0.0584
Spatial*Radiometric	1	5.780	5.62	0.0261
Spectral*Radiometric	1	18.605	18.09	0.0003
Spatial*Spectral*Radiometric	1	1.361	1.32	0.2613
Total Model	7	529.029	73.49	<0.0001
Error	24	24.680	MSE= 1.028	

Table 5. Pairwise Comparisons, by the Tukey Method, of Differences in Treatment Means
Due to the Spectral Factor

Treatment Pair	Difference in Percent Accuracy	Studentized Range; $q(8,24)$	α *
A minus E	+ 7.7%	15.2	<0.01
B minus F	+ 5.5%	10.8	<0.01
C minus G	+ 7.1%	14.0	<0.01
D minus H	+ 3.3%	6.5	<0.01

Table 6. Pairwise Comparisons, by the Tukey Method, of Differences in Treatment Means
Due to the Quantization Factor

Treatment Pair	Difference in Percent Accuracy	Studentized Range; $q(8,24)$	α *
A minus C	+ 5.5%	10.8	<0.01
B minus D	+ 8.0%	15.9	<0.01
E minus G	+ 3.3%	6.5	<0.01
F minus H	+ 4.2%	8.3	<0.01

Table 7. Pairwise Comparisons, by the Tukey Method, of Differences in Treatment Means
Due to the Spatial Factor

Treatment Pair	Difference in Percent Accuracy	Studentized Range; $q(8,24)$	α *
A minus B	- 1.2%	2.4	>0.10
C minus D	+ 1.3%	2.6	>0.10
E minus F	- 1.8%	3.6	>0.10
G minus H	- 1.0%	2.0	>0.10

*(NOTE: α is the probability of committing a Type I error.)
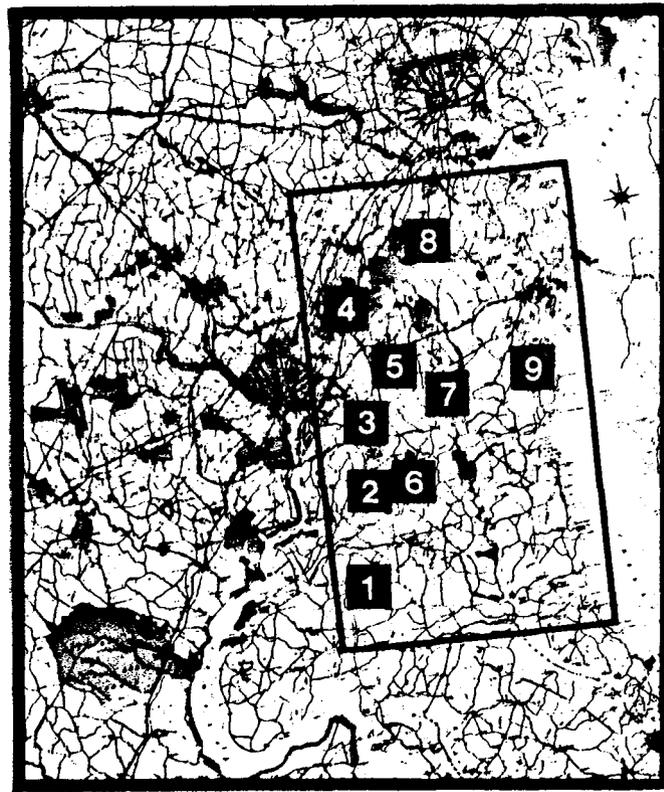
Figure 1. Location of the general study
area (within box) and the nine
study sites randomly chosen
for detailed analysis.
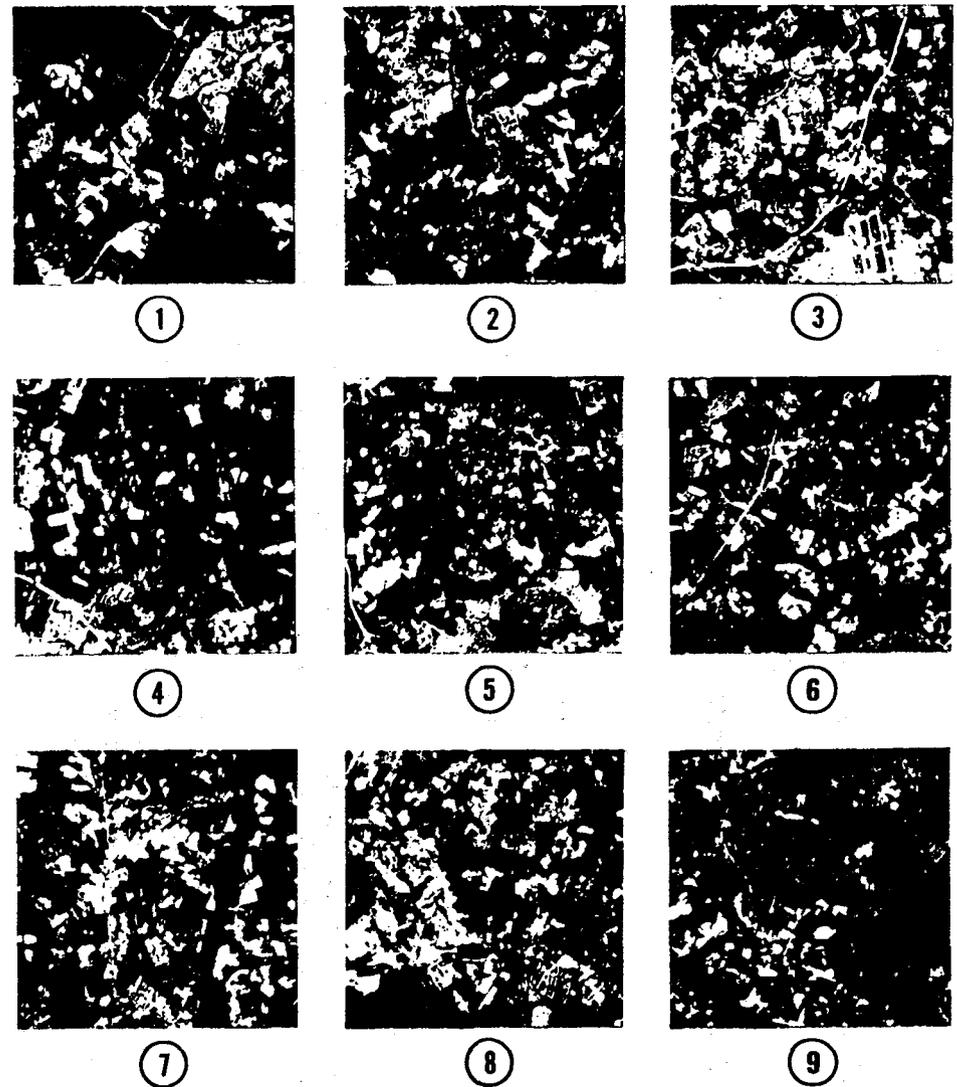
Figure 2. Thematic Mapper band 3 (0.63-0.69 µm) sub-images
for the nine study sites shown in Figure 1. Each
image is 256-by-256 pixels in size.

ANALYSIS AND EVALUATION OF THE LANDSAT-4 MSS AND TM SENSORS

AND

GROUND DATA PROCESSING SYSTEMS--EARLY RESULTS

Ralph Bernstein
Jeffrey B. Lotspiech
IBM Palo Alto Scientific Center
1530 Page Mill Road
Palo Alto, CA 94303-0821

1.0 INTRODUCTION

The Landsat-4 was launched in July 1982, and contained as its payload an advanced new sensor, the Thematic Mapper (TM) in addition to the Multispectral Scanner (MSS). The TM sensor was designed on the basis of user requirements defined at a NASA Workshop (Ref. 1), and successfully built and launched into space by NASA. This is the first of a series of papers reporting the results of a principal investigation activity under NASA Contract NAS5-27355 (Ref. 2). The purpose of the contract is to assess the performance of the Landsat-4 sensors and the associated ground processing, and to recommend improved algorithms and procedures to process the data. In addition, image science experiments to improve information extraction were conducted and are included. This paper provides results to date, recommendations for changes and improvements to the processing of the data, and a discussion of work planned for the future.

2.0 LANDSAT-4 SENSORS' CHARACTERISTICS

The MSS sensor principle of operation is discussed in detail in Reference 3, and the TM in Reference 4. These devices use mirror systems and detectors to convert the earth radiance and temperature values into digital numbers that are transmitted to the ground. The MSS sensor has 24 detectors, 6 per band and the TM has 100 detectors, 16 for each visible and infrared bands and 4 for the thermal band. The MSS and TM sensor performance were evaluated by studying both the sensors and the characteristics of the data. This included information content analysis, image statistics, band-to-band registration, the presence of failed or failing detectors and sensor resolution. This section will address these categories.

2.1 Sensor Data Entropy

The Landsat-4 TM uses eight-bit analog-to-digital (A/D) converters for each band. The MSS only uses a six-bit A/D converter. Are the extra two bits of the TM effectively used? One way to try to answer this question is to calculate the

entropy of the signal.

Entropy is a measure of the amount of information (in bits) in an arbitrary signal where the ith code word has a probability p(i) (Ref. 5). With eight-bit TM data, there are 256 possible intensity counts for each pixel for each band. From the histogram of a scene, one can calculate the probability that any count will be sent (in that scene). The entropy H is the expected value of the base 2 logarithm of the probabilities of the counts:

$$H = - \sum_i p(i) \log_2 p(i) \qquad\qquad (1)$$

The entropy yields the lower bound on the average number of bits required to encode each pixel in that scene if an ideal coding scheme were found and used.

Table 1 shows the entropy (per pixel) of the Chesapeake Bay scene imaged on November 2, 1982. To avoid invalid or extraneous pixels, a sub-image from TM column 1000 to TM column 5600 was used. Also, non-geometrically corrected data were used; geometric correction increases the entropy by creating new intensity values. The entropies have been calculated per detector for both the MSS and the TM. The table shows the average entropy for all the detectors in the band.

Table 1 - Sensor Entropy by Band
Chesapeake Bay November 2, 1982 Scene (E-40109-15140)

	TM[1]	TM spectrum[2]	MSS[1]	MSS spectrum[2]
Band 1	4.21	0.45-0.52	-	-
Band 2	3.78	0.52-0.60	-	-
Band 3	4.55	0.63-0.69	-	-
Band 4	5.19	0.76-0.90	2.91	0.5-0.6
Band 5	5.92	1.55-1.75	3.57	0.6-0.7
Band 6	3.53	10.4-12.5	4.29	0.7-0.8
Band 7	5.11	2.08-2.35	3.63	0.8-1.1

([1]average bits per pixel)
([2]wavelength in micro-meters)

An interesting aspect of Table 1 is the comparison between the MSS and the TM entropies in corresponding spectral regions (i.e., TM 2 vs. MSS 4, TM 3 vs. MSS 5, and TM 4 vs. MSS 7). Since the instruments were imaging the same area at the same time, any difference in entropy should only be due to the slightly different spectral regions (minor) or the finer quantization levels of the TM A/D converter.

TM bands 2 and 3 appear to have about one bit more entropy than their corresponding MSS bands, and TM band 4 appears to have about one and a half bits more entropy. Therefore, it appears that the additional two bits of the TM converter provide not only an improved quantization within the existing MSS range, but also increase the range as well. In other words, it appears that of

the two new TM bits, roughly one bit is a new high order bit while the other bit is a new low order bit.

2.2 Sensor Data Analysis

Histograms - The histograms of each detector in the Chesapeake scene are shown in Figures 1-7. In most bands, the radiance/temperature counts are clustered in a narrow intensity region of the 0-255 count range. This is consistent with the results of the entropy calculations. It is also expected due to the low sun elevation angle and characteristics of that scene.

Figures 1-7 are histograms from the "A-tape" data (radiometrically calibrated but not yet geometrically corrected). Gaps (zero counts) are visible in several histograms (for example see Figure 1). These are a normal and an expected result of the radiometric calibration processing. We call these gaps "empty buckets" and we will discuss them further.

The histograms show that the detectors are well calibrated with the exception of TM band 6 (Figure 6). The four detectors show significant differences at the histograms peaks. (Note that the detector outputs are replicated four times resulting in sixteen histograms). This is most likely caused by an improper radiometric calibration gain. In fact, NASA discovered after this image was processed that the gain factors for band 6 were being applied to the detectors in the wrong order.

We also calculated the histograms for the "B-tape" data--the data that was not yet radiometrically calibrated. They are very similar to the A-tape histograms (if you remove the gaps, they would be identical).

A/D Converter Non-Linearity - Table 2 illustrates the distribution of pixel intensities as a function of the low order two bits of each band's A/D converter (from the B-tape histograms). NASA has reported that the spacecraft's A/D converters are not strictly linear in these bit positions. Table 2 supports this conclusion for this data set. Pixel counts ending in 01 or 10 binary occur more frequently than pixel counts ending in 00 or 11 binary. Statistically, there should be an equal frequency of occurance of each low order bit position. However, Table 2 has some scene dependency in it: for bands that have a sharp peak at the same count in most detectors, Table 2 could be reflecting that peak rather than an A/D non-linearity.

Table 2 - Distribution of Samples as a Function of Low Order Two Bits
Chesapeake November 2, 1982 Scene (E-40109-15140)

Low order bits:	00	01	10	11
Band 1	17%	31%	29%	22%
Band 2	18%	29%	29%	24%
Band 3	18%	34%	23%	24%
Band 4	18%	32%	32%	18%
Band 5	21%	25%	34%	20%
Band 7	24%	29%	26%	21%

2.3 Sensor Band-to-Band Registration

The TM has a primary and a secondary focal plane. Also, multiple detectors are used to image the earth in parallel scans. Thus the potential exists for band-to-band misregistration of the individual detectors and bands. The relative registration of the TM sensors was performed in two different ways: 1) visual assessment using digitally enlarged data, and 2) cross- correlating the bands.

Visual assessment - Data that included features characterized by points or edges were selected and used in this study. Band 1 was arbitrarily used as the reference band. The sub-images were enlarged by a factor of 8 times using a cubic convolution resampling algorithm and the relative positions of various features measured manually using a high resolution interactive display. Figure 8 shows the features that were selected for this analysis. The cursor was programmed to read out its position to 1/100 of a pixel in this step, allowing the feature to be located to about that precision. Table 3 on the following page provides the results of this analysis. Bands 1-4 appear to be in registration to within 0.1 pixels, while bands 5 and 7 exhibit about 0.7 pixel misregistration in the along-scan direction and about 0.3 pixel misregistration in the cross-scan direction. The TM thermal band appears to have a 1.5 pixel misregistration in the along-scan direction and 1.9 pixel misregistration in the cross-scan direction.

In order to independently assess the band-to-band registration, additional experiments were conducted using a cross-correlation algorithm.

Cross-correlation - Sub-images from six of the seven TM bands were cross-correlated using a computer algorithm. The thermal band, band 6, was not used. The algorithm was a simple "template matching" approach to find the best registration point (Refs. 6, 7). The algorithm worked as follows:

1. We extracted a 70x70 sub-image centered at each registration point (i.e., at the Washington Monument, the Jefferson Memorial, etc.)

2. The pixel intensities in the bands to be registered (i.e., bands 2-7, called the "test data") were then intensity normalized, that is, adjusted with a gain/bias so that their means and standard deviations were identical to the reference band (band 1).

Table 3 - TM Band-to-Band Visual Registration Analysis Results
Chesapeake Scene, ID: E-40109-15140, November 2, 1982

Features		1	2	3	4	5	6	7
Visible and IR Features								
Lincoln Memorial	Pixel	0	0.0	0.0	0.0	0.38	-	0.50
	Line	0	0.10	0.10	0.25	0.50	-	0.38
Jefferson Memorial	Pixel	0	0.0	0.10	0.25	0.75	-	0.75
	Line	0	-0.10	-0.10	0.10	0.10	-	0.10
Washington Monument	Pixel	0	-0.10	0.10	-0.10	1.0	-	0.75
	Line	0	-0.10	0.0	0.0	0.25	-	0.10
White House	Pixel	0	0.0	0.0	0.0	-	-	0.75
	Line	0	0.0	0.0	0.0	-	-	0.63
Thermal IR Features								
Wash. Channel	Pixel	0					1.13	
	Line	0					-1.75	
Park Area	Pixel	0					1.5	
	Line	0					-2.13	
Tidal Basin	Pixel	0					1.88	
	Line	0					-1.88	

Average Error		1	2	3	4	5	6	7
	Pixel	0	0.03	0.07	0.03	0.71	1.50	0.69
	Line	0	0.03	0.0	0.10	0.29	1.92	0.32

Note: Results relative to band 1 features (address of band i-band 1)

3. Then, for the test data only, we selected a centered 48x48 sub-image from the larger intensity normalized 70x70 sub-image.

4. For each possible registration of a 48x48 test data sub-image within the 70x70 reference data sub-image (529 registrations total) we calculated a score based on the sum of the absolute values of the pixel intensity count differences between the normalized test data and the reference band. A minimum sum represents maximum similarity.

5. The registration result with the lowest score (sum) was chosen as the best registration coordinates.

The results of the cross-correlation by the above algorithm are shown on Table 4 and agree well with the visual analysis results.

Table 4 - TM Band-to-Band Cross-Correlation Results
Chesapeake Scene, ID: E-40109-15140, November 2, 1982

Features		Misregistration of TM Band						
		1	2	3	4	5	6	7
Visible and IR Features								
Lincoln Memorial	Pixel	0	0.10	0.25	0.25	0.62	-	0.62
	Line	0	0.00	0.00	0.10	0.38	-	0.25
Jefferson Memorial	Pixel	0	0.10	0.10	NA	0.88	-	0.88
	Line	0	0.10	0.10	NA	0.38	-	0.25
Washington Monument	Pixel	0	0.00	0.10	NA	0.10	-	-0.62
	Line	0	0.25	0.00	NA	0.38	-	1.00
White House	Pixel	0	0.25	0.10	NA	1.00	-	0.88
	Line	0	0.00	0.10	NA	0.62	-	0.25
Average Error		1	2	3	4	5	6	7
	Pixel	0	0.10	0.14	0.25	0.66	-	0.44
	Line	0	0.09	0.05	0.10	0.44	-	0.44

2.4 Temporal Registration

Scene-to-scene registration is important for both image correction and information extraction operations. Limited experiments were conducted to assess the degree that TM data acquired at different times could be

cross-correlated. As two or more images with the same path and row numbers were not available at this date, we used the overlapped areas of the Modesto (December 8, 1982) scene and the San Francisco (December 31, 1982) scene not obscured by cloud cover. Unfortunately, the Central Valley of California was covered by fog at 9:30 AM on December 31 and much potential overlap was lost.

However, the town of Morgan Hill, California (a small town on US route 101 about 20 miles southeast of San Jose) was excellently imaged in both scenes. Furthermore, there are four small reservoirs that form a rough box around the town and whose dams make excellent registration points. The reservoirs are Anderson Lake, Coyote Lake, Uvas Reservoir, and Chesbro Reservoir and are shown on Figure 9.

Using a high resolution color display and digital enlargement, we located the northernmost point of each dam in each scene. We then performed a digital cross-correlation using an automatic algorithm. We used the same simple template matching algorithm described in the previous section. The results, shown in Table 5, demonstrate a 100% success rate: the automatic registration did not differ by more than a pixel from the manual registration. We ran the automatic registration for every reflective band; the best registration point found for each band never differed by more than a pixel from the other bands' points or from the manually determined point. In fact, because of the high band-to-band agreement, we consider the automatic registration to be more accurate than the manual registration for this experiment. The excellent success rate can be attributed, in part, to close acquisition dates (23-day separation) between the San Francisco and Modesto scenes. Further work is planned in this area as multiple data sets for the same ground area with greater temporal separation become available.

Table 5 - Results of Temporal Registration Experiment
Modesto Scene E-40145-18082 to San Francisco Scene E-40168-18143

Sub-image	Registration Results	
	Visual	Cross-Correlation
Anderson Lake	-1,-1	-2, 0
Coyote Lake	-5,+6	-5,+6
Uvas Reservoir	-9,-3	-9,-2
Chesbro Reservoir	-5,-3	-6,-3

(x,y pixels from nominal)

2.5 Failed Detectors

The TM contains a total of 100 detectors (16 for each of the six visual and infrared bands, and 4 for the thermal band). Two of the detectors either failed, or were considered to have been performing inadequately and their output was not used by the NASA ground data processing system. The result of not having a detector output is essentially a null value along scan line and produces a pathological histogram response. The failed detector 3 of band 5 is quite evident in the band 5 histogram shown on Figure 10. In this case the detector is

outputting an intensity count of 0 for all radiance input values. It was presumed that detector 4 of band 2 had also failed; however, it appears to provide a normal histogram as shown on Figure 11. The current ground processing approach is to use the output from the preceding detector, that is, to repeat the line directly above the failed detector. Improved techniques to compensate for failed detectors are discussed in Section 4.2

2.6 Sensor Resolution

The resolution of the TM and MSS data was assessed by visual and edge analysis methods. There was concurrent data acquired from these sensors and a sub-image over Dulles airport was used to determine the smallest linear feature that could be discerned and to conduct absolute and relative edge analyses.

Visual Analysis - Figure 12 shows a Dulles airport sub-image from the Chesapeake scene. This figure also shows a map of the airport and a high altitude aircraft photo in addition to the MSS and TM data. It should be noted that these data sets were all geometrically corrected and enlarged to be a conformable data set using an interactive geometric correction program (Ref. 10). The runways of this airport are 150 feet (45.7m) wide, and the parallel taxi strips are 75 feet wide. They can be easily seen on both the TM and the MSS data. Cross-sections of a corresponding point of the runway of the enlarged and registered images are shown on Figure 13; it is apparent from the images and the cross-sections that the TM data has significantly improved resolution and feature discernability relative to the MSS data. The TM cross-section data exhibits a sharper slope and narrower width, as would be expected from the smaller TM aperture. In the TM subimage of Dulles airport, linear features as small as about 25 feet (about 1/4 pixel) can be easily discerned.

Edge Analysis - Multiple edge analyses were conducted on TM linear features and plotted. A cross-section region of the Dulles airport runway were selected and ten contiguous lines of data were plotted. This was done in order to obtain a range of sample lines over the runway edges. Figure 14 show the edge traces that were produced from TM band 1 and Figure 15 the edge traces produced from TM band 2. These traces show a rapid transition from the radiance value of the grassy area into the concrete area. The runway is 45.7m wide and the radiance counts show a rapid transition from the grassy area into the concrete region (within two pixels). In a few cases, this transition occurs within a pixel. This is consistent with the expected transient response, taking into consideration the finite aperture size (30m) and the filtering effects of the atmosphere, aperture, presampling filter and the digitizing process. Further analysis will be conducted to determine precisely the transfer function and spatial frequency response of the TM sensor.

2.7 Sensor Noise

Figure 16 shows a section of the Pacific Ocean from the December 31, 1982 San Francisco scene. It is a monochrome representation of the TM band 1 data portrayed with a high contrast stretch. It was chosen as it visually exhibits

every noise defect that we have found in any image. The near uniform radiance value of the ocean does not "mask" out the noise.

In the vertical dimension, two sources of noise are apparent: 1) there are alternating light and dark regions ("bands") varying from 60 to 180 detector lines in length, and 2) there are alternating light and dark detector lines ("stripes"). The second effect can be easily explained by inaccuracies in detector calibration processing, and will be covered in more detail in the next section when we discuss ground processing.

The "banding" effect is more difficult to explain. There is no known noise source that can account for it. It is possible that the detector offset voltage becomes unstable in certain images; this will be studied further at a later time.

In the horizontal dimension there are also two sources of noise: 1) a waveform with a spatial period of about 17 pixels that can be seen as a "ripple" effect in Figure 16, and 2) a waveform with a spatial period of 3 pixels. The 3 pixel frequency is most easily visualized in Figure 17, which shows the result of subtracting each pixel count from its left neighbor's count. If the noise were perfectly formed and perfectly in phase from line to line, one would see continuous vertical stripes in Figure 17. Of course, the noise is not that well behaved, but one can see a definate "vertical texture" in the figure. This 3 pixel noise typically shows up as a repeating "+1 -1 0" pattern over the background average intensity count.

Figure 18 shows the energy at each spatial frequency in the top line of the Figure 16 image. There are peaks that correspond to both of the noise spatial frequencies actually observed. The 3 pixel peak (at 325 cycles per 1024 pixels) is the larger; the 17 pixel peak (at 59 cycles per 1024 pixels) is still very noticable. These peaks indicate that the actual spatial periods of the 3 pixel and 17 pixel noise sources are 3.15 and 17.35 pixels respectively in this image.

A waveform with a 3 pixel spatial period has a time frequency of about 32 kHz. This corresponds to the chop frequency of a switching power supply on board the space craft, so it is reasonable to assume that the 3 pixel noise is due to this electrical noise source adding to the signal. Later in this paper, we will present a computationally efficient algorithm to reduce this noise effect.

The source of the longer period pixel noise (17.35) is unexplained at this time.

3.0 LANDSAT-4 GROUND DATA PROCESSING

As the TM is a new sensor, with different principles of operation and improved data characteristics, this investigation explored the data from the point of view of adequacy of the ground processing and improvements that could be made to compensate for sensor problems and deficiencies. This included investigating the radiometric correction processing, compensation for a failed detector, and geometric correction processing.

3.1 Radiometric Correction Processing

The sixteen detectors in a band respond fairly uniformly to identical inputs, varying by no more than 1 part in 30 between them. However, the human eye is very sensitive to linear features and this variation can cause objectionable "striping" over uniform radiance features, such as bodies of water. To compensate for this variation, NASA ground processing transforms each detector's output by separate gain/bias factors derived either from the spacecraft calibration data or from averages of readings over the ground:

$$I_o(i,j) = gI(i,j) + b \tag{2}$$

where g is the gain factor and b is the bias.

The B-tape data is transformed to A-tape data by multiplying the B-tape pixel value by the appropriate gain, adding the appropriate bias, then rounding the result to the nearest integer number. The process is illustrated in Figure 19, using actual calibration values for one detector from the Chesapeake scene. This figure also illustrates a side effect of the process: the "empty bucket" effect. The output value 64 is an "empty bucket"; the input count 63, when transformed, was rounded to 63, and the input 64, when transformed, was rounded to 65. Nothing was mapped to output 64, so it is empty. Similar empty buckets can be seen for almost every detector in the A-tape histograms.

Incidentally, the multiplying/rounding process is only calculated once for each possible input value 0-255. The correct output is placed in a table (one table for each detector), and the B-tape to A-tape conversion of the millions of input pixels then becomes a simple matter of using the input to fetch the correct output from the table. For this reason this processing technique is often called the "table lookup" approach.

NASA's radiometric processing does not completely remove the stripes (measured subjectively by that unsurpassed stripe detector, the human eye). We wondered whether the observed stripes might be solely due to an empty bucket effect, not to any error in the calibration factors. We looked at an area of the Potomac River in the Chesapeake scene that showed striping in band 1 (see Figure 25). The counts were in the range 63-65. In band 1, one detector had an empty bucket at 64 and another detector had an empty bucket at 65. If we take the detector with the empty bucket at 64 as an example, NASA's ground processing prevented it from indicating that the radiance count was 64. Judging from the rest of the detectors in this area, this must have frequently been the true scene radiance.

Later in this paper, we will present a statistical algorithm that radiometrically corrects the data but does not leave empty buckets.

3.2 Failed Detector Data Compensation

When a detector has failed, NASA ground processing replaces the failed detector scan line with the scan line of the detector immediately above it prior to geometrically correcting the data. This scheme can cause very observable

distortions in the final image products, especially images of high contrast cultural features. Figure 20 shows an aerial view of RFK Stadium in Washington, D.C. Figure 23a shows a greatly expanded TM image of the same stadium acquired on November 2, 1982. The stadium shows up as a bright donut-shaped object with a diameter of about 8 picture elements. In this true color image using bands 1, 2, and 3, the southern stands show up as a bright magenta feature with green fringing. This is a data defect due to the failed detector in band 2; in reality, the southern stands are identical to the northern stands. Figure 21 shows band 2 in a three dimensional presentation where the height corresponds to pixel brightness. One can clearly see that the repeated line due to the failed detector is in line with the southern stands. Therefore the stadium appears to be horseshoe-shaped rather than donut-shaped in band 2.

The Dulles Airport TM sub-images (Figure 12) show the same kind of defects in band 2 that were observable in the RFK sub-image. For example, in the true color (3-2-1) image, there are periodic magenta colored gaps in the taxiway of the east/west runway where the failed detector tracks over it. Throughout the image, the failed detector can be spotted as smears of magenta or green color. Any linear feature that lies at a significant angle to the spacecraft's line of flight shows the failed detector problem clearly.

Later in this paper, we will present some new algorithms that work better for computationally replacing a failed detector.

3.3 Geometric Correction

A preliminary investigation was performed to assess the geometry of a TM image. Both TM and MSS data were acquired over Washington, D.C. on November 2, 1982. Both scenes were processed to be in the Space Oblique Mercator (SOM) projection (Ref. 8). In the absence of SOM projection maps, we decided to use the MSS image as a SOM reference and to evaluate the geometry of the TM data relative to that reference, as the MSS data processed by NASA, NOAA and DOI was assumed to have had more geometric checks made on it.

Background - An image may have geometric errors from a number of sources:

* sensor-related errors,

* platform attitude and altitude deviations from nominal,

* scene or cartographic related errors.

Transformations of varying complexity may be required depending on the geometric corrections needed. For example:

* zero-order transformations provide a translation correction,

* first-order transformations provide a coordinate axes rotation or scaling, and

• second or higher order transformations correct for non-linear errors or implement cartographic projection transformations.

Image registration - This technique is used to register different images taken of the same scene or images taken at different times with the same or differing sensors. The registration can be performed automatically or can involve manual mensuration of ground control points. Registering two images requires correlating a number of points in both images. There must be a sufficient number of points to accommodate an accurate mathematical model of the relative geometric distortions existing between the images.

Image mapping - Image mapping transforms or converts the image from one geometric space to another. This can be done with a two-dimensional or a three dimensional transformation. In the former, the information relating the scene projection onto a plane is used, neglecting vertical relief data (mountains, etc.). Three dimensional transformations are the more precise as they provide vertical relief displacement corrections.

Approach used - The MSS image data and the TM image data have differing pixel sizes. The MSS data is processed by NASA so that the pixels correspond to 57 meters square on the ground, and the TM data is processed so that the pixels correspond to 28.5 meters square. We processed both MSS and TM images so that the new pixel sizes of each sensor were 25.4 meters square (chosen because it allows a precise 1:250,000 scale factor on our 4 mil plotting device). This processing only influenced a single linear term in each of the mapping equations, and did not change the image geometry other than pixel size (Ref. 10). Corresponding features were accurately located in each digital image using an interactive high resolution display (IBM 7350). A relative geometry table was generated and is shown on Table 6. It relates the x (along scan) and y (across scan) coordinates of the same point in both the MSS and TM space. Table 6 summarizes the average displacements in six regions of the image and approximately where those regions were located. The averages were made up of about five ground control points for each region. Table 7 on the following page shows the actual ground control points and their locations.

Table 6 - Average Displacements of MSS to TM Points
Chesapeake Bay November 2, 1982 Scene (E-40109-15140)

(+2.1,+0.5)	(+2.0,-0.4)	(+2.1,-0.3)
	(+2.0,-0.6)	
(+2.1,-0.8)		(+2.1,-0.7)

- all measurements in (x,y) kilometers -

Results of TM and MSS Registration - These two images, acquired from the same spacecraft at the same time, processed (by NASA) to be in the same map projection (SOM), and processed (by us) to be at the same scale, should in conformance throughout the image except for a uniform displacement introduced because we did not register the images before scaling them. Table 6 shows the effect of this displacement, but it also shows that there are other higher order distortions. These distortions are greater in the y dimension (totalling 1.3 kilometers). The upper left hand portion of the image shows the greatest relative distortion.

It is surprising that the y dimension shows the greater error. The x dimension is scanned by the mirror systems, which are different in the two instruments; the y dimension is scanned by the motion of the satellite itself, which, of course, is common to the instruments. The following two dimensional mapping functions are the best first order fit for the 33 registration points shown in Table 7:

$$X = -2.00 + 0.9995x + 0.0005y \tag{3}$$
$$Y = -0.11 + 0.0023x + 1.0056y \tag{4}$$

They indicate a slight rotation combined with a scale expansion of about 0.5% in the y dimension. Unfortunately, they fail by as much half a kilometer in predicting the y displacements.

The following equations are the best second order fit for the 33 registration points in Table 7:

$$X = -2.10 + 1.0039x - 0.000028x^2 + 0.000002xy - 0.0009y + 0.000004y^2 \tag{5}$$
$$Y = -0.81 + 0.0215x - 0.000093x^2 - 0.000065xy + 1.0066y + 0.000042y^2 \tag{6}$$

These equations produce registered images accurate to within 120 meters in both x and y. This result indicates that either the MSS or the TM have both scale and non-linear distortions remaining.

Table 7 - Relative Registration Between MSS and TM Data
Chesapeake Bay November 2, 1982 Scene (E-40109-15140)

Name	MSS x	y	TM x	y	Delta x	y
REGION A						
River bend	14.17	9.86	12.14	9.40	2.03	.46
Pointed field	18.85	7.87	16.76	7.37	2.08	.51
Field corner	17.78	16.64	15.70	16.18	2.08	.46
Valley	7.11	15.24	5.03	14.78	2.08	.46
REGION B						
Donut	71.09	67.54	69.09	68.12	2.01	-.58
White dot	72.24	69.32	70.23	69.90	2.01	-.58
Platform	88.14	62.53	86.16	63.07	1.98	-.53
Moon	89.36	66.04	87.35	66.60	2.01	-.56
Torpedo	90.27	69.14	88.24	69.72	2.03	-.58
REGION C						
Finger	145.72	130.45	143.61	131.11	2.11	-.66
Stirrup	140.18	122.53	138.05	123.19	2.13	-.66
Channel	142.09	121.11	139.95	121.77	2.13	-.66
Thumb	148.18	124.33	146.05	125.02	2.13	-.69
River/lake	135.71	114.63	133.55	115.32	2.16	-.69
REGION D						
Dog	76.30	20.96	74.35	21.39	1.96	-.43
Siamese	81.10	14.66	79.15	15.04	1.96	-.38
River	90.63	7.42	88.65	7.80	1.98	-.38
Black hole	86.94	23.14	84.96	23.60	1.98	-.46
Eastern hole	89.36	22.43	87.43	22.83	1.93	-.41
Lake	77.42	5.79	75.44	6.17	1.98	-.38
REGION E						
Ruin	138.96	5.87	136.83	6.15	2.13	-.28
Nose	144.02	4.06	141.88	4.34	2.13	-.28
Appendix	148.95	16.21	146.89	16.48	2.06	-.28
River intersect.	134.59	21.03	132.56	21.39	2.03	-.36
Hook	138.96	19.48	136.73	19.91	2.24	-.43
Triangle	150.65	5.87	148.49	6.17	2.16	-.30
White square	137.62	14.27	135.46	14.63	2.16	-.36
REGION F						
Gold tooth	6.17	121.97	4.06	122.76	2.11	-.79
Radio	8.59	118.36	6.53	119.15	2.06	-.79
Road intersect.	13.39	121.39	11.30	122.12	2.08	-.74
Barn	17.98	112.70	15.88	113.39	2.11	-.69
Lake point	26.82	119.81	24.74	120.65	2.08	-.84
Snake eyes	20.55	122.81	18.44	123.57	2.11	-.76

• Note: names are mnemonics for the appearance of a feature, and do not correspond to actual place names.

4.0 EXPERIMENTAL ALGORITHMS AND RESULTS

This section describes algorithms developed to improve radiometric processing, to reduce striping, to compensate for failed detectors, and to reduce the noise of the TM sensor data.

4.1 Radiometric Correction/Striping Removal

As has been described previously, NASA's radiometric correction processing leaves "empty buckets" in the output data. Also, there is reason to believe that these empty buckets contribute to the striping observed in some images.

We decided to process the Potomac River sub-scene from the November 2, 1982 Chesapeake image and eliminate this source of striping. An alternative to NASA's lookup table approach is diagrammed in Figure 22. It can be described as a probabilistic approach. If a detector's calibrated output of an input 64 count is 64.504, for example, we randomly place 50.4% of the input 64's into the 65 output bucket and 49.6% of the input 64's into the 64 output bucket.

There is a concern that the probabilistic approach "destroys" the original input data. This is true in the sense that it is no longer possible to determine uniquely what the B-tape data value must have been from the calibrated A-tape data. However, it is not true that the existing lookup approach yields a "better" estimate of the actual ground radiance. An input 64 on the B-tape could actually correspond to any radiance between 63.5 and 64.5. Therefore the true output could be anywhere (in this detector's example) between 64.000 and 65.008 and only on the average would it be 64.504. What is the best guess for the output count? Unfortunately, there are two good answers:

1. Guessing it always to be 65 is "best", in the sense that it minimizes the average error (although most of the time the guess will be higher than the actual radiance). This is what NASA's standard processing would do.

2. Guessing it sometimes to be 64 and sometimes to be 65 is "best", in the sense that the accumulated bias of the error will be zero (although the average magnitude of the error will be greater). This is what our alternative would do.

We applied the probabilistic estimating approach to the Potomac sub-scene. The striping was noticeably reduced (see Figure 25c) but not altogether eliminated. We conclude that:

• Empty buckets can cause striping in an image even when the calibration is otherwise perfect.

• The calibration factors used by NASA in the Chesapeake scene were not perfect.

Incidentally, in using the probabilistic approach to adjusting pixel itensities, it is not necessary to calculate a new random number for each pixel operation. It is adequate to keep a table of random numbers and simply cycle

through them. A table of about 1000 numbers is enough. In addition to saving computation, this modification to the algorithm allows the input data to be reconstructed from the output (assuming the random number table is published).

In fact, just as with the current NASA scheme, no multiplications need be carried out for each pixel--only fixed point additions. This is done as follows:

1. Build a table for each detector for each of the 256 input possibilities where the output is represented as a 16 (not 8!) bit quantity of the form XX.XX (base 16).

2. Store the random numbers in the form $0.XX_{16}$. (The random numbers should be evenly distributed in the range 0.00_{16} to $0.FF_{16}$.)

3. To find an output value, add the indicated output in the table with the next random number then truncate the decimal part of the result (i.e., the low order 8 bits).

4.2 Failed Detector Data Compensation

We have seen from the previous section how the current NASA failed detector replacement scheme can cause image defects. It has been suggested that the ground processing, instead of merely replacing the failed detector with the line above, should linearly interpolate between the line above and the line below to calculate the failed detector line. This does not solve the problem; RFK stadium still ends up looking like a horseshoe instead of a donut. Even interpolation with higher order curves, such as quadratic fit, are of no help. Figure 23b demonstrates this. In fact, it is difficult to imagine any algorithm that could correctly deduce the donut shape from the existing band 2 data--after all, many stadiums actually have a horseshoe not a donut shape.

We have been experimenting with the idea of replacing the failed detector scan line under the control of the same scan line in a "template" band--a nearby band with no failed detectors that is fairly well correlated with the failed detector's band. The results are very encouraging. We use band 1 as a template with which to generate new intensity values for the failed detector in band 2. The following three algorithms are different methods for doing this:

Algorithm 1 - Template Replacement

This is the simplest template algorithm that we have devised. In this algorithm we directly substituted detector 4 of band 1 for detector 4 of band 2, after scaling its output intensity so that its range was similiar to the other detectors in band 2. The band 1 to band 2 conversion is of the form:

$$I_2(i,j) = aI_1(i,j) + b \tag{7}$$

where $I_n(i,j)$ is the pixel value in band n (n = 1 to 7) at line i, column j, and

where the gain, a, and the bias, b, are calculated from the statistics of the two bands:

$$a = \sigma_2 \div \sigma_1 \qquad\qquad b = \mu_2 - a\mu_1 \qquad\qquad\qquad (8)$$

where μ_n and σ_n are the mean and standard deviation of band n respectively.

Algorithm 2 - Template Replacement with Error Adjustment

In this algorithm, band 1 data is substituted for band 2 data as in algorithm 1, with an error count value added to each pixel. The error value is a measure of how different band 1 and band 2 are in the neighborhood of a failed pixel.

Specifically, the error signal ε is the average of the difference between normalized band 1 signal and the actual band 2 signal at the pixel above and the pixel below the failed detector pixel. That is:

$$\varepsilon(i,j) = [I_2(i-1,j) - (aI_1(i-1,j)+b) + I_2(i+1,j) - (aI_1(i+1,j)+b)] \div 2 \quad (9)$$

where a and b are calculated as in algorithm 1. The final output pixel is:

$$I_2(i,j) = aI_1(i,j) + b + \varepsilon(i,j) \qquad\qquad\qquad (10)$$

Algorithm 3 - Quadratic Vertical Fit with Template Data

The final algorithm fits a quadratic equation to a five pixel vertical (across scan) slice centered around each failed detector pixel. The relative pixel intensity values are considered to be a quadratic function of the line number, "i":

$$I(i) = a_0 + a_1 i + a_2 i^2 \qquad\qquad\qquad (11)$$

The coefficients of the quadratic are determined by a least squares fit to the actual data in each vertical slice. The data value used for the failed (center) pixel in the slice is the scaled template value from the nearby band calculated as in algorithm 1.

Once the coefficients are determined, the missing pixel value is simply the value of the quadratic at the i value of the missing detector line. (In the five pixel centered vertical slice the i value of the missing pixel is always 3.) Note that new coefficients must be calculated for each pixel that needs to be replaced.

We programmed these three algorithms in APL and ran them on the RFK and Dulles sub-images. The results were excellent. Figure 24 shows the algorithms applied to the RFK stadium sub-image. Both the RFK and Dulles sub-images can be corrected so that the casual observer sees no defects in any circular or linear

feature using any of these algorithms. If you wish to replace a failed detector with another detector's output and are concerned with maintaining the shape of geometric features, you are far better off using the same detector's output from a nearby band than a nearby detector's output from the same band.

A detailed examination of the failed detector lines does show some defects with the template algorithms, although in no cases are they as extreme as the defects observable with the current failed detector scheme. These defects are in two classes:

1. In flat, low contrast regions, the failed detector line frequently shows up as a slightly off color stripe with algorithm 1. Algorithm 2 exhibits this same property, but much less frequently and less pronounced. We have never seen stripes with algorithm 3.

2. In high contrast man-made features, algorithm 3 usually yields a lower contrast value than would be best for the scene. This can be observed as slightly off-color (e.g, pale magenta or green) pixels near or on the man-made feature. We have never seen this problem with algorithms 1 or 2.

When table lookup programming techniques are used, only algorithm 3 requires per pixel multiplications and divisions (to perform the least squares fit). Even then, the computer calculations required are not more than those that are required for a geometric resampling, and, of course, need only be performed for the failed detector pixels, not for every pixel.

4.3   Reduction of 32 KiloHertz Noise

There appears to be a high frequency coherent noise signal in the TM data. There are two ways to remove a coherent noise source of a known frequency:

1. Transform the incoming signal to the frequency domain and filter out the noise frequency, then transform the signal back to the spatial domain.

2. Process the signal in the spatial domain by subtracting a waveform of the noise frequency directly from the incoming signal.

The first method can require a prohibitive amount of processing without special Fourier transform hardware. The second method, although it requires much less processing, is very sensitive to the relative phases of the subtractive noise waveform and the actual noise in the data--if you are not careful, you may end up doubling the noise rather than zeroing it out. So, determining the phase of the noise in the data is a key factor in successfully reducing or removing it by the second method. The problem is complicated because the noise period is not necessarily an integral number of pixels and the noise may not be stationary (e.g., may drift slightly with time). Knowing the precise noise phase at a certain point in the input signal is no guarantee that you will know it later on.

In this section we will present an algorithm for eliminating the 3 pixel (32 kiloHertz) noise from the images that is based on the second method above. In this algorithm we arbitrarily partition the incoming signal line into adjacent

"cells" containing three pixels each. Within the cells, the pixels are called "A", "B", and "C". The algorithm then attempts to determine, for each cell, whether the noise signal is in synchronization with the A, B, or C pixel. To do this, we "differentiate" the signal by subtracting each pixel from its left-hand neighbor. The noise signal now typically looks like a "+2 -1 -1" pattern. The cells are now assigned to one of four states:

1. "A sync" - a positive transition was found in the A position only.

2. "B sync" - a positive transition was found in the B position only.

3. "C sync" - a positive transition was found in the C position only.

4. "Undecided" - either no positive transition was detected in the cell or more than one transition was detected.

At this point with a typical input signal we probably have equal numbers of A, B, and C sync cells. However, because the phase of the noise signal does not change rapidly, cells will tend to be in the same sync as their neighbors. Therefore the cells will be grouped in regions of similiar sync, and between the regions the cells will be predominantly undecided. Also, scattered throughout the line will be cells whose sync has been incorrectly assigned: for example, an isolated "B" in the middle of a group of "A"s.

Now we enter an iterative algorithm that attempts to grow the regions of sync by assigning the undecided cells to one of the three definite sync states. The decision flow for an undecided cell to become decided is shown on Figure 26, and depends on the state of its neighboring cells. If neither its left nor right neighbor has decided on a sync, then a cell remains undecided. If only one has decided on a sync, then the cell decides to be in sync with it. If both have decided on a sync, then the cell arbitrarily decides to be in sync with its left neighbor.

Each time we apply the decision algorithm to the cells, more cells become decided. The regions of sync grow as they convince their undecided neighbors to be in sync with them. The decision algorithm can be applied iteratively until all undecided cells have become decided; however, we recommend setting an upper bound on the number of iterations at four. This is adequate for uniform intensity regions (like the Pacific Ocean). Over structured land features the algorithm will neither be as accurate nor as important, so there is no need to force it with extra iterations.

After we have grown the regions as much as we want, we can now go and re-label some of the cells that were obviously mislabeled in the first step. If a cell is surrounded on both sides by neighbors that agree on a sync state, but the cell itself is in a different sync state, we change the state of that cell to be in agreement with its neighbors.

After synchronization is determined, the magnitude of the noise can be estimated. This is simply a matter of averaging the signal of all the pixels in the first position, the second position, and the third position after the sync point (A, B, or C). These correlated averages are subtracted from the signal average to determine the difference due to the noise. Then this difference is subtracted from the original signal, using the synchronization points

determined for each cell. If a cell is still undecided, no noise correction is done for that cell.

Figure 27 shows the results of this algorithm applied to the Pacific Ocean sub-image of the San Francisco December 31, 1982 scene. The top half of the image has been compensated, the lower half is the original data. Figure 28 shows the same repaired sub-image represented as pixel-to-pixel differences, a representation which enhances the 32 kHz noise. It can clearly be seen that the noise (the "vertical texture") is reduced in the upper half of the image.

Figures 37 and 38 show the same image with the noise reduced by the more conventional approach of transforming the image with an FFT algorithm, eliminating the noise frequency in the frequency domain, then transforming the image back to the spatial domain. It can be seen that the algorithm presented above performs at least as well as the FFT approach, and takes significantly less processing (assuming the special FFT hardware is not available).

4.4 Digital Enlargement of Sub-Image Areas

Registration to a map - an experiment was conducted to enlarge and to register a TM sub-image area with a map. The objective was to ascertain the degree of enlargement that could be used before the data became unusable, and also to determine the the amount of distortion in the original data. This experiment was accomplished by digitizing an available street map of the downtown Washington, DC region, and then registering a TM sub-image of the same area to the map (Ref 10). In this experiment, the digitally enlarged TM image was expanded by a factor of about 7 times and rotated in order to match the geometry of the map. Figure 32 shows the reference map that was used, Figure 33 the source TM sub-image that contained the same area, and Figure 34 the geometrically registered, rotated and enlarged TM image. Of interest is the detail of the enlarged TM image. Clearly visible are the Capital, White House, Space Museum, the Washington monument including its shadow, and the Lincoln memorial. This data was also overlayed on the map, and is shown on Figure 35. A linear first order mapping function was used to enlarge and rotate the image using cubic convolution re-sampling (Ref. 11). The mapping function is:

$$X = 230.58 + 0.14565x + 0.02473y \qquad (12)$$
$$Y = 373.75 - 0.00240x + 0.14573y \qquad (13)$$

A second experiment was done to register the data to a 1:24,000 scale USGS map. This was also successful, and showed regions on the map that needed updating (for example, the Kennedy Center for the Performing Arts had been built after the map was published).

It appears that the data is of good enough resolution and quality to be useful for land use analysis and evaluation.

Resampling experiment - an experiment was conducted to evaluate the performance of resampling algorithms to support the TM enlargement. Figure 39a shows the Dulles airport band 1 sub-image, and Figures 39b, c, and d show a portion of the sub-image enlarged, rotated, and resampled with nearest neighbor, cubic

convolution, and bilinear interpolation (Ref. 11). Clearly, the nearest neighbor resampling results in undesirable structured data due to the replication of data values. Surprisingly, bilinear interpolation gave similar results to the cubic convolution resampling. It should be noted that the source data was P-tape data--data previously cubic convolution resampled in the SOM correction process. The edge enhancement resulting form this process is maintained in both the bilinear interpolation enlargement and the cubic convolution enlargement, although additional edge enhancement can be seen on inspection in the cubic convolution enlarged image.

Generally, users should be able to enlarge P-tape data in many applications using bilinear interpolation, with attendant savings in processing time. However, higher order resampling algorithms should be used for A-tape to P-tape data geometric correction.

5.0 INFORMATION EXTRACTION EXAMPLES

Several experiments were conducted to assess the utility of the TM data for information extraction purposes. These experiments included using differing band combinations for Red-Green-Blue color presentation, combining bands to display more than three bands at one time, and principal component transformation of the original bands.

5.1 Color/Band Selection for Color Composites

A subimage from the Modesto scene was selected for color presentation experiments. Shown on Figures 29 and 30 are the seven bands of the Modesto subimage used for this experiment. This subimage provides a representative sample of geological, agricultural and urban land use categories. Various band combinations were used and recorded, and are shown on Figure 30. It is apparent that many possibilities are possible, as there are three bands from seven possible bands that can be used. It appears that bands 4 and 5 are important bands, from the point of view of their contribution to the color and separation of categories. Shown on Figure 31 are the map of that region and also a land use map produced by the USGS. It is interesting that the TM images show far greater detail than the map and provide current land use data.

5.2 Band Ratioing

Experiments were conducted to combine multiple bands into one color presentation. This was done in order to display more information for image viewing and analysis than would be possible in the usual red-green-blue color presentation of 3 of the bands. A subimage from the Modesto scene and centered on Tracy, CA was used in these experiments.

Image ratioing was performed by simply dividing corresponding pixels from one band into another. The resultant ratio would then be combined with a similar operation on the other bands. In this manner, a color composite could be

produced that effectively had six TM bands of information included in the result. Figure 30 shows the results of these processing operations. As a reference, real and false color images are also shown. It is noted that very good separation of land use and crop types result.

5.3 Principal Components Processing Results

A principal component analysis was performed on the 7-band Tracy sub-image extracted from the Modesto scene. The purpose of this analysis was to assess the "dimensionality" of the TM data. Multispectral images frequently exhibit high correlation between the spectral bands. Thus, a great deal of data redundancy can occur. This reduces the effectiveness of color presentation as only three conventional spectral bands can usually be shown at one time. The computation of principal components provide a set of component images that are far less correlated with each other, and can be ranked with increasingly lower variance. This usually results in fewer "bands" and can be used for color presentation with maximum information content (Refs. 5,8).

The results of the analysis are shown on Table 8 on the following page. From this table one can see that the first three components contain 97.2% of the variance. It is also apparent from the correlation matrix that there is significant correlation between TM bands 1, 2 and 3. Band 4 is quite uncorrelated with these bands, and accounts for the good color composites that are produced when this band is used. Band 7 is significantly uncorrelated with band 4, and thus the combination of band 4 with bands 7 and 1,2 or 3 should provide good image presentations. Clearly, Landsat-4 TM data has at least three significant principal components, as contrasted with Landsat 1-3 which usually exhibits two components. It should be noted, however, that in spite of these statistical results, the higher order components frequently provide interesting and surprisingly good information, in spite of the apparent low variance that they show mathematically. This is discussed further in Reference 12.

5.4 Thermal Image Processing

A night time TM scene of the Buffalo, New York area acquired August 22, 1982 was digitally processed. This band 6 thermal infrared scene is shown on Figure 36 in a gray scale representation. The image was edge enhanced, and the result of this processing is also shown. It is of interest to note that individual streets can be seen in the enlarged edge enhanced subimage as well as several canals that are located in the region. Various false color enhancements of the image were used to improve the information extraction potential of the data, and three experimental color products are shown on Figure 36. The dynamic range of the data spans about 32 counts, and color encoding is very helpful in enhancing the thermal contours and temperature distribution.

Table 8 - Results of Principal Component Processing of Tracy Sub-Image

Modesto December 8, 1982 Scene (E-40145-18082)

	1	2	3	4	5	6	7
Statistics:							
Means	55.57	23.45	23.37	36.91	48.23	92.11	23.97
Std. Dev.	4.80	3.14	5.00	1.05	1.29	2.09	8.63
Eigenvalues:							
	270.70	107.80	23.20	5.20	4.00	1.60	0.70
Percent Variance:							
	65.50	26.10	5.62	1.27	1.00	0.40	0.10
Cumulative Percent Variance:							
	65.60	91.60	97.20	98.50	99.50	99.90	100.00
Eigenvectors:							
	0.193	-0.176	0.596	-0.351	0.018	-0.671	-0.050
	0.149	-0.064	0.333	-0.136	-0.064	0.362	0.842
	0.230	-0.212	0.464	-0.100	-0.085	0.623	-0.530
	0.282	0.897	0.272	0.195	0.030	-0.010	-0.052
	0.768	-0.005	-0.489	-0.385	-0.148	-0.013	-0.011
	0.017	0.038	-0.048	-0.275	0.951	0.123	-0.006
	0.466	-0.337	-0.060	0.765	0.246	-0.122	0.062
Correlation Matrix:							
	1.000	0.891	0.915	0.022	0.553	-0.004	0.732
	0.891	1.000	0.918	0.216	0.680	0.012	0.773
	0.915	0.918	1.000	-0.003	0.665	-0.036	0.850
	0.022	0.216	-0.003	1.000	0.404	0.207	0.046
	0.553	0.680	0.665	0.404	1.000	0.152	0.852
	-0.004	0.012	-0.036	0.207	0.152	1.000	0.030
	0.732	0.773	0.850	0.046	0.852	0.030	1.000

6.0 SYSTEMS USED FOR DIGITAL IMAGE PROCESSING

Two digital image processing systems were used to support the analysis and processing of the Landsat-4 data. Much of the image processing analysis and display was performed on the IBM 7350 Image Processing System, and some experimental work was done on the IBM Personal Computer. Programs were written in Fortran, APL, and Basic.

6.1 The IBM 7350 Image Processing System

The IBM IPS is an integrated image processing system and display work station directly attachable to IBM 370 architecture computers (Ref. 13). It consists of the following units:

7351 Control Unit - This device contains the memory, channel support and processors need to support the display. It has a standard S/370 channel interface and cabling and the control unit support a 7352 Color Image Display Station, a 7353 Conversational Display Station, and can support up to six additional terminals. The Image Processor subsystem contains special logic for high speed programmable image processing and includes an image processor arithmetic unit, six band buffer look up tables, a classification look up table, interpolator, XY generator, mask buffer, and eight megabytes of memory for working image storage.

Display Subsystem - This system has three 5-bit digital-to-analog converters driving the high resolution RGB display, 4096 shades of color, a 1024 x 1024 x 13 bit refresh buffer, a pseudo color look up table, and an overlay plane for text / graphics annotation.

7352 Color Image Display Station - The color display is a high quality, high resolution (1024x1024) color monitor with the means for the attachment of a user provided color hardcopy device. The image quality is nearly photographic in nature.

7373 Conversational Monitor Station - This monitor is used to support user interaction with the system and includes an 87-key keyboard, and a joystick interface controlled by a programmable micro controller.

Host Basic User Subroutines - The support software consists of host resident library of subroutines for high level interface control of 7350. It is callable from FORTRAN, PL/I, assembler, PASCAL languages.

Operational Use - When performing interactive image processing, the six band buffers are loaded with six 1024x1024 8-bit subimages. Image presentation involves the selection of three of the six bands for color presentation using Blue-Green-Red or Intensity-Hue-Saturation color modes. The look-up tables are used for color enhancement, and the arithmetic processors use used for spatial operations such as enhancement or enlargement. The basic cycle time is about 3.5 seconds, so that edge enhancement or enlargement of a three band 1024x1024 subimage occurs in about 11 seconds. Principal component processing can be performed in about 1/2 minute using the arithmetic unit, compared to about 20-40 minutes on a general purpose computer.

6.2 Experimental Use of the IBM Personal Computer

A demonstration image processing system was developed for the IBM Personal Computer (PC), and shown at the Landsat-4 Symposium (Ref. 14). The purpose of this effort was to determine if meaningful digital image processing could be performed on a small inexpensive computer. This section will briefly describe the results of our experiment.

Summary Description - The IBM Personal Computer is a computer designed for an individual user. It has a 16K-256K byte memory, 40K byte of read-only memory and uses an 8088 microprocessor. The auxiliary memories are two 320K diskette drives and/or a 10M byte disk drive. An 83 key keyboard and high resolution 80 column monochrome display provide the means for an interactive terminal. An 80 to 132 character/line printer can be attached for hard copy output.

Software and Functions - The demonstration programs for the PC were written principally in Advanced BASIC with some assembly language code. The BASIc programs handle all the screen control and user-interface functions and many of the simple calculations that need floating point arithmetic. Table 9 on the following summarizes the various BASIC-coded functions. The assembly language code is provided to handle computationally intensive operations and is summarized in Table 10, also on the following page.

Structures - The general design for the demonstration was to select a fixed size subimage that would correspond to the capabilities of the display screen, i.e. 320 x 200 pixels. A subimage of suburban Detroit and Windsor, Ontario was extracted from LANDSAT-4 TM/P data tapes. An IBM 370/158 was used to extract a four-band subimage which was then transmitted over a local network (RS-232 interface) at 2400 baud to the IBM PC, and recorded on the PC 5-1/4" diskettes. A separate program in BASIC computed intensity histogram data and formatted the four-band histogram display. This display was then stored on the same diskette as the images. One double-sided diskette holds 322K bytes of data, which is sufficient for five 64K images. For the demonstration program the diskette contained one copy each of 4 bands, one histogram for each band, the 4-histogram display, and a text file containing a brief narrative description of the data. About 40K bytes of free space remained on the diskette.

Image Processing Programs - The main demonstration program is menu driven, and can thus be run with little or no user training. The program also supplies to the user information about both the hardware and software. The application part of the program allows the user to select among several sequences of processing of the subimage data.

Application demonstration - The application program consisted of the following functions and events:

1. Display Description of sample image
2. Display Histogram
3. Allow user to select 1 band of 4

TABLE 9 - BASIC Functions

INIT	Condition screen, create cursors and read menus to memory
SCOLOR	Set the Color display as the active screen
SMONO	Set the Monochrome display as the active screen
SFLIP	Flip active screen between color and monochrome
ERM	Write error message on current screen
LOADB	Load Image Band B (check for already in memory)
LOADH	Load Histogram (pre-created as a 1-record file)
INKEY	Wait for user to key in, then normalize key and return it to caller (allow debugging escape)
INKEY/COLOR	Like INKEY but intercepts color change requests
BLINK	Blink current cursor while waiting for user input
PUTCURSOR	Manages current cursor
SHOWTXT	Display selected menu or image description
SELBAND	Select working band from histogram display
PARTCOLOR	Elicit color partitions from user, build TRT
GETCOLOR	Get foreground/background colors from user
CVIMG	Call ASM color mapping function
FUNCOLOR	Elicit (linear) coloring functions from user, build TRT
BOXCAR	Do Boxcar classification
PUTCROSS	Cross hair manager for BOXCAR
MARKAREA	Mark selected training area
PUTDATA	Puts intensity values on screen
MAXMIN	Get maximum/minimum values for each class
CLASS	Control ASM classification functions

TABLE 10 - Assembler Language Functions

MAPBITS(TRT)	Convert all pixels via TRT into color and place on screen
CLASS0	Set all class codes to 1
CLASS(MINMX)	Compare all pixels to min/max and determine class
CLASSE(TRT)	Convert all class codes via TRT to color and place on screen
RDFILE(IMID)	Read image file into image buffer

4. Allow user to select intensity coloring method
   a) Color by partitioning
   b) Color by linear functions
5. Select foreground and background color combinations
6. Display
   a) Selected band using above options.
   b) Numeric data relating to coloring method.
7. Modify foreground and background colors as desired
   while displaying current image.
8. Select from the following options:
   a) Re-color (go back to step 2).
   b) Return to MAIN MENU.
   c) Do box-car classification (step 9).
9. Using the image currently displayed the user may:
   a) Select classifier training areas (up to 5
      rectangular areas for each of three classes).
   b) Display intensity values of current band within
      user-specified rectangle.
   c) Process the training information (step 10)
10. Construct classification image
   a) Use the training areas to construct parameters for
      each of the 4 bands.
   b) Apply the parameters to the 4 bands an display a
      composite image of 3 classes.
11. Modify foreground and background colors as desired
   while displaying current image.

Program Size - The BASIC program is about 750 statements long and the assembler programs contains about 200 instructions. The BASIC program takes about 15K bytes on a diskette. Once it is loaded and space allocated to variables, there are about 17K bytes left for program expansion. The assembler code and its internal data areas takes about 450 bytes.

System performance - We were quite surprised to see how fast the PC could perform image processing functions. Once the data was loaded onto the diskettes, the system was capable of interactive image processing. Table 11 shows the approximate timings for significant functions.

Table 11 - Timing for Selected Image Processing Functions

Function	Time	Comment
MAPBITS	0.6 sec	Translate table mapping 64K pixels
CLASS	6.0 sec	Compare 64K pixels with each of 6 numbers
RDFILE	5.0 sec	Read 64K pixels from diskette

Use of Printer for Hardcopy Output - As an experiment, the PC dot matrix printer was programmed to output an image, using a 4x4 dot matrix pattern. This provided effectively 17 levels of grey for image presentation. Shown on Figure 40 is a dot matrix representation of a TM band 1 subimage of the Detroit airport.

Individual picture elements can thus be represented in a pseudo grey-scale form, and can be produced in minutes on the low-cost output device.

Future Plans for Image Processing on the IBM PC - Experiments are being conducted to improve both the functional capabilities of the system, and the resolution of the displayed image. Because of the excellent image processing performance of the PC, more functions and capabilities are being added to the application programs. In addition, experiments are being conducted to increase the image display size by adding a larger screen. To date, a screen with 1080 pixels by 809 lines has been used, and the color range has been extended to 512 different colors by the addition of a special memory card.

7.0 PRELIMINARY CONCLUSIONS

7.1 TM Sensor Performance

The following conclusions can be drawn on TM sensor analysis conducted to date:

* The data exhibit very good feature discernability; one can identify high contrast features of 0.25 pixels (about 7.5m).

* The full 8-bit dynamic range does not appear to be adequately used at this time (based, unfortunately, only on winter scenes). The entropy of the TM data indicates only a 1-bit dynamic range improvement of the TM data relative to the MSS data. A presampler variable gain amplifier would be effective in utilizing the full dynamic range of the sensor, or an A/D converter with more bits (eg. use of an on-board 9-bit A/D converter) could be used.

* The data exhibit some striping. There are at least three sources of this striping: 1) Per detector calibration has variability, 2) ground processing has introduced null values at various count positions that occur in different count positions for adjacent detectors, and 3) coherent noise from a satellite subsystem has added to the sensor detector output causing additional striping to the data.

* The A/D converter exhibits a degree of non-linearity in the two least significant bits. It is unlikely that this can be corrected.

* The band-to-band registration of the primary focal plane bands (TM Bands 1-4) is within 0.1 pixels in the along-scan and the cross-scan directions. The band-to-band registration of the secondary focal plane bands (TM Bands 5,7) is about 0.7 pixels in the along-scan direction and 0.3 in the cross-scan direction relative to the primary focal plane. The thermal IR band (Band 6) registration is about 1.5 pixels in the along-scan direction and 1.9 pixels in the cross-scan direction relative to the primary focal plane.

* A number of cosmetic defects exist. A dominant cause of one defect is the algorithm used to compensate for failed detectors.

7.2 MSS Sensor Performance

The following conclusions can be drawn on the MSS sensor:

*   The entropy of the MSS data indicates that the dynamic range is efficiently
    utilized.

*   The data appear to be well calibrated, and show little striping
    characteristics.

7.3 TM Ground Processing

Although the TM ground processing has produced data of very good quality,
several improvements could be achieved:

*   The current method of replacing a failed detector output by the output of an
    adjacent detector is a computationally simple method. Although adequate in
    the macroscopic sense, it causes cosmetic defects in linear and geometric
    features in the microscopic sense. For applications that require that
    features be more truly represented, a higher order operator that
    computationally determines a "best" estimate of the failed detector output
    would be desirable. Experiments conducted to date indicate that several
    algorithms can provide better compensation for a failed detector and should
    be refined and used.

*   Statistical intensity allocation during radiometric correction processing
    yields images with fewer observable defects (i.e., it contributes to a
    reduction in striping).

*   Spatial and/or frequency domain ground processing can reduce or
    substantially eliminate certain noise defects present in the sensor data.
    This applies in particular to the coherent noise in the TM data. Although
    computationally expensive, special purpose processors can be
    microprogrammed to implement these algorithms to achieve high speed and low
    cost.

*   The geometric processing of TM data to date has only compensated for
    systematic errors. No ground control data have yet been used. However, the
    current processing has been done fairly well, and the images do not show
    significant mirror non-linearities or defects. The data are in a SOM
    projection only and there is evidence that there is both scale and
    non-linear errors in the products. Limited experiments to date provide
    strong indications that TM data will cross-correlated very reliably. Given
    a library of TM ground control points, there will then be the means to
    correct the data to other projections and thus provide users with
    geometrically correct data in standard map projections.

*   The TM data have been digitally enlarged using higher order resampling
    algorithms to about 1:10,000 scale on an interactive display and 1:24,000 on
    film. Good feature definition is still evident, and large buildings can be

discerned and identified. It is likely that the TM data can be used to improve and update 1:24,000 land use and cartographic maps.

- The TM data, when processed using Principal Component processing, exhibit at least 3 dominant components. This is a significant improvement over the MSS data, and provides additional color spaces for image presentation.

- Ratioing techniques can be used to combine and enhance the seven TM data bands for image analysis and interpretation purposes.

- Special purpose processors such as the IBM 7350 Image Processing System allow interactive image processing and information extraction which results in improved user productivity.

7.4 MSS Ground Processing

Limited evaluation has been conducted on the MSS ground processing. Therefore, only these results can be reported at this time:

- The MSS data have only been produced in a SOM projection, with only systematic corrections made. No ground control has yet been used to correct the data. Relative geometric comparisons of the TM to the MSS data indicated that the data has some residual scale and non-linear errors that could be eliminated by the use of ground control points.

7.5 Use of Personal Computers

There are many who feel that they do not have the financial or computational resources to process the new TM sensor data. The low cost and high speed of the PC have demonstrated the following:

- The PC offers a cost-effective approach to small area image processing for many standard image processing operations and techniques.

- With the rapid availability of inexpensive memory and high resolution displays for these computers, the PC technology will become increasingly important for remote sensing applications.

8.0 RECOMMENDATIONS

Based upon the work to date, the following recommendations can be made:

- Use a higher order failed detector algorithm for processing TM data.

- Implement statistical radiometric calibration processing to reduce striping.

- For future sensors, use a variable gain presampler amplifier and/or provide an A/D converter with more bits (9 bit A/D converter).

- Refine and use spatial or frequency domain filters to reduce coherent noise present in the TM data.

- Use ground control points to accurately correct the MSS and TM data to standard map projections.

- The secondary focal plane bands should be put into registration with the primary focal plane bands by sub-pixel geometric correction. This correction should be combined with the geometric correction/mapping operation so that only one resampling need be performed.

- Consider the use of pixel sizes that would produce standard scale data with commonly used film recorders (eg., 25m TM and 50m MSS pixels).

9.0 ACKNOWLEDGEMENTS

9.0 ACKNOWLEDGEMENTS

10.0 REFERENCES

1. NASA Workshop for Definition of Landsat-D Thematic Mapper Sensor Characteristics, Purdue University, 1975.

2. "Landsat-D Sensor and System Data Analysis and Image Science," IBM Proposal and Contract, NASA/GSFC, Contract No. NAS5-27355.

3. Landsat Data Users Handbook (revised edition), U.S. Geological Survey, United States Department of the Interior, 1979.

4. Engel, J.L., "Thematic Mapper - An Interim Report of Anticipated Performance," AIAA Paper 80-1915, 1980.

5. Moik, J.G., "Digital Processing of Remotely Sensed Images," NASA Publication SP-431, U.S. Government Printing Office, Washington, D.C. 1980.

6. Bernstein, R., and Silverman, H., Digital Techniques for Earth Resource Image Data Processing, AIAA paper no. 71-978, AIAA 8th Annual Meeting and Technical Display, Washington, D.C., October 25-28, 1971.

7. Barnea, D.I., Silverman, H.F., "A Class of Algorithms for Fast Digital Image Registration," IEEE Trans. Comput., vol.C-21,pp. 179-186, Feb. 1972.

8. Snyder, J.P., "Space Oblique Mercator Projection," Geological Survey Bulletin 1518, U.S. Government Printing Office, Washington, D.C. 1981.

9. Pearl, J., Andrews, H.C. and Pratt, W.K., "Performance Measures for Transform Data Coding," IEEE Trans. Commun., vol.COM-20, pp. 411-415, June 1972.

10. Bernstein, R., Lotspiech, J.B., and Marks, S., "Interactive Geometric Correction System," IBM PASC Report GXXX-XXXX (to be published as a Palo Alto Scientific Center Report, 1983).

11. Bernstein, R., "Digital Image Processing of Earth Observation Sensor Data," IBM Journal of Research and Development, Vol. 20, No. 1, January 1976

12. Myers, H.J., "Image Processing on the IBM Personal Computer," IBM Palo Alto Scientific Center Note, March 3, 1983.

13. Franchi, P., Gonzalez, J., Mantey, P., Paoli, C., Parolo, A. and Simmons, J., "Design Issues and Architecture of Hacienda an Experimental Image Processing System," IBM Journal of Research and Development, Vol. 27, No. 2, March 1983.

14. Dave, J.V., Bernstein, R., Kolsky, H.G., "Importance of Higher-Order Components to Multispectral Classification," IBM Journal of Research and Development, Vol. 26, No. 6, Nov. 1982.

FIGURES

Number
of
Occurances

Figure 1

Detector   Pixel Intensity
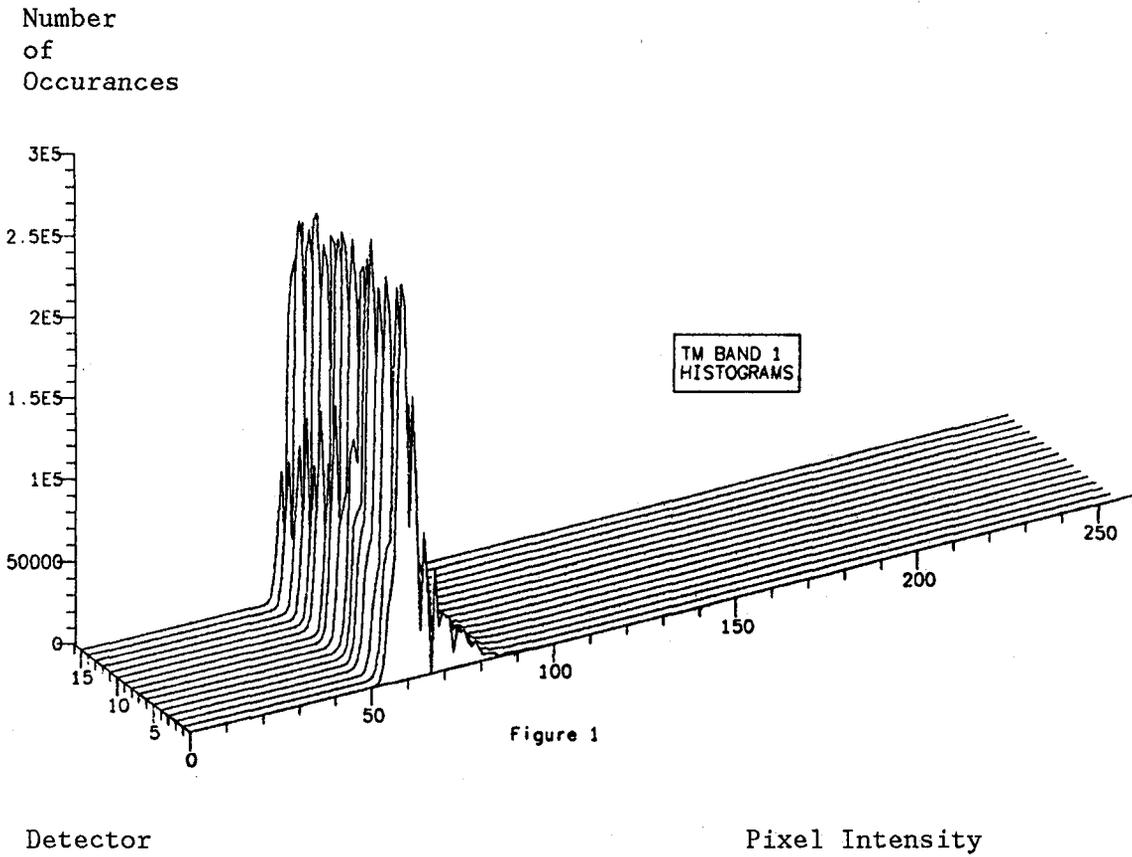
Figure 1 - Band 1 Histograms
Chesapeake November 2, 1982 Scene (E-40109-15140)

Number
of
Occurances
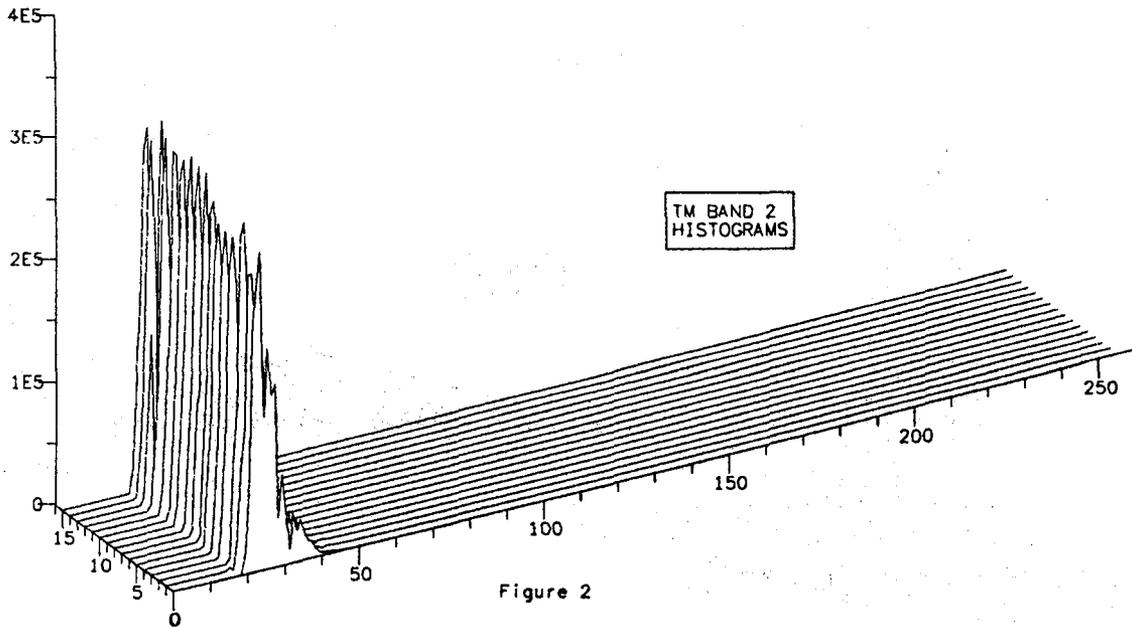
Figure 2

Detector

Pixel Intensity

Figure 2 - Band 2 Histograms
Chesapeake November 2, 1982 Scene (E-40109-15140)
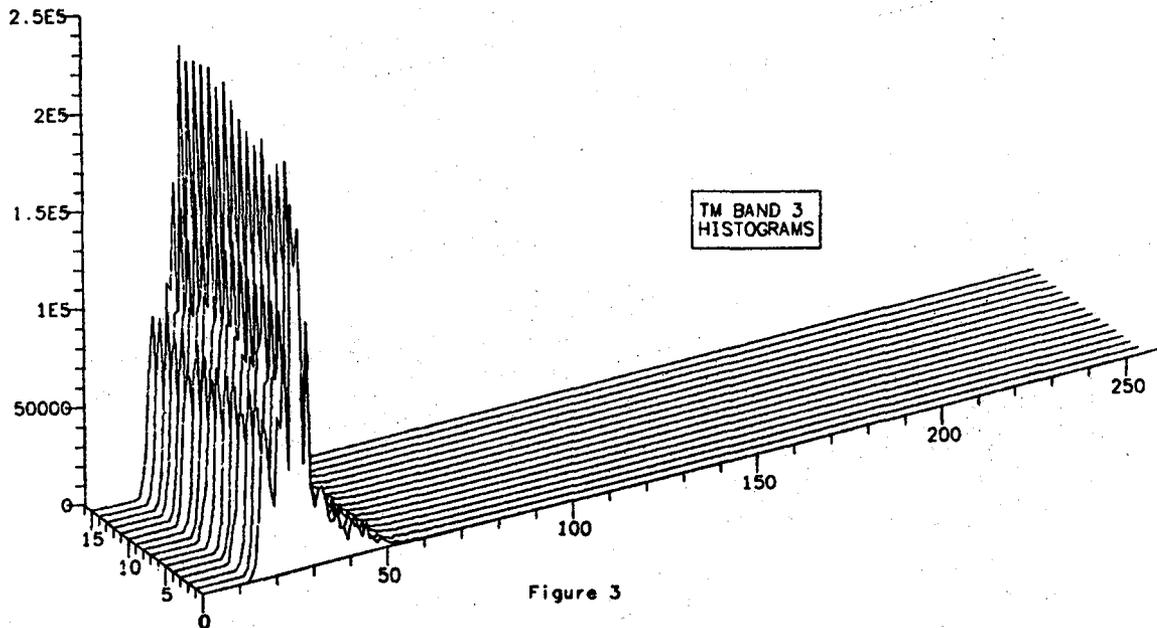
Number
of
Occurances

Detector   Pixel Intensity

Figure 3 - Band 3 Histograms
Chesapeake November 2, 1982 Scene (E-40109-15140)

Number
of
Occurances

2E5

1.5E5

1E5

TM BAND 4
HISTOGRAMS

50000

250

200

150

100

50

15

10

5

0
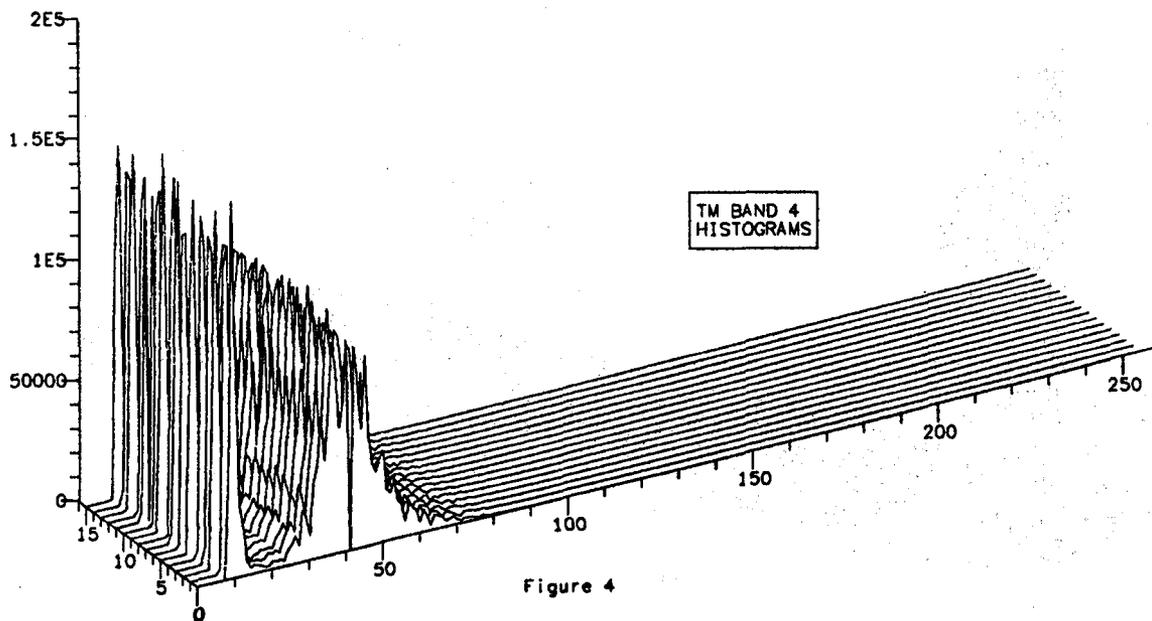
Figure 4

Detector

Pixel Intensity

Figure 4 - Band 4 Histograms
Chesapeake November 2, 1982 Scene (E-40109-15140)

Number
of
Occurances
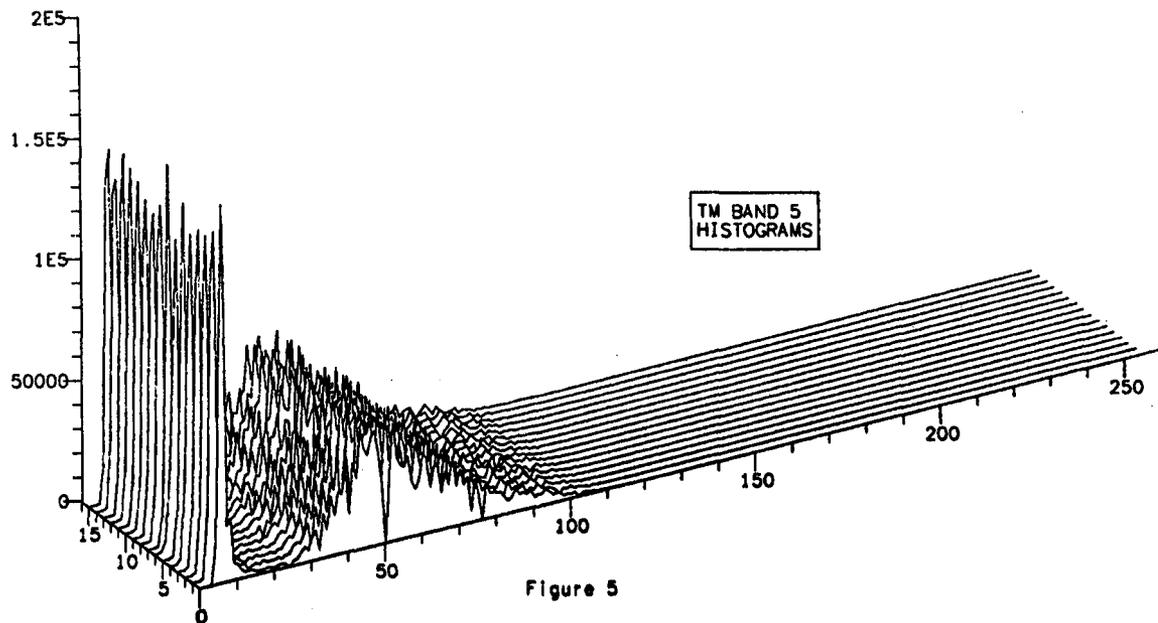
Detector   Pixel Intensity

Figure 5 - Band 5 Histograms
Chesapeake November 2, 1982 Scene (E-40109-15140)

Number
of
Occurances
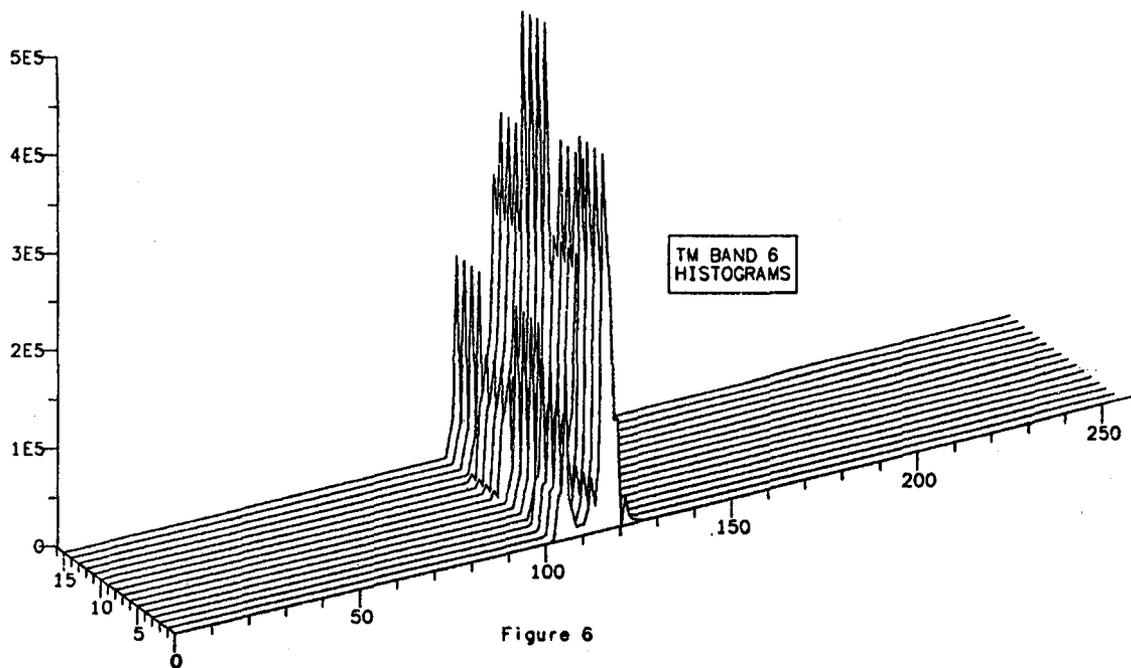
Detector   Pixel Intensity

Figure 6 - Band 6 Histograms
Chesapeake November 2, 1982 Scene (E-40109-15140)

Number
of
Occurances
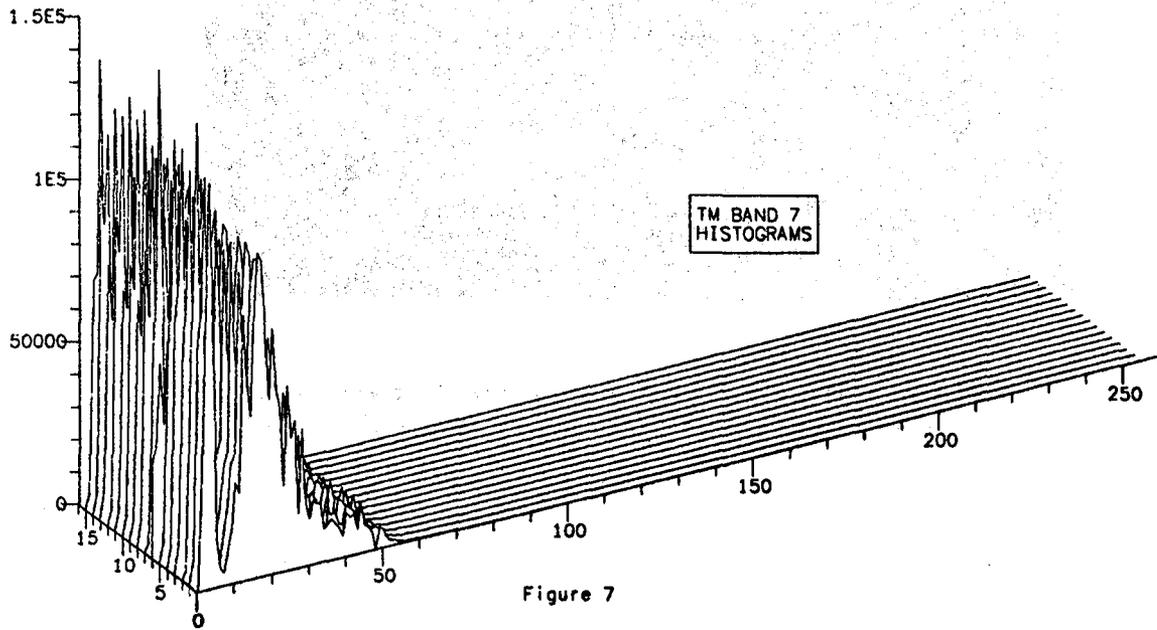
Figure 7

Detector

Pixel Intensity

Figure 7 - Band 7 Histograms
Chesapeake November 2, 1982 Scene (E-40109-15140)
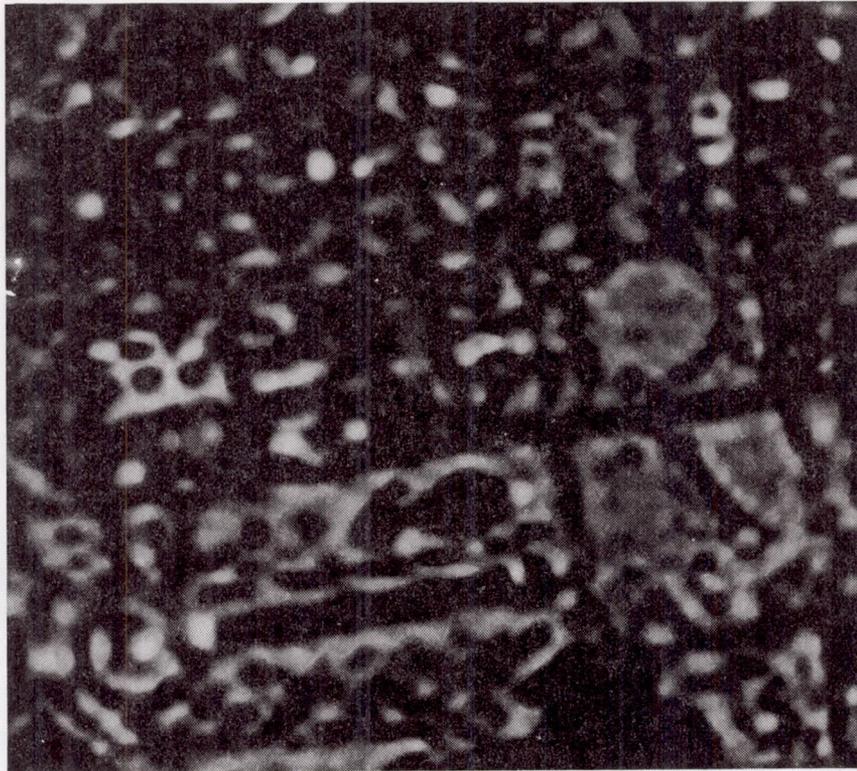
Figure 8 - Greatly Expanded Sub-Image of Washington D.C.
Chesapeake November 2, 1982 Scene (E-40109-15140)

San Francisco Scene
E-40168-18143

Modesto Scene
E-40145-18082

Anderson Lake
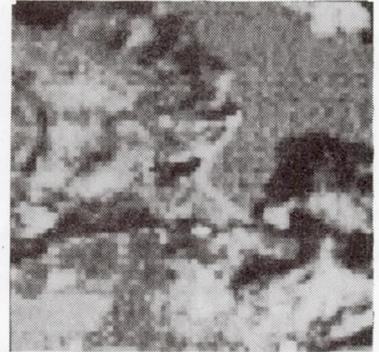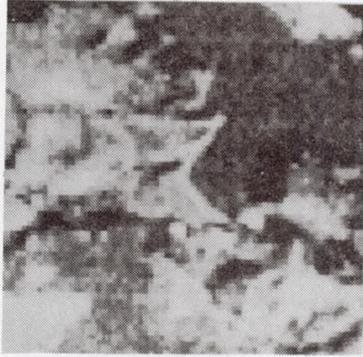
Coyote Lake
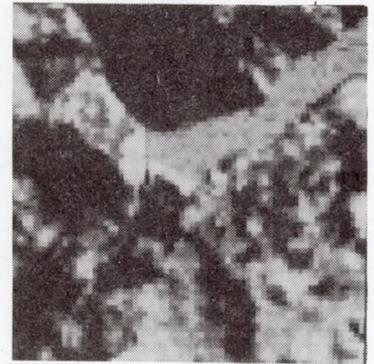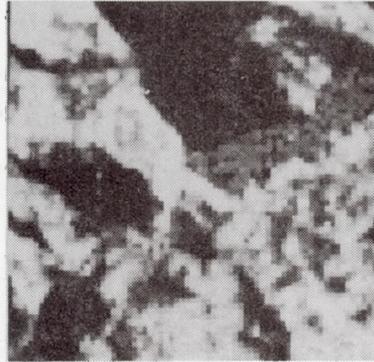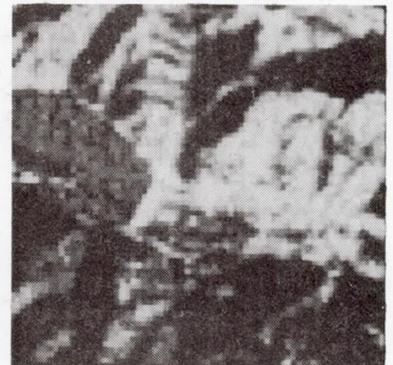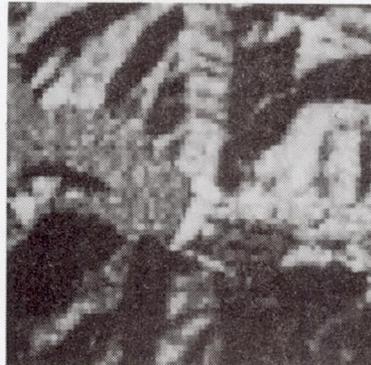
Uvas Reservoir

Chesbro Reservoir

Figure 9 - Reservoirs Around Morgan Hill, California
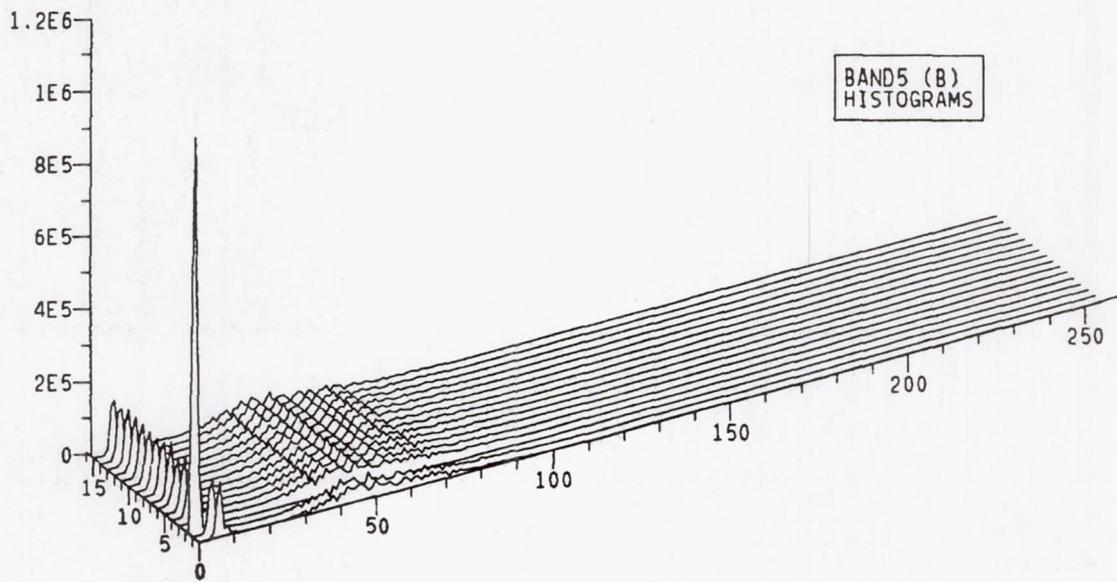
Figure 10 - Histograms of Uncalibrated Band 5 Data
Chesapeake November 2, 1982 Scene (E-40109-15140)
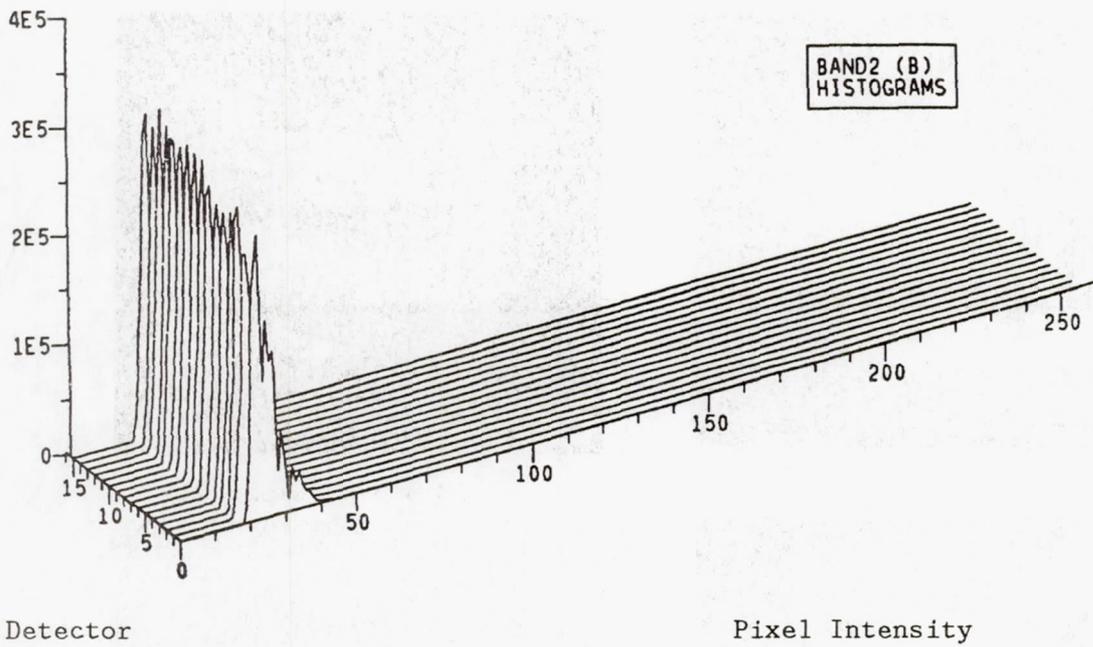
Figure 11 - Histograms of Uncalibrated Band 2 Data
Chesapeake November 2, 1982 Scene (E-40109-15140)
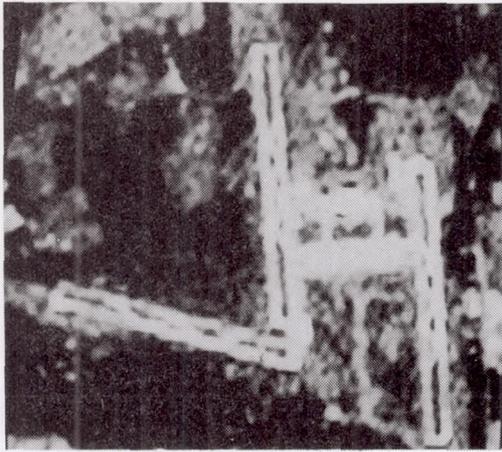
MSS 7-5-4

TM 4-3-2
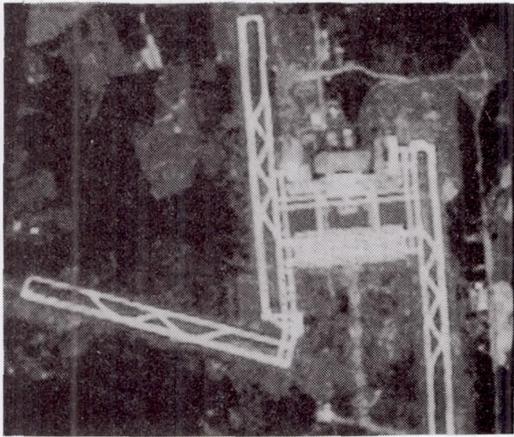
TM 3-2-1
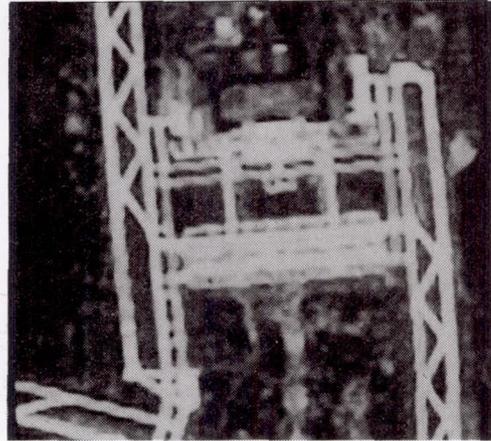
TM 4-3-2 (expanded)
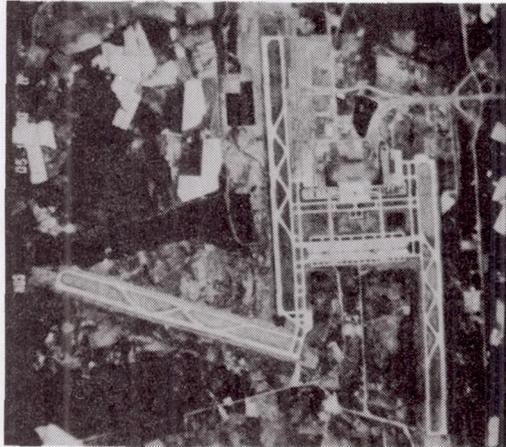
Aircraft Photo
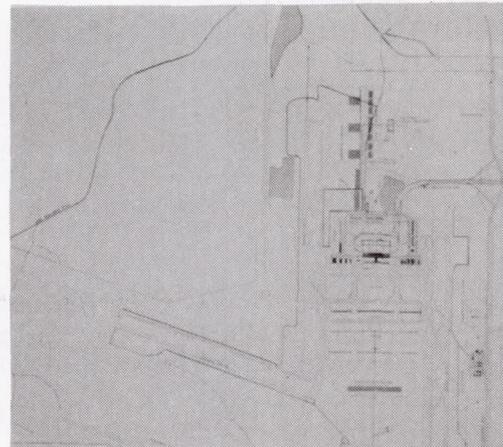
Map

Figure 12 - Various Views of Dulles Airport
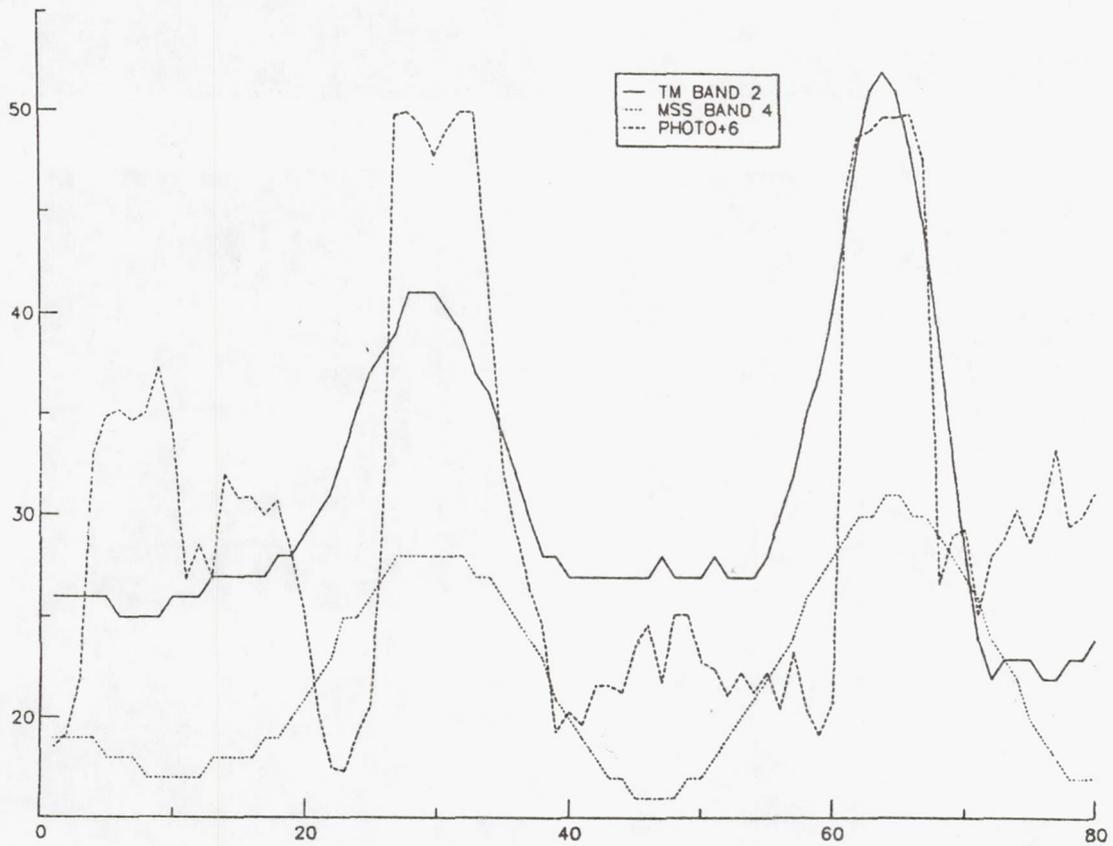
Figure 13 - Cross-Section of Dulles Airport Runway
Chesapeake November 2, 1982 Scene (E-40109-15140)
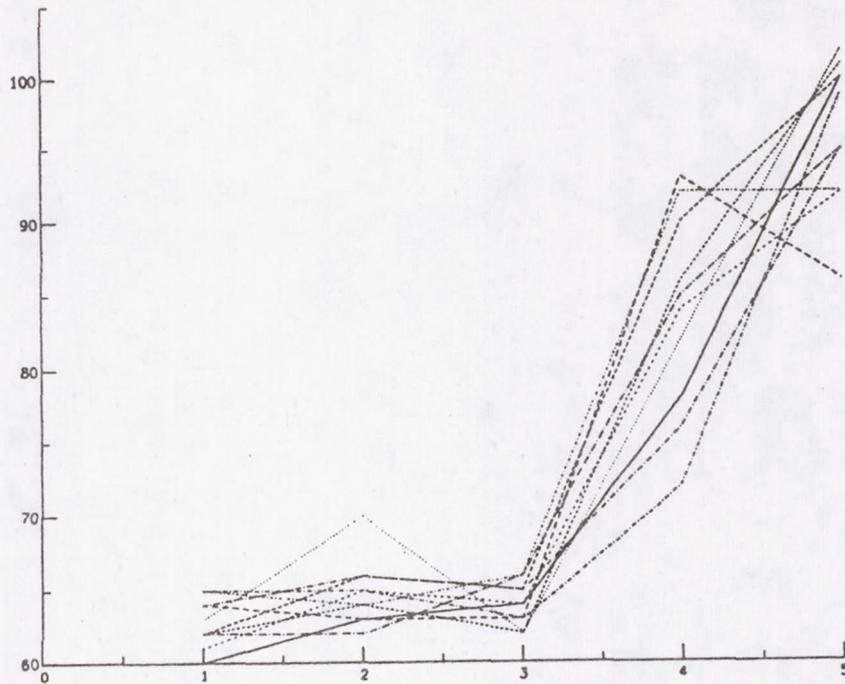
Figure 14 - Crossings of a Linear Edge (Band 1)
Chesapeake November 2, 1982 Scene (E-40109-15140)
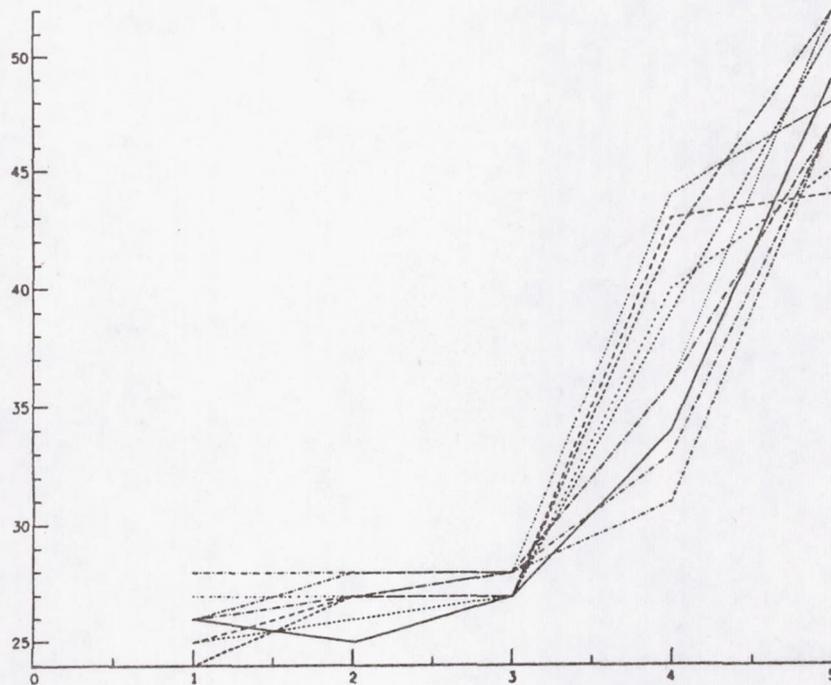
Figure 15 - Crossings of a Linear Edge (Band 2)
Chesapeake November 2, 1982 Scene (E-40109-15140)
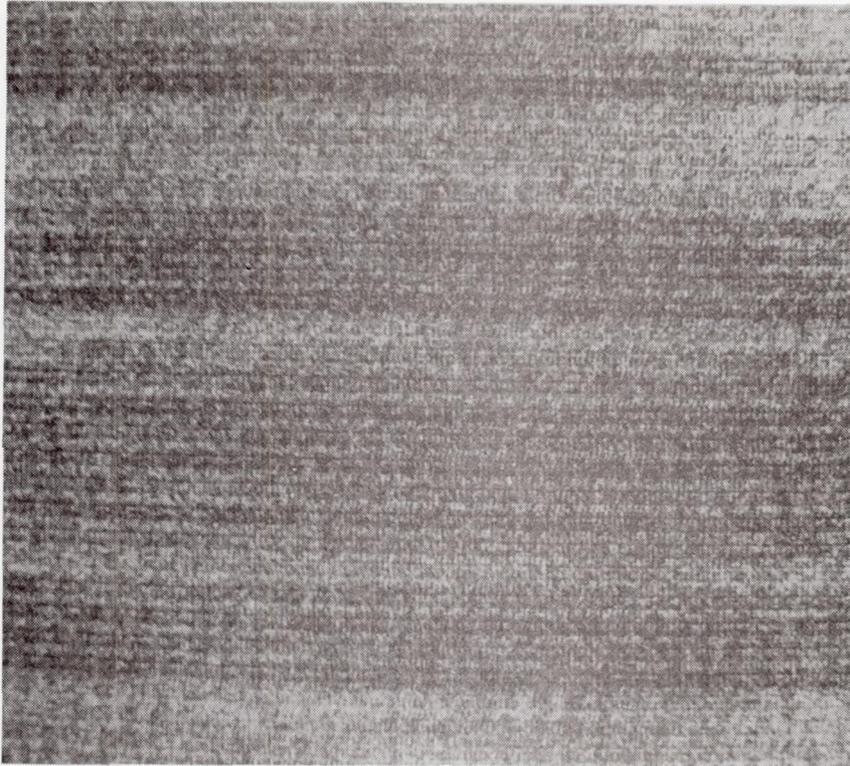
Figure 16 - Pacific Ocean
San Francisco December 31, 1982 Scene (E-40168-18143)
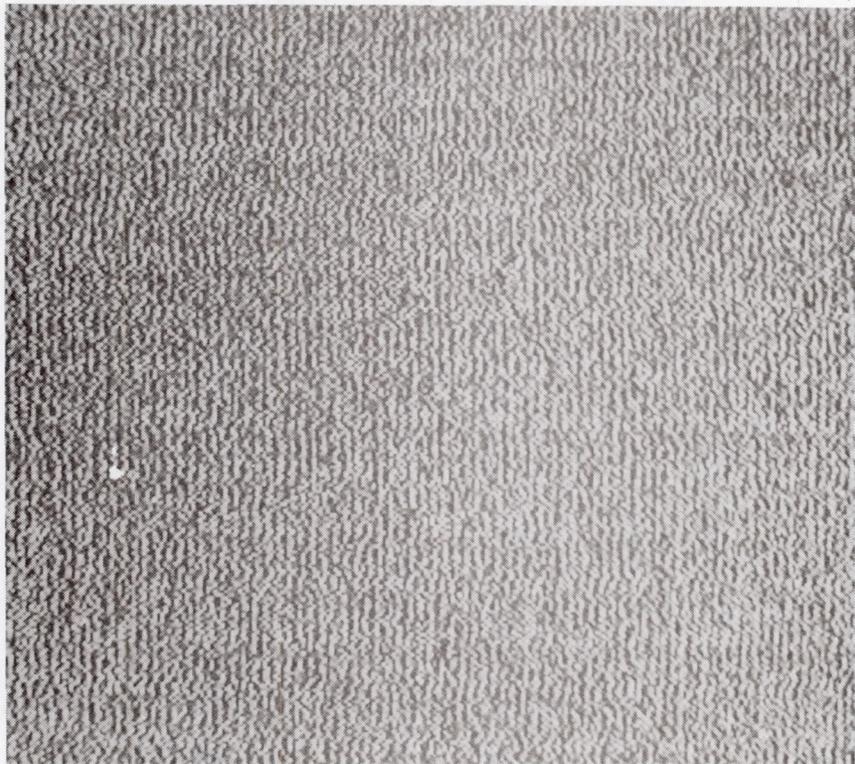
Figure 17 - Pacific Ocean (Pixel-to-pixel Differences Along Scan)
San Francisco December 31, 1982 Scene (E-40168-18143)
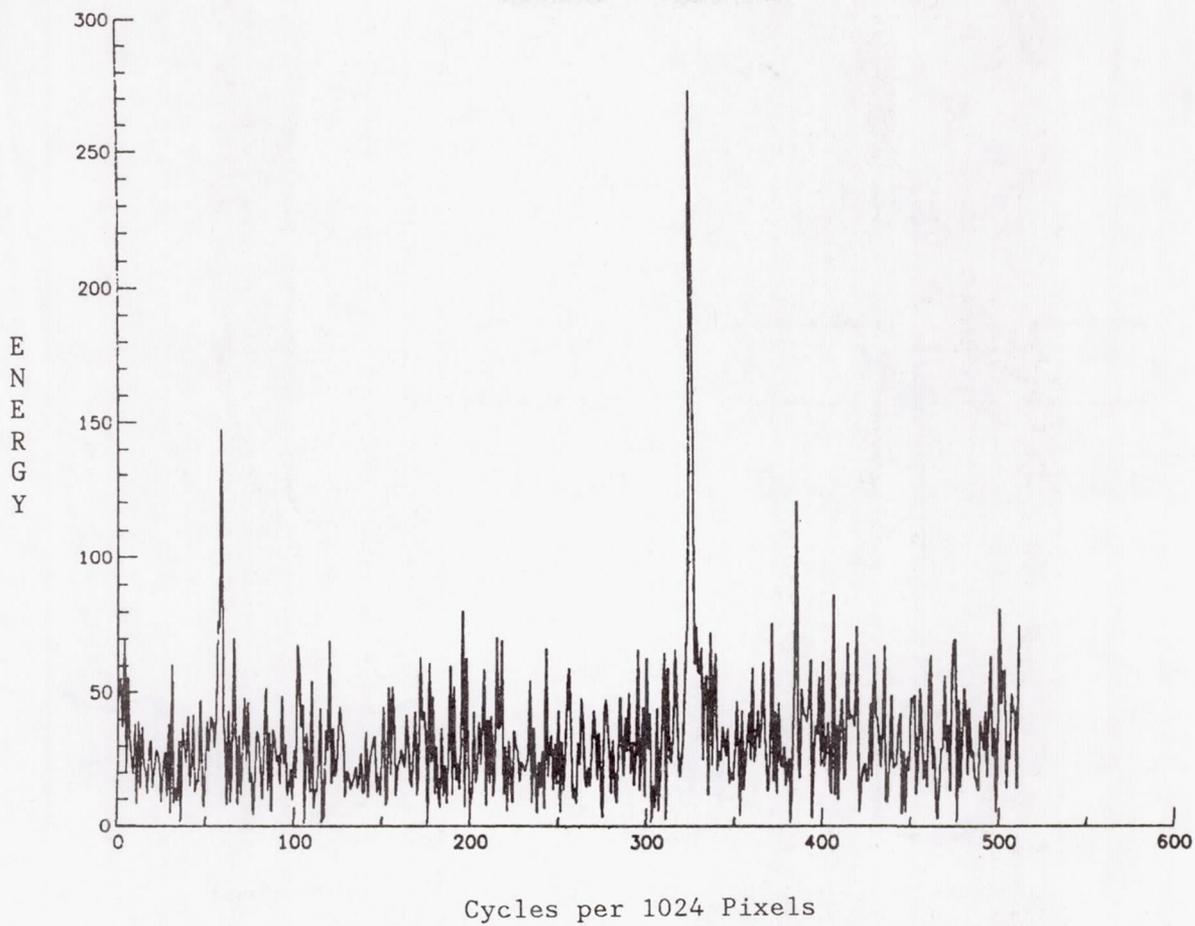
Figure 18 - Horizontal Fourier Transform of Pacific Ocean
San Francisco December 31, 1982 Scene (E-40168-18143)
(DC Component Omitted)

INPUT

63   x1.0079   64   63.496   65   64.504   65.512

OUTPUT

63   64   65   66
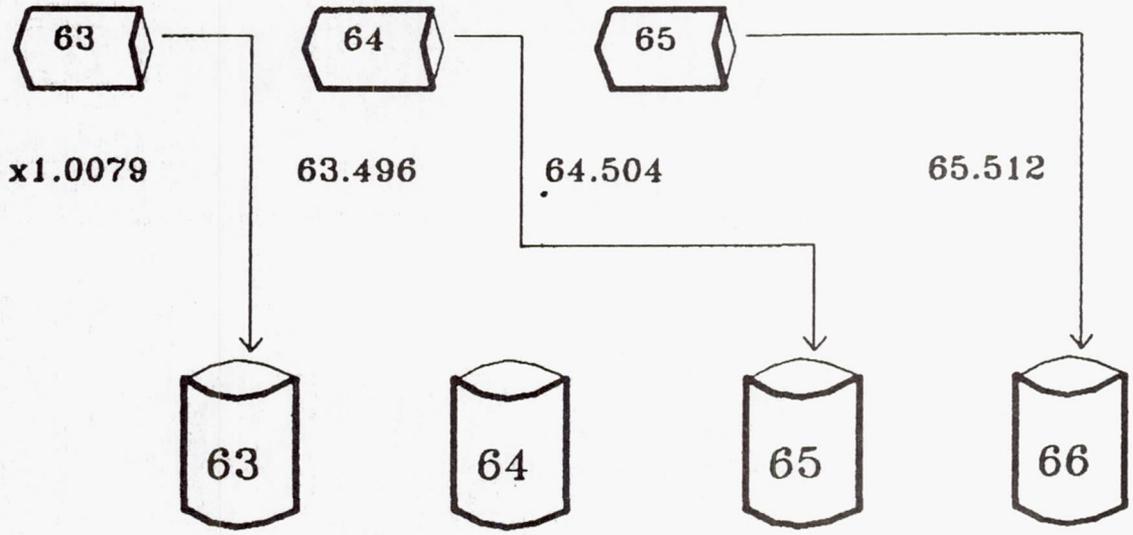
OUTPUT

(Detector 5, Band 1)

Figure 19 - NASA Radiometric Calibration Procedure

Figure 20 - Aerial View of RFK Stadium, Washington D.C.
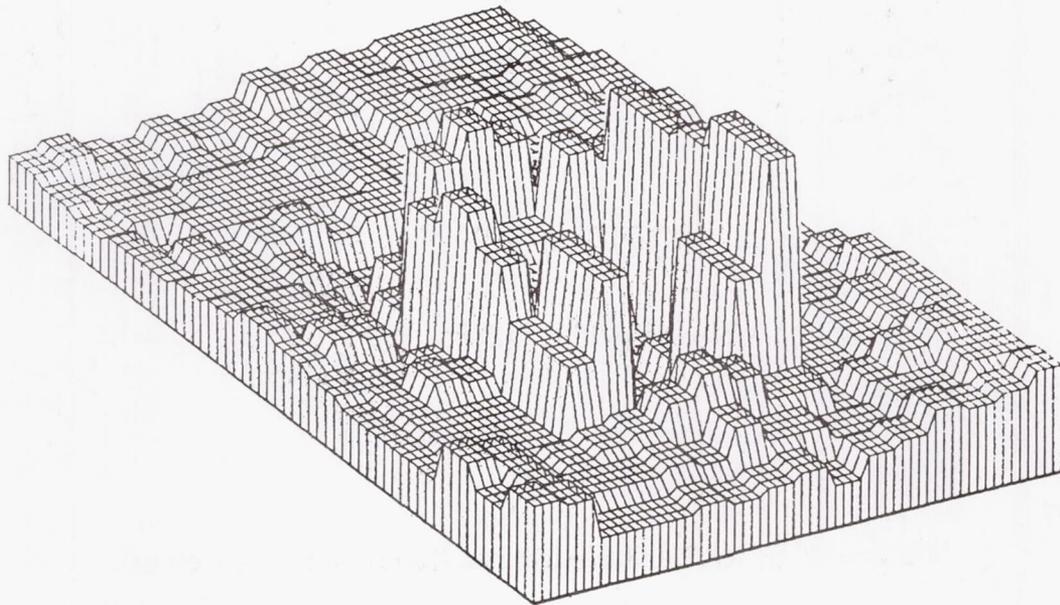
Figure 21 - Three Dimensional View of RFK Stadium Band 2
Chesapeake November 2, 1982 Scene (E-40109-15140)

INPUT

x1.0079

49.7%   50.3%
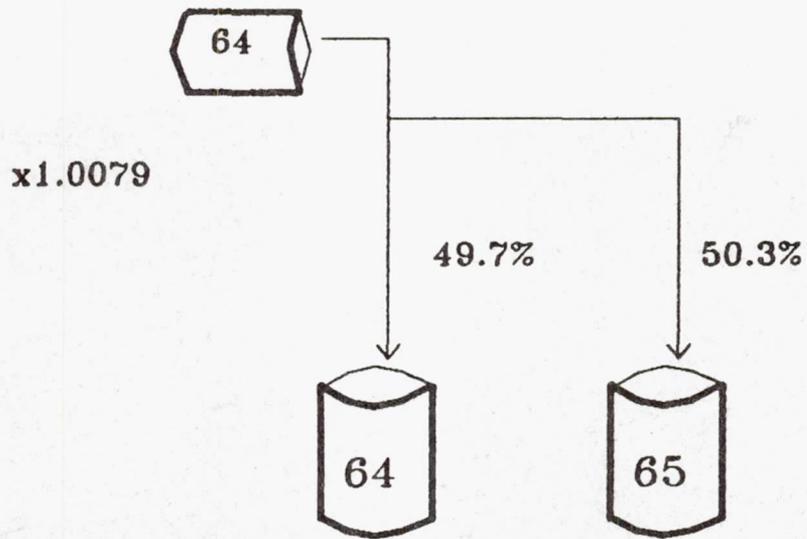
OUTPUT

(Detector 5, Band 1)

Figure 22 - Probabilistic Radiometric Calibration
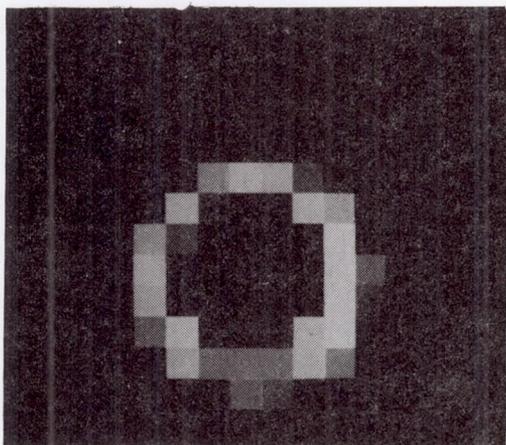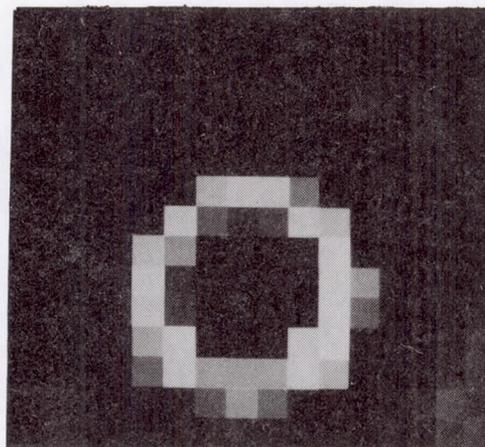
NASA's Scheme   Quadratic Interpolation

Figure 23 - Unsuccessful Failed Detector Replacement (RFK Stadium)
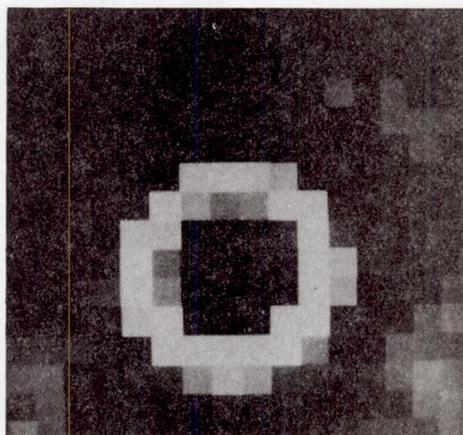
Algorithm 1
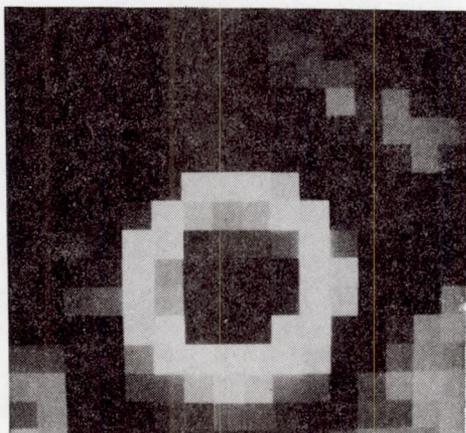
Algorithm 2
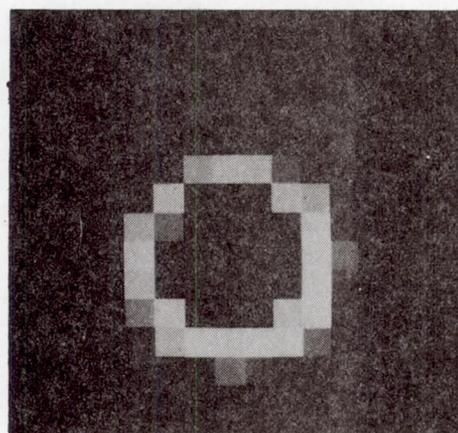
Algorithm 3

Figure 24 - Successful Failed Detector Replacement (RFK Stadium)
Chesapeake November 2, 1982 Scene (E-40109-15140)
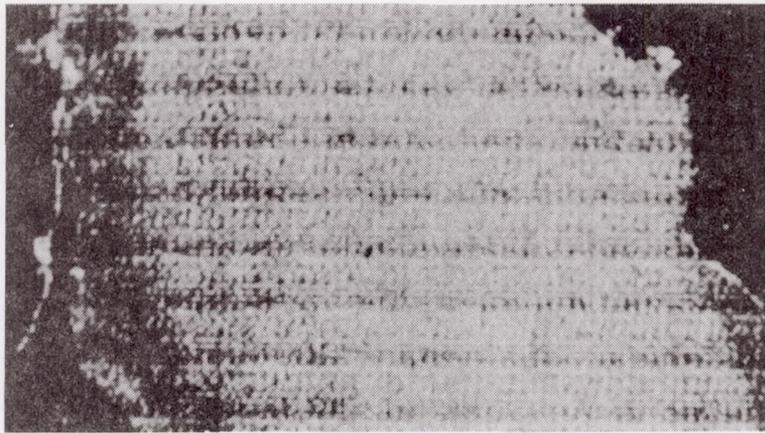
"B-Tape" Data - Not Radiometrically Calibrated
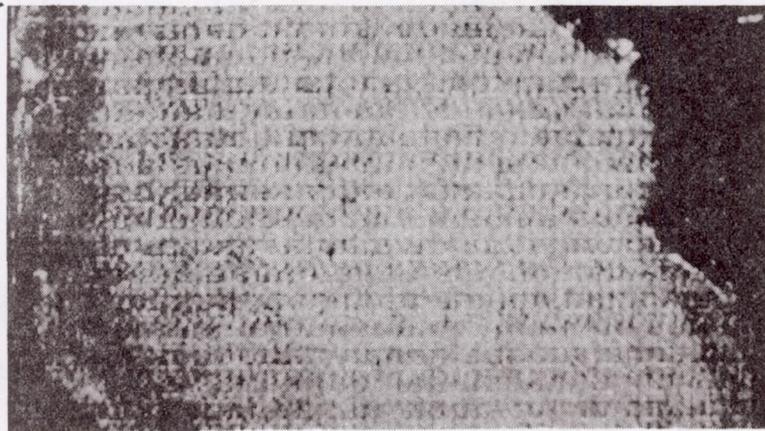
"A-Tape" Data - Radiometrically Calibrated by NASA
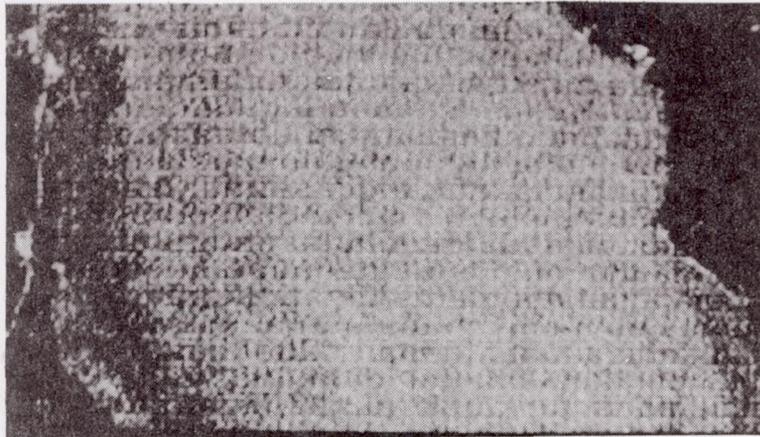
Radiometrically Calibrated with NASA's Factors
But by Probabilistic Calibration

Figure 25 - Three Views of the Potomac River
Chesapeake November 2, 1982 Scene (E-40109-15140)
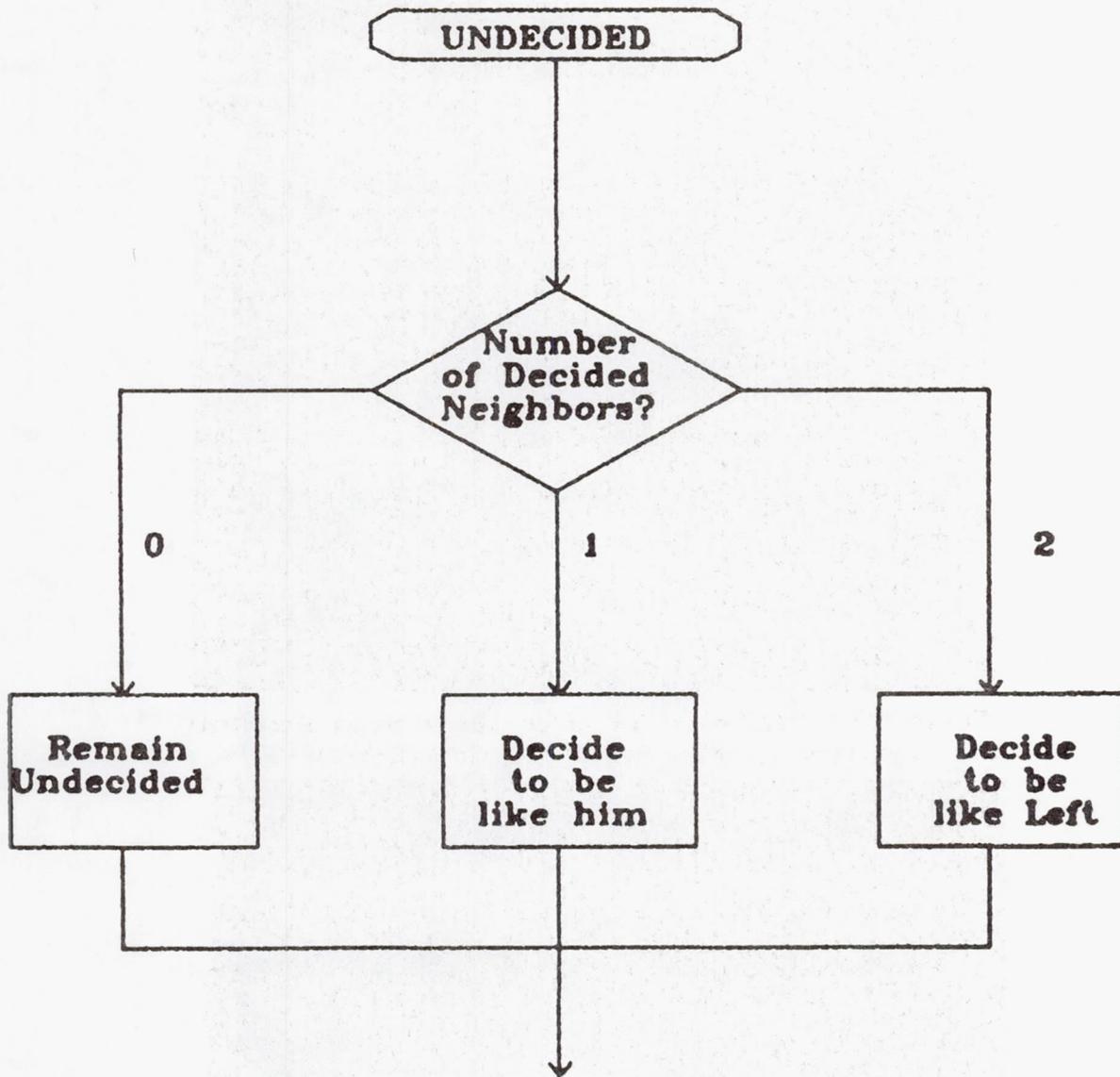
Figure 26 - Decision Flow for Undecided Cell
32 kHz Noise Removal Algorithm
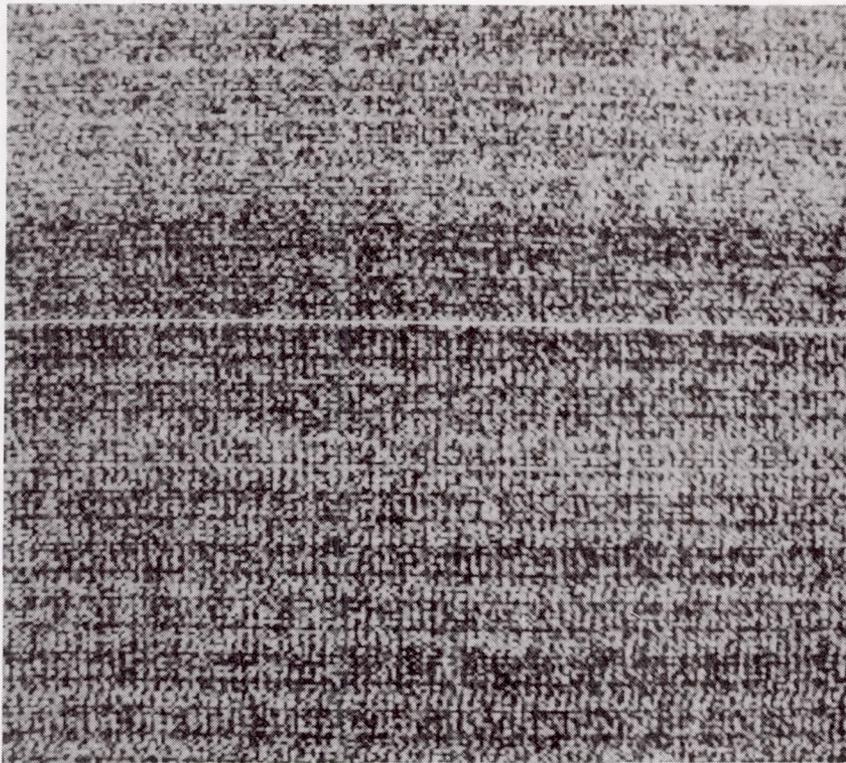
Figure 27 - Pacific Ocean After 32kHz Noise Removal
San Francisco December 31, 1982 Scene (E-40168-18143)
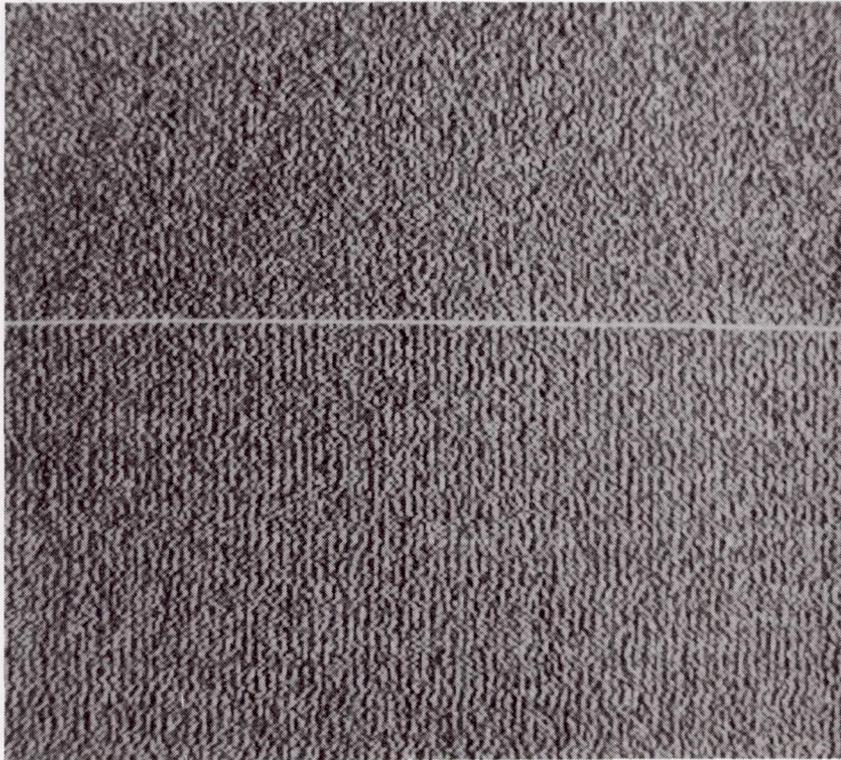
Figure 28 - Noise Removal (Pixel-to-pixel Differences Along Scan)
San Francisco December 31, 1982 Scene (E-40168-18143)

Band 1   Band 2
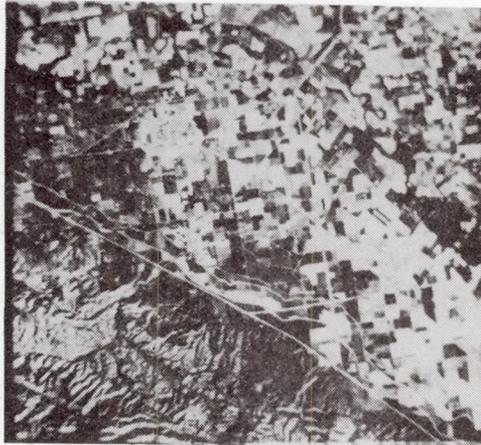
Band 3   Band 4
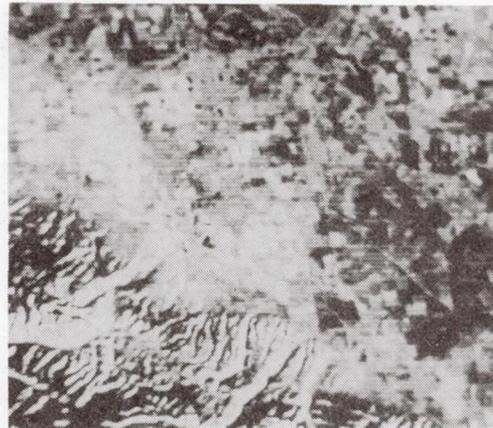
Band 5   Band 6

Figure 29 - Sub-Image Around Tracy, California (Monochrome Bands)
Modesto December 8, 1982 Scene (E-40145-18082)
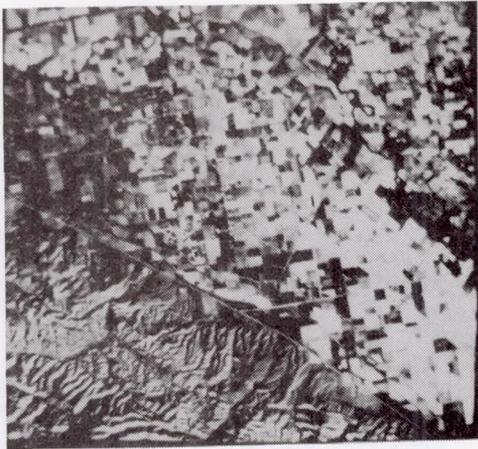
Band 7
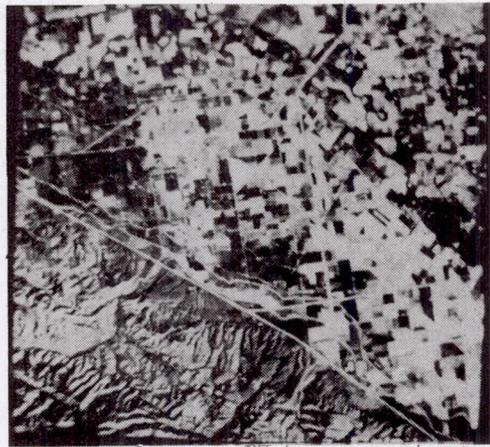
Bands 3-2-1
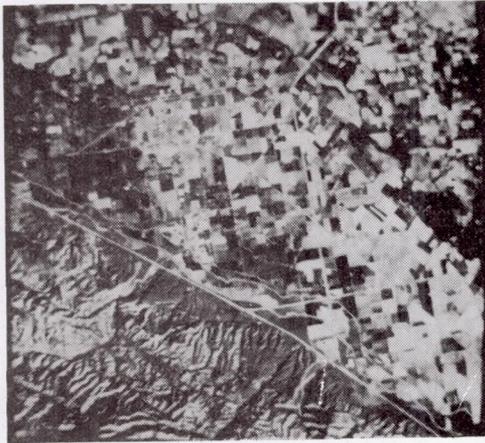
Bands 4-3-2

Bands 4-2-1
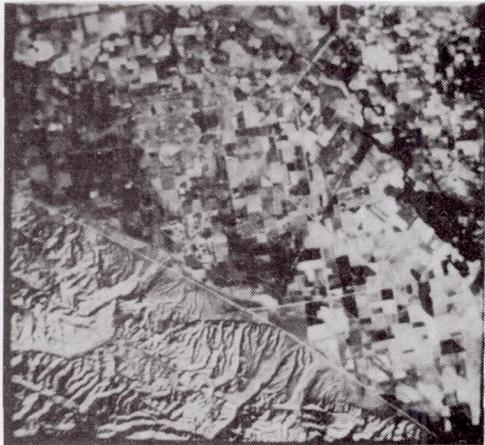
Bands 4-5-1

Bands 7:1-5:2-4:3

Figure 30 - Tracy, California (Color Composites)
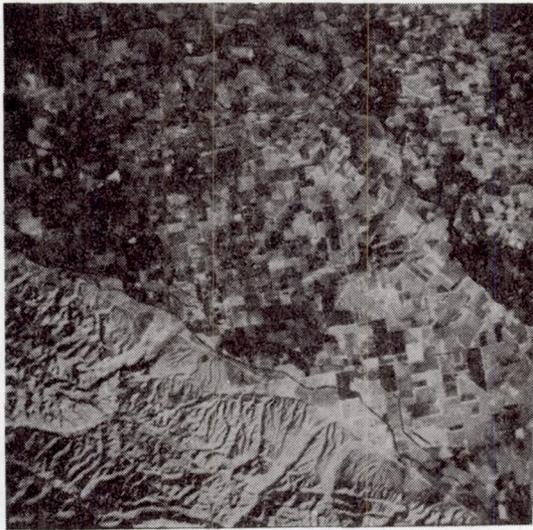
PC Image 1

PC Image 2
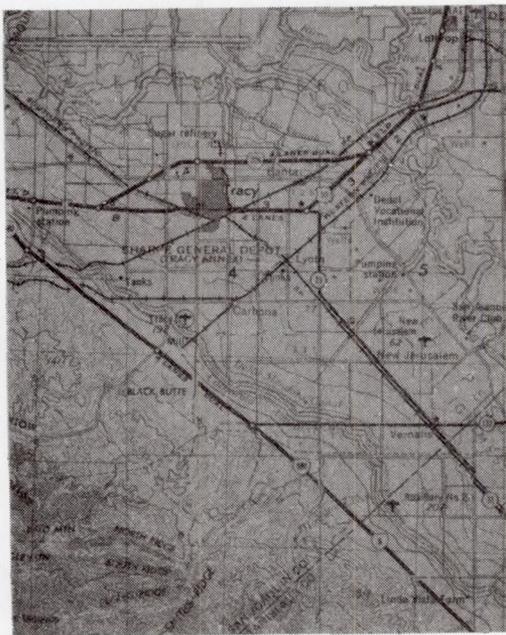
USGS Map

Land Use Map

Figure 31 - Tracy, California (Principal Component Images and Maps)
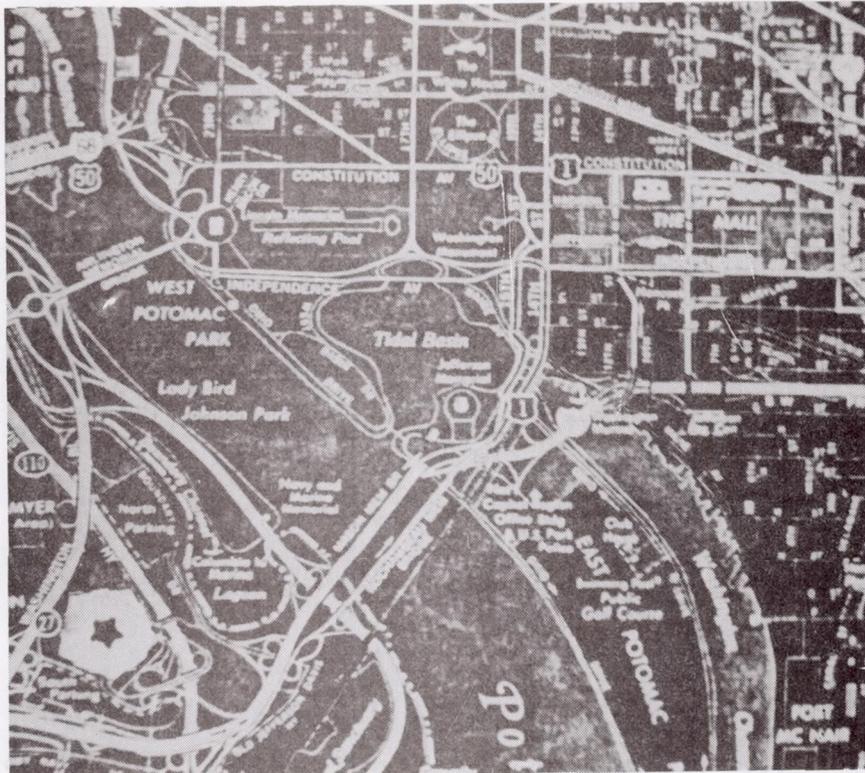
Figure 32 - Reference Map for Registration

Figure 33 - Source TM Sub-Image
Chesapeake November 2, 1982 Scene (E-40109-15140)
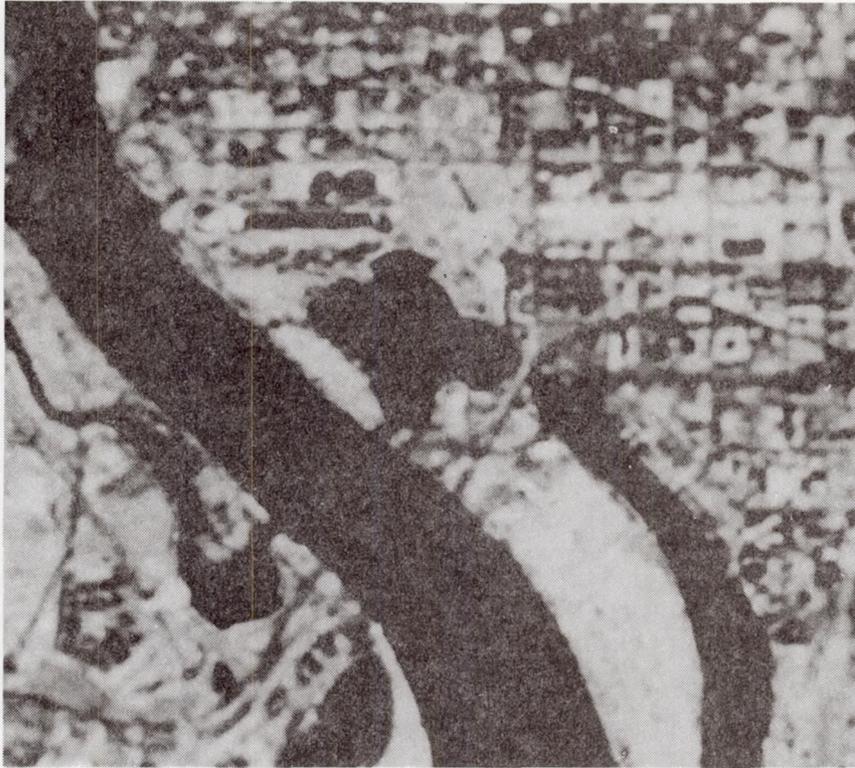
Figure 34 - Geometrically Corrected Sub-Image
Chesapeake November 2, 1982 Scene (E-40109-15140)
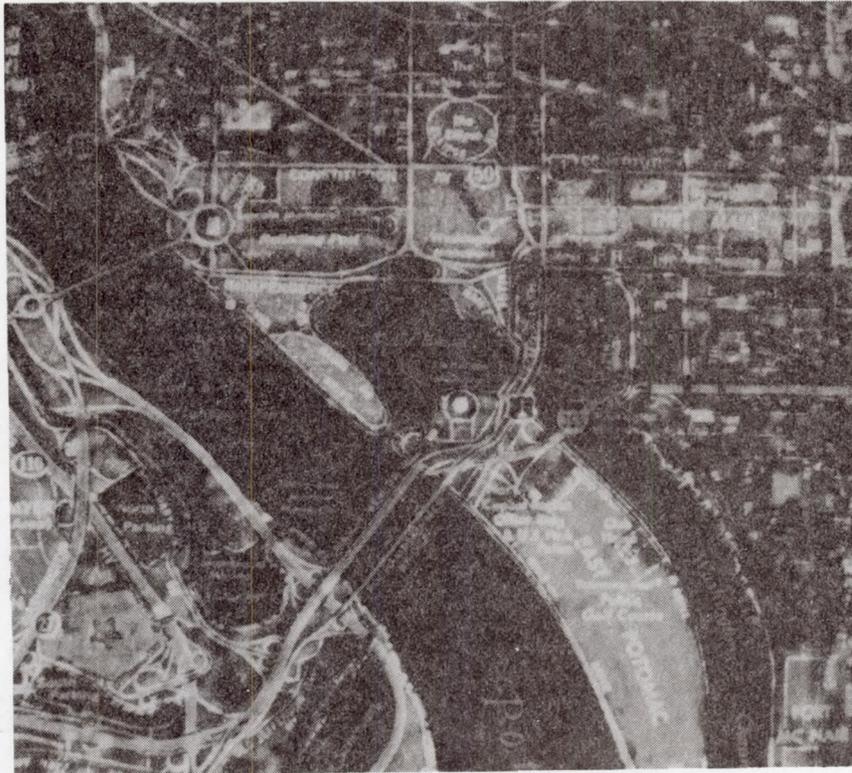
Figure 35 - Geometrically Corrected Sub-Image Overlayed on Map
Chesapeake November 2, 1982 Scene (E-40109-15140)
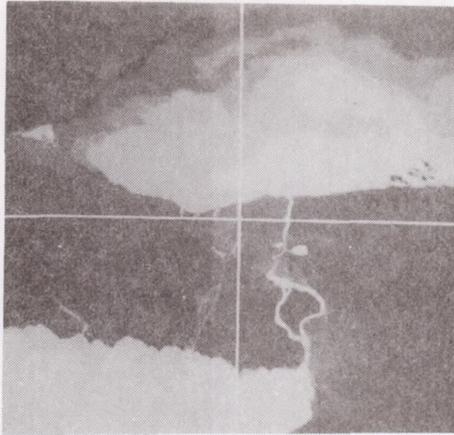
Black/White
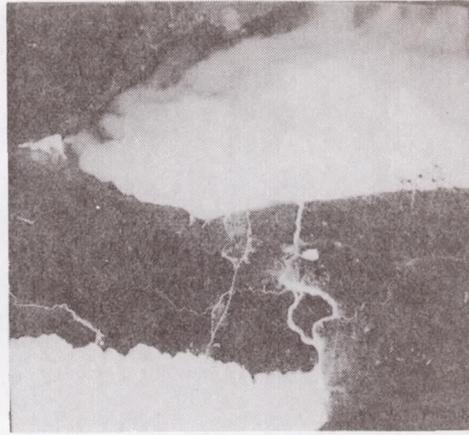
Black/White (Enhanced)

Pseudo Color 1

Black/White
(Enhanced and Enlarged)

Pseudo Color 2

Pseudo Color 3

Figure 36 - Thermal Night Images of Buffalo, New York
Buffalo August 22, 1982 Scene (E-40037-02243)
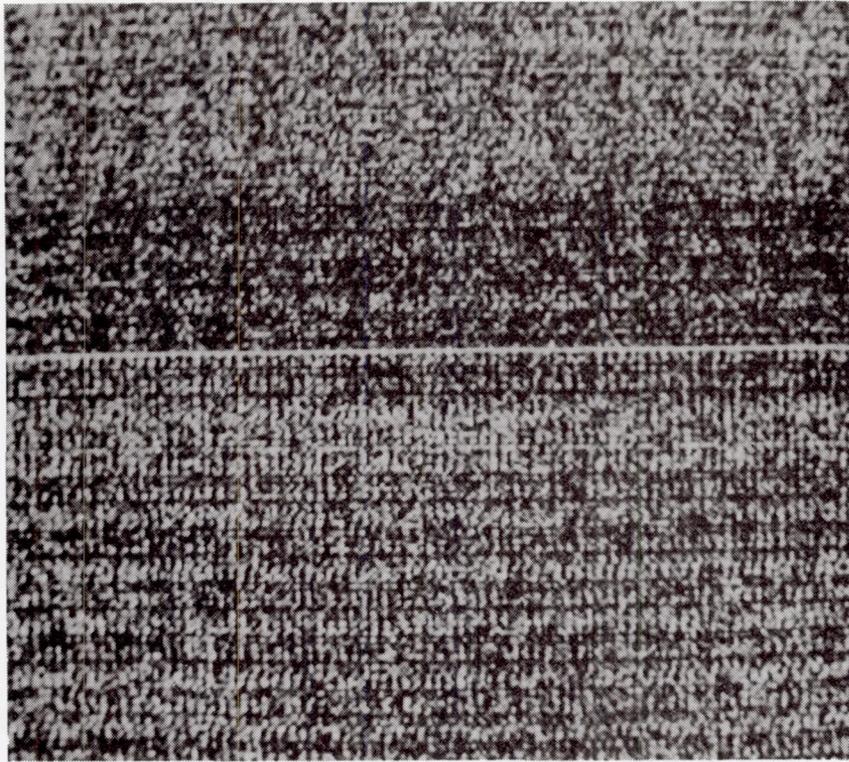
Figure 37 - Pacific Ocean After 32kHz Noise Removal by FFT
San Francisco December 31, 1982 Scene (E-40168-18143)
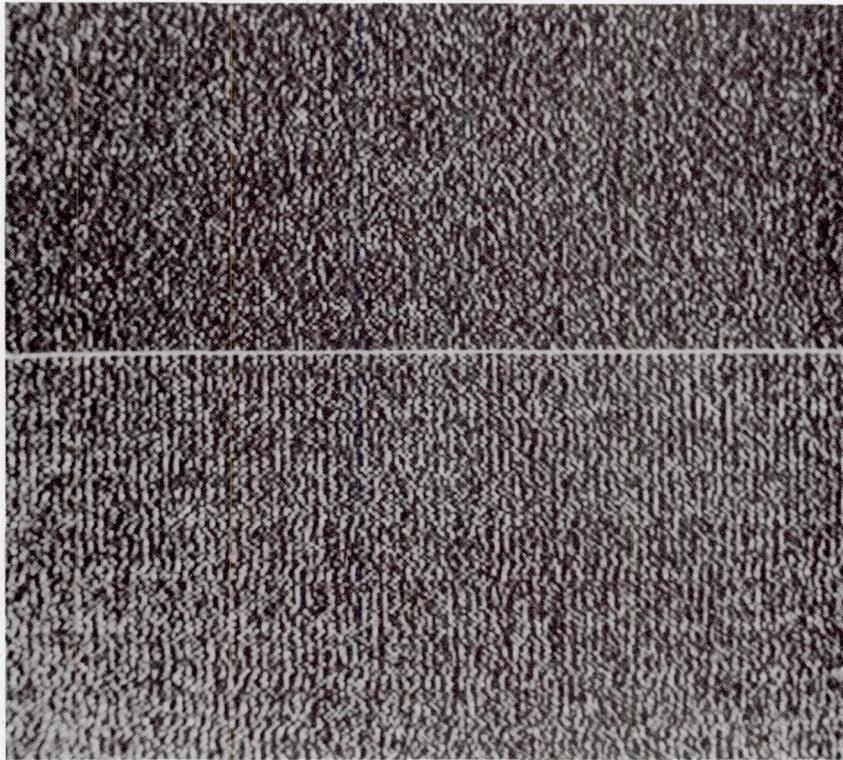
Figure 38 - Noise Removal by FFT (Pixel-to-pixel Differences Along Scan)
San Francisco December 31, 1982 Scene (E-40168-18143)

Original   Nearest Neighbor
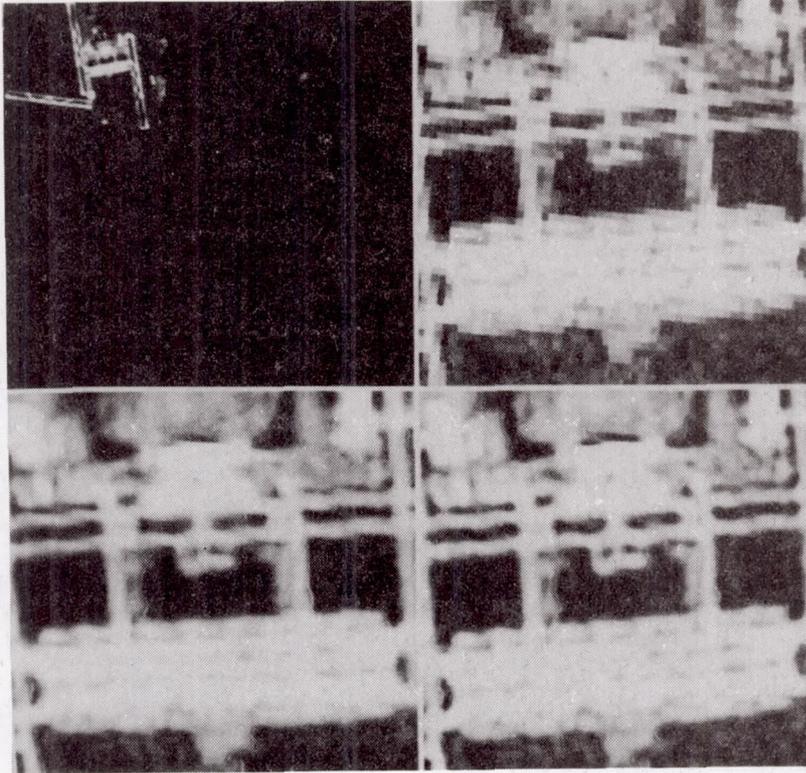
Bilinear Interpolation   Cubic Convolution

Figure 39 - Different Methods of Re-Sampling
10x Expansion of Dulles Airport Terminal, TM Band 1
Chesapeake November 2, 1982 Scene (E-40109-15140)

LANDSAT-4 IMAGE OF DETROIT AIRPORT
Processed on IBM Personal Computer
IBM Palo Alto Scientific Center
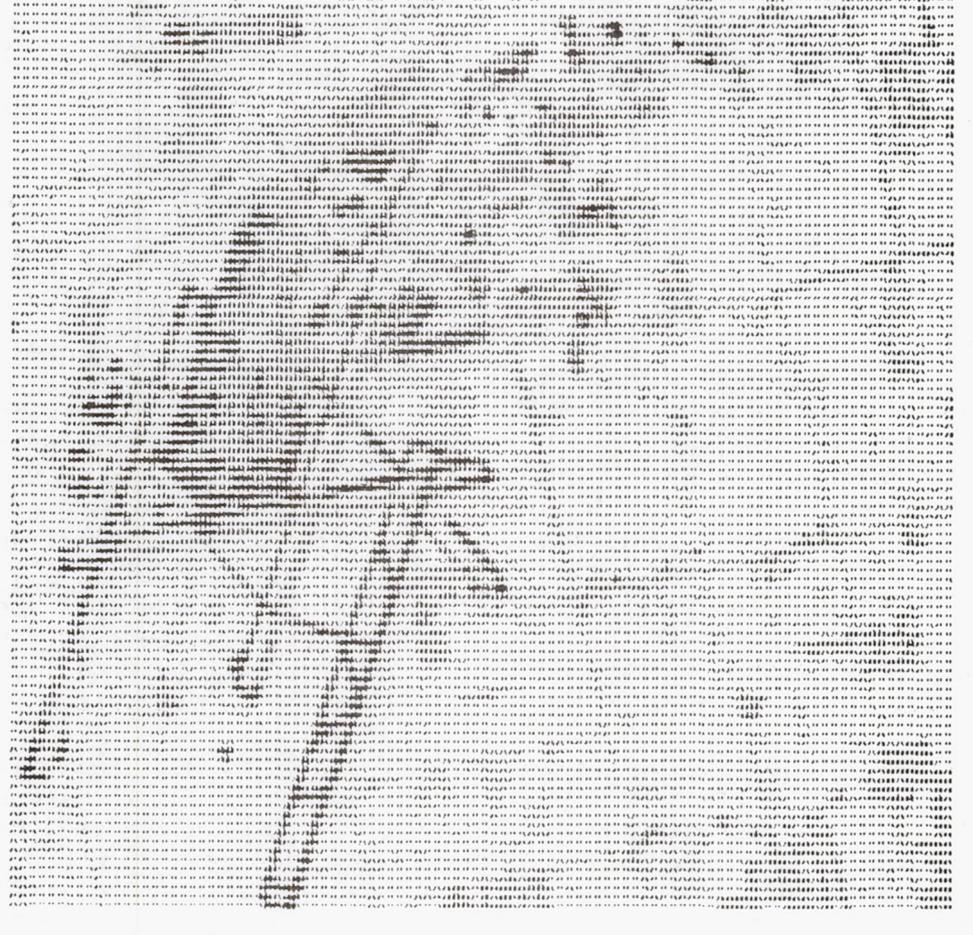
Figure 40 - Detroit Airport - Personal Computer Printer

CHARACTERIZATION OF LANDSAT-4 TM AND MSS IMAGE QUALITY FOR THE INTERPRETATION OF CALIFORNIA'S AGRICULTURAL RESOURCES

Stephen D. DeGloria
Robert N. Colwell

Remote Sensing Research Program
University of California
Berkeley 94720

INTRODUCTION

The primary goal of our research is to characterize the performance of Landsat-4's Multispectral Scanner (MSS) and Thematic Mapper (TM) in terms of spectral and spatial resolution, radiometric sensitivity, and geometric fidelity. A major objective is that of determining how these characteristics affect the utility of the data for natural resource applications. Our overall approach for characterizing the quality of Landsat-4 MSS and TM data entails: (1) analyzing Landsat-4 TM spectral and spatial performance in terms of spectral variability of natural targets and the TM-ground instantaneous field-of-view (IFOV) variability in level and mountainous terrain; and (2) determining the suitability of TM and MSS image products for characterizing renewable resource features.

For the early phases of our research, as reported upon in this paper, our objectives are to: (1) develop a basic understanding of the TM data in terms of spectral and spatial characteristics, CCT and film formats and products, and special problems in data handling; (2) determine the extent to which major agricultural resources and conditions can be detected and identified on TM image products and field-specific spectral statistical summaries; and (3) evaluate the quality of TM image products in comparison to simultaneously-acquired MSS image products.

During this phase of our research, our focus is on evaluating the quality of TM and MSS data for the interpretation of California's most important resource-- agriculture. Table 1 lists the major attributes of California agriculture which make California the leading agricultural state in the nation (Reference 1). In California, there is a diversity of crop types and practices, field sizes and shapes, and soil and landform conditions, which provides numerous opportunities for evaluating the quality of Landsat-4 data for meeting the inventory objectives of agricultural statisticians and resource managers.

APPROACH

The approach for accomplishing our objectives is as follows:

(1) Acquire the first available Landsat-4 scene of an active test site in California's Central Valley. An active agricultural test site is one in which ongoing projects are collecting detailed field data. These data consist of ground and aerial photographs and descriptions of specific field conditions and cropping practices.

(2) Acquire, process, and catalog small format, low altitude, color oblique aerial photography of selected areas within the scene to document major agronomic conditions including cropping practices, ground cover, and field conditions at the time of the Landsat-4 overpass. Acquisition of this photography should occur coincident with the overpass.

(3) Compile the available ground data for the area imaged to reconstruct, as accurately as possible, the environmental conditions prevalent at the time of the overpass. The sources of ground data for our research include: a) Land Use Survey Maps of the California Department of Water Resources (DWR), published at a scale of 1:24,000 and including individual field boundaries which are outlined and labeled (Reference 2); b) the U.S. Department of Agriculture's statistical summaries for crops and climate (Reference 3), and c) field crew notes and data, as compiled by personnel of our own Remote Sensing Research Program (RSRP) at the University of California.

(4) Produce TM and MSS black-and-white and color composite image products for interpretation.

(5) Locate the field data and aerial photographic coverage on the TM and MSS imagery.

(6) Relate the environmental conditions to the TM and MSS spectral data in both analog (film) and digital (numeric) formats.

(7) Determine the interpretability of major agricultural crops using these Landsat-4 spectral data based on established techniques (References 4,5). Interpretability requires that the image products allow both the detection and the correct identification of features of interest. Detection requires, at a minimum, the simple recognition or awareness that a feature is present. To identify the feature requires a synthesis of spectral, spatial, textural and temporal characteristics (Reference 6).

Our objectives call for interpreting diverse agricultural features using image products. Such products have both advantages and limitations in that photo-like imagery provides the best format for evaluating spatial and textural characteristics, but has limited usefulness for analyzing detailed spectral and temporal characteristics (Reference 6). When an image is created, whether in black-and-white or in color, from digital data, the data must be compressed into a limited number of gray (or color) levels thus obscuring subtle spectral differences of a feature of interest. In addition, color variation due to photographic processing may obscure data critical for feature identification. Inasmuch as these conditions suggest that some of the analyses of Landsat data can best be made using the original numeric data rather than images produced from these data (Reference 7), such an analysis is being included in our investigations.

RESULTS AND DISCUSSION

The first available Landsat-4 scene for one of our active test sites was acquired on December 8, 1982. This site is located in San Joaquin County, California. The importance and diversity of agricultural production in this county is shown in Table 2 (Reference 1). The image data were received by the Prince Albert Station in Canada and forwarded to NASA-Goddard Space Flight Center (GSFC) for subsequent processing. The scene identification number is #84014518082X0, World Reference System (WRS) Path 43, Row 34. Figure 1 shows the location of this scene in Northern California (solid line). It also shows the three other principal scenes covering U.C. Berkeley's primary study areas (dotted lines). The TM data were processed as a "P" tape by the Landsat Assessment System (LAS) at GSFC using the interim SCROUNGE image processing system. The "P" tape product is both radiometrically and geometrically corrected. The computer compatible tape (CCT), at 6250 bpi, was forwarded to the IBM Palo Alto Scientific Center, c/o Mr. Ralph Bernstein, for subsequent processing and analysis by IBM and U.C. Berkeley. The MSS data were purchased at the EROS Data Center as a CCT-AM ("A" tape) which is radiometrically, but not geometrically processed. Table 3 summarizes the basic Landsat-4 spacecraft and sensor constants. Reference is made to source documents which should be consulted for more detailed information on satellite and ground processing operations (References 8,9,10). Table 4 gives the spectral range of the TM and MSS sensors.

Due to winter ground fog in the Central Valley, the first opportunity during which to acquire small format, low altitude color oblique photography after the December 8 Landsat pass occurred on January 20, 1983. On that day, several pre-selected transects within San Joaquin County were flown and specific fields photographed using dual 35mm cameras. One camera contained natural color film and the other, color infrared film. The aircraft altitude was 500 m. The film was processed commercially, and each transect and frame was labeled and annotated on DWR land-use maps at 1:24,000 scale. An example of the quality of this photography is shown in Figures 2a and 2b.

Given the vast area covered by each Landsat frame, two 21,000 hectare study areas within the County were selected for detailed analysis due to the diversity of their agronomic and pedologic conditions. The Vernalis Study Area is dominated by alluvial and low terrace soils supporting orchards, field crops, and native pasture. The Caswell Study Area is dominated by basin and alluvial soils supporting mixed pasture, field crops, some orchards and vineyards, and extensive native vegetation in Caswell State Park (Reference 11). Detailed agricultural land use maps and legends for the Caswell and Vernalis study areas are shown in Figures 3 and 4, respectively (Reference 2).

By thoroughly examining these detailed land use maps along with the oblique aerial photographs and published agronomic and climatic data, we were able to determine environmental conditions prevalent at the time of the overpass. Climatic conditions one week prior to the overpass were varied. A series of Pacific Ocean storms had crossed the State with over one inch of precipitation falling in northern San Joaquin County. No precipitation fell during the week of the overpass, and temperatures were near normal for the study area. Precipitation was heavy during the period between the overpass and the acquisition of the oblique aerial photography. As periodic storms and cool temperatures preceeded both the satellite and aerial photography acquisitions, variations in surface

soil moisture between the two dates of data acquisition were minimal. Agronomic conditions were dominated by slow growth of small grains, which were 50% emergent, statewide, at the time of the overpass. Preparation for planting the remaining small grain fields was in progress with much moist, fallow soil present. Field preparation included weed control, pre-irrigation and planting. Harvesting of grain sorghum and corn had recently been done in some fields. This is indicated in both study areas by the presence of grain and corn stubble fields. Some limited alfalfa cutting was in progress, and many overwintered sugar beet fields were evident. Pruning and weed control were the dominant field activities in the deciduous orchards and vineyards. Many spectral variations in the orchards resulted from the high spectral reflectance of the grass canopy understory in orchards of varying age. Pasture growth and conditions were above normal due to favorable climatic conditions prior to the overpass. Both native and irrigated pasture experienced rapid herbaceous growth prior to the overpass. The cool, wet conditions that prevailed after the overpass retarded grass growth; conditions documented on the aerial obliques acquired six weeks after the overpass were very similar to those present at the time of the overpass.

Image products and numeric data were extracted from both the TM and MSS data. TM image products were generated using the IBM 7350 Image Processing System at the IBM Palo Alto Scientific Center (Reference 12). Various single band and multi-band images were displayed on the 7350's color monitor; 35mm slides were used to image the data displayed on the screen. Initial analysis of the TM data was accomplished using these 35mm slide products. MSS image products were generated using the Remote Sensing Image Analysis Computer System at the Space Sciences Laboratory on the U.C. Berkeley campus. Digital displays were copied onto 35mm and Polaroid (Type 809) color film using a Matrix Color Graphics Camera. Images of individual TM and MSS spectral bands for the Caswell and Vernalis study areas are shown in Figures 5 and 6, respectively. Through the use of these and color image products, direct comparisons of tone and textural signatures were made between the oblique photography and the ground data in order to determine the TM and MSS spectral characteristics of major agricultural fields in the area, and to locate specific fields for extracting numeric data from both the TM and MSS CCT's. Using these numeric data, we estimated the within-field and within-region spectral variability, by band, for both of the Landsat-4 sensors. These numeric data for the Caswell Study Area are summarized in Figure 7 where spectral data for each of the TM spectral bands are plotted. The thermal band (TM6) displays the lowest variability and range of values for this area. This is expected given the 120-meter IFOV and limited radiant temperature variability of the area sampled. In the reflective bands, the spectral variability increases with wavelength. Field-specific spectral data for the Caswell study area are tabulated in Table 5, and plotted in Figure 8. The fields and crops selected are those which dominate the study area in terms of spectral, spatial, and textural characteristics.

Systematic analyses of both image products and numeric data for these study areas have yielded the following early results:

(1) The overall quality of the TM data are excellent. This quality is illustrated for all bands as shown in comparison to the MSS data in Figures 5 and 6. Both study areas contain fields of variable shape, size, orientation and cropping practices on contrasting soil groups. Spectral variations in fallow fields are primarily the result of soil moisture and surface roughness variability due to various stages of field preparation for planting small grains.

(2) There is extensive coherent noise in the MSS data for all bands. This noise is illustrated in Figures 5 and 6. The noise affects data quality in Bands 1 and 2 to a greater extent than in the two near-infrared bands. We anticipate this noise will cause significant classification errors for mapping small fields and specialty crops in California when using MSS data. This noise is also apparent in TM Band 1 for both Study Areas (Figure 5a). The period of this MSS and TM noise has not been determined by these investigators.

(3) Spectrally, the addition of the first short-wave infrared band (Band 5) has significantly enhanced our ability to discriminate different crop types as shown in Figure 8. In the visible and near infrared bands, there is no significant difference between the sugar beet and alfalfa spectra. In the middle infrared band, however, we see significantly different spectral values resulting from the increased absorption of the radiation by the higher content of leaf water of the sugar beet plant. Several other spectral crossovers (tone shifts) between the visible and the middle infrared regions are also displayed. These crossovers provide enhanced capabilities for discriminating and identifying major crop groups and land cover conditions that are commonly confused spectrally in the visible and near-infrared regions on single-date imagery. These obvious crossovers occur between orchard and bare soil; between mixed pasture, sugar beets, and alfalfa; and between grain stubble, mixed pasture, alfalfa, and sugar beets. All of these numeric crossovers are illustrated in Figure 5b-e as shifts in gray tones on the image products. The accuracy of crop group or crop type classification using single-date or multi-date Landsat-4 data will increase if TM Band 5 is used in conjunction with TM Band 4 and/or Band 3 as simple ratios, linear combinations, or other commonly used transformations.

Photographic images of the thermal data acquired by the TM sensor for both study areas are shown in Figure 6e. The dark tones on this image are those land surfaces which have low radiant temperatures at the time of the overpass (0908 hours, PST), and represent primarily fields of grain stubble and bare soil which have high moisture conditions. The light tones are those surfaces which have high radiant temperatures at the time of the overpass, and represent fields of deciduous orchards, field crops and mixed pasture which have relatively lower moisture conditions than the bare soil fields. Improvements in the processing of the TM thermal data are still needed to reduce the radiometric striping resulting from the bi-directional scanning.

(4) Spatially, the twofold decrease (28.5 m vs. 57 m) in interpixel distance, and fourfold decrease in area per pixel of TM data allow for improved spectral characterization of individual features due to a reduction in measurement errors. This reduction results from the ability to extract a higher number and proportion of "pure" pixels that are minimally contaminated by "boundary" pixels. Mapping at more detailed levels of classification will also be enhanced by using the spatially improved TM products. The improved spatial resolution of the TM sensor is best illustrated in Figures 6a-d of the Vernalis Study Area. Numerous linear features and various angles are depicted on the image products with minimal scan-angle effects. Small linear features such as light-duty roads, water canals, and subtle field boundaries are easily resolved on the TM image product, but are not consistently resolvable on the MSS products. Several examples in the Vernalis area illustrate this point. The New Jerusalem Airport is shown on the right hand margin of each image in Figures 6a-d as two parallel, concrete runways located alongside cropped fields. Running parallel to the runways are taxi strips separated from the runways by bare soil fields; these taxi strips are not resolvable

on either image product due to the spatial resolution of the sensors and lack of sufficient contrast between the concrete and bare soil. The field crop growing on both sides of the upper runway allows sufficient contrast for both sensors to resolve this feature. The lower runway, however, is bounded both by a field crop, creating a high contrast upper boundary, and by a bare soil field, creating a low contrast lower boundary. This variable contrast boundary makes the lower runway barely resolvable on the TM image products and not resolvable on the MSS image products with the exception of the portion of the runway where there is sufficient contrast between the concrete and bare soil to be resolved by the near-infrared channel, MSS Band 3 (Figure 6c).

(5) The 8-bit signal quantization level of the TM provides an image that is rich in detail, optimizing the textural characteristic--a major attribute used in feature identification. The improved tone contrast and increased sharpness of feature boundaries on the TM image products, in comparison to the MSS products, is readily apparent from a careful viewing of Figures 5 and 6.

(6) No geometric comparisons were made between the MSS and TM data because the MSS data had not been geometrically corrected. Qualitative comparisons between the TM data and USGS 7½' topographic quadrangles, however, appear to indicate that the geometric quality of TM data is sufficient for updating land use maps and field boundaries at this scale (1:24,000).

SUMMARY

Even at this early stage of our research we find the quality and utility of the TM data to be excellent for meeting most of the inventory objectives of the agricultural resource specialist. The TM data will be extremely valuable for crop type and area proportion estimation, updating agricultural land use survey maps at 1:24,000-scale and smaller, field boundary definition, and determining the size and location of individual farmsteads.

Ongoing research activities are focused on making spectral and spatial analyses of both MSS and TM analytical film products. Based on the improved spectral, spatial and radiometric quality of the TM data, we see a renewed emphasis and interest in direct visual interpretation of these image products, both for updating and improving land stratification in support of resource inventory and for enhancing the image analyst's contribution to computer-assisted analysis procedures.

ACKNOWLEDGEMENTS

REFERENCES

1. California Department of Food and Agriculture. 1982. California Agriculture--statistical review for 1981. Sacramento, 18p., July.

2. California Department of Water Resources. 1982. Land use survey maps, Vernalis and Ripon quadrangles. Sacramento.

3. U.S. Department of Agriculture. 1982. California crop-weather. Vol. 2, Nos. 21, 22, 28. Statistical Reporting Service, USDA, Sacramento, December 1982, January 1983.

4. Colwell, R. N. 1978. Interpretability of vegetation resources on various image types acquired from earth-orbiting spacecraft. J. Appl. Photogr. Eng. 4(3):107-117.

5. Benson, A. S. and K. J. Dummer. 1983. Analysis of photo interpretation test results for seven aerospace image types of the San Juan National Forest, Colorado. Proc. 49th ASP Annual Mtg. Washington, D.C. pp.121-130.

6. Hay, C. M. 1982. Remote sensing measurement techniques for use in crop inventories. pp.420-433. In C. Johannsen and J. Sanders (eds.) Remote Sensing for Resource Management. Soil Conservation Society of America, Ankeny, Iowa.

7. Odenweller, J. B. and K. I. Johnson. 1982. Crop identification using Landsat temporal-spectral profiles. Proc. Symp. Machine Processing Remotely Sensed Data, Purdue University, West Lafayette, IN. pp.469-475.

8. Goddard Space Flight Center. 1982. Landsat-D to ground station interface description, Rev. #4, February. GSFC #435-D-400. Nat. Aeronautics and Space Admin., Greenbelt, MD. 91p., Appendices.

9. U.S. Geologic Survey. 1982. Landsat data users notes #23, July EROS Data Center, U.S. Dept. Interior, Sioux Falls, SD. p. 5.

10. Personal communication with Mr. Kent Hegge, EROS Data Center, Sioux Falls, South Dakota.

11. Weir, W. W. 1952. Soils of San Joaquin County, California. Agric. Exp. Station, College of Agric., University of California, Berkeley. 137p.

12. Niblack, W. 1982. IBM 7350 Image Processing System: A tool for earth resources data processing. Proc. Symp. Machine Processing Remotely Sensed Data, Purdue Univ., West Lafayette, IN. pp.533-537.

Table 1.

IMPORTANCE OF CALIFORNIA'S AGRICULTURAL RESOURCES

Leading Agricultural State in U.S.
200+ Commercial Crops
14 Million Hectares in Farm Production
Leads U.S. in 48 Crop and Livestock Commodities
50% of U.S. Fruit and Nut Crop Production
33% of U.S. Vegetable Crop Production
$13.9 Billion Crop and Livestock Production Value
$4.2 Billion Export Value (Cotton, Rice, Wheat, Others)

Table 2.

AGRICULTURAL STATISTICS FOR SAN JOAQUIN COUNTY, CALIFORNIA

365,200 Hectares
6th Leading Agricultural County in California
$770 Million Crop and Livestock Production Value
Major Crop Groups:
    Tree Fruits and Nuts
    Vineyards
    Field and Truck Crops
    Range Pasture, Irrigated and Non-Irrigated
Average Field Size $\sim$25ha
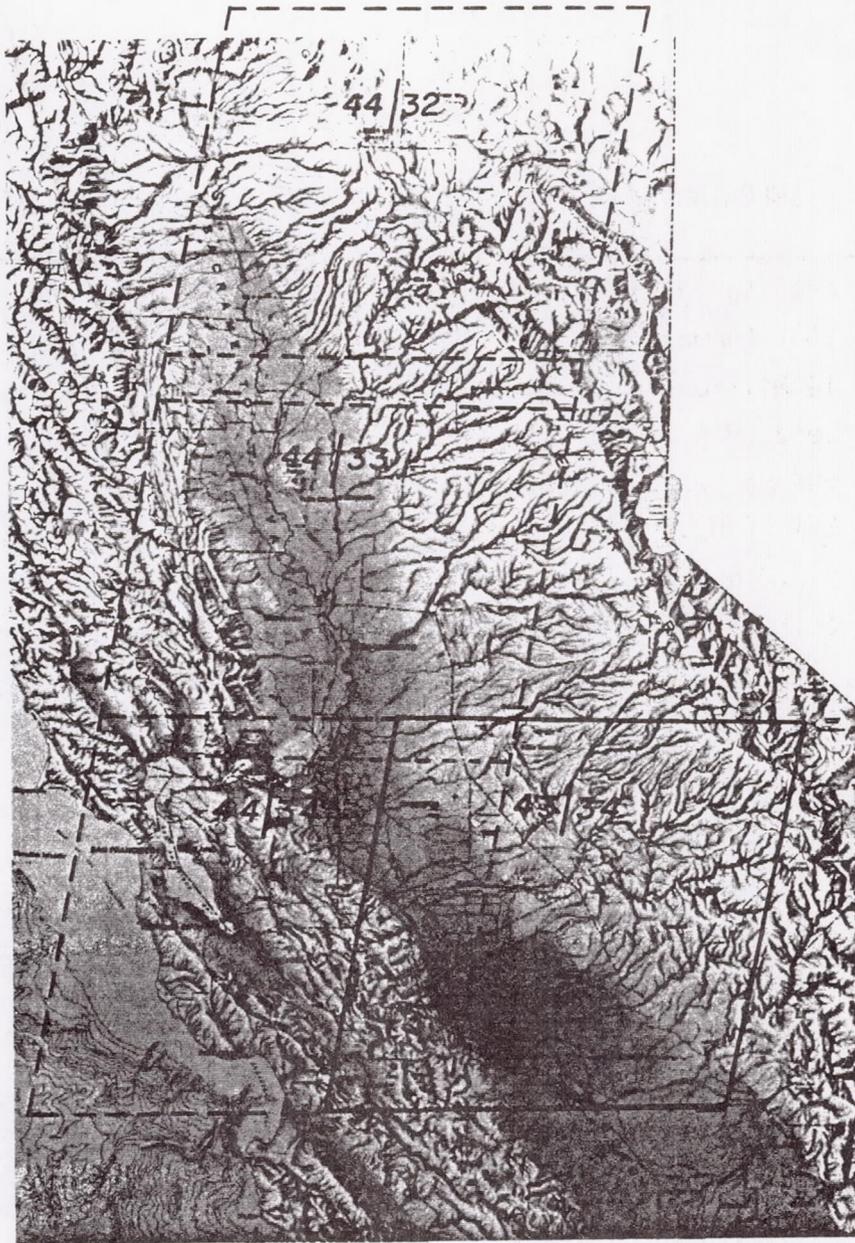
Figure 1.   Location of the principal Landsat-4
scenes covering U.C. Berkeley's
study areas.

Table 3.

BASIC LANDSAT-4 SPACECRAFT AND SENSOR CONSTANTS

SPACECRAFT

    Sun Synchronous
    Nominal Altitude   705.3 km
    Nominal Swath Width   185.0 km
    Orbit Inclination   98.2°
    Orbit Period   98.9 min
    Repeat Period   16 days
    Sidelap (at equator)   7.6%
    Sidelap (at 40° Latitude) 29.0%

SENSOR

    MSS (partially processed image; CCT-AM)

        Nominal number of pixels/line   3240
        Number of lines   2400
        Nominal interpixel distance   57.0m
        Nominal interline distance   82.7m

    MSS (fully processed image; CCT-PM)

        Number of pixels/line   3548
        Number of lines   2983
        Interpixel distance   57.0m
        Interline distance   57.0m
        Signal quantization levels   127

    TM (fully processed image; CCT-PT)

        Number of pixels/line   6967
        Number of lines   5965
        Interpixel distance   28.5m
        Interline distance   28.5m
        Signal quantization levels   256

Table 4.

SPECTRAL RANGE OF THE SENSORS ON LANDSAT-4

THEMATIC MAPPER (TM)	
Band	Spectral Range, μm
1	0.45 - 0.52
2	0.52 - 0.60
3	0.63 - 0.69
4	0.76 - 0.90
5	1.55 - 1.75
7	2.08 - 2.35
6	10.40 -12.50

MULTISPECTRAL SCANNER (MSS)	
Band	Spectral Range, μm
1	0.5 - 0.6
2	0.6 - 0.7
3	0.7 - 0.8
4	0.8 - 1.1
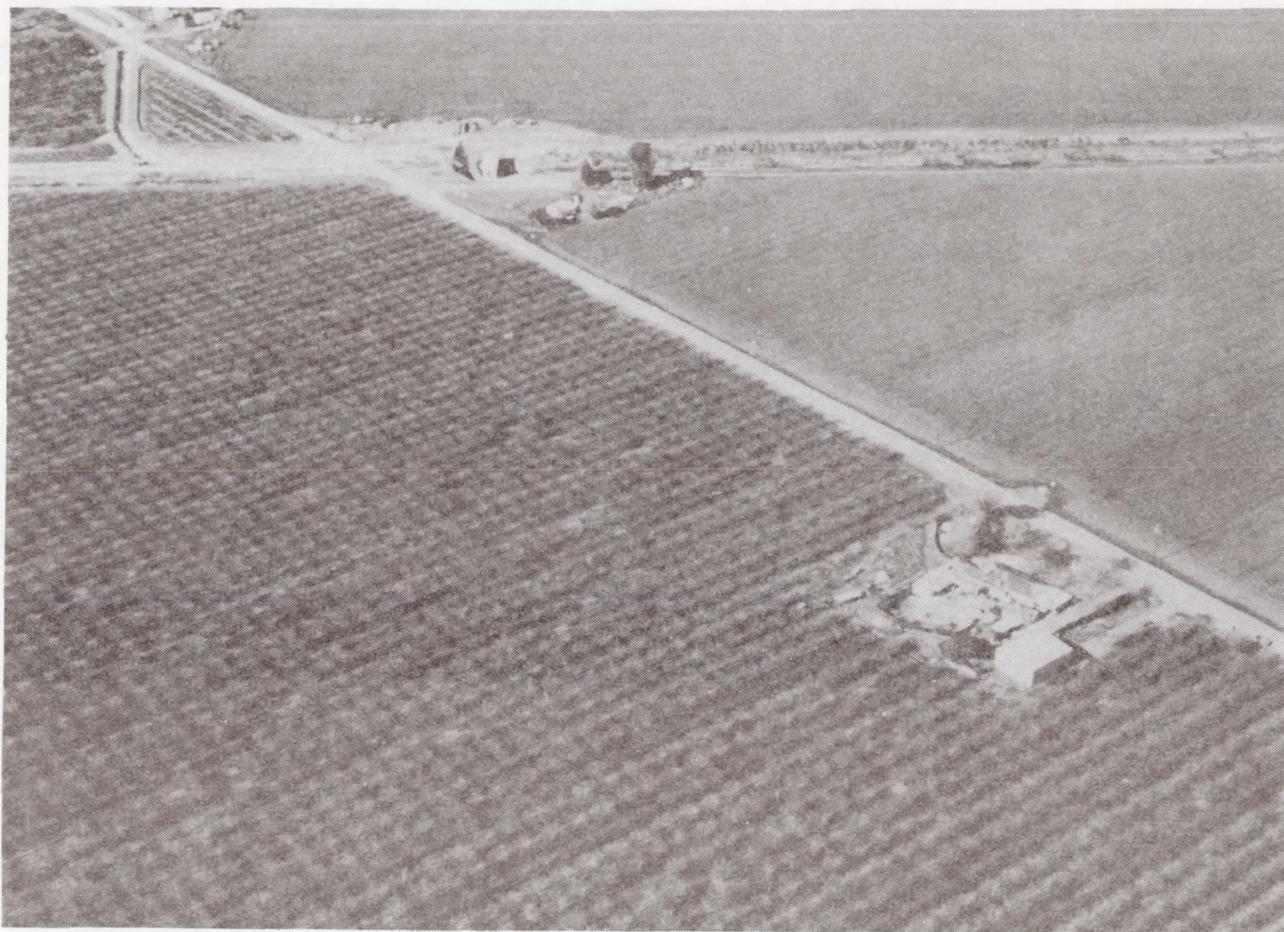
Figure 2a. Example of low altitude, 35mm aerial oblique photography acquired on January 20, 1983 for assessing land cover conditions. This image shows a deciduous orchard with an herbaceous vegetation understory (left), and an emerging small grain field (upper right) where bare soil dominates the spectral response. The location and direction of this photograph are illustrated in Figure 6c. Variations in orchard canopy density are evident in the TM image products.
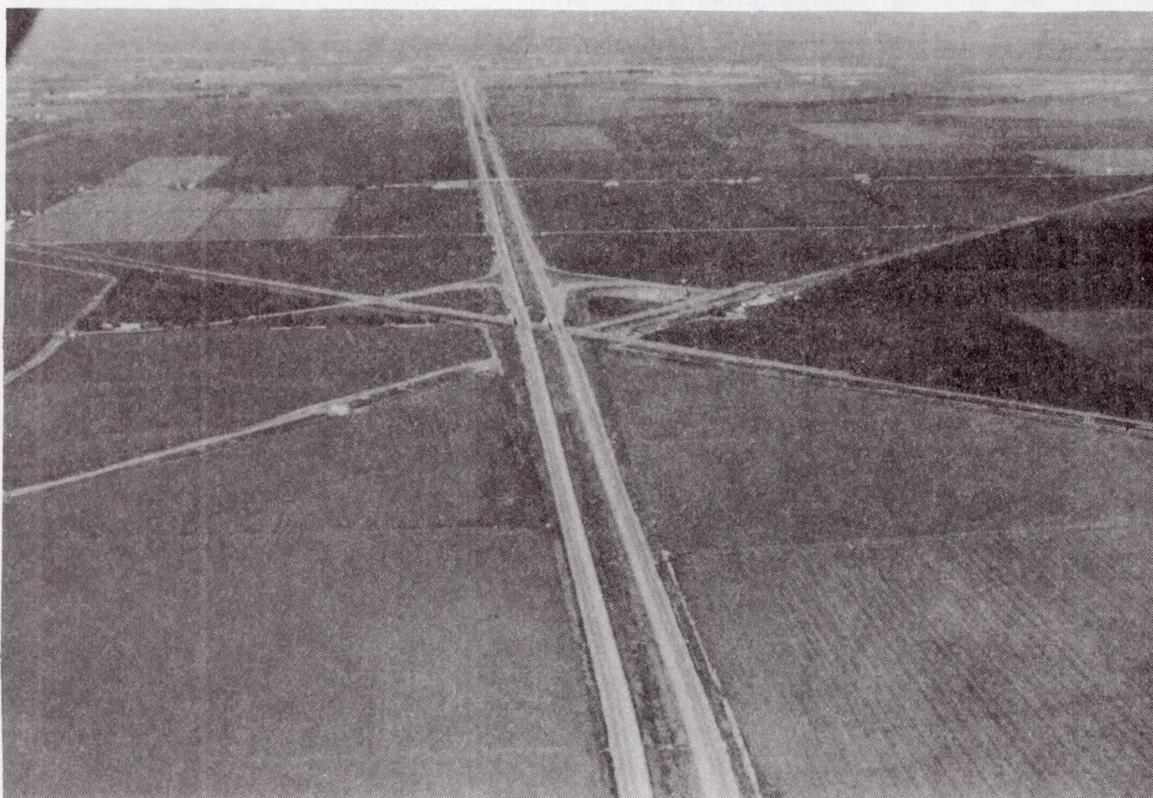
Figure 2b. Low altitude oblique photography of the Caswell Study Area (top) and the Vernalis Study Area (bottom).
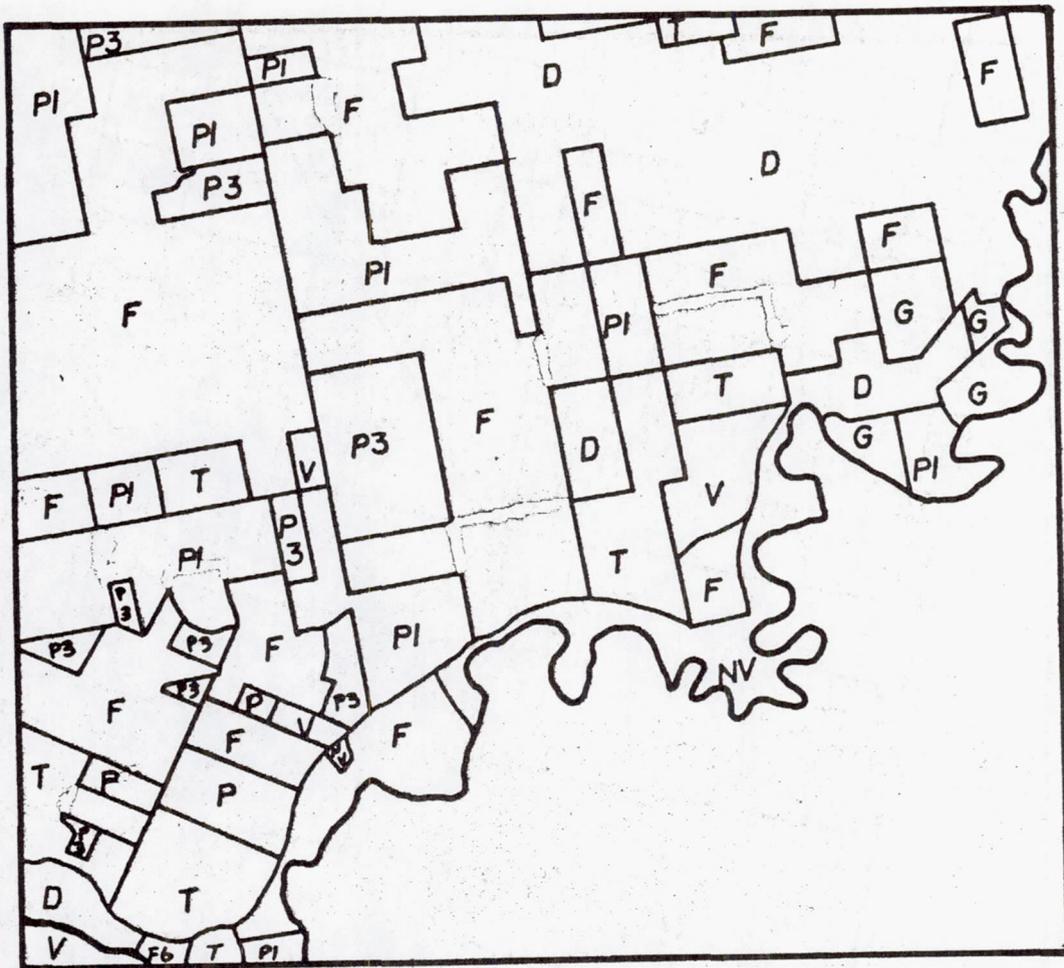
AGRICULTURAL CLASS KEY

D - Deciduous Fruits and Nuts

F - Field Crops

G - Grain and Hay Crops

NV - Native Vegetation

P - Pasture

    P1 - Alfalfa and Alfalfa Mixtures

    P3 - Mixed Pasture

T - Truck and Berry Crops

V - Vineyard

Figure 3. Agricultural land use map and legend for the Caswell Study Area.
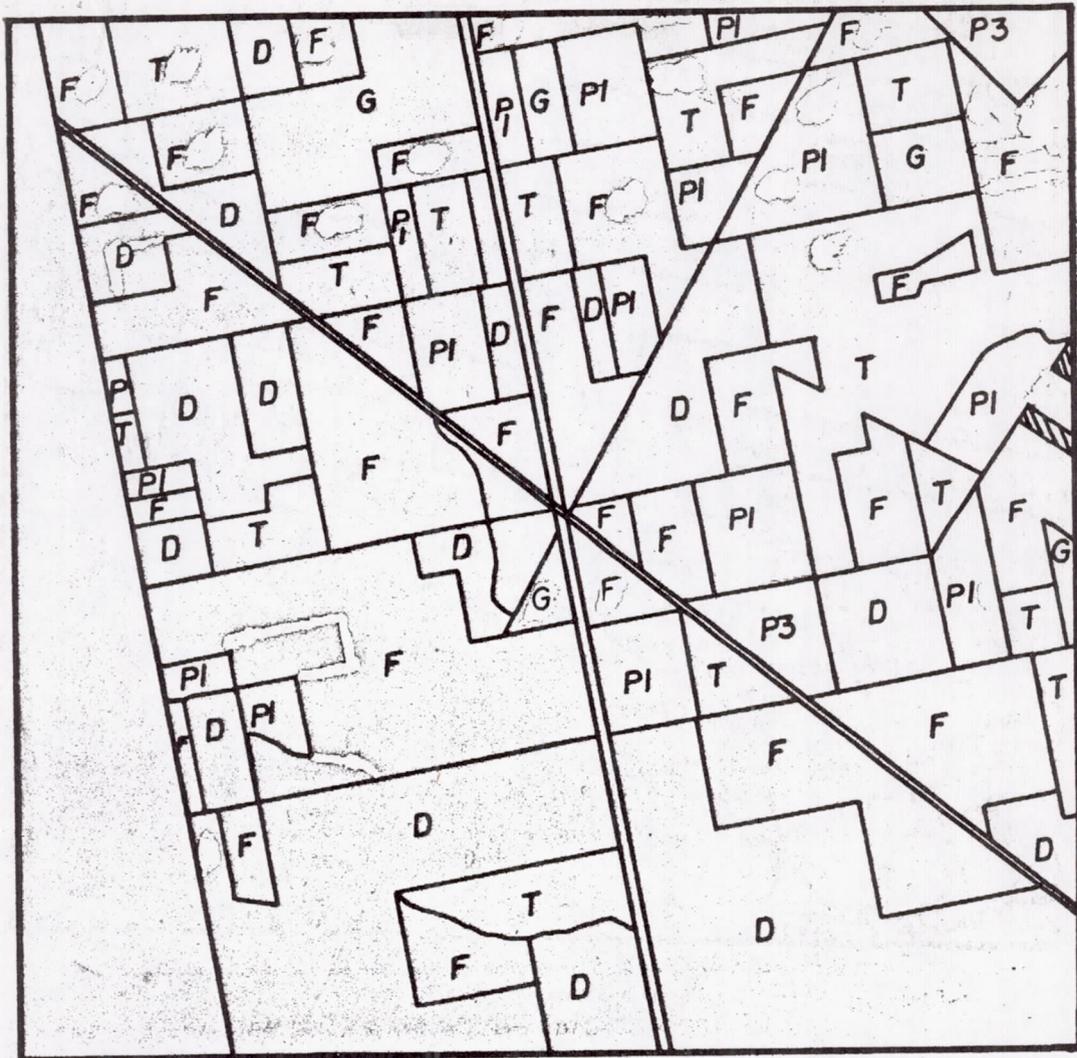
AGRICULTURAL CLASS KEY

D   -   Deciduous Fruits and Nuts

F   -   Field Crops

G   -   Grain and Hay Crops

NV -   Native Vegetation

P   -   Pasture

      P1   - Alfalfa and Alfalfa Mixtures

      P3   - Mixed Pasture

T   -   Truck and Berry Crops

V   Vineyard

Figure 4.   Agricultural land use map and legend for the Vernalis Study Area.
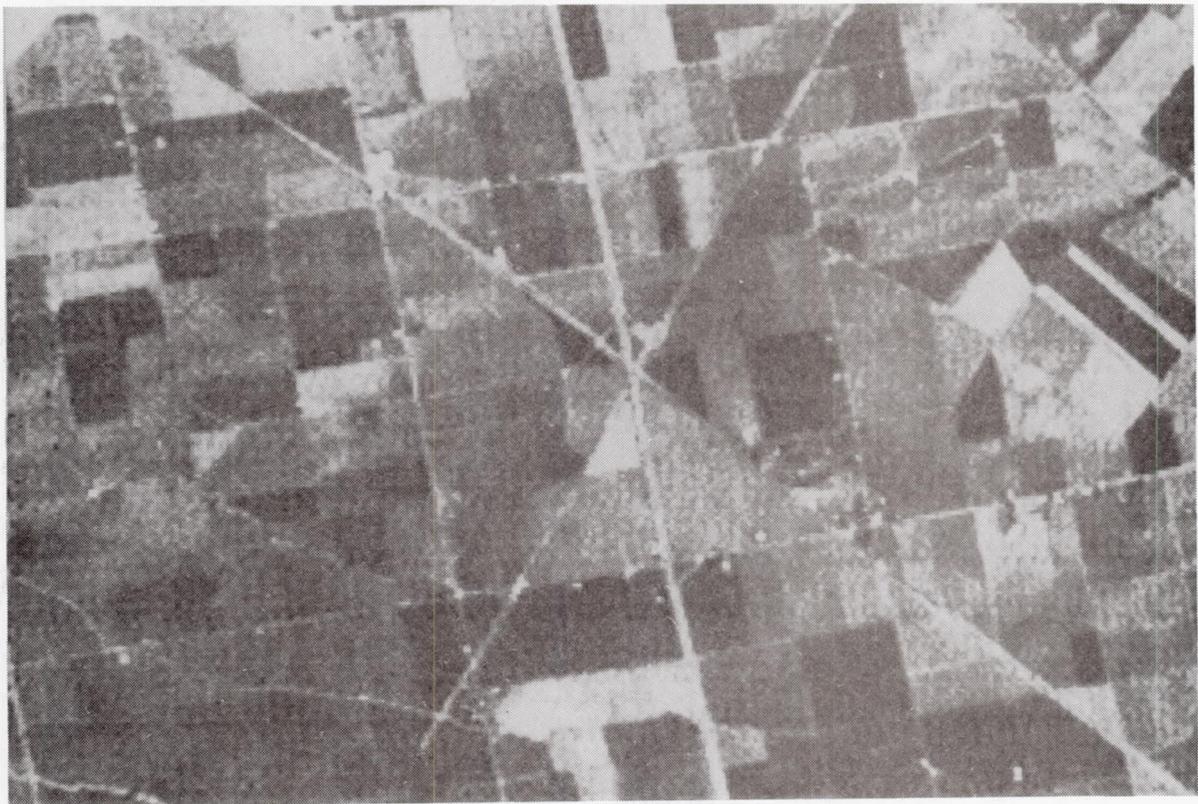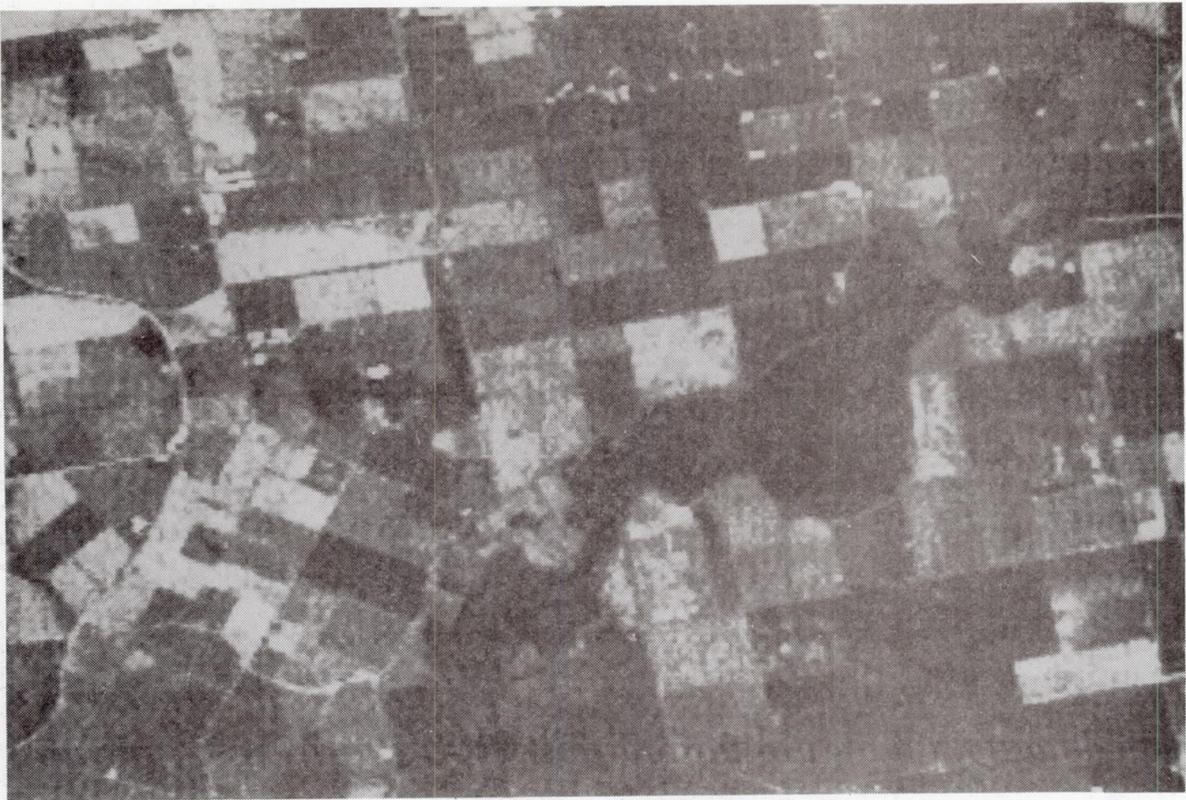
Figure 5a. TM Band1 (Blue) for the Caswell (top) and Vernalis (bottom) Study Areas. Coherent noise is evident on both images.
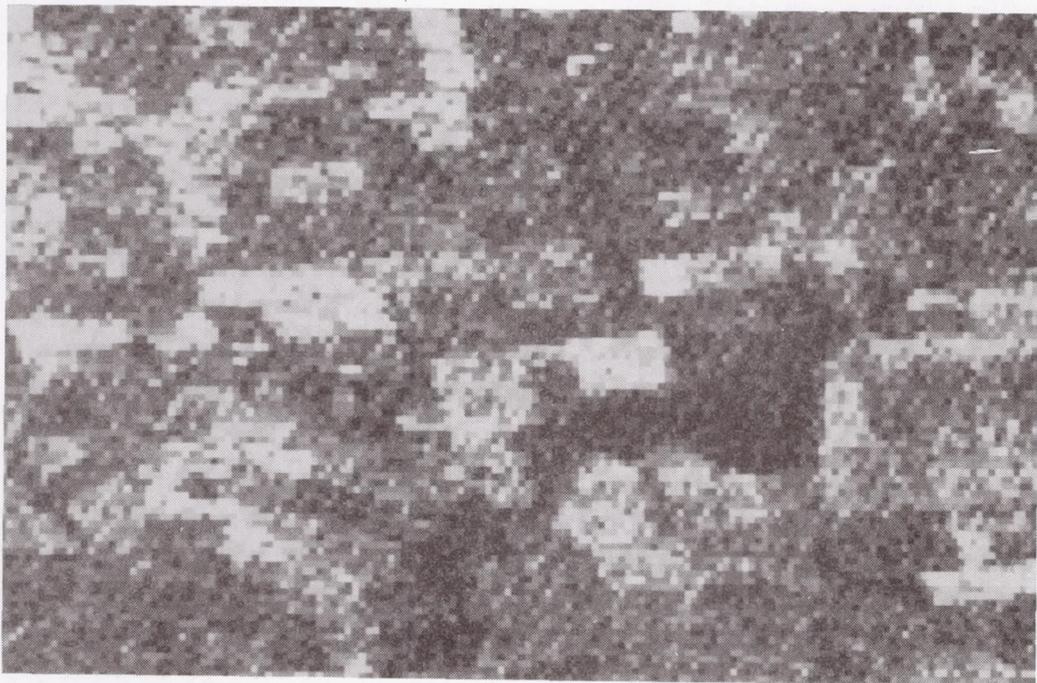
Figure 5b. Comparison of the image quality in the green region of the spectrum.
TM Band 2 (top) and MSS Band 1 (bottom) for the Caswell Study Area.

Figure 5c. Comparison of image quality in the <u>red</u> region of the spectrum. TM Band 3 (top) and MSS Band 2 for the Caswell Study Area.

Figure 5d. Comparison of image quality in the near-infrared region of the spectrum. TM Band 4 and MSS Band 3 (bottom) for the Caswell Study Area.
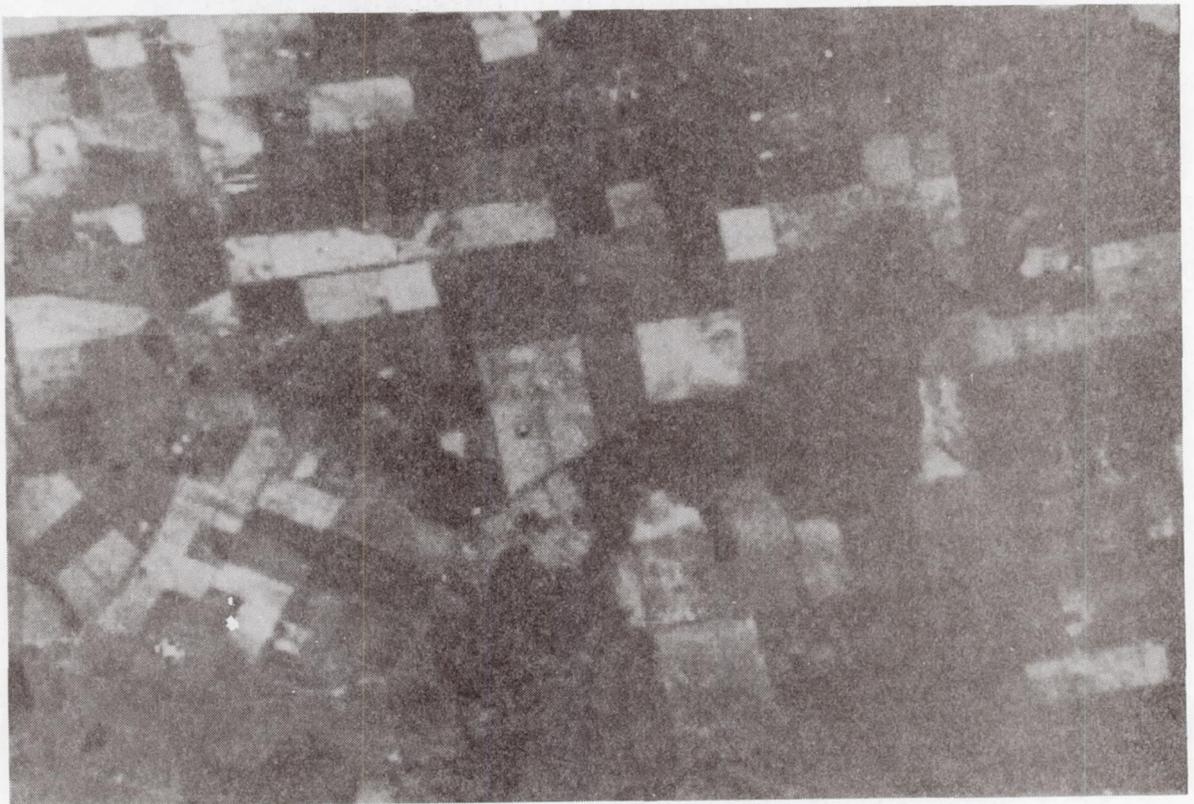
Figure 5e. TM Band 5 (top) and TM Band 7 (bottom) for the Caswell Study Area.
The delineated area indicates the look direction of the oblique
aerial photograph shown in Figure 2b. (top).
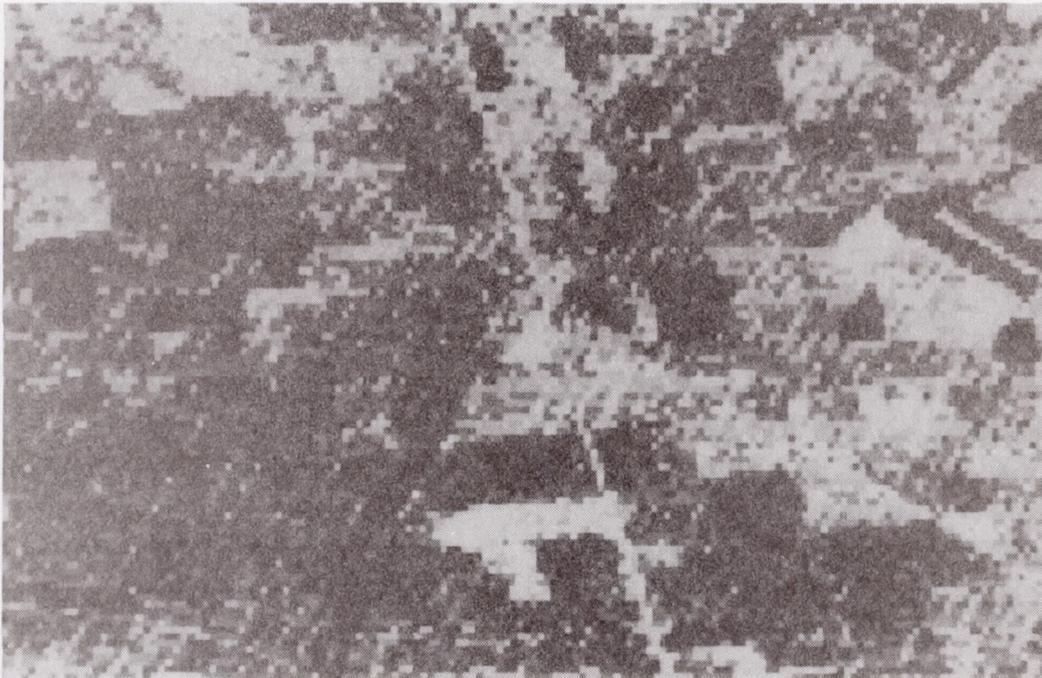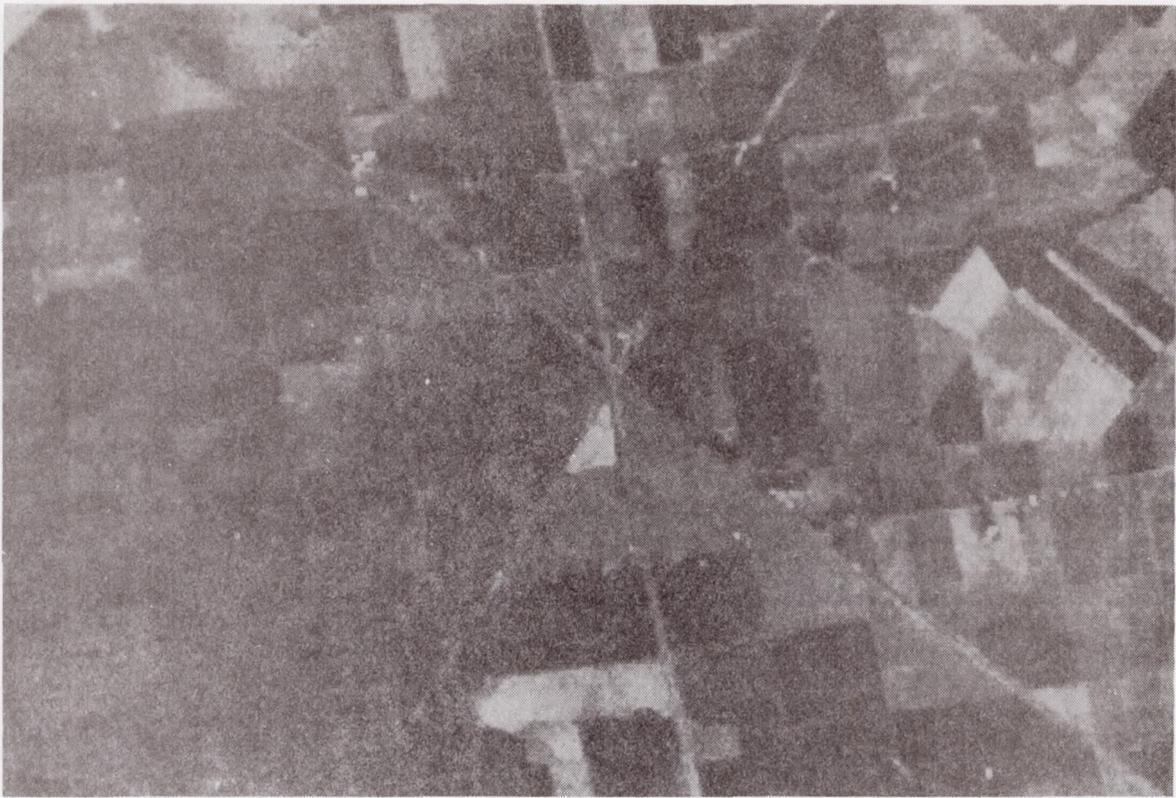
Figure 6a. Comparison of image quality in the green region of the spectrum. TM Band 2 (top) and MSS Band 1 (bottom) for the Vernalis Study Area.
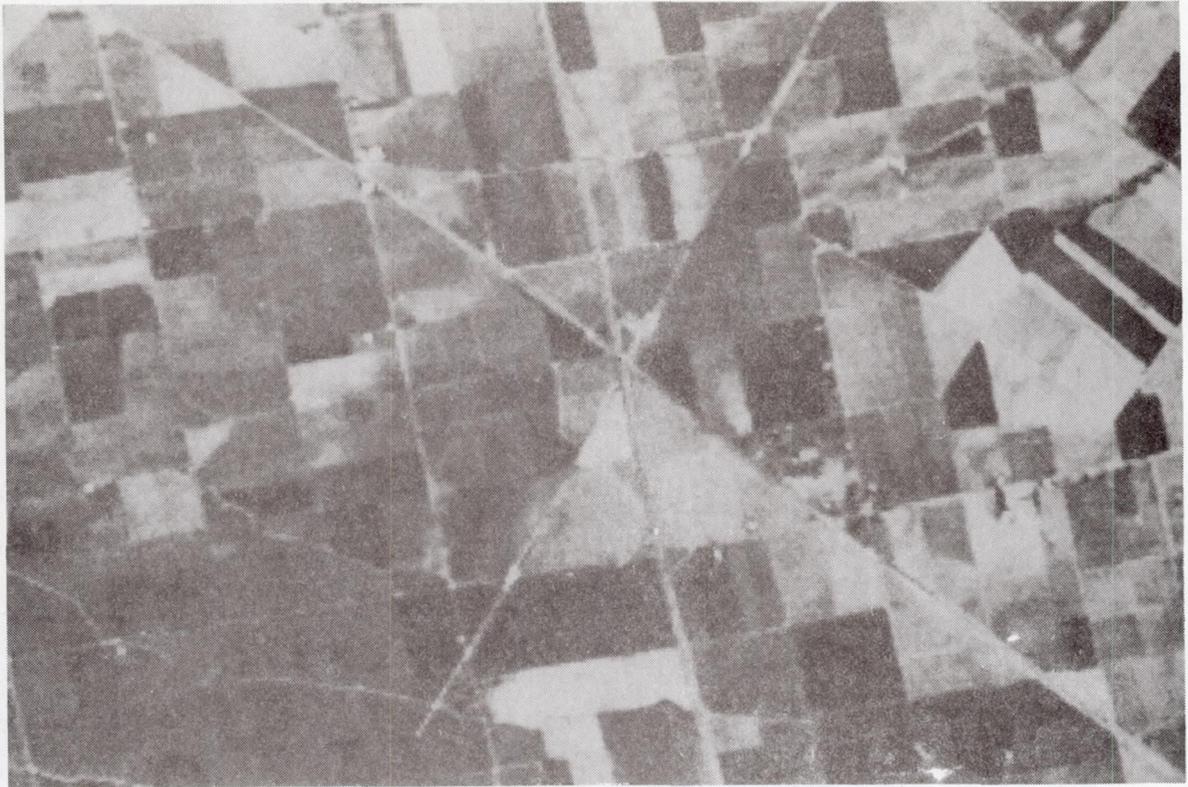
Figure 6b. Comparison of image quality in the red region of the spectrum. TM Band 3 (top) and MSS Band 2 (bottom) for the Vernalis Study Area.
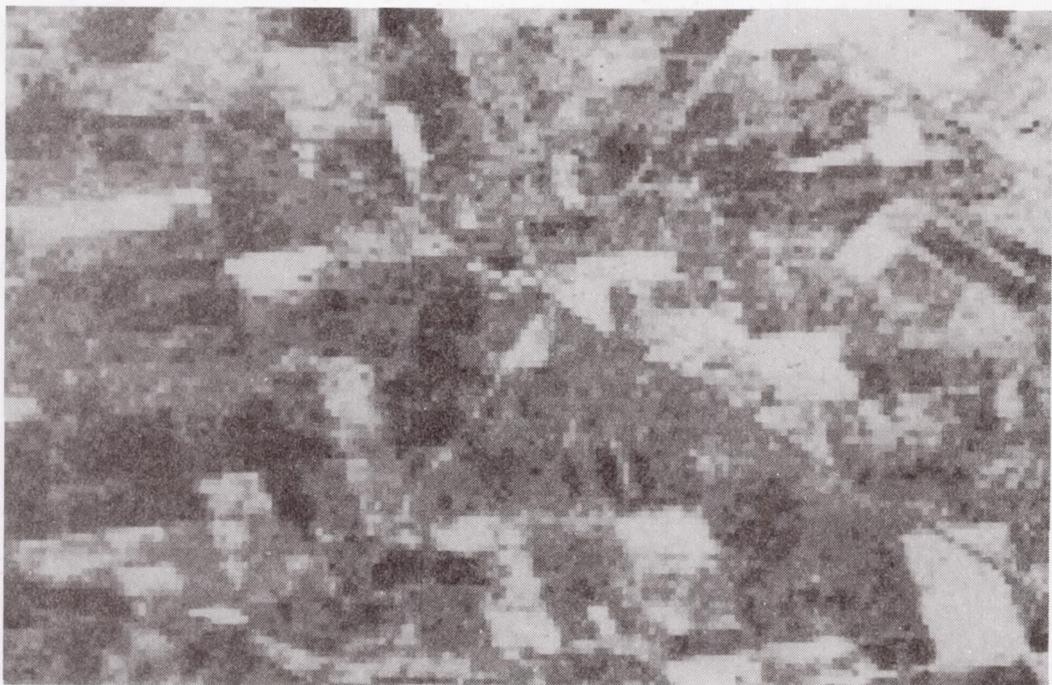
Figure 6c. Comparison of image quality in the near-infrared region of the spectrum. TM Band 4 (top) and MSS Band 3 (bottom) for the Vernalis Study Area. The delineated area indicates the look direction of the oblique aerial photograph shown in Figure 2a.

Figure 6d. TM Band 5 (top) and TM Band 7 (bottom) for the Vernalis Study Area. The delineated area indicates the look direction of the oblique aerial photography shown in Figure 2b. (bottom).
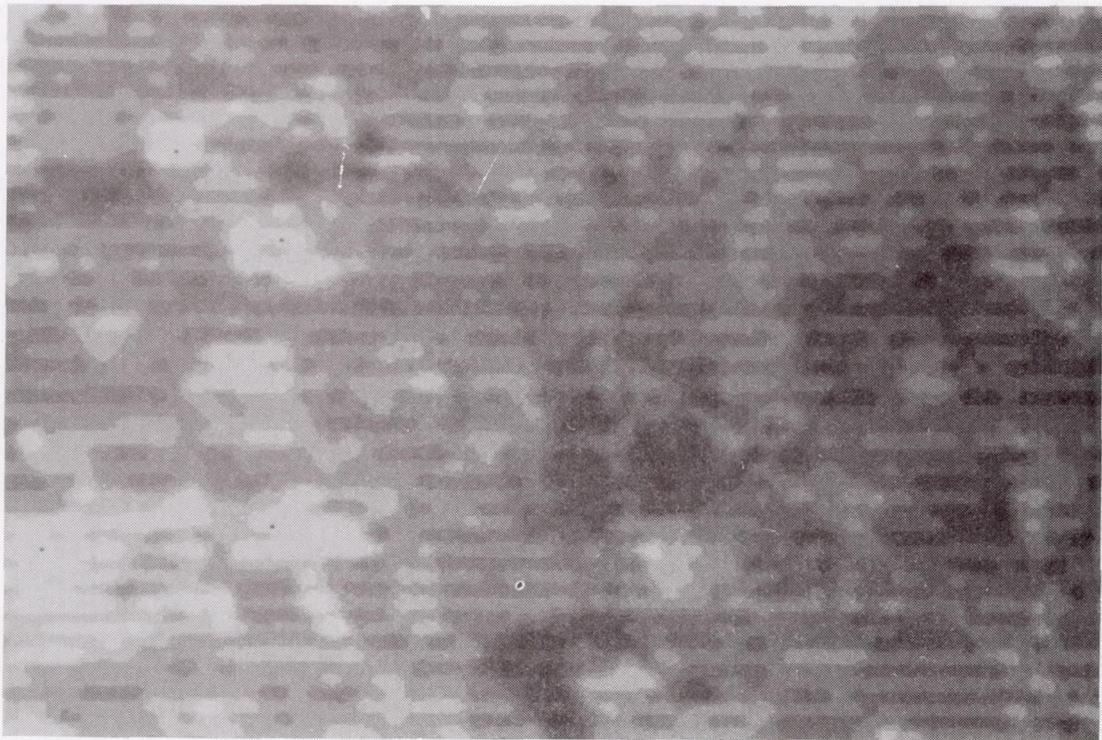
Figure 6e. Image quality in the thermal infrared region of the spectrum.
TM Band 6 for the Caswell Study Area (top) and for the Vernalis
Study Area (bottom).

CASWELL STUDY AREA

(632 x 404)

BAND	MIN	MAX	$\bar{x}$	s	CV
1	44	149	54.0	4.3	8.0
2	15	74	22.2	2.7	12.2
3	12	90	21.8	4.3	19.7
4	5	105	37.3	9.8	26.3
5	1	220	44.9	9.5	21.2
7	0	252	21.9	7.1	32.4
6	77	102	91.9	1.2	1.3
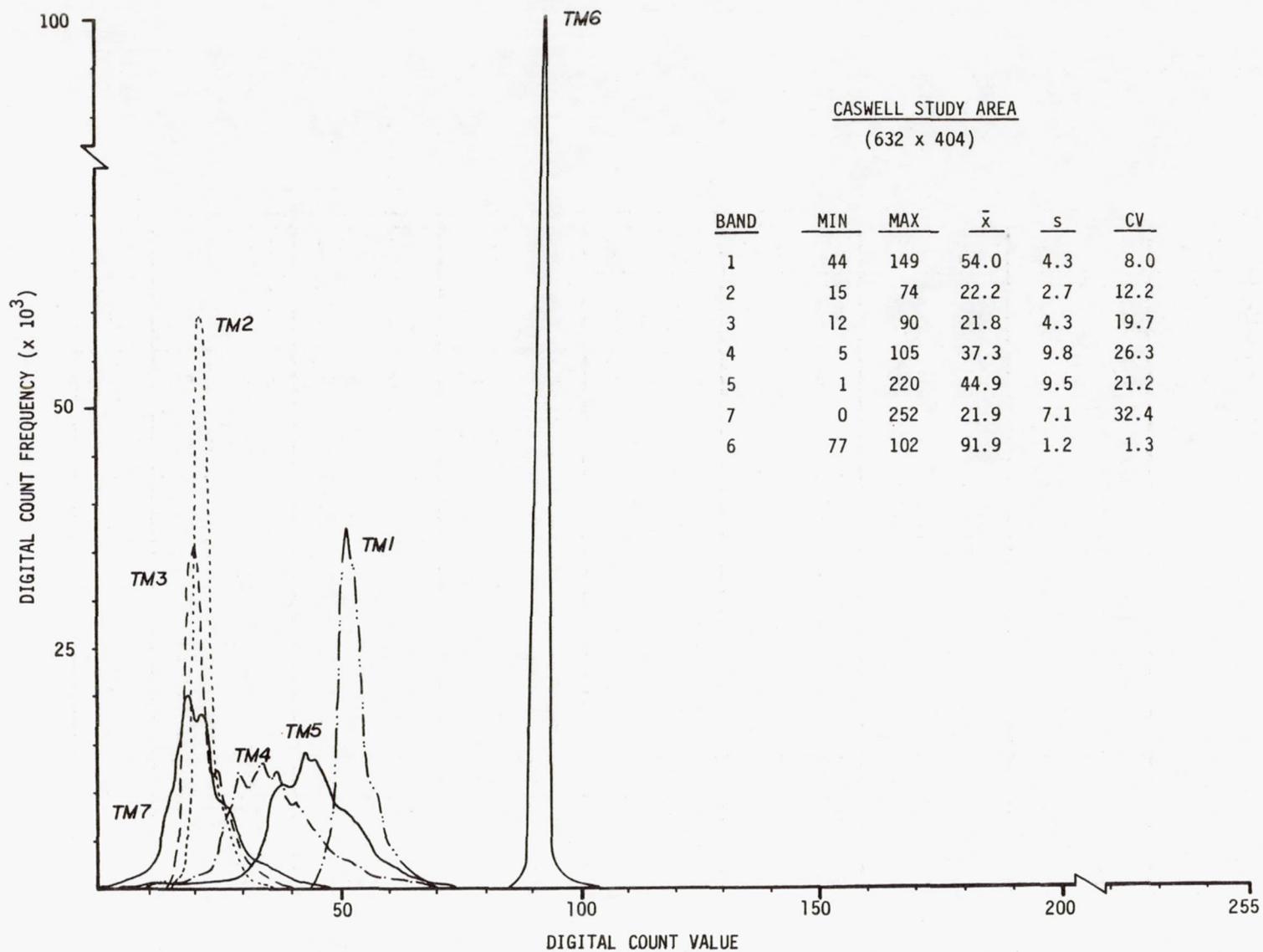
Figure 7. Spectral data plot for each of the TM spectral bands using the Caswell Study Area.

Table 5.

TM AND MSS SPECTRAL STATISTICS FOR THE CASWELL STUDY AREA

	SUGAR BEETS		ALFALFA		MIXED PASTURE		ORCHARD		VINEYARD		GRAIN STUBBLE		BARE SOIL		NATIVE VEGETATION	
	$\bar{x}$	CV	$\bar{x}$	CV	$\bar{x}$	CV	$\bar{x}$	CV	$\bar{x}$	CV	$\bar{x}$	CV	$\bar{x}$	CV	$\bar{x}$	CV
TM1	50.4	2.5	50.1	2.3	53.8	2.8	51.4	2.6	52.5	3.1	65.2	2.6	56.4	2.5	50.6	3.2
TM2	20.3	3.9	20.5	3.6	22.5	4.1	20.2	3.8	21.3	3.8	29.9	4.3	23.4	4.0	18.9	3.9
MSS 1	13.8	7.4	14.4	7.5	15.1	7.8	14.1	8.3	14.7	6.8	21.4	7.1	16.1	7.5	13.4	9.2
TM3	16.9	4.0	17.1	3.7	22.4	5.4	19.4	4.4	21.5	5.4	36.3	4.4	24.9	3.8	18.0	6.1
MSS 2	8.8	12.0	9.3	11.5	12.0	8.5	10.4	8.6	11.8	8.3	21.6	6.7	14.2	9.1	9.5	11.4
TM4	60.4	3.9	58.8	3.8	46.2	5.6	30.4	3.5	33.3	5.1	38.6	4.9	28.2	7.1	25.4	11.1
MSS 3	37.2	7.3	38.4	7.0	30.4	1.8	20.1	5.9	22.4	8.9	30.3	5.6	20.8	8.6	15.7	14.7
MSS 4	34.4	7.5	35.4	2.9	28.0	1.8	18.5	5.6	18.9	1.6	22.8	6.8	16.2	8.8	13.4	18.7
TM5	28.0	5.0	44.8	2.8	53.9	4.8	37.5	4.6	46.4	6.7	65.8	4.2	43.8	4.5	33.7	13.2
TM7	9.1	11.1	15.2	9.1	21.5	8.2	17.5	10.6	23.8	7.8	43.7	5.4	25.7	6.4	16.2	18.2
TM6	91.8	0.5	92.7	0.7	93.4	0.6	92.1	0.6	92.7	0.7	91.8	0.6	90.9	1.0	92.0	0.7
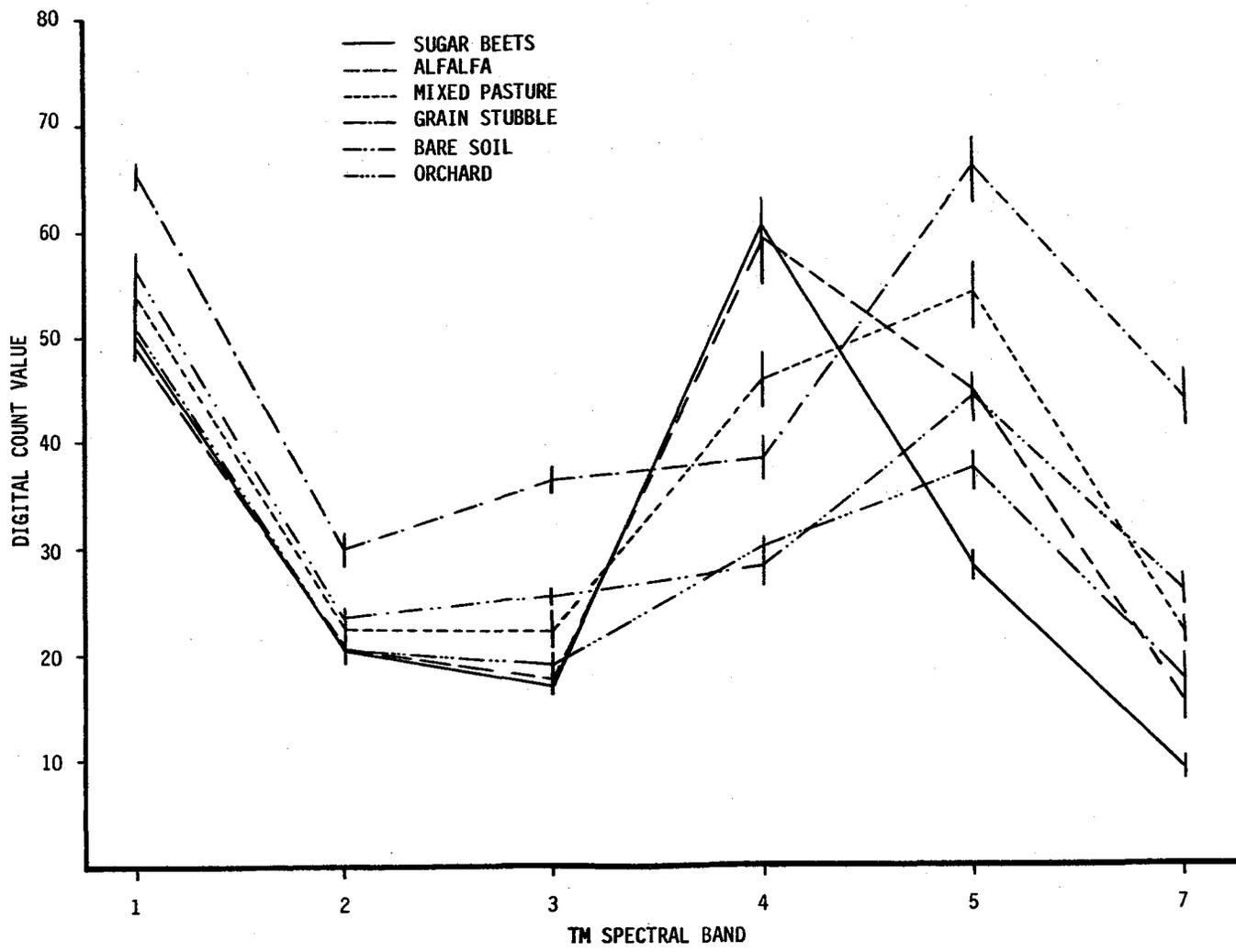
Figure 8. Plot of the spectral values for several crops for each of the reflective TM bands.
Data values represent field means (± 1 s.d.) using one or more fields per crop.
Values are tabulated in Table 5.

EVALUATION OF THEMATIC MAPPER PERFORMANCE
AS APPLIED TO HYDROCARBON EXPLORATION

Dr. John R. Everett, Dr. Charles Sheffield, Dr. Jon Dykstra
Earth Satellite Corp., 7222 47th Street, Chevy Chase, MD 20815

TM AND GEOLOGIC EXPLORATION

Since the early 1960's, the science of geology has been undergoing a major
revolution. The new paradigm of plate tectonics and seafloor spreading is
replacing the older paradigm of a rigid, stable earth. Inherent in the
acceptance of plate tectonic theory is a growing appreciation of the role of
plate motion in determining the location of mineral deposits and hydrocarbon
accumulations. It is fortunate that developments in spaceborne remote
sensing have paralleled these developments in geologic thinking. As a con-
sequence, we have remote sensing tools that view the earth with appropriate
scale and scope to enable us to appreciate and map the regional structures
that reflect the motions of continent-sized segments of the earth's crust.
We received our first glimpses of the earth from space with photos from the
Apollo and Gemini flights. The first three Landsat satellites gave us near
ubiquitous high resolution (80 metre) coverage in four spectral bands. These
data have had and continue to have enormous impact on all facets of the per-
ception and management of renewable and non-renewable natural resources and
the environment.

Before speculating on the impact of the new data types from Landsat-4, it is
useful to take a look at the role data from the first three Landsat satellites
have in geologic exploration and their current level of acceptance. In a
general sense, Landsat data has made its major contribution to hydrocarbon
exploration in the spatial domain. In mineral exploration, Landsat has
revealed some spectral information, but again the major contribution is
spatial. The synoptic view of over 34,000 square kilometres of the earth's
surface on a single Landsat image permits the detection and mapping of major
regional structures associated with the geologic development of entire geo-
logic provinces. It is also possible, through special digital enhancements,
to map some of the more subtle surface expressions of fracturing, folding and
alteration associated with buried hydrocarbon accumulations and the emplacement

of mineral deposits. The data make it possible to interrelate widely sepa-
rated geologic features and detect subtle changes that occur over tens of
miles and, hence, have gone unnoticed on conventional types of data. Perhaps
most important of all, the new perspective that the view from space provides
stimulates us, even forces us, to think of geology in new ways and perceive
new possibilities. Truly it isn't a panacea but it is an extremely powerful
tool. It has not by itself "found" an oil field or mine, but it has made
significant contributions to the exploration thinking that led to the discovery
of millions of barrels of oil and millions of tons of ore.

At this point, it is appropriate to consider how industry regards this new
tool. Bob Porter (President, Earth Satellite Corporation) once characterized
the oil and gas and mineral exploration industries' acceptance of Landsat
data or any technical innovation as progressing through three stages:

1. An initial "Gee Whiz" stage;
2. An "Interesting but not yet commercial" stage; and finally
3. Full acceptance and integration of the innovation as a bona fide
   exploration tool.

The progression through these stages appears to be a direct function of the
geologists' and geophysicists' experience and familiarity with the tool; in
this instance, satellite data. Consequently, not all exploration groups
progress through each stage in unison.

In the earlier "Gee Whiz" stage, the geologist may be impressed by the
presence of a familiar structure or landform that is visible on the imagery,
or by a subtle feature visible on an exotic digitally enhanced color image.
At this stage, some are tempted to see satellite data as the answer to all
exploration woes, and the potential to "oversell" its capabilities is a real
danger.

This stage is usually quickly replaced by the "Interesting but not yet
commercial" stage where imagery produced from the Landsat data is viewed
mainly as a cheap, low resolution, aerial photo substitute. To so view
Landsat imagery is to miss both the unique geologic perspective of the
imagery and the potential contribution available through computer processing
and data base integration of the digital data.

The final stage is characterized by the integration of the geologic information
gleaned from the Landsat imagery with a complete oil and gas or minerals
exploration model. At this point, the exploration geologist fully appreciates
the potentials and limitations provided by the satellite system and routinely
applies the satellite data to the design and execution of exploration pro-
grams. This whole process takes time. It took the gravity meter and the
seismograph about 40 years to make the transit; the digital computer has
progressed more rapidly.

At present, I think a healthy percentage of the exploration community is
working out of the second stage of acceptance. There is a great promise that
the Thematic Mapper data will provide the results necessary to convince the
exploration geologist and, more importantly, the exploration financial managers,

to move fully into the final stage. However, in order for this to occur, there must exist a continuity of data and, equally important, an availability of data at a reasonable (that is, user justifiable) price.

The two major advantages of Thematic Mapper data over that of the MSS system are its increased spatial resolution and its greater number of narrow, strategically placed, spectral bands (Table 1). The 30 metre pixel size will permit finer definition of ground features and thereby improve the reliability of photo-geologic interpretation of geologic structure. Of equal importance is the increased homogeneity of the types of surface material within a given pixel. The less mixed the pixel, the greater the potential of extracting useful spectral information. The increased spectral resolution is allowing geologists to map altered zones associated with mineralization based not only on iron oxides, but on the basis of recognizing rocks and soils rich in hydroxyl groups, such as many of the clays formed as a product of the mineralization process.

The increased spectral sensitivity also promises the ability to detect some types of vegetation changes that are associated with anomalous mineralization. This will be particularly helpful where soil and plants obscure the bedrock. This capability is not definitely proven, but it is theoretically possible and highly anticipated.

In addition to plate tectonics, there is a second revolution going on in the geologic thinking of petroleum exploration. The old paradigm of tightly sealed hydrocarbon traps which retain for long periods of time petroleum that was generated and migrated in the distant past is giving way to a newly evolving paradigm which envisions a much more dynamic scenario in which most, if not all, traps leak, and the generation and migration of hydrocarbons is a continuing process. This implies that there is very little, if any, really old oil or gas, rather, only new hydrocarbons generated from old rocks or retained in old traps. The hydrocarbon leaked from these imperfect traps moves vertically through the overlying rocks to the surface and, in the course of its movement, produces a host of chemical changes. The near surface environment manifests this leakage in a variety of geochemical, biological, geobotanical, or geomorphological anomalies and by the simple presence of hydrocarbon itself.

This new paradigm also has important significance to the mineral explorationists. The chemical environment created by leaking hydrocarbon has caused the emplacement of a vast amount of lead, zinc, uranium, and silver and has potentially played a role in localizing some deposits of gold, copper, and barite.

In the remainder of the talk, I would like to give you an appreciation of a few of the ways that the increased spectral and spatial resolution of the Thematic Mapper will affect geologic exploration. First, the increased spatial resolution. It is clear to us that, with careful computer and photographic processing, the quality of the TM digital data enables sharp photographic enlargements to a scale of 1:50,000 and, in some cases, larger. With clearly interpretable imagery at these scales, exploration geologists are able to significantly refine their structural interpretations compared to those made from 80 metre resolution MSS imagery.

°   What was detectable only as a lineament on MSS imagery might be able to be confidently mapped as a fault.

°   More importantly, some of the smaller features that indicate direction of movement along faults will be identifiable in the TM imagery, where they are lost in the lower resolution MSS imagery.

Southern Ontario (Example)

There are relatively few TM scenes available of areas with strong oil and gas interests, however, the July 25 image of Detroit does include some of the oil and gas fields of southern Ontario, Canada.

Thematic Mapper False Color Composite of Southern Ontario

On the false color image of the Ontario area, we have delineated some of the more prominent linears along with the location of the Malden, Colchester and Leamington oil and gas fields. At the Malden and Colchester fields, the hydrocarbon accumulations are in fractured, dolomitized, Ordovician limestones. The fractures trend WNW. It's a safe bet that the lineament marked on the imagery is the surface expression of a major through-going structure which is controlling the subsurface fracturing.

The Leamington field is a little younger and is located in ancient reef deposits. Reefs are known to prefer the high edge of structural blocks. The intersecting lineaments mapped on the imagery may well define two intersecting normal fault zones responsible for the uplift of a block edge and the locali- zation of the Silurian reef.

Cement, Oklahoma (Example)

The most exciting potential contribution of the TM data is the availability of seven carefully placed spectral bands. For oil and gas exploration, these spectral bands will be extremely useful for the detection of possible surface rock alteration and geobotanical anomalies associated with microseepage of hydrocarbons from buried oil and gas accumulations. As the leaking hydro- carbons find their way to the surface, they alter the chemistry of the rocks through which they pass. At the surface, several things can occur: the altered surface chemistry may change the spectral and erosional characteristics of the surface rocks and soils and/or it may create variations in the density, type or vigor of any vegetation growing in the altered soils.

As a portion of our TM investigations, we are assessing TM's ability to identify and delineate areas of surface alteration due to microseepage of hydrocarbons at the Cement oil and gas field. The Cement field is overlain on the surface by the Rush Springs Sandstone. The Rush Springs Sandstone is a characteristic red color due to an abundance of ferric iron-oxides. The reducing chemical environment associated with the hydrocarbon microseepage appears to have altered the insoluble ferric iron to soluble ferrous iron, allowing it to be leached out of the sandstone. The result is a bleaching of the sandstone overlying the oil and gas field. We have only recently received our TM coverage of the Cement area. Our spectral analyses are therefore in their earliest stages. These next few images are pictures of our interactive

image processing system and demonstrate our first cut approach at delineating the bleached area associated with the Cement field.

Cement NCC/HSV

The iron oxide rich areas are delineated on the imagery as areas of orange to red color. The quarter frame image shows the location of the red coloration following closely the outcrop of the Rush Springs Sandstone. However, the area overlying the Cement oil and gas field is one of those areas where the Rush Springs appears to have lost its strong iron oxide signature.

DEATH VALLEY, CALIFORNIA (EXAMPLE)

The first place to assess potential of TM data to map different rock types is in an area of low vegetation density and diverse rock types. Within the present range of the TM system there is clearly no more vegetation free area than Death Valley, California.

(Death Valley NCC/Death Valley FCC) - (Eigen/HSV)

The following imagery are of an approximately 1/3 TM scene area of the Death Valley, California overpass on 17 November, 1982. The scene includes a natural color, false color, eigen and HSV image.

The Hue, Saturation and Value (HSV) image is one of the more exciting images for geologic applications. Through the use of two ratios as hue and saturation, and the first eigenband as the value, the resulting HSV image possesses the spectral information of a ratio image and the spatial integrity of the first eigenband.

The hue of the image is controlled by the ratio of TM5 (1.6 microns) over TM2 (0.56 microns). The color assignments are such that high ratio values are red with decreasing values passing through the spectrum ending with the lowest values in blue. The saturation of the image is controlled by the ratio of TM5 (1.6 microns) over TM7 (2.2 microns).

TM2 was chosen for its sensitivity to ferric iron oxides; TM7 for its sensitivity to hydroxyl bands and TM5 for its high variance and broad information content. The 5/2 ratio will have high value (red hue) over areas of high ferric iron content, vegetation, as well as an assortment of other surface materials. The 5/7 ratio will have particularly high values (high saturation on the output image) over areas which contain hydroxyl bearing minerals or surface materials containing free water (e.g., clays, hydrated salts and vegetation). The first eigenband represents a positively weighted sum of the seven TM bands and thus provides excellent geomorphologic information allowing for precise geographic locations of the image's spectral information.

We suggest comparison of this image with the 1:250,000 scale Death Valley sheet of the Geologic Map series of California. Through comparison with the geologic map, some interesting examples of the unique information content of the HSV image appear along the northeastern flank of the Panamint Mountains, the eastern Funeral Mountains and the northern portions of the Resting Spring

Mountains. The lower Paleozoic marine section along the northeastern flank of the Panamints is clearly distinguished from the older (PC?) section to the west. The small outcrops of Tertiary volcanics overlying the Paleozoic section are also clearly distinguishable. Note, however, that the Paleozoic marine section to the north (Tucki Mountain area) is spectrally "confused" with the Tertiary volcanics. The Tucki section is distinctly different from the Paleozoic sediments to the south of Black Water Wash, however, it is not immediately clear why its 5/2 ratio should be so spectrally similar to that of the Tertiary volcanics. Along the eastern portions of the Funeral Mountains and the Resting Spring Range, there are several examples of stratigraphic horizons which are clearly mappable on the HSV imagery and have been grouped into the Cambrian marine unit on the 1:250,000 scale geologic map. Although such groupings are obviously necessary during geologic mapping, the ability to map the individual lithologic beds on the HSV imagery significantly augments the information available on the geologic maps.

SUMMARY

We in the exploration industry find ourselves in a very challenging situation. World consumption of energy and mineral commodities is ever increasing, while at the same time, we are at a point where most of the large easy-to-discover, cheap-to-produce petroleum accumulations and mineral deposits have been located and many of these already exploited and depleted.

However, on the bright side, our technology is continuing to develop new tools with which geologic explorationists can evolve and test new geologic concepts. These new concepts allow the geologist to view exploration challenges with a new set of glasses, leading to such discoveries as finding oil in fractured volcanic rocks in the Great Basin of Nevada and to the thought of drilling through igneous and metamorphic rocks to find underlying oil in the Appalachian Mountains.

The improvements of Thematic Mapper data over multispectral scanner data brings us to the point that we are able to exploit satellite imagery at about the same scale that we have used aircraft data in the past. Certainly, improved spatial and spectral resolution and wider spectral coverage would be welcomed and stereoscopic imagery will be a great boon. However, it appears to us that the present TM system offers a near optimum balance between resolution requirements and data handling capabilities.

In summary, we feel confident that specially enhanced Thematic Mapper imagery will make a very significant contribution to the oil and gas and mineral exploration industries. The TM's increased spatial resolution will enable the production of larger scale imagery, which will greatly increase the amount of geomorphic and structural information interpretable. TM's greater spectral resolution, combined with the smaller, more homogeneous pixels, should enable a far greater confidence in mapping lithologies and detecting geobotanical anomalies from space. The results from its applications to hydrocarbon and mineral exploration promise to bring the majority of the geologic exploration community into that final stage of acceptance and routine application of the satellite data.

Table 1

COMPARISON OF LANDSAT -1, -2, -3 AND -4 MULTISPECTRAL
SCANNER CHARACTERISTICS WITH THOSE OF LANDSAT-4 THEMATIC MAPPER

	MSS	TM
Resolution:	~ 80m	~ 30m

Wavelength Bands:

MSS	TM
4 = 500 - 600nm	1 = 450 - 520nm
5 = 600 - 700nm	2 = 520 - 600nm
6 = 700 - 800nm	3 = 630 - 690nm
7 = 800 - 1100nm	4 = 760 - 900nm
	5 = 1550 - 1750nm
	6 = 10400 - 12500nm
	7 = 2080 - 2080nm

Page intentionally left blank

GEOLOGIC UTILITY OF LANDSAT-4 TM DATA

Michael Abrams, Anne Kahle, Alan Gillespie,
James Conel, Harold Lang
Jet Propulsion Laboratory
Pasadena, CA 91109

INTRODUCTION

The present LIDQA study is being conducted in several phases to quantify the performance of the TM vis-a-vis various geological applications. These phases include: (1) analyses of the geological utility of the data with respect to the increased spatial resolution and number of bands (compared to the MSS); (2) analysis of geometric accuracy; (3) analysis of radiometric performance of the TM scanner.

Preliminary analyses have been performed on two TM scenes: E-40124-17495 over Death Valley, California, and E-40128-17263 over southern Arizona. Both scenes were acquired in CCT-PT format, where the data were geometrically and radiometrically corrected. Overall, the TM data appeared to contain a marked increase in geologically useful information; however, a number of instrumental or processing artifacts may well limit the ability of the geologist to fully extract this information.

DEATH VALLEY SCENE

In order to examine the utility of the TM data at full usable spatial resolution, several small areas were extracted from the TM scene for further image processing. A 27 by 18 km area was examined covering the east side of the Panamint Mountains, alluvial fans descending to the valley floor, part of the Death Valley salt pan, and Trail Canyon. Data were processed using band ratioing, color-enhanced band composites, and principal components transformations. Lithologic interpretation maps were prepared and compared to published geologic maps of the area. More detail and delineation of alluvial fan units were evident on the TM scene. Relative ages of the fans could be inferred based on geomorphic appearance. The oldest fans had dendritic drainage patterns developed on their surfaces, while younger fans were characterized by the

presence of parallel to braided drainage patterns. The 28.5 m pixel size was more than sufficient to resolve these drainage features. Spectral contrast between fans was related to differences in source rock composition and variable development of weathering and varnish surfaces. In combination with the spatial details, all mapped fan units were separable, and additional separations based on spectral differences could be made. Of the three different enhancement procedures used, ratioing produced the least useful images due to exaggeration of noise and artifacts (discussed later).

A second area, 15 by 15 km over the Tucki Mountains at the northwest end of Death Valley, was extracted from the TM scene to examine the utility of the data for separating sedimentary rock types. The Tucki Mountains have exposed quartzites, shales, dolomites, limestones, and sandstones. The beds dip 50°-90°, and topographic relief is rather severe. However, exposures are excellent as vegetation cover is minimal to absent. Again the principal components composites and enhanced-band composites were the most satisfactory for display of the data. Many of the mapped rock types were separable based on spectral differences. Problems occurred along north-facing slopes due to deep shadows resulting from the low sun angle (27°) during the November data acquisition; no lithologic information was discernible in these shadowed areas.

The same two areas were extracted from Landsat-2 MSS data for comparison to the TM data. The improvement in spatial resolution of the TM was patently apparent. No details of the drainage patterns on the fans were discernible on the MSS data, making interpretation of geomorphic information impossible. In addition, the limited spectral band coverage reduced the amount of lithologic separations displayed on the images.

A larger area (60 by 40 km) was processed to examine the effects of using different spectral channels in false color composites. The data were processed using decorrelation stretching (Soha and Schwartz, 1978) and combined in various triplets to produce a color composite (described in a later section). The most useful combination examined was created using bands 4, 5, and 7--the three infrared bands. This is not surprising, as the major spectral contrast between different rock types occurs in the infrared part of the spectrum. This points out one of the main advantages of the TM over MSS data--the presence of channels beyond 1.0 μm.

We have digitally registered the TM data to a topographic map base, then registered Seasat radar data and six channels of thermal multispectral aircraft data (8.2-12.2 μm range) to this data base. The objective is to assess the improvement in material separation possible using this multivariable data set. Each data set measures a different surface physical property--the TM is sensitive to reflectance characteristics which are mainly controlled by the presence of iron, water, hydroxyl ion, and carbonate ion, and overall brightness or albedo; the thermal data are sensitive to the presence of free silica, hydroxyl ion, density, albedo, conductivity, and diffusivity; the Seasat data are sensitive to surface roughness, orientation, and moisture content.

A principal components transformation was applied using 13 input variables: six TM bands excluding thermal, six thermal multispectral scanner bands, and one Seasat channel. Composites were created using various triplets of the eigenpictures, and two were selected for separation of fan units and rock units.

Both composites had more information displayed using the combined data set than was apparent in images created from any of the data sets alone. Further processing and analysis of these data will continue to assess the contribution of the data types for separating various types of materials.

SILVER BELL AREA

A 30 by 45 km area was extracted from the southern Arizona TM scene over the Silver Bell porphyry copper deposit. This area was intensively studied in the past during the Joint NASA/Geosat test case project (Abrams et al., 1983). A number of extrusive and intrusive rocks are exposed, in addition to limestone and alluvium. A major hydrothermal alteration event produced a varied assemblage of minerals related to hydrothermal activities and deposited copper and molybdenum. These minerals have spectral characteristics which occur in the 0.4 to 2.5 μm wavelength region, and were detectable using Thematic Mapper Aircraft Simulator data.

A number of processing techniques were applied to the TM data; the most satisfactory (least objectionable noise) was decorrelation stretching. Color composites produced using visible and infrared channels reproduced the alteration separation derived from the aircraft data. This confirmed the earlier predictions that the TM data, at a resolution of 30 m, would be useful for detecting mineralogical features associated with this type of ore deposit.

PROCESSING TECHNIQUES AND NOISE

Band ratioing, a technique which has produced satisfactory results with the MSS data, suffers from a severe noise problem using the TM data. Specifically, the ratioing process exaggerates the presence of striping in the TM data. This striping is apparent in the individual TM channels; it has a 17 line periodicity, and in some bands consists of a pair of bad data lines, with the appearance of salt-and-pepper noise. The bad lines occur at the joins between the forward and reverse scan directions. The cause of the 17 line periodicity may be a result of the geometric resampling performed on the data to produce 28.5 m pixels from 30 m data. Notice that the ratio 28.5/30 = .950, and 16/17 = .941. This suggests that the interpolation algorithm used to produce the added lines of data is functioning improperly. Also, the bad lines occur where differences in the radiometry between the forward and reverse scans would be most apparent--at the join between them. This type of noise--coherent, along-line striping--can be readily removed using the following procedure:

1) The average of each line is computed and retained as a one-column image = A;

2) This image is low-pass filtered with an equal weight filter = B;

3) The one-column difference picture (A-B) is calculated, and then expanded to the full picture dimensions. That is, a picture with the same number of columns as the original is created, with each of its columns being identical with (A-B);

4) The above picture is subtracted from the original to produce the end result, an image without striping.

Principal components analysis applied to the 6 visible and near-infrared channels produced eigenpictures with the striping distributed in the last three components (the fourth, fifth, and sixth). A composite using the first three components was devoid of striping; however, the last three contained meaningful information. Composites made with any of these added striping into the color composite.

The most generally useful display technique, which enhanced the information content without exaggerating the striping, is a procedure called decorrelation stretch. The six TM channels were input to a principal components transformation; the data were stretched to equalize the variance between components; the inverse rotation was performed, which rotated the data back to the original coordiante space. The effect of this procedure is to greatly exaggerate saturation and intensity variations, while preserving the hue content. Any triplet combination of enhanced channels can then be used to produce a false color composite.

REFERENCES

Abrams, M., Conel, J., and Lang, H., 1983, "The Joint NASA/Geosat Test Case Project," Jet Propulsion Laboratory Technical Report, Pasadena, CA, in press.

Soha, J. and Schwartz, A., 1978, "Multispectral Histogram Normalization Contrast Enhancement," Proceedings of 5th Canadian Symposium on Remote Sensing, Victoria, August 1978, pp. 86-94.

AN INITIAL ANALYSIS OF LANDSAT-4 THEMATIC MAPPER DATA FOR THE DISCRIMINATION OF AGRICULTURAL, FORESTED WETLANDS, AND URBAN LAND COVER

Dale A. Quattrochi
NASA
National Space Technology Laboratories
Earth Resources Laboratory
NSTL Station, Mississippi 39529

INTRODUCTION

This paper describes the results of initial work at the NASA, National Space Technology Laboratories, Earth Resources Laboratory (ERL) on evaluating Landsat-4 Thematic Mapper (TM) data for the delineation and classification of agricultural, forested wetland, and urban land covers. The paper's contents have been digested from an ERL report which[1] details the methodologies employed to achieve the results outlined below. All TM data have been extracted from scene ID #40037-16031 which was collected on August 22, 1982 and encompasses portions of Tennessee, Kentucky, Arkansas, and Missouri. There are three sections to the discussion presented here - one for each of the specific land cover investigations. In the first section a comparison is made between a classification derived from Landsat Multispectral Scanner (MSS) data for agricultural land covers in Poinsett County, Arkansas, with a TM classification of the same area. The next section of the paper describes the application of TM data for delineating forested wetland species within Reelfoot Lake located in northwestern Tennessee. Lastly, the ability of the TM to discriminate urban features is addressed using Union City, Tennessee as a study area.

COMPARATIVE EVALUATION OF MSS AND TM DATA FOR CLASSIFICATION OF THE AGRICULTURAL STUDY AREA

This investigation had as its purpose: (1) to examine the potential of Landsat-4 TM data for providing information on agricultural land covers; and (2) to compare the general capabilities of Landsat TM and MSS data for crop mensuration and mapping. The Powers Slough and Otwell 7-1/2' topographic quadrangles located in Poinsett County, Arkansas in the northeastern part of the state have been used as a study area for analysis (Figure 1). The primary crops produced in Poinsett County include cotton, rice, soybeans, wheat, and to a lesser degree, grain sorghum and hay.

MSS Data Processing Procedure and Classification Evaluation:

Multidate MSS data of the study area were obtained for three periods during the growing season: (1) for pre-planting conditions and winter wheat mapping (February 26, 1981); (2) for midseason vigor (July 20, 1981); and

MAP OF POINSETT COUNTY, ARKANSAS STUDY AREA
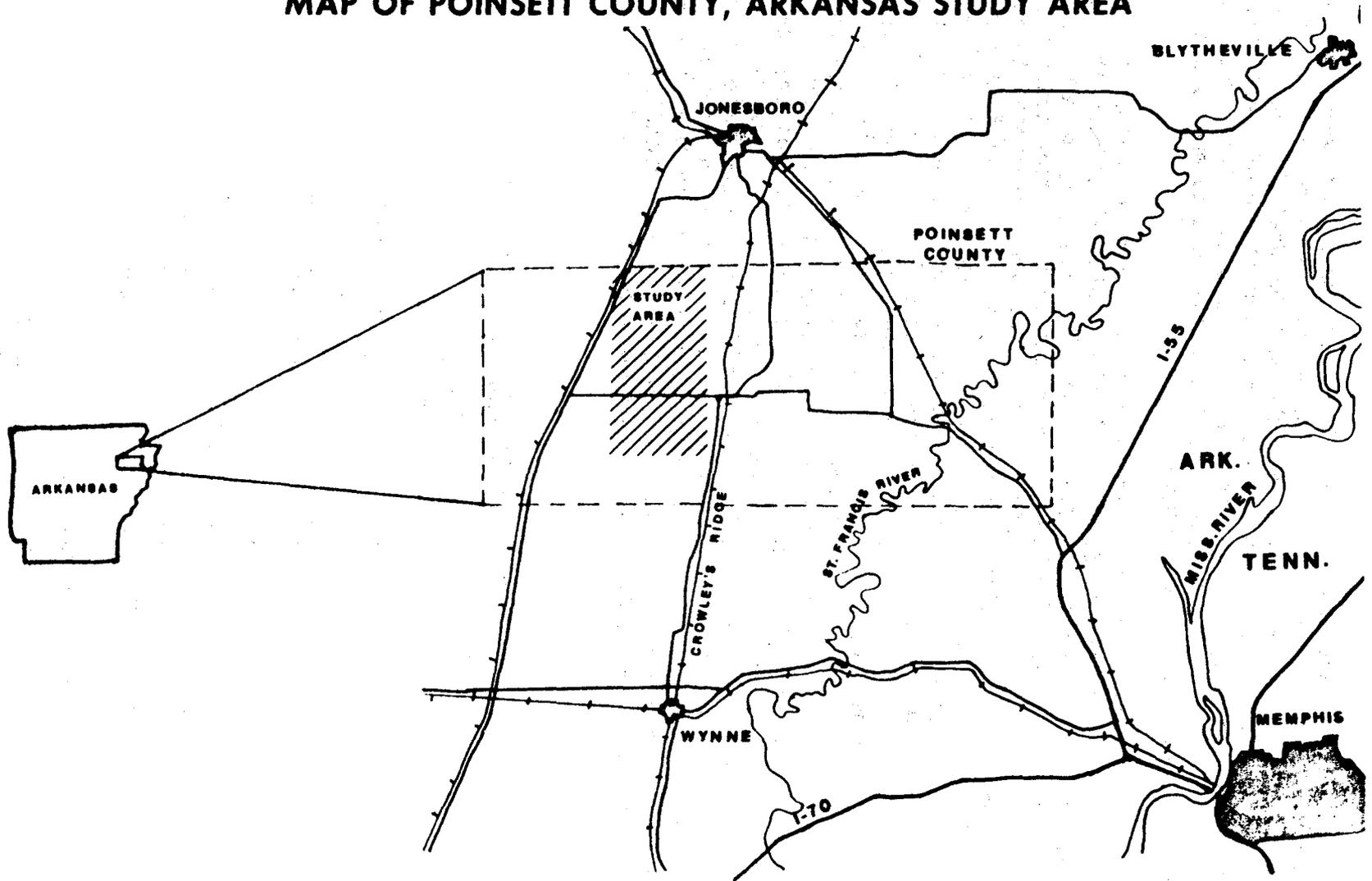
FIGURE 1

for senescence (September 30, 1981). These data were used to give the broadest possible range of spectral values for the target land cover types. In preparation for data processing, the multitemporal data were registered to a base data set; the February scene was used as the base with the other data sets overlayed or registered with these data. After registration, channels 2 and 4 were extracted from the overlayed data and used to create a six-channel data set for analysis.

Data processing was accomplished using an unsupervised signature development algorithm which passes a 3 x 3 pixel "window" through the data to derive spectral statistics. For the 75,053 acres (30,386 ha) within the study area, 30 spectral signatures were obtained. These spectral statistics were then classified using gaussian maximum likelihood techniques; subsequently, six specific land cover types were identified from this classification process (Figure 2). Each class was then evaluated in relation to ground verification information to determine classification accuracy. These accuracies have been listed in Table 1. The highest percentages of classification accuracies were recorded for the hardwood, rice, and soybean categories with percentages of 100, 98.74, and 89.69, respectively. Low accuracies were recorded for double-cropped areas of winter wheat and soybeans (18.63%) and water (22.81%). Seventy-three percent of the double-cropped areas of winter wheat and soybeans were classified as soybeans. The relatively smaller fields of winter wheat in the study area did not contribute a significantly large number of pixels for signature development, which resulted in reduced accuracies. Also, impoundments within the study area are normally smaller than 10 acres and are usually bordered by hardwoods. This makes discrimination of water bodies difficult and contributes to the low accuracies listed in the table.

TABLE 1: ACCURACY OF CLASSIFICATION FOR MSS DATA - POINSETT COUNTY, ARKANSAS STUDY AREA

LAND COVER CATEGORIES

MAPPING ACCURACY

		HARDWOOD	RICE	SOYBEANS	WINTER WHEAT/ SOYBEANS	WATER	NO. OF PIXELS
		1	2	3	4	5	
GROUND VERIFICATION CLASSES	1	307 100.00	0 0.00	0 0.00	0 0.00	0 0.00	307
	2	0 0.00	2191 98.74	28 1.26	0 0.00	0 0.00	2219
	3	0 0.00	149 10.31	1296 89.69	0 0.00	0 0.00	1445
	4	0 0.00	41 8.78	339 72.59	87 18.63	0 0.00	467
	5	44 77.19	0 0.00	0 0.00	0 0.00	13 22.81	57

PERCENT CORRECT OVERALL 80.91

CLASS	%CORRECT
1 Hardwood	100.00
2 Rice	98.74
3 Soybeans	89.69
4 Winter Wheat/Soybeans	18.63
5 Water	22.81

POWERS SLOUGH/OTWELL QUADRANGLES

AN AUTOMATED CLASSIFICATION OF LANDSAT II MSS DIGITAL DATA DERIVED FROM SRCH GENERATED STATISTICS

LANDCOVER CATEGORY		ACREAGE
HARDWOOD		5,001
FALLOW		117
RICE		28,740
SOYBEANS		31,510
WINTER WHEAT/SOYBEANS		575
WATER		717

CLASSIFICATION DERIVED FROM MSS DATA SETS
ACQUIRED 2/26/81 7/20/81 9/30/81

NASA
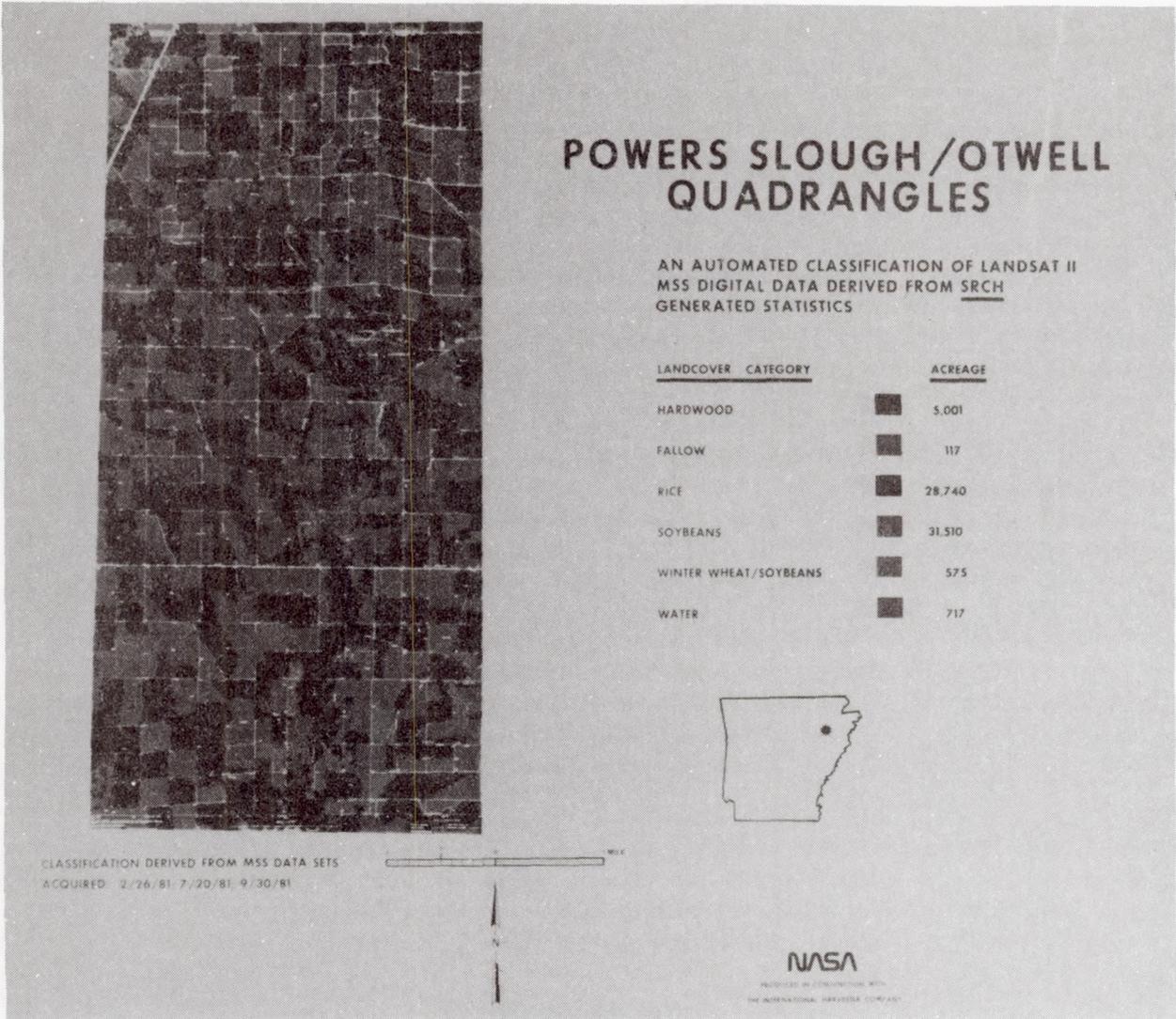
FIGURE 2

Although a fallow category has been defined in Figure 2, no ground verification sites were selected for this class. Field conditions within the study area precluded delineation of verification sites; thus, the class could be identified, but no accuracy statistics have been produced for inclusion in Table 1.

TM Data Processing and Classification Evaluation:

TM data from the August 22, 1982 data used in the investigation were subjected to the same automated signature development procedure used to derive spectral statistics from the MSS data. This process resulted in 43 spectral signatures utilizing TM channels 2, 4, and 5 as input data. All ground verification sites established for the MSS evaluation were revisited in August 1982 and were used to: (1) establish the relationship of spectral signatures with specific land covers; and (2) develop estimates of accuracy. Because of crop rotation practices, land uses in the study area had changed in the intervening one year time period between MSS and TM data acquisition. The distribution of land cover types for TM analysis, therefore, was not identical to that found in the MSS evaluation. Consequently, the 43 spectral signatures developed from the data were classified into the five land cover categories shown in Figure 3. These classes were subsequently assessed for accuracy in relation to ground verification information, with the results listed in Table 2.

TABLE 2: ACCURACY OF CLASSIFICATION FOR TM DATA – POINSETT COUNTY, ARKANSAS
STUDY AREA

LAND COVER CATEGORIES

MAPPING ACCURACY

		HARDWOOD 1	FALLOW 2	RICE 3	SOYBEANS 4	WATER 5	UNCLASSI-FIED	NO. PIXELS
GROUND VERIFICATION CLASSES	1	194	0	0	0	0	0	194
		100.00	0.00	0.00	0.00	0.00	0.00	
	2	0	149	0	1	0	11	161
		0.00	92.55	0.00	0.62	0.00	6.83	
	3	9	0	4783	18	0	1	4811
		0.19	0.00	99.42	0.37	0.00	.02	
	4	45	0	212	4672	0	1	4930
		0.91	0.00	4.30	4.77	0.00	.02	
	5	0	0	0	0	83	0	83
		0.00	0.00	0.00	0.00	100.00	0.00	

Percent Correct Overall   97.06

CLASS	%CORRECT
1. Hardwood	100.00
2. Fallow	92.55
3. Rice	99.42
4. Soybeans	94.77
5. Water	100.00
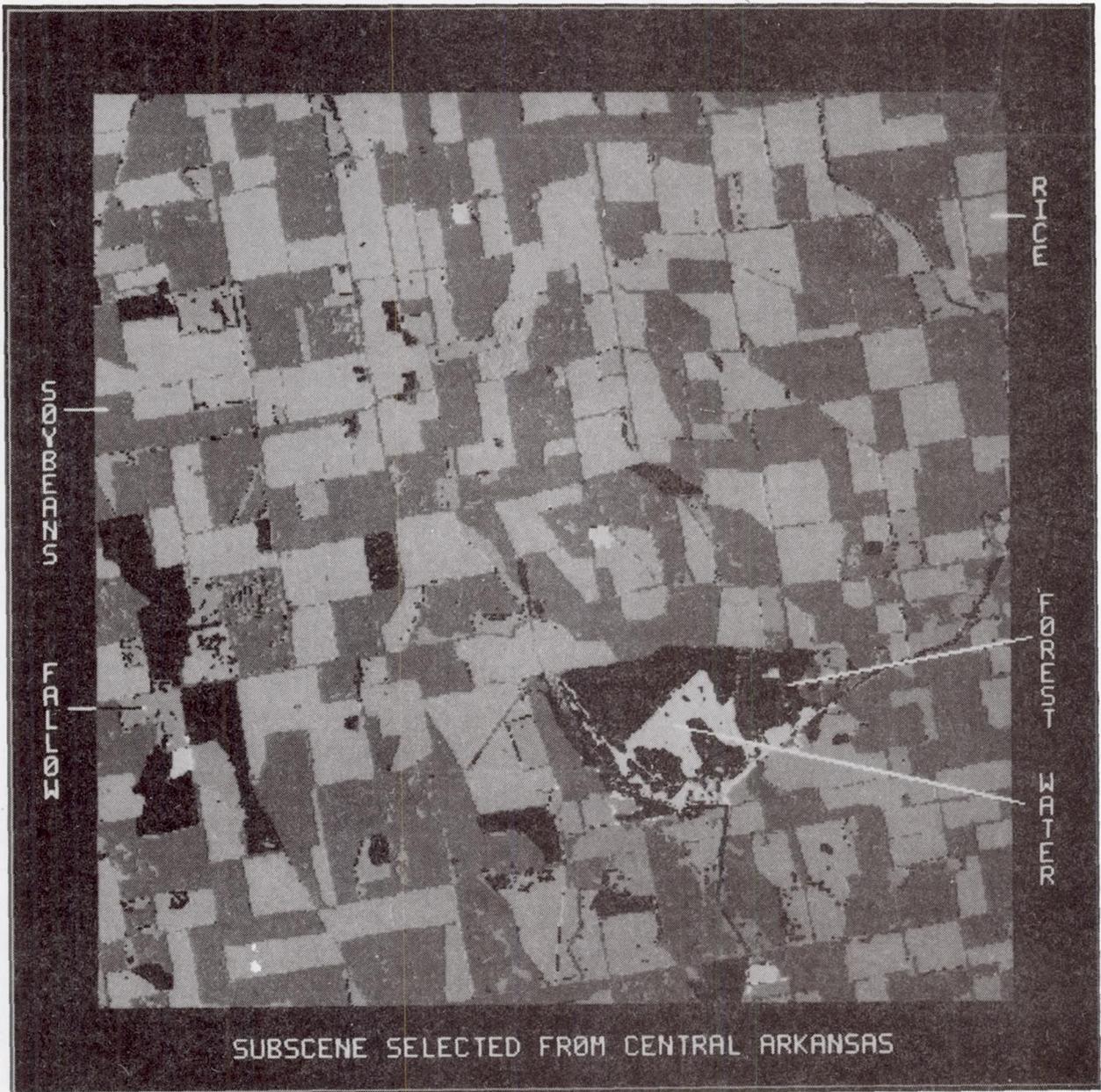
FIGURE 3

Comparison of MSS and TM Classification Results:

The accuracies listed in Tables 1 and 2 have been used to compare the performance of the MSS versus the TM within the Poinsett County study area. Results from a Newman-Keuls test of comparative accuracies based on the arcsine $\sqrt{p}$ tranformation at the .05 significance level, illustrate the following: (1) the TM did significantly better than the MSS in an accuracy assessment of the water class; (2) the MSS and TM performed equally well (i.e., no statistical signficant difference in accuracies) in the soybeans, rice, and hardwood categories; (3) and most importantly, the TM performed significantly better in an overall comparison of accuracies. (Unlike in the MSS evaluation, however, an accuracy assessment for a fallow/bare soil category was derived for the TM data because land uses within the study area allowed delineation of ground verification sites).

EVALUATION OF TM DATA FOR CLASSIFICATION OF FORESTED WETLANDS IN THE REELFOOT LAKE AREA OF NORTHWESTERN TENNESSEE

The goal of this investigation was to analyze Landsat-4 TM data collected on August 22, 1982 for the discrimination and inventory of forested wetlands in the vicinity of Reelfoot Lake, Tennessee. Because of its unique aquatic ecology the Reelfoot Lake area offers an unusual opportunity to test the capabilities of the TM for delineating specific biomes within the freshwater wetland regime. The lake is situated within the Mississippi River floodplain of western Tennessee and contains approximately 8,117 acres (3,245 ha) of wetlands (Figure 4). These wetlands are comprised mainly of cypress mixed with other hardwoods, exposed mudflats vegetated with aquatic grasses and shrubs, and shallow water with emergent and floating aquatic plants.

TM Data Processing and Classification Evaluation:

To focus attention on areas where wetland heterogeneity was most prominent, a polygon was delineated around the lake and only data which fell within this polygon were actually processed for the study. Preliminary evaluation of the data for the Reelfoot Lake area, based on the analysis of spectral scattergrams for selected ground truth plots, indicated that TM channels 1 (.45-.52 μm) and 6 (10.40-12.50 μm) did not contribute a significant amount of information which could be used to spectrally separate wetland classes. Consequently, these channels were eliminated from consideration and data analysis was restricted to channels 2, 3, 4, 5, and 7.

Spectral signatures were derived for the study area utilizing the unsupervised 3 x 3 pixel sliding window approach, and also on a pixel-by-pixel basis; this latter process was employed to separate those signatures that were spectrally distinct, but could not be spectrally separated using the 3 x 3 pixel sliding window. Sixty spectral statistics were produced by these algorithms and they were then classified using gaussian maximum likelihood techniques. The 60 classes were ultimately grouped into five primary cover types: cypress; mixed hardwoods; willow and cypress; brush, grasses, and emergents; and floating aquatic vegetation. For display purposes, the five
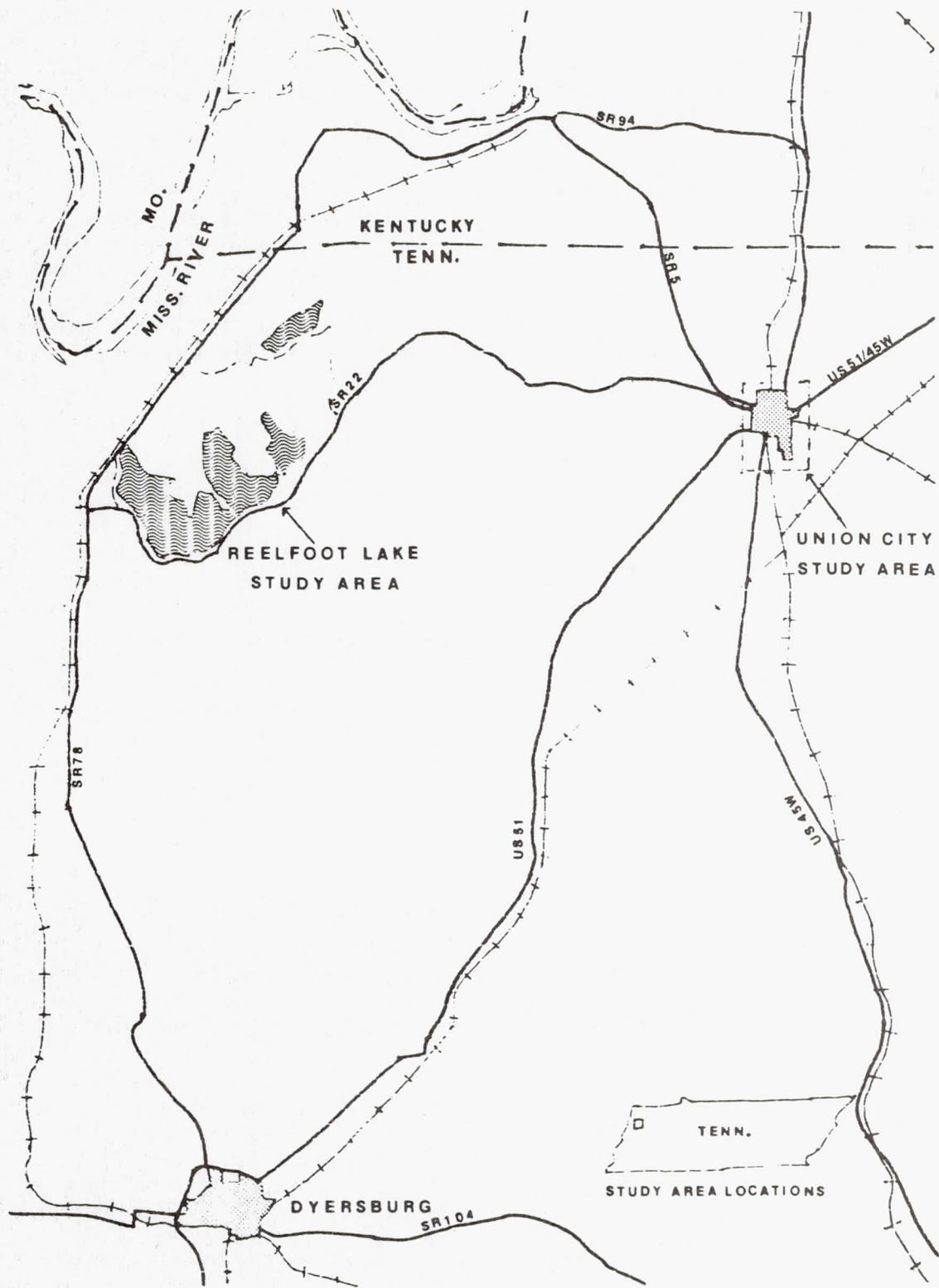
FIGURE 4

primary cover types were further refined into the nine specific classes illustrated in Figure 5. This nine-category classification was not used to assess the accuracy of the TM data because ground truth sites could not adequately be defined within some of the classes; i.e., the nine classes in Figure 5 were interpreted from the data, but sites with areal extents large enough for ground truthing could not be defined.

Independent of the class naming procedure, ground verification samples were established for use in determining associated accuracy estimates for each of the five primary cover types. These verification samples were identified using ground observation information, U.S. Fish and Wildlife Service timber stand maps of the Reelfoot Lake area, and recently acquired aerial photographs. Table 3 summarizes the results generated from accuracy assessments of the data, predicated on an evaluation of the TM-derived classification against known cover types within the ground verification samples.

TABLE 3: SUMMARY OF "PERCENT CORRECT" ACCURACY VALUES ASSOCIATED WITH THE FIVE LAND COVER TYPES OF INTEREST — REELFOOT LAKE STUDY AREA

| | | LANDSAT-4 TM CLASSIFICATION LAND COVER CLASS | | | | | |
		CYPRESS	MIXED HARDWOOD	WILLOW CYPRESS	BRUSH, GRASS, EMERGENTS	FLOATING AQUATICS	UNCLASSI-FIED
GROUND VERIFICATION CLASS	CYPRESS	98.75	0.83	0.0	0.0	0.42	0.00
	MIXED HARDWOOD	5.75	94.25	0.00	0.0	0.0	0.00
	WILLOW CYPRESS	7.07	0.0	91.92	0.0	0.0	1.01
	BRUSH, GRASS, EMERGENTS	2.38	1.79	0.0	93.45	2.38	0.00
	FLOATING AQUATICS	0.0	0.0	0.0	0.0	97.20	2.80
	OVERALL PERCENT CORRECT						95.36

COMPUTER IMPLEMENTED LAND
COVER CLASSIFICATION OF
THE REELFOOT LAKE AREA
IN WESTERN TENNESSEE
DERIVED FROM LANDSAT-4
THEMATIC MAPPER DATA

CYPRESS
CYPRESS/HARDWOOD
MIXED HARDWOOD
CYPRESS/WILLOW
BRUSH/GRASSES
GRASSES/EMERGENTS
FLOATING AQUATICS
CYPRESS/AQUATICS
AQUATICS/CYPRESS

FIGURE 5

It appears from the high percentages of correct classification listed in Table 3, that the signatures developed using TM channels 2, 3, 4, 5, and 7 precisely defined the five wetland land covers. Also, where confusion (i.e., misclassification) existed, it could logically be explained. For example, the willow/cypress class have been confused only with land covers classified as cypress; this sort of misclassification is plausible because of the extreme heterogeneity of land covers within the study area.

EVALUATION OF TM DATA FOR CLASSIFICATION OF A SMALL URBAN AREA IN NORTHWESTERN TENNESSEE

The last segment of this paper deals with the evaluation of Landsat-4 TM data for analysis of a small urban area in northwestern Tennessee. With its improved spatial and spectral resolution over what has previously been afforded by the Landsat MSS, it is anticipated that the TM will provide new and better information for discriminating urban features. Several researchers have used Thematic Mapper Simulator (TMS) data to assess the capabilities of these data for delineating and mapping urban areas. Toll[2] compared TMS data acquired from the NS-001 airborne scanner collected over the Denver, Colorado metropolitan area with Landsat MSS data. His research indicated that the TMS data provided additional urban land cover mapping capabilities particularly at the urban/rural fringe in comparison to the type of information that could be derived from MSS data over the same study area. Rangaswamy and Lien[3] utilized NS-001 data for a suburban area near Washington, D.C. to simulate and assess the TM's spatial, spectral, and radiometric characteristics. Their results showed that data from the TM would give acceptable classification accuracies for hydrologic applications where land covers were an important component in the overall landscape. Clark[4] employed data from selected channels of a 24-channel airborne MSS acquired over a portion of Los Angeles, California to simulate three channels (green, red, and infrared wavelengths) of the Landsat 4 TM. One of Clark's main goals was to vary the spatial resolution of the 24-channel scanner data and assess the resulting classifications obtained for the Los Angeles test site. From his results, he concluded that a spatial resolution of approximately 30 meters would be best for multispectral classification of urban scenes.

Given the potential value of TM data for urban analysis as demonstrated by work with simulated data, an initial evaluation of Landsat-4 TM data has been conducted for a small city in western Tennessee. Union City, located in the extreme northwestern portion of the state, was chosen as a study area (Figure 6). The city has a population of approximtely 14,650 according to the preliminary estimates from the 1980 census. It is the major commercial center of northwestern Tennessee and has about eight square miles (20.7km^2) within its city limits. The land surrounding the town is predominantly agricultural, with soybeans, corn, wheat, and small grains the principal crops. Although the city is in a rural area, it does support a number of diverse light industries.
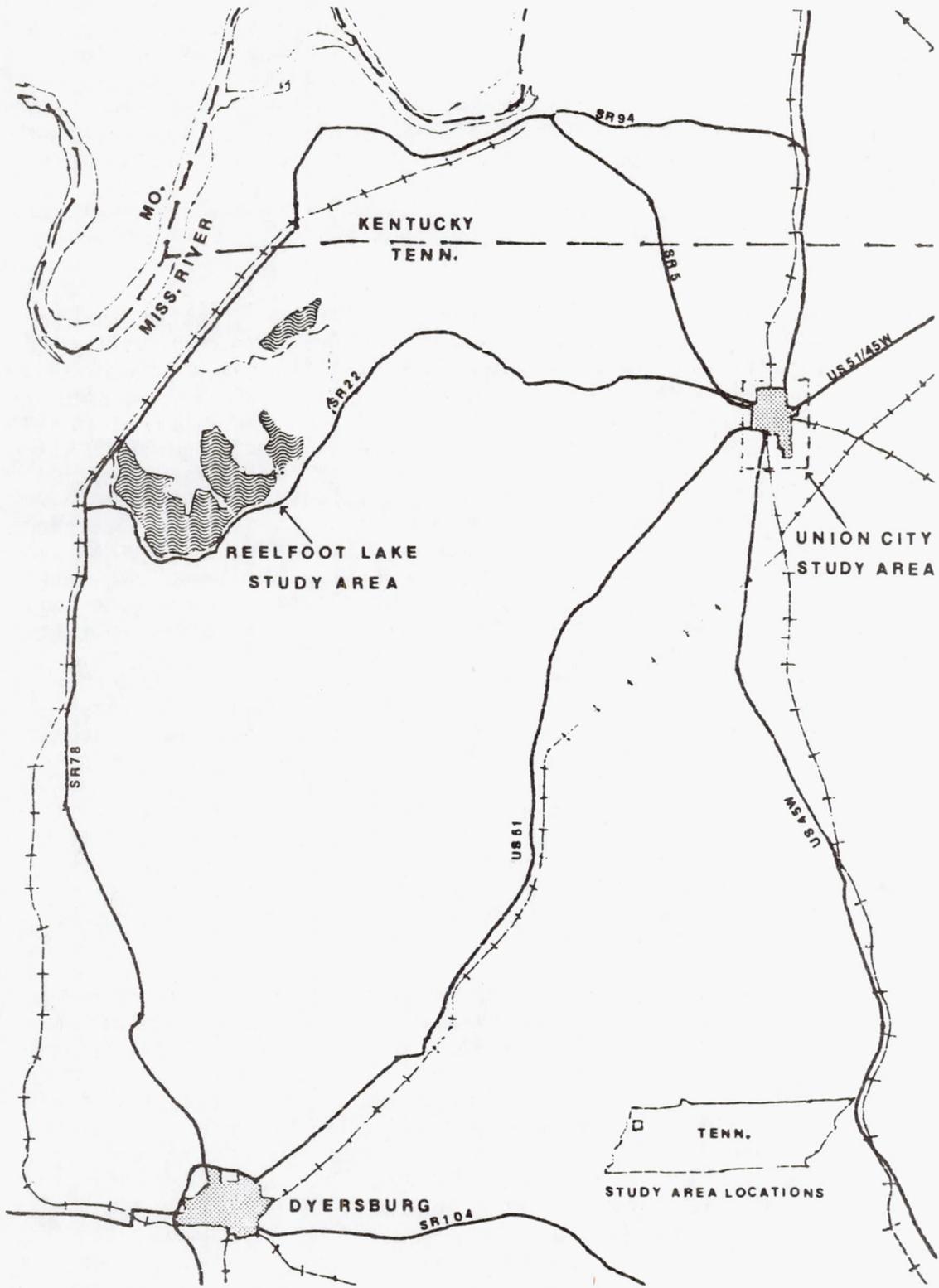
FIGURE 6

A pixel-by-pixel automated signature development algorithm was used to derive spectral signatures within a polygon defined from the August 22, 1982 TM data used in the study. This polygon was selected to encompass the majority of the Union City urban area. An analysis of the seven-channel TM data, predicated on the evaluation of spectral scattergrams for selected ground truth plots, indicated that channel 1 (.45 μm to .52 μm) did not contribute a significant amount of information which could be used to separate urban signatures. Thirty-nine spectral signatures were derived from the unsupervised signature development procedure utilizing the six channels of data as input.

These spectral responses were then classified via the gaussian maximum likelihood technique. Ultimately, the classes were grouped utilizing ground truth and ancillary data into six specific land cover categories: (1) roads and inert materials; (2) commerical and industrial development; (3) residential development; (4) agriculture and bare soil; (5) transitional or grassland areas; and (6) forested areas. Figure 7 represents the classification of Union City as delineated by the polygon that was used to define the urban area for signature development purposes.

Accuracies were computed for the classification based on the evaluation of 45 ground verification polygons with known land covers selected from the data. Because of the difficulty in defining precise ground truth polygons for the transitional/grassland and roads/inert materials classes, polygons for these categories were combined with the agriculture/bare soil, commercial/industrial, or residential categories. Table 4 gives the accuracies for the resulting four major land cover types used to estimate classification accuracy.

TABLE 4: COMPUTED CLASSIFICATION ACCURACIES - UNION CITY STUDY AREA

CLASS CATEGORY

(% Correct by Class and No. of Pixels Classified by Class)

		Agriculture	Commercial	Residential	Forest	Total No. of Ground Truth Pixels Used
GROUND VERIFICATION CLASS	Agriculture	89.97 1570	8.37 146	1.66 29	0.00 0	1745
	Commercial	.90 5	95.68 532	2.88 16	.54 3	556
	Residential	13.73 198	.49 7	83.50 1204	2.29 33	1442
	Forest	1.19 8	0.00 0	.15 1	98.66 662	671

Percent Overall Correct = 89.90%   TOTAL =   4414
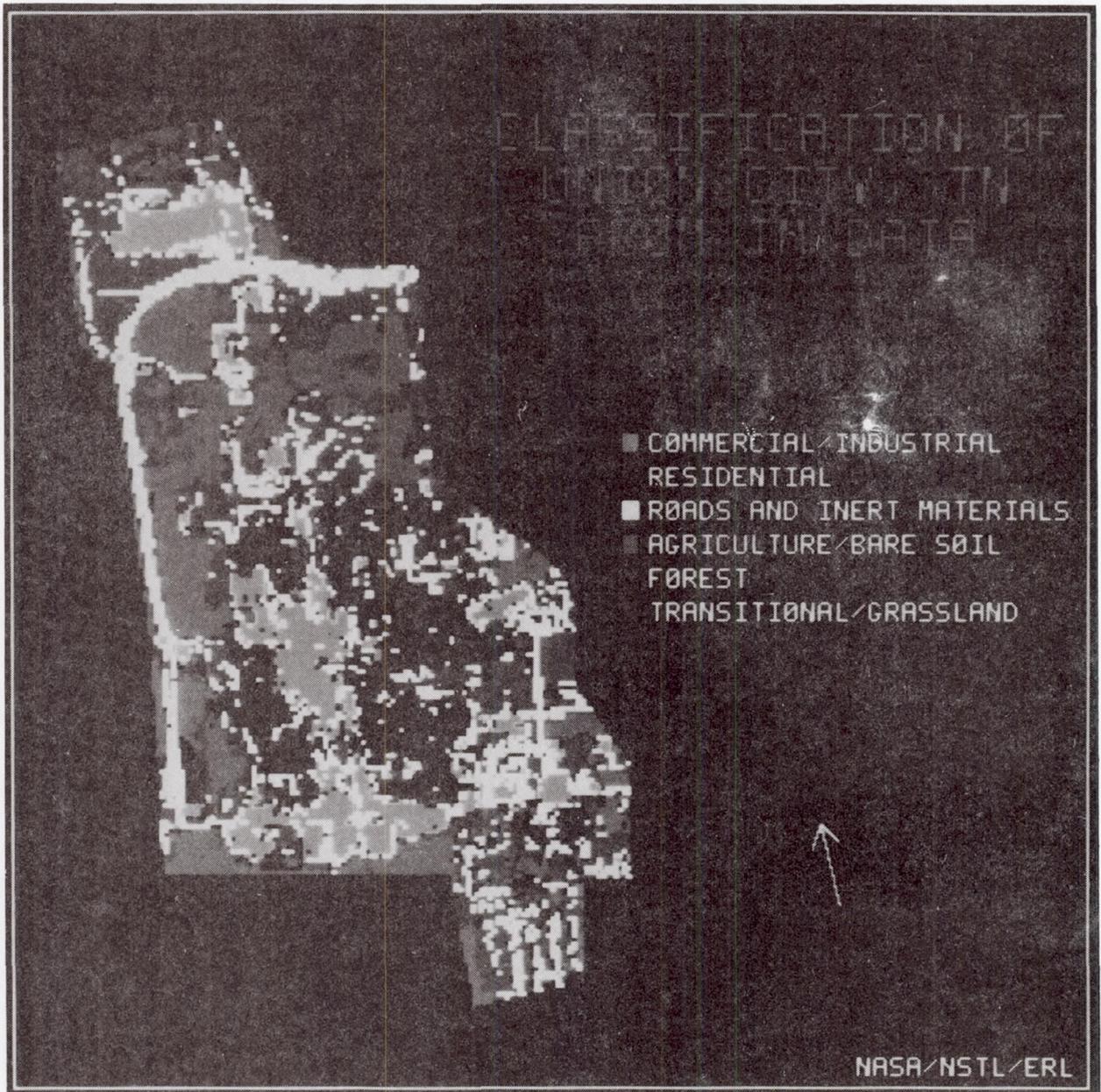
FIGURE 7

The accuracy figures in the table indicate the amount of within-class confusion that occurred for each of the four ground truth categories. Table 4 shows that the agriculture/bare soil class had an accuracy of approximately 90%, while the commercial/industrial class produced an accuracy of about 96% correct classification. Residential areas had an accuracy of 83.50% The confusion of the residential class with agriculture was predominantly due to the overlap of spectral signatures within the transition category. Newer residential areas have fewer trees than older, more established neighborhoods. These newer subdivisions appeared spectrally similar to grassland or shrubland areas and were confused with the transition land component of the agriculture class. Forested areas produced the best classification accuracy, with a percentage correct of almost 99%. The overall accuracy for the four major classes as compared to the ground verification data totaled 89.90% correct.

Concurrent with the digital assessment of the TM data for classification of the Union City study area, a photointerpretative analysis employing digital enhancement techniques was also performed. This empirical analysis of the data was conducted to augment the results obtained through digital classification and to evaluate the photointerpretative characteristics of the TM data for urban feature discrimination. It was hypothesized that the TM's improved spatial and spectral resolution over that offered by the MSS would be more conducive for photointerpretation of urban areas. In many situations, it may in fact be advantageous to bypass digital classification of the data and employ photointerpretation methodologies to derive the required information. This would be particularly true for areas where only certain or specific land covers may need to be observed for changes in the direction or intensity of urban growth patterns. It would be unnecessary in most of these cases to apply gaussian maximum likelihood or similar techniques for classifying the data; the desired information instead could be obtained through photointerpretation.

The three black and white products for the Union City area (Figures 8-10) illustrate how the increased spatial and spectral characteristics of the TM greatly augment the photointerpretative qualities of the data. To enhance the spectral contrast within the urban area, principal components analysis (PCA) was applied to the original seven channels of TM data. In addition to its data enhancement characteristics, PCA has been effectively used to eliminate confusion between agricultural and residential signatures in MSS data[5].

The first principal component (PC1) has in the past been commonly referred to as "brightness" because it emphasizes surface reflectance albedo; thus, highly reflective materials such as those in the Central Business District (CBD) and in other commercial areas appear as bright white tones (Figure 8). Note in Figure 8 that individual buildings are evident as exhibited by the reflectances from the Starite Company and Kinkead Industries located north of the Union City CBD. The Starite Company has a roof that is high in reflectance (e.g., a roof comprised of very light-colored gravel) while the Kinkead Industries building has relatively low response from its black, tar-coated roof.

1ST PRINCIPAL COMPONENT FROM THEMATIC MAPPER DATA
UNION CITY, TENNESSEE

NASA/NSTL/ERL

FIGURE 8

2ND PRINCIPAL CØMPØNENT FRØM THEMATIC MAPPER DATA
UNIØN CITY, TENNESSEE

NASA/NSTL/ERL

FIGURE 9

QUALITY SEED CO.
GOODYEAR TIRE PLANT
HWY 51
LAKE
BROWN SHOE CO.
KINKEAD INDUS.
STARITE CO.
OLD RESIDENTIAL
ARMORY
COURTHOUSE
CBD
HIGHLAND SUBDIV.
TRAILER PARK
HIGH SCHOOL
HWY 22
OBION CO. HOSPITAL
REELFOOT MEAT CO.
NEW RESIDENTIAL
DIXIE GUN WORKS

RATIO OF 1ST AND 2ND PRINCIPAL COMPONENTS FROM
THEMATIC MAPPER DATA --- UNION CITY, TENNESSEE

NASA/NSTL/ERL

FIGURE 10

PC2 exhibited some equally interesting photointerpretative characteristics. This component has frequently been alluded to as "greenness" since it emphasizes vegetative characteristics, or in the case of urban areas, the absence of vegetative response (Figure 9). Street patterns can be detected in this image because they have a low greenness reflectance in the second component. As in PC1, the individual structures can also be discriminated from PC 2.

To maximize the information content contained in PC's 1 and 2, these transformed data channels were ratioed (Figure 10). The ratioing of PC1 and PC2 has been shown to be useful for enhancing the target-to-background contrast of features with heterogeneous land cover compositions such as surface mines[6]. PC's 1 and 2 contain uncorrelated data, with each component contributing a significant amount of useful information; ratioing these data, therefore, permits optimization of data content which leads to an improved overall contrast level within the image. This is illustrated in Figure 10, where the contrast between highly reflective buildings and more subdued urban components, such as streets or residential areas, has been increased by ratioing PC's 1 and 2. Although both PC1 and PC2 enhanced cultural features within the city, the ratioed data augmented the detailed discrimination of urban features, particularly in the identification of specific structures.

From analysis of the classified and photointerpretative data products, it is evident that the TM can provide significant information for detection of urban features. It is enticing to see from this initial evaluation of the data that discrete urban land covers can be discriminated using digital techniques while maintaining accuracies as high as those established in Table 4. More importantly, a town the size of Union City could barely be discriminated through photointerpretation, let alone be digitally classifed as an urban area, from MSS data. Yet with the TM, it is possible to classify components of the city and visually locate and discriminate individual buildings. It definitely appears, therefore, that the TM will significantly advance interpretation of the urban milieu in comparison to what formerly could be obtained through evaluation of MSS data.

SUMMARY AND CONCLUSIONS

The investigations described in this paper have explored the capabilities of TM data for discriminating land covers within three particular cultural and ecological realms. Although the work presented here has been initial in scope, the results indicate how useful the Landsat 4 TM will be in providing researchers with a new capability to monitor the Earth's environment and landscape. One scene of TM data collected on August 22, 1982 over portions of Arkansas, Missouri, Tennessee, and Kentucky, has set the background for the studies that have been outlined here.

The agricultural investigation in Poinsett County illustrated that TM data can successfully be used to discriminate a variety of crop cover types within the study area. Moreover, in comparison with a classification

derived from a multitemporal MSS data set of the same area, the single-date TM classification produced results that were significantly better than those developed from the MSS.

For the Reelfoot Lake area, TM data processed using unsupervised signature development techniques produced a detailed classification of forested wetlands with excellent accuracy. In fact, the nine-category classification generated for the study suggests that it is possible to extract so much detail within the wetlands that delineation of areas of sufficient size for use in ground truth verification is difficult.

It also appears that the TM is very well suited to deriving information on specific urban land cover classes. As indicated by the evaluation presented in the last section of this paper, even in a small city of approximately 15,000 people, TM data can successfully be used to spectrally distinguish specific urban classes. Furthermore, the principal components analysis evaluation of the data shows that through photointerpretation, it is possible to distinguish individual buildings and roof responses with the TM.

In conclusion, the investigations discussed here have explored the digital classification and enhancement of TM data for three land cover applications. Although the TM offers a significant improvement in spectral resolution over what has previously been available on the Landsat MSS, the increased spatial resolution of the TM presents even more interesting opportunities for research. Since the TM is a new sensor, it is axiomatic that further work be conducted to understand the spectral properties and characteristics of the system. To fully exploit the capabilities of the TM, however, both the spectral and spatial attributes of the data must be examined. The next step in the evaluation process, therefore, should assess the interrelationships of these factors by employing new spectral pattern recognition techniques along with spatial, textural, and contextural classifiers.

REFERENCES

1. Dale A. Quattrochi, James E. Anderson, David P. Brannon, and Charles L. Hill, An Initial Analysis of Landsat 4 Thematic Mapper Data for the Classification of Agricultural, Forested Wetland, and Urban Land Covers, NASA, Earth Resources Laboratory, National Space Technology Laboratories, NSTL Station, Mississippi, Report No. 215, November 1982.

2. David L. Toll, "An Evaluation of Simulated Thematic Mapper Data and Landsat MSS Data for Discriminating Urban Area Land Cover," draft of manuscript submitted for publication in Photogrammetric Engineering and Remote Sensing, NASA, Goddard Space Flight Center, 1981.

3. S. Rangaswamy and T. Lien, Evaluation of the Improved Spatial, Spectral and Radiometric Capabilities of the Thematic Mapper Sensor, Final contractor report NAS5-25766 prepared for NASA, Goddard Space Flight Center by Research and Data Systems, Inc., Lanham, Maryland, March, 1981.

4. Jerry Clark, The Effect of Resolution in Simulated Satellite Imagery of Spectral Characteristics and Computer-Assisted Land Use Classification, NASA, Jet Propulsion Laboratory, Pasadena, California, Report No. 715-22, January 1980.

5. Darrel L. Williams and F. Yates Borden, "A Reduction in Agriculture/Residential Signature Conflict Using Principal Components Analysis of Landsat Temporal Data," Proceedings, American Society of Photogrammetry Fall Technical Meeting, Little Rock, Arkansas, American Society of Photogrammetry, Falls Church, Virginia, 1977, pp. 230-238.

6. Dale A. Quattrochi, A Technique for Using Multidate Landsat MSS Data to Discriminate Small, Heterogeneous Surface Mine Features in Eastern Kentucky, NASA, Earth Resources Laboratory, National Space Technology Laboratories, NSTL Station, Mississippi, Report No. 206, March 1982.

Page intentionally left blank

PRELIMINARY EVALUATION OF THEMATIC MAPPER IMAGE DATA QUALITY

R. B. MacDonald, F. G. Hall, D. E. Pitts, and R. M. Bizzell
NASA Johnson Space Center
Houston, Texas

S. Yao, C. Sorensen, E. Reyna, and J. Carnes
Lockheed Engineering and Management Services Company, Inc.
Houston, Texas

OBJECTIVES OF THE JSC LIDQA

The objective of this investigation is to determine the quality and utility of
the TM data, in particular to evaluate and understand the improvements in the
ability to monitor renewable resources/vegetation due to improvements in the
spatial, spectral and radiometric resolution of TM data. The analysis effort
at the Johnson Space Center was initiated in the fall of 1982 upon receipt of
the first TM data. The results presented here are from the first 4 months of
analysis and include: (a) geometric performance, (b) band-to-band registration,
(c) modulation transfer function, and (d) crop separability performance.

Future work will place these results on a more firm foundation and the scope
will be expanded to include:

a) the identification of TM features which enable vegetation information to be
    extracted from TM scenes,

b) the stability of vegetation TM signatures as affected by diverse geograph-
    ical, cultural, climatic and meteorological conditions,

c) radiometric performance, and

d) improvement in local vegetation identification and separability due to the
    additional middle infrared bands and the thermal bands.

CROP SEPARABILITY

Mississippi County, Arkansas:

Both TM (Thematic Mapper data)(seven bands) and MSS (Multispectral Scanner data)
were collected by Landsat 4 on August 22, 1982, over Mississippi County, Arkan-
sas. In preparation for such an acquisition, USDA-SRS collected a detailed

inventory and agronomic observations over this 5x6 n.mi. site. Shown in figure 1 are the TM and MSS data for this scene in Mississippi County, Arkansas. This segment is predominantly soybeans (80%) with small amounts of rice (5%) and cotton (5%). Since the soybeans are both single and double cropped (following winter wheat), there is a wide range of soybean crop stages (ranging from >V-5 (indicating that 5 nodes are present) to beginning seed). The rice had the flag leaf visible and the cotton had green bolls. This segment has a wide range of soils with the soils in the west loamy and sandy throughout, while the soils in the east have a thick clayey subsoil and are sandy or clayey in the upper part.

Mississippi County, Arkansas
Landsat-4, Segment 306
August 22, 1982

TM   MSS

Spatially registered Landsat-4 Thematic Mapper and Multispectral Scanner Images acquired on August 22, 1982 over a 9x11-mile agricultural area in Mississippi County, Arkansas; predominant crops are soybeans and rice. Irrigation ditches within fields are visible in the TM images. Images and registration were produced by the Data Systems Branch of the Earth Resources Research Division.

Results of feature selection for agriculture/crop classes in this scene show best performance is achieved when measurements from each of the three groups (visible, near infrared, and mid infrared) are utilized. However, for optimum classification of a single class (e.g., rice or soybeans at different growth stages) a different combination of bands may be required. This is scene dependent but for the cases examined in the current studies the MIR bands certainly play a significant role.

TM "MSS equivalent bands" show improvement over MSS due to increased spatial resolution and increased signal/noise. Moreover the mid IR bands add additional separability between rice and soybeans. A 25% improvement in soybean classification accuracy was noted when the mid IR was incorporated in the classification from the Mississippi County, Arkansas, scene.

While investigations into the relationship of thermal band physics to crop type are just beginning, some evidence has been found that the thermal band is going to prove useful in distinguishing between crops. In spite of the misregistration of the thermal band we have observed that sorghum (which can be confused

with many classes, especially the late soybeans) was separated when we added the thermal band, figure 2.

S82 41471

POTENTIAL FEATURE SEPARATION ENHANCEMENT
USING THEMATIC MAPPER THERMAL BAND

ARKANSAS SCENE
AUGUST 22, 1982

THEMATIC MAPPER IMAGE USING VISUAL AND NEAR INFRARED BANDS (1, 2 & 4)

THEMATIC MAPPER IMAGE USING THERMAL BAND (6) COMBINED WITH VISIBLE MID-INFRARED BANDS (3, 5 & 6)

RIPE SORGHUM IS NOT SEPARABLE FROM EMERGING SOYBEAN FIELDS USING VISUAL AND INFRARED LANDSAT BANDS.
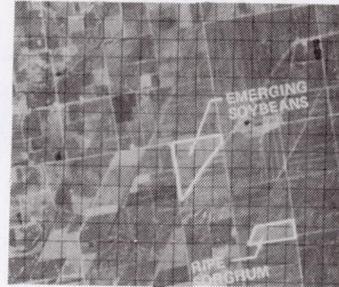
RIPE SORGHUM SEPARATES FROM EMERGING SOYBEAN FIELDS USING THERMAL BAND (6) IN COMBINATION WITH VISIBLE AND MID INFRARED BANDS.

NASA
Lyndon B. Johnson Space Center

Expectations based upon field research data, helicopter spectrometer data, and thematic mapper simulated data over the last 5 years may be confirmed using TM data. The middle infrared added significant additional information over the MSS bands (three principal components of TM data account for 97% of the variance in the scene, whereas two principal components of MSS data usually account for about 99% of the variance present in MSS data).

The principal components for the Caruthersville scene as shown in associated images of the first three principle components, figure 3, and the last three (thermal band excluded), show clearly that there is information in even the last three components. Note, the distinction between the inland water and the Mississippi River and the separation of two different crop classes in the last three components.

EXAMPLE OF ADDITIONAL INFORMATION AVAILABLE WITH THEMATIC MAPPER, BASED ON PRINCIPAL COMPONENT ANALYSIS

FIRST THREE COMPONENTS   LAST THREE COMPONENTS
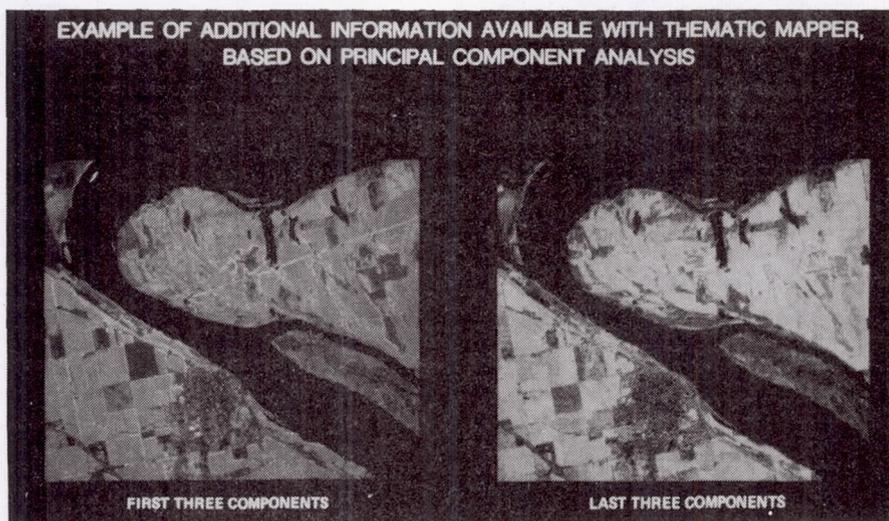
Webster County, Iowa:

The initial TM acquisition over Webster County, Iowa, occurred on August 2, 1982. Neither the Landsat 4 MSS nor the cold focal plane bands of TM (bands 5, 6, and 7) were active on this date. This region of Iowa is predominantly corn and soybeans (80%). Since there is a narrow range of planting dates in the scene, the crop stages have a narrow distribution (90% of the corn was in Blister stage and the 100% of the soybeans were in flowering).

Since the MSS data were not collected on this date from Landsat 4, the nearest Landsat 3 MSS data were utilized. Both the TM and MSS data were clustered using the CLASSY unsupervised clustering algorithm and each cluster was assigned a label based on the SRS ground truth enumeration (figure 4). Even though the TM data only include the visible and near infrared bands, the higher spatial resolution and increased signal to noise cause several classes to be more distinct on the TM: roads, senesced vegetation, and homesteads. However, more within field variability is apparent with the higher spatial resolution TM data.

CLUSTERING EVALUATION OF SPECTRAL SEPARABILITY
WEBSTER COUNTY, IOWA

AN UNSUPERVISED CLUSTERING ALGORITHM (CLASSY) WAS APPLIED
TO RAW CHANNEL VALUES TO OBJECTIVELY DETERMINE THE
CLASSES PRESENT IN THE DATA.

INCREASED SPATIAL RESOLUTION OF THE THEMATIC MAPPER ALLOWS
SEPARATION OF SPECTRAL CLASSES NOT SEPARABLE USING MSS DATA.

COLOR CODE
CORN—BLUE, SOYBEANS—RED, MIXTURE PIXELS—GREEN

COLOR CODE
CORN—BLUE, SOYBEANS—RED, TREES—GREEN, NON-AG—WHITE, SENESCENT VEGETATION—LIGHT BLUE

MSS (JULY 28, 1982)

TM (AUGUST 2, 1982)

While the TM proportion estimates are very close to the SRS ground enumerations it is unknown now much of this is due to commission errors and omission errors balancing out.

Category	Ground Truth Proportion	Estimate
Corn	43.57	39.4
Soybeans	37.98	36.40
Trees	4.45	3.03
Nonagriculture	4.49	3.03
Roads	—	13.21

IV-156

Analysis of TM simulator data flights over this site since 1979 has shown that bands 1-4 of TM are not optimum for separability of corn and soybeans in Iowa in early August. However, the mid IR bands are thought to be critical during this period, since the corn and soybeans apparently have different amounts of leaf water content. This hypothesis will be verified in the near future by analyzing the middle IR bands from the TMS data collected only 2 days prior to the August 2, 1982, TM data.

Recently JSC has received additional TM data for this site. Both MSS and all seven bands of TM data were collected on September 3 and October 21 and these data have now been multitemporally registered. Analysis of these data will provide additional information as the corn was beginning to full dent and the soybeans were beginning to full seed on September 3. On October 21, both corn and soybeans were at physiological maturity, but only the soybean harvest had started.

Preliminary analysis of the cause of the within field variability seen in the cluster maps indicates that poorly drained low yielding soil appears coincident with these confusion areas within the fields (figure 5). At this time it is not known what effect the soil is having on the crop. However, it is thought that the poor soil is causing a lower Leaf Area Index. Upon examination of the September 3 scene, it can be seen that much of this variability has decreased, thereby adding credence to this hypothesis.

TM RESOLVES WITHIN FIELD SOIL STRUCTURE
SEGMENT 893 WEBSTER COUNTY, IOWA
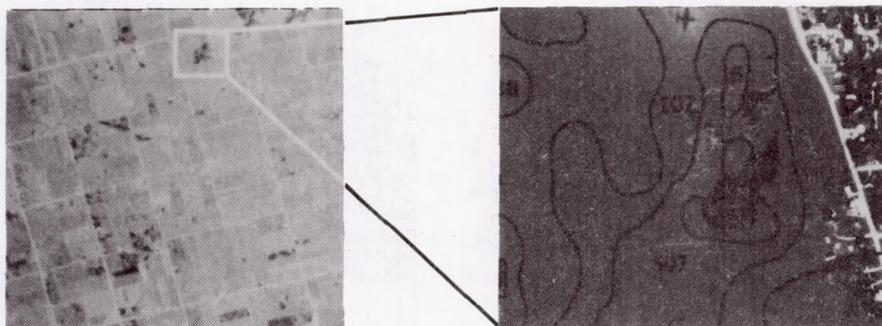
THEMATIC MAPPER DATA
AUG. 2, TM BANDS 2, 3, 4

COLOR INFRARED PHOTOGRAPH
AUG. 19, 1980 (1,500 FT ALTITUDE)

SOIL TYPE	POTENTIAL FIELD (BU/YIELD)	
	CORN	SOYBEANS
6	84	32
507	105	40
107	110	42
55A	118	45

Multitemporal Registration of TM Data

Both tie point registration (using the JPL VICAR system) and an edge correlation technique are used at JSC. The tie point registration is used to remove gross differences in rotation (>5°) and scale so that the automatic, more accurate, edge correlation technique can be applied. To use the edge correlation technique, clouds, cloud shadows and data dropout areas are removed from the data, and a gradient is calculated for each remaining pixel of the scene. These gradients are then histogrammed and the highest 15% are utilized to form the edge image in each data set (different channels or different sensors). Iterations are then performed to estimate correlation peak positions using a fourth order bivariate polynomial. Tests show the procedure will give an accuracy of better than 1/15 pixel when an image is registered to itself.

The August 2, September 3, and October 21 scenes of Webster County, Iowa, were multitemporally registered using TM band 4 and the edge correlation technique described above. Tests of the accuracy were conducted by measuring the line and pixel offsets in 40 patches (each of which is 40 pixels by 40 pixels). The accuracy of the misregistration from August 2 to September 3 was about .25 pixels rms and the accuracy of the registration from the August 2 to the October 21 was about 1 pixel rms (which does not meet our need for 0.5 pixel rms). The exact cause of this unacceptably large error is not known at this time; however, it is expected that different edges are apparent in the October 21 scene when most of the vegetation is senesced as compared to the August 2 scene when the corn is at full silk and the soybeans are flowering.

Band-to-Band Registration Accuracy

The Thematic Mapper contains two focal planes, the first contains bands 1 thru 4 (blue, green, red, and near infrared channels) where the second focal plane contains the mid IR (bands 5 and 7) and the thermal (band 6). Thus, the purpose of this analysis was to compare bands to show the registration within each focal plane and between each focal plane.

The September 3, 1982, scene over Webster County was analyzed using three pairs of channels: 2 and 4 (within the first focal plane); 4 and 5 (between the first and second focal plane); and 4 and 6 (between the first and second focal plane).

The scene was divided into collections of 40-by-40 pixel regions each of which was registered using the edge gradient procedure described in the previous section. Each 40-by-40 pixel region line and pixel misregistration was then plotted and the mean and variance compared to the specification. As seen in figure 6, bands 2 and 4 were well registered (within the specification of 0.2 pixels, 6 meters) whereas bands 4 and 5 were found to have almost one pixel misregistration. Furthermore, the thermal band (band 6) was found to have an additional bias along the scan line of about 3-4 pixels (the specification for the thermal band is also 6 meters). The multitemporal registration of TM at JSC has a goal of 0.5 pixels rms from one scene to another. Misregistration on the order of that observed in the mid infrared and thermal infrared will severely degrade the analysis of spatial and temporal features in the TM data. This will affect classification, crop stage estimation, emergence date estimation, and estimation of Leaf Area Index of vegetation canopies.

GEOMETRIC FIDELITY OF THEMATIC MAPPER

TWENTY-ONE COMMON POINTS WERE LOCATED ON THE THEMATIC MAPPER IMAGE AND THE 1:24,00-SCALE TOPOGRAPHIC MAP
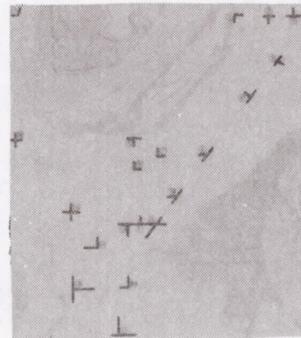
SIMPLE ROTATION, TRANSLATION, AND SCALING (NO STRETCHING) GAVE LESS THAN ONE-TENTH OF A PIXEL ABSOLUTE ERROR

TM · AUGUST 22, 1982
BLUE · TM2, GREEN · TM7, RED · TM5

Geometric Fidelity

The P-tapes received from GSFC to date have not been corrected for ground control, only system corrections have been applied. Nevertheless, the imagery appeared to have high geometric accuracy. The 7-1/2 minute Tiptonville, Tennessee, quadrangle was extracted from the August 22, 1982, Arkansas TM scene and 21 control points were chosen on well defined edges that were apparent in both the scene and the USGS quad sheet (figure 7). A least squares fit was

EVALUATION OF
TM BAND TO BAND REGISTRATION

WEBSTER COUNTY, IOWA
SEPTEMBER 3, 1982 ACQUISITION
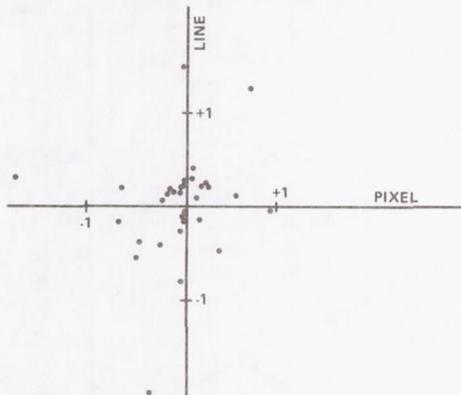
BAND 2 VS BAND 4
LINE AVERAGE OFFSET 0.013 PIXEL
COLUMN AVERAGE OFFSET -0.17 PIXEL
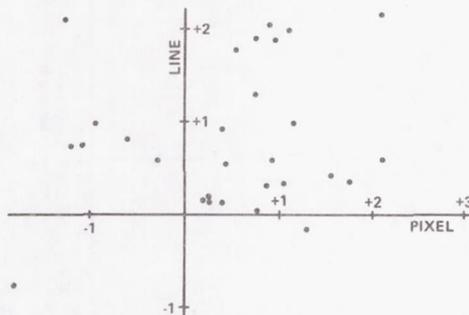
BAND 4 VS BAND 5
LINE AVERAGE OFFSET 0.79 PIXEL
COLUMN AVERAGE OFFSET 0.89 PIXEL
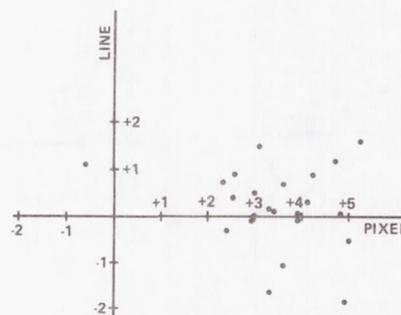
BAND 4 VS BAND 6
LINE AVERAGE OFFSET +0.53 PIXEL
COLUMN AVERAGE OFFSET +3.68 PIXEL

determined which allowed for scale change and rotations, but did not allow for differential changes (e.g., rubber sheeting). The resultant rms error was <1/10 pixel which indicates that the geometric fidelity of the scene is excellent, certainly better than that expected a year ago when mechanical interference between MSS and TM was a major concern. If this is true this will certainly expand the utility of TM data and will significantly reduce the cost of multitemporal TM analysis.

Modulation Transfer Function

The response of the Thematic Mapper was determined prior to launch by collecting imagery of Bar patterns. In order to determine the response of the TM after launch, a group of north-south edges in band 5 were chosen which had homogeneous fields extending at least three TM pixels from the edge. The MTF was obtained by taking the Fourier Transform of the gradient across each edge. These estimates were obtained using VICAR software. The overall MTF shows a more rapid fall-off than was observed in the protoflight measurements (figure 8). However, when modified to account for the cubic convolution resampling done by GSFC and the spread function due to the atmosphere (Pearce, 1977) better agreement is achieved. Better agreement could be achieved if the optical depth of the atmosphere were known, the position of samples were known relative to the edge and better contrast existed across the edges analyzed.

MODULATION TRANSFER FUNCTION FOR TM CHANNEL 5

PROTOFLIGHT MEASURMENTS (UPPER)
3 TIMES NORMAL ATMOSPHERIC TURBIDITY(PEARCE)-(LOWER)

RANGE OF ABOVE WITH GSFC CUBIC CONVOLUTION

RANGE OF SYSTEM MTF ESTIMATED FROM 4 GOOD TM SCENES

METERS PER CYCLE
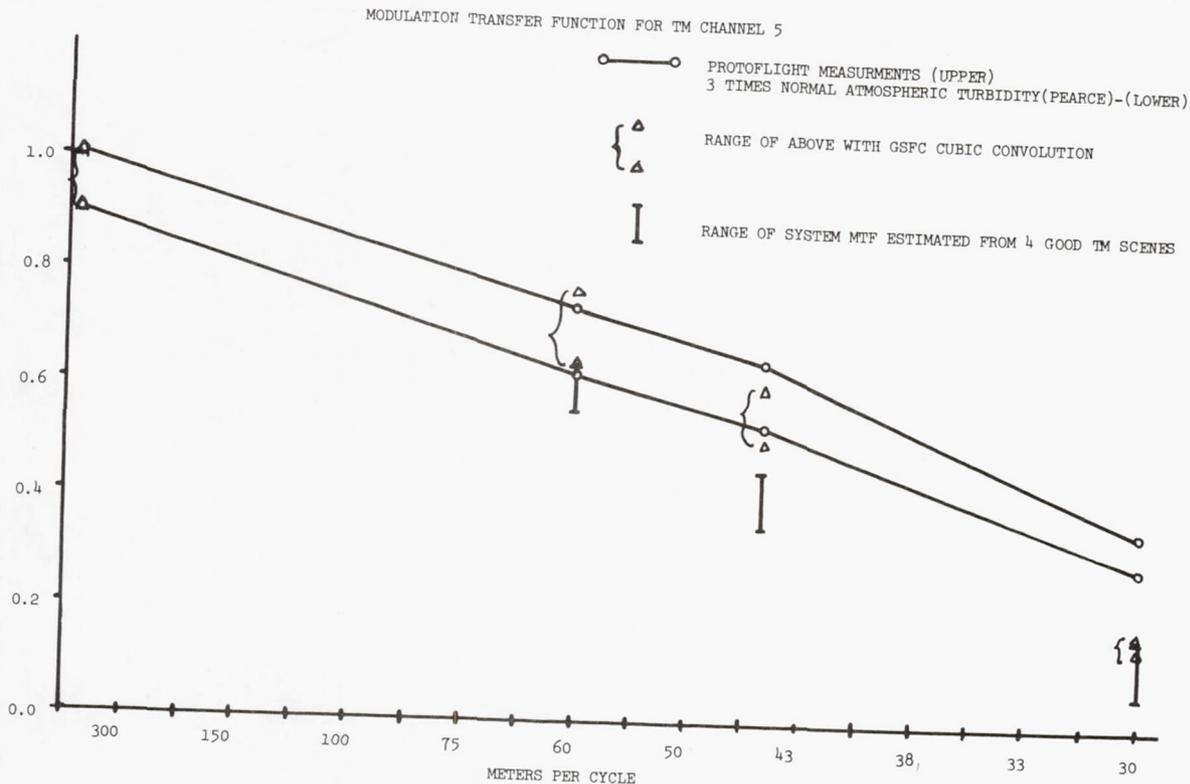
Conclusion

Although a few problems exist with the registration of the middle infrared and thermal infrared, the overall quality of the thematic mapper data appears excellent. The improvements in spatial resolution, signal to noise, quantization accuracy, geometric accuracy, and the inclusion of new and better placed spectral bands make TM a welcome and badly needed improvement over MSS.

Reference

Pearce, W.A. 1977. "A Study of the Effects of the Atmospheric or Thematic Mapper Observations." Report No. 004-77 EG&G/Wash. Anal. Ser. Center.

Page intentionally left blank

ASSESSMENT OF COMPUTER-BASED GEOLOGIC MAPPING OF ROCK UNITS

IN THE LANDSAT-4 SCENE OF NORTHERN DEATH VALLEY, CALIFORNIA

Nicholas M. Short

Code 922
Goddard Space Flight Center
Greenbelt, MD 20771

Abstract

Geologic mapping of stratigraphic units by use of aerial-photointerpretation methods has been the established practice for nearly four decades. Mapping by means of multispectral remote sensors on aircraft and, since the first Landsat in 1972, on spacecraft should in principle be a more efficient procedure. Classification mapping of stratigraphic units within Landsat scenes by computer-based statistical analysis of spectral data has achieved relatively low and generally unacceptable accuracies of typically 40-60% in semi-arid mountainous terrains. Rock unit identification by ratio and principal components analysis may reach higher accuracies in terrains dominated by good exposures of rock materials and sparsity of vegetation. However, none of these methods is likely to attain consistently high accuracy in any favorable terrain because of two fundamental differences between conventional geologic maps and those derived from remote sensing data. These are:

1) only spectral categories of rock materials can be separated by remote sensing, allowing some rock units to be specified, but geologic maps depend on stratigraphic discrimination in which relative <u>ages</u> must be recognized by some time criterion that normally requires close examination, and

2) much of the area represented by a stratigraphic unit is actually covered by soil, debris, vegetation, etc. and is mapped by extrapolation whereas a remote sensing map shows only what is at the immediate surface.

Improved classification accuracies have been predicted for Landsat-4 because of the four additional spectral bands, higher resolution, and greater sensitivity of the Thematic Mapper (TM). This has now been verified for land use and agricultural classifications but has not been fully tested for geologic classes. This paper reports results from a series of classifications conducted on a subscene of the northern Death Valley, California, acquired by the TM on November 17, 1982. These are summarized as follows:

Type of Classification	Image Size (pixels)	Bands Used	No. of Classes
↑ Supervised (subsampled)	300 x 320	1,2,3,4,5,7	21 (19)
Supervised (full size)	1500 x 1600	1,2,3,4,5,7	18
Unsupervised (32 cluster)	300 x 320	1,2,3,4,5,7	17
Supervised	"	1,5,7	19
"	"	2,3,4	18
Unsupervised (16 cluster)	"	1,2,3,4,5,7	11 (8)
"	"	2,3,4	9 (7)

(Left margin, vertical label:) Increasing Apparent Accuracy

Measurements of accuracy are made through comparison with the 1977 edition of the Death Valley geologic sheet. This employs a simplified map version which is registered by computer to the image data base, allowing a pixel by pixel match with the classified scene. The results from this study show accuracy ranges from 36 to 79% depending on the type of classifier used and the statistical adjustments made to the data. Accuracy values in identifying geologic units were 2 to 3 times higher for those in the relatively flat valleys than for units in the rugged mountainous terrain. Improvements in accuracy will be sought by correcting for slope/aspect variations in mountainous terrain using topographic data recorded in Defense Mapping Agency (DMA) tapes. The above classification results will also be compared with ratio and principal component image classifications made from the same scene.

Introduction:

Geoscientists who apply computer-based analysis to Landsat scenes have established a hierarchy of preferred processing techniques ranked according to the relative success of each in recognizing geologic units and features of practical interest. Generally, processing of digital data through Principal Components Analysis and by ratioing selected band combinations has proved most effective for discrimination of rock and alteration units where rock units are homogeneous and well exposed. Band-pass filtering and edge enhancement techniques are considered best for improving detectability of lineaments and other structural features. In some instances, just a simple image enhancement procedure, involving spatial filtering and radiometric adjustments, may be sufficient to yield a visual product which discloses optimal geologic information suited to straightforward photointerpretation.

Several disciplines that use Landsat and other remote sensing data have found digital classification techniques to be the most informative approach to identifying features and materials at the earth's surface. Agronomists apply these techniques in categorizing crop types. Land cover/land use specialists find statistically-based classification reliable for mapping first- and second-level geographic classes. When measured by quantitative accuracy standards,

accuracies of 80-95% have been attained for individual crop types, and sometimes several crops, as well as for major subdivisions of forest types and for other principal ground cover classes. In contrast, geologists have rarely exceeded accuracies of 40-60% using various methods of classification to reproduce Landsat-derived maps of stratigraphic units made from Multispectral Scanner (MSS) data for comparison with published maps made by conventional methods that include field studies (Siegal and Abrams, 1976). Several reasons can be cited for this "low score", chief among which are:

1) A fundamental difference exists between remote sensing classification maps of materials actually at the surface and most geologic maps. Geologic maps record rock type as recognized from hand specimen examination and from relative geologic age based on time criteria derived from fossil evidence, radioactivity measurements, or superposition relations distinguished in the field or by photointerpretation.

2) Another characteristic of geologic maps is that the mapped units are frequently extrapolations of the usually low percentage of surface outcrop observations (generally only 1-2% of the eastern U.S. and 10-30% of the western U.S. ground surface is actually bedrock; most of the remainder is soil, vegetation, water, and cultural features), so that the actual "ground truth" is largely inferential, and,

3) The immediate surfaces of exposed rock units are often strongly weathered or otherwise altered so that the spectral signatures of the fresh materials comprising diverse rock types are in effect replaced by those of more uniform end product alteration. In very arid areas where mechanical weathering dominates, it appears possible to relate specific alluvial classes to the lithology of their provenance (Blodget and Brown, 1982).

These three factors, and others, are particularly troublesome in efforts to classify the rock materials in the same way as conventional mapping, although they likewise may adversely influence results in recognizing these materials by ratio and principal components methods. These limitations prompted a comment by Michael Abrams of the Jet Propulsion Laboratory during his oral presentation at the Landsat-4 Early Results Conference which, to paraphrase him, stated that "the scientists at JPL find ratio and principal components images to be superior to their attempts at recognizing rock units by direct unsupervised or supervised classification methods".

While the "track record" for computer classifications of geologic units has not yet been outstanding, one might infer that part of the difficulty arises from inadequate spatial resolution. Certainly, higher interpretation accuracies can be achieved in geologic mapping from aerial photos. In addition, other regions of the electromagnetic spectrum may be more efficient in differentiating rock types than the visible-near IR region sensed by the MSS on the Landsats. Thus, the Thematic Mapper (TM) on Landsat-4 should be capable of acquiring data from which a greater number of surface rock units would be discriminated, allowing a more reliable geologic map with accuracy exceeding 60% to be generated.

To test this hypothesis, this paper will describe an experiment to classify a subset of the November 17, 1982 TM image of the Death Valley scene along the

California-Nevada border, employing procedures developed for the IDIMS computer system operating at the Goddard Space Flight Center. The principal objectives of the study are to:

1) Determine the extent, if any, of accuracy improvement in using classification methods to map meaningful geologic units brought on by the higher resolution, additional spectral bands, and their greater sensitivity, of the Thematic Mapper relative to results reported by Siegal and Abrams for the Landsat MSS as the standard of reference.

2) Evaluate the relative efficiencies of the supervised versus unsupervised approaches to computer-based geologic mapping; likewise, the effectiveness of two common classifiers is examined.

3) Compare classification maps with ratio and principal components images to ascertain the types and degrees of information provided by each.

4) Shed more light on the reasons for the low accuracies in correctly identifying and mapping geologic units by remote sensing techniques and to suggest possible avenues for improvement. The results reported here must still be considered preliminary in that even more sophisticated processing has yet to be applied and that the standard for success in terms of agreement with published maps needs further refinement.

Data Processing Procedures:

A series of supervised and unsupervised classifications were performed on the reflectance bands data subset taken from the Death Valley scene (Landsat 40124-17495) as outlined in the following sequence. The thermal band 6 (10.4-12.5 μm) was not used because of difficulties in registration of its larger pixels with those of the other bands.

CL1:   Supervised; Bands 1, 2, 3, 4, 5, 7 (subsampled partial scene)
CL2:   Supervised - 6 Bands (partial scene)
CL3:   Supervised - Bands 2, 3, 4
CL4:   Supervised - Bands 1, 5, 7   Subsampled
CL5:   Unsupervised - Bands 2, 3, 4 (16 clusters)   Partial
CL6:   Unsupervised - Bands 1, 2, 3, 4, 5, 7 (16 clusters) Scene
CL7:   Unsupervised - Bands 1, 2, 3, 4, 5, 7 (32 clusters)

All of the above except CL2 utilized a resampled 300x320 pixel subscene; CL2 was performed on a subscene containing all original pixels. A Maximum Likelihood classifier was applied to all seven CLs; in addition a Minimum Distance classifier was applied to CL1.

Ratio: 5/7; 3/4; 5/2

PCA: Six components; various combinations of three.

A more detailed summary of the steps involved in the classification is given here.

1) The reference partial area chosen from the full Death Valley scene covers a 60 (N-S) by 45 (E-W) km equivalent subset of the TM scene, occupying

roughly the upper left 1/16th of the full image. Represented are the northern section of the Death Valley basin, the northern end (known locally as the Tucki Mountain) of the Panamint Range, most of the Grapevine Range, and some of the Funeral Mountains, as located in Figure 1.

2) Control in setting up classes was supplied by the 1977 Death Valley Sheet (hereafter referred to by the initials DVS), a 1:250,000 scale geologic map published by the California Division of Mines and Geology. Most of these classes are based on the stratigraphic units depicted in the 1977 geologic map; several classes are combinations of units shown on the map. A generalized version of the 1977 map appears in Figure 1. This latter map serves as the accuracy reference.

3) All computer analyses were performed on the Interactive Digital Image Manipulation System (IDIMS) at NASA/Goddard Space Flight Center. This system is tied to a Hewlett-Packard HP3000 Series II minicomputer with 512 kilobytes of core memory. Landsat-4 data are introduced from 6250 bpi CCTs and stored on disc during processing. Images are commonly displayed as resampled data arrays on a 1024 raster line DeAnza monitor, from which most illustrations shown in this paper were produced using a Calumet 4x5 inch View Camera to photograph directly off the screen.

4) The first subset image was created from all pixels in the TM data set within the represented 1/16th portion of the scene. This image size is 1500 by 1600 pixels. After carrying out several functions on that subset, it was concluded that the total number of data points was too large to be handled efficiently on IDIMS. To create a more manageable data set, the initial subset was resampled to 300 by 320 pixels by selecting every 5th line and 5th sample (pixel) within that line.

5) For all analyses save one, only the six reflectance bands were applied to the classification. Three combinations of bands were examined, namely Bands 2, 3, 4 (to approximate the MSS configuration), Bands 1, 5, 7 (to investigate classification using the non-MSS bands only), and Bands 1, 2, 3, 4, 5, 7 (to test the assumption that more bands will improve discrimination and accuracy).

6) The classification functions were just those developed by the IDIMS supplier (ESL, Inc. of Sunnyvale, California) as the recommended routines using the software programs provided for the system. For <u>unsupervised</u> classification, the normal steps are:

A. Run RANDSAMP, which randomly selects a large number of data points (pixels) from the set, from which to build up the statistics needed for clustering. However, in this experiment, this step was obviated by considering the 5 line – 5 sample resampling to have accomplished a similar task. The validity of this alternative was not tested.

B. Run ISOCLS, to gather statistical information using a clustering algorithm from which a number of (initially unspecified) separable classes are selected. Output includes a statistical file containing the number of points (pixels) in each cluster, digital count (or DN) means and standard deviations, and covariance matrix for each cluster and each co-associated band, and the intercluster distance (in DN units) in multidimensional space for cluster pairs. For two

experiments the following defaults for mandatory and optional parameters were accepted:

   Number of Iterations = 8
   DLMIN = Minimum distance required between clusters = 3.2 DN
   STDMAX = Standard deviation limit above which clustered values will be split into separate clusters = 4.5 DN
   NMIN = Minimum number of data points to accept a cluster = 30
   MAXCLS = Maximum number of classes sought = 16
   CHNTHS = Threshold at which clusters may be optionally combined = 3.2 DN

The parametric conditions for a third experiment will be specified later (p. 22)

C. Run CLASFY, which assigns each pixel in the subset to the most similar of the clusters established in ISOCLS according to the criteria developed in the statistics file, using a maximum likelihood decision rule. The number of classes thus specified will be less than or equal to the number of assigned clusters. Numerical output consists of a determinant value, a constant term, and the inverse covariance matrix for band pairs. An image is produced consisting of pixels assigned to each cluster, expressed in grey levels at increments of preset DN values (a narrow range, which can be made more "seeable" by contrast stretching). A second image, based on Chi-square statistics, showing the relative confidence in the classification of each pixel, is also formed.

For supervised classification, these steps are taken:

A. Run TSSELECT, in which training areas within the image are delineated (by cursor-drawn lines) as named classes. Maps and other identification sources are used to specify these classes. The training sites are selected carefully to insure that they are typical of the class and possess reasonable spectral homogeneity.

B. Run TSDEFINE, by which appropriate statistics, analogous to those developed for ISOCLS, are calculated from the pixel DN values within each training site. Documented output includes means and standard deviations for each identified class arranged by band, covariance matrix and correlation matrix values, and histograms of the data point distribution by class and band. An optional program, called STATPLOT, allows two dimension (bands as axes) plots of the means and standard deviations; the resulting ellipses resemble smoothed depictions of the clusters produced by ISOCLS.

C. Run CLASFY, using the TSDEFINE statistics instead of ISOCLS.

7) After a CLASFY image is displayed on a color monitor, the final step consists of assigning (also called "alarming") colors to each class or cluster using the TCC function on IDIMS to produce the Classification Map (referred to hereafter by its CL number, as for example CL4). Several combinations are usually tried out to find the most pleasing and informative color pattern. Only 24 colors are available from TCC for this purpose; when classes exceed about 12 it is difficult to find enough contrasting colors to set off some of the classes, as is evident from some of the illustrations in this paper. Color assignments were worked out first for the supervised classes and these same colors were then applied to clusters in the unsupervised CLASFY images that appeared to be equivalent as judged from their geographic distributions. Color assignments for several classes had to be "juggled" to find a discernible combination.

8) Following presentation of the first results of the Death Valley study at the Landsat-4 Conference, two additional, more sophisticated classifications were performed on IDIMS. For one (CL7), the program utilized a more rigorous unsupervised procedure. This approach, preferred by land use specialists at Goddard, requires specificaton of a larger number of initial clusters and more iterations. In the other (CL2), a smaller subset from the original 1500 by 1600 pixel subscene was classified in toto. The conditions chosen for these special classifications are discussed further in the results section.

9) A series of Principal Components Analysis (PCA) images were produced on IDIMS through the KLTRANS (Karhuuen-Loeve Transformation) function developed by ERIM. By using the six reflectance bands in TM, a set of six component images (black and white) were generated. These typically were "flat" as displayed, i.e., showed little grey level variation, so that each was arbitrarily stretched to a high contrast version. Various combinations of three such stretched images were displayed in red, green, blue color composites on the monitor. A similar approach was used in producing a set of ratio images. The DIVIDE function was applied to pairs of reflectance bands to give 7/5, 5/2, and 3/4 ratio images. Stretched images were then superimposed and each assigned a primary color to form color composites.

Development of the principal components and ratio composite images was a secondary objective of the study. No statistical data were extracted nor were possible refinements in the procedures attempted. The purpose was simply to provide a visual comparison between patterns of distinguishable ratio and component units them and the classification image units, as produced on the same image processing system, and to tie in with ratio composite images formed by R. Haydn and other TM investigators (see this Proceedings Volume).

10) Following production of all of the classification products, the results were field-checked during a one-day trip by car on April 21, 1983 through northern Death Valley. Observations and implications from this on-site visit are reviewed in the Discussion section. The author gratefully acknowledges the assistance of Dean James V. Taranik of the Mackay School of Mines, University of Nevada and Mr. Marcus Bornegasser, a graduate student in remote sensing there in conducting this "ground truth" excursion.

Analysis Results:

The end product images of four supervised and three unsupervised classifications of the Death Valley subscene are reproduced in Figure 2. Tables 1 and 2 summarize the class and cluster means produced as statistical files by TSDEFINE for CL1-4 and by ISOCLS for CL5-7. Analytical interpretation of the information given in these figures and tables is reported in this section.

At the outset, a conceptual framework for this analysis can be erected by gaining a visual understanding of the geology and geomorphology of the northern Death Valley through a brief review of scene content in a series of photos taken during the one-day field trip through the area on April 21, 1983. Look again at the geologic map and legend of Figure 1 and then examine Figure 3A and B and their captions with this in mind.

The interpretations can best be communicated by visually "walking through" the class distributions in each of the seven classification maps shown in Figure 2, pointing out both similarities and differences among the various renditions. CL1 is taken as the standard of reference. Before treating each map in some detail, three general comments about certain classifications are in order:

1) For the CL3 and 4 supervised classifications, the numerical DN means for each of the two 3-band cases (2, 3, 4; 1, 5, 7) are identical with those listed for the 6 bands in Table 1 which records the values derived for CL1. This must be simply because the values are just those calculated for the same training sites which are used in all three classifications.

2) The unsupervised Band 2, 3, 4, classification created 9 distinct clusters under the standard default conditions. These clusters were initially assigned a selection of contrasting colors so that their spatial distribution was visually defined. Subsequently, these clusters were correlated with certain of the classes set up during the first supervised classification, by comparing their DN numbers with those in the supervised statistics files and by establishing equivalency in spatial distribution. New colors compatible with those of CL1 were then assigned.

3) When all six reflectance bands were applied to the default unsupervised classification, most of the same 9 clusters were created, although the DN mean for each is slightly different in value. In addition, two new clusters were established, both of which could be correlated with two more classes as specified in CL1.

Each of the CL mappings and the Ratio and PCA results are now considered. By far, the most attention is given to CL1, inasmuch as that is designated the best product to which all other classifications are compared.

CL1: The CL1 map is shown in Figure 2A (left page), together with the other three supervised classification maps for easy visual comparison. However, the CL1 map is also reproduced on a full page (Figure 2C) to depict finer details. The CL1 map versions (see also Figure 7A) are judged to be the most "believable" of any of those reviewed in this section. Considerable care was exercised in locating suitable training sites. Tracings of the polygons outlining one or more sites for each class are reproduced in Figure 4; the classes are identified by the symbol patterns used in Figure 1 as defined in the accompanying legend. Table 1 records the 6-band means for each of these classes.

An interpretation map showing the distribution of recognized classes (mainly stratigraphic units) appears as Figure 5, again using the symbols presented in the Figure 1 legend. This map was generated by tracing the class units from a copy of the CL1 map made as a transparency. Each unit has been assigned an identifying color (see legend in Figure 2B). The boundaries between units, as shown in Figure 5, are somewhat arbitrary, representing the author's choice for dominant color in parts of CL1 where several colors are mixed owing to misclassification and other factors. A revised CL1 map, shown in Figure 7A and discussed later, aided in selecting some class boundaries.

A qualitative appraisal of the accuracy of this classification can be drawn from comparison between the Figure 1 and Figure 5 maps of geologic units.

TABLE 1

6-BAND SUPERVISED CLASSIFICATION

Class	Color	1	2	3	4	5	7	Unit
				DN Values Band				
1	Orange	97.5	48.4	60.6	52.8	87.0	55.1	QD
2	Pink	107.2	54.1	68.1	59.9	97.1	59.8	QL
3	Black	54.1	19.3	18.6	12.8	13.2	7.2	SHAD
4	Red	156.6	75.3	90.8	76.5	120.9	77.5	QLB
5	Peach	75.6	36.5	44.9	41.6	76.5	45.8	VO
6	Yellow	108.2	55.5	71.3	61.3	102.6	65.2	QS
7	Purple	75.6	34.4	42.0	36.1	62.0	36.7	PPN
8	Brown	74.9	33.0	39.1	33.3	54.5	32.0	PNM
9	Aqua	81.3	39.8	49.8	44.4	83.2	46.5	IPC
10	Bluegreen	82.6	41.7	54.0	48.8	94.2	52.4	PCC
11	Blue	76.5	36.1	44.6	40.8	81.2	46.5	C
12	Blue	75.5	35.2	44.3	40.1	80.9	47.7	OP
13	Ltgreen	77.0	35.6	42.1	48.4	59.3	27.8	VEG
14	Dkgreen	82.2	41.2	53.9	52.3	96.9	55.6	TV
15	Grey	86.4	39.5	47.3	39.7	66.2	39.1	QA
16	White	88.8	43.3	54.6	47.8	88.7	51.2	QAB
17	Blue	74.5	35.4	44.0	40.0	75.2	43.0	MP
18	Dkgrey	81.7	37.0	43.5	35.2	51.7	26.8	QCS
19	White	170.6	85.6	104.7	87.6	61.9	24.9	QSB
20	Ltred	101.5	48.2	58.6	48.6	59.2	27.1	FPD
21	Sand	108.5	56.0	73.7	69.4	111.9	58.1	TN

CP

Comments on the identification and distribution of units in the CLl classification maps are introduced here:

1) As expected, all units defined from the DVS map as generalized are found in the CLl map, simply because each was specified as a class located at its own training site. Of course, some classes represent combinations of two or more geologic formation units as mapped on the DVS. Combining is necessary because some of these formations occur in outcrops of limited lateral extent owing to complicated faulting evident in the mountain terrain. Thus, a sequence of formations ranging from upper Cambrian to Pennsylvanian in age is exposed as repeating fault slices in the eastern Tucki Mountain, as shown in the original Death Valley Sheet. These units are not distinguishable in the images displayed on the IDIMS TV monitor nor could they be recognized by consistent differences in DN values when a cursor on the IDIMS display is placed at locations within the subscene where each formation should occur. For this reason primarily, these units were combined as a single composite labelled CP. In actuality, CP was first subdivided into two classes (CD and OP), but inspection of the DN means for each (Table 1) shows them to be nearly identical, so that the same color and pattern is assigned to both and the composite is labelled CP (undivided).

The class (unit) labelled C, represented by a cross-hatch pattern, dominates the Grapevine Mountains in Figure 1 and is mapped also within Tucki Mountain. When DN means for this unit were obtained independently in a test run, these values were determined for the two Grapevine Mountain sites shown in Figure 4:

1	2	3	4	5	7
77.9	37.0	43.3	41.6	72.8	41.6

The values from this site pair do not differ significantly for the first four bands compared with those reported for CD and OP in Table 1. However, notable differences are evident in Bands 5 and 7. Yet, when a blue was assigned on the screen to the CP unit (which includes a proportion of the C units) derived from training sites solely at Tucki Mountain and the C unit 10 was alarmed as blue green, there was no strongly discernible difference in color distribution between Tucki Mountain and the Grapevine Mountains inasmuch as both blues and blue-greens were similarly dispersed and intermixed over each mountain block. Therefore, it was decided to "lump" the C unit in with the remainder of CP, coloring each blue, even though improved separation might have been accomplished by better training site selection and additional statistical manipulations. The subsequent field examination offered some justification for this combination in that a diversity of lithologies was observed at each mountain, leading to "overlap" of spectral values resulting from similarities of rock types that make up formations of different stratigraphic ages. In fact, the Cambrian (C) unit is described in the Explanatory Data supplement to the DVS as a complex of 14 or more formations ranging in lithology from dolomites through shales to orthoquartzites. Comparable lithologies comprise the younger units from Ordovician to late Paleozoic.

Likewise, an attempt was made during the test run to distinguish a group of Mississippi and Pennsylvania rocks (CM) exposed at the easternmost end of Tucki Mountain. These take on a more reddish color in the false color composite for this subscene. However, again only small differences in DN values mark the means for a training site established during the test for this group. When assigned a separate color, both the training site area and areas where the group does not occur display that color on the monitor. For these reasons the group was included in the CP combination by coloring the alarmed areas as blue rather than being called out as a mappable class.

Looking at the distribution of Tucki Mountain units as a whole, inspection of CL1 indicates only a broad distinction between CP (blue) on the east and the IPC and PCC units (aqua/blue green) on the west. The photo reproduction in Figure 2A fails to clearly separate the aqua from blue-green but this was more apparent directly on the monitor. Most of the pixels in the Funeral Mountains are indeed aqua/blue-green which corresponds to the dominance of Precambrian and lower Cambrian units in that terrain. No one color prevails in the Grapevine Mountains, perhaps the consequence of the variability of units in the Cambrian (C) class; the use of the C pattern in Figure 5 is therefore a subjective interpretation rather than a conclusion from the statistics or color display.

The problems in distinguishing similar units in a mountainous setting where the geologic structure is also complex are considered further in the Discussion section.

2) There are eight classes--QAB, FPD, QSB, QCS, QLB, VO, VEG, and SHAD--- not established or mapped in the Death Valley Sheet nor shown in Figure 1. Most have been defined by photointerpretation and spectral data analysis of the Landsat-4 subscene. The last--SHAD--is artificial and self-evident. VEG, or vegetation, is, of course, not usually represented on a geologic map. The only areas within the northern Death Valley, having vegetation dense enough (in excess of 40% ground cover), to produce the vegetation signature (light green) are around Furnace Creek (an area of trees, including date palms, bushes, and grass, as well as a golf course, lodging, and a resort associated with the National Park) and along an intermittent stream channel and spring east of Stovepipe Wells.

The classes called QLB and QSB are picked from the false (and natural) color displays as areas having even brighter reflectances than their associated lake and saline beds respectively. Both classes are nearly vegetation-free and can be singled out by the eye in the field, although their boundaries with the adjacent related units are gradational where observed. They appear definable mainly by their spectral rather than compositional properties. However, they can be regarded as facies units and, as such, are worthy of mapping as separate entities. The QLB pattern (red) in the southwestern part of Mesquite Flat is anomalous in that it sometimes appears in darker tones in black and white aerial (vertical and oblique) photos, possibly an indication of increased vegetation cover at certain times of year.

The units designated QCS and FPD were established by correlating reflectance patterns in the color composites with units defined in a geologic map of Death Valley produced originally by Hunt and Mabey (1966) and modified for use in the Seasat SAR report (JPL Publ. 80-67). The latter map is shown in

Figure 6. The QCS unit colored dark grey in CL1 corresponds to the group
of facies units shown by a diagonal line pattern. Most of this facies lies
within carbonate zones among the saline deposits. On the ground, the surface
of the units appears dark and rough, with silt and sparse vegetation contributing
to this lower reflectance. On the CL1 map the dark grey pattern coincides
with the QCS unit on the south and east of Cottonwood Basin but that unit
fails to be classified on the northwest side. The FPD unit is in reality a
saline playa deposit that forms a very smooth surface (minimal backscatter
in radar images); on the color composite the unit has a bluish cast. Its
occurrence in CL1, indicated by a light red, is nearly coincident with the
map distribution in Figure 6; part of the FPD unit in that map is accounted
for by the QSB pattern in CL1 which suggests a genetic or compositional
kinship.

Two new classes, QAB and VO, were set up on a "hunch" after viewing
the color composites of the subscene. Both are located within the pediment
and alluvial wash slopes between mountain flanks and valley floors. The
Death Valley Sheet and, for the part of the image (upper right) within
Nevada, the map in "Geology of Southern Nye County, Nevada" (Nev. Bur.
Mines and Geology Bull. 77, 1972), label the areas in which these units
occur as Quaternary Alluvium (QAL). But, the unit QAB appears conspicuously
lighter in the Landsat imagery and VO shows up as redder in the natural
color composite. The author postulated that the QAB unit consists of lighter-
colored rocks derived from IPC outcrops in the western Funeral Mountains.
The VO unit is explained as outwash from volcanic (TV) units making up much
of the eastern side of the Grapevine Mountains. Both suppositions proved
correct when the areas containing the units were inspected in the field.

3) The source of the volcanic outwash is a series of volcanic rocks of
Tertiary age, shown as TV on the DVS and as several units on the Nye County,
Nevada map. The units are a mix of rhyolite and dacite flows and pyroclastic
deposits; most are characterized by reddish to buff tones. As rendered (in
dark green) in CL1, the distribution of TV is generally similar but more
widespread than shown on the two geologic maps. The TV unit appears along
the northeast corner of the Funeral Mountains where, in fact, it is nearly
absent on the geologic maps. This green color also shows up sporadically
in other parts of the Grapevine Mountains and at Tucki Mountain as an obvious
misclassification. A pair of small isolated blocks of Paleozoic rock off
the southeast end of the Grapevine Mountains, known locally as Death Valley
Buttes, is classed as a mix of TV and C units in CL1, again a partially
erroneous identification. However, in the lowermost left (SW) corner of
CL1, the green color of the TV unit once more is found; here, the equivalent
area on the DVS is a volcanic unit of basaltic composition. Another elongate
thin dark line just east of Emigrant Wash coincides with a small basalt
flow remnant not shown on the DVS.

Adjacent to the TV outcrop area in the Grapevine Mountains is a unit
of nonmarine tuffaceous sandstone, mudstones, and other sedimentary rocks
comprising the Titus Canyon Formation, which could not be singled out as a
discrete unit for classification. This unit (labelled OLN in Figure 1) is
slightly younger than the TV units and probably contains material derived
from the volcanics. If the Titus Canyon is spectrally similar to the TV
rocks, as is suggested by its lack of distinction in the image, that could
account for some of the apparent increase in distribution of the TV unit
within CL1.

IV-174

4) Several units specified in the DVS map, likewise chosen as classes for this classification, are relatively well mapped in CL1. The QA unit (grey) is properly located in CL1 with respect to DVS as reference. The QL unit (pink) is somewhat less accurately defined but occurs generally where it should at Mesquite Flat. The QS unit (yellow) appears in the interior of Cottonball Basin, where it belongs, but the eastern third of Mesquite Flat also displays this class in CL1, inconsistent with the geologic map. The sand dunes (QD) unit, colored orange, is somewhat more extensive in CL1 in the areas west of Stovepipe Wells and is less in areal extent to the east and north relative to the DVS map. The map may be imprecise here, since the sand dunes cannot be clearly seen along the eastern margin of the Flat in the color composites. Orange tones on the west side of Cottonball Basin are a misidentification, with saline-playa deposits being confused as dunes. The standard deviations for QD and QS overlap in value so that lower than average DN's for QS pixels might be mistaken for those of the QD unit.

5) Two units--PPN (QP in DVS) and PNM (QC)--that represent hill-forming deposits and fan deposits respectively, have proved the most difficult to correctly identify and locate in CL1. In CL1 the purples of the older PPN unit are interspersed in some places with the browns of the PNM unit. The latter appears as brown-dominated patterns having fan-like shapes along the southern edge of the Grapevine Mountains and again around Emigrant Wash, in good coincidence with the DVS. It is sporadic to absent in parts of CL1 southwest of the Funeral Mountains. There, the DVS indicates it should co-exist as an older surface criss-crossed by QA deposits laid over the more dissected alluvial fans containing the cobbles and fragments (often of darker lithology and/or coated with desert varnish) comprising the PNM unit. In general, this PNM=QC unit occurs in flat to tilted surfaces having little relief.

In contrast, the PPN unit produces hills (relief of several hundred meters) of highly dissected soft sediments that in places are almost badlands-like in character. The unit (QP) is represented in the northern Death Valley by the Funeral Formation, described as gravels, fanglomerates, and mudstones of continental origin that are variably lithified. In natural color, the units range from brown through buffs to reddish-grey members.

Training sites for PPN were pinpointed in the Kit Fox Hills and along the west side of Tucki Mountain (where the unit is known as the Nova Formation fanglomerate). The statistics for the two sites were combined for purposes of classification. The DN values for each site are:

	1	2	3	4	5	7
Kit Fox Hills	76.7	34.8	42.6	36.9	63.8	38.5
W. Tucki Mountain	75.7	33.4	39.1	32.5	49.1	27.1

Although similar in the first four bands, the reflectances from this unit show real and significant differences in the two SWIR bands (5 and 7) between the two sites. In an earlier version (1958) of the DVS map, the unit at Kit Fox Hills was different in age (TC on that map) from that at West Tucki Mountain (QP). This difference persists in the CL1 map: much of the Kit Fox Hills is rendered purple but the area at W. Tucki Mountain is shown as an irregular mix

of purples and browns. Both localities "appear" similar in color and topographic expression in the field, but PPN outcrops elsewhere show greater differences.

East of Cottonball Basin, the DVS indicates PNM to prevail, with patches of PPN. In CL1, the purple of PPN dominates, with an increase in the browns of PNM along the periphery of this area of low hills. Three isolated outcrop areas of PPN (QP) appear in the color composites as rounded, isolated prominences of dissected terrain located beyond the northeast boundary of Cottonball Basin. In CL1, each is expressed as a mottling of purple and brown. This, in miniature, focuses on the problem of discriminating between these two classes whose spectral properties are so much more similar than their actual appearances in the field. Apparently, variations in slope angles and aspect for the surfaces making up the hilly PPN unit can produce spectral responses that are easily mistaken for those coming from the flatter PNM terrain. This is reenforced by the prevalence of purples in the fan deposits emanating from Tucki Wash at the east end of Tucki Mountain. The mapped unit on the DVS is QC (PNM) which should have been displayed as brown in CL1.

Other investigators in the Landsat 4 TM program have reported that ratio images can distinguish among several different outwash deposits within the fans flanking mountains that bound Death Valley. Three and even four different outwash units, each representing contributions from different source areas and/or different times of formation, have been discriminated. These ratio images, produced by workers at JPL, Earthsat Corp., the University of Munich, and others, duplicate with impressive accuracy the patterns of the fan gravels shown in the generalized map after Hunt and Mabey (Figure 6). It is safe to say that the present level of classification exhibited in CL1 does not single out these several fan gravel units with any reasonable accuracy nor does it match the discrimination efficiency shown in the ratio images. However, none of the gravel units was established individually during specification of training sites; the more general QA and PNM units include these gravels which were simply undifferentiated when combined within individual training sites.

6) Two units listed in the legend of Figure 1 as TN and PN have also proved challenging to identify. TN corresponds to a unit labelled TC (Tertiary nonmarine) in the DVS. It outcrops in several small areas along the southwest and northeast flanks of the Funeral Mountains and again along the Tucki Wash. The training site for TN lies along the Keene Wonder fault zone at the southwest end of the Funeral Mountains. This site was observed through binoculars during the one-day field trip as an area of light buff rocks at the base of the mountain. In the DVS explanatory supplement, TC is described only as a multicolor assemblage of sandstones, mudstones, fanglomerates, and limestones comprising the Artist Front Formation. Another publication, Death Valley Geology by W. Hildreth, lists this outcrop area as containing travertine deposits at the Keene Wonder Spring. In CL1, the training site is precisely defined by the sand color assigned to it. That color appears again in a small patch on the eastern side of the Funeral Mountains, falling within one of the two outcrop patterns shown in the DVS (the other was not recognized). On the IDIMS monitor, the sand color is evident in Tucki Draw as well. Thus, this distinctive unit was picked out in CL1 at most of its outcrop areas.

The PN unit corresponds to the PC unit in the DVS. During the classification runs, the importance of this unit, which occurs only at the Salt Creek Hills and around Furnace Creek in the study area, was not appreciated, so that it was not set up as a class to be sought. In the field, this omission was judged to be a serious oversight. The PC unit is the Furnace Creek Formation, probably the single most distinctive rock unit in Death Valley, and one quite frequently included in scenic photographs because of its characteristic and photogenic coloring. The formation is predominantly mudstones and sandstones with subordinate tuff, gypsum and borate deposits, that together are marked by bright yellowish-grey, brown, and red colors well exposed in badlands topography (Figure 3B-E).

Despite its absence as a defined class, the PN unit is expressed in CL1 generally at the places where it occurs. When the IPC unit is assigned its aqua color, that same color is also "alarmed" in terrain near Furnace Creek and in the area within the Salt Creek Hills. This would seem to imply that spectral reflectances for PN are similar to IPC. To test this, DN values were later taken within small training site polygons astride PN outcrop areas in the displays of individual bands on the IDIMS monitor. The average of 5 such readings for PN is as follows:

Band

	1	2	3	4	5	7
Av. DN Values	114.5	60.4	75.3	65.3	116.6	70.5

These values are quite different from those of IPC and PCC units listed in Table 1. No explanation can be offered to account for this "false alarming" of aqua pixels indicative of the mountain terrain units at just those areas in the valley where the few PC-dominated hills also occur.

Note that the aqua color also occurs at several places along the southwest edge of the Kit Fox Hills and the fans to their northwest. In the field, several exposures in the QP (PPN) units making up these hills were of notably brighter, more buff colored sediments. These, no doubt, are spectrally similar to the PC unit.

7) A major structural feature, the Furnace Creek wrench fault, is defined in the geologic map. Its presence can be deduced in CL1 (and less so in several of the other class maps) but its trace is faint. It cuts diagonally through the map downward from left to right, passing through the image center. Visually, it affects the color patterns by sharply truncating the purple PPN unit against the orange QD unit; further definition is afforded by a few aqua pixels representing the buff lithologic phase in PPN. The Keene Wonder fault, along the southwest edge of the Funeral Mountains, is nebulously expressed in this and other class maps except where its presence might be inferred from the juxtaposition of aqua/blue pixels against other colors, especially in maps containing bands 1, 5, 7 inputs.

8) Following completion of the series of classifications described in this section, two special classifications were applied to the CL1 data set to test (1) the potential improvement in map quality through a "smoothing" operation, and (2) the relative efficiency of a second type of classifier. The results

are depicted in Figure 7.

The classification shown in Figure 7A utilizes the IDIMS function RECLASS. The function changes the DN (grey level) value of a pixel to the DN (grey level) value occurring most frequently in the pixel neighborhood. This is accomplished by defining a moving window with odd number dimensions (in this case, a 3x3 pixel array) about each data point (pixel) and noting the frequency of occurrence of each DN value within that window. The center point of the window is assigned a new value computed from the chosen multiplicative weights by which frequencies are increased or decreased. The end product of this smoothing or averaging is to "clear out" many of the misclassified pixels within a class boundary, giving rise to an apparent improvement in accuracy. Inspection of Figure 7A seems to confirm this result, despite the replacement of linear class boundaries with blocky or jagged boundaries that result from the squares formed by the windows.

The map generated for Figure 7B uses the RECLASS procedure as well. However, in the CLASFY step, a minimum distance classifier substitutes for the maximum likelihood classifier normally used in this step. The function MINDST works on the same TSSELECT or STAT statistics file that was developed from the same training sites used in the initial CL1 procedure. Comparison of the Figure 7B map with that of 2C shows, from visual examination, that the MINDST result yields some similar class distributions as CLASFY but also introduces many significant misclassifications. Prominent examples include (1) improper locations of the TV unit, which largely disappears within the Grapevine Mountains only to reappear in draws and washes along mountain flanks, (2) notable redistributions between the PPN (purple) and PNM (brown) units which for the most part are now incorrect, and (3) disappearance of aquas and blues from much of the mountainous terrain and reappearance of the aquas in patterns within the valley.

The refined classification map shown in Figure 7A is judged to be the optimum in terms of "believability" produced in the CL series.

9) Before leaving the CL1 effort, one more representation of data quality is in order. An insight into the degree of separability among various classes can be gained by inspecting scatter plots for each class. Typically, the plots show the position of each class in 2- or 3-dimensional spectral space, with each dimension set as the range of DN values for a band or channel of a multispectral sensor. The mean value of the spread of DN values for each band is plotted on an X, Y (and Z) orthogonal axis diagram. The covariance between bands defines an ellipse or ellipsoid centered on the mean point.

On IDIMS, the function STATDP uses STATS data to generate a printer plot for 2 and 3 band multispectral data. The plots for DN values from two different bands, using the TSSELECT statistics compiled for CL1, are shown as Figure 8A and 8B. The first is produced from bands 3 vs. 4; the second from bands 2 vs. 7. In both cases, most of the classes plot close together in spectral space. Only classes 3(SHAD), 4(QLB), and 19(QSB), and to a lesser extent 20 (FPD) are discretely separated both from each other and the remaining, more closely clustered classes. The classes for the Band 3 vs 4 plot all align along a straight line (not shown) and have ellipses with narrow minor axes; those for Band 2 vs. 7 deviate from a single straight line and are composed of broader ellipses. These differences are indicative of the degree of autocorrelation

(or redundancy) between bands. Bands 3 and 4 are strongly cross-correlated; Bands 2 and 7 are notably less so. This conclusion is supported by evaluation of some of the TSSELECT statistics, which are not recorded in this paper.

CL2: Two questions can be posed after consideration of the information gleaned from the CL1 map:

(1) Is the accuracy of class definition and location improved if all pixels in a subscene are included in CLASFY instead of the resampled subset?

(2) Can more be seen and interpreted by enlarging the image (or in effect, using a still smaller subscene)?

To answer these, a simple modification of the CL1 procedure was executed. A subset was selected from the test scene to include a 700 x 730 pixel array centered on Cottonball Basin; this array was not resampled, i.e., it contains all data points. Applying the same TSSELECT training sites and derived statistics, this subset was processed by CLASFY and the resulting classes were assigned the same colors as CL1. The image so produced is shown in Figure 2A. Changes in image content are summarized in this way:

1) At first glance, this new image appears to be just an enlargement of the equivalent part of CL1. However, careful scrutiny shows a finer detail within class patterns and at their boundaries and some small areas are identified as containing classes not evident in the larger subscene. Thus, inclusion of all pixels leads to modest improvement in class pattern sharpness and local detail, but this increase is not significant. Whether the use of all pixels is justified in view of the need to process much more data, will be explored in the Discussion section.

2) The most notable change in CL2 is the recognition of vegetation in places not easily seen in CL1. The light green of VEG now appears along several boundaries (still not obvious in Fig. 2., but evident in full enlargement) between units making up the saline and associated deposits. These are plausible locations in that the vegetation patterns occur at contact zones where ground water is likely to surface.

3) It was hoped that the higher spatial resolution of the full pixel array would better define the different outwash deposits extending over the fans. Overall, the improvement was not conspicuous, although some streamer-like patterns along the fan surfaces were better resolved and one color frequently dominates. Some differentiation between PPN and PNM units in areas where purple and brown intermix does happen but does not lead to notably better definition of the two classes. Of special interest is the presence of blue and bluegreen patterns on the fan surface southwest of the Funeral Mountains. These seem to tie into source areas containing PCC and C units and thus represent more recent contributions to the outwash deposits. Bluegreen dominates in the Tucki Wash as well; the drainage in that draw originates at higher elevation where PCC is the principal outcropping unit.

4) North of Tucki Wash, there are patterns of white which lie within the QA unit. These do not appear when the QSB unit is alarmed but are evident when QAB is alarmed. They are therefore identified as alluvial materials containing a higher percentage of light-colored rocks.

5) The aqua of the Furnace Creek (PN) unit is more readily seen in the valley topography in CL2. The positions thus pinpointed coincide quite well with the DVS map.

CL3: As expected, all 21 classes specified for CL1 are present in this 3-band MSS-approximation case. Classes making up mountain terrain are rather poorly segregated in this version. The aquas and blues depicting the IPC and CP units respectively are crudely clustered in the western and eastern halves of the Tucki Mtn., but some intermixing occurs and the blues are concentrated (incorrectly) in the IPC area. Separation between these units is even poorer in the Grapevine-Funeral Mountain blocks; splotches of peach (VO) also are found in these mountains. In this, as in all other supervised and unsupervised cases discussed in this section, the uplifts are characterized by a speckled pattern of colors suggesting considerable misclassification. The Tertiary Volcanic (TV) unit, in dark-green, is fairly well defined along the east side of the Grapevine Mountains where it occurs; this color is noted further east along pediment slopes and in the VO outwash, as would be expected from redistribution of weathered materials into the northern end of the Amargosa River valley. Presence of this color at the east end of Tucki Mtn. is, in this instance, an incorrect identification. The actual units there are late Paleozoic sedimentary rocks that have some spectral similarity to the TV unit.

The QA unit once more has the broad distribution observed in the CL1 case. In general, most units within the valley floor and mountain flanks have a more splotchy character than they show in CL1, implying a greater degree of misclassification when the Bands 2,3,4 combination is used. Note in particular the presence of white and pink pixels in the red QLB pattern in Mesquite Flat and the widespread interspersion of pink (QL) and yellow (QS) pixels. The unit labelled PPN (purple) has a more limited and scattered distribution in the CL3 map. Only a fraction of the image corresponding to the DVS map unit QP is expressed in purple. Purple patches are developed elsewhere in places where this unit should be absent. The areas noted as PNM seem somewhat more sparse than in CL1. The areas classed as QD (dunes) appear more accurately fixed in CL3 than in other classifications. The FPD unit, however, is more poorly defined in CL3. At the northwest end of Tucki Mtn., the increase in area occupied by QRS is not realistic, in that this unit is almost certainly absent anywhere on the fan slopes. The class VEG, in light green, is confined to patches around Furnace Creek and a long patch around the Jaywalker Spring at Stovepipe Wells, near the CL3 map center. This may be the most accurate assessment of the very limited distribution of vegetation in this subscene.

CL4: Overall, the CL4 image yields a distribution of classes more like that of CL1 than of CL3. However, several significant differences are evident in the CL4 map. In the Tucki Mtn. area, distinction between the IPC and CP units--not particularly good in the CL2 case--becomes even less meaningful when only the blue (1) and shortwave infrared (SWIR) (5 and 7) bands are used. Somewhat better separations are discerned in the Grapevine-Funeral Mountain chain. Aqua and bluegreen colors mark part of the IPC outcrop area and bluegreen is conspicuous where the C unit occurs; a patch of blue suggests the presence of one or more members of the CP sequence of units in part of the Funeral Mountains field mapped as IPC. Pixels for IPC and C units are

reduced in number in the Grapevine Mountains, with a corresponding rise in CP pixels (better displayed on the IDIMS monitor) in areas mapped on DVS. Dark greens signifying the TV unit almost vanish in the CL4 rendition. The PPN class is now more diffusely widespread and again is shown as present in areas (such as the upper right corner) in which it almost certainly is absent or sparse; this is especially evident in the fan and alluvial deposits along the northeast flank off Tucki Mtn. and at the edge of the Amargosa Valley.

CL5: For both this and the CL6 maps, each representing the standard default condition for unsupervised classification on IDIMS, only a small number (9 for CL5) of clusters are generated. These are far less than the 20-21 classes established for the supervised classifications. Moreover, there is not a one to one correspondence between clusters and classes. For some clusters, assignment of a color during alarming causes a pattern indicative of the class given that color in CL1 to appear in CL5 or CL6 in roughly the same places as in CL1, but misclassified areas invariably are also alarmed in that color. Several clusters, when assigned the same class-identifying color, give better agreement in pattern distribution for that class as thus combined despite some erroneous areas also being alarmed. The DN values for such cluster combinations indicate probable kinship, even though taken together the composite DN spread may be high for the class.

Units in the mountain blocks are not differentiated or otherwise effectively mapped in CL5. Comparison of DN values for Bands 2,3,4 in Table 2A with Table 1 reveals that only Cluster 7 can be closely matched to IPC, C, or CP units. When a blue color is assigned to cluster 7, it shows up in the valley at locations where PNM is dominant. Only Cluster 6 pixels prevail in the mountains; blue is assigned to these even though their DN values are well below those in most mountain units.

Colors associated with several valley units (mainly PNM) occur in the Tucki Mtn., Grapevine, and Funeral Mountains, along with the blacks representing the SHADOW class defined in the supervised classifications. Initially, the Plio-Pleistocene unit PPN shows up where it really occurs but also appears (probably as "false alarms") in many places within the rugged mountain terrain and in parts of the valley, and so was rejected. Elsewhere, the distribution of PNM is realistic if both Clusters 2 and 7 are assigned a brown color. The sand dunes unit (QD) (Cluster 5) is more widespread in this case than indicated on the DVS map but its overall locations within the valley are plausible. The grey assigned to the QA alluvium unit recurs both at the left (west) for Cluster 3 and center of the map for Cluster 5 - again a reasonable interpretation based on both geologic map and the false color composite patterns. The red assigned to Cluster 1 for QSB (not subdivided) occupies a smaller surface area but if Cluster 10 is likewise colored red, the result is a good match to the pattern noted in CL1 for QSB in the southwest part of Mesquite Flat but an excess of red elsewhere. The QLB unit, colored pink, occupies much of Mesquite Flat but also is predominant in the Cottonball Basin interior where saline deposits recur instead.

CL6: Eleven clusters are called out when all six reflectance bands are used in this unsupervised classification. Again, within the mountains only one unit, shown in blue, is present. Its distribution is different from that noted in CL5. The PNM unit becomes slightly more widespread in the 6-band case, and once more some areas where it is actually absent are incorrectly alarmed. The light-toned alluvial QA deposits, named QAB in CL1, here stand out in orange when QD is alarmed. Even though two more clusters resulted in this 6-band case, they were not useful in designating two more classes. When, for example, Clusters 2, 7, and 10 were each assigned different colors in a test to see which class best fits the distribution patterns in CL1, the least erroneous color combination was the choice of brown (PNM) for all three.

Thus, the 6-band unsupervised classification yields very few improvements over the 3 bands alone. Neither CL5 nor CL6 does an effective job in recognizing and properly locating most of the classes set up in the supervised cases, although a moderately successful placement of some of the valley units ensues. It is obvious that a more sophisticated unsupervised approach is needed.

CL7:. After the data and image products from the preceding six classifications had been scrutinized and evaluated, the author was persuaded by colleagues to modify the conditions under which the unsupervised classification had been carried out. Several analysts in the ERRSAC group at Goddard claim that they find the unsupervised approach superior to supervised classification. This may be a valid conclusion if a large enough number of clusters (between 16 and 64 for most cases) is initially specified and if they can be systematically combined into a smaller number of clusters. These clusters must then be converted into classes by correlating those which are spectrally similar and spatially in juxtaposition or distributed such that they most probably come from the same classes or subclasses. This correlation usually requires some independent "ground truth", from maps, aerial photos, or famiarity with the scene gained from field work, in making the decisions. Thus, in a sense the procedure is a variant of supervised classification in that clusters are identified as classes after the distribution of pixels in each cluster is determined by displaying them on the monitor and noting their spatial relations to known classes. The statistics associated with each cluster become, in effect, analogous to those obtained from training sites. The major difference is that the full number of pixels believed to represent a class (or combined clusters assumed to belong to that class) are incorporated in the statistics employed in classification rather than just those from the training sites. The analyst also retains the option of setting up one or more subclasses within each class if their spatial distribution warrants this. Conversely, new classes can be established from these clusters if supporting evidence for their reality is found.

The ERRSAC analysts have gained considerable success in this procedural strategy when they apply it to scenes in which land cover/use categories are relatively straightforward. Terrains in the eastern U.S. characterized by forests, farmlands, and metropolitan areas are especially amenable to the approach. To test the effectiveness of this procedure to geologic terrains

TABLE 2A

UNSUPERVISED (DEFAULT) CLASSIFICATION

Cluster	Color	3-Band			6-Band						Unit*
		2	3	4	1	2	3	4	5	7	
1	Red	74.0	92.6	79.0	129.2	65.2	82.3	71.3	114.0	70.5	QLB
2	Brown	31.3	36.0	32.0	71.1	31.6	37.2	32.2	56.4	32.2	PPN
3	Grey	40.8	50.5	44.2	83.1	39.4	49.0	43.5	79.0	45.9	QA
4	Black/White	19.3	18.5	12.8	19.4	10.9	13.0	10.9	21.3	12.3	SHAD
5	Orange/Aqua	46.4	58.6	52.2	85.1	43.2	56.7	53.2	113.7	64.1	QD/MT
6	Aqua/Black	25.9	28.5	23.4	54.4	20.0	19.5	13.8	16.8	8.9	MT/SHAD
7	Brown	36.0	43.7	38.3	76.9	35.4	43.0	37.9	66.9	38.7	PPN
8	–	–	–	–	–	–	–	–	–	–	Margin
9	Pink	55.0	69.6	61.1	108.7	54.4	68.5	59.8	98.1	60.3	QL
10	Red/Brown	69.0	79.0	62.4	65.4	27.6	31.1	25.9	39.7	22.2	QLB/PPN
11	Grey				89.4	41.5	50.0	42.1	62.8	35.6	QA
12	Orange				94.1	45.8	57.2	50.4	84.8	50.4	QD

MT = Mountain Terrain

* / = 3/6 Unsupervised

with little ground cover, the Death Valley subscene was re-examined in this manner:

The mandatory and optional inputs to ISOCLS are modified prior to running that function on the 300 x 320 pixel subset. The number of iterations is increased from 8 to 12. The maximum number of clusters sought is raised from 16 to 32. The minimum distance between clusters (DLMIN) is changed from 3.2 to 5.0 DN units. The latter modifications will have the effect of "breaking apart" each individual cluster (some with a large standard deviation) into two or more smaller cluster ellipses, which can then be identified as classes.

After ISOCLS is re-run on the subset created from these parametric changes, a two-dimensional cluster diagram (STATPLOT) is run on several combinations of band pairs. This plot aids in organizing clusters into classes equivalent to those set up in supervised classification by comparing the spatial distribution of pixels represented by each cluster with that of one or more likely classes. To accomplish this, a cluster number is entered into the pseudocolor (TCC) display program, assigned an arbitrary color, and displayed. Its pixel distribution is noted and matched with pixel positions in CL1 to decide whether the cluster is similar to some class. If so, the identity can be confirmed by reference to class mean data in Tables 1 and 2B. The arbitrary color is then changed to that of the correlative class and an output map is then produced.

This reliance on data and class distribution from the supervised classification to identify the clusters does not fundamentally compromise the unsupervised approach. In supervised classification, the statistical parameters needed to establish classes are derived from selected training sites; in unsupervised, the clusters are based on statistics provided from the entire scene without a priori correlation with ground classes. The clusters can become classes when they can be identified, usually with ancillary information. That information can come from published maps, previous classifications, and other sources.

The Bands 1 vs 5 pairing appears to achieve effective separability, as do 1 vs 7 and others. The plot of the means for Bands 1 and 5 (in Table 2B) and their covariances in X-Y space gives rise to the cluster diagram shown as Figure 9.

A perusal of the CL7 output map (Figure 2B) leads to the following observations:

1) The definition of units in the mountain terrain is still generally poor--inferior to previous supervised classifications. No well-defined concentration of color indicative of Precambrian and Paleozoic units is apparent. The data in Table 2B show the IPC, PPC, and CP units to have a wider dispersion or spread of values in the classification than in the others. The aqua (IPC) seems the only consistent and ubiquitous of the colors indicating mountain terrain units. However, this color is also found in two areas near the upper right corner of the image, roughly coincident with the outcrop pattern of the TV unit. The TV unit itself (Cluster 17), shown in dark green, does appear as a narrow pattern along the east side of the Grapevine Mountains. The upper limit for PPC (Cluster 4) lies beyond the range of DN values for that class obtained from the CL1 statistics, casting doubt on its assignment to that unit except for the spatial location of many Cluster 4 pixels within PPC "territory". The dark blue associated with CP occupies some of the pediment

UNSUPERVISED (EXPANDED) CLASSIFICATION

Class	Band 1	2	3	4	5	7	Probable Unit
			DN Values				
1	157.1	77.0	94.5	79.9	127.6	82.0	QLB
2	69.7	31.9	38.3	34.5	72.2	41.0	VO
3	93.0	44.5	55.1	47.9	79.6	47.2	QAB
4	94.7	50.2	67.8	64.1	136.9	76.4	PCC
5	61.6	26.0	28.6	24.2	49.9	27.0	OP
6	75.8	36.6	46.3	42.7	93.4	52.8	C
7	–	–	–	–	–	–	Margin
8	166.7	81.8	100.7	84.5	70.1	27.5	QSB
9	70.0	30.4	35.3	29.7	43.4	25.0	PNM
10	86.2	39.8	48.0	40.7	64.2	36.5	QA
11	99.4	49.0	61.1	53.7	88.2	53.7	QD
12	54.6	20.3	20.0	14.5	20.6	10.9	SHAD
13	77.6	35.4	42.8	37.1	62.5	36.1	PNM
14	117.9	59.6	75.2	65.3	107.0	67.2	QL
15	69.1	30.3	35.5	30.7	52.7	30.1	PNM
16	84.3	39.8	49.5	43.5	77.2	44.9	QA
17	81.4	40.7	53.0	49.7	108.5	61.4	TV
18	61.4	24.3	25.9	20.1	22.0	12.5	SHAD
19	79.0	36.7	45.0	39.8	70.5	41.0	PPN
20	107.4	53.9	68.0	59.3	98.3	61.0	QD
21	67.2	28.4	32.0	26.3	32.8	18.8	CP
22	94.1	44.8	54.2	45.2	36.0	15.9	FPD
23	86.2	42.4	54.1	48.9	90.9	52.2	IPC
24	52.1	18.3	17.1	11.3	10.7	5.5	SHAD
25	78.3	35.3	41.9	35.5	51.8	29.6	QCS
26	127.5	65.2	83.1	72.3	119.6	74.8	QS
27	70.8	31.8	37.8	33.5	60.3	35.0	PPN
28	93.6	43.7	52.9	44.5	68.9	40.2	QA
29	89.5	45.9	60.6	56.5	115.5	65.1	IPC
30	58.4	23.4	24.8	19.9	35.7	19.2	SHAD(?)
31	75.7	35.8	44.5	40.6	78.8	45.3	PPN
32	120.0	57.7	70.4	59.2	70.2	32.6	FPD

area north (upper right) of the Grapevine-Funeral Mountains, suggesting that there at least Cluster 4 is misidentified as belonging to CP when, in fact, it might be closer to valley units (see below). There is widespread occurrence in the mountains of the purple color associated with the PPN unit. This color occurs sporadically within one outcrop area of PPN (west side of Tucki Mtn.), but presence within the several other ranges is another misclassification. However, the purple pattern shows up again in the hills north and west of Furnace Creek, where the 1977 geologic map (DVS) indicates QP (PPN) to be present.

2) The valley units are better defined, for the most part, in the areas where they are known to occur. QA appears west of Mesquite Flat and again south of that area and in low washes north of Furnace Creek. The conspicuous south-trending, light-colored outwash deposit (QAB) is distinguishable from QA by its higher values of Bands 5 and 7 DNs and is again set apart as a separable unit, shown in white. The PNM unit (in brown) is found generally where it is supposed to be but its distribution is excessive in the Amargosa Valley. None of the PNM Clusters 9, 13, or 15, when colored peach (VO) instead, effectively reduced the brown in the Amargosa Valley without introducing the VO unit into Death Valley where it is likely to be totally absent. Cluster 2 is exclusive to the Amargosa Valley; it is alarmed there in grey instead of peach. The orange associated with QD is distributed in generally the same areas noted in most of the other classifications; in all such instances this unit is more widespread than indicated on the DVS map but the Qs unit of that map is closely defined by the morphological expression of the sand materials as distinct dunes.

3) The units within Mesquite Flat and the salt flats in and around Cottonwood Basin are also well defined. The QL unit (pink) appears where expected in Mesquite Flat but it shares some of the area there, as well as at Cottonwood Basin, with QS (Cluster 26). Cluster 1 when shown in red corresponds to QSB but occupies a smaller area than in CL1. Cluster 8 is quite different owing to the much lower values for Bands 5 and 7 digital counts. This cluster defines the small areas (in white) along the east perimeter of Cottonwood Basin. Not only is the material for QSB in those areas spectrally different from that making up Cluster 1 (mainly a difference brought about by much greater amounts of saline minerals relative to playa clays), but it remains largely free of any vegetation cover during the year whereas QLB seems to vary considerably with the seasons owing to vegetation changes. Both Cluster 1 and 8 materials are different from those making up Clusters 22 and 32. When pixels representing Clusters 22 and 32 are displayed alone on the IDIMS monitor, they concentrate in the parts of Cottonwood Basin coincident with FPD units (light red) in CL1. Cluster 25 pixels largely coincide with the QCS unit defined in CL1.

4) The net result of this 32 cluster unsupervised classification can best be surmised from inspection of Table 2B in which those supervised classification units presumably recognized in CL7 are listed. Classes established for CL1 that are not recognized in CL7 are: C, TN, PN, and VEG.

Ratios and PCA: Before embarking on a discussion and evaluation of the information presented in this section, a brief analysis of two other image products is now considered.

The first is a color ratio composite made by combining (superimposing) ratio images for bands 5/7 (projected as red), 3/4 (green), and 5/2 (blue), shown in Figure 10A. The IDIMS function DIVIDE which creates each ratio image (which is then stretched for higher contrast) does not produce numerical output of ratio values. These can be roughly estimated from the supervised 6-band data in Table 1 to aid in determining possible relationships between resultant color patterns and classes and geologic features recognized in the scene (Table 3).

Podwysocki et al. (1982) used the same ratio and color combination as above to characterize the spectral response of materials comprising the mineralized/altered geologic units and associated vegetation in the Marysvale, Utah mining district. They noted these associations between colors and rock and vegetation classes:

Cyan to Light Blue	= Limonite	Green	= Spectrally Flat
Yellow	= Argillitic Alteration	Magenta	= Pine/Juniper
White	= Argillite + Limonite	Deep Blue	= Sagebrush
		Red/Orange	= Grasses

These color-class associations may offer some guidance in interpreting the Death Valley ratio composite but the arbitrary contrast stretches, the differences in rock materials and vegetation, and other factors introduce uncertainties that limit the extrapolation of the Podwysocki classification to this Death Valley scene.

The vegetation near Furnace Creek, around the Jaywalker and Stovepipe Wells, and wells and springs in northern Mesquite Flat all are rendered in the red/orange colors predicted from the list above. The yellow tones are present in places where argillitic weathering products are compatible with the inferred geologic materials present in the outwash deposits. The cyan color in the valleys may express the occurrence of limonitic pigments in the alluvial deposits but this color also appears where the geologic map indicates saline crust and other evaporite deposits. The magenta pattern around Cottonball Basin corresponds in large part to carbonate and salt units on the Seasat geologic map (Figure 6), representing both light and dark reflectance units evident in the false color composites. But, magenta is also characteristic of the PPN and PNM units and of the IPC unit on the west side of Tucki Mtn. as well. However, mysteriously this color is not evident in the outcrop areas along the southwest flank of the Grapevine Mountains. The deep blue associated with both QA and QLB unit locations around Mesquite Flat may represent sagebrush (noted in the field), as suggested from the list above, or more likely is indicative of the spectral responses of the surface materials themselves. All of these tentative identifications are speculative and must await more study.

TABLE 3

BAND RATIOS

Class	5/2	3/4	5/7	Unit
1	1.80	1.15	1.58	QD
2	1.79	1.37	1.62	QL
3	0.68	1.45	1.83	SHAD
4	1.61	1.19	1.56	QLB
5	2.10	1.08	1.67	VO
6	1.85	1.16	1.57	QS
7	1.80	1.16	1.69	PPN
8	1.65	1.17	1.70	PNM
9	2.09	1.12	1.79	IPC
10	2.26	1.11	1.80	PCC
11	2.25	1.09	1.75	C
				CP
12	2.30	1.10	1.70	OP
13	1.66	0.87	2.13	VEG
14	2.35	1.03	1.74	TV
15	1.68	1.19	1.69	QA
16	2.05	1.14	1.73	QAB
17	2.12	1.10	1.75	MP
18	1.40	1.24	1.93	QCS
19	0.72	1.20	2.49	QSB
20	1.23	1.21	2.18	FPD
21	2.00	1.06	1.93	TN

Figure 11 contains the black and white images of each of the six numbered Principal Components produced by the KLTRANS function on IDIMS. The first (1) component image is essentially an expression of the relative albedos of the surface materials and classes. In the second component (2) image, vegetation is singled out by its light grey tone while some of the brightest tones in component 1 now are quite dark. In component 3 the light tones in the mountain terrain correspond to shadows (dark in component 1 and largely removed in the ratio image) while the saline and alluvial deposits become dark and those identified as FPD appear in conspicuous light tones. The light outwash deposit QAB is defined by a dark tone and the PNM unit west of Tucki Mtn. is expressed by a light tone (dark in component 1). The hills composed of the PPN unit are emphasized by a speckled tone pattern. Still different tonal patterns emerge in component 4 and 5 images where details of the salt flats are brought out by contrasting light and dark tones and subtle drainage patterns on the pediments now stand out. Component 6 shows mainly "noise" effects.

In Figure 10B, the images of the first three components have been combined into a color composite using the colors shown. The version reproduced in the figure is not as varied in color contrasts as the image itself directly on the IDIMS monitor, where the vegetation shows as a more pronounced green and the QAB outwash deposit takes on a yellow-orange distinct from its surroundings.

Neither the ratio composite nor Principal Components images prove especially helpful in discriminating different rock units in the mountains. Their chief contribution comes from the color patterns evident in pediment and fan slope terrain and the flatter valley floor.

Quantitative Measurements of Accuracy:

Presumably the best determination of accuracy in geologic units mapping is to match the computer classification units map with the corresponding geologic map. This is true provided the units on the classification map bear a one-to-one relation to those on the geologic map and allowances are made for surface cover that differs from the units as conventionally mapped or consists of non-geologic features and materials. This approach to accuracy measurement will be pursued later in the present study. Here I report another quantitative measure that represents a good approximation to the estimation of accuracy by means of a digital matching of classification units and geologic maps.

The calculations are here referred to as the back classification method. Two sets of polygons within the image are established: (1) the original training sites, with units chosen from geologic maps, image interpretation, and field study, and (2) verification sites, composed of units mapped by the classifiers and named according to the units expected at each site after utilizing the same controls stated in (1). The verification sites are outlined on the image in the same manner as used to select and define the training sites. Errors of commission are then determined for training sites and for verification sites. In effect, the procedure computes the percentage of class X in the training or verification polygons (Figure 4) assigned to that class. The percentage is just 100 times the ratio of the number of pixels identified as X from the statistical parameters to the total of X and non-X pixels (non-X representing all those from the non-X classes confused with X).

Results of these calculations are recorded in Table 4. The class names by symbol comprise the rows. Each of the four columns consists of percentages for training sites (left set of numbers) and for verification sites (right set). The first and second columns treat the data obtained using the maximum likelihood classifier; the first column denotes the standard classification values and the second treats the percentages using the RECLAS procedure. The same arrangement describes the third and fourth columns which however consist of percentages obtained from minimum distance classifier results. Averages are computed at the bottom of the table; those in the maximum likelihood columns are further subdivided into percentage for 13 valley classes and 6 mountain classes (excluding SHAD and also VEG).

Six general observations can be drawn from these data:

1) The "purity" of the training sites is greater than that of the verification sites.

2) The maximum likelihood classifier is clearly superior to the minimum distance classifier in this study.

3) The RECLAS function significantly improves accuracy.

4) The accuracies for valley geologic units is 2 to 3 times better than for those in mountain terrains.

5) Accuracies for several mountain units are "ridiculously" low. Reasons for this are extreme variation in slope and aspect and presence of shadows in the polygons even though care was taken to avoid these during site selection.

6) The verification values for classes TN, QSB, and QD are anomalously low because most of the area actually occupied by these units was "used up" in the training sites, leaving little more to be verified by extension; VEG was eliminated completely because the class was found almost exclusively at the training sites.

Discussion of Analytical Results:

One conclusion stemming from the Death Valley study stands out as paramount in assessing the impact of the results reported in the previous two sections:

In spite of the anticipated improvements in accuracy expected from the superior resolution, broader spectral coverage, and greater sensitivity inherent to the Thematic Mapper, the actual measured accuracy for TM was in the same narrow range (35-60%) recorded for MSS data from the earlier Landsats. Of course, the specific measurement techniques applied in this paper differ in general from those reported by Siegal and Abrams (1976) which are typical of the few accuracy determinations for computer-based classification to be found in the open literature. However, both those results and the accuracy values given in the present study are based on measures of errors of commission between geologic (stratigraphic) map units and sought-after equivalent units recognized by remote sensing from Landsat. The two sets of results are therefore believed to be comparable.

TABLE 4

Method Class Site	Maxlike Verif.	 Train. %	Maxlike Reclass Verif.	 Train. %	Mindist Verif.	 Train. %	Mindist Reclass Verif.	 Train. %
QD	27.0	81.5	50.7	97.4	28.4	70.8	48.4	90.6
QL	57.0	57.7	70.2	72.2	26.3	18.1	28.3	14.8
SHAD	94.4	92.2	100.0	99.3	95.7	94.9	100.0	99.7
QLB	90.3	98.8	100.0	100.0	96.8	92.0	100.0	95.4
VO	85.0	89.5	97.7	99.2	14.0	24.8	11.7	30.5
QS	72.1	79.6	79.8	94.3	46.6	40.6	51.6	40.6
PPN	36.4	48.7	53.2	78.7	16.0	20.1	14.0	28.4
PNM	55.1	78.7	69.7	96.2	46.6	50.0	50.6	48.5
IPC	8.7	12.5	9.3	14.6	5.9	6.8	4.2	3.9
C	8.7	42.9	33.3	61.6	8.5	9.3	3.7	5.1
CD	25.2	35.2	43.2	58.8	1.6	2.0	1.1	0.3
OP	25.2	45.2	27.9	67.8	9.9	6.9	6.3	0.9
VEG		88.8		97.2		59.7		73.6
TV	28.6	48.2	35.7	67.6	34.3	33.5	52.8	55.2
QA	65.2	73.6	74.7	80.1	49.1	58.1	56.9	63.3
QAB	70.4	93.3	77.2	99.4	45.1	75.5	49.4	91.1
CM	16.9	32.6	18.0	49.5	6.7	10.1	1.9	4.4
QCS	76.3	86.6	93.5	99.4	61.3	68.3	80.6	81.1
QSB	59.1	90.0	72.7	97.5	75.0	90.0	93.2	97.5
FPD	80.4	68.0	91.3	76.0	45.8	42.0	52.7	45.7
TN	7.6	85.1	0.5	100.0	16.7	62.9	15.1	81.4
	49.5	65.1	59.9	79.0	36.5	39.4	41.1	43.2
Valley (13)	60.1	79.3	71.8	91.6				
Mountains (6)	18.9	36.1	27.9	53.3				

A valid question is "Why was there no significant increase in accuracy attributable to the TM improvement?". A speculative answer is put forth, as one representing the author's hunch--almost conviction--but one as yet without substantive proof. Stated succinctly, the reason may well be that there is an intrinsic upper limit to accuracy that is largely independent of sensor quality or efficiency. The limit is set instead by geologic constraints or factors. These were alluded to in the introductory section of the paper and will be expanded upon in the next paragraphs. In essence, they relate to fundamental differences between geologic maps (and the units therein) and remote sensing-derived classification maps (and the surface-dominant units these depict).

A published map, such as the DVS used to establish training sites, would seem a strong condidate as the "ground truth" reference. However, it fails to provide an objective basis of comparison, for the several reasons already touched upon in this paper and reconsidered here:

1) As mapped, geologic units are time-dependent or stratigraphic in nature; remote sensing units (specified classes) are a mixture of surface materials and features that a) can be visually tied to geologic map units as expressed by outcrops, correlative soils, topographic expressions, and vegetation associations, and b) are separable by differences in multispectral characteristics.

2) Despite variations in rock composition, texture, age, and degree of surface weathering or alteration, many different geologic units show remarkable similarity in spectral reflectances even if measured under controlled conditions in the laboratory or on the ground. Significant differences may only exist for fresh surfaces; the spectral curves for different rock types reported in the literature usually fall into this category. Convergence of soil types with maturity in a given climatic regime, mass wasting redistribution, superposition of vegetation across lithologic boundaries and other factors serve to modify diverse geologic materials as seen at the surface, such that they begin to resemble one another as they come to share in the homogenizing conditions prevailing around the rock/atmosphere interface. In the Death Valley area, as in much of the desert southwest, rocks of many types tend to be covered with "desert varnish"--an alteration product rich in silica gel, iron, and manganese derivatives. The spectral response of these units is governed more by this coating than by the particular lithology of a unit.

3) Accuracy must necessarily decrease in dissected terrain consisting of steep, variable slopes whose orientations (aspect) may well "box the compass", unless corrected for by normalizing the spectral reflectances to a reference (usually flat) surface. The statistical values derived from the training sites for each class will apply only to identical terrain. Any other parts of the classified scene containing this class will likely consist of assemblages of surfaces with different (non-equivalent) averages of aspect and slope angles. The deviations, which can be non-systematic, will be considerable and hence a prime source of error.

4) Accuracy is strongly conditioned by the "purity" of training sites. Those chosen for this study show, at best, a maximum purity of 79% (p 29). At Landsat scales (effective resolution), sites large enough to provide adequate statistical control will almost certainly be both stratigraphically and spectrally heterogeneous. A specified stratigraphic unit in reality may consist of members with varied lithologies in a sequence that might lie entirely within an area of exposure

which is of ground-equivalent pixel dimensions. This may be further complicated by structural complexities. Units within the eastern Tucki Mtn. are severely faulted, with repeated sections of diverse lithology that will fall within any reasonably-sized training site.

5) Because multispectral images and derivative classifications usually present a new perspective that tends to focus attention on certain characteristics of rock units not evident from air or field inspection, these can frequently be defined as new remote sensing units. The units may have some equivalence to mappable attributes of the geologic/stratigraphic units but often represent surface states or conditions without direct counterparts among those units. The remote sensing units are valid, however, as map units insofar as they can be recognized as meaningful, either in some geologic sense or in terms of a non-geologic class of materials/objects/features of signficance to the geologic purpose underlying the mapping. By introducing classes not already defined on the reference map, this "usurpation" of available surface by these "extra" classes must inevitably reduce overall accuracy. This has happened in the CL1 and other classifications by inserting such units as QAB, QSB, VO and others through photointerpretation and by adding units like QCS and FPD from other maps. Likewise, when units such as OLN are not found, or PN is overlooked, or various lithologic units of Paleozoic age are not differentiated, the accuracy is bound to diminish even further.

If this interpretation holds up and indeed expresses a truism, then what are the consequences and is there any recourse open to solve the problem? The response to the first query is that geologists may simply have to learn to live with the below optimum accuracy of remote sensing classification maps and use them mainly as reconnaissance level aids, or, if the geologic community judges accuracy level as too low for acceptability (as I believe 50-60% to be), we will just abandon them as surrogates for geologic maps and continue to rely on the more conventional methods for making maps with suitable accuracy. A more tractable recourse will be to consider the classes to be <u>remote sensing units</u> only--valid as indicators of what is actually at the surface. With this philosophy, the geologist must then learn how to utilize and interpret remote sensing unit maps <u>per se</u>. He must change his attitude and way of thinking about surficial geology by adopting a new framework based on surface manifestations alone. Eventually, the geologist may become adapt at establishing connections between indirect surface expressions of three-dimensional geology and the bedrock geology below the "noise" of the soil and vegetation that masks the geologic features of interest.

Another conclusion, true certainly for this study, is summarized in the following statement:

> The supervised classification approach appears to be superior to the unsupervised approach when applied to vegetation-sparse surfaces composed of spectrally contrasting rock/soil units distributed in relatively flat to low relief terrain.

For geologic purposes, this statement seems to favor settings in arid country in which a variety of rock units are well exposed in valleys, plateaus, or other terrain consisting of gentle slopes. It implies a potential for reaching a high level of accuracy in terms of correspondence between remotely-sensed units and

formations or other geologic units displaying distinctive differences in material properties that correlate well with spectral parameters. It further implies a range of lower accuracies for rugged terrains in a typical western U.S. setting and even lower accuracies in an eastern U.S. physiography. For both situations, the presence of heavier vegetation cover and perhaps thicker soils accounts for much of this reduction in accuracy. These generalizations have already been reported by other Landsat investigators; this study merely re-enforces these observations.

The 32 cluster unsupervised classification CL7 approaches the quality of CL1 but some glaring misidentifications and omissions compromise the CL7 accuracy. That classification, furthermore, is really a variant of the supervised approach in that the alarmed pixels for each cluster are identified from prior knowledge. The ground truth in that case is the distribution of classes determined directly in CL1 and, in turn, controlled ultimately by the DVS reference map.

Problems in correctly identifying the class relative to its ground truth-equivalent unit will be greater for some units than for others. This is clearly evident in the Death Valley subscene for such readily confused and poorly separated units as PPN/PNM, QL/QS/QD, and IPC/C/CP. Each of these "look alikes" groupings is marked by spectral similarity in terms of means and by rather large variances. In the field, the characteristics of the units involved--mainly in regard to topographic variability--accounts for much of the misidentification.

Other problems affecting accuracy are inherent to such elements of the remote sensing approach as sensor performance, processing methodology, and image display. The availability of six reflectance bands on TM certainly improves the apparent accuracy. The optimum results are associated with CL1 and CL7, both six band classifications. The three new bands on TM (1, 5, 7) seem to do a better job on rock identification than the three MSS-equivalent bands but the proper test of that conclusion should consist of a comparison with a classification performed on actual MSS data. One can speculate with curiosity on the influence of thermal band 6 data on classification accuracy; further improvement seems likely.

There appears to be a systematic pattern in the variability of DN values for any given class as a function of spectral band (but not necessarily of wavelength). This is revealed by calculating a statistic called the Coefficient of Variation (CV), defined as the quotient obtained by dividing the standard deviation by its mean, and commonly presented as a percent by multiplying the CV by 100. The CV simply expresses the idea that, numerically, the value of the standard deviation will increase in proportion to the increase in the value of the mean. For a series of related measurements over different intervals in a spectral range, equivalent and constant performance of each sensor channel (band) would be indicated by a uniform CV regardless of the differences in DN mean values from one band to the next. The trend for TM bands 1 through 7 is typified by the CVs for four classes chosen at random from the 21 classes in CL1 (most other classes follow the same pattern):

Band:	1	2	3	4	5	7
Class						
QD	4.0	5.5	6.1	6.7	8.1	8.9
SHAD	10.9	19.7	30.2	46.1	88.4	98.1
PPN	11.2	13.1	17.6	20.9	23.4	24.8
CD	15.6	23.5	34.0	34.1	41.3	41.4

The CVs consistently rise going from Band 1 through 7. Some of the variation can be ascribed to the different gains and offsets applied to each channel. The sensitivity of each band may also play a role. The variations in atmospheric backscatter radiance with wavelength also contribute. But, the precise cause(s) of the increase in CV with band number remains to be determined.

The effect of higher spatial resolution seems to be that of a moderate improvement in accuracy relative to a resampled image in which data points are now separated by 150 meters along scan lines (every fifth sample). This does not in itself simulate lower resolution; instead, only a reduced number of samples characterizes the terrain, so that the accuracy must decrease if the variability among classes is of higher spatial frequency than the 5 pixel separation distance as is likely true for some classes. Again, analysis of MSS data for the scene--preferably obtained on the same day as the TM data--using identical training sites and classification methods must be carried out to achieve a suitable comparison.

The relative merits of the particular classifiers used in the CLASFY function in terms of resulting accuracies were surprising in this study. The maximum likelihood classifier was significantly better than the minimum distance classifier (p. 28) in extrapolating the classifications from the training sites to the rest of the scene. The reason(s) for this must still be explored.

The best classification maps (CL1 and CL7) have more readily interpretable information than do the Ratio and Principal Components Analysis images produced for this paper. This is logical in that the geologic units are specified at the outset of the classification procedure whereas in Ratio and PCA processing the patterns of ratio and component levels or steps (which are usually contrast stretched arbitrarily in forming the images) must be correlated with known units. The patterns show highly variable correlation with units: some coincide closely but others are poorly matched or may even lack meaningful relation to the units. Ratio images in particular can be misleading in that certain band pairs have nearly identical ratios for some classes even though the DN values of each band may be dissimilar for different units (e.g., for bands X and Y, Unit A = 50/25 and B = 70/35, or 2.00 for each). Obviously, the availability of six bands from TM increases the probability of finding more individual band combinations with different DN values that give non-equivalent ratios. These band combinations may still need to be used because certain other (rock) classes can be discriminated by them.

Inspection of the Table 3 ratios derived from CL1 means points both to sets of units that tend to yield similar ratios and to band combinations that are not redundant and hence should afford improved separability. Thus, the classes IPC, C, CD, OP, and CM (before grouping) all show similar 5/2, 3/4, and 5/7 values; one would predict difficult separability among these units--a fact born out by both ratio and classification image results--unless other band pairings prove more favorable. Conversely, such units as SHAD, VEG, QCS, and FPD have one or more distinct ratios that minimize confusion. Likewise, the DN values of TV indicate it to have the highest 5/2 and lowest 3/4 ratios, implying efficient separability which, unfortunately, does not occur in the color ratio composite. Three duos of units--QD and QLB, QA and QAB, and PPN and PNM--all show very similar 3/4 and 5/7 ratio values but notably different 5/2 values, suggesting that they can be effectively separated by color differences in the ratio composite. In fact, however, this fails to happen in the color composite shown in Figure 10. Overall, then, that composite does not achieve the quality of units definition and separation evident in ratio composites made by other investigators, for reasons still obscure but undergoing examination.

Concluding Statement:

The results from this experimental study of the efficacy of computer-based classification using Landsat-4 data to map a favorable geologic terrain have been sufficiently encouraging and positive to warrant expansion of the investigation. The work will continue with additional research on the Death Valley image and subsequent examination of scenes from other parts of the U.S. and the world. The following tasks are now underway or planned:

(1) Application of classification techniques to the Ratio and PCA images.

(2) Classification of MSS imagery for Death Valley, for comparative purposes.

(3) Use of DMA topographic data tapes to attempt to improve classification accuracy, particularly in the uplands.

(4) Digitization of the 1977 DVS and the Hunt and Mabey maps, and consequent determination of classification accuracy.

(5) Selection of other subscenes from Death Valley, including at least one with extensive mineralization/alteration.

(6) Testing of the developed classification methodologies and experience on other Landsat scenes (Wyoming; Utah).

These further studies will no doubt bring about better quantification of accuracies, an increase in accuracy levels themselves, and improved understanding of the factors that influence the classification process. However, evaluation of the work done in this paper prompts the author to reaffirm one of his previous general conclusions, which here serves also as a prediction. Thus, classification of remotely sensed data pertinent to geologic mapping but without concommittant field work will by itself probably never lead to levels of accuracy that meet the demanding standards of the professional community. These levels, while seldom explicit, should exceed 90% in conventional larger-scale maps; levels below that may be acceptable in reconnaissance geologic maps. The inherent

inability of remote sensing to decipher the stratigraphic nature of rock units will prevent multispectral classification from becoming a stand-alone approach. Nevertheless, as spatial resolution improves and optimal spectral bands for identifying rock materials are specified, use of classified multispectral remote sensing data from air and space when coupled with supporting field calibration and checks will quite likely become the dominant way in which geologic mapping is carried out in future decades.

REFERENCES

Blodget, H.W. and G.F. Brown, Geological Mapping in Western Saudi Arabia
   by Use of Computer-Enhanced Imagery, USGS Professional Paper 1153, 1982.

Cornwall, H.R., Geology and Mineral Deposits of Southern Nye County, Nevada,
   Nev. Bur. of Mines and Geology, Bull. 77, 1982.

Hildreth, W., Death Valley Geology, Death Valley Natural History Association,
   1976.

Hunt, C.B. and D.R. Maybe, Stratigraphy and Structure, Death Valley, California,
   U.S. Geol. Survey Professional Paper 494-A, 1966.

Podwysocki, M.H., D.B. Segal, and M.J. Abrams, Use of Multispectral Scanner
   Images for Assessment of Hydrothermal Alteration in the Marysvale, Utah,
   Mining Area, U.S. Geol. Survey Open File Report 82-675, 1982.

Siegal, B.S. and M.J. Abrams, Geologic Mapping Using Landsat Data, Photogrammetric
   Eng. and Remote Sensing, v. 42, no. 3, 1976, pp. 325-337.

Streitz, R. and M.C. Stinson, Geologic Map of California: Death Valley Sheet
   (1:250,000), Calif. Div. of Mines and Geology, 1977.

FIGURE CAPTIONS

Figure 1:   Generalized geologic map of the Northern Death Valley study
            site, drawn from the 1977 Death Valley Sheet (1:250,000).

Figure 2:   The classification maps produced by Supervised (left page)
            and Unsupervised procedures; see text for details.

Figure 3A: A. This panoramic view is taken from the highway north of Tucki
            Mountain looking northeast across Mesquite Flat towards the Grapevine
            Mountain. QA deposits make up the foreground. QD appears as a
            line of dunes in the middle. Beyond are its PPN units, including
            the light colored phase, and dark PNM units against the mountains.
            The Death Valley Buttes block is seen near the center right.

            B. A closer view of the dune field near Stovepipe Wells. The
            vegetation may correspond to part of the VEG class in that vicinity.

            C. This scene shows the western end of Mesquite Flat looking
            north along the valley bounded by the Cotton Wood Mountains on
            the west and the Grapevine Mountains to the east. The tapering
            strip of grey in its middle is typical QA. Limepan Playa lies
            beyond where the light tone is present. No equivalent of QLB
            is visible in this photo and it defied detection through binoculars.
            The gravelly surface in the foreground makes up part of the QA
            unit.

            D. The west end of Tucki Mountain is viewed to the south showing
            part of the QA fan deposits, hills of PPN beyond and IPC and PPC
            units toward the upper left. A dark unit at the base of the hills
            is a lobe of PNM.

            E. The north face of Tucki Mountain exposes several of the Precambrian
            and Paleozoic formations characteristic of the uplifts. Units on
            the left are probably Cambrian through Devonian in age. Reddish
            quartzites are exposed in the lower right, with Precambrian units
            above and to the west.

            F. The northeast end of Tucki Mountain is seen in the distance. A
            large fan of QA deposits lies against the flank. Hills of PN stand
            out in light colors in the valley. Part of the Kit Fox Hills comprised
            of PPN lies somewhat closer. At right center is the terrain of
            Death Valley Butte.

Figure 3B: A. The strongly dissected terrain of the Kit Fox Hills in the middle
            ground is composed of PPN. The gravel surface is QAB.

            B. Looking eastward from the highway 58 cutoff one sees the northern
            end of the Funeral Mountains, where IPC units occupy the lower region
            and Cambrian units the higher ridges. The broad light colored area
            at the base is the PN training site locality, where travertine,
            sediments, and tuff are exposed. The brownish hills are probably
            the PNM unit. The foreground gravels are QAB.

C. The southern end of Cottonball Basin includes the FPD unit (bright) and QCS. This view looks northeast from the Furnace Creek Inn across the tree-covered Furnace Creek Ranch now occupied by tourist facilities and the National Park Service buildings.

D. The center of Cottonball Basin is visible from low hills (foreground) of PNM; QCS, FPD, and QS units make up the flat areas within the basin.

E. At a preserved historial site of a 19th century borax processing station just north of the NPS exhibit building, the scene extends across a tongue of saline deposits, a QA surface, and isolated hills comprised of the bright PN unit. A spur of Cambrian rocks appears to the right, with the Funeral Mountains against the skyline.

F. Along the east side of the Grapevine Mountains (with Cambrian units in the background) are lower hills of the reddish TV unit. The soil in the foreground is typical of the VO unit. The dark hills at the right may be the OLN unit.

Figure 4: Location of training sites for CL1 through CL4.

Figure 5: Classification map drawn from interpretation of CL1 map; see Figure 2 for Legend.

Figure 6: Map of geologic units at Cottonball Basin and environs, produced for 1982 Seasat report, modified from Hunt and Mabey, 1966.

Figure 7: RECLASS and MINDST images of Northern Death Valley study area, made from CL1 data set.

Figure 8: Cluster plot of Bands 3 vs 4 and 2 vs 7 DN means and standard deviations for CL1 data set.

Figure 9: Cluster plot of Bands 1 vs 5 means and covariances made from CL7 data set.

Figure 10: Left - Color ratio composite image of Northern Death Valley study area, using 5/7 (red), 3/4 (green) and 5/2 (blue) projection; Right - Color composite made by combining the first three Principal Components as (1) red, (2) green, (3) blue.

Figure 11: Black and white versions of the first six Principal Component images of the Northern Death Valley study area.

1977 GEOLOGIC MAP OF DEATH VALLEY

Figure 1

LEGEND

(QD) DUNE SAND (ORANGE)

(QAB) QUATERNARY ALLUVIUM
BRIGHT   (WHITE)

(QA) QUAT. ALLUVIUM (GREY)

(FPD) FLOOD PLAIN DEPOSITS (LT RED)

(QSB) QUAT. SALINE BRIGHT (WHITE)

(QS) QUAT. SALINE (YELLOW)

(QCS) QUAT. CARBONATE/SALT (DK GREY)

(QLB) QUAT. LAKE DEPOSITS
BRIGHT   (RED)

(QL) QUAT. LAKE DEP. (PINK)

(VO) VOLCANIC OUTWASH (PEACH)

(VEG) VEGETATION (LIGHT GREEN)

(PNM) PLEISTOCENE NONMARINE (BROWN)

(PPN) PLIO-PLEIST NONMARINE (PURPLE)

(PN) PLIOCENE NONMARINE (AQUA)

(OLN) OLIGOCENE NONMARINE (NR)

(TN) TERTIARY NONMARINE (SAND)

(TV) TERTIARY VOLCANICS (DK GREEN)

(OP) ORDOVICIAN — PENNSYLVANIAN
MARINE   (BLUE)

(C) CAMBRIAN MARINE (BLUE)

(PCC) PRE-CAMBRIAN-CAMBRIAN MARINE
(BLUE GREEN)

(IPC) LATE PRE-CAMBRIAN META./SED.
(AQUA)

U = UNDIVIDED
B = BASALT
NR = NOT RECOGNIZED
S = SHADOW

LOCALITIES

AD = AMARGOSA DESORT
CB = COTTONWOOD BASIN
CCF = COTTONWOOD CANYON FUN
EW = EMIGRANT WASH
FC = FURNACE CREEK AREA
FM = FUNERAL MOUNTAINS
GM = GRAPEVINE MOUNTAINS

KF = KIT FOX HILLS
KW = KEANE WONDER SPRINGS
LP = LIME PAN PLAYA
MF = MESQUITE FLATS
SC = SALT CREEK HILLS
SW = STOVEPIPE WELLS
TM = TUCKI MOUNTAIN

Figure 1 (Continued)
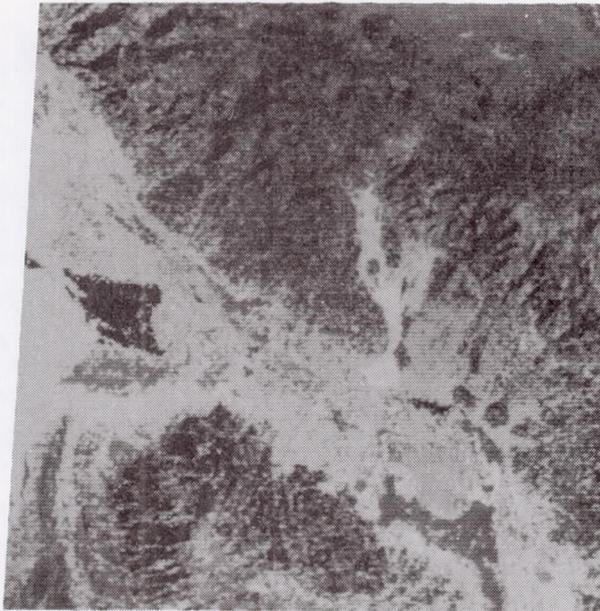
CL1 — SUPERVISED CLASSIFICATION:
BANDS 1, 2, 3, 4, 5, 7
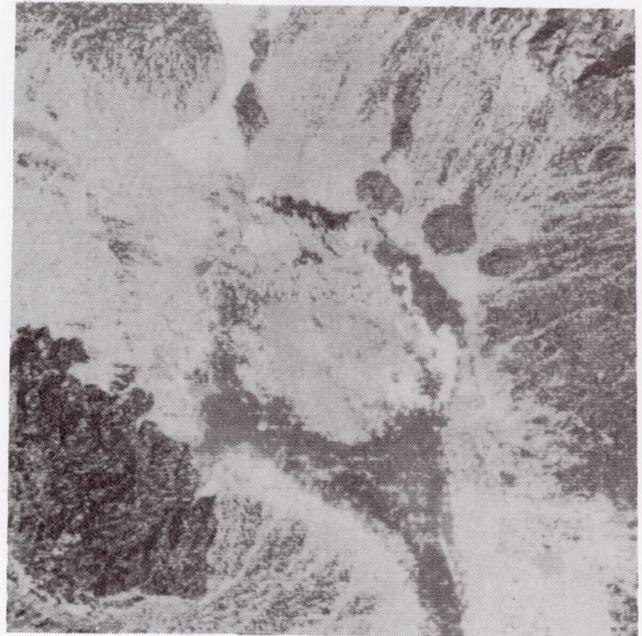
CL2—SUPERVISED 6—BAND ENLARGED

CL3 — SUPERVISED CLASSIFICATION:
BANDS 2, 3, 4
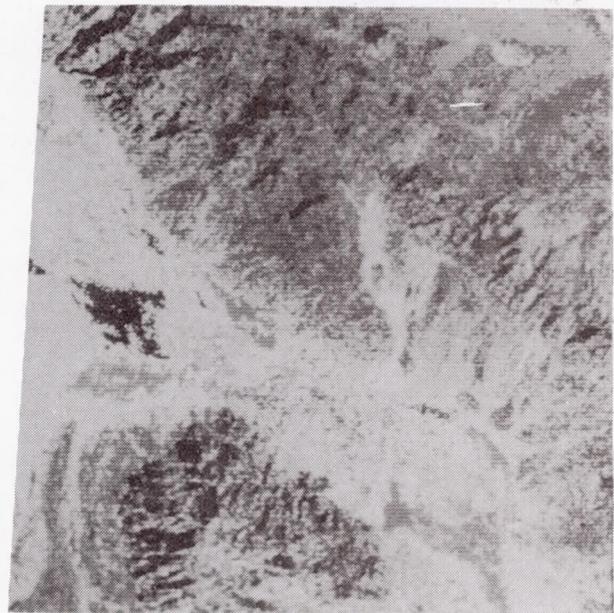
CL4 — SUPERVISED CLASSIFICIATION:
BANDS 1, 5, 7

Figure 2A

**CL5 — UNSUPERVISED CLASSIFICATION:
BANDS 2, 3, 4**
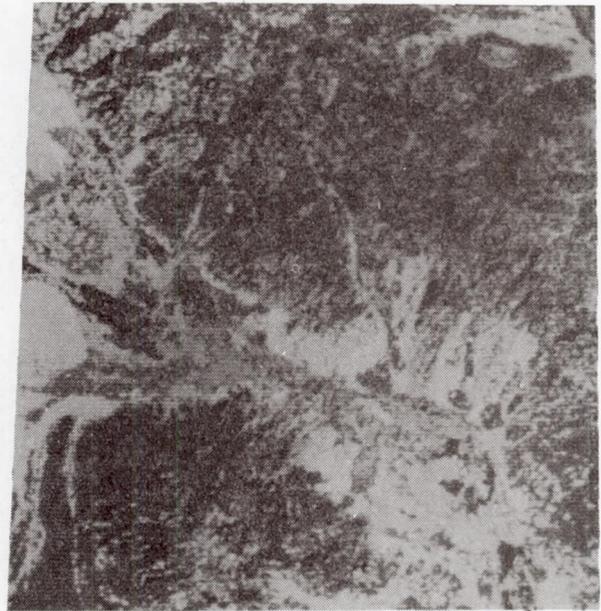
**CL6 — UNSUPERVISED CLASSIFICATION:
BANDS 1, 2, 3, 4, 5, 7**

LEGEND

	(QD)	DUNESAND
	(QAB)	QUATERNARY ALLUVIUM BRIGHT
	(QA)	QUAT. ALLUVIUM
	(FPD)	FLOOD PLAIN DEPOSITS
	(QSB)	QUAT. SALINE BRIGHT
	(QS)	QUAT. SALINE
	(QCS)	QUAT. CARBONATES/SALT
	(QLB)	QUAT. LAKE DEPOSITS BRIGHT
	(QL)	QUAT. LAKE DEPOSITS
	(VO)	VOLCANIC OUTWASH
	(PNM)	PLEISTOCENE NONMARINE
	(PPN)	PLIO-PLEIST. NONMARINE
	(PN)	PLIOCENE NONMARINE
	(TN)	TERTIARY NONMARINE
	(TV)	TERTIARY VOLCANICS
	(OP)	ORDOVICIAN-PENNSYLVANIAN MARINE
	(C)	CAMBRIAN MARINE
	(PCC)	PRE-CAMBRIAN-CAMBRIAN MARINE
	(lPC)	LATE PRE-CAMBRIAN-CAMBRIAN META./SED.
	(VEG)	VEGETATION
	(SHAD)	SHADOW

CL7 — UNSUPERVISED (32 CLUSTER) CLASSIFICATION

Figure 2B
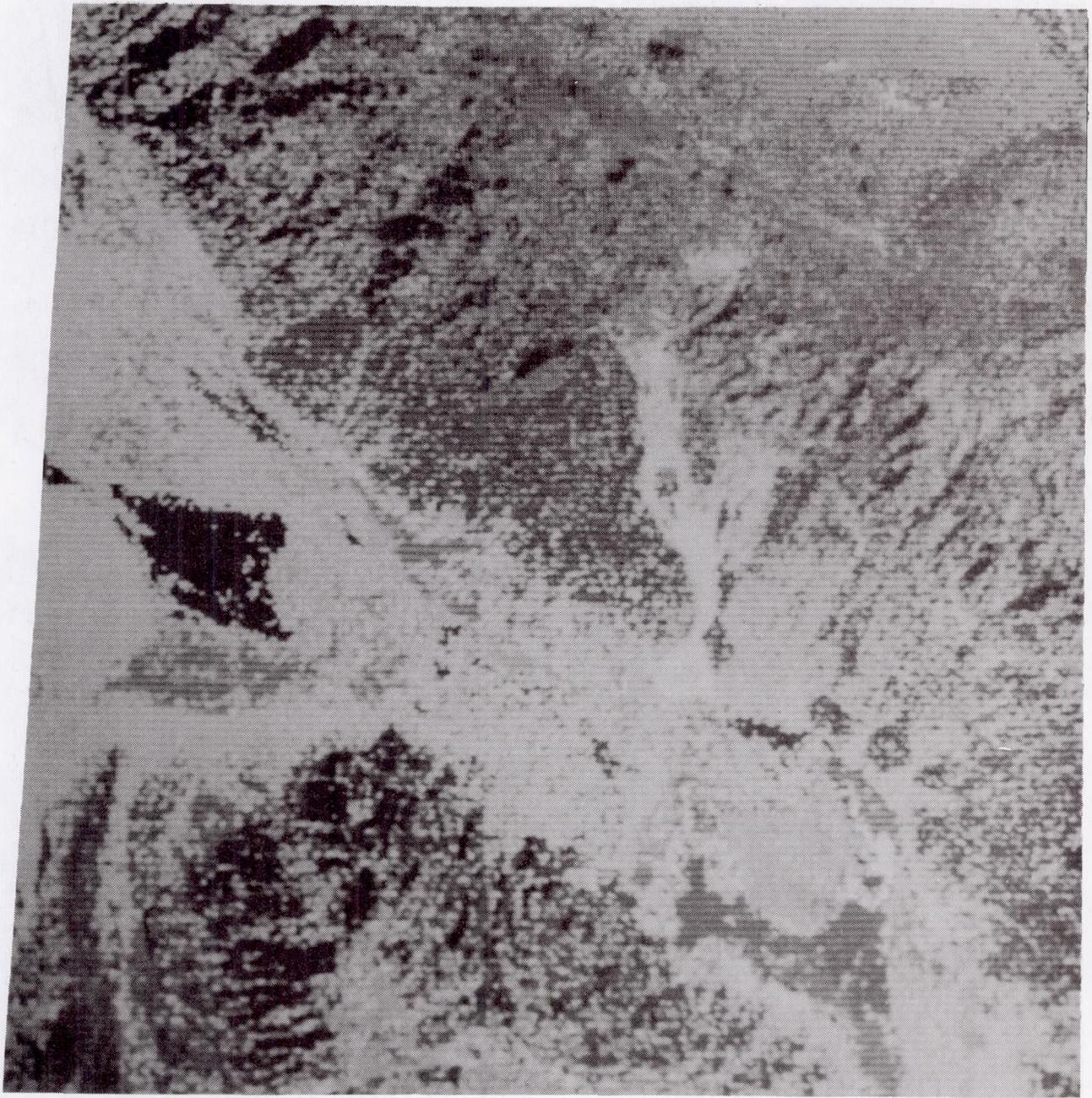
Figure 2C

A

D

B

E

C

F
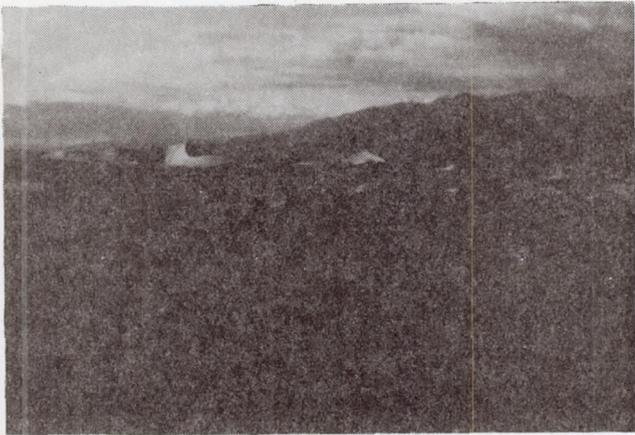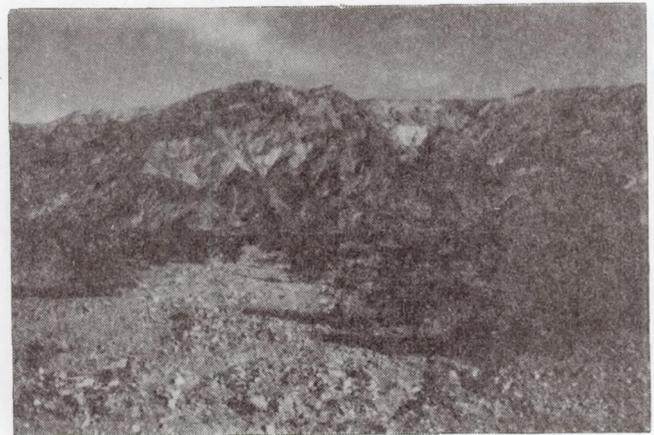
Figure 3A
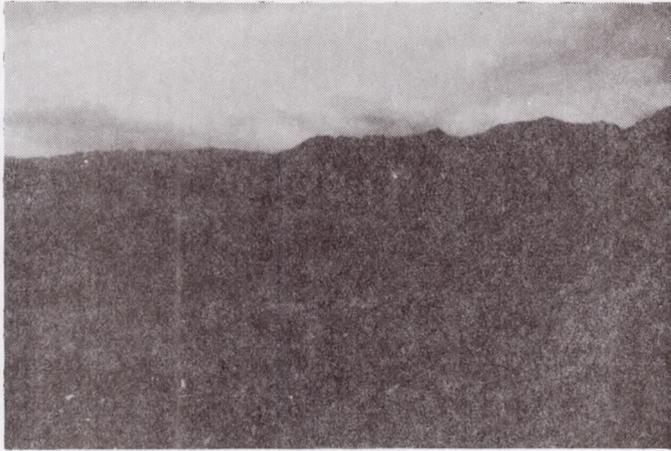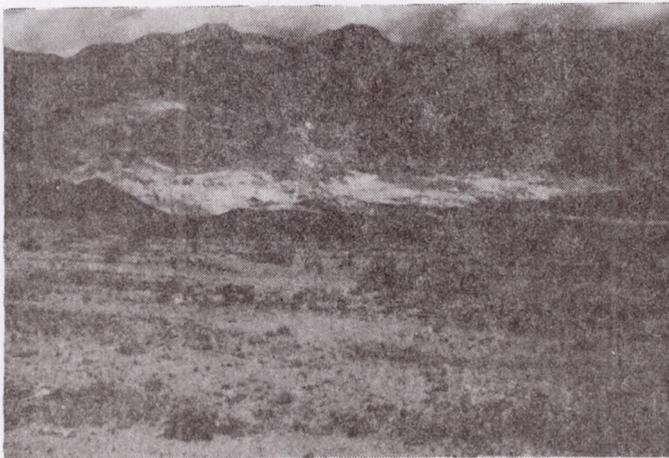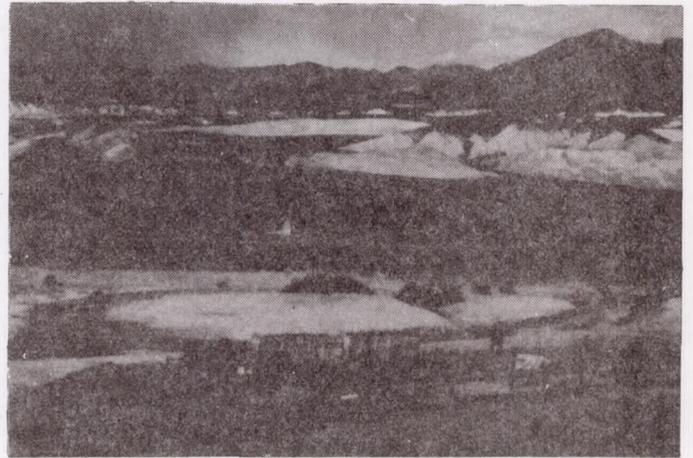
Figure 3B

TRAINING SITE LOCATIONS
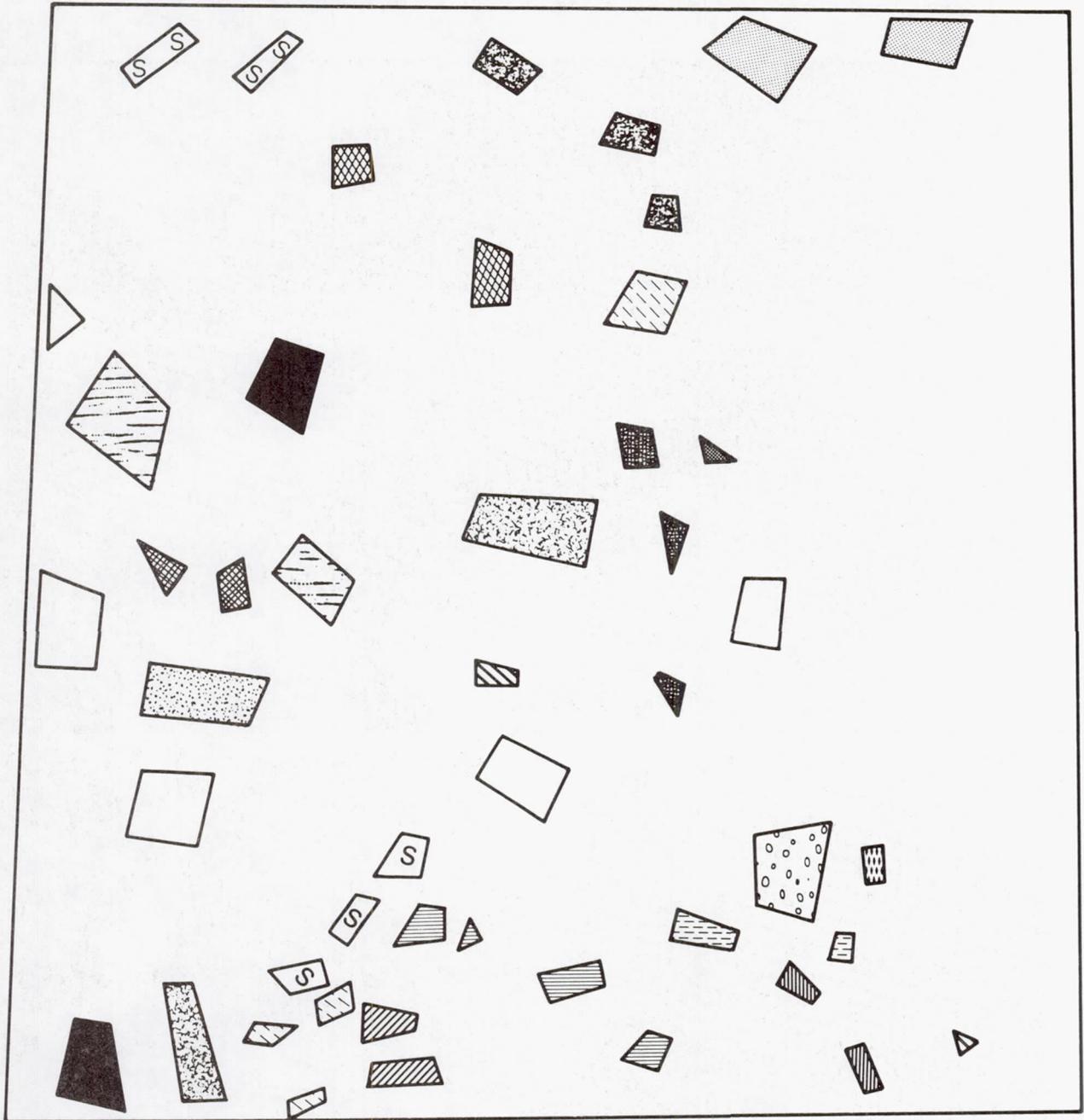
Figure 4

DEATH VALLEY: SUPERVISED 6-BAND

Figure 5

EXPLANATION

	Qse	ERODED SILTY ROCK SALT
	Qsr	SILTY ROCK SALT, ROUGH FACIES
	Qss	SILTY ROCK SALT, SMOOTH FACIES
	Qs	MASSIVE ROCK SALT
	Qsg	MASSIVE GYPSUM
	Qsn	MARSH DEPOSITS, SULPHATE ZONE
	Qcl	SALINE FACIES, CARBONATE ZONE
	Qss	SALINE FACIES, SULPHATE ZONE
	Qcm	MARSH DEPOSITS, CARBONATE ZONE
	Qcs	SAND FACIES, CARBONATE ZONE
	Qcsi	SILT FACIES, CARBONATE ZONE
	Qq4	NUMBER 4 FAN GRAVEL
	Qf	FLOOD PLAIN DEPOSITS
	Qq3	NUMBER 3 FAN GRAVEL
	Qq2	NUMBER 2 FAN GRAVEL
		PRECAMBRIAN TO PLIOCENE ROCKS, UNDIVIDED

QUATERNARY — RECENT
PLEISTOCENE

N

0   10   20 km

Figure 6

SUPERVISED (RECLASS): 6 BANDS   **SUPERVISED (MIN DIST): 6 BANDS**

Figure 7
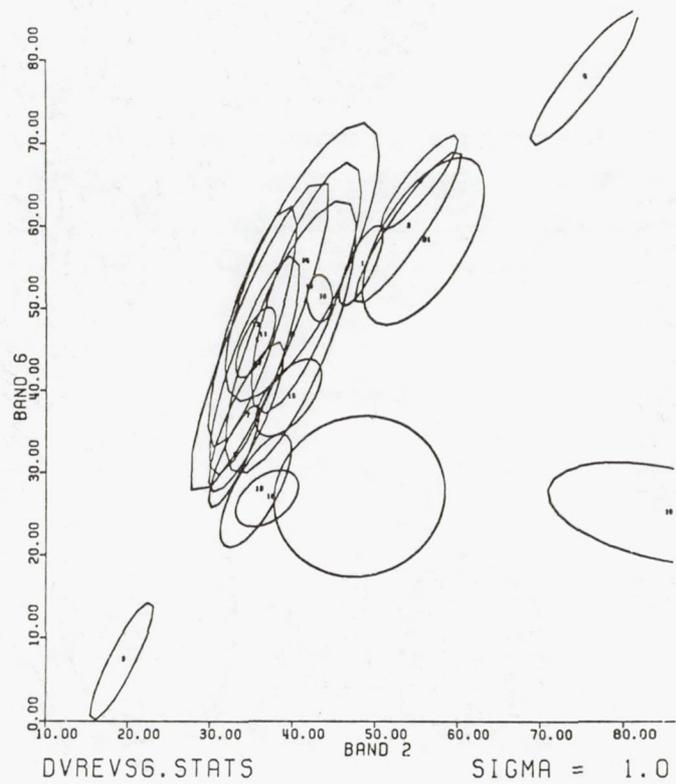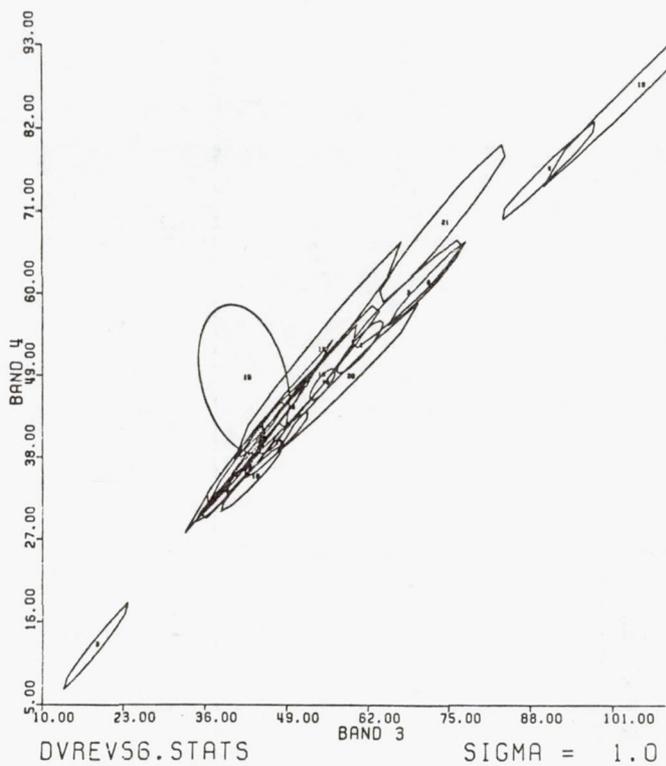
Figure 8

CLUSTER PLOT
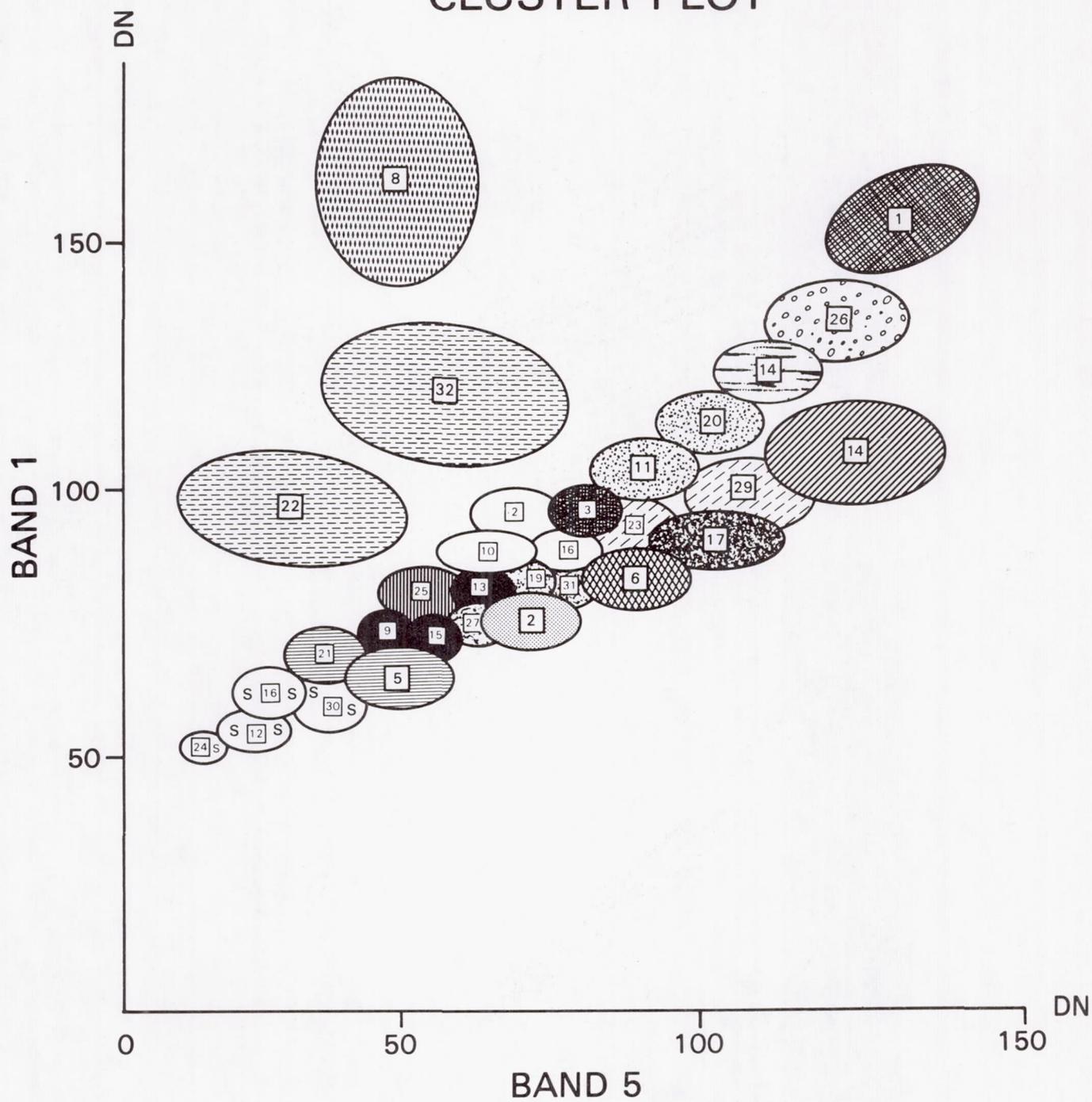
Figure 9

BAND RATIO COMPOSITE:
5/7 (RED), 3/4 (GREEN), 5/2 (BLUE)

PRINCIPAL COMPONENTS:
PC 1 = RED, PC 2 = GREEN, PC 3 = BLUE

Figure 10
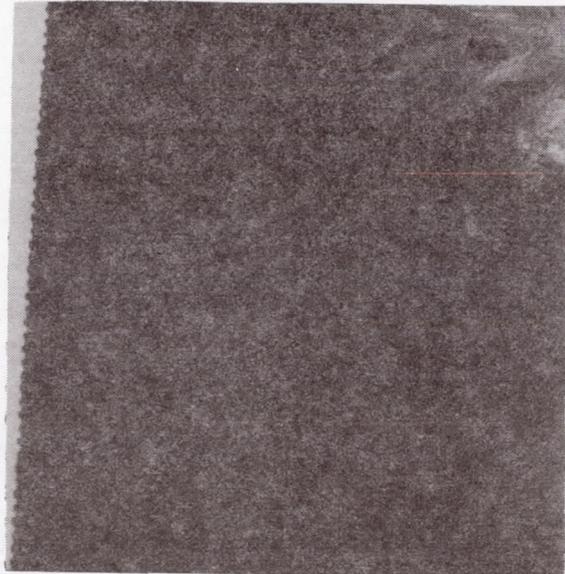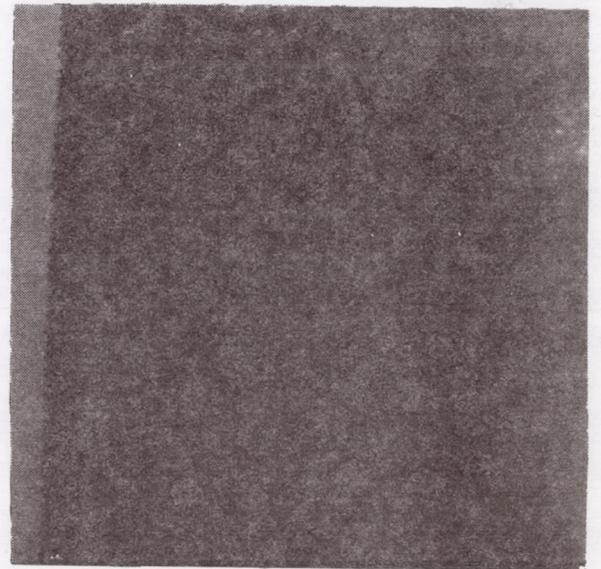
Figure 11

Page intentionally left blank

A CONCEPT FOR THE PROCESSING AND DISPLAY OF THEMATIC MAPPER DATA

Dr. Rupert Haydn

University of Munich
Faculty for Geosciences
Luisenstr. 37, D - 8000 München 2

INTRODUCTION

With the successful launch of the Thematic Mapper on Landsat-4, NASA has
implemented a system which will have tremendous impact on the future of
spaceborne remote sensing. The improved capabilities of this scanner
in comparison to the LANDSAT-MSS form an important basis for evaluating the
operational aspects of remote sensing from space and also for exploring
its implications to the earth sciences, especially in terms of information
acquired within the so called short-wave infrared regions (SWIR) of the
electromagnetic spectrum.

In keeping with the overall goals of this program, it is essential to
improve data availability not only to the existing remote sensing com-
munity but also to potential users with new applications. Therefore,
topics such as image distribution networks and image formats in terms
of optimizing the data content and extractable information within com-
monly available standard products should be emphasized. The purpose of
this paper is to discuss this concept of optimization and to show ways
in which preliminary Thematic Mapper image products might represent a
feasible approach towards the above cited "commonly available
standards".

User Requirements Versus LANDSAT Thematic Mapper Data

With respect to the availability of Thematic Mapper image products, one
must specifically consider the needs of the large potential earth-science
user community, which is not necessarily interested in remote sensing re-
search per se, but in the utilization of remote sensing products as one
of many tools. For the near future, the link between remote sensing

technology and the potential user community has to be established on a level
which adequately meets its requirements on a non-experimental or operational
basis. This can probably be best fulfilled through addressing existing and
well established capabilities for interpretive analysis of image data.

The LANDSAT-4 Thematic Mapper system represents an ideal platform from which
to promote the establishment of such a link. The high resolution capability
of TM brings spaceborne remote sensing into the realm of high altitude aerial
photography. Therefore, the traditional methods in photointerpretation can
now be applied more directly than was possible with lower resolution data. This
poses a challenge for the potential user community which has to be met.
The spectral information acquired by multispectral scanners is a feature
unique to remote sensing technology. The diversity of spectral bands on
TM offers new capabilities for identifying and classifying earth materials
that must be considered in any utilization scheme.

Generally, it can be stated that multispectral information can best be
accessed and evaluated through digital and interactive image processing
techniques. The potential user community, however, has not reached the
level where image processing is being used routinely as a standard tool.
Therefore, for the time being, special effort must be put into development
of strategies that will guarantee optimal utilization of the spectral
information contained in remote sensing data acquired under the varying
conditions affecting each scene. The Thematic Mapper system provides
spectral information in seven carefully selected spectral bands, covering
the visible, near IR, short-wave IR and thermal IR region of the electro-
magnetic spectrum. The challenge is to devise the best approach for pre-
senting this complex spectral information in a pictorial format which can
be understood and accepted as a standard by the growing user community.

Currently, natural and false color images are the standard display products
with which the user community has become familiar. But, if we incorporate one
or both of the short wave IR bands of the TM (bands 5, 7) into the production
of a color image, that community should be willing to accept this as another new
standard which supplements rather than replaces the imagery already in use.

The mere display of individual TM-bands in the form of black and white ren-
ditions cannot be regarded as an optimum standard product because the
actual recorded spectral information is not easily assessed by visual means.
Thus, unique spectral characteristics recorded in one band are most
effectively displayed and identified when considered in combination with or
contrast to other spectral bands. Therefore, the generation of improved
standard products requires a certain amount of image processing in order
to take full advantage of the multispectral information recorded. Taking
advantage of the spectral information means also to generate pictorial
presentations which can be readily understood and "spectrally deciphered"
by the interpreter.

A more detailed discussion on the above requirements is presented in the
following paragraphs.

Some Basic Considerations About the Interpretation of Multispectral Data

For interpretive purposes, multispectral image data can be characterized by two levels of information. These levels will be further referenced as INTERPRETIVE COMPONENTS and they can be subdivided into a PANCHROMATIC COMPONENT and into one or more SPECTRAL COMPONENTS.

Panchromatic Component

This component is characterized through image attributes which a photo-interpreter knows how to handle on the basis of his experiences in the traditional fields of aerial photo interpretation. Panchromatic black and white aerial photographs can still be regarded as the classic data source for photo interpreters. Through a careful analysis of tonal variations, textures, shapes and other image attributes, these pictures provide important information for multidisciplinary earth scientific applications.

Within the context of this paper, the term "Panchromatic Component" is used to specifically address, in a symbolic way, those features of multi-spectral remote sensing data that retain strong ties to the concepts applied in conventional photointerpretation. Thus, the panchromatic component describes basically the first-order effects of image brightness due to surface topography and albedo.

Because of long established methodologies and experience in this dis-cipline, many users of remote sensing data continue to work on straight-forward black and white renditions of the individual spectral bands.

Spectral Components

The term "Spectral Components" indicates a level of information which ex-hibits subtle spectral reflectance contrasts of surface phenomena. Normally, the Spectral Component of a multispectral data set is dis-played through additive colors. However, a Spectral Component can also be presented as a set of black and white images, exhibiting relative differences in spectral information.

In order to further discuss the significance of Spectral Components within the overall concept, it is necessary to point out some simple relationships between multispectral characteristics, color and how color is being incorporated into interpretation schemes.

> The most straightforward and understandable approach
> in the interpretation of the "information source"
> color is based on aerial color photographs. Color
> photographs can be regarded as produced by a multi-
> spectral sensor operating within the visible wavelength
> region. According to the previously given definition,
> the color displayed can be related to the Spectral

Component. Using such photographs, the interpreter is
able to directly relate and compare the displayed colors
with the environment as it is being experienced by him.
Therefore, in this case, color is used on a rather in-
tuitive and empirical basis. It supports directly the
recognition and identification of surface phenomena.
Although it is a fact that color is an expression of
spectral properties, an interpreter of natural color
photographs normally does not think in terms of
spectral categories.

A different situation occurs when analyzing an IR-
false color rendition. The expression "false color"
indicates already that the above intuitive and em-
pirical approach is no longer feasible. Color now
acts as a more abstract source of information. It
becomes involved in the process of analysis in order
to distinguish between various surface categories on
a purely phenomenological basis. However, if the in-
terpreter is experienced in the analysis of IR-false
color renditions, he is able to additionally derive
diagnostic and understandable spectral information
for a limited number of spectrally unique surface
categories.

A typical example along this line is the red appear-
ing vegetation cover on IR-false color composites.
This example serves to demonstrate the transition
from the previously discussed intuitive-empirical
approach to a phenomenological and finally to a
spectral-diagnostic oriented utilization of color.

The empirical approach is based on the simple know-
ledge that healthy vegetated areas appear always red
on false color IR renditions. From a phenomenologi-
cal point of view, one would only identify red colored
areas, without being able to draw conclusions on the
nature of the phenomenon. However, using color in its
spectral diagnostic sense, the corresponding analy-
sis could be described as follows. Red colors in-
dicate increased Near-IR reflectivity in comparison
to the reflectance characteristics in the visible.
Such a spectral pattern can be related to vegetation.

For interpreting multispectral data, especially from the broader spectral
coverage such as the Thematic Mapper System provides, the applicability of
the spectral-diagnostic approach is regarded to be of utmost importance;
likewise, the interpretation of multispectral images from a purely phenomeno-
logical aspect is not an adequate substitution for the above intuitive-
empirical approach. Unfortunately, the spectral-diagnostic approach does

not always work well on IR-false color and other multispectral color composites. The reason for this can be found in the correlative properties of multispectral data. This means that most surface features exhibit similar variations in their wavelength-dependent reflectivity (similar shapes of spectral curves). The combination of highly correlated spectral bands into additive color renditions leads correspondingly to images characterized by subtle color variations that are difficult to perceive and to understand.

Because of these effects, it is important to enhance the Spectral Components to improve their interpretability on a spectral-diagnostic basis.

Conventional Processing Techniques Versus Interpretive Components

From an interpreter's point of view, both the Panchromatic as well as the Spectral Components are equally important drivers for an optimum visual analysis of multispectral data. Therefore, it is essential that any enhancement scheme consider individually the various Interpretive Components. In regard to commonly applied digital image enhancement and display techniques, this requirement is in most cases not being fulfilled. In the following section the relationship between some processing techniques and the above Interpretive Components is given.

RATIO ENHANCEMENT means essentially an enhancement of the Spectral Component. Multiplicative effects caused by changing illumination due to topography are minimized and subtle variations in the spectral slopes between the two ratioed bands are enhanced. A ratio image can be directly used to interpret spectral relationships independent of morphology. This means, however, that the Panchromatic Component must be sacrificed. The creation of color ratio images and also hybrid ratios does not reestablish a Panchromatic Component in the previously defined sense.

CONTRAST ENHANCEMENT of individual spectral band images as a necessary preprocessing step takes advantage of the full dynamic range of the display medium. It affects both components in a positive sense. The disadvantages inherent in the additive color process resulting from highly correlated spectral bands, however, cannot be overcome.

EDGE ENHANCEMENT improves the interpretability of the Panchromatic Component (texture). Color composites of edge enhanced spectral bands are characterized by a slightly degraded Spectral Component.

LINEAR TRANSFORMATIONS and the principal components transformation as a special case may affect both components, depending on the weighting factors applied. Additions of spectral bands enhance the Panchromatic Component but diminish the Spectral Component.

In summary, the commonly applied approaches to the enhancement and display of multispectral data cannot be regarded as a good solution for the generation of optimized image products. The photo interpreter gains the most

intelligible presentation of multispectral data when he bases his analysis of a Panchromatic Component on a scenario with which he is familiar while relying on Spectral Components to provide him with additional spectral-diagnostic information. This requirement has a strong impact on the overall approach in the processing of multispectral and especially of Thematic Mapper data. The approach is based on the following steps:

1. Independent definition and optimization of individual Interpretive Components.

2. Combined display of individual Interpretive Components in a perceivable manner.

Definition and Optimization of Interpretive Components

The definition of the individual Interpretive Components depends, of course, mainly on the number and the characteristics of spectral bands available but also on target areas, as well as on intended applications.

The Panchromatic Component as an information source for image attributes, as described earlier, can be represented by a single band, preferably with a good dynamic range and signal to noise ratio. For processed TM data, as will be demonstrated in this paper, the near IR band 4 has been selected. For optimization purposes, edge and contrast enhancement algorithms were applied. Another possible approach which gives an even better illustration of the Interpretive Components concept is to equate the Panchromatic Component to a First Principal Component image derived from the three visible TM bands.

In order to appreciate the rather simple implications in the definition of enhanced Spectral Components one needs to keep in mind the above requirement of being able to base the analysis on a spectral-diagnostic approach. Thus, each defined Spectral Component has to be characterized by intelligible spectral meanings. Intelligibility, however, is reached if only a limited number of spectral bands are being considered at a time.

The best means for displaying enhanced spectral information lies in the generation of spectral ratios. In this way, the spectral slope between any two bands can be displayed and interpreted independent of the first-order brightness effects that are accounted for by the Panchromatic Component. The Spectral Component may also be defined in terms of thermal or thermal inertia data.

For some applications the Spectral Component can be assigned to more complex ratio transforms which include more than two spectral bands. Such ratios are defined in order to quantify certain surface phenomena which need to be monitored, as for example, the development of vegetation. The ratio transforms are referred to as vegetation or soil brightness indices. In this instance, the Spectral Component will exhibit data on the nature of certain phenomena rather than spectral-diagnostic information.

Pictorial Presentation of Interpretive Components

In the previous section we noted that a multispectral data set can be separated into various "information planes" referenced as Panchromatic and Spectral Components. Each of these components has to be individually defined. In order to improve the value of these components for interpretation purposes, they also need to be individually enhanced. A logical approach to implementing the components concept is to merge and display the defined components within a single image. Figure 1 exhibits a schematic representation of the various steps.

An important boundary condition at this point is, however, that the individually defined components be perceived independently on the basis of the final image product. The use of additive color processes to combine the Interpretive Components would obscure the previously defined and separated information planes. Two alternative approaches for generating image products that display the Interpretive Components in a non-confusing manner are based on: 1) the application of a color coordinate system described as Intensity, Hue and Saturation (IHS), and 2) the generation of synthetic stereo (SST) effects. Both techniques are well established in the field of multispectral image processing. The IHS transforms in one or another modification can be used to analyze color images or to combine multisensor data. The introduction of a synthetic parallax function is applied to generate true stereo images on the basis of digital terrain models or to display other kinds of non-imaging data such as geophysical and geochemical measurements. For a better understanding of the utilization of these techniques, a short summary is given.

Intensity, Hue and Saturation (IHS) Color Coordinate System

In the theory of the IHS-color coordinate system, any color image triplet based on the red, green and blue (RGB) primaries can be represented alternatively by three independent parameters which describe color in terms of its Intensity (I), its Hue (H) and its Saturation (S). These parameters will be perceived independently by the human observer. From a processing point of view, Intensity, Hue and Saturation can be represented as three data fields or grey tone images in which each field is individually manipulated. In order to visualize the effects of IHS-manipulations on the corresponding color presentation, they have to be retransformed into an RGB-system (Figure 2a). A specific scheme for combining Panchromatic and Spectral Components through an IHS-RGB retransformation is shown in Figure 2b.

By treating any three images, A, B, and C respectively as Intensity, Hue and Saturation components and decoding these images into an RGB color rendition, the intensity or brightness of the resulting color image is controlled solely by image A, the hues by image B, and the saturation by image C. The fact that intensity, hue and saturation are controlled individually, so that they can be perceived independently, makes such a model a powerful tool for jointly displaying individual Interpretive Components in a non-confusing way.

Synthetic Stereo (SST)

In color presentations, there will always be only three variables or Inter-
pretive Components which can participate in generating the final display
product. This is valid for the RGB as well as for the IHS system. Owing
to the increased number of spectral bands provided by the Thematic Mapper
system, an even larger number of Interpretive Components are available to
contribute to a color display. To incorporate additional components in a
color display limited to three variables requires innovative processing
techniques.

An interesting and useful solution for this is to generate synthetic
stereo pairs in IHS color in which the 3-D effects is modulated by infor-
mation provided by a Spectral Component rather than by the real topography.
This permits the interpretability of the original color display to be
preserved, while the additional introduced Component accounts for a fourth
variable that can be analyzed together with three other Interpretive Com-
ponents. The quasi stereo representations are calculated by displacing
the pixels of a scene along the scan lines by amounts proportional to the
DN values of one of the previously defined Spectral Components.

Taking into account the large number of Interpretive Components extractable
from TM-data and the manifold possibilities in their presentation through
IHS and SST, one should follow a certain strategy in order to avoid con-
fusion. Such a strategy is based on a priori decision as to the Inter-
pretive Components to be displayed and is further tempered by certain basic
rules of assignment.

Some Rules in the Handling of IHS and SST

Based on the implicit meaning of intensity, hue and saturation and the infor-
mation exhibited through the Interpretive Components, the Panchromatic Com-
ponent is best treated as intensity. As color perception is strongly degra-
ded with decreasing intensity or image brightness, a mapping table must be
applied which offsets the histogram in order to avoid completely dark areas
on the final product.

For some applications involving observables such as water areas, it will be
necessary to apply more complex enhancement techniques to the Panchromatic
Component. A typical example within this context would be to increase the
DN-values of pixels representing water. This can be achieved through piece-
wise linear mapping tables. Cosmetic operations, however, should not
destroy the meaning of the Panchromatic Component for interpretation pur-
poses in the previously defined sense.

Spectral Components can be best displayed through hue, saturation and syn-
thetic stereo. The way in which color is perceived by the human observer
and the application-oriented significance of a given Spectral Component
have a strong impact on their final assignment. It can be generally stated

that an interpreter will have difficulties in visually differentiating among various subtle levels of saturation or pastels. Therefore, those Spectral Components which exhibit significant spectral information mainly in their extreme values should be considered as drivers for saturation. For the presentation of highly differentiated spectral components it is necessary to use hue or synthetic stereo as the basis for display.

The approach in making the final assignment of Spectral Components through hue and saturation can be simply demonstrated by an example applied to vegetation. If one specifically wants to visualize the effect of vegetation on the slope between spectral regions in the red (TM-band 3) and near IR (TM-band 4), the corresponding Spectral Component will be best represented through hues. In such a case, saturation could be used to additionally highlight the high degree of correlation between the green (TM-band 2) and the red (TM-band 3) – "greenness factor" – or between the near IR (TM-band 4), and short wave IR (TM-band 5), which might provide diagnostic data on water absorption characteristics.

Special treatment is needed to handle thermal data when combined with reflectance data through IHS recording. When, in the normal case, thermal patterns are restricted to only one Spectral Component (e.g., TM-band 6 or HCMM ATI), best results will be achieved by assigning the corresponding thermal and reflectance components to hue and saturation respectively.

The above examples also demonstrate the value of the proposed concept in actually constructing image data, which will provide a priori defined intelligible spectral information.

Preliminary Thematic Mapper Image Products

Relying on past experiences in the processing of LANDSAT MSS and other multispectral data through IHS and SST, a Thematic Mapper scene (40124-17495, Nov. 17, 1982), covering the Death Valley and parts of Nevada has been processed under various conditions. However, there has been only limited experience-mainly with aircraft data-in the shortwave infrared bands (Bands 5 and 7) data from Thematic Mapper, so that their utility for lithological mapping using the concepts presented in this paper, is a prime objective in the study.

Therefore, the bulk of the experiment to process these TM images was devoted to specifically displaying spectral surface characteristics recorded in these wavelength regions. This has resulted in the definition of Spectral Components exhibiting correlative spectral information between the TM-bands 4 and 5, 4 and 7, and also between 57 and 7. Additional Spectral Components were calculated to enhance "color" in terms of looking at the slopes between green and red (TM-bands 2 and 3) and in order to display thermal characteristics as recorded in TM-band 6. A more detailed description of image products generated so far is given by Table 1 through 5.

CONCLUSIONS

Processing of the Thematic Mapper data within the framework of Interpretive Components requires the application of special display techniques, referred to as IHS and SST. The results to date using these techniques demonstrate improved visual separability of spectral surface categories relative to standard multispectral color composites as well as a greater potential for conducting meaningful spectral-diagnostic analysis.

The overall concept discussed in this paper may also serve as a sound basis for defining IHS-SST Thematic Mapper images as superior standard products. The establishment of optimum standards, however, requires more experiences in the application of TM-data.

ACKNOWLEDGEMENTS

REFERENCES

Batson, R. M., K. Edwards and E. M. Eliason, 1976, Synthetic Stereo and Landsat Pictures, Photogramm. Engin. and Rem. Sens., Vol. 42, No. 10, pp. 1279-1284.

Haydn, R., G. W. Dalke, J. Henkel and J. R. Bare, 1982, Application of IHS colour transform for processing of multispectral data and image enhancement. Int. Symp. Rem. Sens. of Arid and Semi-Arid Lands, Cairo, Egypt.

Haydn, R., G. W. Dalke, J. Henkel and H. Kauffman, 1982, Multidisciplinary investigations on HCMM data over Europe and Morocco. NASA-HCMM type III, Final Report, Contr. No. HCM-053, p. 82.

Haydn, R. and M. Youssef, 1982, The Application of Processed Landsat Imagery in Photo-Interpretation, Intern. Geoscience and Remote Sensing Symposium (IGARSS 82) IEEE Catalog No. 82CH14723-6.

Haydn, R. (1982), Some Aspects of the Presentation of Remote Sensing Data, EARSeL-ESA Symposium, Igls, Austria, 1982 (ESA SP-175, June 1982), pp. 77-80.

Hjelkema, J.U., 198_, Remote Sensing Techniques and Methodologies for Monitoring Ecological Conditions for Desert Locust Population Development, Final Report, FAO/ACP, Rome.

Segal, D. B., 1982, Theoretical Basis for Differenciation of Ferric-Iron Bearing Minerals Using Landsat MSS Data, Int. Symp. Rem. Sens. of Exploration Geology, Forth Worth, Texas.

Siegal, B. S. and A. R. Gillespie, Remote Sensing in Geology, J. Wiley & Sons, New York.

Tucker, C. J., 1977, Use of Near Infrared/Red Radiance Ratios for Estimating vegetation Biomass and Physiological Status, NASA/GSFC X-923-77-183.

Zobrist, A. L., R. J. Blackwell and W. D. Stromberg, 1979, Integration of Landsat, Seasat and other geodata sources, 13th Int. Symp. of Rem. Sens. of Env. Proceedings ERIM Ann Arbor, pp. 271-279.

Multispectral data

Optimized Interpretive
Components

Final product

Combination of optimized
Interpretive Components
via IHS and SST

Fig.1.: Schematic representation of processing steps for the
generation of interpretation-optimized TM-images
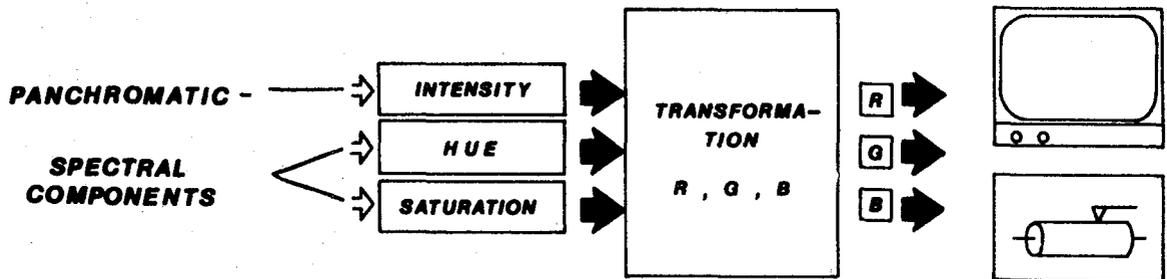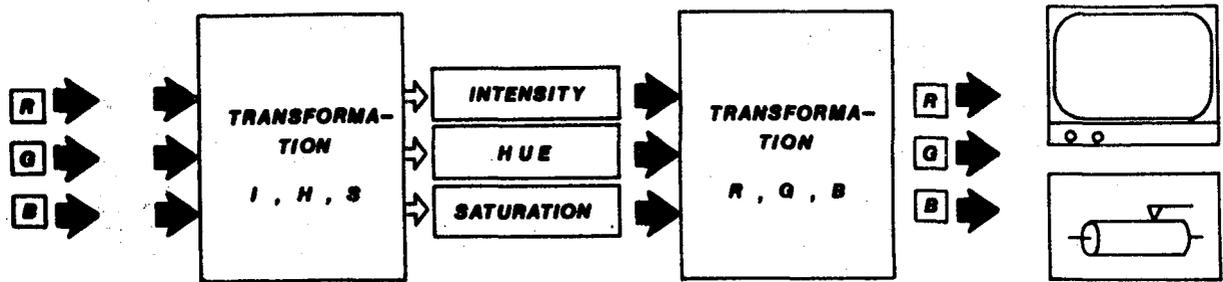
Fig.2ab: Schematic representations of the IHS transformations and their applications in combination with Interpretive Components

TABLE 1

PROCESS   : IHS - NIR/SWIR

PURPOSE   : DISPLAY OF SUBTLE SPECTRAL SURFACE
                  CHARACTERISTICS AS RECORDED WITHIN THE
                  TM - SHORT WAVE INFRARED BANDS (SWIR)
                  VERSUS THE TM - NEAR IR BAND (NIR)
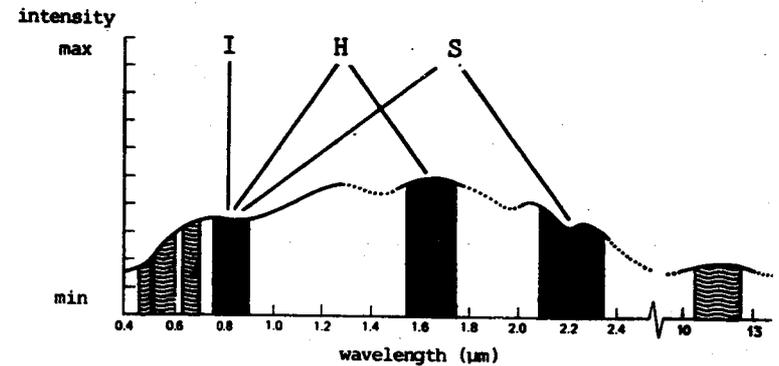
intensity

RGB = additive composite (red,green,blue)
I = intensity
H = colour frequency
S = saturation
SST = synthetic stereo

IMAGE   : INTENSITY - MODULATION THROUGH TM - BAND 4 (= NIR .76-.9 µm)
ATTRIBUTES   HUE   - MODULATION THROUGH RELATIONSHIP BETWEEN TM-5 (1.55-1.75 µm)
                              OVER TM-4 (.76-.9 µm).
                              MAX. TM-5/TM-4 VALUES = RED; MIN VALUES = BLUE
                  SATURATION- MODULATION THROUGH RELATIONSHIP BETWEEN TM-7 (2.08-2.35 µm)
                              OVER TM-4 (.76-.9 µm)
                              MAX. TM- 7/TM-4 VALUES = SATURATED HUES; MIN VALUES = NO
                              SATURATION (NO COLOR)

REMARKS   : THE ENHANCED DISPLAY OF SPECTRAL INFORMATION GATHERED WITHIN THE TM -
                  NIR AND SWIR BANDS LEADS TO A HIGH SEPARABILITY OF LITHOLOGICAL
                  PHENOMENA.
                  THE IMAGE ATTRIBUTES CAN BE USED AS DIAGNOSTIC FEATURES TO VISUALLY
                  DESCRIBE THE SLOPES OF REFLECTANCE SPECTRA OF INPUT BANDS

TABLE 2

PROCESS   : IHS - VIS/SWIR

PURPOSE   : COMBINED DISPLAY OF SPECTRAL SURFACE
              CHARACTERISTICS RECORDED WITHIN THE
              VISIBLE AND SHORT WAVE INFRARED
              WAVELENGTH DOMAINE
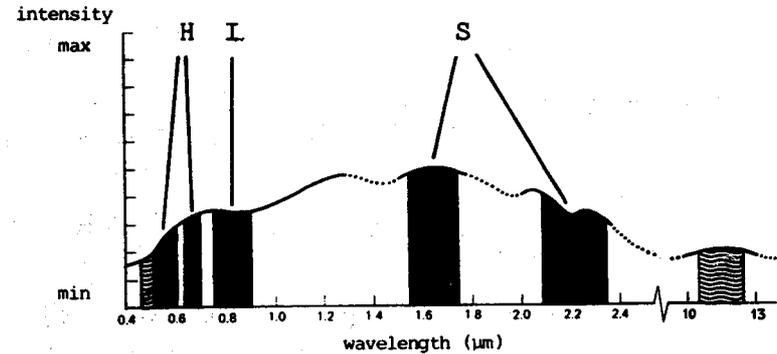
RGB = additive composite (red,green,blue)
I   = intensity
H   = colour frequency
S   = saturation
SST = synthetic stereo

IMAGE   : INTENSITY - MDULATION THROUGH TMS -BAND 4 (.76-.9 µm)
ATTRIBUTES   HUE   - MODULATION THROUGH THE RELATIONSHIP BETWEEN TM-3 (.63-.69 µm)
                           OVER TM-2 (.52-.6 µm).
                           MAX; TM-3/TM-2 VALUES = RED ; MIN. VALUES = BLUE
               SATURATION- MODULATION THROUGH RELATIONSHIP BETWEEN TM-5 (1.55-1.75 µm)
                           OVER TM- 7 (2.08-2.35 µm).
                           MAX. TM-5/TM-7 VALUES = SATURATED HUES ; MIN. VALUE = NO
                           SATURATION (NO COLOR).

REMARKS   : OVERALL REDUCED INTERPRETABILITY DUE TO
              DATA ERRORS "ENHANCED" BY THE UNDERLAYING RATIO PRE-PROCESSING.

TABLE 3

intensity
max

SST   I   H   S

min

0.4 0.6 0.8   1.0 1.2 1.4 1.6 1.8 2.0 2.2 2.4   10   13

wavelength (µm)

RGB = additive composite (red,green,blue)
  I = intensity
  H = colour frequency
  S = saturation
SST = synthetic stereo

PROCESS   : IHS - NIR/SWIR AND SST-VIS

PURPOSE   : TO INDEPENDENTLY DISPLAY A MAXIMUM NUMBER
              OF SPECTRAL INFORMATION FOR AN OPTIMUM
              INTERPRETATIVE ANALYSIS OF SPECTRAL
              SURFACE CHARACTERISTICS AS RECORDED BY
              THE THEMATIC MAPPER
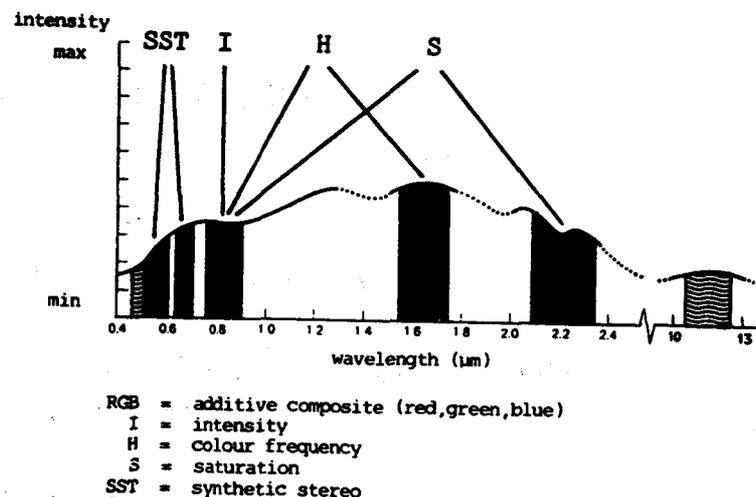
IMAGE   : INTENSITY - MODULATION THROUGH TM - BAND 4 (= NIR .76 -.9 µm)
ATTRIBUTES   HUE   - MODULATION THROUGH RELATIONSHIP BETWEEN TM-5 (1.55 - 1.75 µm)
                              OVER TM-4 (.76-.9 um)
                              MAX. TM-5/TM-4 VALUES = RED; MIN. VALUES = BLUE
               SATURATION - MODULATION THROUGH RELATIONSHIP BETWEEN TM-7 (2.08 - 2.35 µm)
                              OVER TM-4 (.76-.9 um)
                              MAX. TM-7/TM-4 VALUES = SATURATED HUES; MIN. VALUES = NO
                              SATURATION (NO COLOR)
               SST   - MODULATION THROUGH RELATIONSHIP BETWEEN TM-3 (.63-.69 µm)
                              OVER TM-2(.52-.6 µm)
                              MAX.TM-3/TM-2 VALUES = "TOPOGRAPHIC HIGH";
                              MIN. VALUES   = "TOPOGRAPHIC LOW".

REMARKS   : DEGRADED 3D EFFECT DUE TO ERRORS IN TM - DATA WHICH ARE ENHANCED BY THE UNDERLAYING
               RATIO PREPROCESSING

IV-233

TABLE 4

PROCESS : RGB - SST VIS / THERMAL

PURPOSE : DISPLAY OF LOW RESOLUTION THERMAL DATA
(DAY, NIGHT, INERTIA) IN COMBINATION
WITH HIGH RESOLUTION MULTISPECTRAL
DATA SETS.
(BY THE INTRODUCTION OF THERMAL DATA
VIA A SYNTHETIC STEREO EFFECT AS ADDI-
TIONAL AND INDEPENDENT SOURCE OF
INFORMATION, THERMAL CHARACTERISTICS CAN
BE DIRECTLY COMPARED WITH SPECTRAL
FEATURES.)

RGB = additive composite (red,green,blue)
I = intensity
H = colour frequency
S = saturation
SST = synthetic stereo

IMAGE : RGB - ADDITIVE COLOR RENDITION ON THE BASIS OF TM-1 (.45 - .52 μm),
ATTRIBUTES TM-2(.52 - .6 μm) AND TM-3 (.63 - .69 μm).

SST - MODULATION THROUGH TM-6 (10.4 - 12.5 μm) MAX. TEMP. VALUES = "TOPOGRAPHIC
HIGH"; MIN. TEMP. VALUES = "TOPOGRAPHIC LOW".

REMARKS : STRONG AND ABRUPT TEMPERATUR CHANGES (SNOW; CHANGES IN EXPOSITION AT LOW SUN
ANGLE IMAGES) CAUSE CONFUSING EFFECTS.
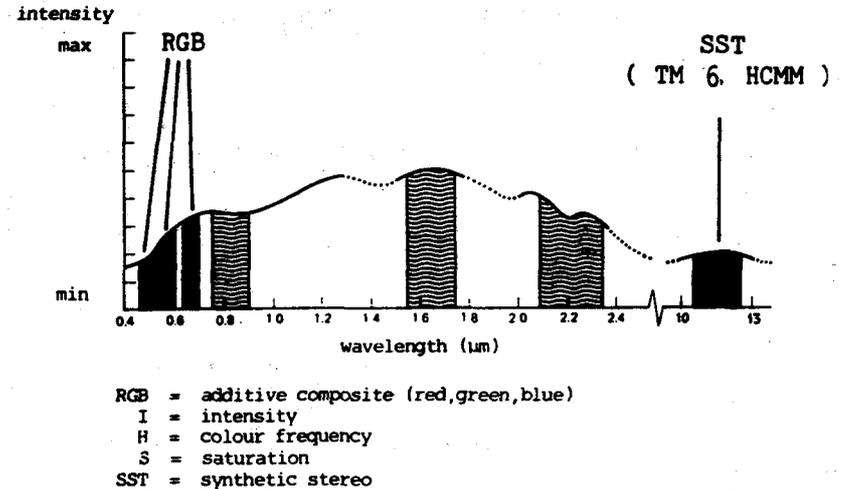
TABLE 5

PROCESS : IHS - TM / THERMAL

PURPOSE : DISPLAY OF LOW RESOLUTION THERMAL
           INFORMATION (DAY, NIGHT, INERTIA) IN
           COMBINATION WITH HIGH RESOLUTION TMS-
           DATA. THE SELECTED TM -BAND SERVES AS
           SCENARIO FOR A BETTER INTERPRETABILITY
           OF HEAT SENSOR DERIVED (TM- /HCMM)
           INFORMATION.

intensity

max   I   H,S
                                              (TM 6 , HCMM)

min

0.4 0.8 0.8 1.0 1.2 1.4 1.6 1.8 2.0 2.2 2.4   10   13
                    wavelength (µm)

RGB = additive composite (red,green,blue)
  I = intensity
  H = colour frequency
  S = saturation
SST = synthetic stereo
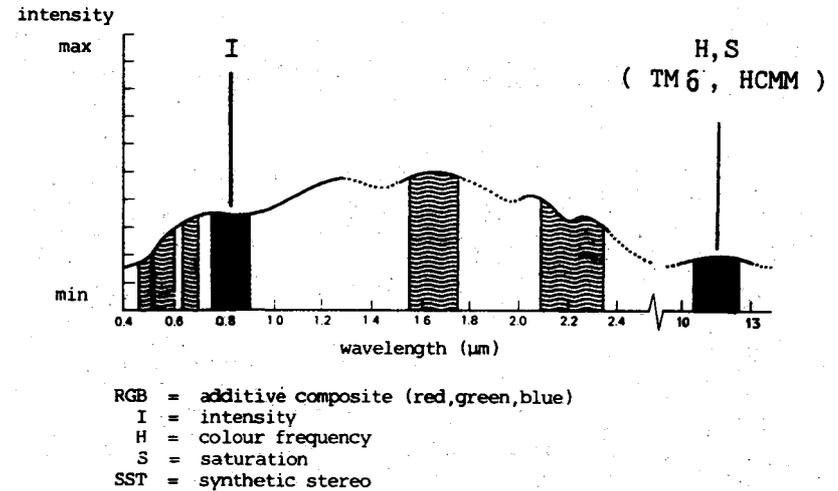
IMAGE   : INTENSITY - MODULATION THROUGH TM-4 (.76 - .9 µm)
ATTRIBUTES   HUE   - MODULATION THROUGH THERMAL DATA
              SATURATION- MAX. TEMP. VALUES = RED; MIN. TEMP. VALUES IS BLUE.

REMARKS : STRONG INFLUENCE OF TOPOGRAPHY ON TM- THERMAL PATTERNS DUE TO LOCAL TIME OF
           ACQUISITION; IMPROVED MATERIAL DEPENDENT THERMAL CHARACTERISTICS ON HCMM MERGE.

Page intentionally left blank

QUICK LOOK ANALYSIS OF TM DATA OF THE WASHINGTON, D.C., AREA

Darrel L. Williams
James R. Irons
Brian L. Markham
Ross F. Nelson
David L. Toll

NASA/Goddard Space Flight Center
Earth Resources Branch
Greenbelt, MD   20771

Richard S. Latty

University of Maryland
Department of Civil Engineering
College Park, MD   20742

Mark L. Stauffer

Computer Sciences Corporation
Silver Spring, MD   20910

INTRODUCTION

With the launch of Landsat-4 on July 16, 1982, and the successful operation of its new sensor, the Thematic Mapper (TM), a significantly improved source of data became available to the remote sensing community. Relative to the familiar Multispectral Scanner (MSS), the TM offers a finer spatial resolution, new and more optimally placed spectral bands, and improved radiometric sensitivity quantized over eight bits rather than six bits (Table 1). These improvements in sensor capability were designed to significantly increase data quality and information content, and thereby enhance the utility of the data for earth resources observations.

One method commonly used to assess the relative utility of image data acquired by different remote sensing devices is to compare accuracies attained in the classification of pixels into surface feature categories. Numerous studies using data collected by aircraft-mounted Thematic Mapper simulators (TMS) were conducted prior to the launch of Landsat-4 to quantify the overall improvement in classification accuracy to be expected from TM data relative to MSS data[1]. However, few of these studies attempted to isolate the impact or contribution of individual sensor parameters (e.g., spectral, spatial, and radiometric resolution) on classification accuracy.

The effect of altering individual sensor attributes can be anticipated qualitatively. For example, the addition of spectral bands can enable the discrimination of previously inseparable categories by providing data from portions of the spectrum where category reflectivities become disparate. Similarly, improved radiometric resolution and increased signal-to-noise ratios may facilitate discrimination by enhancing between-category boundaries in spectral data space. In contrast, the refinement of spatial resolution can

have offsetting effects on classification accuracy[2]. Finer resolution tends
to decrease the proportion of mixed pixels and thus enhance classification.
Classification is hindered, however, by an increase of within-category spectral
heterogeneity at finer resolutions. The TM is the result of an ambitious
development effort which simultaneously integrated all of these major
improvements into one system. Classification capabilities with TM data result
from the interactive effects of all of the sensor's attributes which complicates
a more quantitative evaluation of the effects of individual sensor improvements.
Such quantitative information could significantly benefit scientists and engineers
in defining sensor parameter requirements and in designing new sensors for
future remote sensing missions.

With the encouragement of the Landsat-4 Project Scientist, a group of discipline
scientists within the Earth Resources Branch at NASA's Goddard Space Flight
Center in Greenbelt, Maryland, conducted an experiment to quantify the effect of
three major TM sensor parameters on classification accuracy. This paper
discusses the experimental design and summarizes the preliminary results obtained
using TM data acquired over the Washington, D.C., area on November 2, 1982.

STUDY SITE/DATA DESCRIPTION

Accurate, detailed ground reference information was an important component of
the study. To facilitate the collection and field verification of the ground
reference data, an area close to Goddard was selected as the general study
area. This area is bounded on the west by Washington, D.C., on the north by
Baltimore, Maryland, on the east by the Chesapeake Bay, and on the south by
northern Charles County, Maryland (Figure 1). The area is characterized by a
diversity of urban, suburban, and rural land cover types. The western portion
of the area includes numerous residential developments associated with suburban
Washington, D.C. The entire area includes intensive urban fringe development,
suburban multifamily and single family residential tract development, low
density single family developments, and rural areas. In addition, numerous
commercial support services such as shopping centers, industrial complexes,
gravel quarries, and airports are scattered throughout the study area. The area
lacks heavy industry, but does include the Fort Meade and Andrews Air Force
Base military complexes.

In addition, the region includes areas of agriculture and forest cover. The
agricultural areas are primarily small, scattered fields. The principal crops
are corn, soybeans, and tobacco, with areas of pasture and grass. The study
site includes the USDA/Beltsville Agricultural Research Center. In terms of
areal extent, forest is the predominant cover type, and consists primarily of
mixed deciduous forest, mixed hardwood-conifer and isolated conifer stands.
The area also includes lowland vegetation communities associated with Chesapeake
Bay estuaries.

To acquire ground reference data, an aerial photographic mission was flown on
July 13, 1982, to obtain color infrared aerial photography in stereo at a scale
of 1:40,000. A random sample of nine frames of photography was selected from
this aerial survey to obtain a representative sample of the range of ground
cover conditions in the area. These frames represent the actual study sites,
and their locations are illustrated in Figure 1.

Although Landsat-4 was launched on July 16, 1982, seven-band, cloud free TM imagery for all nine study sites was not acquired until November 2, 1982. TM and MSS imagery were collected simultaneously, and both data sets were of excellent quality (i.e., no cloud cover, and both sensors operating satisfactorily). Ground cover conditions were less than optimum for category recognition due to the time of year. For example, deciduous trees were undergoing fall leaf coloration, most agricultural crops had senesced, and many fields had been harvested. In addition, total scene illumination was reduced because of low sun angle conditions in November and thus, the full dynamic range and quantization capabilities of the TM were not utilized. However, a decision was made to proceed with the analysis because it afforded the first opportunity to test the experimental design/methodology with real TM data; because a quantitative assessment of the attributes of TM sensor parameters relative to MSS was desired as soon as possible; and because a ground reference data base for an alternate area could not be created in a timely, cost-effective manner. Digital TM data in P-format (i.e., radiometrically and geometrically corrected) were used.

PROCEDURES

The first step in the work presented here was to design an experiment which could isolate the effect of each TM sensor improvement (spectral, spatial and radiometric resolution) on classification performance. The work of Sigman and Craig[3] with TMS data suggested a promising methodology based on multifactor analysis-of-variance (ANOVA). The ANOVA approach permits the evaluation of the effect of three factors (i.e., spectral, spatial, and radiometric resolution), where each factor has two levels (i.e., TM and MSS), on classification accuracy. This approach requires eight data sets as shown in Table 2. Data sets are created by degrading TM data in a manner which approximates the MSS level for each factor (e.g., TM data are spatially degraded to approximate the coarser MSS spatial resolution). The degradations are described in more detail in a subsequent section. The ANOVA design enables the statistical testing of the significance of classification accuracy differences between data sets. The testing results in a quantitative assessment of the effect of each sensor improvement, individually and in combination with other improvements, on classification performance.

The analysis of the eight data sets is not yet completed. However, to obtain preliminary, quantitative results, the data sets labeled A, B, C, and D in Table 2 were generated. Data set A consists of actual TM data where the 120 m thermal band data were deleted. Data sets B, C, and D were derived from the actual TM data by degrading one factor, either spectral, spatial, or radiometric resolution, to the MSS level. These data sets were chosen to provide a preliminary, "quick look" assessment of the effects of improving one sensor attribute at a time. Several major activities were involved in preparing and analyzing the data: photointerpretation of the aerial photography to create a ground reference data set, extraction of the TM data corresponding to the nine study sites, preprocessing of the TM data to simulate MSS spectral bands, spatial resolution, and radiometric characteristics as required by the ANOVA design, selection of training and test sites for each cover type, clustering and classification, and tabulation of results. To maintain brevity, only the highlights and unique aspects of these various procedures will be presented.

Photointerpretation

As previously mentioned, color IR aerial photography at a scale of 1:40,000 was acquired on July 13, 1982, just prior to the scheduled launch of Landsat-D. Nine frames were randomly selected for detailed analysis. Prior to photointerpretation, a decision was made to work with a sub-frame area designated by plus-or-minus 50 mm on either side of the principal point of the 241 mm format photography. The resultant 100 mm square area represented approximately 20 percent of the entire frame. It was felt that this approach would minimize the effects of distortions typically found toward the edges of aerial photographs.

The 1:40,000 scale sub-frame areas were photographically enlarged by a factor of four to attain a nominal scale of 1:10,000 and paper prints were produced. Each 400 mm square, 1:10,000 scale photograph covered an area of 4000 m on a side, or 1600 hectares per photo. Clear acetate film was laid on top of each photograph so that the photointerpretation results could be scribed directly onto the film overlay. The original photography was available and could be viewed stereoscopically with a 7x magnifier in the event questions arose concerning the identity of a particular feature on the paper enlargements. Using this approach and a minimum mapping unit criterion of 15 m (i.e., one-half the instanteous-field-of-view of the TM), thirteen land cover/land use categories were identified on the photos (Table 3). All polygons drawn on the acetate overlays were labeled with the appropriate land cover/land use identification. The photointerpretation and labeling results were verified or updated by field visitation and enumeration during the last week in October, just prior to the TM data acquisition. It should be noted that the land cover/land use categories are not mutually exclusive. For instance, large lawn areas in residential neighborhoods were considered grassland. The land use categories were used in situations where the land cover components of the categories (e.g., the roofs, grass, trees, and asphalt of a residential neighborhood) occupied areas with dimensions smaller than the 15 m minimum mapping unit.

Preprocessing of TM Data

The TM data corresponding to the nine randomly selected study sites were extracted from the original P-format data tapes to facilitate subsequent processing. Each extracted segment of the TM data was 256 by 256 pixels in size and contained all six bands of 30 m resolution data. The thermal IR data, which are collected at a ground resolution of 120 m, were omitted from this study due to the significant difference in spatial resolution. The ANOVA design (Table 2) required the original TM data to be degraded spectrally, spatially, and radiometrically to simulate MSS specifications for each of these sensor parameters. The precise simulation of MSS radiometry, spectral bands, and spatial resolution from TM data is not possible due to inherent differences in spectral band cutoffs, radiometric responses, and across track scanning strategies. The procedures used to degrade TM data for MSS simulation are described below:

(i) Spectral Simulation

The simulation of MSS spectral resolution was achieved by using only TM bands 2, 3 and 4, which closely approximate MSS bands 1, 2 and 4. The inability to

approximate MSS band 3, the first near IR band, was not considered significant because MSS bands 3 and 4 are often highly correlated and provide redundant information.

(ii) Radiometric Simulation

The radiometric analysis consisted of a comparison of quantization levels. The MSS simulation was achieved by mapping the 0 - 225 range of potential bins for the TM data into 0 - 63 bins for MSS data (i.e., each TM datum was divided by four and rounded to the nearest integer). In taking this approach, two simplifying assumptions, that the dynamic range and signal-to-noise ratios of both sensor systems are comparable for the similar spectral bands, were made. Neither assumption is precisely correct. Therefore, this approach simply addresses the issue of six bit versus eight bit quantization, rather than TM radiometric sensitivity versus MSS radiometric sensitivity.

(iii) Spatial Simulation

The simulation of MSS spatial resolution was achieved by computing the simple arithmetic average over a three-by-three pixel window of the TM data. The window was moved across the image two columns at a time to simulate the 57 m along-scan MSS sampling rate relative to the MSS 80 m IFOV. After moving across an image, the averaging window was incremented two lines to approximate the geometric resampling of MSS data to reduce the 80 m nominal pixel dimension in the along-track to 57 m. Thus, the 57 m-by-57 m pixel format of the standard MSS P-tape product distributed by EROS was simulated.

Selection of Training and Test Sites

Training and test sites were chosen in a supervised manner. The TM digital data for each study site were displayed on a cathode ray tube (CRT), compared to the corresponding airphoto/acetate overlay, and representative areas were outlined and labeled on the CRT using interactive cursor training capabilities. A number of training and test sites were identified for each land cover/land use category using this technique. The locations of the training and test sites were identical for all four data sets.

Clustering and Classification

The category statistics required for classification were derived separately for each of the four data sets under analysis. Given a particular data set, the training site data for each land cover/use category were clustered into spectral classes by a well known computer program called ISOCLS[4]. The parameters of ISOCLS were specified in a manner which limited the number of spectral classes to four or less per category. No attempt was made to improve subsequent classification results by the editing of the statistics generated by ISOCLS (i.e., no merging, pooling, or deleting of spectral classes). Editing was deferred to avoid the incorporation of analyst bias into classification results. The intention of the procedure was to allow the characteristics of each data set to be the sole determinants of classification performance. Results, however, are also highly dependent on the algorithms chosen to define category statistics

and to classify the data.

The use of the clustering program produced a different set of category statistics for each of the four image data sets, and each land use/cover category within a data set was represented by up to four spectral classes. For each data set, the pixels from both the training sites and the test sites were then classified according to the category statistics using a per-point Gaussian maximum likelihood classifier.

RESULTS

For this "quick look" analysis effort, the frequency of errors of omission and commission were tabulated for each of the thirteen cover classes for each of the four data set treatments. Omission/commission errors were tabulated by making independent comparisons of the classification results to the ground reference data for both the training site pixels and the test site pixels. Only the "test" results will be presented here as they are unbiased relative to the development of spectral signatures for the various cover classes.

Table 3 lists the omission and commission errors by cover class for each data set. The impact of a specific sensor parameter on the ability to recognize a particular class can be evaluated by comparing the errors listed in the first column (Data set A, original TM data) of Table 3 with the errors listed for the same class in the other columns. Examination of Table 3 in this manner reveals that the reduction of either the number of spectral bands or the number of quantization levels frequently increased the errors. In contrast, the degradation of spatial resolution reduced many of the errors.

Table 4 summarizes the detailed information in Table 3 by presenting the overall classification accuracy (i.e., the number of test pixels correctly classified divided by the total number of test pixels) for each data set. The results can be summarized as follows: the reduction of quantization level from eight bits to six bits caused an overall 7% decrease in attainable accuracy; the use of only three spectral bands covering the visible and near IR portions of the spectrum caused an overall 7% decrease in accuracy; and the degradation of spatial resolution resulted in an overall increase in accuracy of 4%.

DISCUSSION

Evaluation of a sensor's utility must be made in the context of the type of information extracted from the sensor's data and the methodology applied to the extraction. The classification of pixels into land cover/use classes was chosen for the evaluation presented here as a type of information frequently derived from remote sensing data. The selected methodology involved the independent computation of training statistics for each of the four data sets and the subsequent applications of the commonly used per-pixel maximum likelihood classification rule. Thus, the classification decisions were based on the pixel-by-pixel spectral properties of each of the cover classes. No attempt was made to exploit textural, contextural, or spatial properties for identification of the classes. Assessments of the results obtained by this selected methodology cannot be directly extended to the extraction of different types of information or to the application of alternate data analysis techniques.

The results presented in Tables 3 and 4 do indicate that the additional number of spectral bands and quantization levels of the TM relative to the MSS increase capabilities for the recognition and discrimination of land cover/use categories by per-pixel maximum likelihood classification. The refinement of spatial resolution, however, seems to hinder classification. This result may appear surprising, but is not difficult to understand in the context of the data analysis approach. The supervised delineation of training and test sites resulted in the selection of field-center pixels. Studies[2,5] have shown that finer spatial resolution often increases the within-class variability of field-center pixels and hence increases class overlap in spectral data space. The degradation of spatial resolution tends to reduce within-class spectral variability and facilitate the separation of classes by per-pixel classification rules. The results presented here again point to the need for the development of new data analysis techniques which exploit the increased spatial and textural information provided by fine resolution data. The other improved attributes of the TM, the additional spectral bands and quantization levels, appear to be of immediate benefit in the context of a currently available and widely employed method for analyzing remotely sensed digital data.

FUTURE WORK

With the completion of the "quick-look" analyses, a more rigorous examination of the effects of each TM sensor improvement on classification capabilities will be performed using the full ANOVA design. Further processing of the original TM data will produce all eight data sets required by the ANOVA design. The ground reference data will then be digitized and geometrically registered to the eight data sets. The digitized reference data will facilitate the random selection of training and test pixels from each set for each land cover/ land use category. The unsupervised clustering algorithm will be used to derive training statistics for each category from each set. The test pixels will then be classified and classification accuracies tabulated. The ANOVA approach will allow the statistical testing of the significance of classification accuracy differences between treatments. This approach will result in a more comprehensive assessment of the impact of each sensor improvement individually and in combination with other improvements.

ACKNOWLEDGMENT

REFERENCES

1. Irons, J. R. 1982. Summary of Research Addressing the Potential Utility of Thematic Mapper Data for Renewable Resource Applications. NASA Technical Memorandum 83965.

2. Markham, B. L., and J. R. G. Townshend. 1981. Land Cover Classification Accuracy as a Function of Sensor Spatial Resolution. Proceedings of the Fifteenth International Symposium on Remote Sensing of Enviroment. Ann Arbor, MI.

3. Sigman, R. and M. Craig. 1981. Potential Utility of Thematic Mapper Data in Estimating Crop Areas. Proceedings of Fifteenth International Symposium on Remote Sensing of Environment. Ann Arbor, MI.

4. Minter, R. T. 1972. Computer Program Documentation for ISOCLS, Iterative Self-Organizing Clustering Program. Program CO94. Prepared for NASA/JSC under contract NAS 9-12200 by Lockheed Electronics Company, Inc. Houston, TX.

5. Sadowski, F. and J. Sarno. 1976. Forest Classification Accuracy as Influenced by Multispectral Scanner Spatial Resolution. Final Report to NASA/Lyndon B. Johnson Space Center, Houston, TX. Contract No. NAS9-14123.

Table 1. Comparison of Landsat-4 TM and MSS Sensor Capabilities

Band Designation	Thematic Mapper (TM)		Multispectral Scanner Subsystem (MSS)	
	Micrometers	Radiometric Sensitivity (NE$\Delta\rho$)	Micrometers	Radiometric Sensitivity (NE$\Delta\rho$)
Spectral Band 1	0.45 − 0.52	0.8%	0.5 − 0.6	0.57%
Spectral Band 2	0.52 − 0.60	0.5%	0.6 − 0.7	0.57%
Spectral Band 3	0.63 − 0.69	0.5%	0.7 − 0.8	0.65%
Spectral Band 4	0.76 − 0.90	0.5%	0.8 − 1.1	0.70%
Spectral Band 5	1.55 − 1.75	1.0%		
Spectral Band 6	10.40 − 12.50	0.5 Kelvin (NEΔT)		
Spectral Band 7	2.08 − 2.35	2.4%		
Ground IFOV		30 meters (Bands 1-5,7)	82 meters (Bands 1-4)	
		120 meters (Band 6)		
Data Rate		85 megabits/sec	15 megabits/sec	
Quantization Levels		256	64	

Table 2. Characteristics of Data Set Treatments Required for a Complete Two Level (TM, MSS) by Three Factor (Spectral, Spatial, Radiometric) Analysis-of-Variance (ANOVA) Experiment

		SPECTRAL BANDS			
		TM		MSS	
		SPATIAL RESOLUTION			
		TM	MSS	TM	MSS
RADIOMETRY	TM	A 6 bands 30 meters 8 bit	D 6 bands 80 meters 8 bit	C 3 bands 30 meters 8 bit	3 bands 80 meters 8 bit
	MSS	B 6 bands 30 meters 6 bit	6 bands 80 meters 6 bit	3 bands 30 meters 6 bit	3 bands 80 meters 6 bit

Table 3. Classification Error as a Function of Varying Quantization Level,
Number of Bands, or Spatial Resolution

	Data Set A 8 bit 6 bands Real TM Data 30 meters		Data Set B 6 bit 6 bands 30 meters		Data Set C 8 bit 3 bands 30 meters		Data Set D 8 bit 6 bands 80 meters	
	Test		Test		Test		Test	
Class (Pixel Number:Training-Test)	Omission Error (%)	Commission Error (%)	Omission Error (%)	Commission Error (%)	Omission Error (%)	Commission Error (%)	Omission Error (%)	Commission Error (%)
1. Water (915-627)	1.4	0	1.3	0	1.0	0.4	3.7	0.0
2. Grass (2060-2312)	39.2	12.8	35.1	17.6	32.2	36.4	35.6	10.7
3. Plowed (353-293)	42.7	62.0	45.1	70.5	87.3	34.6	31.8	63.4
4. Soybean (433-382)	69.4	78.6	76.7	82.9	60.8	70.9	62.3	75.3
5. Hardwood (3579-5213)	42.1	3.8	57.2	6.5	38.1	4.9	39.3	2.5
6. Corn (807-922)	60.4	34.0	65.5	39.8	59.9	48.5	75.8	49.6
7. Agriculture (296-146)	67.8	96.8	74.7	98.7	83.3	96.4	73.3	97.2
8. Cleared Land (323-533)	45.9	55.6	51.6	56.8	47.1	59.6	36.8	41.3
9. Industrial/Commercial (567-568)	25.5	29.8	22.9	36.3	31.0	35.9	13.6	29.7
10. Hardwood/Conifer Mixture (255-488)	49.2	83.4	69.3	84.6	68.7	84.9	37.5	79.5
11. Conifer (477-356)	39.3	56.5	36.5	54.5	18.3	62.3	39.3	58.5
12. Shrub (590-237)	48.5	88.0	64.6	87.5	76.0	90.9	30.8	79.8
13. Residential (2295-3061)	25.6	8.2	28.8	10.9	55.6	8.2	18.8	2.8
Average	42.8	50.6	48.4	53.3	50.8	52.4	38.3	49.3

Table 4. Summary of Overall Classification Accuracy as a Function of
Data Set Treatment

DATA SET CHARACTERISTICS	Accuracy Obtained With Test Pixels (%)	Difference in Accuracy From Actual TM Data (Data Set A) (%)
A. 30 meter/6 bands/8 bits	61.6	--
B. 30 meter/6 bands/6 bits	54.8	-7 (B minus A)
C. 30 meter/3 bands/8 bits	55.8	-7 (C minus A)
D. 80 meter/6 bands/8 bits	65.2	+4 (D minus A)

Figure 1. Location of General Study Area and the Nine Study
Sites Randomly Chosen for Detailed Analysis

Page intentionally left blank

REMOTE SENSING OF COASTAL WETLANDS BIOMASS

USING THEMATIC MAPPER WAVEBANDS

Michael A. Hardisky
Vytautas Klemas

College of Marine Studies
University of Delaware
Newark, Delaware 19711

ABSTRACT

Spectral data, simulating thematic mapper bands 3, 4 and 5 were gathered in salt and brackish marshes using a hand-held radiometer. Simple regression models were developed equating spectral radiance indicies with total live biomass for S. alterniflora in a salt marsh and for a variety of plant species in a brackish marsh. Models were then tested using an independent set of data and compared to harvest estimates of biomass. In the salt marsh, biomass estimates from spectral data were similar to harvest biomass estimates during most of the growing season. Estimates of annual net aerial primary productivity calculated from spectral data were within 21% of production estimated from harvest data. During August, biomass estimates from spectral data in the brackish marsh were similar to biomass estimated by harvesting techniques. At other times during the growing season, spectral data estimates of biomass were not always comparable to harvest biomass estimates. Reasonable estimates of wetlands biomass are possible during the peak of the growing season (August) using spectral data similar to thematic mapper bands 3, 4 and 5 gathered with hand-held radiometers.

INTRODUCTION

Basic to the understanding of wetland function and value is the quantification of energy fixation. Reduced carbon compounds comprising macrophytic biomass provide the energy necessary to maintain the heterotrophic organisms which feed upon them. Aboveground biomass represents only a portion of total net primary production (belowground production can also be substantial) however, the fixed carbon in this biomass is the surplus available to heterotrophic organisms and is readily detected with remote sensing devices.

Many salt marshes on the eastern coast of the U.S. are dominated by a single plant Spartina alterniflora, Loisel. (Reimold 1977). S. alterniflora biomass can vary from near 100 to over 3000 gdw m^{-2} depending upon substrate type, soil salinity, inundation frequency or other edaphic factors. As interstitial water salinity decreases to the 18-15°/$_{oo}$ range, S. alterniflora is gradually replaced by a variety of plant species. In general, the lower the salinity, the greater the diversity of the resident plant population. The monospecific gramineous canopies of the salt marsh are transformed to brackish marsh canopies comprised of mixtures of gramineous, broadleaf and leafless plants. Spatially and temporally the canopies encountered in the brackish system are complex and dynamic. The morphologic diversity of the plant community produces an equally diverse spectral signature.

The study described herein was designed to develop simple regression models equating spectral radiance indicies with plant biomass. The radiance data were spectrally similar to thematic mapper bands 3, 4 and 5 and have been suggested as being superior to MSS wavebands for vegetation monitoring (Tucker 1978). Our first objective was to use these models to predict biomass and net primary productivity for a salt marsh and to predict biomass for a brackish marsh using ground gathered spectral radiance data. Our second objective was to assess the validity of our biomass estimation by comparing the spectrally estimated biomass values with biomass estimates obtained by traditional harvest techniques.

METHODS

Salt Marsh

A portion of the Canary Creek salt marsh in Lewes Delaware was selected for study (Figure 1). The marsh was dominated by monospecific stands of S. alterniflora with relatively small areas of Distichlis spicata (L.) Greene. Occassionally, Salicornia europaea L. or Limonium sp. occurred mixed with S. alterniflora. Six transects extending from the creek edge to the upland were established. The transects were spaced approximately 210 meters apart and stations were designated every 30m along each transect. A total of 40 stations for the whole marsh were established. By establishing stations in a systematic manner along transects, we sampled a representative cross section of S. alterniflora height forms occurring within the marsh. Beginning on 15 May 1981 and continuing every three weeks until 9 October 1981, four stations were selected, using a table of random numbers, from each transect. For each of the eight sampling dates, 24 stations were sampled yielding a total of 192 for the season.

Brackish Marsh

A brackish marsh near the headwaters of Old Mill Creek at Lewes, Delaware was selected for study (Figure 1). The interstitial water salinity varied from approximately 15-18°/$_{oo}$ at the downstream end to about 12-10°/$_{oo}$ at the upstream end. Plant species comprising the plant community changed with apparent soil salinity. Four transects extending from the creek edge to the upland were established 180 meters apart
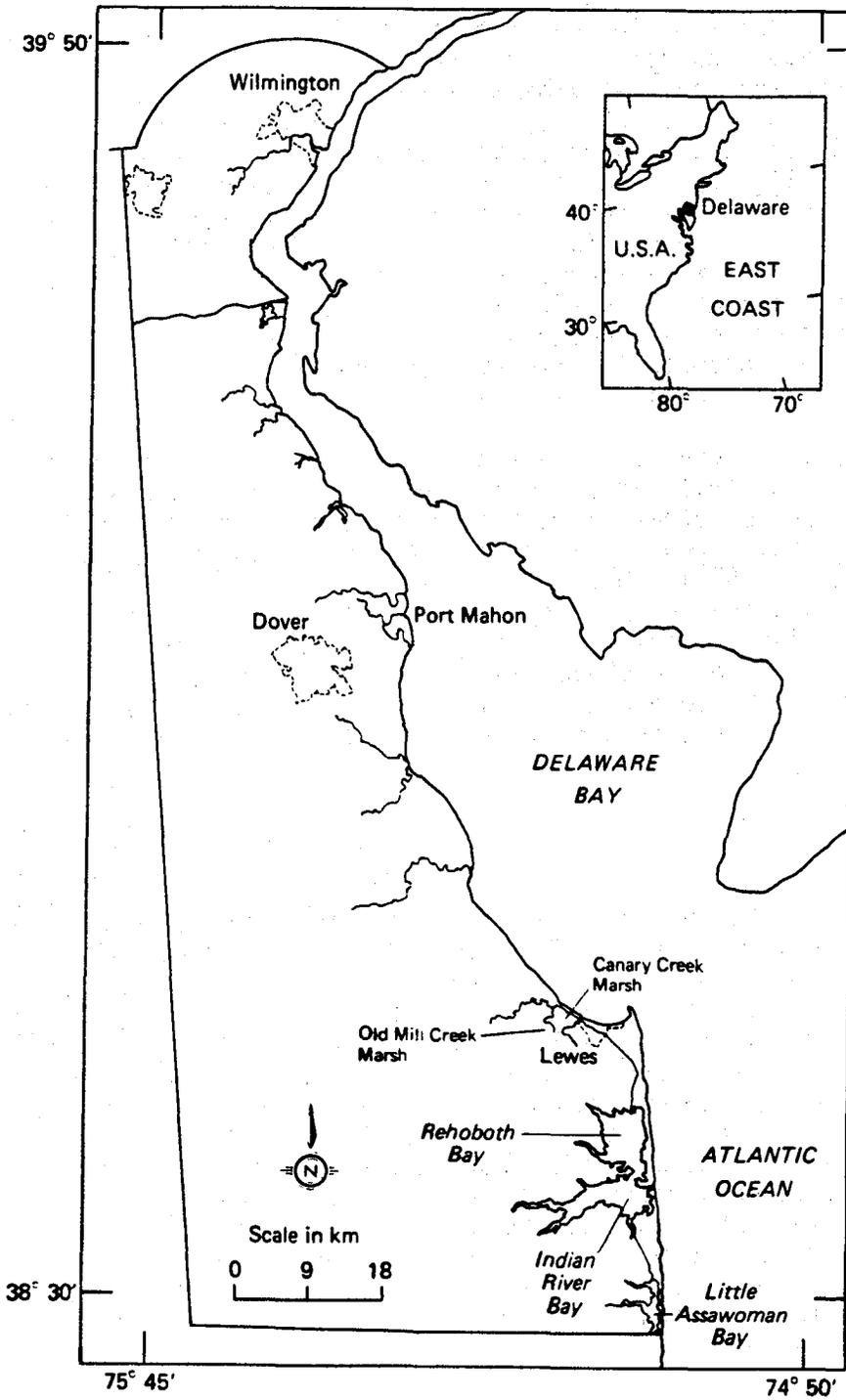
Fig. 1   Location of salt and brackish marsh
test sites near Lewes, Delaware.

along the long axis of the creek. Stations were spaced at 30m intervals along each transect. A total of 29 stations were designated in the marsh. The marsh was sampled 3 times during the growing season (June, August, September) at approximately 6 week intervals. At each sampling date, 4 stations were selected using a table of random numbers from each transect yielding 16 stations and a season total of 48.

Spectral Radiance Data Collection

Before harvesting, a GSFC Mark II hand-held radiometer (Tucker et al. 1981a) was used to measure canopy radiance directly over each area to be harvested. The radiometer contained three wavebands spectrally configured with interchangeable interference filters to match bands 3, 4 and 5 of the Landsat-4 thematic mapper. The sensor head housed a red band (0.63 - 0.69 μm, RED) sensitive to chlorophyll concentration, a near infrared band (0.76 - 0.90 μm, NIR) sensitive to plant tissue structure or biomass and a middle infrared band (1.55 - 1.75 μm, IR) sensitive to leaf moisture. Data were recorded simultaneously for all three bands.

No more than 5 days prior to the actual harvest, spectral radiance was determined for each plot. The radiometer was leveled approximately 1.5 meters above the top of the plant canopy. In the brackish marsh a wooden step ladder was employed to achieve proper instrument height. The radiance was measured 3 times over each plot. Radiance data were not collected under cloudy or very windy conditions and were always collected within 2 hours of solar noon. Radiance data were collected during low tide, however, there were occasions when small amounts of tidal water remained pooled on the marsh. Standing water was avoided whenever possible due to potential specular reflectance from the water surface.

Spectral radiance data were transformed and expressed as a normalized difference of two bands as outlined by Kriegler et al. (1969) and Rouse et al. (1973). The red and near infrared radiance values were combined in the following manner:

$$VI = \frac{NIR - RED}{NIR + RED}$$

where VI is the vegetation index, NIR is the near infrared band radiance and RED is the red band radiance. A similar combination of the near infrared and middle infrared bands was performed (middle infrared substituted for RED in the above expression) and termed the infrared index (II). The infrared index is used here with the understanding that the near infrared and the middle infrared bands are spectrally different and that normalization in this manner may not be totally valid since adjacent, spectrally similar bands were assumed for this transformation (Kriegler et al. 1969). Index values were preferred to raw radiance data because the normalization procedure tends to compensate for changes in solar irradiance caused by seasonal changes in solar zenith angle and/or atmospheric conditions (Tucker et al. 1979a).

Harvesting Procedures

After collection of radiance data, all vegetation (including standing dead material) within a 0.25 m^2 frame was clipped at soil level at each station. The plant material was bagged and returned to the laboratory for processing. A 1/3 subsample (by wet weight) was drawn from the salt marsh samples and sorted into live and dead components. The brackish marsh samples were sorted completely by species, then only plant species with a large volume of material were subsampled and finally live and dead components determined for each species. Most plants in the brackish marsh samples contained little attached dead so the majority of the dead material was considered as a composite of the whole sample. The subsampling procedure for both marsh types greatly reduced processing time. We felt that a representative subsample was sufficient to determine relative proportions of live and dead tissue and by retaining the entire 0.25 m^2 sample for biomass determination, we preserved the best estimate of biomass, given the oftentimes spatially heterogeneous distribution of biomass within the area sampled. Proportions of live and dead tissue determined from the subsample were then extrapolated to the entire biomass sample. All plant material was dried at 60°C to a constant weight, weighed to the nearest 0.1g and expressed as grams dry weight per square meter (gdw m^{-2}).

RESULTS

Salt Marsh - Biomass Estimation

Regression models equating S. alterniflora biomass and spectral radiance indicies were developed during the 1980 growing season (Hardisky et al. 1983a). These models included short and tall form S. alterniflora sampled from June through November using the hand-held radiometer. Table 1 lists the models for the vegetation and infrared indicies. To estimate live and dead biomass, one solves for live leaf biomass (L) in the first equation, for total live biomass (live leaves and stems, T) in the second equation and then substitutes the L value (from equation 1) into the last equation solving for dead biomass (D). Through this sequence, the necessary parameters for annual net aerial primary productivity estimation (total live biomass and dead biomass) are calculated.

Figure 2 depicts biomass estimates from harvesting and computed from the vegetation index for S. alterniflora. For live and total biomass, the predicted values were similar to the harvest values throughout the year. Live biomass estimates using the vegetation index tended to be lower than harvest estimates during the first half of the growing season and were higher than harvest estimates during the latter half of the growing season. Peak biomass was attained in early August at which time canopy development would be the fullest. We would expect the greatest proportion of live biomass compared to dead biomass to occur at this time and for the greatest amount of live tissue to be in the upper portions of the canopy. This may have contributed to the higher vegetation index biomass estimates seen at peak biomass and thereafter. Dead biomass did not vary greatly over the season (from 260 to 400 gdw m^{-2}) however, decomposition of carry-over dead material (from previous growing

season, high in the canopy) and the concurrent addition of dead material from immature culm mortality and leaf senescence (low in the canopy) can change the relative vertical position of the dead biomass without large changes in biomass thereby altering reflectance from this component. It would seem reasonable that this change in the location of dead material contributed to the lower live biomass predictions in the first part of the season (when more dead material was in the canopy) and to the higher live biomass predictions in the latter part of the season (when less dead material was in the canopy).

Table 1

REGRESSION MODELS FOR PREDICTING $\underline{S}$. ALTERNIFLORA BIOMASS

Regression Model	Coefficient of Determination (r^2)
VI = .382 + .068 ln(L)	0.75
VI = .149 + .096 ln(T)	0.64
VI = .760 + .055 ln(L/D)	0.88
II = .178 + .104 ln(L)	0.87
II =-.185 + .148 ln(T)	0.76
II = .752 - .078 ln(L/D)	0.88

L - Live leaf biomass: T - Total live biomass; D - Dead biomass
Units on all biomass = grams dry weight per meter squared
n for all regression models = 96
VI = Vegetation Index; II = Infrared Index

Harvest and infrared index estimates of live and total $\underline{S}$. alterniflora biomass are compared in Figure 3. The infrared index estimates of live biomass were very close to the harvest estimates during the early part of the growing season. After peak biomass, the infrared index estimates of live biomass were lower than harvest estimates. The reasons for the apparent underestimates at the end of the growing season are not clear, however, we would postulate that the lower water content of the plant tissue due to tissue maturity and increased interstitial water salinity at this time in the growing season would cause an increase in the middle infrared reflectance resulting in lower infrared index values. Overall the infrared index and vegetation index estimates of biomass were similar.

Although the mean biomass estimates from harvesting and from radiance indicies were similar, considerable variability existed for individual measurements during some parts of the growing season. Figure 4 presents coefficients of determination (r^2) between harvest estimates and vegetation or infrared index estimates of live (a) and total (b) biomass. High r^2

values indicate good linear association between individual harvest and radiance index estimates of biomass. Low r^2 values indicate considerable variation existed for some samples between the two biomass estimates. From May through June, the most disagreement between harvest and radiance index biomass estimates existed. August was the best time period for agreement of the biomass estimates with the latter part of the growing season as a whole being better than the first part. The harvest and radiance index estimates of live biomass were always in better agreement than the total biomass estimates. Harvest and radiance index biomass means in Figures 2 and 3 were generally very similar. This suggests that during those periods when low r^2 values existed between harvested and predicted biomass, the amount of overestimation and underestimation were similar among the 24 samples, yielding means which were comparable. When using radiance index values for biomass prediction, one should scrutinize the results from individual measurements to assure that each estimate is reasonable, particularly early in the growing season.
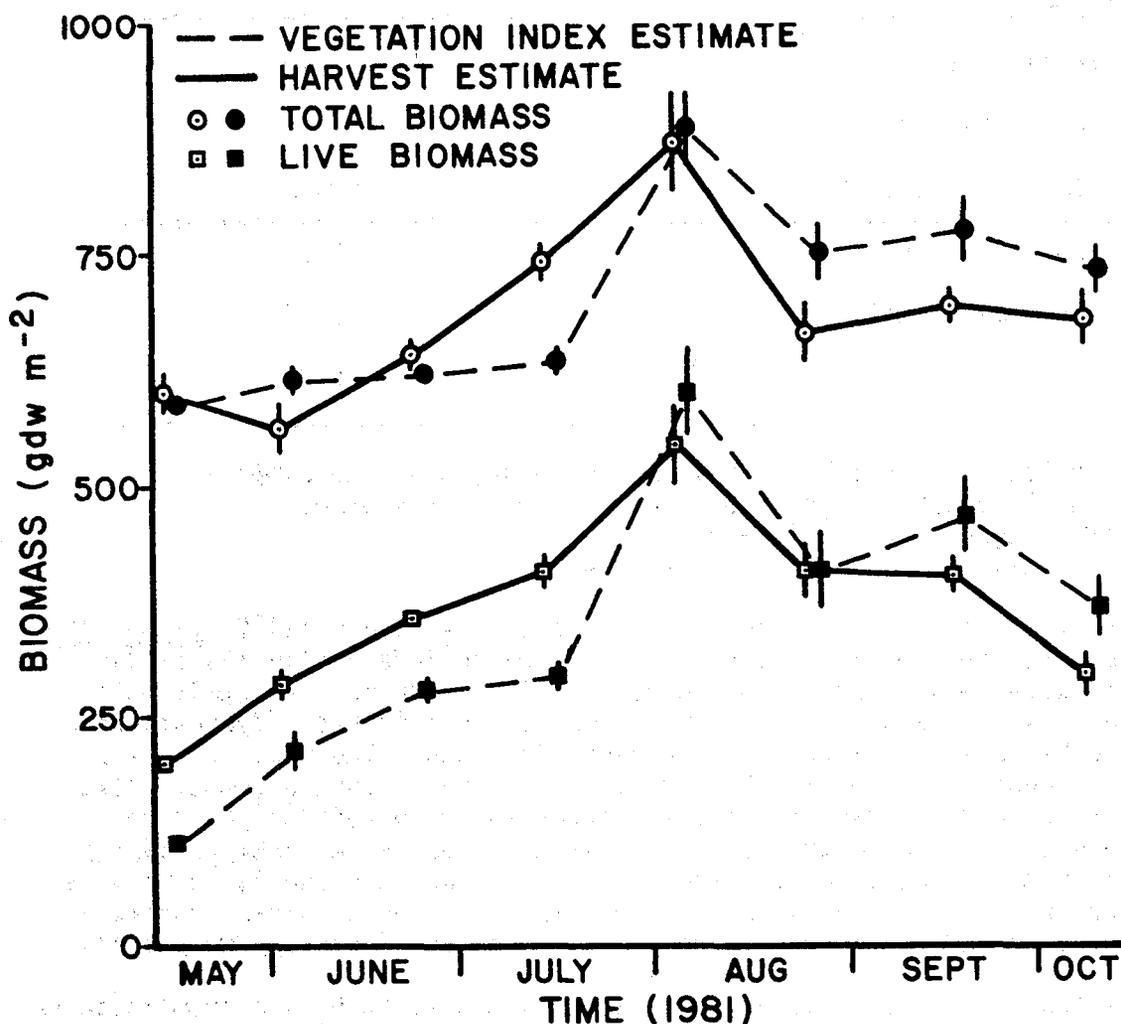
Fig. 2 Vegetation index and harvest estimates of S. alterniflora biomass over the growing season. Bars representing 1 standard error of the mean are shown whenever they exceed the size of the point symbol. Points are slightly offset to improve readability.
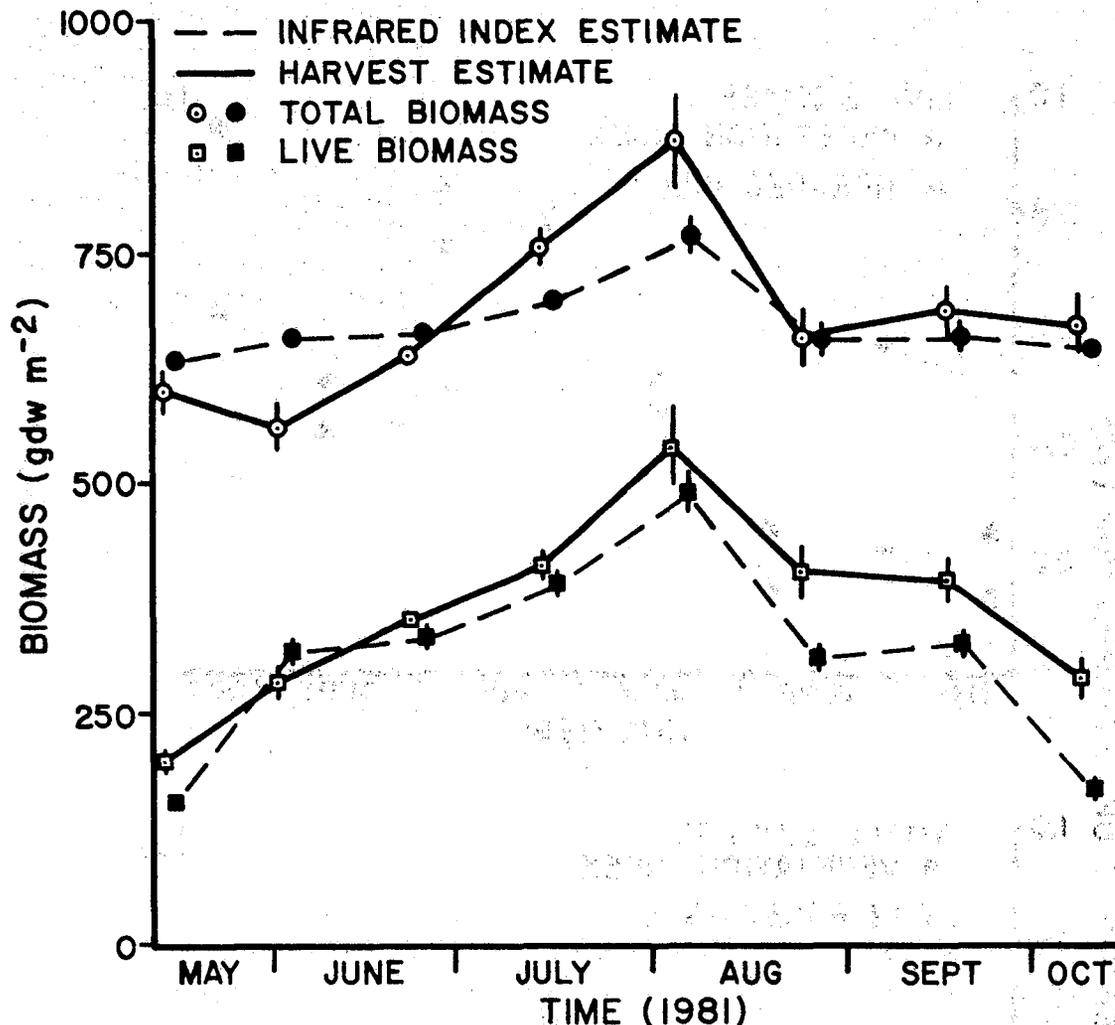
Fig. 3 Infrared index and harvest estimates of S. alterniflora
biomass over the growing season. Bars representing 1 standard
error of the mean are shown whenever they exceed the size of the
point symbol. Points are slightly offset to improve readability.

Salt Marsh - Productivity Estimation

Using the mean biomass estimates shown in Figures 2 and 3, annual
net primary productivity was computed for the S. alterniflora salt
marsh. We employed established production calculation techniques used
widely in salt marsh systems (Table 2). There is some discussion as to
the adequacy of these techniques and we recognize the shortcomings of
each. However, these techniques are widely used and will yield values
comparable to other studies. Linthurst and Reimold (1978) provide an
excellent comparison of various harvest techniques for estimating net
aerial primary productivity in estuarine marsh systems.

Annual net aerial primary productivity estimates for the Canary
Creek marsh are found in Table 2. The vegetation index estimate of
productivity was within 4% of the Smalley (1958) harvest technique and
no more than 21% different from the other techniques. The infrared
index estimates of productivity were within 20% of the Smalley (1958)
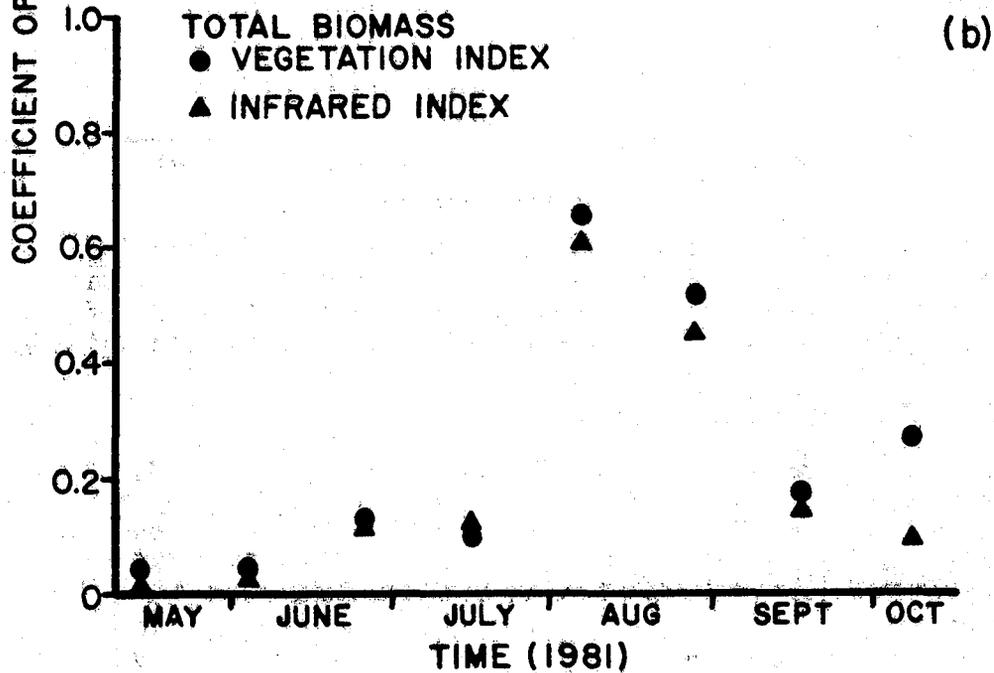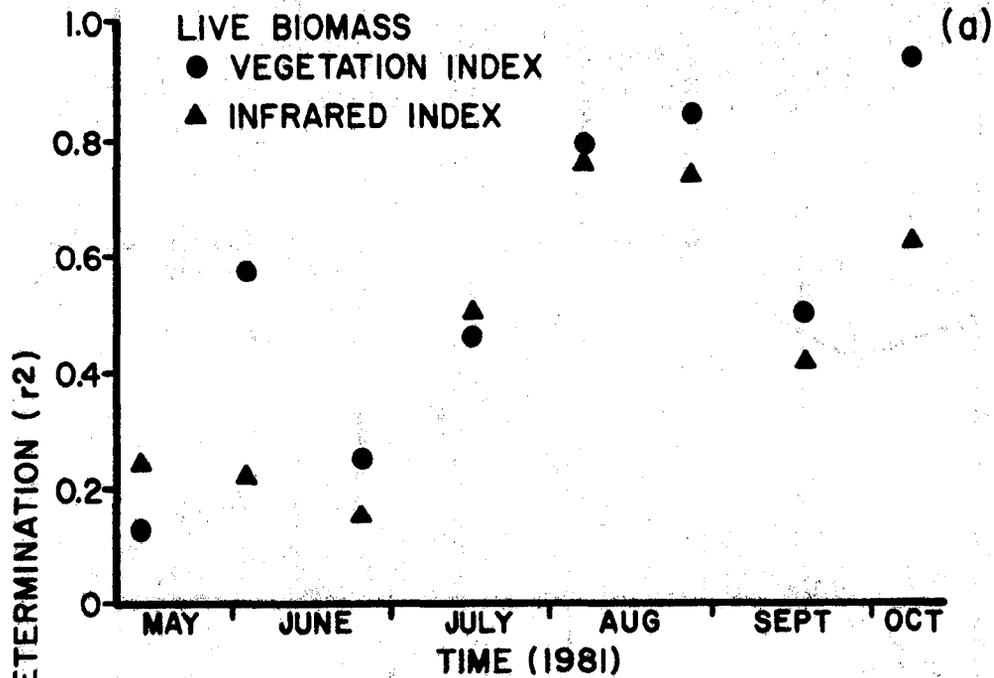
Fig. 4 Coefficients of determination describing the
association between radiance index predictions of
biomass and harvest estimates of biomass over the
growing season.

technique and were 4-5% different from the other techniques. The key to
the agreement between the productivity estimates computed from harvest
and radiance index data was the high correlation between predicted and
harvest biomass during peak biomass (August). For all but the peak
standing crop method of production estimation, successive positive
increments in biomass are summed throughout the growing season, normally
culminating at the point of peak biomass. Therefore, the estimation of
peak biomass is the single most critical measurement in determining
annual production.

Table 2

ANNUAL NET AERIAL PRIMARY PRODUCTIVITY ESTIMATES
FOR SPARTINA ALTERNIFLORA IN CANARY CREEK MARSH

Method	Harvest Estimate	Remote Sensing Estimate	
		VI	II
peak standing crop	517	600	489
Milner & Hughes (1968)	523	661	498
Morgan (1961)	517	600	497
Smalley (1958)	634	661	506

all values are grams dry weight per square meter per year
VI = Vegetation Index; II = Infrared Index

Brackish Marsh - Model Development

Modeling the relationship between spectral radiance indicies and
live aerial biomass in brackish marsh plant communities required consid-
eration of diverse morphologic characteristics among plants residing in
the same community. To illustrate this point, Figure 5 shows the linear
relationship between vegetation index and live biomass for a variety of
wetland plants. Iva, Polygonum, and Solidago represent broadleaf or
deciduous canopies and exhibit rapid increases in vegetation index for
relatively small changes in biomass. This characteristic suggests that
the spectral index can become saturated rapidly. Structurally, these
canopies maintain most leaf surfaces in the horizontal plane and generally
form a complete canopy cover which reduces or eliminates exposure of
dead components or soil background to solar irradiance. This combination
of canopy characteristics yields a very absorptive canopy in the red
region and a very reflective canopy in the near infrared region, thus
the high vegetation index relative to the amount of live biomass present.

The opposite extreme to the broadleaf canopy would be the leafless
canopies represented by Salicornia and Scirpus. Both Salicornia virginica
and Scirpus olneyi possess erect, leafless stems with most green tissue
in the vertical plane and primarily soil background and dead plant material
in the horizontal plane. Normally these canopies are very open with soil

surface characteristics potentially contributing greatly to the observed spectral radiance.

The third canopy type represented in Figure 5 is the gramineous canopy type of Spartina and Typha. Spartina alterniflora exhibits alternate leaves along the length of the stem whereas Typha angustifolia has basal leaves. Both plants form canopies with portions of leaves in the horizontal and in the vertical plane. S. alterniflora exhibits a broad range of canopy configurations as a result of its wide environmental tolerance limits. Both plant canopies can maintain substantial quantities of dead material within the canopy. The amount of live leaf tissue determines to what degree dead material and soil background will influence spectral reflectance. Theoretically, the occurrance of flat leaves (portions of which may be horizontal) in the gramineous canopy would place them somewhere between the broadleaf and leafless canopies in terms of an increase in vegetation index value for an increase in biomass (i.e. an intermediate slope). In practice this does not occur because the measured vegetation index represents the composite of reflectance from vegetation (live and dead) and the soil. In the case of the gramineous canopy, the dead vegetation and soil are oftentimes well illuminated and contribute significantly to the measured vegetation index. The net effect is a lessening of vegetation index increases with increasing biomass.
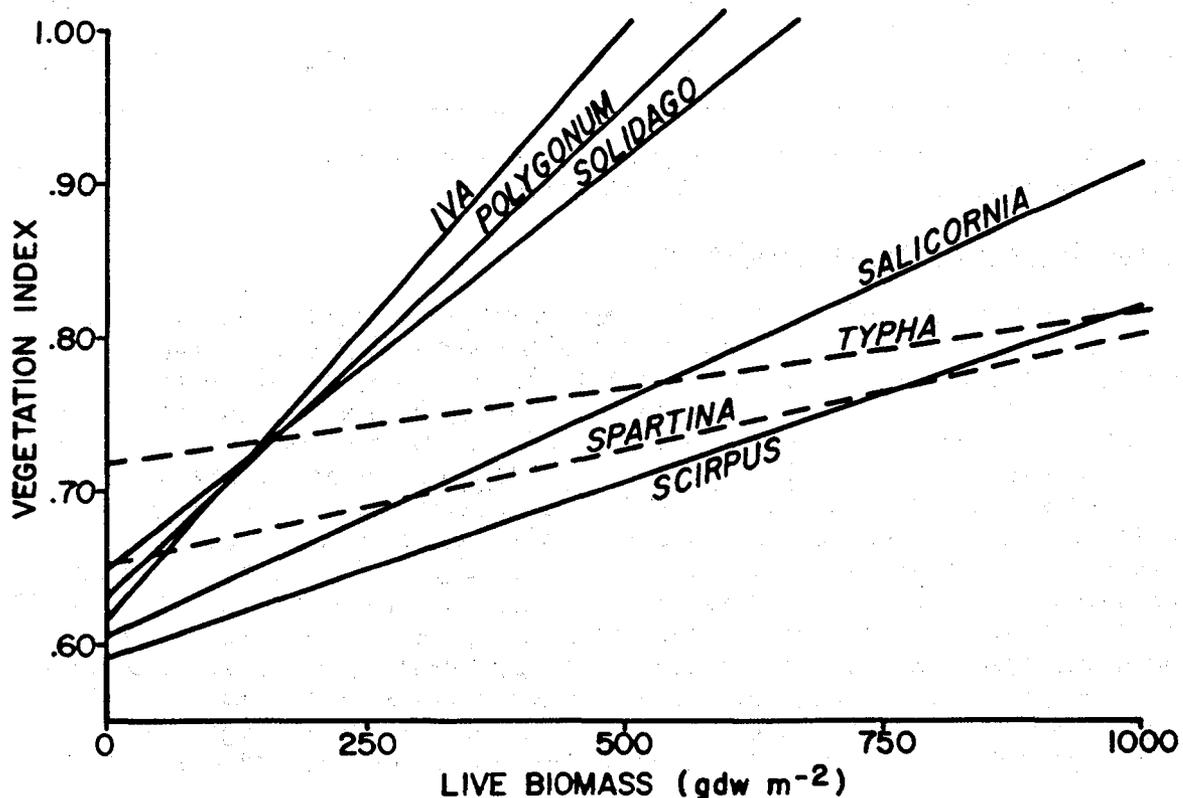
Fig. 5 Comparison of the relationship between vegetation index values and amounts of live biomass for a variety of wetland plants. Iva, Polygonum and Solidago represent broadleaf canopies, Typha and Spartina (dashed lines) represent gramineous canopies and Salicornia and Scirpus represent leafless canopies.

Brackish marsh plant communities are often composed of numerous plant species with morphologies represented by each of the groups discussed. The problem of equating spectral data with live biomass becomes a function of the species composition of the community in question. At present, we lack sufficient data for modeling specific mixtures of the 3 canopy types. So as a first attempt at equating spectral radiance indicies and live aerial biomass, we combined data from each of the morphologic groups into a single model. These data were gathered from stands of Typha angustifolia, Spartina alterniflora, Scirpus olneyi and a broadleaf mixture normally dominated by Acnida cannabina or Hibiscus moscheutos. The areas were sampled monthly from May through August with radiance and biomass data being gathered identical to the brackish marsh samples described in the methods.

Brackish Marsh - Biomass Estimation

The brackish marsh sampled for biomass estimation was diverse in terms of plant species and seasonally dynamic with respect to dominance. Table 3 lists the abundance (expressed as a percent of the total number of samples in which the plant species occurred) and dominance (expressed as a percent of the total number of samples in which the plant species was dominant in terms of biomass) of each plant species encountered during the study. The three most abundant species were Spartina patens, Eleocharis sp. and Acnida cannabina. Grass species dominated most samples during all three sampling periods. There was a slight increase in dominance by broadleaf species in August when most broadleaf plants reached peak biomass.

Simple and multiple regression models equating total live biomass (all species within sample) and the spectral radiance indicies with other canopy descriptors are found in Table 4. Multiple regression models were included for comparison because the percent of total live biomass which was broadleaf biomass (B) and total live biomass expressed as a percent of live plus dead biomass (P) were consistently implicated as important parameters for best fit models. Considering the very different spectral characteristics of broadleaf canopies relative to the gramineous and leafless canopies, and the potential importance of dead vegetation in determining spectral radiance in gramineous and leafless canopies, it was not surprising that these additional parameters (B,P) significantly improved the linear fit (r^2 values) of the models.

Harvest and spectral radiance index estimates of total live biomass for the entire growing season are compared in Table 4. In the case of the vegetation index, the inclusion of B and P reduced the accuracy of the biomass estimate, whereas with the infrared index these two parameters apparently improved the biomass estimate but not to any significant degree. The annual live biomass means predicted with radiance index data were very similar to the live biomass estimated by harvesting. A paired T-test suggested that most harvest and predicted means were not statistically separable at the 0.05 level.

Table 3

ABUNDANCE AND DOMINANCE OF PLANT SPECIES COMPRISING THE OLD MILL CREEK BRACKISH MARSH

Plant Species	June		August		September	
	Abundance[a] (%)	Dominance[b] (%)	Abundance (%)	Dominance (%)	Abundance (%)	Dominance (%)
Acnida cannabina L.	44	6	63	25	44	0
Aster tenuifolius L.	6	0	19	0	25	0
Atriplex patula L.	6	0	19	0	0	0
Carex lurida Wahl.	13	0	13	0	6	0
Distichlis spicata (L.) Greene	50	13	19	0	38	0
Eleocharis sp.	63	0	63	0	50	6
Hibiscus moscheutos L.	44	13	25	6	13	13
Iva frutescens L.	0	0	6	0	0	0
Kosteletzkya virginica (L.) Presl	0	0	13	6	0	0
Panicum virgatum L.	0	0	0	0	6	6
Pluchea purpurascens (Swartz) DC	0	0	0	0	6	0
Polygonum punctatum Ell.	38	0	25	0	19	0
Scirpus olneyi Gray	19	0	13	6	25	6
Spartina alterniflora Loisel.	31	19	44	19	31	25
Spartina cynosuroides (L.) Roth	13	6	19	13	6	6
Spartina patens (Ait.) Muhl.	81	44	69	19	56	38
Unidentified grass	19	0	6	0	6	0

[a]Abundance is based upon presence or absence within a sample and expressed as a percent of the total plots harvested.

[b]Dominance is based upon biomass and expressed as a percent of the total plots harvested.

Table 4

REGRESSION MODELS EQUATING RADIANCE INDICES
AND BRACKISH MARSH CANOPY PARAMETERS.

Model[a]	Annual Live Biomass (gdw m^{-2})		
	Harvest[b]	Predicted	Difference
T = (3278) VI - 1939	691(68)	647(33)	45
T = (4319) VI - (7.12)B - 2682	691(68)	550(49)	142*
T = (4025) VI - (7.16)B + (1.85)P - 2562	691(68)	553(49)	138*
T = (3877) II - 2181	691(68)	727(45)	36
T = (4242) II - (4.06)B - 2402	691(68)	680(51)	12
T = (3902) II - (4.41)B + (2.35)P - 2294	691(68)	674(52)	18

[a] T = total live biomass (gdw m^{-2}), VI = vegetation index, II = infrared index,
B = live biomass of broadleaf species expressed as a percent of total live biomass,
P = total live biomass expressed as percent of total live and dead biomass,
n for all models is 57.

[b] Values are the mean and one standard error, in parenthesis, of 47 samples.
Difference = the numerical difference between the harvest and predicted means.
An asterisk indicates the difference between means was statistically significant
at the 0.05 level.

    The regression models were then used to estimate biomass at each of
the 3 sampling dates (Table 5). Although there was good agreement
between annual harvest and predicted biomass means, substantial deviation
was noted over the growing season. Vegetation index biomass estimates
were very good during June and August but unacceptable during September.
The infrared index only produced acceptable biomass estimates during
August. The failure of the models to yield good biomass estimates
during September was probably related to the rapid senescence of the
marsh plants at this time. The brackish marsh, unlike the salt marsh,
contains annual broadleaf plants which after seed production senesce
rapidly. The larger amount of dead vegetation in the canopy and the
senescence of broadleaf leaves altered the canopy spectral characteristics
sufficiently to invalidate the predictive models at this time of year.
The infrared index estimates of biomass were high in June and low in
September. The high percentage of moisture in young, productive leaf
tissue (June) as opposed to the low percentage of moisture in dead or
senescing leaf tissue (September) probably contributed to the observed
fluctuations in biomass estimation for the infrared index.

Table 5

COMPARISON OF LIVE BIOMASS ESTIMATES FOR A BRACKISH MARSH BY MONTH

Variables[a] in Model	29 June 1981			12 August 1981			19 September 1981		
	Harvest[b]	Predicted	Diff.	Harvest	Predicted	Diff.	Harvest	Predicted	Diff.
VI	609(113)	739(54)	130	649(80)	697(49)	48	814(148)	507(55)	307*
VI, B	609(113)	678(55)	70	649(80)	585(64)	64	814(148)	387(110)	427*
VI, B, P	609(113)	674(56)	66	649(80)	590(66)	60	814(148)	398(111)	416*
II	609(113)	876(48)	267*	649(80)	772(76)	123*	814(148)	537(84)	277*
II, B	609(113)	846(47)	238*	649(80)	712(78)	62	814(148)	484(107)	330*
II, B, P	609(113)	828(52)	220*	649(80)	707(79)	58	814(148)	488(109)	326*

[a] VI = vegetation index, II = infrared index, B = live biomass of broadleaf species expressed as a percent of total live biomass, P = total live biomass expressed as a percent of total live and dead biomass.

[b] Values are the mean and one standard error, in parenthesis, of 16 samples.
Values are live biomass (gdw m^{-2}). Diff. = the difference between harvest and predicted means.
An asterisk indicates the difference between means was statistically significant at the 0.05 level.

DISCUSSION

Other investigators have found good correlations between marsh plant biomass and reflectance in the red and near infrared spectral regions (Drake 1976, Bartlett and Klemas 1981). We have reaffirmed this relationship for S. alterniflora using thematic mapper bands 3 and 4. Previous studies in salt marshes (Budd and Milton 1982), pasture land (Curran 1982) and in agricultural vegetation (Tucker et al. 1981b) suggest a strong relationship between plant biomass and the combination of red and near infrared spectral data. These studies also imply that biomass could be predicted using spectral data. Very few investigators have actually tested models equating biomass and spectral data using a data set independent of the data set used to establish the model. Jensen (1980) working with the salt marsh shrub (Halimione portulacoides) and Curran (1980) working with pasture vegetation have done this with reasonable success. Our data also suggest that spectral radiance models are useful for nondestructive estimates of salt marsh biomass.

The brackish marsh regression models predicted biomass well during the peak of the growing season. The models presented represent an oversimplification of the complex interactions of live and dead vegetation, horizontal and vertical leaf area index, and soil reflectance which are compressed and treated as a single reflecting surface. Brackish marsh canopies are normally much deeper and much more diverse in terms of plant morphologies than salt marsh canopies. It is, therefore, very encouraging when representatives of the 3 most common canopy types measured in relatively pure stands can be combined into a regression model which yields good estimates of biomass for mixed plant stands. The hypothesis that plant morphology (canopy type) is more important in determining measured spectral radiance than consideration of each particular plant species, appears to be valid. For example, Typha canopies were included as input to the predictive regression models, yet in the data set used to test the model, no Typha was present. On the other hand, many plant species were found in the test data set (notably S. patens, Eleocharis sp., D. spicata and P. punctatum) which were not included in the model development data set. The dissimilarities in species composition between the model development and model testing data sets apparently had little effect upon the outcome of live biomass predictions from radiance indicies.

The vegetation index was usually a better spectral transformation for biomass estimation than was the infrared index. The vegetation index has been well established as a useful transformation for monitoring vegetation (Tucker 1979, Tucker et al. 1979a,b) but the infrared index is relatively new. Kimes et al. (1981) and Markham et al. (1981) were among the first to work with the middle infrared band (TM5) using hand-held radiometry. In both studies, they concluded that the middle infrared band contained the same information as the red band. They did acknowledge that their sampling precluded any water stress and that the middle infrared band should undergo additional testing when changes in leaf moisture were expected. More recent work by Hardisky et al. (1983b) suggests that the infrared index may have moisture detection capabilities and therefore, will probably be useful in wetland systems for discriminating

vegetation exposed to varying soil salinity conditions. We believe that additional research must be conducted to determine the worth of the infrared index for vegetation monitoring. The large seasonal variation in biomass predictions in the brackish marsh by the infrared index suggest moisture content or the moisture contrast between live and dead vegetation may have contributed to the results. If our observations are a result of canopy moisture differences, this would indicate a larger seasonal fluctuation in canopy moisture relative to biomass than in chlorophyll content relative to biomass. This could potentially be a very useful tool in monitoring wetlands vegetation.

CONCLUSIONS

Regression models equating total live biomass and spectral radiance indicies were developed and tested for salt and brackish marsh vegetation. Comparisons of biomass predicted using spectral radiance indicies and biomass estimated by traditional harvest techniques were very similar for S. alterniflora biomass. The vegetation index was slightly better for predicting biomass than was the infrared index. The best agreement between predicted and harvested biomass occurred during August (at peak biomass) with a considerable amount of variability at other times of the year. Annual net aerial primary production estimates were also very similar using either predicted or harvest biomass estimates.

Three morphologically distinct canopy types were identified in the brackish marsh vegetation. Data gathered from broadleaf, gramineous and leafless canopies were combined into a single regression model for estimating brackish marsh biomass. The models provided similar estimates of biomass compared to harvest estimates of biomass during June and August for the vegetation index and only during August for the infrared index. Percent broadleaf biomass and percent live biomass were identified as being important parameters for determining total biomass with spectral data. In practice, these additional parameters did little to improve live biomass predictions over the live biomass predictions using only the spectral radiance index.

The thematic mapper bands 3, 4 and 5 used in this study successfully provided the spectral information necessary for nondestructive biomass estimates in coastal marshes. The ground-based radiometric technique described can provide the data necessary for estimates of productivity for some marsh systems. Spectral data gathered with hand-held radiometers from low altitude aircraft and thematic mapper simulator data are presently being tested using the models described in this paper. Preliminary results indicate that with an atmospheric correction, the models work well with spectral data gathered from higher altitude platforms. It seems plausible that the models presented here can be modified for use with thematic mapper spectral data.

ACKNOWLEDGMENTS

LITERATURE CITED

Bartlett, D. S. and V. Klemas. 1981. In situ spectral reflectance studies of tidal wetland grasses. Photogram. Eng. and Remote Sensing 47: 1695-1703.

Budd, J. T. C. and E. J. Milton. 1982. Remote sensing of salt marsh vegetation in the first four proposed Thematic Mapper bands. Int. J. Remote Sensing 3: 147-161.

Curran, P. 1980. Multispectral photographic remote sensing of vegetation amount and productivity. Proc. of the 14th International Sym. on Remote Sensing of Environment, Univ. of Michigan, Ann Arbor, pp. 623-637.

Curran, P. J. 1982. Multispectral photographic remote sensing of green vegetation biomass and productivity. Photogram. Eng. and Remote Sensing 48: 243-250.

Drake, B. G. 1976. Seasonal changes in reflectance and standing crop biomass in three salt marsh communities. Plant Physiol. 58: 696-699.

Hardisky, M. A., R. M. Smart and V. Klemas. 1983a. Seasonal spectral characteristics and aboveground biomass of the tidal marsh plant, Spartina alterniflora. Photogram. Eng. and Remote Sensing 49: 85-92.

Hardisky, M. A., V. Klemas and R. M. Smart. 1983b. The influence of soil salinity, growth form and leaf moisture on the spectral radiance of Spartina alterniflora canopies. Photogram. Eng. and Remote Sensing 49: 77-83.

Jensen, A. 1980. Seasonal changes in near infrared reflectance ratio and standing crop biomass in a salt marsh community dominated by Halimione portulacoides (L.) Aellen. New Phytol. 86: 57-67.

Kimes, D. S., B. L. Markham, C. J. Tucker and J. E. McMurtrey III. 1981. Temporal relationships between spectral response and agronomic variables of a corn canopy. Remote Sensing of Environment 11: 401-411.

Kriegler, F. J., W. A. Malila, R. F. Nalepka and W. Richardson. 1969. Preprocessing transformations and their effects on multispectral recognition. Proc. Sixth International Symp. on Remote Sensing of Environment. Ann Arbor, Michigan. pp. 97-131.

Linthurst, R. A. and R. J. Reimold. 1978. An evaluation of methods for estimating the net aerial primary productivity of estuarine angiosperms. J. Appl. Ecol. 15: 919-931.

Markham, B. L., D. S. Kimes, C. J. Tucker and J. E. McMurtrey III. 1981. Temporal spectral response of a corn canopy. Photogram. Eng. and Remote Sensing 47: 1599-1605.

Milner, C. and R. E. Hughes. 1968. Methods for Measurement of the Primary Production of Grasslands. Blackwell, Oxford. 70 p.

Morgan, M. H. 1961. Annual angiosperm production on a salt marsh. Master's Thesis, University of Delaware, Newark, DE. 34 p.

Reimold, R. J. 1977. Mangals and salt marshes of eastern United States. In: V. J. Chapman, ed. Wet Coastal Ecosystems, Elsevier Scientific Publ. Co., Amsterdam. pp. 157-166.

Rouse, J. W., R. H. Hass, J. A. Schell and D. W. Deering. 1973. Monitoring vegetation systems in the Great Plains with ERTS. Third Earth Resources Technology Satellite-1 Symposium. NASA, pp. 309-317.

Smalley, A. E. 1958. The role of two invertebrate populations, Littorina irrorata and Orchelimum fidicinum in the energy flow of a salt marsh ecosystem. Ph.D. Dissertation, University of Georgia, Athens, GA, 126 p.

Tucker, C. J. 1978. A comparison of satellite sensor bands for vegetation monitoring. Photogram. Eng. and Remote Sensing 44: 1369-1380.

Tucker, C. J. 1979. Red and photographic infrared linear combinations for monitoring vegetation. Remote Sensing of Environment 8: 127-150.

Tucker, C. J., J. H. Elgin, Jr., J. E. McMurtrey III and C. J. Fan. 1979a. Monitoring corn and soybean crop development with hand-held radiometer spectral data. Remote Sensing of Environment 8: 237-248.

Tucker, C. J., J. H. Elgin, Jr. and J. E. McMurtrey III. 1979b. Temporal spectral measurements of corn and soybean crops. Photogram. Eng. and Remote Sensing 45: 643-653.

Tucker, C. J., W. H. Jones, W. A. Kley and G. J. Sundstrom. 1981a. A three-band hand-held radiometer for field use. Science 211: 281-283.

Tucker, C. J., B. N. Holben, J. H. Elgin and J. E. McMurtrey. 1981b. Remote sensing of total dry-matter accumulation in winter wheat. Remote Sensing of Environment 11: 171-189.

Page intentionally left blank

A PRELIMINARY COMPARISON OF THE INFORMATION CONTENT OF DATA
FROM THE LANDSAT 4 THEMATIC MAPPER AND MULTISPECTRAL SCANNER

John C. Price
USDA-ARS Hydrology Laboratory
Beltsville, Maryland

I. INTRODUCTION

In the past two decades great advances have occurred in man's ability to
monitor agriculture from space. The 1972 launch of Landsat 1 began a new
era as the multispectral scanner (MSS) acquired 80 meter spatial resolution
data in four spectral channels on a repetitive basis. This instrument has
subsequently been flown on Landsats 2, 3, and the recently launched
Landsat 4.

This latter satellite also carries an improved imager, the thematic mapper
(TM), which acquires 6 spectral channels at 30 meter resolution as well as
a thermal IR channel at 120 meter resolution. Because both MSS and TM can
acquire data simultaneously it is possible to make direct comparisons of
the advantages and disadvantages of the new instrument vis-a-vis the old.
In this paper the information content[1] of the two instruments is compared
for areas in a representative agricultural region. Although the parameter
"information" does not equate in an obvious way to the value or utility of
the data, it provides a basis for physical interpretation in the same
sense that the mathematically defined variables "brightness," "greenness,"
"yellowness," etc., are ascribed significance in current research. By
focusing on the redundancy of the digital data the estimation of
information content suggests possibilities for algorithms dealing with
subsets of the image data, as well as transformations which reduce the
total volume of data to be analyzed. To the degree that a satisfactory
description by a reduced data set is possible there exist implications
both for design of future satellite instruments and for analysis
procedures.

II. THE MATHEMATICAL FORMULATION OF INFORMATION THEORY

The choice of words used to describe the subject of information theory has an unfortunate history which naturally leads to confusion. I will attempt to describe the existing situation, which presents only undesirable choices for identifying the mathematical quantity which is the principal subject of this paper.

The classic papers in information theory date from the late 40's and early 50's. In these papers Shannon[1] of Bell Laboratories, introduced the quantity "information" as defined by

$$H = - \sum p_i \, Log_2(p_i) \quad \text{(bits)} \quad\quad\quad (1)$$

where p is the probability of a specific numerical value in a series of numbers (i.e., measurements). Although this definition pertains to both continuous and discrete data, it is most commonly applied to discrete data. Thus for a series of random 0's and 1's transmitted over a communication line one finds 1 bit of information per digit.

$$H = -1/2 \times Log_2(1/2) - 1/2 \times Log_2(1/2) = 1 \text{ bit per digit}$$

Shannon's application, and that commonly discussed today, is to the storage, communication, and retrieval of digital information. It naturally falls in the realm of signal processing and computer technology. The word "information" was generally used in early literature in the field, e.g., Schwartz[2].

Implicit in the definition (1) is the fact that a highly variable or random signal contains more information than a constant or low amplitude varying signal. More general formulations of information theory also consider the conditional probability of a series of numbers, with a random sequence resulting in more information than a predictable series. Thus the technical definition of information is directly associated with the disorder or randomness in a series of numbers.

This definition is somewhat contrary to the conventional meaning of the word, resulting in possible confusion. Thus by definition "noise" or static from a radio carries more information to the listener than a complete musical piece, which could be completed by memory by the listener with the radio off, once the first few bars are recognized. Similarly a "noise" image comprised of highly textured speckles would contain more "information" than a picture of a checkerboard.

Possibly realizing this source of confusion Shannon (apparently, i.e., Ter Haar[3]) later adopted the word entropy to describe the previously defined quantity. Thus (Ter Haar, p. 161) "entropy has figured largely in recent discussions in information theory. It must be stressed here that the entropy introduced in information theory is not a thermodynamical quantity and that the use of the same term is rather misleading" (emphasis in the original).

The original use and definition of the word entropy dates to the period 1850–1860, when Clausius and Kelvin considered the mechanical work which could be extracted by a heat engine from a working fluid such as steam. This definition is

$$S = \int \frac{dq}{T} \qquad \text{(Joules/K)}$$

where dq is an element of energy and T is temperature. The definition is appropriate for a reversible process; a more complicated form is necessary when irreversible processes are considered. In the 1930's principles introduced by quantum mechanics demanded a more general formulation of the concept of entropy. This led to a theory based on the foundations of statistical mechanics[4]. The appropriate definition is

$$H = -\sum p_i \log p_i \qquad (2)$$

where the p_i are probabilities associated with energy states (i) of the physical system. For a brief yet complete description see Kittel[5]. The physicist's entropy always involves physical variables relating to the forms of energy, with the quantities in the dimensionless form (2) being expressed as a ratio to Planck's constant. The concept of entropy occupies a central place in thermodynamics and statistical physics.

Until the present day the existence of two conflicting definitions of "entropy" has not been troublesome because the intellectual disciplines have been broadly separated – one is concerned with forms of energy, the other with communication and storage of data. This situation is about to change as the efforts to produce molecular size computer logic circuits, i.e., "chips", will force the consideration of both subject areas at the same time. In general the thermodynamic entropy has many physical applications, the engineering entropy very few.

Evidently at the present time no satisfactory word applies without reservation to the quantity H as given in equation 1. In this paper I will use the letter H and the technical word 'information' when referring to the quantity of equation 1.

III. COMPARISON OF INFORMATION CONTENT OF THE MSS AND TM ON LANDSAT 4.

A prime concern in the estimation of H for image data is the type of landscape being viewed. For example, a uniform featureless scene, such as a desert area, has a low value for H, while a busy scene, such as a city, has a higher value of H. Similarly a scene having no spectral variability, i.e., all wavelength channels having a common brightness value at each point – a black and white scene, has a lower value for H than one in which brightness values differ from one spectral channel to another in a spatially varying way – a multicolored scene.

In this report H is computed for subareas from a scene obtained simultaneously by TM and MSS over an area centered at 36–02 north, 90–02 west in northeast Arkansas. The acquisition date was August 22, 1982.

This area was selected as a test site because it is representative of intensive agriculture in the United States, having relatively small fields, 10 to 80 acres, and a great diversity of field crops. It is not representative of dryland agriculture in the Great Plains, where fields are much larger and several crops account for most agricultural land use. In general one would expect the thematic mapper to lead to smaller advantages compared to MSS in such areas, although this remains to be shown. In urban areas the TM would probably yield even greater advantages over the MSS because the high spatial resolution of the TM resolves many cultural features such as suburban developments, city blocks, etc., which would be averaged out by the coarse resolution of the MSS.

The information per pixel was computed for a number of areas within the scene in order to obtain a statistical representation of the variability in the 185 x 185 km^2 area. Calculations are for areas of 256 x 256 picture elements taken in cropped areas, i.e., water, swamps, forests, etc., were avoided. Table 1 presents the computed values of H for the 6 reflective channels of the TM (1-5, 7), and the 4 channels of the MSS.

Table 1.

a. Multispectral Scanner

Channel 1	3.48	4.04	3.62	3.30
2	4.15	4.34	4.24	3.75
3	5.36	5.46	5.08	4.88
4	4.75	4.75	4.54	4.43
Total	17.74	18.59	17.48	16.36

b. Thematic Mapper

Channel 1	4.30	4.63	4.72	4.09
2	3.92	4.23	4.33	3.77
3	4.66	4.77	4.84	4.25
4	6.84	6.63	6.11	6.27
5	5.51	6.23	6.34	5.43
L6	5.24	5.45	5.51	4.82
Total	30.47	31.94	31.85	28.63

MSS and TM information content per pixel for 256 x 256 areas in the August 22, 1982, scene from northeast Arkansas. In this preliminary analysis the areas do not match; this is not possible for 256 x 256 areas due to the difference of scale.

For historical reasons the NASA nomenclature for the order of the spectral bands is out of sequence. Thus in the NASA ordering the sequence (1, 2,.., 6, 7) corresponds to wavelength values described roughly as 0.4, 0.5, 0.6, 0.8, 1.5, 11., and 2.2 micrometers, so that bands 6 and 7 are out of order. In this paper we shall refer to the bands in logical order (L), so that NASA bands 6 and 7 become L7 and L6, respectively. The inclusion

of the thermal infrared data (L7) in the analysis would be mathematically straightforward. However, the physical processes accounting for radiance values in the thermal IR are quite different from those in the visible and near IR, so that a mixed analysis is potentially misleading[6]. Channels 1-5 and L6 measure the reflected solar radiation from each spot on the ground, providing essentially a picture of the surface. In contrast channel L7 measures emitted thermal radiation from the surface, which results from a balance between a number of energy fluxes, including heat flux into the ground, heating by absorbed solar radiation, transfer of energy from the ground as sensible heating of the atmosphere, etc. The recommended analysis procedure for the thermal IR channel involves modeling surface temperature response to solar heating, meteorological effects, etc.[7, 8, 9]. A formalism is then required for going backward from the modeled temperatures to the surface characteristics which produced these temperatures. In the present work we omit L7 from the analysis, recognizing that L7 provides additional information because it represents an additional physical process.

As table 1 illustrates the information content of all bands of MSS and TM is considerably below the potential capability of the sensor/transmitter system. This results from the bunching of data in a moderately narrow gaussian distribution about a mean value in the lower half of the dynamic range of each instrument. This narrowing and localizing of the data values results in a lower value of H. Although this effect may seem to represent a defect in the instrument design specification, this view is oversimplified. An instrument with a dynamically variable gain could continuously adjust to the range of input radiance values. This would result in an increase in the information content of the data. Higher radiance values could be expected when the sun is high in the sky, lower values in winter. In fact this has been done for scanners on the defense meteorological satellites. However, this additional level of complexity increases cost, and more importantly, complicates greatly the task of providing accurate scientific calibration for the data.

An alternative and much simpler procedure would be to encode the sensor data, e.g., by subtracting off the minimum value of the data and transmitting only enough bits to cover the dynamic range of the result. For example, a data set having values in the range 73-125 could be sent as values 0-53, resulting in a 6 bit transmission rather than the 8 bit range presently used. The constant offset would then be reinserted during ground processing, leaving the output product unaffected in the eyes of the user. Coding procedures of this type will probably be used in future "smart" satellites in order to reduce the cost of the satellite transmitter and data storage devices. The tradeoff of computer components and software in place of satellite hardware becomes more and more desirable as the microelectronics industry evolves.

The most striking feature of Table 1 is the fact that TM bands 5 and L6 are superior to the shorter wavelength bands numbers 1, 2, and 3, in that they have a higher information content. This is a key factor in the conclusion to be developed: the TM provides a substantial improvement over the MSS.

Although the results expressed in Table 1 are suggestive they do not represent a definitive comparison. It is well known that substantial redundancy exists between the spectral bands in Landsat MSS data. This redundancy corresponds to a smaller information content than that obtained by considering the bands separately. The estimate of this redundancy may be carried out in several ways, but the standard technique for multispectral imagery is to apply a principal components transformation to the data[10]. A linear transformation of variables utilizes the correlation coefficients of the various spectral channels to produce new variables which are orthogonal to each other in the sense of an inner product, and aligned with the dominant axes of variability in the data. Redundancy of the original spectral channels equates with decreased variability in some of the new ones. Table 2 illustrates the information content of the transformed variables, where the new components are ordered in terms of decreasing variance, as is conventional. We note that the transformed channels are combinations of those of Table 1, so that a one to one correspondence can not be established between the new and the old channels of data.

Table 2.

a. Multispectral Scanner

P. C. 1	5.77	5.81	5.78	5.40
2	4.32	4.61	4.59	3.97
3	2.44	2.59	2.43	2.46
4	2.20	2.17	2.27	2.19
Total	14.73	15.18	15.07	14.02

b. Thematic Mapper

P. C. 1	6.86	6.67	6.56	6.33
2	5.86	6.41	6.13	5.73
3	4.27	4.45	4.80	3.69
4	3.36	3.52	3.44	3.21
5	2.63	2.60	2.67	2.50
L6	2.25	2.27	2.25	2.07
Total	25.23	25.92	25.85	23.53

Information content for the subscenes of table 1 following a principal components transformation.

Evidently the redundancy of the original spectral channels does produce a substantial overestimate of information in the calibrated data. The three bits difference for MSS corresponds to a factor of $2^3 = 8$, while the 5 bit decrease in the information for TM (from approximately 30 to 25) corresponds to a factor of $2^5 = 32$ in the number of probable combinations of digital values in the respective data sets.

A second form of redundancy exists in image data: that due to spatial correlations. If the Landsat digital values are in a random sequence as

the scanner images the earth then each individual pixel has no predictive value for its successor. Conversely, if large areas (long sequences of values) have a uniform reflectivity value (constant digital value) then with high probability of success one may assign to each pixel value that of its predecessor. The reduction in information due to this effect will be estimated here by use of the difference operator which replaces each value (except the first of a sequence) by its difference. Thus $x_i' =$ $x_i - x_{i-1}$ where i indicates the pixel number along a line. This replacement is called a delta transformation[11]. The information content of the differenced data is given in Table 3.

Table 3.

a. Multispectral Scanner

1	4.50	4.07	4.57	4.38
2	3.64	3.73	3.81	3.37
3	2.44	2.59	2.43	2.46
4	2.20	2.17	2.27	2.19
Total	14.73	12.56	13.08	12.40

b. Thematic Mapper

1	5.09	5.46	5.38	5.19
2	4.72	5.47	5.00	4.59
3	3.74	4.15	4.04	3.52
4	3.11	3.43	3.36	3.16
5	2.63	2.60	2.67	2.50
L6	2.20	2.27	2.25	2.07
Total	21.49	23.38	22.70	21.03

Information content of principal component data after spatial differencing. Underlined values are from table 2 - the spatial differencing produced an apparent increase in the information content of these channels.

For both MSS and TM the spatial redundancy due to large uniform fields is evidenced by the reduction of H in the differenced data. This is most apparent in the first and second principal components of the transformed data. In some of the lower order components a reverse situation exists. These components are dominated by low level random variations which represent noise, either in the scanning instrument, or caused by small variations of spectral response due to insignificant differences in surface cover. For example, localized patches of weeds, crop density variations due to differing soils, scattered bushes, etc., cause minor variations in surface appearance which are essentially uncorrelated with large scale land use and surface type. In the principal components analysis these low level random variations are represented in the higher numbered components. Spatial differencing these components is like differentiating noise - the amplitude of the differentiated signal is greater than that of the original. For this reason the lower of the

values (H, or dH/dx) is given in the third table, with the H values, as opposed to those from the delta transformation, underlined.

It appears that the higher precision of the TM (8 bits as compared to 7 for MSS 1-3), does produce incremental improvement in the ability to resolve spatial differences. Note that in only 7 of 28 cases does spatial differencing increase the computed information value for the principal components of the TM data.

The principal result of the analysis is expressed in the row "total" for the two instruments in Table 3. These numbers permit the assessment of the efficiency of the two instruments as given by the ratio (total information in the data)/(possible information in the data). For the scene studied this ratio is of the order of 13/27 = 0.48 for MSS, and 22/48 = 0.45 for TM. The numbers are esentially equal so the efficiency of the TM is equivalent to that of the MSS.

A factor of some importance has not been studied to this point. Some of the variability in the digital data from both instruments is due to instrument noise and to surface variability as a spatial scale and magnitude too small to be meaningful for analysis purposes. This fraction of the information content of the data is effectively useless and could be discarded without harm. Of course, there is no clear line dividing good from bad data, so this division is a subjective one. However, it is likely that the highest order principal components, i.e., 4 for MSS and 5 and 6 for TM, are not physically significant. This subject deserves further attention. The commonly heard expression, "one man's signal is another man's noise" is pertinent here, but this statement does not have unlimited applicability. It is already known that some of the Landsat 4 images are marred by measurable noise in the data. A 1 or 2 bit variation due to instrument noise effectively reduces the information content of the data by this amount, if one considers applications by the user community.

In view of these factors one may say that for the northeast Arkansas scene the MSS acquires about 10 bits of information per pixel, the TM about 20.

IV. DISCUSSION

The results are more encouraging than expected. Generally the MSS has adequate spatial resolution to resolve most fields in this representative agricultural area. To the extent that this is true the TM would provide only a modest improvement in information content compared to MSS because the main effect would be to decrease border pixels or mixed pixels as a fraction of the total area of the scene. Evidently this effect is quite substantial.

A second somewhat surprising observation is the fact that the new channels, TM 5 and L6, have greater values of H than the visible bands. This is surprising only in the sense that data in these spectral intervals has not previously been generally available. However, there is no a priori reason to expect the middle infrared variability to be so large. These new channels provide not just a marginal improvement, but a substantial gain in information.

The implications of this work may be stated broadly, but further analysis must be carried out. Certainly it is reasonable to expect several possibilities.

   a. The compression of TM and MSS data (e.g., more imagery per physical tape) by a factor of at least two.

   b. Specification of observing instruments which acquire substantially the same information with fewer spectral channels (e.g., 2 channels in the visible as opposed to 3 or 4.

Evidently continued study of additional data sets is desirable; the general outlook is promising.

V. REFERENCES

1. C. E. Shannon, "A Mathematical Theory of Communication," Bell System Tech. J., 27, 1948 pp. 379-423 and 623-656.

2. M. Schwartz, Information Transmission, Modulation and Noise, McGraw Hill, Inc., New York, 1959, 461 pp.

3. D. Ter Haar, Elements of Statistical Mechanics, Rinehart and Company, New York, 1954, 468 pp.

4. J. W. Gibbs, The collected works of J. Willard Gibbs, V. 2, Longmans, Green, New York, 1928.

5. C. Kittel, Elementary Statistical Physics, John Wiley and Sons, New York, 1958, 228 pp.

6. Price, J. C., "The contribution of thermal data in Landsat multispectral classification, Photogrammetric Engineering and Remote Sensing," 47, 1981, pp. 229-236.

7. T. N. Carlson and F. E. Boland, "Analysis of Rural-Urban Canopy Using a Surface Heat Flux/Temperature Model," J. Appl. Met. 17, 1978, pp. 998-1013.

8. J. C. Price, "The Potential of Remotely Sensed Thermal Infrared Data to Infer Surface Soil Moisture and Evaporation," Water Resources Research, Vol. 16, No. 4, 1980, pp. 787-795.

9. J. C. Price, "Estimation of Regional Scale Evapotranspiration Through Analysis of Satellite Thermal-Infrared Data," IEEE Transactions on Geoscience and Remote Sensing, GE-20, 1982, pp. 286-292.

10. H. Hotelling, 1933, "Analysis of a Complex of Statistical Variables into Principal Components," J. Educ. Psychol. 24, pp. 417-441 and 498-520.

11. C. Gonzalez and P. Wintz, "Digital Image Processing," Addison Wesley, Reading, Mass., 1977, 431 pp.

Page intentionally left blank

EARLY RESULTS OF INVESTIGATIONS OF LANDSAT 4 THEMATIC MAPPER AND MULTISPECTRAL SCANNER APPLICATIONS

F. G. Sadowski
J. A. Sturdevant
W. H. Anderson
P. M. Seevers
J. W. Feuquay
L. K. Balick
F. A. Waltz
Technicolor Government Services, Inc.
EROS Data Center
Sioux Falls, South Dakota 57198

D. T. Lauer
U.S. Geological Survey
EROS Data Center
Sioux Falls, South Dakota 57198

INTRODUCTION

The EROS Data Center's mission includes integrating satellite and aircraft remote sensing technology into the operational programs of the resource management agencies within the Department of Interior. In pursuit of this mission, scientists at the EROS Data Center (EDC) have begun to evaluate newly acquired Landsat 4 Thematic Mapper (TM) data for their potential utility in Earth science and land mapping applications. The overall objective is to compare the value of TM data to Multispectral Scanner (MSS) and other types of remotely sensed data, for providing information that can help to meet Department of Interior resource information needs.

This paper summarizes the early results of studies using data from the first available Landsat 4 TM scene of Washington, D.C., which was acquired November 2, 1982 (Scene ID 4019-15140). These results were reported at the Landsat 4 Early Results Symposium at Goddard Space Flight Center on February 22 to 24, 1983.

The results are organized into four sections. The first presents some of the characteristics of TM digital data that were observed for five broad classes of land cover. Some comparisons are drawn between coincident Landsat 4 TM and MSS data. The second section presents an evaluation of TM spectral data as single-band, black-and-white images, and in several three-band color-composite images. The remaining two sections describe demonstrations of TM data transformations which can be used to present the data in a manner that is potentially more useful for analysis or display. These transformations enable generating (a) hue, intensity, and saturation data space from red, green, and blue color space, and (b) perspective view images.

CHARACTERISTICS OF THEMATIC MAPPER DIGITAL DATA

The TM digital data were evaluated for their potential to provide improved land cover information. The analyses included (a) testing for information that may be offered by the new TM spectral bands and (b) comparing data characteritics for equivalent spectral bands of the TM and MSS sensors. The analyses were conducted on several large samples of pixels corresponding to five broad land cover classes.

Methods

The TM digital data characteristics were evaluated for a portion of the Washington, D.C. scene that included the vicinity of Dulles Airport, the Potomac River, and the central District of Columbia. This subscene was approximately 1000 lines north-south by 3,000 pixels east-west. The coincident MSS subscene was spatially registered to the TM subscene to allow analysis of pixels for common ground areas. The TM data were resampled to 25- by 25-meter pixel size via cubic convolution, and registered to a Universal Transverse Mercator (UTM) map projection. The MSS data were resampled to 50- by 50-meter pixel size via cubic convolution. Following an appropriate shift of the MSS data relative to the TM data, the 50- by 50-meter MSS pixels were then replicated to produce four 25- by 25-meter pixels in place of each larger pixel. This replication of MSS pixels created an expanded data set of equal dimensions with and registered to the TM data.

The TM and MSS digital data were analyzed for five broad classes of land cover. Pixels were selected to include a wide variation of conditions within each class so that spectral band relationships could be observed in response to variations in fundamental land cover properties. The five land cover classes (and the associated fundamental properties) were:

a. Forest (species and density),
b. Herbaceous vegetation (species and percent cover),
c. Bare soils (brightness),
d. Impervious surfaces (brightness), and
e. Water (turbidity).

Pixels in the TM subscene were grouped into land cover classes by level-slicing one (or more) spectral band(s). This parallelepiped method of classification was repeated several times to create a separate image for each land cover class. Each image was then spatially edited to remove the boundary pixels of clusters as well as individually occurring pixels. Images of land cover classes which contained large proportions of the original scene (i.e., the forest and herbaceous classes) were sampled to reduce the number of pixels to approximately 20,000. Finally, the images created for TM data were used to mask equivalent locations of pixels in the MSS data.

<u>Results</u>

1. Information potential of the TM spectral bands.

    Information content of a spectral band may be directly related to the
    range of data values recorded for a scene. The presumption here is that
    a large range of data values will occur in spectral bands which are
    particularly responsive to variations in land cover. If there are no
    band-dependent sources of noise within a sensor system, the range of data
    values (and related statistical parameters, i.e., variance) may provide a
    straightforward measure of information content that is readily comparable
    among several spectral bands.

    The relative variabilities of data values in individual TM spectral bands
    for each land cover class are compared in Table 1. The coefficients of

Table 1

RELATIVE VARIABILITY IN DATA VALUES ASSOCIATED WITH TM SPECTRAL BANDS

Numbers in table are coefficients of variation (CV)*. Superscripts denote
ranking of bands for each land cover class according to magnitude of CV.

Land Cover Class	Band 1	Band 2	Band 3	Band 4	Band 5	Band 6	Band 7
Forest	$.03^6$	$.04^5$	$.08^3$	$.08^4$	$.17^2$	$.01^7$	$.21^1$
Herbaceous Vegetation	$.04^6$	$.06^5$	$.09^4$	$.13^2$	$.12^3$	$.01^7$	$.16^1$
Bare Soils	$.09^3$	$.15^2$	$.22^1$	$.22^1$	$.22^1$	$.02^4$	$.22^1$
Impervious Surfaces	$.22^4$	$.29^2$	$.32^1$	$.29^2$	$.28^3$	$.02^5$	$.32^1$
Water	$.03^6$	$.06^5$	$.08^4$	$.13^3$	$.50^1$	$.03^6$	$.48^2$

*where CV = standard deviation/mean.

    variation (CV) in the table normalize for the differences in mean data
    values between bands. The large CVs noted for bands 5 and 7 in all land
    cover classes may provide evidence for the value of these mid-IR bands.
    The CVs for these two bands are generally similar to the CVs of other

bands (e.g., 2, 3, and 4) for nonvegetated land areas (bare soils and impervious classes). However, the CVs for at least one of these two bands are larger than the CVs of all other bands for the two vegetated land cover classes and water. This suggests that the mid-IR bands provide an improved capability to detect variable conditions within vegetated land areas and water areas. The blue band (band 1) has a CV smaller than all other reflective spectral bands (bands 1-5, and 7). The thermal band (band 6) exhibits a very small CV in all bands for all land cover classes.

Correlations among the TM spectral bands can provide insight into information potential. Generally, high correlations between two bands imply redundancy of information, while low correlations indicate that different information is present in each band. The correlations among the visible and reflective-IR bands of TM data for all land cover classes

Table 2

CORRELATIONS* AMONG VISIBLE AND REFLECTIVE-IR BANDS IN TM DATA

Spectral bands	Forest (20,000 pixels)	Herbaceous vegetation (20,000 pixels)	Bare soils (33,000 pixels)	Impervious surfaces (5,000 pixels)	Water (15,000 pixels)
Visible bands					
2 with 3	.28	.62	.97	.96	.72
1 with 3	.31	.65	.95	.91	.51
1 with 2	.38	.66	.95	.95	.50
Reflective-IR bands					
4 with 5	-.11	.15	.87	.81	.44
4 with 7	-.18	-.14	.82	.80	.40
5 with 7	.89	.83	.93	.95	.69
Reflective-IR with visible bands					
4 with 1	.08	-.03	.88	.84	.23
4 with 2	.25	.25	.91	.91	.25
4 with 3	.05	-.26	.92	.97	.36
5 with 1	.34	.31	.85	.57	.11
5 with 2	.28	.41	.87	.69	.14
5 with 3	.74	.48	.89	.78	.21
7 with 1	.39	.44	.87	.58	.14
7 with 2	.33	.44	.88	.70	.13
7 with 3	.65	.65	.90	.78	.20

* All correlations significant at the 99-percent level of confidence.

are provided in Table 2. The following observations are noted:

a. Visible bands have low to moderate correlations for vegetated land
    areas (forest and herbaceous vegetation classes). The low
    correlations for the forest theme are probably the result of greater
    variations in color for the tree crown foliage which was in the midst
    of fall color change.

b. Visible bands are highly correlated for nonvegetated land areas,
    probably because the major variation within these areas appears to be
    brightness. Dramatic color variations are not evident.

c. Correlations among visible bands for water areas suggest a particular
    advantage for using the blue band (band 1), because of its lower
    correlation with both the green band (band 2) and red band (band 3).

d. Mid-IR bands (5 and 7) have generally low correlations with the
    visible and near-IR bands (1 through 4) for vegetated areas and water
    areas.

e. Mid-IR bands (5 and 7) have generally high correlations with the
    visible and near-IR bands (1 through 4) for bare soils areas and
    moderate correlations for impervious surfaces.

f. Mid-IR bands (5 and 7) are most highly correlated with each
    other for nonvegetated land areas. High correlations also occur for
    vegetated land areas. A moderate correlation occurs for water areas.

The correlations in Table 2 do not enable statements about combinations
of spectral bands which optimize information for particular land cover
classes. Furthermore, the correlations observed are scene-specific and
thus possibly not illustrative of more general considerations that have
influenced spectral band selection for the Thematic Mapper. Nevertheless,
the correlations noted here indicate that:

a. There are situations in which the mid-IR bands (5 and 7) may
    provide a greater amount of new and different information for
    vegetated land areas than for nonvegetated land areas.

b. Information contained in the two mid-IR bands (5 and 7) may be
    largely redundant for some applications.

c. The blue band (band 1) may be more useful for certain applications
    involving water and vegetated land areas than for nonvegetated areas.

Principal components analyses were conducted to evaluate the differences
in dimensionality exhibited by TM and MSS data and to assess the
contributions to total variance that are offered by the additional TM
spectral bands (Ref. 1). Principal components were computed for a single
image file from each of the TM and MSS data sets that contained a sample
of pixels from all five land cover classes. (The analysis of the TM data
treated the six reflective spectral bands only.)

The principal components computed for each data set are presented in Table 3. The transformed MSS data appear to be principally

Table 3

PRINCIPAL COMPONENTS (PC) FOR TRANSFORMED MSS AND TM DATA SETS

MSS Data

Spectral band	PC1 (80.8)*	PC2 (16.2)	PC3 (1.9)	PC4 (1.1)
1	.203	.452	-.294	.818
2	.212	.810	.421	-.348
3	.768	-.071	-.535	-.344
4	.569	-.367	.671	.303

TM Data

Spectral band	PC1 (73.4)*	PC2 (18.8)	PC3 (6.4)	PC4 (0.7)	PC5 (0.5)	PC6 (0.2)
1	.262	.195	.608	.411	.534	.264
2	.199	.070	.342	-.042	-.028	-.914
3	.278	.287	.396	-.045	-.784	.257
4	.398	-.871	.205	-.170	-.031	.105
5	.728	.122	-.561	.370	-.020	-.058
7	.355	.317	-.030	-.813	.312	.118

* Percent of total variance accounted for by each component.

two-dimensional because 97.0 percent of the total variance is included in the first two components. This has been a commonly observed characteristic of most MSS data. However, the transformed six-band TM data show the potential for providing a significant third dimension of information that, in combination with the first and second components, accounts for 98.6 percent of the total variance.

The first two components in the transformed MSS data have coefficients that are more or less characteristic of many agricultural scenes. These two dimensions are frequently referred to as "brightness" and "greenness" (Ref. 2). The first two components in the transformed TM data have coefficients also suggestive of brightness and greenness. Coefficients for the first component (PC1) are all positive, suggesting an overall brightness contribution by all of the original spectral bands. The second component (PC2) shows the near-IR band (band 4) contrasted with the visible bands, much as occurs for the second component in the MSS data. The third component (PC3) of the TM data, accounting for 6.4 percent of the total data variance, shows that bands 5 and 7 contrast with all other bands. This suggests that new and different information is present in the TM reflective spectral bands to an extent that may contribute significantly to the overall variability of the scene.

2. Data characteristics for equivalent spectral bands of the TM and MSS sensors.

The preparation of a spatially registered digital data set containing coincident TM and MSS data allowed comparison of data characteristics over common ground areas for equivalent TM and MSS spectral bands. For example, probability density ellipses for the .68 level of probability around the mean value of each land cover class in TM and MSS data respectively, are shown in Figs. 1 and 2. The figures enable comparing the separation between the mean values of the land cover classes and the variance within classes for the equivalent pair of spectral bands in each data set.

The separation between means is greater in both the red and near-IR bands of the TM data (Fig. 1) than in the comparable MSS bands (Fig. 2). Although not shown here, the separation is also greater for the green band of TM data than for the green MSS band. Variances within most land cover classes are also greater in the TM data (water is an exception). However, when compared on a relative basis, the variations in data values for many of the classes in TM data are less than those in equivalent spectral bands in MSS data. Table 4 compares coefficients of variation for equivalent spectral bands by land cover class. (The CVs can be used to compare among bands and sensors to determine which contain the greatest relative variation.) Most (12 out of 15) CVs for the TM spectral bands are less than or equal to the CVs for equivalent MSS spectral bands.

The combination of greater mean separation and generally lower relative variations in data values suggests an improved capability for multispectral discrimination of land cover classes in TM bands 2, 3, and 4 over the equivalent MSS bands. However, due to the presence of an artifact noted in the MSS data, the results noted above may be limited to the MSS data of Landsat 4 only, and thus not be representative of MSS data in general. The artifact occurred as a pattern of systematic banding oriented diagonally (from northeast to southwest) across the image. To quantify the severity of the banding, we computed a coefficient of
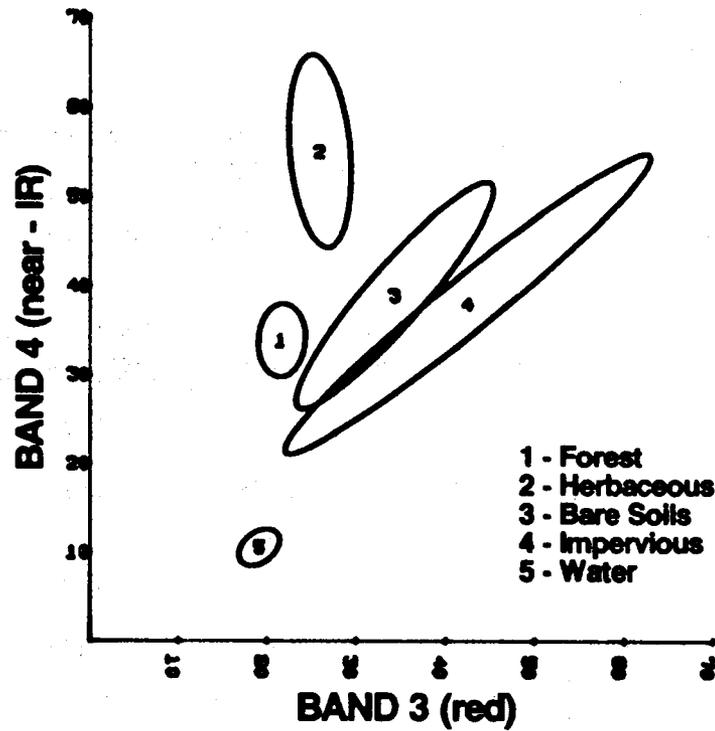
Fig. 1 One standard deviation, covariance ellipses for land cover classes in TM data.
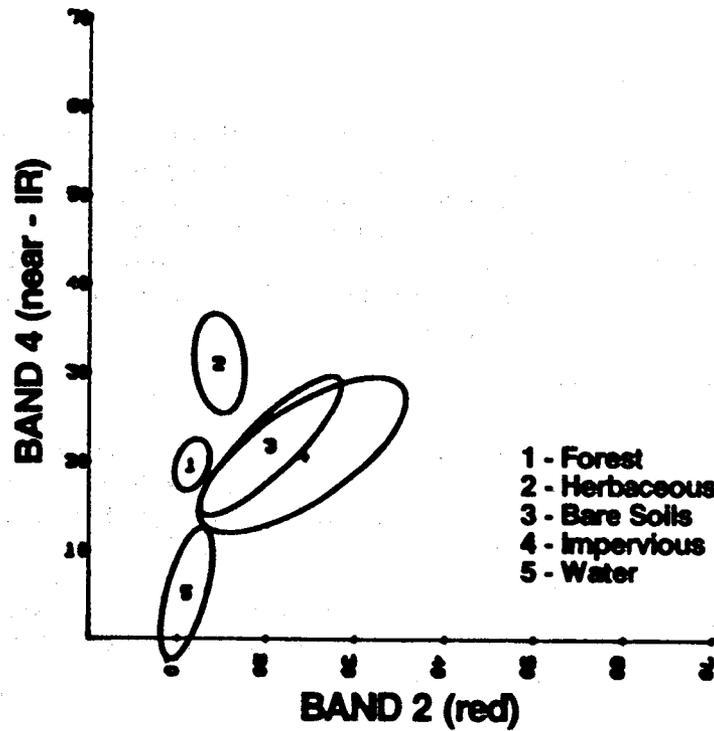
Fig. 2 One standard deviation, covariance ellipses for land cover classes in coincident MSS data.

Table 4

RELATIVE VARIABILITY IN DATA VALUES FOR EQUIVALENT SPECTRAL BANDS
OF THE TM AND MSS SENSORS

Numbers in table are coefficient of variation (CV) for pixels of common
ground area in both data sets.

Sensor and spectral region	Forest	Herbaceous vegetation	Bare soils	Impervious surfaces	Water
MSS green (band 1)	.08	.08	.17	.25	.10
TM green (band 2)	.04*	.06*	.15*	.29	.06*
MSS red (band 2)	.12	.13	.26	.32	.18
TM red (band 3)	.08*	.09*	.22*	.32*	.08*
MSS near-IR (band 4)	.10	.12	.24	.28	.95
TM near-IR (band 4)	.08*	.13	.22*	.29	.13*

* TM (CV) $\leq$ MSS (CV)
  where CV = standard deviation/mean.

    variation for an area of water common to both data sets. Water was
selected as a region having low relatively homogeneous reflectance where
the effect of the banding would be most pronounced. Our results showed
the CVs for water in the MSS data to be three to five times greater than
the CVs for equivalent spectral bands in the TM data. This observation
explains the much greater size for the ellipse for water in MSS data
(Fig. 2) than in TM data (Fig. 1).

TM IMAGE INTERPRETATION TESTS

Because seven different black-and-white images can be generated from TM data,
the question arises as to which single-band image is best suited (from the
visual interpretation standpoint) for a particular application. Similarly,
what combination of three TM bands would likely produce the most interpretable
color-composite image? To gain insight into the answers to these questions, a
test was designed to evaluate the relative interpretability of TM spectral
bands as single-band, black-and-white images, and in several three-band
combinations as color-composite images.

Methods

Black-and-white images of the six reflective TM bands, and six three-band color-composite images were prepared from digitally-enhanced data. Digital enhancements included contrast-stretching the digital data values to fill the entire dynamic range and spatial filtering to increase edge definition. The six color-composite images were:

a. A simulated natural-color image (bands 1, 2, and 3 printed as blue, green, and red, respectively),

b. Two simulated color-infrared images (bands 2, 3, 4 and 1, 3, 4),

c. Two images using each of bands 5 and 7 in combination with bands 3 and 4, (bands 5, 3, 4 and 7, 3, 4), and

d. An image using the same three bands as the 5, 3, 4 composite listed above but with the sequence of compositing (printing) changed to 3, 5, 4.

Eleven different commonly encountered interpretation categories were defined for interpretation on all images. Examples of each category were located throughout the entire image area of the Washington, D.C., TM scene. For each example, a set of image chips was cut out of the six individual black-and-white images and the six color-composite images. The chips, approximately one inch in diameter, were cut from 1:94,000-scale paper prints of the images. Each chip within the set showed the same area on the ground. Each set, in turn, showed features and conditions pertaining to a particular example of an interpretation category.

A total of 420 image chips within 11 categories were submitted to three interpreters for evaluation. The interpreters were asked to rank the black-and-white chips within each set on a scale of 1 to 6 and similarly for the six color composite images. A ranking of 1 was to indicate most interpretable (or best) for that particular interpretation category.

Results

The average scores of interpreter preferences for images in all categories are shown in Tables 5 and 6. Because the selection of a best or most interpretable image is likely dependent on the subject of interpretation, the results are presented by category.

Rankings of interpretability for the individual bands (Table 5) suggest that images of the mid-IR bands (5 and 7) may be very useful for supplying information in many of the interpretation categories. One of these two bands was ranked first in 8 of 11 categories that included both vegetated and nonvegetated scene areas. Interpreters had generally low preferences for images of the blue band (band 1) in most categories.

Table 5

AVERAGE SCORES[1] FOR INTERPRETABILITY OF INDIVIDUAL TM BAND BLACK-AND-WHITE
IMAGES

Superscripts denote ranking of bands for each
category from highest (1.0) to lowest.

Interpretation category[2]		Band number					
		1	2	3	4	5	7
Natural vegetation differentiation	(5)	5.6^6	5.2^5	3.1^3	3.8^4	1.1^1	2.3^2
Forest drainage pattern recognition	(3)	6.0^6	5.0^5	3.8^4	1.7^2	1.3^1	3.2^3
Among fields vegetation variation	(3)	5.7^6	4.3^5	3.6^4	1.8^1	3.3^3	2.3^2
Within field vegetation variation	(2)	5.7^5	4.2^4	4.2^4	3.8^3	2.0^2	1.8^1
Soil/vegetation differentiation	(1)	5.0^5	4.0^4	2.7^3	6.0^6	2.3^2	1.0^1
Among fields soils variation	(1)	2.7^2	4.7^4	4.0^3	6.0^5	1.0^1	2.7^2
Within field soils variation	(3)	3.7^4	2.9^1	3.1^2	3.8^5	4.0^6	3.6^3
Residential details	(3)	3.3^4	4.0^5	5.9^6	2.9^2	3.1^3	1.8^1
Business core details	(3)	5.1^6	4.6^5	3.4^4	2.9^3	2.8^2	2.2^1
Water/vegetation differentiation	(4)	6.0^6	4.8^5	4.2^4	2.2^2	1.6^1	2.3^3
Water turbidity variation	(3)	3.8^4	2.1^2	1.1^1	3.7^3	5.2^5	5.1^6

[1] Average of three interpreters' ranking of the number of examples indicated.

[2] Number in parentheses indicates number of examples interpreted.

Table 6

AVERAGE SCORES[1] FOR INTERPRETABILITY OF TM COLOR COMPOSITE IMAGES

Superscripts denote ranking of composites for each
category from highest (1.0) to lowest.

Interpretation category[2]		Band combination[3]					
		123	134	234	534	734	354
Natural vegetation differentiation	(6)	5.8^6	4.2^5	3.1^2	3.3^3	3.6^4	1.1^1
Forest drainage pattern recognition	(3)	5.8^6	2.2^2	1.7^1	4.8^5	2.6^3	4.0^4
Among fields vegetation variation	(3)	6.0^6	3.8^5	2.6^2	3.6^4	3.4^3	1.7^1
Within field vegetation variation	(3)	6.0^6	3.5^5	3.2^3	3.3^4	2.3^1	2.7^2
Soil/vegetation differentiation	(2)	4.0^4	4.7^5	2.8^2	3.5^3	3.5^3	2.5^1
Among fields soils variation	(2)	5.0^5	3.0^3	2.0^1	3.7^4	5.0^5	2.3^2
Within field soils variation	(3)	1.7^1	3.7^3	2.8^2	5.3^5	4.0^4	3.7^3
Residential details	(3)	3.0^1	3.3^2	3.0^1	3.3^2	4.0^3	5.3^4
Business core details	(3)	2.0^2	3.7^3	1.3^1	4.0^4	4.0^4	6.0^5
Water/vegetation differentiation	(4)	6.0^6	3.8^4	4.0^5	3.3^3	2.4^2	1.4^1
Water turbidity variation	(3)	1.2^1	2.7^2	3.0^3	4.7^5	3.6^4	5.9^6

[1] Average of three interpreters' ranking of the number of examples indicated.

[2] Number in parentheses indicates number of examples interpreted.

[3] All composites printed with blue-green-red filters in the order of bands shown.

Rankings of interpretability for the three-band color composites (Table 6) showed generally high interpreter preferences for the simulated color-infrared composite (bands 2, 3, and 4) in many interpretation categories. This color composite was ranked first or second in 8 of 11 categories. For many categories, interpreter preferences were lower for the color composite consisting of bands 1, 3, and 4. These results suggest that replacement of the green band (band 2) in a color-infrared composite with the blue band (band 1) may reduce the interpretability of the resulting composite for many applications.

Of three color-composite images containing a band from each of the visible, near-IR, and mid-IR spectral regions, the band combination of 3, 5, and 4 showed highest interpreter preferences in 6 of 11 categories. This particular band combination was ranked first over all other combinations in four categories, suggesting the utility of having a band from each of these three spectral regions in a color composite for several applications. However, the varying degrees of interpreter preference evident in Table 6 for the color composite images of bands 3, 5, 4, bands 7, 3, 4, and bands 5, 3, 4 show that the colors assigned to each band in the compositing process may have a significant effect on image interpretability.

The natural-color composite image (bands 1, 2, and 3) ranked generally high in interpreter preference for categories involving distinctions among nonvegetated areas. This type of color composite may have its greatest potential utility for applications where color variations in water, soils, and inner urban areas are of interest.

HUE, INTENSITY, SATURATION TRANSFORMATION

Methods

Color raster images are typically displayed by varying the intensities of three primary colors (red, green, blue) at each pixel location. This approach is simple to implement using computer hardware and is similar to processes used in other image display schemes such as photography or printing. While it is true that color-sensitive receptors in the human eye are most responsive to light centered about the red, green, and blue (RGB) wavelengths, the responses of the eye/brain system to light can best be described by the perceptual variables--hue, intensity, and saturation (HIS) (Ref. 3).

A procedure to create and manipulate color images in these dimensions has been implemented at the EROS Data Center. The procedure consists of transforming an image from the red, green, and blue domain to hue, intensity, and saturation space, manipulating the HIS image, and then performing an inverse transformation back to a red, green, and blue image.

The transform procedure examines the red, green, and blue values of a pixel in a three-band input image and determines hue, intensity, and saturation values for that pixel. Each pixel in the input image is transformed,

resulting in a three-channel data set with the channels representing hue, intensity, and saturation which can then be manipulated in HIS color space. This also affords the opportunity to merge other information with the original three bands. (The operative assumption is that the information contained in the RGB bands is distributed throughout the HIS channels. It is, therefore, possible to replace one of the HIS channels with another data set and not lose one-third of the information content of the original image.)

Results

The result of replacing the intensity channel of the HIS transform of TM bands 2, 3, and 4 with band 7 and then retransforming to the red, green, blue domain is presented in Fig. 3. This particular rendition appears to facilitate the visual perception of roads and streets in urban areas. The substitution of each of the bands 1, 5, and 6 in turn shows promise for enhancing other features. Evaluation of these other transformations is not yet completed.
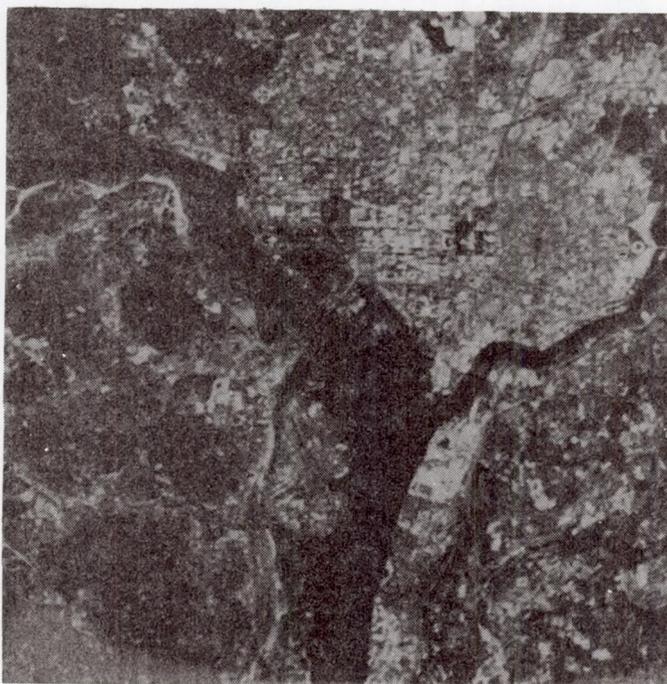
Fig. 3   TM color composite image of Washington, D.C., November 2, 1982. The image is derived from a transformation of spectral bands 2, 3, and 4 into hue, intensity, and saturation data space. The intensity dimension has been replaced by spectral band 7. (Original figure in color.)

PERSPECTIVE VIEW TRANSFORMATION

Methods

A perspective projection creates the illusion of depth in a two-dimensional image; distant objects appear smaller than near objects of the same size. The result is a natural-looking image, similar to an oblique photograph. One of the products of research into flight simulators and robotic vision is an economical method for calculating and displaying perspective images of digital terrain data.

The EROS Data Center has recently implemented a capability to create perspective images by registering digital elevation data and pixel positions. It is depicted here with spatially registered TM data and Digital Elevation Model (DEM) data of the Washington, D.C., area. The user can specify an x, y location in the input scene, a height above the terrain, the look angle, and a field of view that can vary between wide and narrow angle (Ref. 4 and 5).

Results

A perspective view image of central Washington, D.C. appears in Fig. 4. Bands 2, 3 and 4 of TM data have been draped over the digital elevation data.
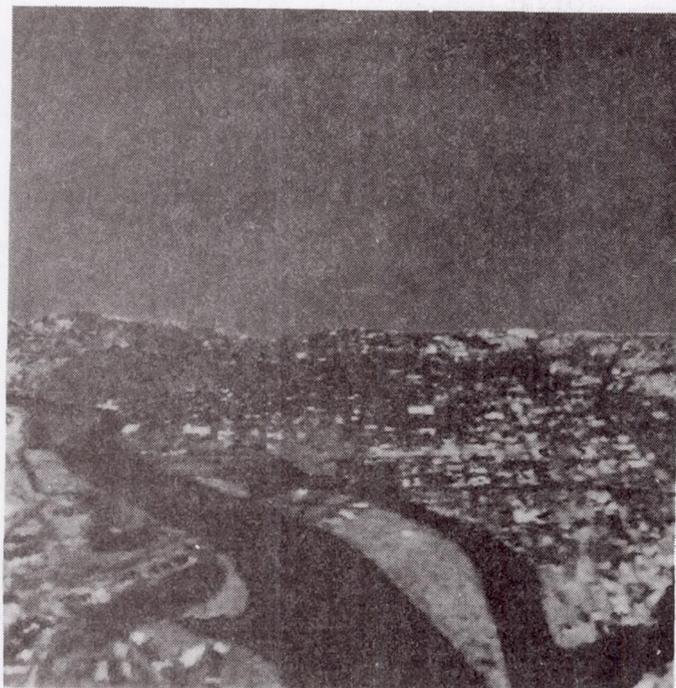
Fig. 4 Composite perspective image of Washington, D.C.,
November 2, 1982. The image shows TM spectral bands
2, 3, and 4 spatially registered to DEM data.
(Original figure in color).

SUMMARY OF RESULTS

Some early results of evaluating newly available TM data for providing
improved land cover information have been obtained. These results were
derived from coincident TM and MSS data of the Washington, D.C., area that
were acquired by Landsat 4 on November 2, 1982. The limited extent of the
analyses performed to date are summarized as follows:

In general, the results of digital data analyses suggest the potential for TM
data to provide improved land cover information due to the addition of data
channels in new spectral regions. The mid-IR bands (5 and/or 7) may be
especially useful because of (a) the large range of variability for digital
values in five broad land cover classes, and (b) low correlations with other
spectral bands for vegetated land cover classes and water areas. The mid-IR
bands may also play a role in providing a significant third dimension to data
space that has been transformed into its principal components. Low
correlations between the blue band (band 1) and other spectral bands suggest
its utility for applications involving water and vegetated land areas.

The separability among the mean data values of several land cover classes was
shown to be greater for TM spectral bands 2, 3, and 4 than for the equivalent
MSS bands 1, 2, and 4. In addition, the relative variabilities in data
values associated with the classes were more often lower for the TM bands than
for the corresponding MSS bands. These observations could indicate a
contribution to better multispectral discrimination of land cover classes by
TM bands 2, 3, and 4. However, an artifact in the MSS data noted herein may
have contributed substantially to the greater relative variabilities observed
in the MSS spectral bands.

The large variabilities noted for the digital values in the mid-IR bands
(5 and 7) likely contributed to the results of interpreting black-and-white
images of the six reflective TM bands. Interpreters indicated a preference
for images of bands 5 and/or 7 over other bands for making distinctions in 8
out of 11 of the interpretation categories that were addressed. Results of
interpreting six color-composite images showed highest interpreter preferences
for a standard color-infrared composite (bands 2, 3, and 4) or a color
composite consisting of bands 3, 5, and 4 in 8 out of 11 categories. A
natural-color composite image (bands 1, 2, and 3) showed high interpreter
preferences for three interpretation categories involving distinctions within
predominantly nonvegetated areas.

Finally, two types of data transformations were demonstrated. A
transformation from red, green, and blue color space into hue, intensity, and
saturation space has the potential for offering enhanced interpretability for
TM color-composite images. A perspective view transformation could be useful
for presenting registered layers of spatial data in an oblique-view format.

REFERENCES

1. S.K. Jenson and F.A. Waltz, "Principal Components Analysis and Canonical Analysis in Remote Sensing," Proceedings of American Society of Photogrammetry 45th Annual Meeting, Vol. I, 1979, pp. 337-348

2. R.J. Kauth and G.S. Thomas, "The Taselled Cap -- A Graphic Description of the Spectral-Temporal Development of Agricultural Crops as Seen by Landsat," Proceedings of Machine Processing of Remotely Sensed Data Symposium, Laboratory for Applications of Remote Sensing, Purdue University, West Lafayette, Indiana, June 29-July 1, 1976, pp. 4B-41 to 4B-51

3. SIGGRAPH-ACM, "Status Report of the Graphics Standards Planning Committee," Computer Graphics, Vol. 13, No. 3, 1979, pp. III6 to III-11

4. T.M. Strat, "Shaded Perspective Images of Terrain," M.I.T.-A.I. Memo 463, MIT Artificial Intelligence Laboratory, Cambridge, Massachusetts, 1978

5. B. Schachter and B. Fishman, "Computer Display of Height Fields," General Electric Tech. Pub., Daytona Beach, Florida, 1979

Page intentionally left blank

THEMATIC MAPPER DATA QUALITY AND PERFORMANCE
ASSESSMENT IN RENEWABLE
RESOURCES/AGRICULTURE/REMOTE SENSING

R. M. Bizzell
and H. L. Prior
NASA/Johnson Space Center

INTRODUCTION

The launch of Landsat-1 on July 23, 1972, provided a new perspective for man's view of the Earth; the assessment of its "quilted" surface, and their associated interface "seams". For the past decade, scientists, engineers and technicians have been successfully processing the telemetered signals and extracting information from multispectral scanners (MSS) aboard the three Landsat platforms. Their success has effected the transfer of routine utilization of the MSS and associated information extraction technology in both the public and the private sector. With the launch of the Landsat-D satellite on July 19, 1982, a new challenge was presented to these technologists. In addition to the familiar MSS, a new sensor (Thematic Mapper) was included that incorporated significant improvements in the radiometric and geometric aspects of the multispectral data. At the Johnson Space Center (JSC) where research and development (Ref. 1) of technology to address significant issues in the incorporation of remotely sensed data for global crop inventory has been a major task, the receipt of the TM data to assess its utility for solving critical elements of this technology has been enthusiastically awaited.

Significant effort will be required to gain understanding of the improved information content due to the increased spectral and spatial data and, early identification of the major effects, i.e., increased within field variability due to detection of subtle variations in vegetation canopy and associated soils background and/or soils and leaf moisture.

This paper represents the results of basically qualitative investigations designed to help formulate the specific research and development tasks to assess the TM in the context of large area renewable resources science objectives.

TM DATA QUALITY ASSESSMENT

Upon receipt of the inital TM imagery a very subjective evaluation was made of the JSC imagery products to detect and report any degradation which may have occurred during extraction and processing, and to report any excessive geometric distortion or image degrading factors that might negate the informational value of the TM imagery.

It was not intended that this evaluation would overlap with other qualitative studies being made at the same time. The evaluation was based on a single multiband Thematic Mapper scene with the imagery products being visually examined by an image analyst to determine the extent of mechanical, electro-optical, film processing, or atmospheric effects noted on the TM image products. Shape and alignment of features identifiable in the imagery were compared with corresponding features on available maps to detect any distortions in shape and direction.

Results of the preliminary evaluation (Ref. 2) indicated the TM imagery has the characteristics as expected from the simulated imagery with respect to pixel purity (and resolution), within-field variation, scan line clarity, etc. In summation, the simulators did a fine job of simulating Thematic Mapper imagery. The quality of the geometric corrections appeared to be excellent in

the areas evaluated (Fig. 1) from a visual standpoint. Straight lines appear as straight lines, as evidenced by section line roads, airport runways, etc. Circular/oval features such as stadiums, drive-in theaters, oval race tracks in the Detroit scene all appeared nominal.

In examining the radiometric characteristics of TM, an analysis of the signal to noise ratio and increased quantization in each spectral band was conducted. Figure 2 shows essentially that the performance is as good or better than specified (which is improved over Landsat 1, 2, 3 MSS). These results are based on analysis of approximately 35 water and 20 vegetation sites from an August 22, 1982, TM scene over Missouri and Arkansas where ground observations were available. Thermal band results are inconclusive in this limited result because the homogeneity of the selected sites could not be ascertained.

In examining the TM system spatial and geometric characteristics, several studies were performed. In the initial image quality assessment, numerous small objects of essentially known dimensions were measured to ascertain that the spatial resolution meets or exceeds slightly the 30 meters specified in all bands except the thermal where results were not obtained (Figure 3).

SPATIAL RESOLUTION INVESTIGATIONS

Pre-Landsat 4 Thematic Mapper crop inventory technology (MSS based has experienced an as-yet-to-be resolved effect from pixels that contain more than one category of interest. Figure 4, a TM simulator scene from Webster County, Iowa, demonstrates this boundary/mixed pixel effect. This was due primarily to category boundaries and category intermixing which was beyond the resolution capability of the system. Thus, the impact due to the increased spatial resolution of the TM is a very important factor in potential solution of the problem.

To evaluate the effect of the improved spatial resolution we categorized an agriculture area of the Detroit TM scene by noting the types and relative content of boundary pixels utilizing a currently existing field definition algorithm. Using an MSS scene for the same area, although not concurrent dates, a comparison was made of boundary pixel proportions in the TM and the associated MSS scene.

Results of this one scene comparison indicate the TM scene boundary pixel content is approximately 37 percent of that found with the MSS scene. A boundary pixel being one not readily identifiable with any field or category, but tending to lie in a line falling between two fields or categories. Stated alternatively, the MSS scene has a boundary pixel content that is 2.7 times greater than that of the TM scene. If these results are indicative of the range of TM scene types it will be a significant step in easing the boundary/mixed pixel effect. Where many scenes contain of as much as 50 percent mixed pixels this can offer a significant reduction in the classification and subsequent proportion estimation error.

The finer spatial resolution of TM gives imagery which was found to be a sufficient base, unlike MSS, for ground cover/land use ground observation collection (Ref. 3) and annotation, (Figure 5). Replacing high altitude aircraft photography for this purpose which also required a registration step to Landsat for digital ground data is not required with TM. This also clearly implies TM

imagery can be used in stratification of land into agricultural or non-
agricultural in commodity production forecasting sample frame development.
Field size distribution with TM imagery by country and crop region can also be
expected to be improved over earlier MSS-based estimates.

SPECTRAL RESOLUTION STUDIES

In examining the spectral characteristics of TM, a principal components (PC)
analysis was conducted using data from the Mississippi Co., AR, scene (August
22, 1982). An example of the results in figures 6 and 7 shows: (1) that TM
bands 2, 3, and 4 provide data correlated to the MSS bands but with greater
dynamic range, and (2) that TM bands 1, 5, 7, and 6 offer potential for
improved identification of land cover classes as can be seen in the informa-
tion available in PC images of the 4-6 components, which is not available in
PC images of the first 3 components (Figure 8). Further, as opposed to MSS
(with its essentially 2 intrinsic dimensions of greenness and brightness in
the fixed linear transform space of Kauth-Thomas' Tasseled Cap, when viewing
vegetation and soils) the TM exhibits essentially 4 intrinsic dimensions plus
a potential fifth of thermal information where the first two dimensions are
highly analogous to MSS greenness and brightness (Ref. 4). The scene detail
found in thermal images indicates the potential of this region even though the
data are not taken at the maximum of the dynamic range or contrast. This
larger dimensionality of the TM data structure with its potential for more ac-
curate information carries with it the need to analyze this larger dimension-
ality to achieve the information gain. Also, this represents added information
from a single TM acquisition. An additional increase in information content
with multitemporal data is expected to be evident.

Although initial studies have been limited by time-since-launch, data quantity
and quality (mainly availability of adequate "ground truth" for quantitative
assessment), the indication of additional information for agricultural purposes
is encouraging. One such analytical evaluation (Ref. 5) of a sampled scene in
Mississippi Co., AR, of August 22, 1982, where field inventory ground observa-
tions were collected by the USDA revealed several significant results. Both
Landsat-4 MSS and TM data were acquired which allowed insight into the poten-
tial increase in information content with the TM data. Separability measures
were calculated for several features (crops, water, trees, soil) from the six
reflective bands. The results were consistent with other quantitative studies,
i.e. principal component analysis, in that 95 percent of the average separa-
bility between cell classes was satisfied by using four bands for pairwise
separation (one class vs. another) approximately the same separability was
achieved with three bands. Figure 9 is an example of the "best" bands for
soybeans which made up 70 percent of the scene. Significant observations from
the feature separability studies and associated classification results are:
(1) "best" three bands for separability of classes generally always come from
these three groups- visible (bands 1, 2, 3), Near IR (Band 4) and middle IR
(Bands 5 and 7), (Figure 10), (2) separability between classes was approximate-
ly the same if one band from each group was used, (3) if no mid-IR band was
used in classification the overall performance was significantly degraded
(Figure 11). These separability results are consistent with principle compo-
nents analysis (Figure 12), in that the first component represents a
"brightness" measure liken to the visible bands, the second component is
"greenness" as is band 4 (Near IR), and the third component represents the
variation in the brightness plane due to soils/soil moisture variability which

takes advantage of the mid-IR bands (5 and 7). One clear message from these analyses is that the TM mid-IR bands significantly contribute to the extraction of agricultural information.

The increase in information content due to the added TM spectral bands over the MSS would, however, be lessened were it not for the increase in the spatial resolution (approximately 30 meters vs. 80 meters). Mere visual comparison of the scenes (Figure 13) exhibits the obvious within field variability (information) captured by the TM, i.e., irrigation ditches in rice fields, drainage patterns, texturing from crop canopies and/or soils. The "good news-bad news" aspect of this is that the technology to derive large area estimates of some important crops with MSS is understood and, importantly, in use within the USDA. However, the limits may have been reached. Similar understanding and associated information extraction technology to take advantage of the TM will require extensive research and development resources.

SUMMARY AND CONCLUSIONS

Analysis of the early TM data indicate the TM sensor and associated ground processing are performing equal to the high expectations and within advertised specifications. The overall TM system with improved resolution, together with additional and more optimumly placed spectral bands shows much promise for benefits in future analysis activities.

Simulations of TM data, using the Thematic Mapper Simulator (TMS) were collaborated by the early TM scenes. These simulations did an excellent job of simulating the TM, and thereby providing meaningful pre-TM studies plus enabling adequate data systems and analyses techniques to be available to support early evaluation of the TM.

By selecting man-made features of known dimensions (e.g., highways, airfields, buildings, and isolated water bodies), an assessment was made of the TM performance relative to the specified 30-meter (98-foot) resolution. Indications are that this resolution was achieved or exceeded.

The increase of spatial resolution of TM (30 m) over MSS (80 M) appears to be significant not only in resolving spectrally distinct classes that were previously undefinable (e.g., roads, small fields) but also in distinguishing within-field variability. This increased spatial resolution, therefore, decreases the effect of the mixed pixels on the boundaries and accurately represents variations within a field due to soils, topography, planting, and density. The TM produced imagery was found to be sufficient base for ground cover/ land use ground truth collection in most cases. If this TM image can be substituted for the high altitude aerial photo base presently used, it could provide a more timely and cost effective approach in the collection of the ground data.

The additional spectral bands, particularly those in the middle infrared region have added a significant improvement to the dimensionality of the data. This larger dimensionality of the TM data structure with its potential for more accurate information carries with it the need to analyze this larger dimensionality to achieve the information gain. Earlier TMS studies and preliminary TM analysis have shown this represents added information from a

single TM acquisition. An additional increase in information content with multitemporal data is expected to be evident.

Four potentially useful components for crop separability were obtained from the TM spectral bands. The first two principal components appear to be highly analogous to the MSS greenness and brightness components, leading to the expectation that the second two components will contain other useful information when viewing agricultural scenes.

An important result of the early TM evaluation and pre-TM analyses was the development of an integrated system to receive Landsat-4 TM (as well as MSS) data and analyze the data via various approaches. This system provides a capability for rapid manipulation of small volumes of TM data including data extraction, digital data manipulation, image display, and film generation as well as performing many sophisticated pattern recognition and image analysis functions.

REFERENCES

1. This research was carried out as part of the Agriculture and Resources Inventory Surveys Through Aerospace Remote Sensing "AgRISTARS" Program, a joint program of the U.S. Department of Agriculture, Interior, Commerce (NOAA) and State (Agency for International Development) and the National Aeronautics and Space Administration. AgRISTARS Research Report-APJ20393 (available from NASA-JSC, Mail Code SK, NASA-Lyndon B. Johnson Space Center), Data was provided by NASA, Goddard Space Flight Center - Landsat LIDQA.

2. Bizzell, R. M., Prior, H. L., Trichel, M. C., et al, "Thematic Mapper Performance Assessment in Renewable Resources/Agricultural Remote Sensing-Initial Scene Quick Look Analysis". JSC-18579, September 15, 1982.

3. Prior, H. L., Henninger, D. L., and Trichel, M. C., "Landsat Thematic Mapper: A New Perspective on Agriculture from Space" - Agronomy abstracts, 1982. p. 231.

4. E. P. Crist and R. C. Cicone, Proceedings, Landsat-4 Scientific Characterization Early Results Symposium, February 1983.

5. Nedelman, K. S., Cate, R. B., and Bizzell, R.M., "Automated Vegetation Classification using Thematic Mapper Simulation Data", Technical papers at

Figure 1. **THEMATIC MAPPER RESOLUTION**

TM resolution is sufficient to allow detection
of golf course fairways, subdivision streets,
athletic fields, shopping areas, small buildings,
bridges, airport taxiways and other small
(near-pixel-size) features.

Ann Arbor, Michigan   Detroit Metropolitan Airport   West Toledo, Ohio   Central Toledo, Ohio

Additional detail provided by TM data
will improve performance of analysis
techniques in areas where problems
have been encountered due to small fields.

Webster County,
Iowa
(Simulated TM)

Pseudo Fields
(White pixels are
boundary/mixed.)

MSS-size pixel
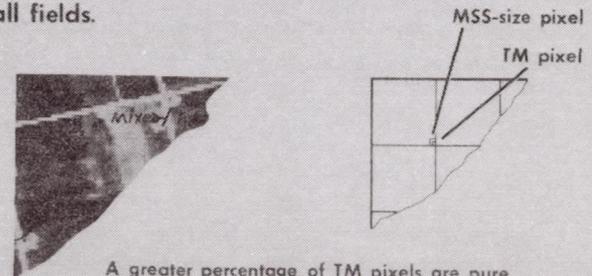
TM pixel

A greater percentage of TM pixels are pure.

MSS - 72.1% pure

TM - 93.2% pure

Field-finding algorithm indicates the percentage
of boundary/mixed pixels is smaller on TM data
than on MSS.

NASA

AgRISTARS

Figure 2. Observed S/N Noise Equivalent Temperature Difference (NETD) by Pre-Flight Specifications
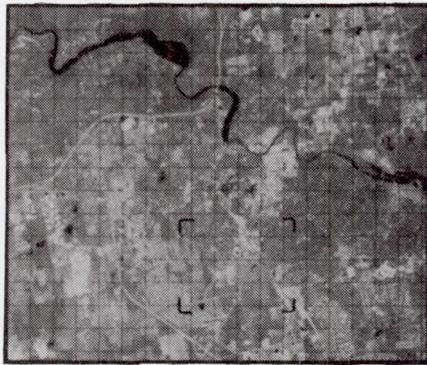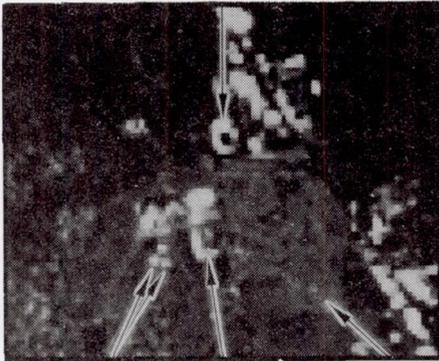
Figure 3. Example of TM Spatial Resolution

AN ENLARGEMENT OF THE TOP LEFT-
HAND CORNER OF THE TMS SCENE

A TMS SCENE OF WEBSTER COUNTY,
IOWA, SEGMENT 893, AUGUST 30, 1979
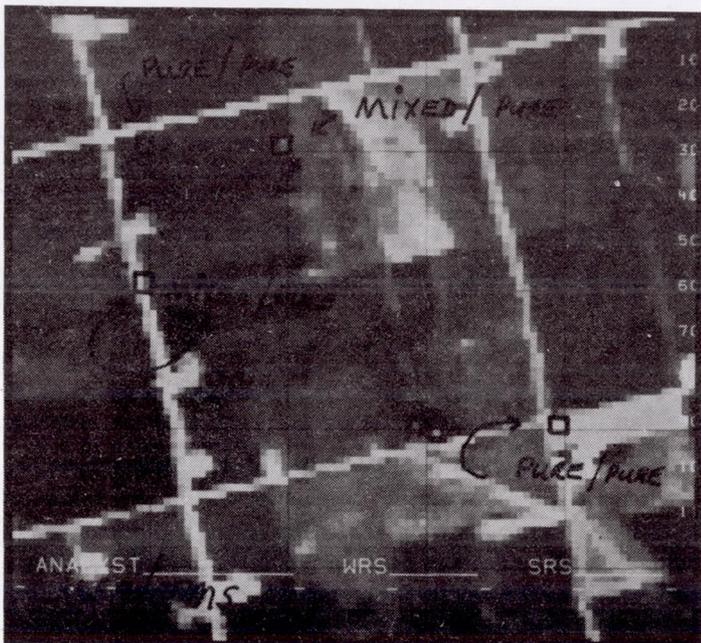
Figure 4. Boundary/Mixed Pixel Effect as Demonstrated by
TM Simulator Image
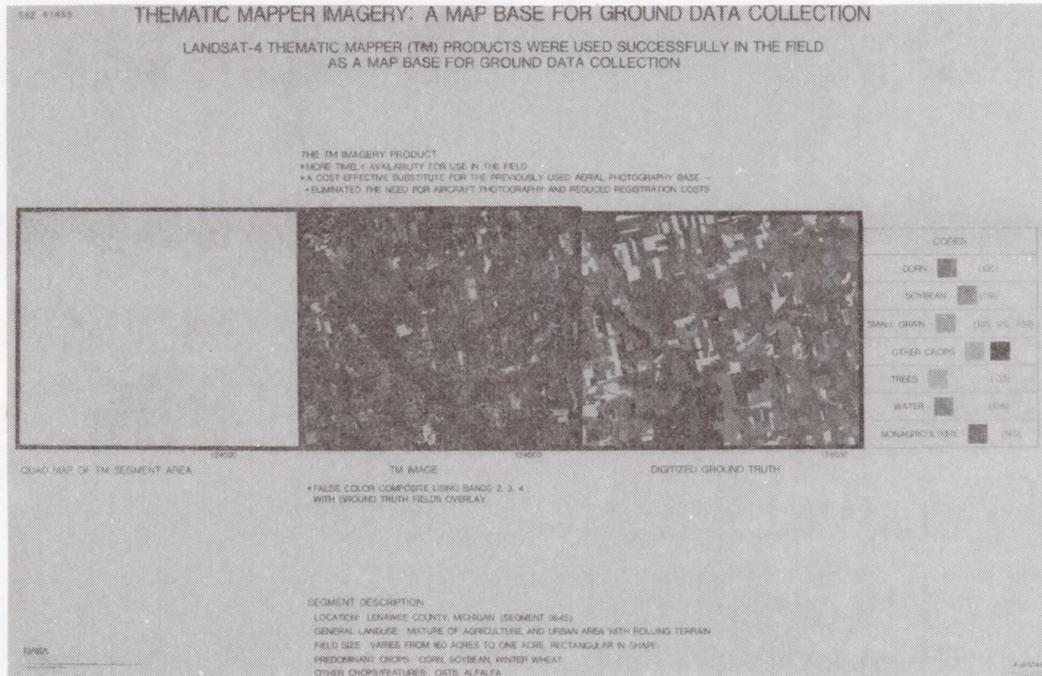
Figure 5. Assessment of Landsat-4 Thematic Mapper (TM)
Products as a Map Base for Ground Data Collection

CORRELATED COEFFICIENTS

MSS

1	.93	.99	.94	-.01	.79	.78
2	.91	.96	.99	-.22	.74	.78
3	-.01	.21	-.03	.97	.15	-.09
4	-.15	.02	-.21	.99	.05	-.20
TM	1	2	3	4	5	7
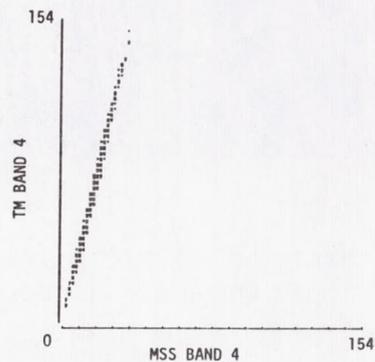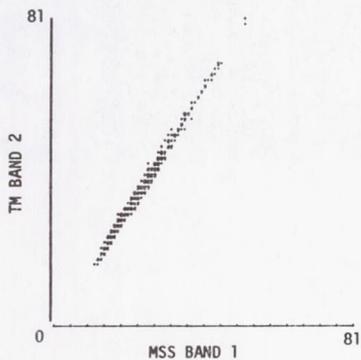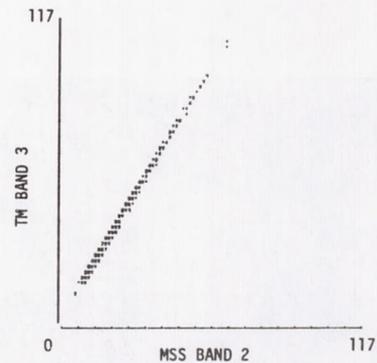
Figure 6.   Regression Analysis: Prediction of New TM Bands from MSS Equivalent

REGRESSION R²

BAND	LOWEST R^2	HIGHEST R^2
1	.85	.95
5	.55	.88
6	.12	.31
7	.59	.87
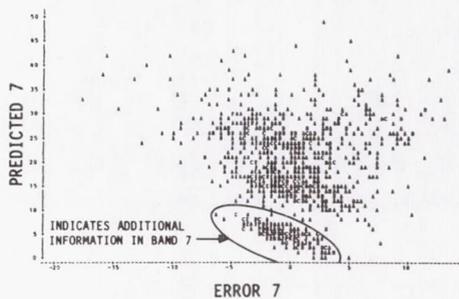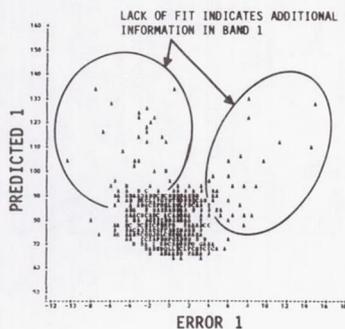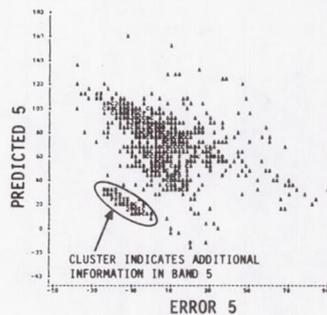
o EVIDENCE OF LACK OF FIT

o CLUSTERS NOT IDENTIFIABLE USING ONLY PREDICTED VALUES

Figure 7.   Correlations of MSS and TM Bands
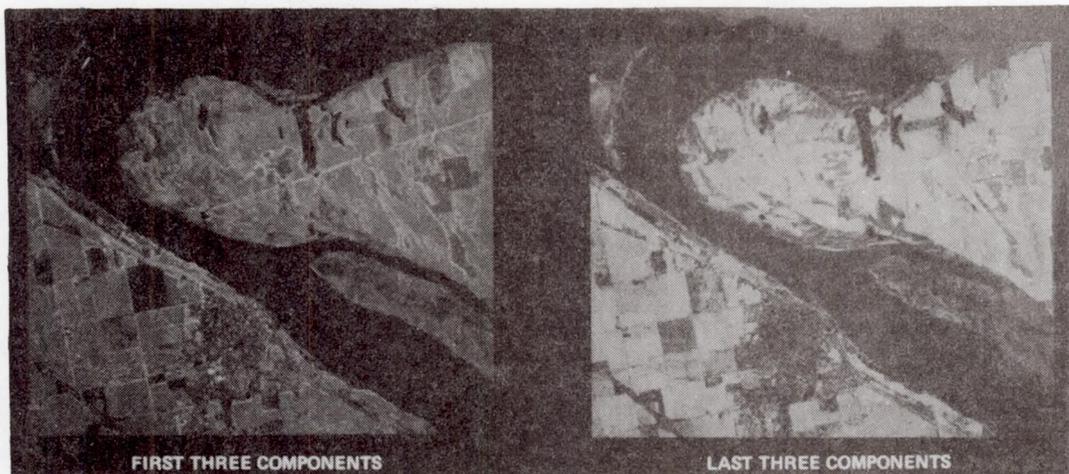
Figure 8.   Example of Additional Information Available with TM Based
on Principal Component Analysis
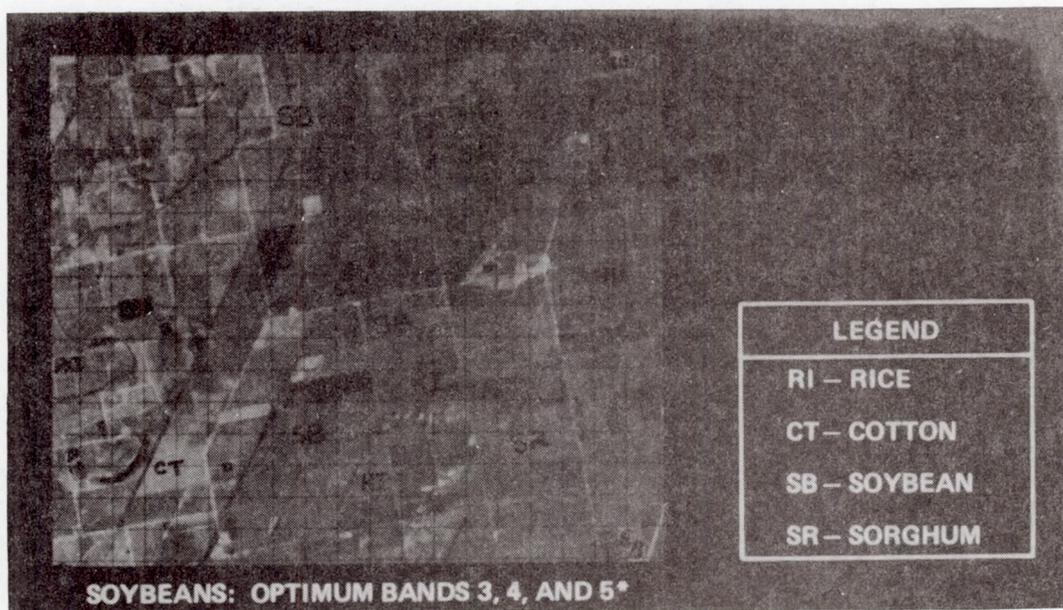
Figure 9.   The Best Three-Band Combination for Crop Discrimination
Using A Single-Date (August 22, 1982) Missouri/Arkansas
TM Scene
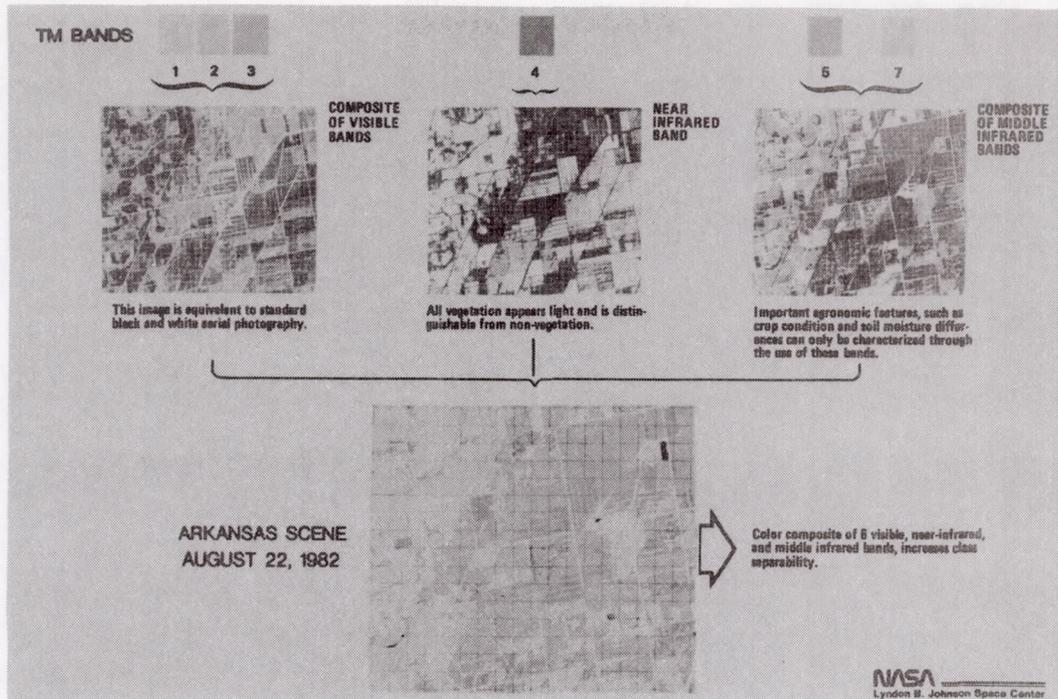
Figure 10. Example of Classification Using Linear Combination
of TM Reflective Bands
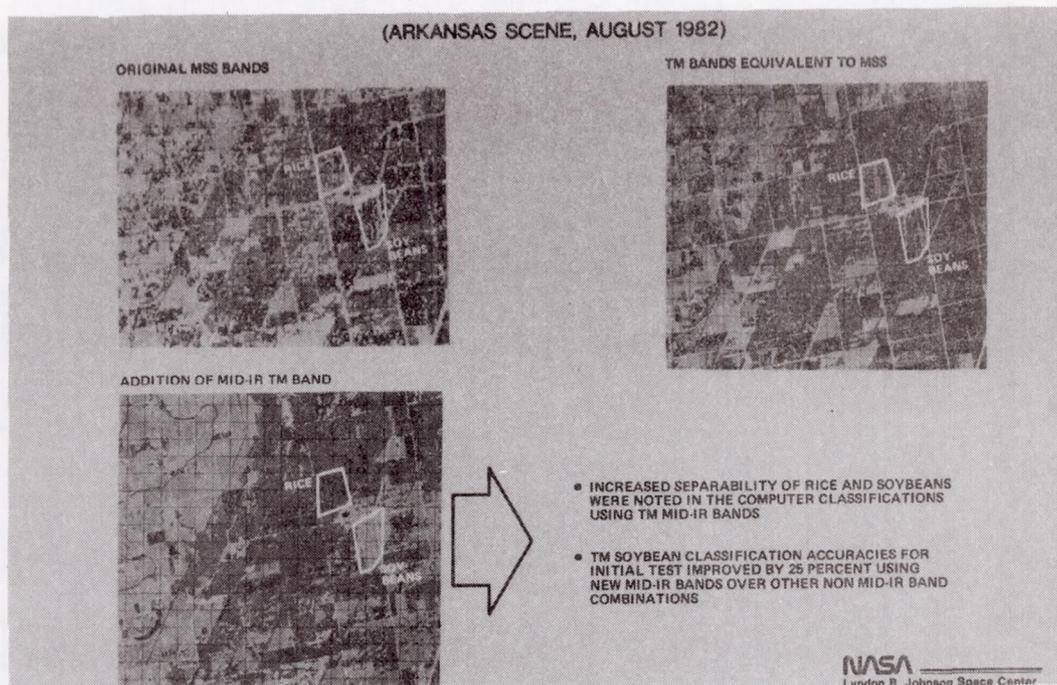
Figure 11. Example of Improved Proportion Estimation Results
with Incorporation of TM mid-IR Bands

% VAR. EXP.	BAND 1	BAND 2	BAND 3	BAND 4	BAND 5	BAND 7
.71	0.4664	0.4515	0.4748	-0.2636	0.2881	0.4482
.21	-0.0376	-0.0966	-0.1174	0.6807	0.6798	0.2239
.05	-0.2761	-0.5448	-0.1300	-0.5646	0.3031	0.4469
.97						

- THE DATA SET FORMED BY THE FIRST THREE PRINCIPAL COMPONENTS (P.C.) WAS PROCESSED THROUGH THE "CAUSE" SOFTWARE TO PRODUCE THIS IMAGE

- GENERATING IMAGES FROM P.C.'S ALLOWS PRESENTATION AND ANALYSIS OF INFORMATION FROM ALL CHANNELS

TM 306	
COLOR	P.C.
BLUE	1
GREEN	2
RED	3

Figure 12.   Example of Analysis Technology Developed to take Advantage of Thematic Mapper Dimensionality

TM   MSS

Spatially registered Landsat-4 Thematic Mapper and Multispectral Scanner Images acquired on August 22, 1982 over a 9x11-mile agricultural area in Mississippi County, Arkansas, predominant crops are soybeans and rice. Irrigation ditches within fields are visible in the TM images. Images and registration were produced by the Data Systems Branch of the Earth Resources Research Division.

Figure 13.   MSS and TM Data over Mississippi County, Arkansas, Site Acquired by Landsat-4, August 22, 1982.

PRELIMINARY COMPARISONS OF THE INFORMATION CONTENT AND UTILITY OF TM VERSUS MSS DATA

Brian L. Markham
Earth Resources Branch
NASA/GSFC
Greenbelt, MD 20771

INTRODUCTION

The Landsat-4 Thematic Mapper (TM) instrument is a second generation electro-mechanical scanner with numerous upgrades over the familiar MSS's. Of particular interest to the user community were the improved spatial resolution, increased radiometric sensitivity, refined locations and widths of the green, red and near-infrared spectral bands, and new spectral bands in the blue, mid-infrared and thermal-infrared regions. Pre-launch simulation studies indicated that TM data would provide significant enhancements over MSS data for various applications.

The objective of this study was to provide some preliminary indications as to the relative merits of actual TM data versus MSS data for land cover mapping related applications. Three analyses were designed which had sensitivity to the differences in spectral, spatial and radiometric parameters between the TM and the MSS. In the water body analysis, a primarily spatially related test, the detectability of small uniform targets was examined. The principal components analysis, an examination of the inherent dimensionality of the data, was more spectrally and radiometrically related. The spectral clustering analysis, also heavily spectrally and radiometrically influenced, provided information on the types of targets separable on TM versus MSS data.

These analyses were to be conducted with simultaneously collected Landsat-4 complete TM (7 band) and MSS (4 band) data. In actuality, 4-band TM data, and archived Landsat-2 MSS data of the same area were used. This situation resulted from the combined effects of:

1. the need for data over a local area (Washington, DC) with good reference data,

2. the delayed activation of the cooled focal plane (bands 5-7) of the TM,
3. the unavailability of Landsat-4 MSS data collected prior to mid-September and
4. the lack of any reasonably clear Landsat-4 scenes of Washington, DC after the activation of the complete TM complement of spectral bands in mid-August and before the end of the growing season.

MATERIALS/PREPROCESSING

The TM data used were July 29, 1982 4-band P-data of the Washington, DC area (Path 15 Row 33). A 512 x 512 subscene covering an area east of Washington, DC including LaPlata, MD was selected for analysis. This area was one of the few cloud free portions of the scene that was covered by July 13, 1982 1:40,000 color infrared (CIR) aerial photographs. A mixture of forest, agricultural and urban/suburban land cover types occurred in this area. An MSS scene, July 11, 1981, of the Washington, DC area was selected for comparison to the TM. From this scene (A-tape) the LaPlata area was extracted. Ten control points on each subscene were identified and the MSS data was transformed into TM coordinates using a first order transformation and were resampled by cubic convolution to 57 meter square pixels. This resulted in roughly a MSS P-type product of 256 x 256 pixels, approximately registered to the TM data.

WATER BODY ANALYSIS

Methods

The objective of this test was to provide a quantitative comparison of TM and MSS for the detection of small uniform targets. Water bodies were selected because of their uniformity, high contrast with surrounding materials and variability in size.

All water bodies greater than 10 meters in size were located on the CIR aerial photography. Each water body was categorized by the diameter of the largest circle that could be inscribed within it. Four categories were established: 10-30 m, 30-80 m, 80-160 m and greater than 160 m. Water bodies in areas of active surface mining were not categorized, as they were characterized by high turbidity and were particularly subject to change between the two dates of imagery.

The TM and MSS subscenes were separately clustered using the ISOCLS program on an IDIMS image processing system (ESL, 1978). The MSS was scaled from 0-255 prior to clustering and the clustering parameters were set equally for the two runs with the exception that for the MSS run the minimum number of pixels per cluster was set one quarter of the TM value to account for the lower number of MSS pixels.

The results of the clustering were displayed on a CRT and compared to the aerial photographs on which the water bodies had been delineated. If comparison to the reference data indicated that the majority of a cluster's pixels imaged water (either totally or partially, i.e., were pure or boundary water pixels) the cluster was called "water," otherwise "non-water."

Each water body identified on the aerial photographs was then checked to determine whether it was detected by the TM and/or MSS. Detection was defined as a minimum of one "water" pixel at the water body's location. "Water" pixels at non-water body locations were considered commission errors.

RESULTS

Two clusters represented water on the TM data; three on the MSS data. The about 10% greater range of digital counts in the stretched MSS data than in the TM data and the greater effect of boundaries on the MSS data may have resulted in the larger number of MSS clusters. The "water" pixels for TM and MSS are illustrated in Figure 1 and the results of the detection analysis are presented in Table 1.

Table 1
WATER BODY ANALYSIS RESULTS

PONDS CORRECTLY DETECTED

POND SIZE (Max. Inscribable Circle)	AIR PHOTOS #	TM	MSS
10-30 m	29	7 (24%)	0 (0%)
30-80 m	22	19 (86%)	5 (23%)
80-160 m	7	7 (100%)	7 (100%)
>160 m	1	1 (100%)	1 (100%)
TOTAL	59	34 (58%)	13 (22%)

COMMISSION ERRORS

TOTAL	--	6 (15%)	3 (19%)

The commission errors for TM and MSS were similar, suggesting that the water/non-water decision boundaries were comparable for the TM and MSS data sets, and thus allowing direct comparison of the detection accuracies (omission errors). The MSS and TM detection accuracies were comparable down to 80 meter water bodies. Ponds smaller than 80 meters were rarely detected with MSS data, though one 40 meter pond was detected. With TM data, the majority of the ponds down to 30 meters was detected. Below 30 meters the detection accuracies decreased; the smallest pond detected on TM data was 16 meters.

The ratio of the minimum consistently detected pond size on MSS data (~80 m) to TM data (~30 m) is commensurate with the ratio of the advertised resolution of MSS (79 m) to TM (30 m). Although this appears to indicate that the improved spatial resolution translates directly to an equivalent small target detection improvement, it should not be forgotten that the spectral and radiometric differences between TM and MSS may have also made a contribution.
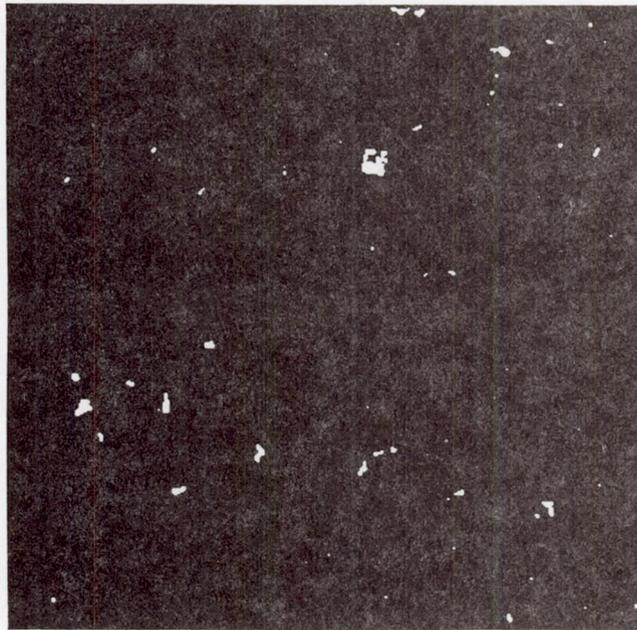
TM
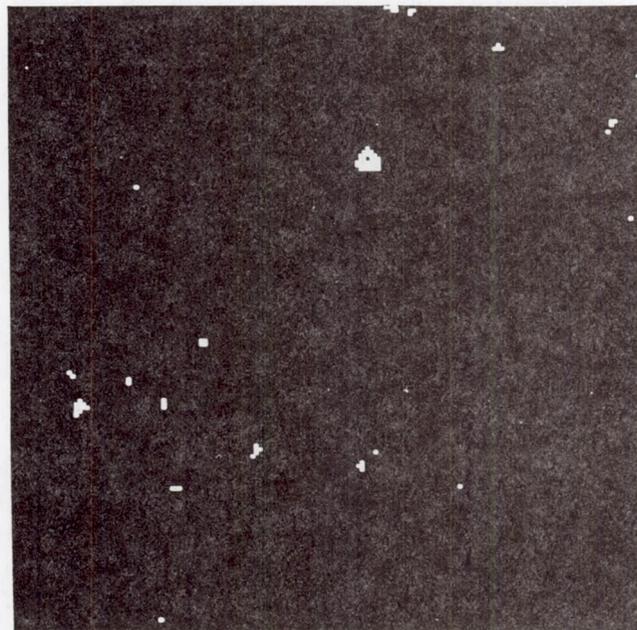
MSS

Figure 1. Pixels in "water" clusters for TM and MSS data.
"Water" pixels in white.

PRINCIPAL COMPONENTS ANALYSIS

Methods

The objective of this analysis was to compare the information content in terms of inherent dimensionality of the TM data to MSS data. The Karhunen-Loeve (K-L) transform to principal components provides a new set of component images that are uncorrelated and ordered in terms of decreasing variance. The principal components reveal the dimensionality of the data, the relative importance of each dimension and the relationship of each dimension to the original data.

To perform the K-L transform, first the variance-covariance matrix was generated for each image. Then the transformation matrices were generated from the variance-covariance matrices and the principal component images produced. The resulting images were contrast-stretched to enhance their visual interpretibility.

Results

The variance-covariance and correlation matrices (Table 2) illustrate the frequently observed high correlations between the two visible MSS bands and between the two near-IR MSS bands, and the low correlations between the near-IR bands and visible bands. For the TM bands, the situation is similar, with high intra-visible band correlations and low visible to near-IR correlations.

The first principal component (PC) of the MSS scene is an overall amplitude-like feature, with positive weighting from all 4 bands (Table 3). The second MSS principal component is a Near-IR/Visible contrast with positive weighting from the two near-IR bands and negative weighting from the visible bands. The third principal component is primarily a band 3 to band 4 contrast with some negative contribution from the visible bands. The fourth principal component is a green (band 1) to red contrast (band 2).

From the transformation matrices (Tables 3,4), the first and second TM principal components appear similar to the first two MSS principal components, containing an overall amplitude and a Near-IR/Visible contrast, respectively. Principal component #3 for TM is similar to PC#4 for MSS containing a blue-green to red contrast. The 4th TM principal component is dominated by the green band (2) with some negative red band contribution.

The principal component images, contrast stretched for display (Figs. 2,3) also show the similarity of the first two components of the MSS and TM scenes. In each case, these first two components account for almost all of the scene variance (97% for TM, 98% for MSS). The third and fourth MSS principal components are dominated by striping and appear to contain little useful information. In MSS PC#4 there appears to be some contrast between the urban/suburban areas (lighter) and the rural areas (darker). The third TM principal component, though containing only 2.6% of the image variance, is relatively noise-free and contains information clearly useful for separating urban/suburban areas (darker) from rural/bare soil areas (lighter). The fourth TM principal component is relatively noisy, containing periodic striping. On this early TM scene the bad detector replacement algorithm for band 2 had

Table 2
MSS AND TM CORRELATION MATRICES

	MSS					TM			
	1	2	3	4		1	2	3	4
1.	1.00				1.	1.00			
2.	0.97	1.00			2.	0.93	1.00		
3.	0.52	0.48	1.00		3.	0.87	0.95	1.00	
4.	0.06	0.00	0.83	1.00	4.	0.37	0.29	0.15	1.00

Table 3
MSS TRANSFORMATION MATRIX (EIGENVECTORS)

	MSS				CHARACTERIZATION	
	BAND 1	BAND 2	BAND 3	BAND 4	MATRIX	IMAGE
PC #1	0.26	0.42	0.65	0.58	AMPLITUDE	"BRIGHTNESS"
PC #2	−0.39	−0.71	0.11	0.57	NIR/VIS CONTRAST	"GREENESS"
PC #3	−0.15	−0.26	0.75	−0.58	NIR 1/NIR 2 CONTRAST	STRIPING – NOISE
PC #4	0.87	−0.49	−0.01	−0.02	GREEN/RED CONTRAST	NOISE – BUILT-UP AREA LIGHT BARE AREAS DARK

Table 4
TM TRANSFORMATION MATRIX (EIGENVECTORS)

	TM				CHARACTERIZATION	
	BAND 1	BAND 2	BAND 3	BAND 4	MATRIX	IMAGE
PC #1	0.57	0.36	0.49	0.56	AMPLITUDE	"BRIGHTNESS"
PC #2	−0.27	−0.23	−0.45	0.82	NIR/VIS CONTRAST	"GREENESS"
PC #3	−0.75	0.13	0.63	0.13	RED/ BL-GREEN CONTRAST	BUILT-UP AREAS DARK BARE AREAS LIGHT
PC #4	−0.19	0.90	−0.40	−0.03	GREEN OR GREEN/RED CONTRAST	BAND-2 NOISE MISREGISTRATION
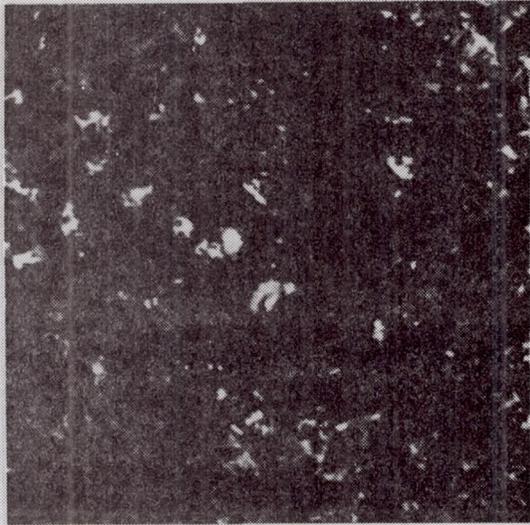
PRINCIPAL COMPONENT 1
(61.2% OF VARIANCE)

PRINCIPAL COMPONENT 2
(37.2% OF VARIANCE)
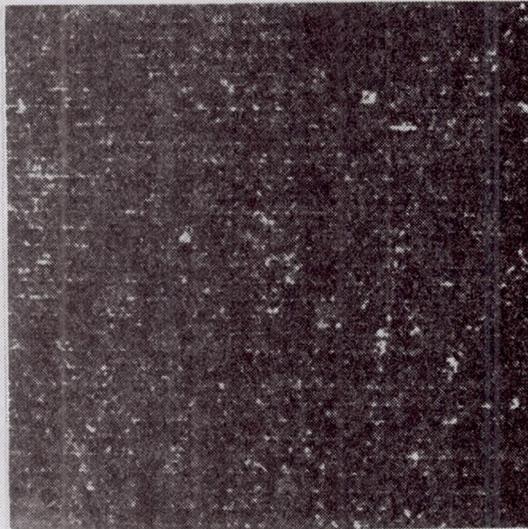
PRINCIPAL COMPONENT 3
(1.2% OF VARIANCE)
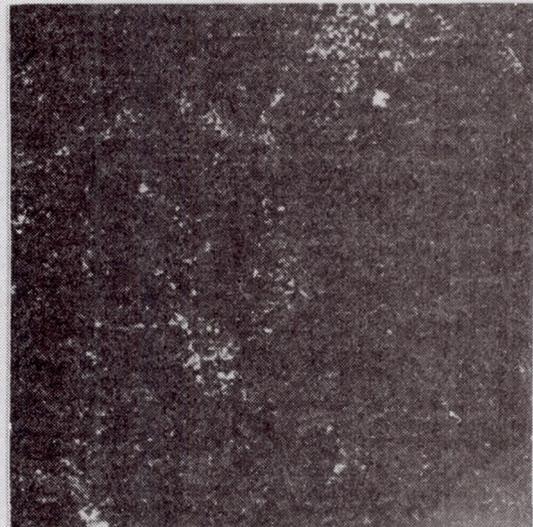
PRINCIPAL COMPONENT 4
(0.4% OF VARIANCE)

Figure 2. MSS Principal Components Images (Contrast - Stretched)
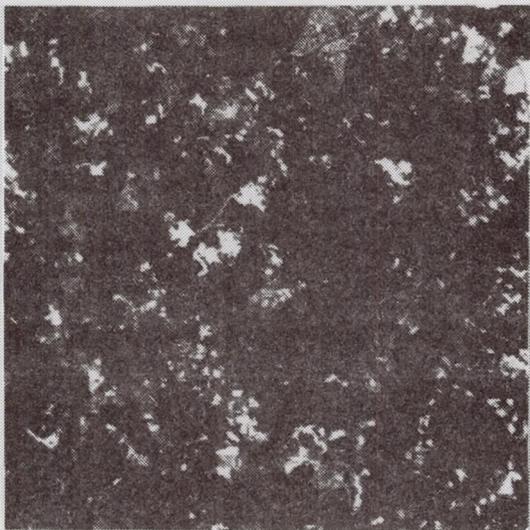
PRINCIPAL COMPONENT 1
(62.6% OF VARIANCE)

PRINCIPAL COMPONENT 2
(34.3% OF VARIANCE)
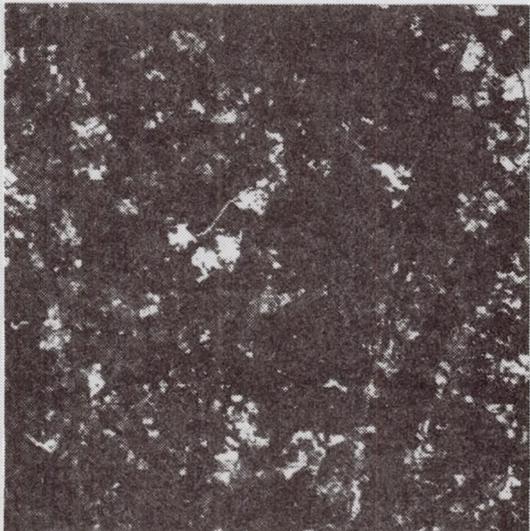
PRINCIPAL COMPONENT 3
(2.6% OF VARIANCE)

PRINCIPAL COMPONENT 4
(0.5% OF VARIANCE)

Figure 3.   TM Principal Components Images (Contrast - Stretched)

not been refined. The level of striping in this component is expected to decrease with enhanced bad detector replacement routines.

Overall the MSS data in this scene appear to contain basically two useful directions of data variability similar to the "brightness" and "greenness" vectors of Kauth and Thomas (1976). The TM data contain three useful dimensions in this scene, the first two similar to "brightness" and "greenness" and the third useful for separating urban from non-urban features. This third principal component is detecting the spectral flatness of construction materials relative to bare soil surfaces (i.e., construction materials are various shades of gray--low red/blue ratio and soils are various shades of brown--high red/blue ratio). The greater useful dimensionality of TM data in this scene is thought to be due to the new TM band 1, the improved TM radiometric calibration (decreased striping) and the improved TM radiometric sensitivity.

SPECTRAL CLUSTERING ANALYSIS

Methods

The objective of this analysis was to provide a preliminary comparison of the types of targets identifiable with spectral clustering on TM versus MSS. The same clustering runs used for the water body analysis were used for this analysis. Each resulting class was assigned to a land-cover class by a majority rule.

Results

Fifty clusters resulted from each clustering run (Fig. 4). Each of these clusters could be assigned to one of the following classes (or mixtures thereof) on both the TM and MSS data: water, conifers, mixed wood, hardwood, agricultural/ grass, residential/commercial, asphalt/turbid water and bare soil/building roofs (Fig. 4a, b). All of the fifty MSS clusters were defined by essentially two bands (band 4 and band 2), i.e., there was little overlap at the one sigma level between the clusters when band 4 was plotted versus band 2. For the TM, however, several bare soil/building roof clusters had large overlaps in a band 4 versus band 3 two band plot (Fig. 4a), signifying that a third band was needed to separate all the clusters. Band 1 in TM contains the separability of these clusters (Fig. 4c). The building roofs had a higher band 1 response for a given band 3 response than the bare soil areas. Thus, in TM data better separability of bare from built-up areas is indicated (Fig. 4c versus Fig. 4d), corroborating the principal components analysis. Note that this improved separability may not have been totally a result of spectral factors; e.g., the small size of the built-up features in this scene may have given the clustering algorithm an insufficient number of MSS pixels to adequately separate them from bare soil.

CONCLUSIONS

A preliminary comparison of 4-band TM data to archival MSS data has indicated: (1) an improved small target detection ability for TM over MSS data, and (2) an increased data dimensionality for TM. With TM data, high-contrast targets
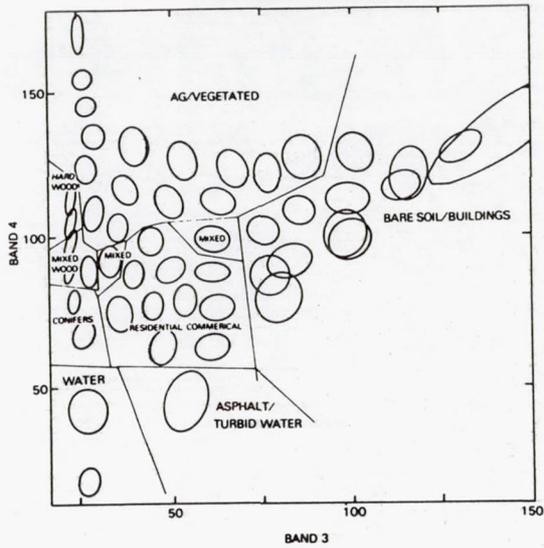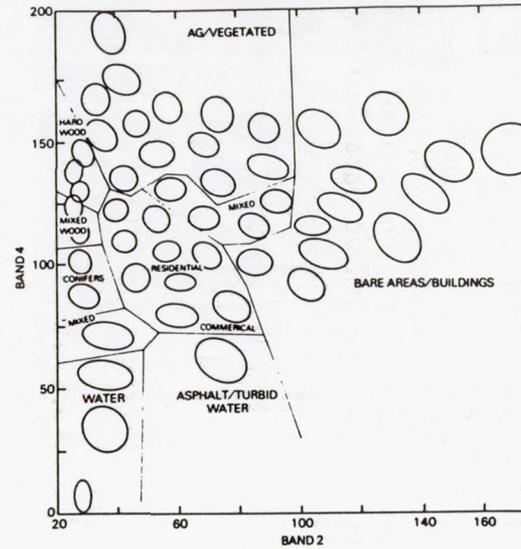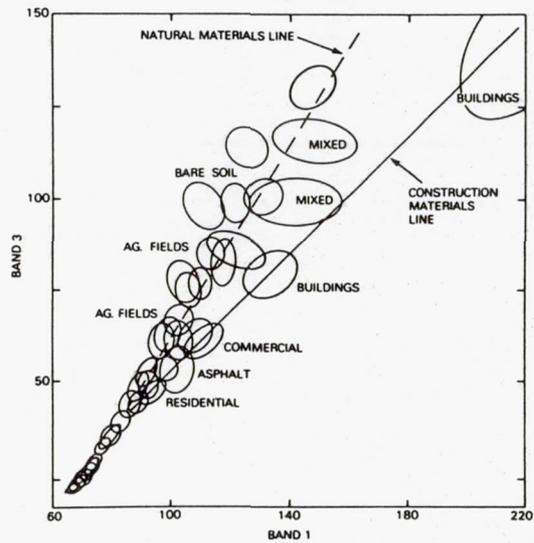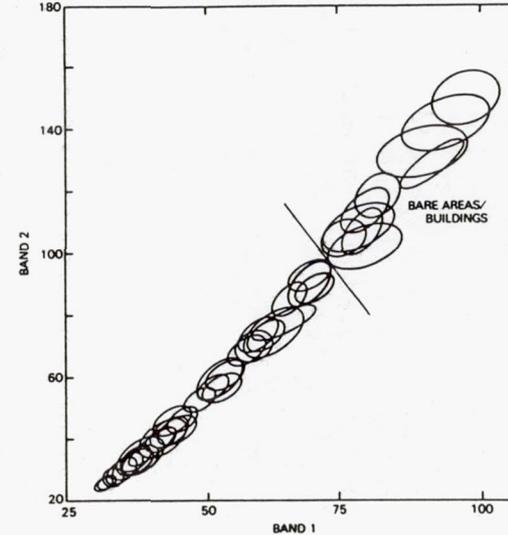
Figure 4. Spectral Clustering Analysis Results

down to 16 meter could occasionally be detected, whereas the comparable figure for MSS data was 40 meters. Whereas MSS data were basically two-dimensional in the scene analyzed, even 4-band TM data showed a third dimension apparently useful for discriminating urban for non-urban features. More detailed TM to MSS comparison studies are ongoing to better quantify TM incremental improvements over MSS and to trace the improvements to system design parameters.

REFERENCES

Kauth, R.J. and G.S. Thomas. 1976. "The Tasselled Cap--A Graphic Description of the Spectral - Temporal Development of Agricultural Crops as Seen by Landsat." Proceedings of Machine Processing of Remotely Sensed Data, Purdue Univ., W. Lafayette, IN. pp. 4B-41, 51.

ESL,Inc. 1978. "IDIMS Functional Guide, Vol. I." Electromagnetic Systems Laboratory, Sunnyvale, California.

Page intentionally left blank

ASSESSING LANDSAT TM AND MSS DATA
FOR DETECTING SUBMERGED PLANT COMMUNITIES

Steven G. Ackleson
Vytautas Klemas

College of Marine Studies
University of Delaware
Newark, Delaware 19711

INTRODUCTION

This research is concerned with assessing the spectral, spacial, and radiometric characteristics of LANDSAT TM and MSS data for detecting and monitoring submerged plant communities. The following preliminary results focus upon the spectral aspects of the problem in which a submerged plant canopy is to be distinguished from a surrounding bottom of sand or mud.

METHOD

Radiative transfer theory is used to model upwelling radiance that would be received by an orbiting sensor viewing a hypothetical estuarine environment, shown in Figure 1. The environment is composed of a clear maritime atmosphere, an optically shallow estuary of either clear or turbid water, and three possible bottom types: vegetation, sand, or mud.

The Atmosphere

A clear maritime air mass is selected and is described by Guttman (1968). Using solar irradiance data (Gast et al., 1965) as input, solar and sky irradiance is calculated at sea level as well as path radiance that would be received by an orbiting sensor. These calculations assume a solar zenith angle of $50°$.

The Water Column

Irradiance reflectance of the water column and bottom is calculated using a quasi-single scattering model developed by Philpot (1981).

$$R_I = \frac{B_d}{K_t} (1 - e^{-K_t d}) + A_b e^{-K_t d} \qquad (1)$$

where R_I = irradiance reflectance of the water and bottom,

B_d = irradiance backscatter coefficient,

K_t = total irradiance attenuation coefficient (the sum of the attenuation coefficients for upwelling and downwelling irradiance),

d = water depth,

A_b = irradiance reflectance of the bottom.

Equation (1) is used, at the expense of slightly lower accuracy, rather than a two-flow or Monte Carlo approach because the two necessary terms, B_d and K_t, are easily calculated from simple field measurements available in the literature and the amount of computer time required is relatively small.

The water column is assumed to be vertically homogeneous and the water surface calm and flat. Two very different water qualities are considered; clear ocean water and turbid fresh water. Measurements representing clear oceanic water are documented in Tyler et al. (1972). Measurements representing very turbid water were made in San Vincente, a man-made lake NE of San Diego, and are documented in Tyler and Smith (1970). Calculated values of B_d and K_t for both water types are shown in Table 1.

The Bottom Types

Three different reflectance profiles are selected from the literature to represent a submerged plant canopy, sand, and mud. The spectral reflectance of each bottom type is shown in Figure 2.

Upwelling Radiance Above the Earth

The upwelling radiance that would be received by an orbiting sensor is calculated as

$$L_{os} = \left[H_o R_I + P_a L_d \right] T_o + L_p, \tag{2}$$

L_{os} = upwelling radiance at the orbiting sensor,

H_o = the combined effects of the atmosphere and air/water interface upon radiance reflected from the water,

R_I = irradiance reflectance of the water and bottom,

P_a = Fresnel reflectance of downwelling radiance at the water surface,

L_d = downwelling sky radiance,

T_o = optical thickness of the atmosphere in the zenith direction, and

L_p = atmospheric path radiance received by the sensor.

Upwelling radiance values are calculated every 10 nm over the wavelength range 450 nm to 700 nm. Radiance values are then summed over TM bands 1 (450-520 nm), 2 (520-600 nm), and 3 (630-690 nm) and MSS bands 4 (500-600 nm) and 5 (600-700 nm).

Assessment of Spectral Quality

A spectral quality index is defined based upon the work of Lyzenga and Polcyn (1978) as

$$SQI = \left| L_T - L_B \right| L_B^{-\frac{1}{2}} \qquad (3)$$

where L_T = upwelling radiance representing the submerged plant canopy

L_B = upwelling radiance representing a background of sand or mud.

Equation (3) is quite similar to the equation for apparent contrast. Relative values of SQI between bands indicate relative effectiveness in detecting submerged plant canopies.

RESULTS

SQI values are calculated for clear water overlying a sand bottom, clear water overlying a mud bottom, turbid water overlying a sand bottom, and turbid water overlying a mud bottom. The results are shown in Tables 2-5 respectively. In all cases, when the water depth is optically shallow TM band 3 and MSS band 5 are most effective in detecting the submerged vegetation. This is intuitively correct since the inherent contrast between the vegetation and both the sand and mud is a maximum in these two bands. In clear water, as the water depth increased, the optimum band shifts from TM band 3 and MSS band 5 to TM band 1 for both bottom types. Here, the attenuation of bottom signal is less in TM band 1 than in TM band 3 and MSS band 5. In turbid water the relative effectiveness of each band is similar for all depths considered.

Spectrally, MSS band 4 is quite similar to TM band 2 and MSS band 5 is similar to TM band 3. Nevertheless, some unanticipated changes in relative SQI values between these bands are observed with respect to increasing water depth. Shown in Table 4, MSS band 4 is slightly more effective than TM band 2 in discriminating between submerged vegetation and sand at 0.5 meters. When the water depth increases to 1.5 meters, TM band 2 becomes slightly more effective. Similar results are seen in Table 2 and 3 between TM band 3 and MSS band 5.

In most cases, SQI values decrease with increasing depth. This also seems intuitively correct as the apparent contrast decreases with either increasing attenuation or increasing pathlength. In Table 3, SQI decreased in TM band 2 between 0.5 and 1.5 meters and then increased between 1.5 meters and 10.0 meters. To understand what is happening here it is necessary to know something about the variation in the optical characteristics of the water and the bottom types across the band. Figure 3 shows the spectral reflectance of the vegeta-

tion and mud within TM band 2. Whereas, the largest reflectance from the vegetation occurs in the larger wavelength portion of the band, the reflectance of the mud increases towards the shorter wavelength region. The average reflectance of the mud is slightly larger than the vegetation so that in the absence of a water column, the mud would appear brighter. Also shown in Figure 3 is the total attenuation coefficient of the clear ocean water which increases significantly towards the shorter wavelength region of the band. Under these circumstances the signal from the mud decreases more rapidly with increasing water depth than does the vegetation signal. Figure 4 is a plot of SQI without taking the absolute value of the numerator. Values were calculated for several depths between 0 and 20 meters. In very shallow water, the signal from the mud is greater than the signal from the vegetation and the index takes on a negative value. At some intermediate depth slightly greater than 1.0 meter the two signals are equal and SQI is zero. At still greater depths the vegetation appears brighter than the mud and SQI values are positive. As the depth becomes very deep both signals take on the value of optically deep water and SQI again falls to zero. This emphasizes the importance of making optical measurements within natural waters at appropriate spectral resolutions. If all optical measurements were made with a broad band radiometer representing TM band 2, the intermediate zero contrast would never have been noticed and the model predictions of upwelling radiance would have been in gross error.

CONCLUSIONS

The effectiveness of an orbiting sensor in discriminating between submerged features is determined by the inherent contrast between the submerged features and how strongly the bottom signal is attenuated by the water column. In optically shallow water the inherent contrast is the controlling factor. Thus, the optimum sensor band is that which correlates with the greatest inherent contrast between the submerged features. In optically deeper water, the optimum sensor band is that in which the bottom signal is attenuated the least.

In the clear ocean water the optimum band for detecting vegetation on a sand or mud bottom is shown to change with the optical depth of the water. In the turbid San Vicente water the optimum band in optically shallow water remains the optimum band in optically deeper water.

Under certain conditions the apparent contrast between two submerged features will decrease to zero at some intermediate depth and then increase for yet deeper depths. This can only be predicted with detailed knowledge of the spectral variation of optical parameters across the sensor band.

REFERENCES

Austin, R, 1974. The remote sensing of spectral irradiance from below the ocean surface. in Optical Aspects of Oceanography. Jerlov and Nielsen editors. Academic Press, New York. pp. 317-343.

Cast, P. R., 1965. Solar electromagnetic radiation: solar irradiance. in Handbook of Geophysics and Space Environments. S. L. Valley editor. McGraw-Hill Publishing Company, New York. pp. 1-16.

Gates, D. M., H. J. Keegan, J. C. Schleter, and V. R. Weidner, 1965. Spectral properties of plants. Applied Optics. Vol. 4, No. 1, pp. 11-20.

Guttman, A., 1968. Extinction coefficient measurements on clear atmospheres and within clouds. Applied Optics, Vol. 7, No. 12, pp. 2377-2381.

Lyzenga, D. R. and F. C. Polcyn, 1978. Analysis of optimum spectral resolution and band location for satellite bathymetry. NASA Final Report on Contract 7-35176. 59p.

Lyzenga, D. R. and F. Thomson, 1978. Basic remote sensing investigation for beach reconnaissance - bottom features task force. ONR Final Report on Contract N0014-74-C-0273. 36p.

Philpot, W., 1981. A radiative transfer model for remote sensing of vertically inhomogeneous waters. Doctoral Dissertation, College of Marine Studies, University of Delaware, Newark, Delaware, 19711. 140p.

Tyler, J. E., R. C. Smith, and W. H. Wilson, 1972. Predicted optical properties of clear natural water. Journal of the Optical Society of America, Vol. 62, No. 1, pp. 83-91.

Tyler, J. E. and R. C. Smith, 1970. Measurements of Spectral Irradiance Underwater. Gordon and Breach Publishers, New York. 103p.

Table 1

APPARENT OPTICAL CHARACTERISTICS OF CLEAR OCEAN WATER (TYLER ET AL., 1972)
AND TURBID SAN VICENTE WATER (TYLER AND SMITH, 1970).

Wavelength (nm)	Clear Oceanic			San Vicente		
	$K_t (m^{-1})$	$B_d \times 10^{-3} (m^{-1})$	$R_I \times 10^{-2} (d=\infty)$	$K_t (m^{-1})$	$B_d \times 10^{-3} (m^{-1})$	$R_I \times 10^{-2} (d=\infty)$
450	0.111	5.160	4.649	2.403	112.2	4.670
460	0.112	4.760	4.250	2.169	108.7	5.010
470	0.113	4.352	3.851	1.955	116.1	5.940
480	0.114	3.931	3.448	1.751	122.2	6.980
490	0.116	3.364	2.900	1.620	121.2	7.480
500	0.124	2.852	2.300	1.526	121.6	7.970
510	0.139	2.360	1.698	1.397	123.2	8.820
520	0.147	2.058	1.400	1.277	131.3	10.280
530	0.156	1.872	1.200	1.149	127.3	11.080
540	0.164	1.640	1.000	1.106	124.0	11.210
550	0.178	1.511	0.849	1.049	116.3	11.090
560	0.192	1.400	0.729	0.997	112.9	11.320
570	0.220	1.298	0.590	0.978	111.9	11.440
580	0.266	1.197	0.450	0.977	112.0	11.360
590	0.346	1.125	0.325	1.067	104.9	9.830
600	0.486	1.021	0.210	1.235	100.1	8.170
610	0.550	0.935	0.170	1.268	88.9	7.010
620	0.604	0.876	0.145	1.300	86.3	6.640
630	0.662	0.768	0.116	1.329	79.7	6.000
640	0.720	0.619	0.086	1.341	75.0	5.590
650	0.790	0.490	0.062	1.407	68.4	4.860
660	0.860	0.344	0.040	1.621	58.0	3.580
670	0.940	0.207	0.022	1.756	58.5	3.330
680	1.010	0.101	0.010	1.762	67.8	3.850
690	1.100	0.055	0.005	1.793	63.3	3.530
700	1.260	0.025	0.002	2.009	55.2	2.750

Table 2

SQI VALUES* (VEGETATION VS. SAND) FOR THE CASE OF CLEAR OCEAN WATER

Band	d=0.5m	d=1.5m	d=10.0m
TM1	143.8	128.9	49.2
TM2	101.4	79.9	12.5
TM3	235.8	120.7	0.1
MSS4	108.2	88.1	18.6
MSS5	214.1	117.4	0.5

* Units = $(mw/cm^2\text{-}str\text{-}nm)^{\frac{1}{2}} \times 10^{-3}$

Table 3

SQI VALUES* (VEGETATION VS. MUD) FOR THE CASE OF CLEAR OCEAN WATER

Band	d=0.5m	d=1.5m	d=10.0m
TM1	70.5	62.9	23.4
TM2	2.8	1.8	4.2
TM3	151.8	74.5	0.01
MSS4	13.23	8.5	0.2
MSS5	127.5	67.9	0.2

* Units = $(mw/cm^2\text{-}str\text{-}nm)^{\frac{1}{2}} \times 10^{-3}$

Table 4

SQI VALUES* (VEGETATION VS. SAND) FOR THE
CASE OF TURBID SAN VICENTE WATER

Band	d=0.5m	d=1.5m	d=10.0m
TM1	69.4	31.5	14.4
TM2	70.6	42.8	25.6
TM3	174.3	88.9	43.3
MSS4	71.7	42.1	24.5
MSS5	154.8	83.1	42.1

* Units = $(mw/cm^2\text{-str-nm})^{\frac{1}{2}} \times 10^{-3}$

Table 5

SQI VALUES* (VEGETATION VS. MUD) FOR THE
CASE OF TURBID SAN VICENTE WATER

Band	d=0.5m	d=1.5m	d=10.0m
TM1	70.5	62.9	23.4
TM2	3.1	1.6	0.8
TM3	109.0	53.5	25.5
MSS4	8.5	4.3	2.2
MSS5	91.4	46.7	23.3

* Units = $(mw/cm^2\text{-str-nm})^{\frac{1}{2}} \times 10^{-3}$
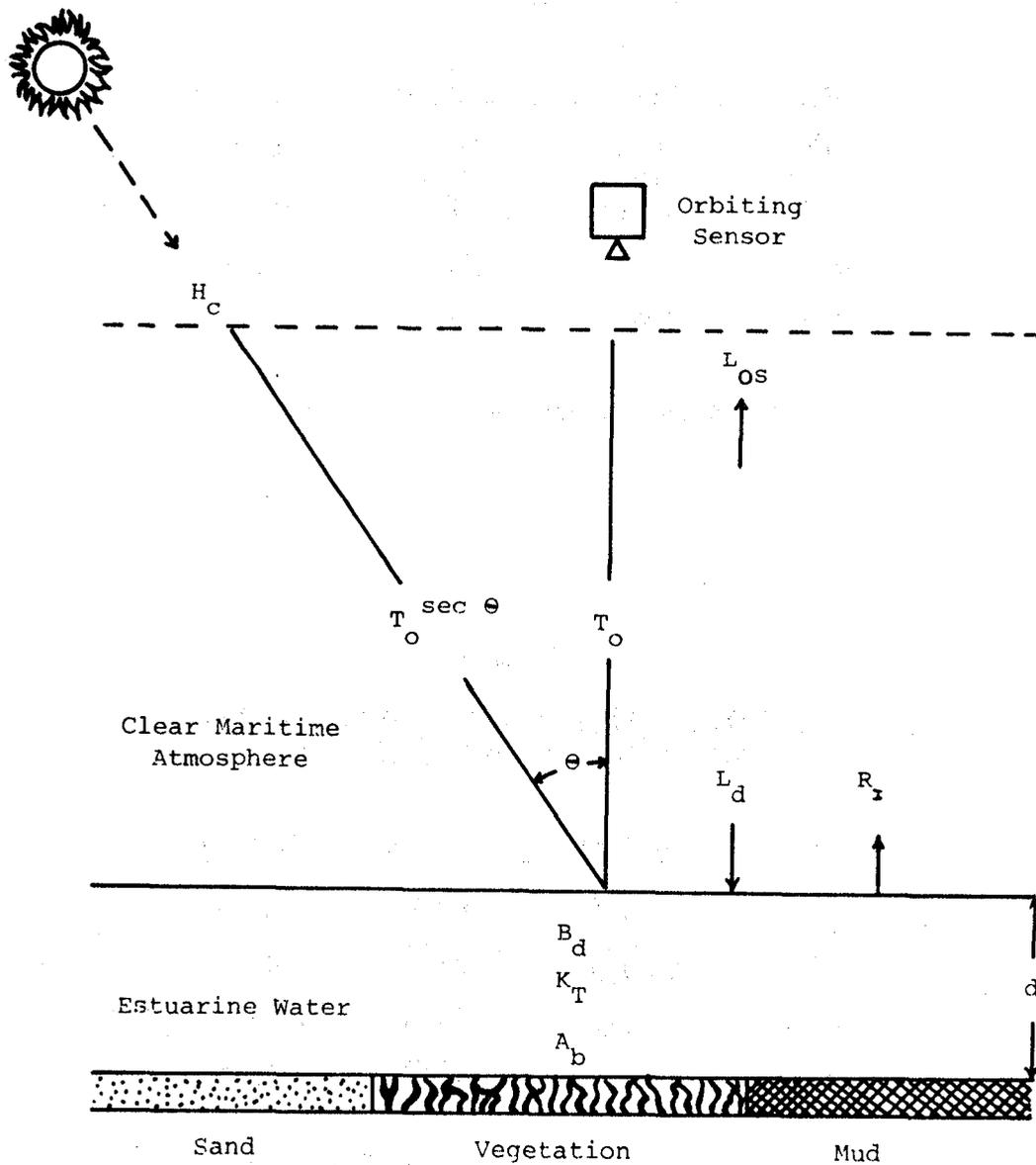
Figure 1. Optical parameters associated with radiative transfer within the estuarine environment.
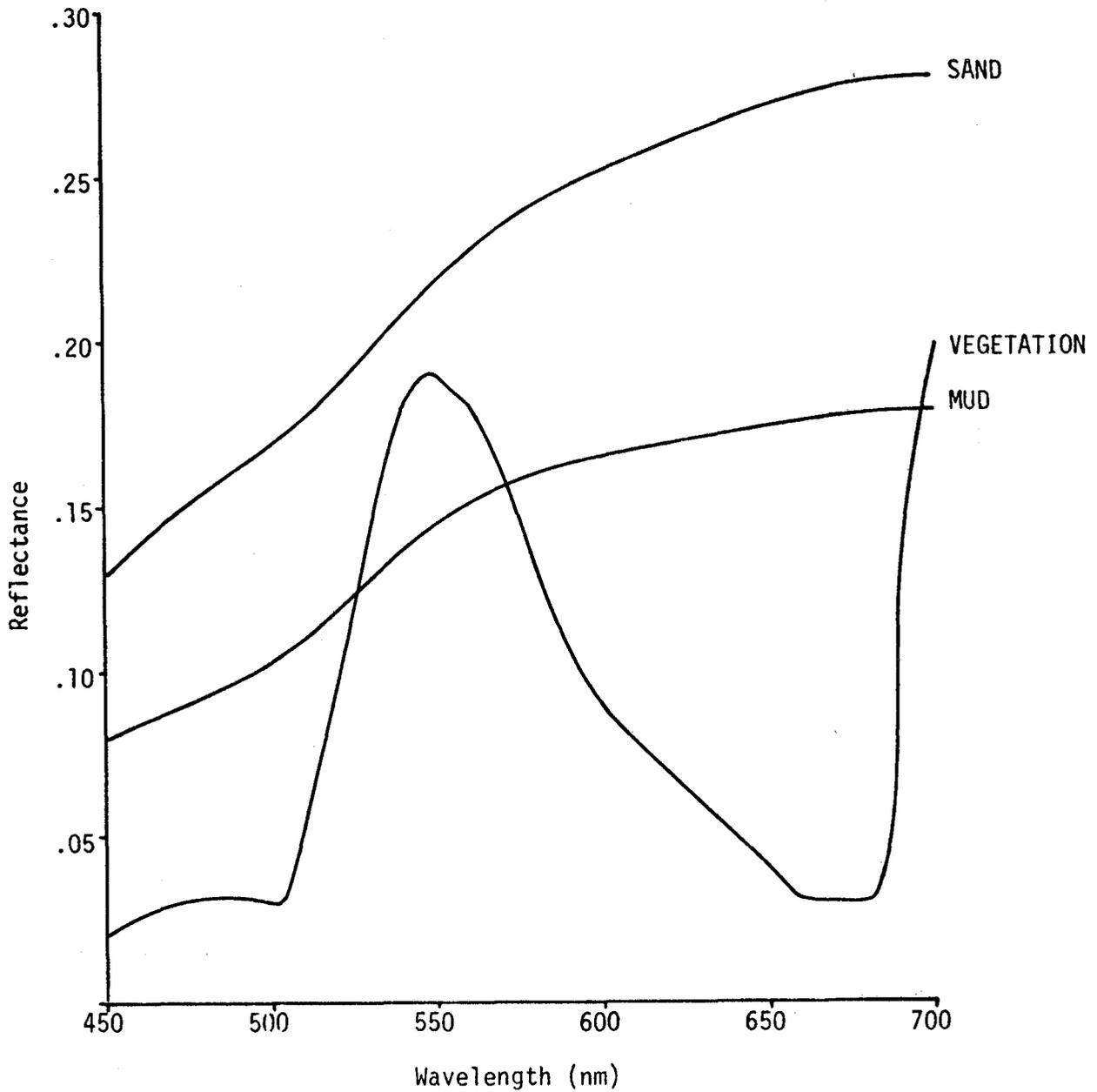
Figure 2. Irradiance reflectance of three bottom types used in the water reflectance model (Philpot, 1981). Sand = beach sand (Lyzenga and Thomson, 1978), mud = dark soil (Lyzenga and Thomson, 1978), and vegetation = an infinitely deep Ilex canopy (Gates et al, 1965).
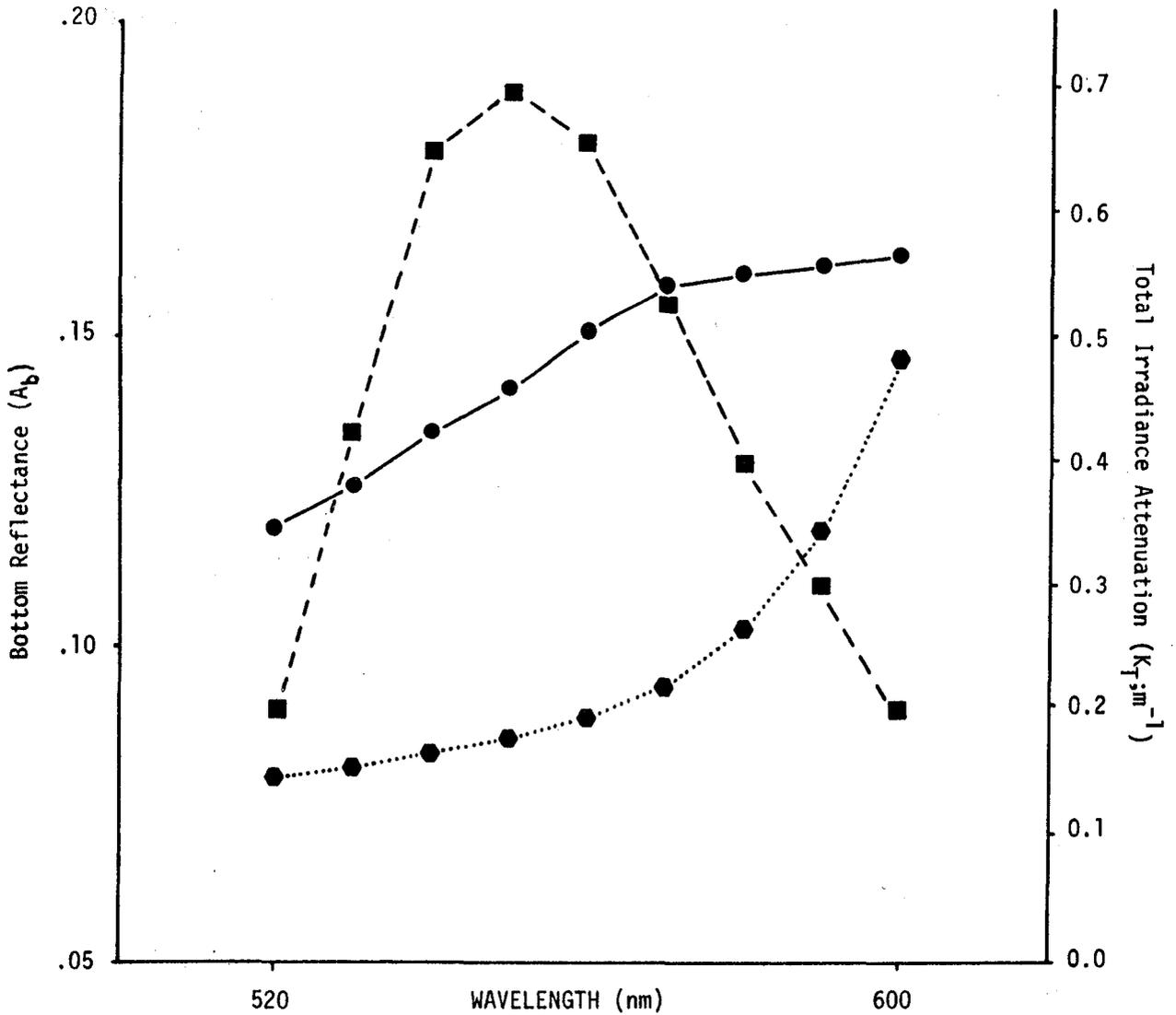
Figure 3. Irradiance reflectance of vegetation (■――■) and mud (●――●) and total irradiance attenuation for clear ocean water (●······●) plotted versus wavelength over TM band 2.
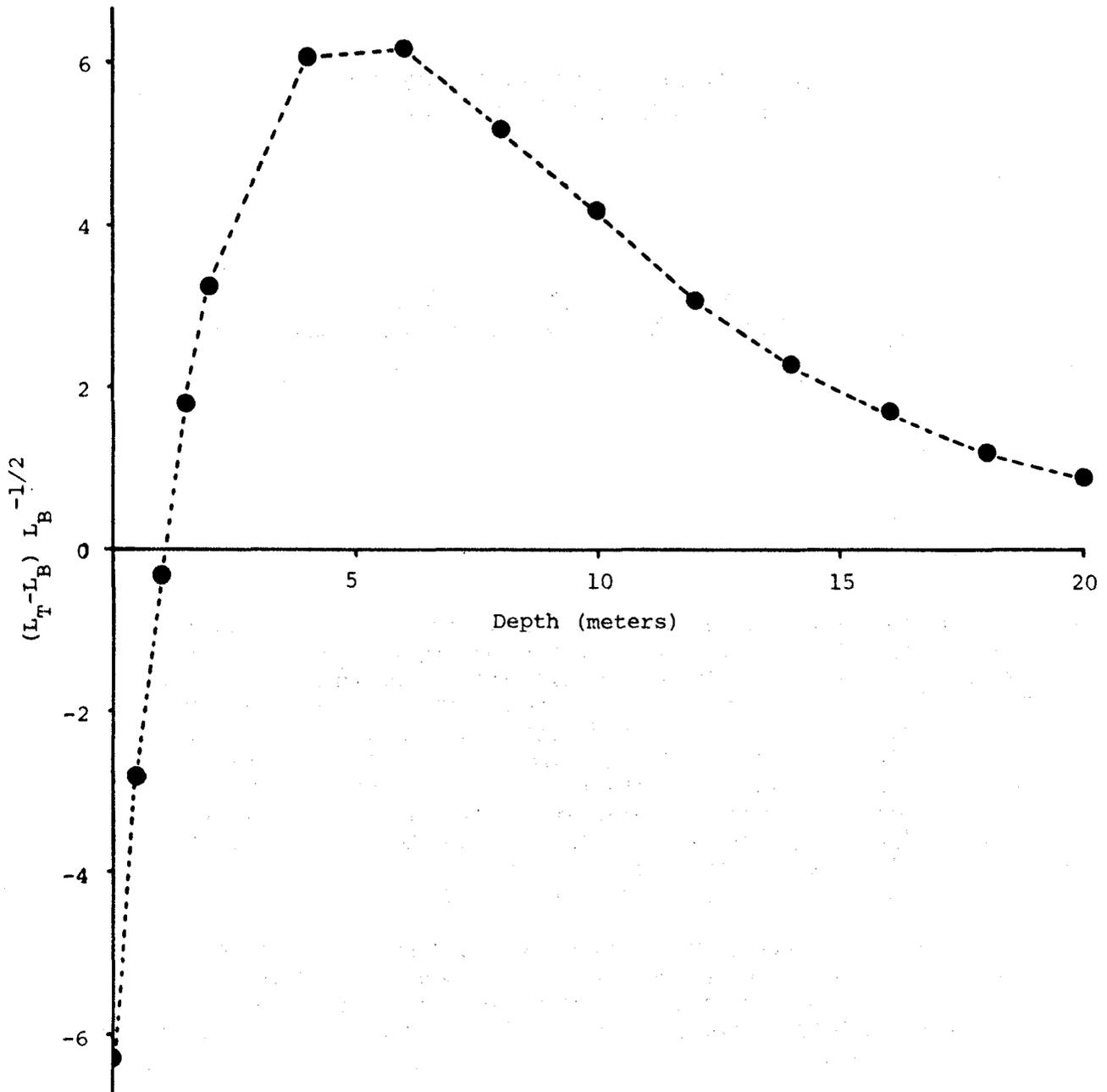
Figure 4. SQI values calculated without the absolute value of
the numerator for TM band 2. The water type is clear
ocean, L_T is the signal representing submerged vege-
tation, and L_B is the background signal representing
a bottom of mud.

A FIRST EVALUATION OF LANDSAT TM DATA TO
MONITOR SUSPENDED SEDIMENTS IN LAKES

F. R. Schiebe, J. C. Ritchie, and G. O. Boatwright
USDA-ARS, Durant, OK; Beltsville, MD; and Houston, TX

INTRODUCTION

Studies have shown that reflected solar radiation measurements obtained with
hand held instrumentation made at ground level (Ritchie et al., 1976; Whit-
lock et al., 1981) can be used to estimate suspended sediments in water
bodies. A linear relationship exists between inorganic sediment concen-
tration and either reflectance or reflected solar energy in the near infrared
band from 700 to 800 nanometers. While portions of the spectrum at shorter
wavelengths were more sensitive, the relationship was not linear and the
reflectance reached saturation levels at relatively low concentrations of
suspended sediment. At wavelengths greater than about 1000 nanometers the
water apparently acts as a black body adsorber and the reflected solar energy
is very low and completely insensitive to any suspended contaminants.

Similar results have been observed by researchers using the Landsat MSS as
the observational platform (LeCroy, 1982). Apparent limitations in the
number of levels of quantization of the radiometric signal and width of the
observed spectral band prevented sensitivity to concentrations much greater
than about 100 mg/l.

With the much improved characteristics of the TM instrumentation, both in the
increase in quantization levels to 256 and the narrowing of the spectral
bands, the capability for measuring suspended sediments in water should be
much improved. The purpose of this paper is to make a preliminary assessment
of the TM package as to its ability to monitor particulates suspended in
water.

STUDY AREA

Lake Chicot, in southeastern Arkansas (33° N latitude and 91° W longitude),
is a large oxbow lake on the lower Mississippi River flood plain. It was

formed by a cutoff of the Mississippi River approximately six centuries ago. Before the 1920's the lake, under natural conditions, was flushed periodically and it was known for its fishery and recreational assets. The location of the lake is indicated on the NOAA 7 scene illustrated in Fig. 1.

During the 1920's, extension of the main line Mississippi River levee cut direct flow between the lake and the river and greatly expanded the lake's watershed. In 1927 a disastrous flood breached the levee and allowed the river to flow into the lake temporarily. Since that time the watershed has been developed and much of it has been cleared for row crops and other agriculture. The lake is divided into two parts by a causeway with the southern or lower portion of the lake receiving most of the runoff.

The lake currently drains a 350 mi^2 (900 sq km) watershed. The lunate shaped lake is 11.25 mi (18 km) long with an average width of 0.5 mi (0.8 km). The average stage of the water surface is 103 ft (31.4 m) with a surface area of 3812 acres (14.5 x 10^{6}m^2) and a volume of 52,802 acre-ft (65.1 x 10^{6}m^3). The maximum and average depths at this surface elevation are 30.2 ft (9.2 m) and 13.85 ft (4.22 m) respectively. A sand-gravel aquifer 70 ft (21.3 m) thick underlies a 20 ft (6.1 m) fertile top stratum in the entire area.

The quality of water in Lake Chicot has deteriorated, particularly as a result of the large diversion of water to the lake and high suspended sediment and nutrient concentration from the largely agricultural watershed. This has affected the lake ecosystem and significantly reduced the fishery and other recreational assets.

The Corps of Engineers has diversion and lake level stabilization facilities under current construction which are intended to prevent an excessive quantity of sediments from entering the lake. Landsat is one of the means proposed to monitor and track changes in the water quality of the lake.

METHODS

Preliminary evaluations were made from a Landsat-4 TM and MSS scene (path 023/row 037) obtained September 23, 1982. Digital tapes for the MSS and TM scene were sampled over nine water sites (Fig. 2). Only water samples were studied in this evaluation. At least 140 pixels were sampled for the TM data and at least 15 pixels for the MSS data. The average pixel signal was calculated for each sample site.

Ground measurement of total suspended sediments, dissolved solids, temperature, dissolved oxygen, Secchi depth, chlorophyll and other water quality measurements were made in conjunction with the Landsat-4 overpass at four (1, 4, 5, 7) of the sample sites. Methods used to make these measurements have been described in an earlier publication (Ritchie et al., 1976).

RESULTS AND DISCUSSION

Total suspended solids in the lake ranged from 168 to 508 mg/l (Table 1). Temperature was relatively uniform ranging only from 27.2 in the lower lake to 29.0° C in the upper lake. Chlorophyll-a content in the upper lake was
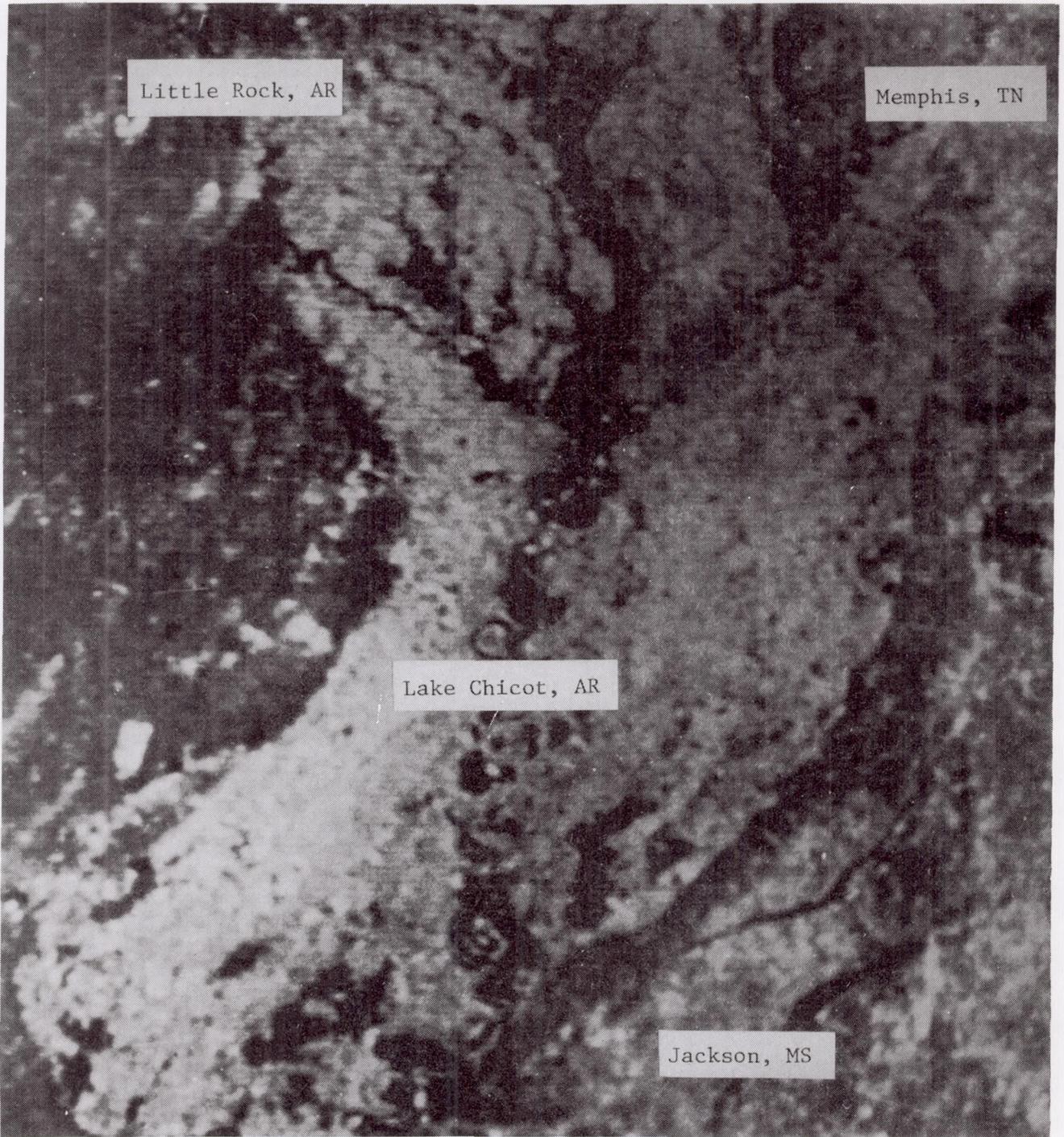
Figure 1. Lake Chicot Location Map
(from NOAA 7, Sept 22,
1982 scene).
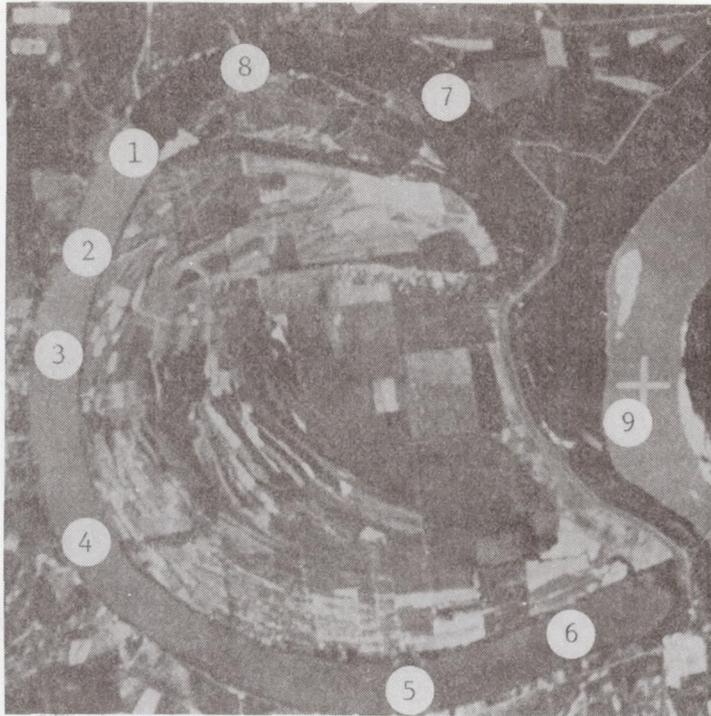
Figure 2. Water Data Site Locations
on Lake Chicot, AR.
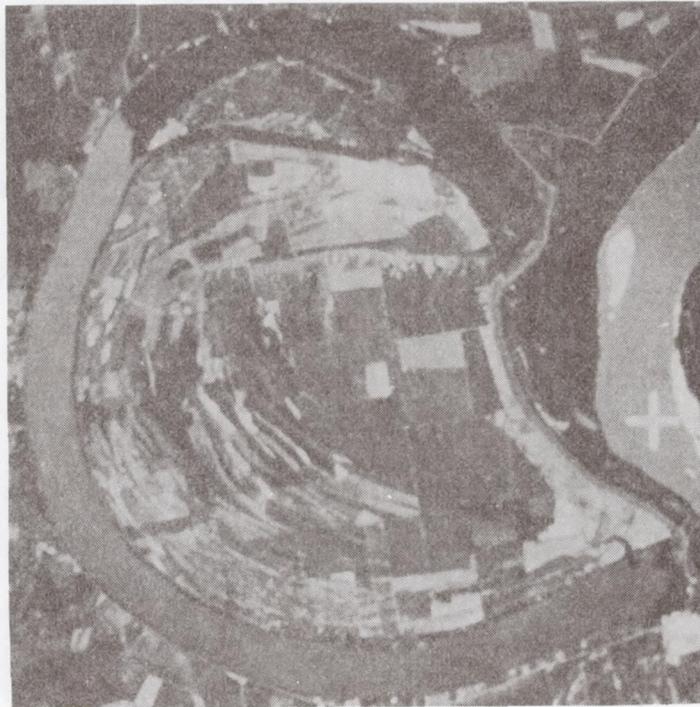
Figure 3. TM Band 1
450–520 nanometers

Table 1
WATER QUALITY MEASUREMENTS FOR LAKE CHICOT

Sample Site*	Temperature °C	Total Solids mg/l	Secchi Disk Depth cm	Chlorophyll a mg/m^3
1	27.2	508	49	22.0
4	27.9	300	66	23.5
5	28.0	314	53	20.0
7	29.0	168	48	55.0

*Sites 1, 4, and 5 are at the inlet, middle and outlet of the lower lake and site 7 is in the middle of the upper lake.

55.0 mg/m^3 which was more than double the chlorophyll-a (20.0 to 23.5 mg/m^3) in the lower lake. During lake August and early September the lake is generally at its clearest condition. By then the sediments from the previous winter rainy season have either settled out or have been flushed out during the summer. On September 12 and 13, 1982, about ten days prior to the overpass, a 58 mm precipitation event occurred on the watershed. This rainfall and the runoff caused near ideal conditions to exist in the lake on September 23, 1982, for a measurable suspended sediment gradient to exist (508 to 300 mg/l) in the lower lake. Measurements at the Stoneville, MS, Agricultural Experiment Station, 35 km east of Lake Chicot, showed solar radiation of 1.04 langley/minute at the exact time of the Landsat-4 overpass and the entire day to be nearly cloud free.

The 512 x 512 pixel (Figs. 3 through 9) subscenes of the TM data show major visual differences in the response of the different TM bands to water. TM Band 1 in the blue portion of the spectrum (0.45-0.52 μm) (Fig. 3) shows the upper lake with a uniform response except for the end of the lake near the Mississippi River which has an extensive cypress grove. The lower lake has a response gradient from the inlet in the north of the lake to the outlet in the south. TM Band 2 indicating reflection in the green (0.52-0.60 μm) (Fig. 4) is similar to Band 1 except that the gradient in the lower lake is more pronounced. TM Band 3 indicating reflection in the visible red (0.63-0.69 μm) (Fig. 5) shows a strong gradient in the lower lake. TM Bands 5 and 7 (Figs. 6 through 9) all appear to have uniform response from water. Basically only TM Bands 1, 2, 3, and 4 appear to contain information relative to suspended particulates in the water and TM Bands 4, 5, and 7 discriminate between water and nonwater.

Basic statistical data derived from the digital reflection values extracted from the nine water sites indicated on Fig. 2 are presented in Tables 2a and 2b. The coefficients of variation and range to mean ratios between sites in TM Bands 1, 2, 3, and 4 indicate that information relative to water quality is possible because backscatter of the suspended particulates caused greater ranges in the digital values and greater coefficients of variation.
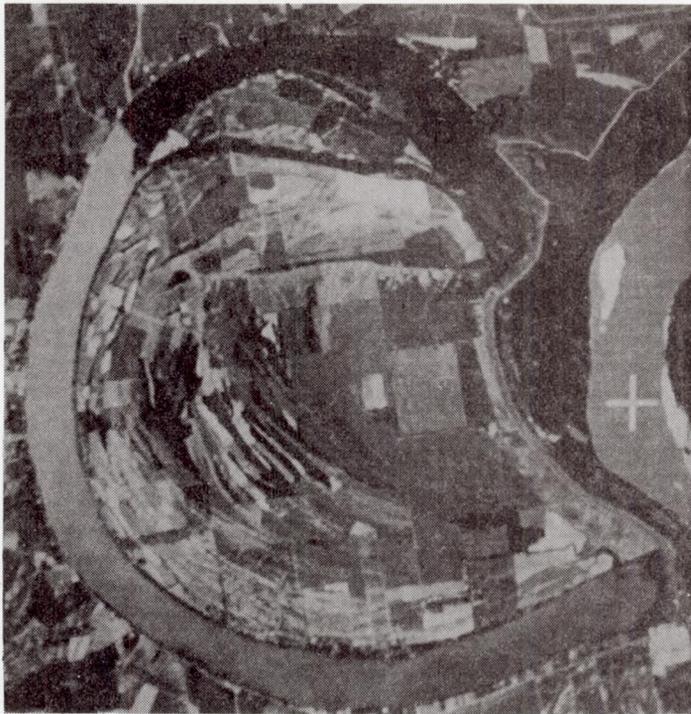
Figure 4.   TM Band 2
            520-600 nanometers

Figure 5.   TM Band 3
            630-690 nanometers

Figure 6.   TM Band 4
760–900 nanometers
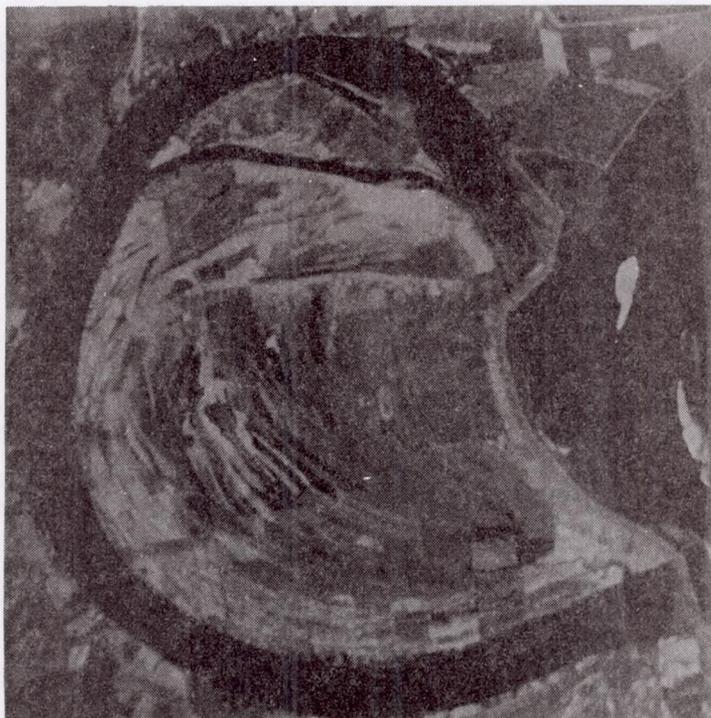
Figure 7.   TM Band 5
1.55–1.75 micrometers
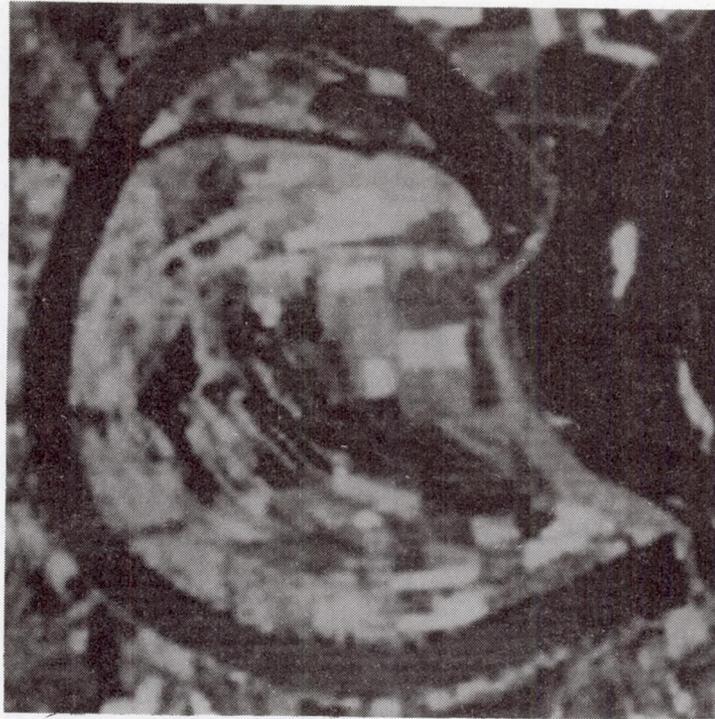
Figure 8.   TM Band 6
            10.4–12.5 micrometers

Figure 9.   TM Band 7
            2.08–2.35 micrometers

Table 2a
AVERAGE TM PIXEL RESPONSE FOR NINE WATER SITES

Band	TM1	TM2	TM3	TM4	TM5	TM6	TM7
Mean	75.4	33.3	29.7	14.5	5.9	127.5	3.2
Standard deviation	8.4	7.2	8.8	2.2	0.3	1.1	0.2
Coefficient of variation	11.2	21.5	29.8	15.3	4.9	0.9	4.6
Range	23.4	19.6	23.6	6.4	1.1	3.4	0.5
Range/mean	.31	.59	.79	.44	.19	.03	.16

Table 2b
AVERAGE MSS PIXEL RESPONSE FOR NINE WATER SITES

Band	MSS1	MSS2	MSS3	MSS4
Mean	23.7	18.6	13.3	2.5
Standard deviation	4.9	6.3	3.5	0.4
Coefficient of variation	20.5	33.8	26.6	15.5
Range	13.8	17.8	10.6	1.2
Range/mean	.58	.96	.80	.48

The average coefficient of variation within individual site were 1.9, 2.2, 2.9, 4.7, 18.0, 0.5, and 31.8 for TM Bands 1 through 7, respectively. This indicates that the pixels in each sample site were uniform. The high coefficients of variation in Bands 5 and 7 were due to low signal response.

Comparison of the TM Bands (Table 3) for water samples shows a high correlation between Bands 1, 2, and 3 and a marginal correlation with Band 4. The data from Band 7 is questionable because of low signal levels. No other significant correlations were found between the different TM bands.

Table 3
CORRELATION MATRIX r FOR LANDSAT-4 THEMATIC MAPPER BANDS FOR WATER (N=9)

Band	1	2	3	4	5	6	7
1	1.00	.99	.96	.61	.13	-.03	-.48
2		1.00	.96	.62	.09	-.04	-.54
3			1.00	.81	.01	-.25	-.60
4				1.00	-.31	-.61	-.72
5					1.00	.26	.74
6						1.00	.45
7							1.00

Comparison of TM bands with MSS bands for water (Table 4) showed TM Bands 1, 2, and 3 to be highly correlated with MSS Bands 1 and 2. This is to be expected because they view the same portion of the spectrum. TM Band 4 was highly correlated with MSS Bands 3 and 4 for the same reason. No other highly significant correlations were found. These correlations show that TM Bands 1, 2, and 3 and MSS Bands 1 and 2 are measuring similar information and that TM Band 4 and MSS Bands 3 and 4 are measuring similar information. Further studies are needed to evaluate the information content of the different sensors in each band.

Table 4

CORRELATION COEFFICIENT (r) FOR LANDSAT 4 THEMATIC MAPPER BANDS vs. MULTISPECTRAL BANDS FOR WATER (N=9)

Band	TM1	TM2	TM3	TM4	TM5	TM6	TM7
MSS 1	.99	.99	.94	.59	.11	-.03	-.51
MSS 2	.97	.98	.99	.77	.06	-.19	-.56
MSS 3	.74	.75	.89	.97	-.20	-.54	-.7
MSS 4	.55	.57	.75	.97	-.28	-.64	-.71

Comparing the ground data (only 4 measurements) with TM data for the same 4 sites indicated that TM Bands 1, 2, and 3 were highly correlated (r >.95) with total suspended solids. TM Band 3 had a r >.98. MSS Bands 2 and 3 also had r >.95. These results are consistent with published reports (Ritchie et al., 1976; Whitlock et al., 1981) and with studies made on Lake Chicot over the past 7 years (LeCroy, 1982; Ritchie and Schiebe, 1979).

TM Bands 1, 2, and 3 also appear to be highly related to chlorophyll-a content of water. However, our chlorophyll data is clumped in two regions (55 and 23 mg/m^3) so more data are needed before any conclusions are reached.

TM Band 6 contains temperature information. It has been shown (Schiebe et al., 1975) that suspended sediment laden water is expected to be a few degrees cooler than clear water, all other factors being equal. Our ground truth indicates that the upper lake temperature (Site 7) was two degrees warmer than at Site 1 on the lower lake where the concentration of suspended sediment was the highest, and about one degree higher than at Site 5 near the lake outlet. Some differences can be visibly seen in Fig. 8. The area where the sediment laden water enters the lake is slightly darker than either the upper lake or the lake near the outlet. The digital data shows only about a two digit difference to indicate the temperature difference. TM Band 6 data indicates that the Mississippi River was apparently somewhat cooler than Lake Chicot on this data although we do not have ground truth to corroborate this information.

CONCLUSIONS

1. TM Bands 1, 2, 3, and 4 appear to be providing information on concentrations of particulate matter suspended in surface waters. These bands are also highly interrelated for water samples.

2. Preliminary evaluation indicates that TM Band 3 showed the best relationship to surface suspended solids.

3. TM Bands 5 and 7 are useful for separating water from nonwater areas.

4. Analysis indicates the MSS Bands 2 and 3 can be related to suspended solids in surface water, as has already been shown from previous Landsat research.

5. Analysis of TM Band 6 indicates that while synoptic temperature patterns may be discerned, the digital sensitivity to a two degree temperature difference is low.

LITERATURE CITED

1. J. C. Ritchie, F. R. Schiebe, and J. R. McHenry. Remote Sensing of Suspended Sediments in Surface Waters, Photogrammetric Engineering and Remote Sensing, Vol. 42, No. 12, 1976, pp. 1539-1545

2. C. H. Whitlock, W. G. Witte, T. A. Talay, W. D. Douglas, J. W. Usry, and L. R. Poole. Research for Reliable Quantification of Water Sediment Concentrations from Multispectral Scanner Remote Sensing Data, Proc. Intl. Symp. on Rainfall-Runoff Modeling, 1981

3. S. R. LeCroy. Determination of Turbidity Patterns in Lake Chicot from Landsat MSS Imagery. NASA Contractor Report 165870, 1982

4. J. C. Ritchie and F. R. Schiebe. Remote Sensing of Suspended Sediments in Lake Chicot, Arkansas, Proc. American Soc. of Photogrammetry, Vol. 1, 1979, pp. 29-39

5. F. R. Schiebe, J. C. Ritchie, and J. R. McHenry. Influence of Suspended Sediment on the Temperatures of Surface Waters of Reservoirs, Verh. Int. Ver. Limnol., Vol. 19, 1975, pp. 133-136

Page intentionally left blank

SNOW REFLECTANCE FROM THEMATIC MAPPER

Jeff Dozier
University of California Santa Barbara

INTRODUCTION

In California 75% of the agricultural water supply comes from the melting Sierra Nevada snowpack. The California Cooperative Snow Survey uses measurements of snow water equivalent from snow courses, snow depth from aerial survey markers, and snowcovered area from satellite data to estimate the amount and the timing of the spring runoff.

Our work on snow reflectance from the TM should lead to improved use of satellites in snow hydrology.

1) Basin-wide albedo measurements from the TM could be used to better forecast the timing of the spring runoff, because these data can be combined with solar radiation calculations to estimate the net radiation budget. The TM is better-suited for this purpose than the MSS because of its larger dynamic range. Saturation still occurs in bands -4, but is only severe in band 1.

2) TMband 5 can discriminate clouds from snow.

3) Measurements of snowcovered area should be better with the TM, because the 20m spatial resolution can be used to estimate the contiguity of the snowcover above the snowline.

SPECTRAL ALBEDO OF SNOW

Calculations of snow reflectance in all 6 TM reflective bands (i.e., 1,2,3,4,5, and 7), using a delta-Eddington Model , show that snow reflectance in bands 4,5, and 7 is sensitive to grain size. An objective in our investigation is to interpret surface optical grain size. An objective in our investigation is to interpret surface optical grain size of snow, for spectral extension of albedo. Our results so far are encouraging.

Table 1 and Figure 1 show calculations of integrated reflectance for snow over all reflective TM bands, and water and ice clouds with thickness of 1mm water equivalent over TM bands 5 and 7. In the blue and green bands (1-2) snow reflectance is not sensitive to grain size, so measurements in these wavelengths will show the extent to which snow albedo is degraded by contamination from atmospheric aerosols, dust, pine pollen, etc. In the red
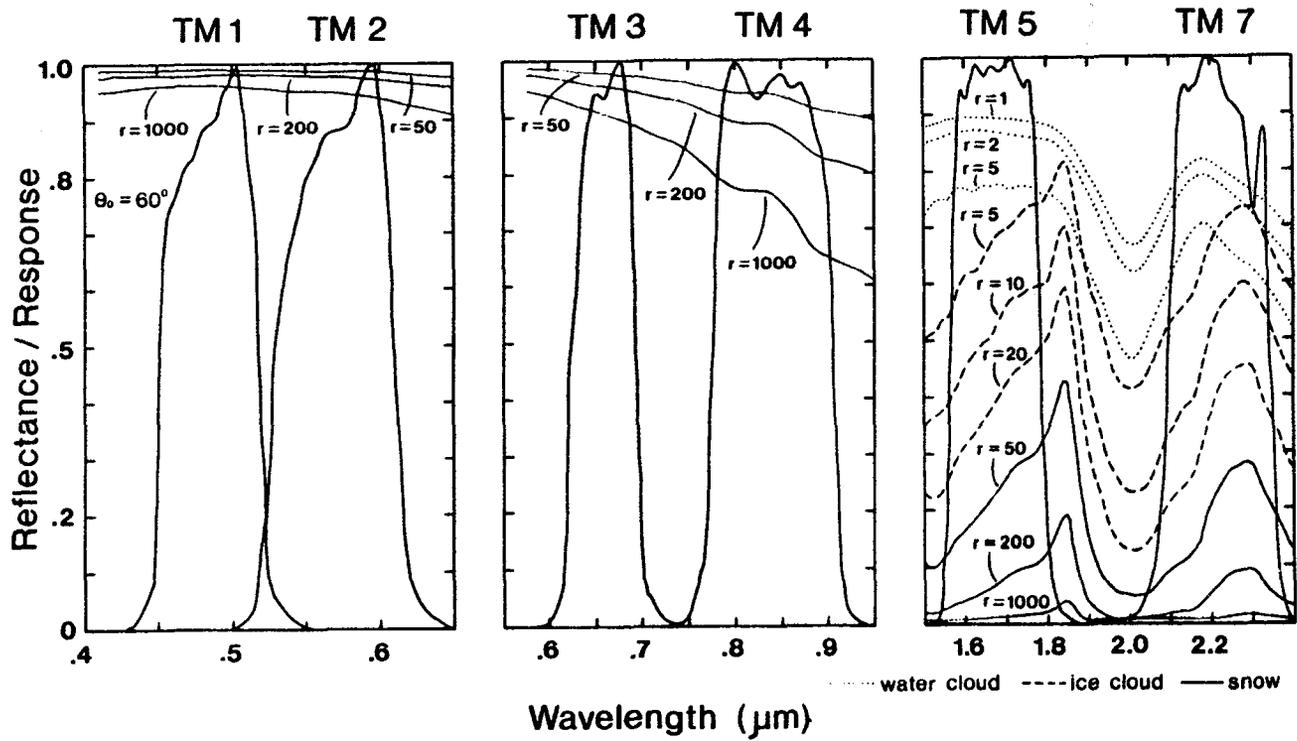
Figure 1. Sensor response functions and snow reflectance, at illumination angle $\vartheta_0 = 60°$ and grain radii r from 50 to $1000\mu m$, for the reflective bands (1-5, 7) of the Landsat-4 Thematic Mapper.

and near-infrared, snow reflectance is sensitive to grain size but not to contaminants, so grain size estimates in these wavelengths can be used to spectrally extend albedo measurements.

<div style="border:1px solid">

Table 1

TM Integrated Reflectances*, $\vartheta_0 = 60°$

band	*clean semi-infinite snow optical grain radius (μm)*				
	50	*100*	*200*	*500*	*1000*
1	.992	.988	.983	.974	.963
2	.988	.983	.977	.964	.949
3	.978	.969	.957	.932	.906
4	.934	.909	.873	.809	.741
5	.223	.130	.067	.024	.011
7	.197	.106	.056	.019	.010

band	*water cloud, 1mm water optical droplet radius (μm)*				
	1	*2*	*5*	*10*	*20*
5	.891	.866	.769	.661	.547
7	.784	.750	.650	.481	.345

band	*ice cloud, 1mm water equivalent optical crystal radius (μm)*				
	1	*2*	*5*	*10*	*20*
5	.817	.780	.665	.513	.383
7	.765	.730	.642	.478	.341

* Integrated reflectance ρ is

$$\rho = \frac{\mu_0 \int_0^\infty \rho_\lambda \, \Phi_\lambda^{(j)} \, E_\lambda \, d\lambda}{\mu_0 \int_0^\infty \Phi_\lambda^{(j)} \, E_\lambda \, d\lambda}$$

where ρ_λ is direct-beam spectral snow reflectance at illumination angle $\vartheta_0 = \cos^{-1}\mu_0$, E_λ is spectral solar constant, and $\Phi_\lambda^{(j)}$ is instrument response function for band j. (The μ_0's of course cancel.)

</div>

The reason that snow reflectance in bands 1 and 2 is not sensitive to grain size is that ice is so transparent to these wavelengths that increasing the size of a snow crystal does not significantly change the probability that a photon impinging on the crystal will be absorbed. Impurities are much more absorptive than ice in these wavelengths, however, so small amounts of contaminants will affect reflectance . In the near-infrared, bands 3 and 4, ice is slightly absorptive, so an incident photon is more likely to be absorbed if the crystal is larger, and snow reflectance is therefore sensitive to grain size. Impurities are not so important in these wavelengths because their absorption coefficients are not much larger than those of ice.

Table 2 gives characteristics of the Thematic Mapper, and, for background information, the Multispectral Scanner and NOAA Advanced Very High Resolution Radiometer. In the radiance columns of the table, the quantization

<table>
<tr><td colspan="6" align="center">Table 2</td></tr>
<tr><td colspan="6" align="center">TM, MSS, and AVHRR Spectral Characteristics
[spectral distribution of solar constant from Ref. 5]</td></tr>
<tr><td colspan="6" align="center"><i>Thematic Mapper</i></td></tr>
<tr><td rowspan="2">band</td><td colspan="2"><i>wavelengths</i>
(50% ampl., μm)</td><td colspan="4"><i>radiances</i> ($W\,m^{-2}\,\mu m^{-1}\,sr^{-1}$)</td></tr>
<tr><td colspan="2"></td><td>NEΔL</td><td>sat.</td><td>solar</td><td>%</td></tr>
<tr><td>1</td><td colspan="2">.452 - .518</td><td>.63</td><td>161</td><td>621</td><td>25.9</td></tr>
<tr><td>2</td><td colspan="2">.529 - .610</td><td>1.24</td><td>316</td><td>540</td><td>58.5</td></tr>
<tr><td>3</td><td colspan="2">.624 - .693</td><td>.95</td><td>241</td><td>468</td><td>51.5</td></tr>
<tr><td>4</td><td colspan="2">.776 - .905</td><td>.92</td><td>234</td><td>320</td><td>73.1</td></tr>
<tr><td>5</td><td colspan="2">1.568 - 1.784</td><td>.13</td><td>31.7</td><td>66.5</td><td>47.7</td></tr>
<tr><td>7</td><td colspan="2">2.097 - 2.347</td><td>.067</td><td>16.9</td><td>24.4</td><td>69.3</td></tr>
<tr><td>6</td><td colspan="2">10.422 - 11.661</td><td colspan="4" align="center">(thermal band)</td></tr>
<tr><td colspan="6" align="center"><i>Landsat-2 Multispectral Scanner</i></td></tr>
<tr><td>4</td><td colspan="2">.5 - .6</td><td>4.0</td><td>259</td><td>574</td><td>45.1</td></tr>
<tr><td>5</td><td colspan="2">.6 - .7</td><td>2.8</td><td>179</td><td>491</td><td>36.5</td></tr>
<tr><td>6</td><td colspan="2">.7 - .8</td><td>2.3</td><td>149</td><td>401</td><td>37.2</td></tr>
<tr><td>7</td><td colspan="2">.8 - 1.0</td><td>3.0</td><td>192</td><td>285</td><td>67.4</td></tr>
<tr><td colspan="6" align="center"><i>NOAA-7 Advanced Very High Resolution Radiometer</i></td></tr>
<tr><td>1</td><td colspan="2">.56 - .72</td><td>.51</td><td>518</td><td>485</td><td>106.8</td></tr>
<tr><td>2</td><td colspan="2">.71 - .98</td><td>.33</td><td>341</td><td>364</td><td>93.7</td></tr>
<tr><td>3</td><td colspan="2">3.53 - 3.94</td><td colspan="4" align="center">(thermal bands)</td></tr>
<tr><td>4</td><td colspan="2">10.32 - 11.36</td><td colspan="4"></td></tr>
<tr><td>5</td><td colspan="2">11.45 - 12.42</td><td colspan="4"></td></tr>
<tr><td colspan="6">For the TM and AVHRR, the solar constant values were integrated over the sensor response functions. We do not have response function data for the MSS, so the sensor was assumed to have a square-wave response.</td></tr>
</table>

and errors and saturation radiances of the sensor bands and compared with the
solar constant, integrated through the sensor response functions. Solar
constant spectral distributions are from the NASA standard , adjusted to fit
the integrated values measured from the Nimbus-7 cavity radiometer of the
earth radiation budget experiment . The last column in the table expresses
thesensor saturation radiance as a percentage of the solar constant,
integrated through the band response function.

Snow will frequently saturate in band 1, but in bands 2, 3, and 4 the
saturation problem is not nearly as severe as with the MSS, so the TM can be
used to measure snow albedo and thus allow basin-wide energy budget snowmelt
calculations. Bands 5 and 7 will not saturate over snow.

Snow does stretch the dynamic range of the TM, however. Figure 2
shows histograms of all 6 reflective bands for the southern Sierra Nevada on
10 December 1982 (northwest portion of path 41, row 35) and Table 3 lists
portions of the image that are saturated in all 7 bands. In band 1 fully 1/8
of the pixels are saturated, and the saturated portion would increase as sun
elevations get higher in the spring.
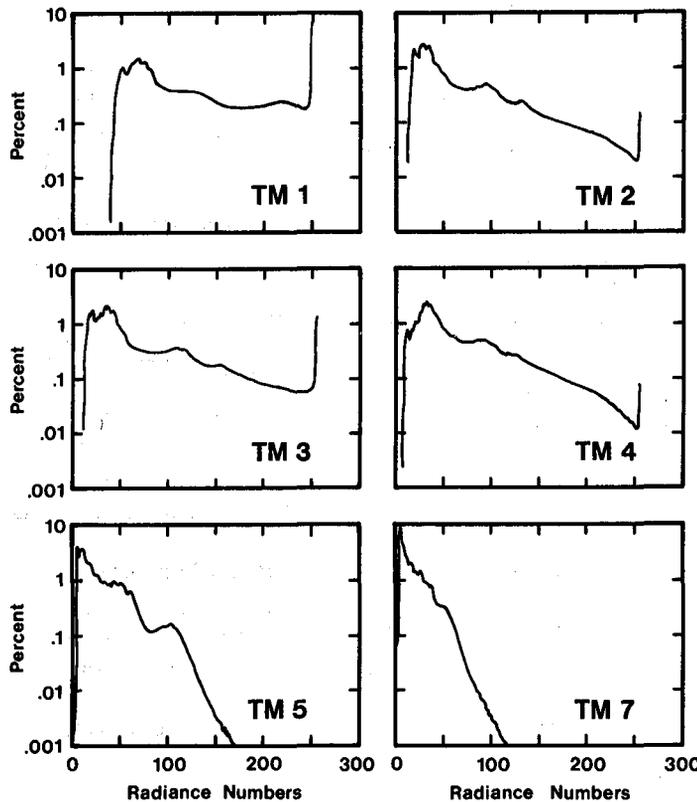
FIGURE 2.   Histograms of digital radiance numbers for all
            reflective bands (1-5,7) for the scene in
            Figure 2. The saturation percentages are in
            Table 3.

Table 3

Sierra Nevada and White Mountains, 10 Dec 1982
Saturation, TM Reflective Bands

band	percentage saturated
1	12.25
2	0.15
3	1.40
4	0.07
5	0.00
7	0.00

SNOW/CLOUD DISCRIMINATION

Figure 3 shows TM bands 2 and 5 of the Sierra Nevada, Owens Valley, and the White Mountains on 10 December 1982 (northwest quarter of path 41, row 35). In band 2 both snow and clouds are bright, while in band 5 the clouds are bright but snow is dark.

Table 1 and Figure 1 also analyze reflectance of snow and ice clouds. In both "shortwave infrared" bands, 5 and 7, snow is much darker than clouds, and water clouds are brighter than ice clouds in band 5. In both of these bands ice is highly absorptive, and snow reflectance is low and sensitive to grain size for small sizes, which explains the higher reflectance of ice clouds than snow. In band 5 water is less absorptive than ice , so water clouds are more reflective than ice clouds.

EFFECT OF RESOLUTION ON SNOWCOVER MAPPING

The major operational use of satellite data in snow hydrology has been in mapping snowcovered area, as an index to the amount of snowmelt runoff   . In mountainous regions the usual approach has been to use the satellite data to identify the snowline (above which the ground is snowcovered, below which it is snowfree) and to then measure the area within the snowline as the snowcovered area.

Unfortunately the elevation of the snowline is not always a good index to the volume of snow (or snow water equivalence) in the watershed. Sometimes a cold storm deposits small amounts of snow over a wide area, whereas a warmer storm will deposit much more snow but over a smaller area. The finer spatial resolution of the Landsat 4 Thematic Mapper might make it possible to use textural information about the snowcovered area, and thereby to

SNOW/CLOUD DISCRIMINATION
SIERRA NEVADA and WHITE MOUNTAINS, 10 DEC 82

TM band 5

TM band 2
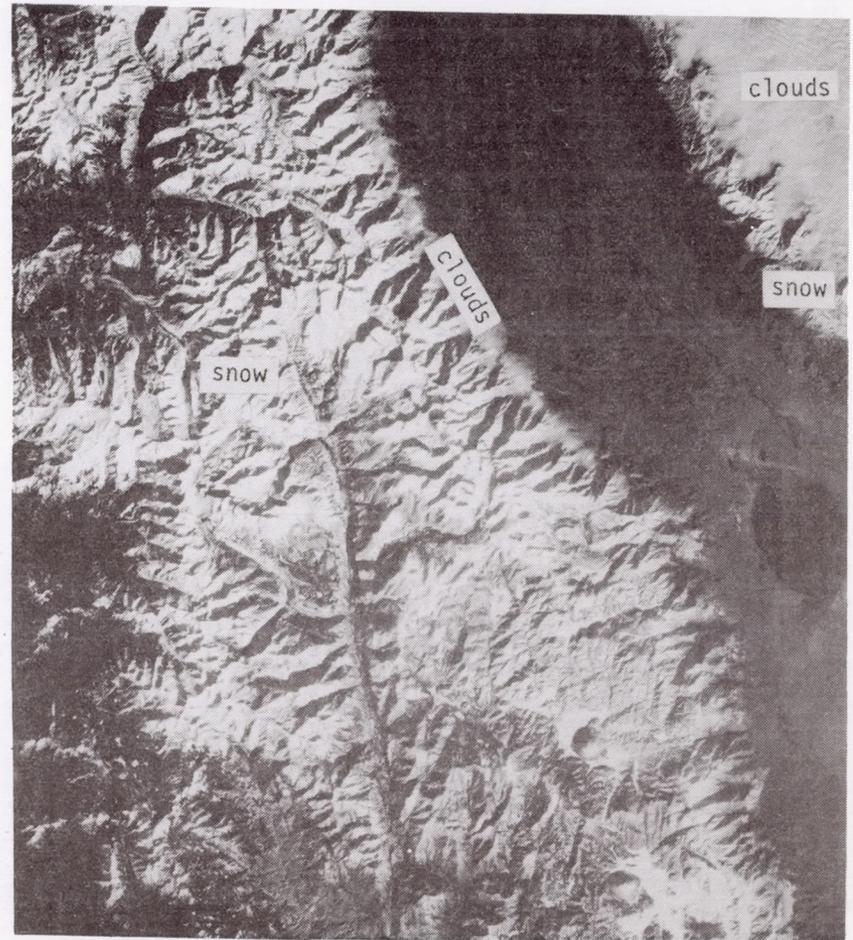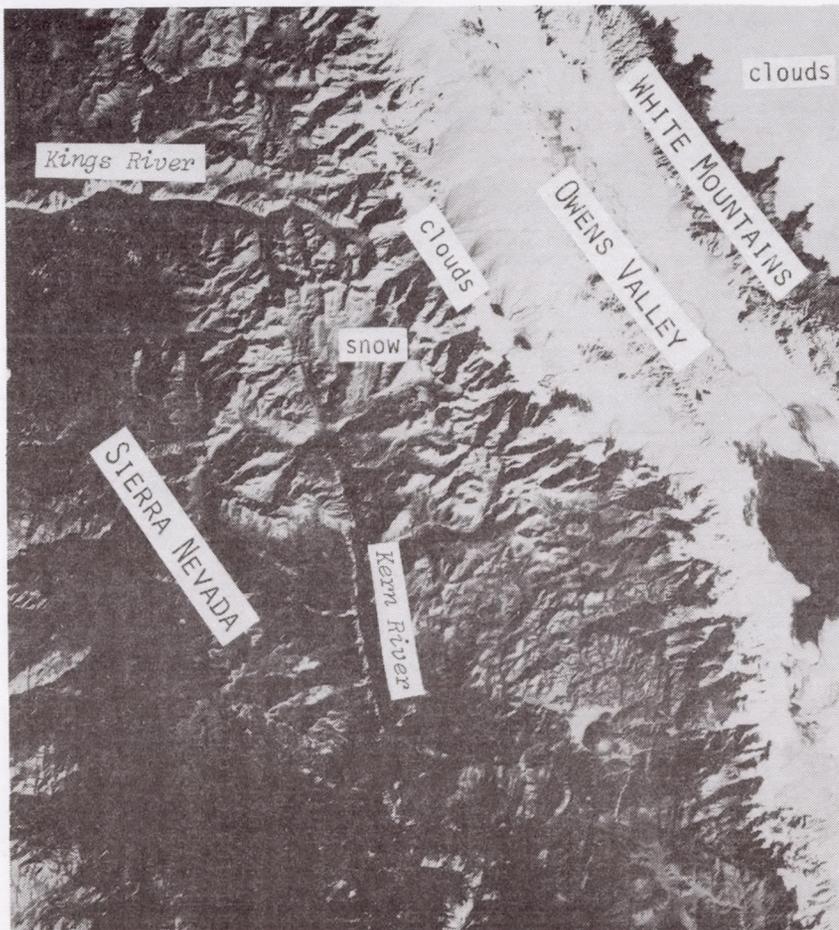
IV-355
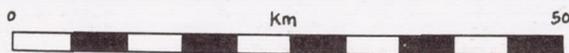
Figure 3. Bands 2 (right) and 5 (left) Landsat-4 Thematic Mapper data for the Sierra Nevada, Owens Valley, and White Mountains on 10 December 1982 (Path 41, Row 35). In band 2 both snow and clouds are bright, but in band 5 snow is dark and clouds are bright.

better use satellite data to estimate the volume of snow in a watershed. Even above the snowline, there are differences between years of large accumulation and normal or lean years. Rocks, bushes, trees, etc. may or may not be covered. Ridges may or may not be blown clean. The spatial contiguity of the snow is also an index of its volume, and the TM should help us estimate this.

CONCLUSION

Landsat-4 Thematic Mapper data include spectral channels suitable for snow/cloud discrimination and for snow albedo measurements that can be extended throughout the solar spectrum. Except for band 1, the dynamic range is large enough that saturation occurs only occasionally. The finer spatial resolution gives much better detail on the snowcovered area.

REFERENCES

1. Hale, G.M., and M.R. Querry, 1973, Optical constants of water in the 200-nm to 200- m wavelength region, "Applied Optics", 12, 555-563.

2. Hickey, J.R., L.L. Stowe, H. Jacobowitz, P. Pellegrino, R.H. Maschoff, F. House, and T.H. VonderHaar, 1980, Initial solar irradiance determinations from Nimbus-7 cavity radiometer measurements, "Science", 208, 281-283.

3. Rango, A., and K.I. Itten, 1976, Satellite potentials in snowcover monitoring and runoff prediction, "Nordic Hydrology", 7, 209-230.

4. Rango, A., and J. Martinec, 1979, Application of a snowmelt-runoff model using Landsat data, "Nordic Hydrology, 10, 225-238.

5. Thekaekara, M.P., ed., 1970, The solar constant and the solar spectrum measured from a research aircraft, NASA TR-R-351.

6. Warren, S.G., and W.J. Wiscombe, 1980, A model for the spectral albedo of snow, 2, Snow containing atmospheric aerosols, "Journal of the Atmospheric Sciences, 37, 2734-2745.

7. Wiscombe, W.J., and S.G. Warren, 1980, A model for the spectral albedo of snow, 1, Pure snow, "Journal of the Atmospheric Sciences", 37, 2712-2733.

Page intentionally left blank

PRELIMINARY EVALUATION OF TM FOR SOILS INFORMATION

David R. Thompson, Keith E. Henderson,
A. Glen Houston, and David E. Pitts

NASA Johnson Space Center
Houston, Texas 77058

INTRODUCTION

The Landsat satellites have been a valuable and prolific source of remotely
sensed Earth resource data since the first Landsat was launched in 1972.
They have been used to make crop acreage estimates[5] and to detect and moni-
tor drought in the U.S., U.S.S.R., and Australia.[8,9] Many soil survey studies
have been conducted using Landsat data. Soil associations and attendant range
sites were identified using Landsat imagery by Seevers et al.[7] Soil associa-
tions have been stratified by manual interpretations from Landsat color com-
posite imagery in regions where polypedons are related to soil drainage[6],
topography[12,13,14], or topography and vegetation[4]. Westin and Frazer[13]
described the characteristics of Landsat imagery that are applicable to its
use in soil survey programs. Using tone, color, land use patterns, and
drainage patterns on a Landsat color composite transparency, they prepared a
low-intensity soilscape map that needed only moderate refinement after field
checking. Weismiller et al.[11] made an inventory of soils in Clariton County,
Missouri, using Landsat and topographic data; however, they did not attempt
to relate soil cover to soil type. In using digital analysis of Landsat data
from Clinton County, Indiana, Kirschner et al.[2] defined 12 soil spectral
classes and 4 vegetation classes. The 12 spectral soil classes were corre-
lated with soil drainage classes and were grouped into 4 drainage classes.
Thompson et al.[10] found that selected soil properties important to plant
growth were separable on natural vegetated landscapes using June and October
Landat data. However, few of the above have significantly advanced the soil
survey process or provided an understanding of the influence of soil on the
spectral signature of vegetation. This lack of progress in using Landsat is
in part due to the coarse spatial resolution (79 m) and the four wide spectral
bands of the multispectral scanner (MSS) aboard every Landsat since 1972. A
new improved second-generation, Earth-sensing satellite called the thematic
mapper (TM) was launched in July 1982. It has a new sensor system with
improved spatial resolution (30 m), spectral separation (seven narrow bands),

geometric fidelity and radiometric accuracy. The selection of bands for TM
were designed such that four bands (0.45-0.52 μm, 0.52-0.60 μm, 0.63-0.69 μm,
and 0.76-0.90 μm) are similar to the Landsat MSS bands (0.5-0.6, 0.6-0.7,
0.7-0.8, and 0.8-1.1). Two new bands in the mid-IR region (1.55-1.75 μm and
2.08-2.35 μm) and one in the thermal region (10.4-12.5 μm) should provide new
information for vegetation and soil monitoring. The improved spatial resolu-
tion (over that of MSS) is also an important attribute of TM. A pixel size
of 30 m (ground resolution) in all but band 6 will allow classification of
areas as small as 2-1/2 to 4 ha. Band 6, a thermal band has a pixel size of
120 m on the ground; however, the band 6 values have been interpolated to give
a value for each 30 m pixel.

The objectives of this study are to evaluate whether Landsat TM provides in-
formation that could be used for soil association maps and if soil properties
(variability within vegetated fields) can be detected with the new bands on
TM.

Materials and Methods

Thematic Mapper (TM) digital data and transparencies were acquired on
August 22, 1982, over a 185 X 185 km area near the corner of the states of
Arkansas, Missouri, and Tennessee. Within this area, Mississippi County,
Arkansas, was selected for evaluation. Transparencies of the seven bands of
TM were made of the county, and a 5 X 6 n mi sample segment was located within
the county. Wall-to-wall crop identification on the 5 X 6 n mi sample segment
was collected by USDA-SRS personnel along with crop condition data from 30
fields. This information included growth stage, percentage of ground cover,
plant height, soil surface moisture, and other agronomic observations. Each
field was outlined and registered to the TM spectral data. A detailed soil
survey was available for Mississippi County, Arkansas.[1] The soils of the
county are derived from alluvium and provide a wide variety of soils.

Results and Discussion

The general soil map of Mississippi County was overlayed onto the images of
the seven TM bands (Figures 1-7). Examination of the tonal patterns of these
soil associations indicate that bands 1, 2, and 3 do not have as much contrast
between the various associations that bands 4, 5, 6, and 7 have. Bands 1, 2,
and 3 are in the visible part of the spectrum while bands 4, 5, and 7 are in
the near and mid IR region with band 6 being the thermal band. The main
difference between the different soil associations is the drainage and soil
texture (Table 1). At the time of the satellite acquisition, the area was
planted in soybeans, cotton, and rice with the majority of the ground cover
being greater than 90 percent. Contrast is apparent in TM band 5 (1.55-
1.75 μm) between soil associations 1 and 2. Association 1 is composed of
soils that are loamy throughout and poorly drained while association 2 is
poorly drained soils that have a thick clay subsoil. However, in TM5, asso-
ciations 2 and 3 have essentially the same tones, but in TM bands 4 (.76-
.90 um) and 6 (10.4-12.5 um), they are different. As the difference in the
two associations is the minor soil, an examination of the available water
holding capacity indicates that the Steele soils have 9.2 inches of available
water in a 60-inch profile while Crowley has 13.2 inches. This difference in
available water holding capacity appears to explain the dark tone (cool) for

association 3 and the light tone (warm) for association 2 in the TM 6 (10.4-12.5 um). The thermal channel indicates that the additional available water holding capacity of association 3 is reflected by the cooler crop canopy and soils. Also, it is apparent that the thermal band is picking up differences within association 1. An examination of the detailed soil survey indicates that the light (warm) area within the association contains a soil complex of sandy soil that is poorly to excessively drained. It appears that the thermal channel along with the IR channels are reflecting the vegetation responses to the available water in the soil. While these indications as to the soil properties being reflected through the vegetation are not supportable by ground measurements at the time of the TM acquisition, it does appear that TM is providing information which is related to soil properties over large areas that are related to characteristics of the crop canopy.

A subset of fields within a 5 X 6 n mi segment located within associations 1 and 2 were selected to determine whether soil properties (as measured by variability within vegetated fields) can be related to TM spectral response and which TM bands are responding to the soil properties.

Ten fields of soybeans were selected such that five fields had uniform soil types (mapping units) and five fields had complex soil patterns. Individual pixel values for each TM band were extracted for each field. The hypothesis is that the uniform soil fields will have less variability in the spectral data within the field than the complex soils if soil properties are being reflected in the vegetation covering the soil. A plot of the coefficient of variation of each TM band for each field shows that the complex soil fields have more within-field variability than the uniform soil fields (figure 8).

A nonparametric quantitative comparison of the distribution of the coefficients of variation (C.V.) of the five uniform soils soybean fields with the distribution of the C.V.'s of the five complex soils soybean fields is provided in Table 2. The Wilcoxon rank-sum statistic[3], in the form of an average rank from the combined distribution of the two types of fields, is used to test the hypothesis that the distribution of C.V.'s for the uniform soils fields is identical to that for the complex soils fields. The hypothesis is rejected if the median of the C.V.'s for the complex soils fields is significantly larger than the median of the C.V.'s for the uniform soils fields. The results of the test of this hypothesis for each TM channel, as shown in Table 2, indicate that the median C.V. for the complex soils fields is significantly larger than the median C.V. for the uniform soils fields for each TM channel except channel 6, the thermal IR channel. However, one of the five uniform soils fields appears as an outlier with respect to the C.V.'s for the thermal channel 6 (see figure 9). If this field is omitted from the analysis, the results become significant, i.e., the median C.V. for the complex soils fields is significantly larger at the .005 level than the median C.V. of the uniform soils fields for band 6. It is believed that the suspect field has an artifically increased C.V. for band 6 due to the interpolation scheme. A significant change in band 6 values occurs near the edge of this field due to the lower band 6 responses in the neighboring field. No such effect was observed for the other TM channels.

For this set of fields, there was no overlap at all between the distributions of the C.V.'s for the uniform and complex soils fields for TM channels 3, 5, and 7 as indicated by the range of these distributions in Table 2. Also, of all the channels, channel 7 shows the largest relative within-field variability for both the uniform and complex soils. It remains to be shown, quantitatively, that this difference in within-field variability between uniform and complex soils fields for the TM channels is in fact due to the different soils associations within the fields. However, these results are supportive of the hypothesis that the TM spectral data are responding to the soils properties being reflected in the vegetation covering the soil.

Summary

Results from this study indicate that the TM bands are providing information that is related to the soil properties within the field. Over large areas, these bands also appear to provide information that is related to the soil properties that are important to plant condition. While these results are only an indication of the information that TM can provide, they do indicate that TM data--especially, the mid-IR and thermal bands--show the capability for separating vegetated soil landscapes on a broad basis. The analysis at the field level with a growing crop also indicates that TM, with its additional and narrower bands and improved spatial and radiometric resolution is influenced by within field variability due to soils that will have to be accounted for in the analysis of TM data.

References

1. Ferguson, D.V. and J.L. Gray, 1971. Soil Survey of Mississippi County, Arkansas. U.S. Department of Agriculture, Soil Conservation Service, Washington, D.C. 58p.

2. Kirschner, F.G., S.A. Kaminsky, R.A. Weismiller, H.R. Sinclair, and E.J. Hinzel. 1978. Map unit assessment using drainage classes defined by Landsat data. Soil Sci. Soc. Am. J. 42:768-771.

3. Lehmann, E.L. 1975. Nonparametrics: Statistical Methods Based on Ranks, Holden-Day, Inc. pp.5-31.

4. Lewis, D.T., P.M. Seevers, and J.V. Drew. 1975. Use of satellite imagery to delineate soil associations in the Sand Hills region of Nebraska. Soil Sci. Soc. Amer. Proc. 39:330-335.

5. MacDonald, R.B. and F.G. Hall. 1980. Global Crop Forecasting. Science 208: 677-679.

6. Parks, W.L. and R.E. Bodenheimer. 1973. Delineation in major soil associations using ERTS-1 imagery. p.121-125. In S.C. Freden et al. (ed) 2nd Symposium on Significant Results Obtained from the Earth Resources Technology Satellite. Goddard Space Flight Center, Greenbelt, Maryland. March 5-9, 1973. Scientific and Technical Information Office, NASA, Washington, D.C.

7. Seevers, P.M., D.T. Lewis, and J.V. Drew. 1974. Applications of ERTS-1 Imagery in Mapping and Managing Soil and Range Resources in the Sand Hills Region of Nebraska. p.225-232. In S.C. Freden et al. (ed.) 3rd Earth Resources Technology Satellite Symp., vol. 1, NASA SP-351, Goddard Space Flight Center, Greenbelt, Maryland, December 10-14, 1973. Scientific and Technical Information Office, NASA, Washington, D.C.

8. Thompson, D.R. and O.A. Wehmanen. 1979. Using Landsat Digital Data to Detect Moisture Stress. Photo. Eng. and Remote Sensing 45:201-207.

9. Thompson, D.R. and O.A. Wehmanen. 1980. Using Landsat Digital Data to Detect Moisture Stress in Corn-Soybean Growing Regions. Photo. Eng. and Remote Sensing 46:1087-1093.

10. Thompson, D.R., R.H. Haas, and M.H. Milford. 1981. Evaluation of Landsat Multispectral Scanner Data for Mapping Vegetated Soil Landscapes. Soil Sci. Soc. Am. J. 45:91-95.

11. Weismiller, R.A., I.D. Persinger, and O.L. Montgomery. 1977. Soil inventory from digital analysis of satellite scanner and topographic data. Soil Sci. Soc. Am. J. 41:1166-1170.

12. Westin, F.C. 1973. Identification of soil associations in South Dakota on ERTS-1 imagery. In Symposium Proceedings, Management and Utilization of Remote Sensing Data. Soc. of Photogramm., Falls Church, Virginia, p.610-629.

13. Westin, F.C. and C.J. Frazee. 1976. Landsat data, its use in a soil survey program. Soil Sci. Soc. Am. J. 40:81-89.

14. Westin, F.C. and V.I. Meyers. 1973. Identification of soil associations in western South Dakota on ERTS-1 imagery. In Second Symposium on Significant Results Obtained from the Earth Resources Technology Satellite. Goddard Space Flight Center, Greenbelt, Maryland, 1:965-972.

TABLE 1. Soil Associations Descriptions for Mississippi County, Arkansas

Map
Symbol   Association Description

1   Amagon-Dundee-Crevasse association: Poorly drained and somewhat
        poorly drained soils that are loamy throughout and excessively
        drained soils that are sandy throughout.

2   Sharkey-Steele association: Poorly drained soils that have a thick
        clayey subsoil and moderately well drained soils that are sandy in
        the upper part and clayey in the lower part.

3   Sharkey-Crowley association: Poorly drained soils that are clayey
        in some part of the subsoil.

4   Tunica-Bowdre-Sharkey association: Moderately well drained and
        poorly drained soils that are clayey in some part of the subsoil.

5   Convent-Morganfield-Crevasse association: Somewhat poorly drained
        soils that are loamy throughout and excessively drained soils that
        are sandy throughout.

6   Alligator-Earle association: Poorly drained and somewhat poorly
        drained soils that have a dominantly clayey subsoil.

TABLE 2. Descriptive Statistics Comparing the Relative Within-Field
          Variability of TM Channel Values for 10 Soybean Fields--
          5 Having Uniform Soils and 5 Having Complex Soils

| TM | C.V. RANGE | | Median C.V. | | Wilcoxon Rank-Sum Statistic | |
Channel	U	C	U	C	U	C
1	(2.2,5.0)	(4.6,7.3)	2.8	5.2	3.3	7.7*
2	(3.2,6.9)	(1.7,11.8)	4.3	9.0	3.2	7.8*
3	(6.3,12.9)	(13.7,25.3)	8.7	18.2	3.0	8.0**
4	(5.4,9.2)	(9.0,13.7)	7.6	11.0	3.8	7.2*
5	(4.4,5.5)	(7.0,9.4)	4.8	8.3	3.0	8.0**
6	(1.0,3.5)	(1.9,2.7)	1.6	2.2	4.0	7.0
7	(9.9,13.8)	(16.7,27.2)	22.6	23.6	3.0	8.0**

U - Fields having uniform soils   * Significant at .05 level
C - Fields having complex soils   ** Significant at .005 level
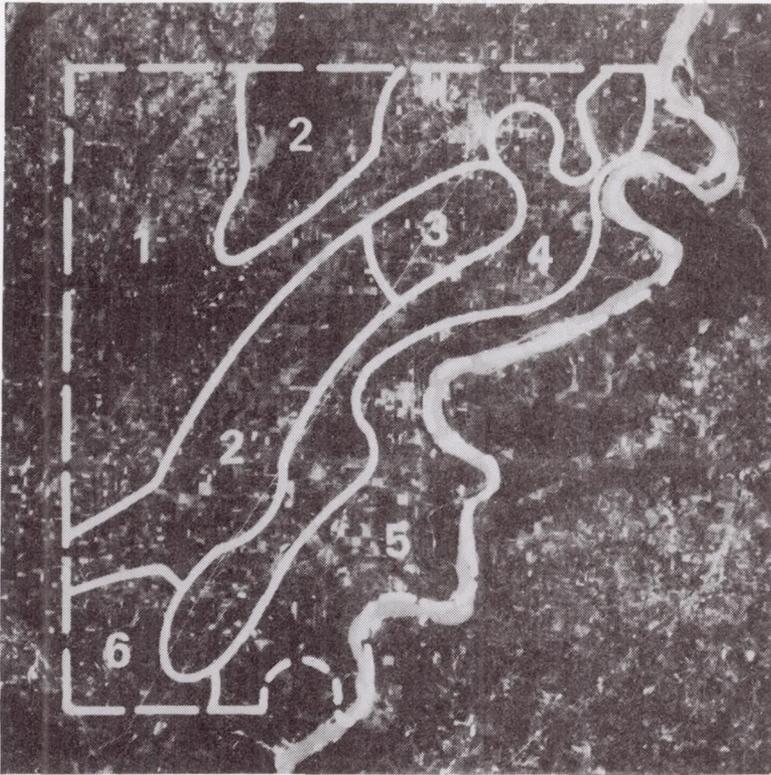
Figure 1:
Soil associations
for Mississippi
County, Arkansas,
overlaid on TM
Band 1 (0.45-0.52 μm)

Figure 2:
Soil associations
for Mississippi
County, Arkansas,
overlaid on TM
Band 2 (0.52-0.60 μm)

Figure 3:
Soil association
for Mississippi
County, Arkansas,
overlaid on TM
Band 3 (0.63-0.69 μm)
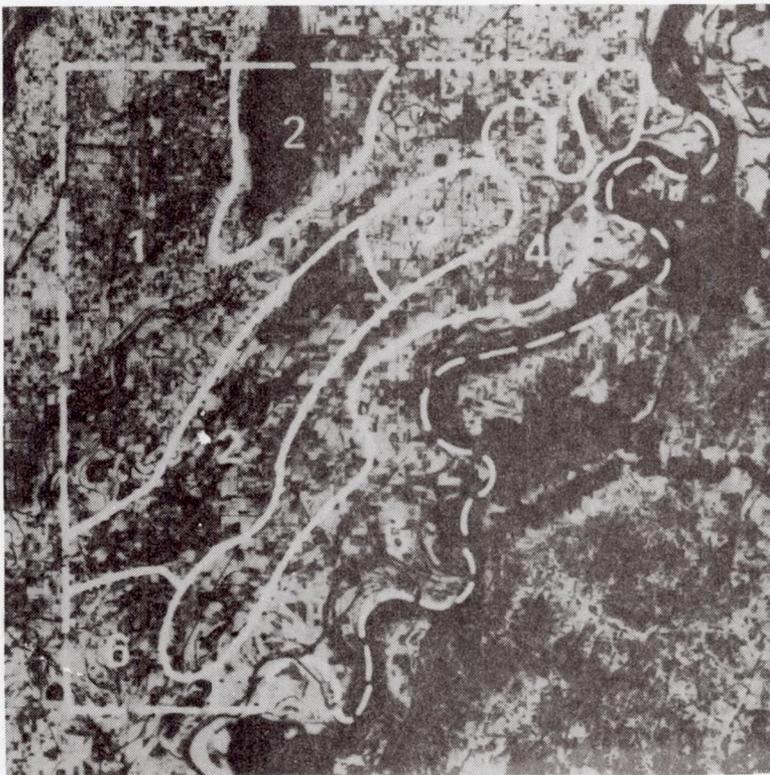
Figure 4:
Soil associations
for Mississippi
County, Arkansas,
overlaid on TM
Band 4 (0.76-0.90 μm)
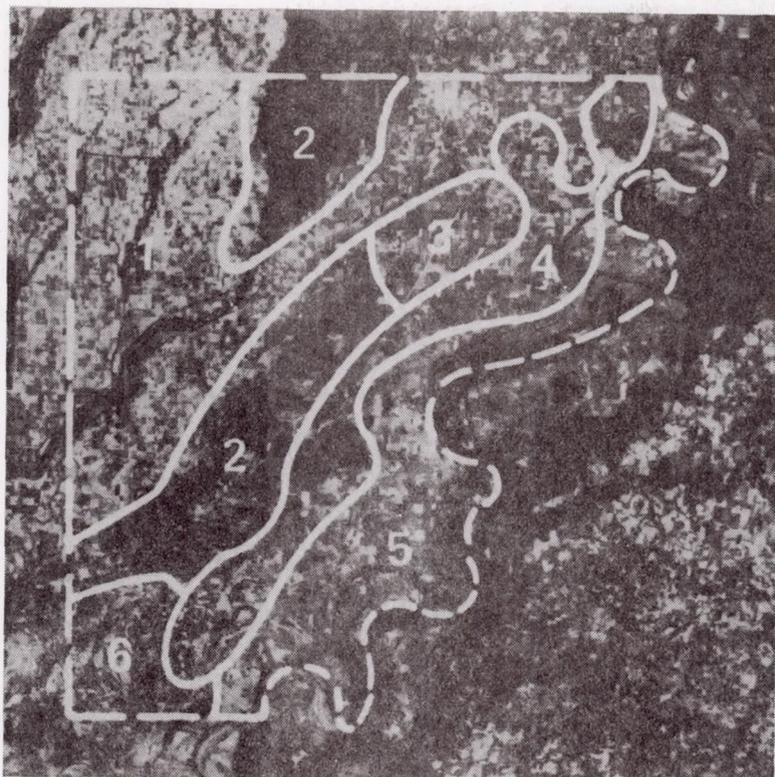
Figure 5:
Soil associations
for Mississippi
County, Arkansas,
overlaid on TM
Band 5 (1.55-1.75 µm)
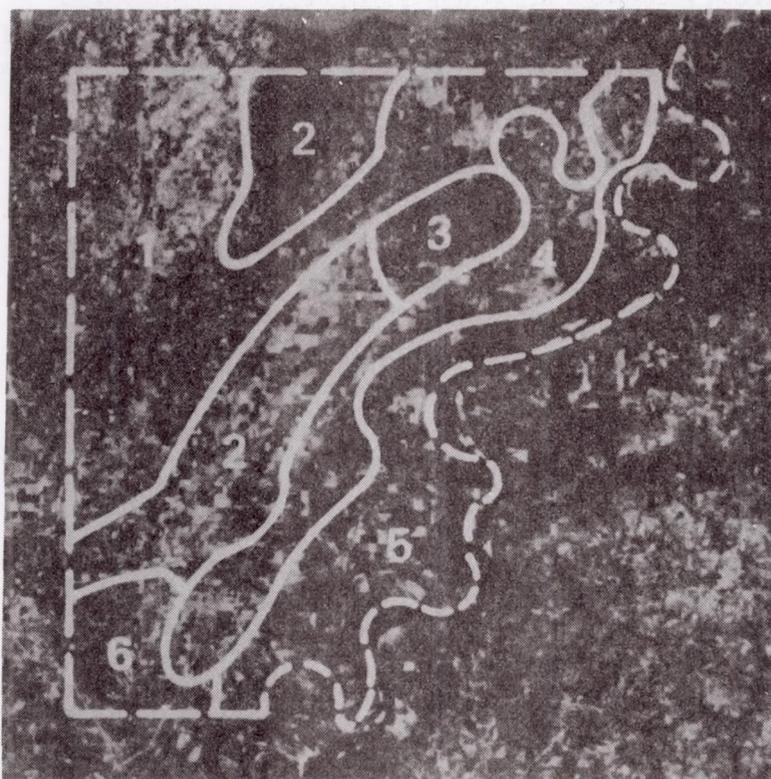
Figure 6:
Soil associations
for Mississippi
County, Arkansas,
overlaid on TM
Band 6 (10.4-12.5 µm)

Figure 7:
Soil associations
for Mississippi
County, Arkansas,
overlaid on TM
Band 7 (2.08-2.35 μm)
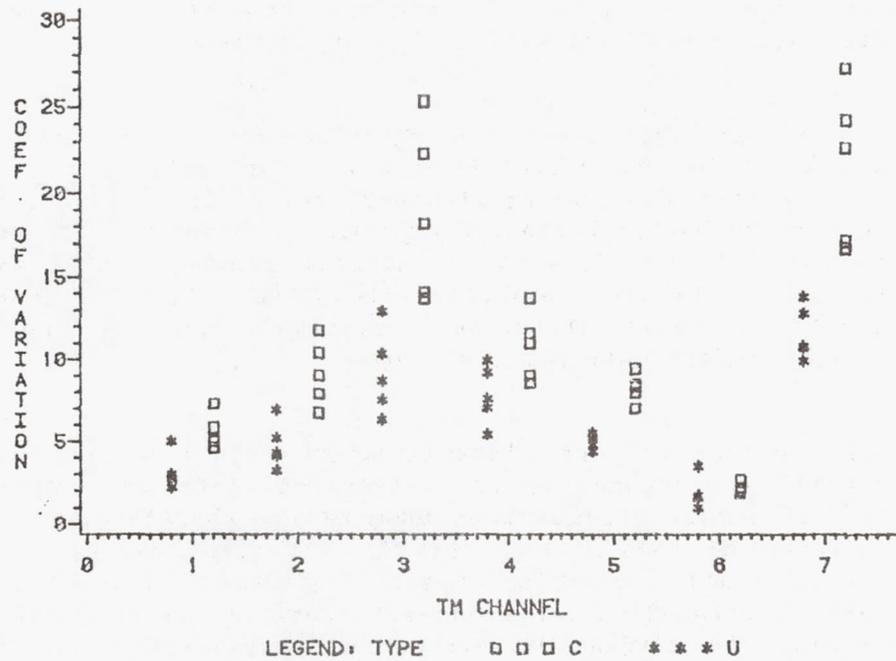
Figure 8: The coefficient of variation for uniform and
complex soils

THE USE OF THEMATIC MAPPER DATA FOR LAND COVER DISCRIMINATION

- PRELIMINARY RESULTS FROM THE UK SATMaP PROGRAMME

M.J. Jackson,
J.R. Baker,

Natural Environment Research Council, UK.

J.R.G. Townshend,
J.E. Gayler,
J.R. Hardy

Reading University, UK.

The principal objectives of the UK SATMaP programme are to determine Thematic Mapper (TM) performance with particular reference to spatial resolution properties and geometric characteristics of the data. Since no data of the UK test sites have been received so far, analysis has been restricted to images from the U.S. and has concentrated on spectral and radiometric properties.

Examination of selected sub-scenes reveals that the visible bands display a narrow range of digital values. For example, for band 2 over 95% of the pixels are found within 25 out of 255 digital counts. The histograms are better balanced for bands 4, 5 and 6. For example for band 4 the 95% limit covers 120 digital counts. For classification purposes it is not considered that the eight-bit quantization available is being effectively utilised, even if one takes account of the limited data set analysed.

In assessing the accuracy of classification techniques for Thematic Mapper data the consistency of the detector-to-detector response is critical. Preliminary studies were undertaken, therefore, to assess the significance of this factor for the TM. The results obtained suggest the existance of striping especially in band 4 for the Detroit scene. This is related to differences in forward and backward scans of the sensor. The average difference is approximately two digital counts and is clearly present from the eastern edge of the Detroit scene to the lake shore near the centre of the image. Examination of Reelfoot Lake in the eastern portion of the Arkansas scene fails to reveal a similar response, nor is it apparent in any part of the Mississippi. Either a change in response of the sensor or a difference in the data processing is therefore indicated.

For all three sub-scenes analysed there are strong correlations between the three visible bands, the coefficients exceeding 0.9 in all cases. Of the other band combinations only bands 4 and 5, 5 and 6, and 6 and 7 show any strong relationships. Negative correlations are found consistently between band 4 in the near infrared and the visible bands though the strength of these relationships varies substantially between the sub-scenes.

The overall structure of the relationships can be examined by principal component analysis. For the first two sub-scenes there are apparently three basic dimensions of variability whereas for the third this is reduced to two dimensions, since band 5, 6 and 7 are missing.

In order to examine the utility of the Thematic Mapper data more carefully, six different land cover classes approximately Anderson level 1 were selected. These included an area of water from the sediment-laden Mississippi, woodland, agricultural land and urban land. A "plume" class was also selected which includes the plume of smoke emanating from the power station and drifting over the Mississipi river.

For the first three bands the overall form of the spectral response is remarkably similar for all classes, whereas for the near and middle infrared bands considerable differences in overall response are found. For the thermal infrared band, the means of the classes are very similar but is worth noting that the standard deviations are also very low suggesting this band may have some discriminatory power.

Considerable differences can be seen between the correlation structure of the different categories and that of the whole sub-scene. For example for water and woodland the correlations between the three visible bands are much weaker; the usual weak to moderate negative relationship between the visible bands and the near infrared band 4 is replaced by strong positive correlations for the industrial and plume categories. For the agricultural and urban land categories bands 5 and 6 have moderate to strong relationships with the other bands except for band 4, whereas the first two sub-scenes as a whole and the water and woodland classes of one sub-scene show much weaker relationships.

If the Eigenvectors of the first two principal components are examined, it is apparent that although the dimensionality of the data is similar for the whole sub-scene and several of the individual land cover categories, the principal components are orientated very differently within the seven dimensional feature space. In other

words different bands contribute to very varying degrees to these
first two components. Relatively speaking bands 2 and 3 contribute
least to the first two principal components, and bands 4, 1 and 5
the most. The results stongly suggest that although there may be
onlt three dimensions within the data, if we wish to depict the
variability within as well as between broad cover categories then
more than three bands will have to be used.

The classification potential of the Thematic Mapper has been examined
by calculating the divergence between the classes.

It is notable that except for band 2 all the bands are indicated as
having significant discriminatory potential for at least two of the
classes. Overall the results indicate the particular significance of
bands 3, 4 and 5 in discrimination between the classes. Additionally
it is interesting that the thermal band, band 7, is of independent
value in discrimination despite its low spatial resolution and a less
than optimal time for sensing with this band.

Advanced classificatory algorithms are being explored to improve
information extraction from TM data. Specifically the use of carto-
graphic digital vector data and other remote sensing data in
registered formats is being investigated to develop classification
techniques which exploit per-pixel, textural and contextual
algorithms within the framework of a probabalistic tree classifier
and an integrated multi-level and multi-parameter data set.

The first TM image of the UK was received via X-band transmission to
Fucino, Italy and was processed by ESRIN, Frascati. Qualitative
analysis of the image clearly shows that in rural areas, there is a
very significant improvement over the MSS, whereas in urban areas
the improvement is much less marked, probably as a result of the
high density of English urban development (Fig. 1).
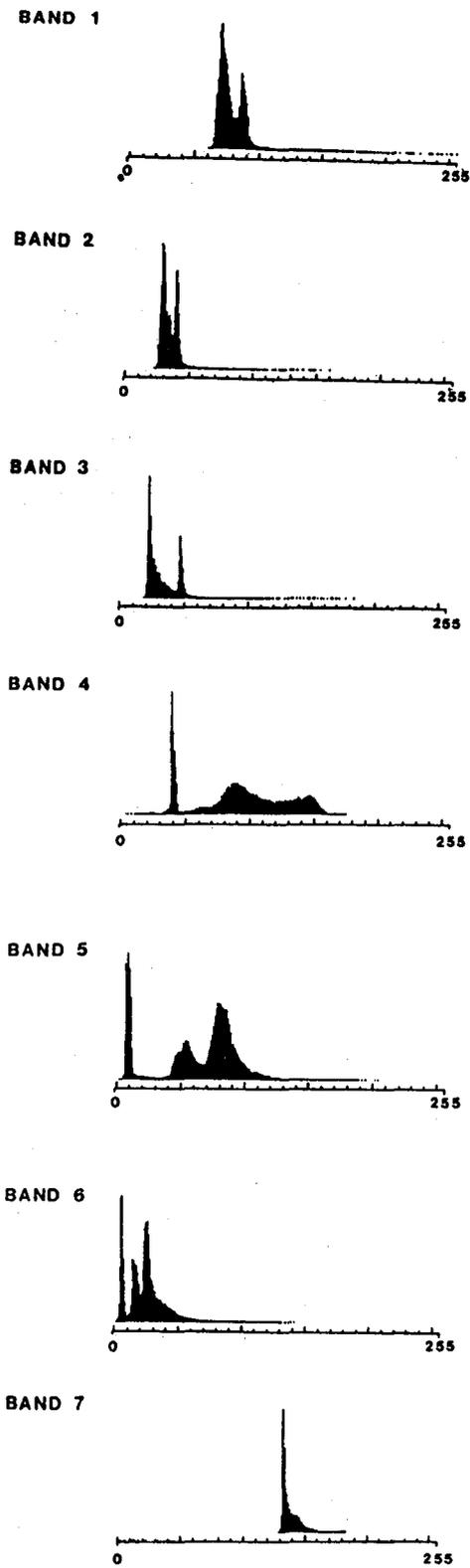
Fig.1   Histograms For Each Spectral Band For Sub-scene 1.
         Note that band 7 is the thermal band.

6. WITHIN BAND VARIATION IN SPECTRAL RESPONSE

In assessing the accuracy of classification techniques for Thematic
Mapper data the consistency of the detector-to-detector response is
critical. Preliminary studies were undertaken, therefore, to assess
the significance of this factor for the TM. The approach taken has
been to examine the spectral response of water bodies where spectral
frequency responses are generally low and where for wavebands longer
than 0.7um reflectance is both very low and stable. The results
obtained suggest the existence of anomalies especially in band 4
for the Detroit scene. Figure 2 shows a profile of band 4 data over
Lake Erie. The striping is related to differences in forward and
backward scans of the sensor. The average difference is approximately
two digital counts and is clearly present from the eastern edge of
the Detroit scene to the lake shore near the centre of the image.
Examination of Reelfoot Lake in the eastern portion of the Arkansas
scene fails to reveal a similar response, nor is it apparent in any
part of the Mississippi. Either a change in response of the sensor
or a difference in the data processing is therefore indicated.

7. INTER-RELATIONSHIPS BETWEEN BANDS

The correlations between the thematic bands are shown in Table 1 for
three sub-scenes. The first two are from the Arkansas scene. The
first sub-scene is the one described above , and the latter includes
an agricultural area and a large region of woodland. The 512 x 512
sub-scene from the Detroit scene is centered on Toledo, and includes
a wide diversity of urban land cover types, agricultural land and a
portion of Lake Erie. At the time the latter was imaged the cooled
detectors (for bands 5, 6 and 7) were not operating. For all three
sub-scenes there are strong correlations between the three visible
bands, the coefficients exceeding 0.9 in all cases. Of the other
band combinations only bands 4 and 5, 5 and 6, and 6 and 7 show any
strong relationships. Negative correlations are found consistently
between band 4 in the near infrared and the visible bands 3 though
as Table 1 shows, the strength of these relationships varies substant-
ially between the sub-scenes. The overall structure of the relation-
ships can be examined by principal component analysis, the Eigenvalues
for the three sub-scenes being shown in Table 2. For the first two
sub-scenes there are apparently three basic dimensions of variability
whereas for the third, this is reduced to two dimensions, since bands
5, 6 and 7 are missing.

8. CHARACTERISTICS OF INDIVIDUAL LAND COVER CATEGORIES

In order to examine the utility of the Thematic Mapper data more
carefully, six different land cover classes at approximately Anderson
level 1 were selected from the first sub-scene. These included an
area of water from the sediment-laden Mississippi, woodland, agricult-
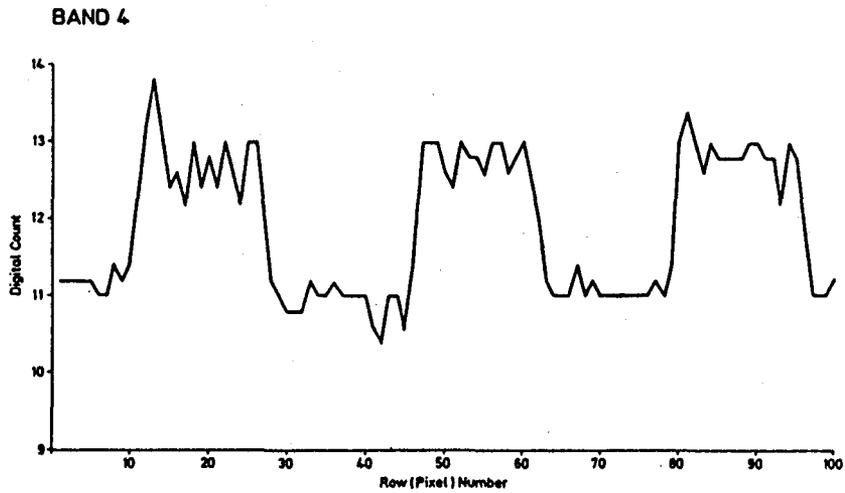
BAND 4

Fig.2 Spectral Response For Band 4 Across Lake Erie (P Tape).
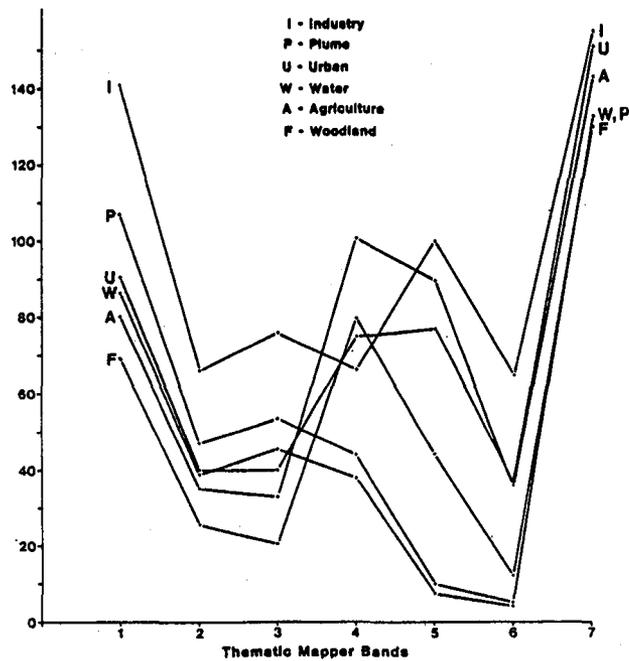
Fig. 3 Spectral Response Of Selected Cover Types From Sub-scene 1
        Note that band 7 is the thermal band.

IV-374

Table 1

CORRELATION ON MATRICES FOR SELECTED LANDSAT 4 THEMATIC MAPPER SUB-SCENES

Correlation Matrix For Sub-scene 1

	1	2	3	4	5	6
1	1.00					
2	.967	1.00				
3	.953	.957	1.00			
4	-.512	-.473	-.631	1.00		
5	-.136	.067	-.245	.713	1.00	
6	.244	.310	.166	.362	.883	1.00
7*	.347	.391	.298	.008	.567	.745

Correlation Matrix For Sub-scene 2

	1	2	3	4	5	6
1	1.00					
2	.950	1.00				
3	.935	.904	1.00			
4	-.148	-.029	-.166	1.00		
5	.089	.207	.088	.849	1.00	
6	.353	.431	.361	.592	.904	1.00
7*	.477	.485	.455	.076	.452	.674

Correlation Matrix For Sub-scene 3

	1	2	3
1	1.00		
2	.923	1.00	
3	.989	.948	1.00
4	-.386	-.330	-.210

Note band 7 is the thermal band*

Table 2

EIGENVALUES FOR SELECTED SUB-SCENES

Sub-scene 1

Eigenvalue	1	2	3	4	5	6	7
	.745	.204	.042	.004	.002	.001	.000

Sub-scene 2

Eigenvalue	1	2	3	4	5	6	7
	.868	.099	.025	.003	.001	.001	.000

Sub-scene 3

Eigenvalue	1	2	3	4
	.822	.175	.003	.000

Note that band 7 is the thermal band.

ral land and urban land. A "plume" class was also selected which
includes the plume of smoke emanating from the power station and
drifting over the Mississipi river. The means and standard
deviations for this class are shown in Table 3 and the spectral
response of each class is summarised in Figure 3. For the first
three bands the overall form of the spectral response is remarkably
similar, whereas for the near and middle infrared bands considerable
differences in overall response are found. For the thermal infrared
band, the means of the classes are closely clustered but it is worth
noting from Table 3 that the standard deviations are also very low
suggesting this band may have some discriminatory power.

9. CORRELATION STRUCTURE OF INDIVIDUAL COVER CATEGORIES

Table 4 shows the correlation between the TM bands for the individual
cover categories. Considerable differences can be seen between
their correlation structures and that of the whole sub-scene (Table
1). For example for water and woodland the correlations between the
three visible bands are much weaker; the usual weak to moderate
negative relationship between the visible bands and the near infrared
band 4 is replaced by strong positive correlations for the industrial
and plume categories. For the agricultural land and urban land
categories bands 5 and 6 have moderate to strong relationships with
the other bands except for band 4, whereas the first two sub-scenes
as a whole (Table 1) and the water and woodland classes of sub-scene
1 show much weaker relationships.

The underlying structure of the relationships is shown in Table 5
for each of the categories. Except for the water and plume
categories the eigenvalues are similar to those of the complete
sub-scenes indicating that there are three basic dimensions. For
the plume category there are only two dimensions and for the water
category apparently as many as seven. The latter may simply stem
from a near spherical distribution of points of this category in the
residual sub-space. If the eigenvectors of the first two principal
components are examined (Table 6), it is apparent that although the
dimensionality of the data is similar for the whole sub-scene and
several of the individual land cover categories, the principal
components are orientated very differently within the seven dimensio-
nal feature space. In other words different bands contribute to very
varying degrees to these first two components. Relatively speaking
bands 2 and 3 contribute least to the first two principal components,
and bands 4, 1 and 5 the most. These results strongly suggest that
although there may be only three basic dimensions within the data,
if we wish to depict the variability within as well as between broad
cover categories then more than three spectral bands will have to be
used.

Table 3

MEANS AND STANDARD DEVIATIONS OF COVER CLASSES FROM SUB-SCENE 1

	1	2	3	4	5	6	7
WATER							
Mean	87.4	38.8	45.4	38.0	7.5	4.4	133.0
Standard Deviation	(1.8)	(1.0)	(1.2)	(2.0)	(1.4)	(1.3)	(.8)
WOODLAND							
Mean	69.7	26.9	21.1	82.4	51.0	14.8	131.5
Standard Deviation	(2.2)	(1.1)	(1.1)	(5.0)	(7.6)	(2.7)	(1.8)
AGRICULTURAL LAND							
Mean	79.2	34.6	31.6	112.5	87.5	32.1	140.0
Standard Deviation	(17.9)	(11.0)	(14.7)	(23.7)	(10.2)	(9.3)	(4.0)
URBAN							
Mean	90.1	39.6	40.0	75.5	76.6	35.9	150.0
Standard Deviation	(11.4)	(7.1)	(10.6)	(12.2)	(13.1)	(10.2)	(4.0)
PLUME							
Mean	111.4	48.9	55.0	45.0	9.5	5.4	133.0
Standard Deviation	(8.5)	(3.7)	(3.6)	(2.2)	(1.0)	(1.1)	(1.4)
INDUSTRIAL							
Mean	144.8	67.3	77.6	68.5	104.9	67.9	153.9
Standard Deviation	(34.0)	(18.5)	(23.1)	(17.2)	(24.4)	(18.2)	(6.6)

Note that band 7 is the thermal band

Table 4

CORRELATION STRUCTURE OF COVER CATEGORIES

WATER

	1	2	3	4	5	6
2	.4					
3	.5	.6				
4	-.4	-.3	-.2			
5	.3	.4	.4	-.1		
6	.3	.2	.3	-.1	.5	
7	.0	-.1	-.2	.1	-.2	-.1

WOODLAND

	1	2	3	4	5	6
2	.4					
3	.5	.7				
4	-.1	.1	-.1			
5	-.2	.3	.1	.6		
6	-.2	.3	.2	.5	.9	
7	-.2	.2	.1	.5	.8	.8

AGRICULTURAL LAND

	1	2	3	4	5	6
2	.9+					
3	.9+	.9+				
4	-.2	-.2	-.3			
5	.5	.5	.6	-.1		
6	.7	.7	.8	-.4	.8	
7	.5	.5	.5	-.7	.3	.6

URBAN

	1	2	3	4	5	6
2	.9+					
3	.9+	.9+				
4	-.2	-.1	-.2			
5	.7	.7	.7	.3		
6	.8	.8	.9	-.2	.8	
7	.5	.4	.5	-.6	.1	.4

PLUME

	1	2	3	4	5	6
2	.9					
3	.9	.9				
4	.9	.9	.9			
5	.5	.5	.5	.5		
6	.1	.1	.1	.1	.3	
7	-.3	-.4	-.3	-.3	-.2	-.1

INDUSTRIAL

	1	2	3	4	5	6
2	.9+					
3	.9+	.9+				
4	.8	.8	.9			
5	.7	.7	.7	.7		
6	.6	.6	.6	.4	.9	
7	-.2.	-.2	-.2	-.1.	-.4	-.4

+ indicates correlation above 0.95

Table 5

EIGENVALUES FOR INDIVIDUAL LAND COVER CATEGORIES

	1	2	3	4	5	6	7
WATER	.40	.25	.13	.08	.06	.04	.03
WOODLAND	.77	.14	.06	.01	.01	.01	.00
AGRI LAND	.59	.33	.06	.01	.00	.00	.00
URBAN	.66	.25	.06	.02	.01	.00	.00
PLUME	.94	.02	.01	.01	.01	.01	.00
INDUSTRIAL	.82	.12	.04	.01	.00	.00	.00

Note that band 7 is the thermal band

Table 6

FIRST 2 EIGENVECTOR/BAND LOADINGS FOR EACH COVER CATEGORY
(Absolute values above 0.5 are underlined)

Band number

Eigenvector		1	2	3	4	5	6	7
WATER	1	.56	.29	.36	-.53	.35	.25	-.00
	2	-.39	-.04	-.14	-.82	-.29	-.21	.12
WOODLAND	1	.06	-.03	-.01	-.42	-.85	-.27	-.16
	2	.03	-.05	-.05	.90	-.37	-.15	-.15
AGRICULTURAL LAND	1	-.53	-.33	-.46	.52	-.19	-.26	-.06
	2	.38	.23	.25	.84	.17	.05	-.06
URBAN	1	-.48	-.30	-.46	.03	-.52	-.44	-.05
	2	.14	.05	.14	-.89	.39	.05	.13
PLUME	1	-.84	-.36	-.34	-.20	-.05	-.01	.00
	2	-.20	.21	.22	.06	.09	-.04	-.92
INDUSTRIAL	1	-.63	-.35	-.43	-.28	-.39	-.26	.00
	2	-.35	-.18	-.21	-.12	.67	.57	-.05
WHOLE SUB-IMAGE	1	-.12	-.06	-.14	.72	.63	.21	-.00
	2	-.26	-.2	-.33	.50	-.54	-.48	-.12

Note that band 7 is the thermal band.

10. DISCRIMINATION BETWEEN COVER CATEGORIES

The classificatory potential of the Thematic Mapper bands may be examined by calculating the divergence between the classes[1]. Table 7 shows the four best bands from the seven TM bands in discriminating between any one class from any of the other classes and the four best bands in simultaneously distinguishing between the classes. It is notable that except for band 2 all the bands are indicated as having significant discriminatory potential for at least two of the classes. Overall the results indicate the particular significance of bands 3, 4 and 5 in discrimination between the classes.

Additionally it is interesting that the thermal band, band 7, is of independent value in discrimination despite its low spatial resolution and a less than optimal time for sensing of this band.

11. IMPACTS ON LAND COVER CLASSIFICATION

Whilst the above comments have naturally stressed the anomalies and error factors associated with the TM it should be clearly stated that the overall performance is considered to be excellent. Considerable potential exists with the TM data for improved classification performance over that available from MSS. This is due not only to the improved spatial resolving capability but to the greater real dimensionality of the data.

The improved land cover classification accuracy will not be achieved, however, merely by applying the traditonal per-pixel classifiers so frequently used with MSS data. In fact in some circumstances such procedures could result in reduced accuracy[2]. Attention is therefore being given to improved techniques and procedure for classification of TM data. The Thematic Information Services (TIS) of NERC incorporates the Experimental Cartography Unit (ECU) which over the last 15 years has acquired large quantities of digital vector data and developed a large body of software for manipulating and overlaying vector/polygon data sets. Software has now been written to allow any of these data contained within the cartographic data-base to be imported and registered with the satellite data[3]. In addition the airborne scanner data acquired in September 1982 is seen as the first acquisition of a regular programme of flying and again the imagery is being input and registered with the map and satellite data. The opportunity therefore exists to apply classification techniques which exploit per-pixel, textural and contextual algorithms within the framework of a probabilistic tree classifier and an integrated multi-level and multi-parameter data set. As for the characterisation of the TM geometry and spatial resolving properties significant further progress awaits TM data of the UK but preliminary results using the airborne Daedelas and MSS data are promising and are being applied in a number of studies ranging from ecology to epidemiology.

Table 7

DIVERGENCE BETWEEN CLASSES: BEST FOUR BANDS FOR
DISCRIMINATING BETWEEN CLASSES

	1	2	3	4	5	6	7
Water			X	X	X	X	
Agricultural Land	X		X	X	X		
Woodland	X		X	X	X		
Urband			X	X	X		X
Plume			X	X	X		X
Industry			X		X	X	X
All classes			X	X	X		X

Note that band 7 is the thermal band.

IV-382

12. PRELIMINARY ANALYSIS OF THE FIRST UK SCENE

The first TM image of the UK was obtained in January 1983. This image was received via X-band transmission at Fucino, Italy and processed at ESRIN, Frascati. Unfortunately the scene includes neither of our UK test areas but does include the towns within which our two research institutes are found. At present only a single, TM band 4 image has been received but some preliminary evaluation is possible. Two obvious defects are found in the image. The first relates to shifts due to a lack of registration between forward and reverse scans. The strength of the shift is up eight pixels though normally it is three or less. This shift apparently arises because precise orbital data have not been used in image processing so that corrections for minor changes in satellite orientation have not been included. A number of drop-outs can be seen thoughout the image. Their origin is not currently understood. Currently steps are being taken to correct these minor defects. These have digital counts between 50 and 80 rather than zero. It should be emphasised, however, that ESA released this scene to European PI's at the earliest possible time with the knowledge that these problems existed. In terms of information content this image represents a very substantial improvement on Landsat MSS data in terms of the detectability of ground targets especially in rural areas. In the upper and lower parts of the scene, it is apparent that individual fields are readily detectable, see figure 4 which certainly was not true in this area with MSS data. In several places narrow hedgerows can be seen which are less than 6m across and most of which are less than 3m across.

The River Thames can be seen meandering across the northern half of the image. The large black areas are gravel pits, now filled with water. The main through route in the area (the M4) can be seen in the southern part of the image. Whereas the image is significantly better in rural areas than the MSS, in the urban areas the improvements are much less marked. The urban area is represented by the mottled dark tones across the full width of the central part of the image. Compared with images of urban areas in the US such as Detroit and Washington D.C., the results are apparently rather disappointing. However it must be noted that the density of urban development is in general much higher in English than American cities and hence much less ground detail will be detectable. For resolution of the details of urban structure of cities like Reading, spatial resolutions of 20m or better will be required.

Fig. 4 Preliminary TM band 4 sub-scene of Reading UK. Scale is
approximately 1:65,000.

REFERENCES

1. P.H. Swain, and S.M. Davis, Remote sensing: the quantitative approach New York: McGraw-Hill, 1978.

2. J.R.G. Townshend, The spatial resolving power of Earth resources satellites: A review. NASA Technical Memorandum. 82020, 1980.

3. M.J. Jackson and J.E. Drummond, The NERC System for the combined analysis of raster remotely sensed image data and vector digital cartographic data. Proceedings of 17th Congress of the International Federation of Surveyors, Sofia, Bulgaria, July 1983 (Preprint).

Page intentionally left blank

PRELIMINARY STUDY OF INFORMATION EXTRACTION OF LANDSAT TM DATA FOR A SUBURBAN/REGIONAL TEST SITE

David L. Toll
NASA/Goddard Space Flight Center
Earth Resources Branch/Code 923
Greenbelt, MD 20771

OBJECTIVE

The primary objective of this study is to assess the TM sensor improvements relative to MSS for use in a land cover discrimination evaluation. The actual TM sensor parameter improvements studied includes: (1) increase in spatial resolution from 80m to 30m; (2) spectral band additions of TM1 (0.45 - 0.52 µm), TM5 (1.55 - 1.75 µm), TM6 (10.4 - 12.5 µm) and TM7 (2.08 - 2.35 µm); and (3) increased quantization level from 6 bits MSS (0-63) to 8 bit TM (0-255). An additional objective was to assess the spectral/spatial information content of TM for regional/suburban land cover discrimination.

STUDY SITE DESCRIPTION

The rapidly urbanizing area north of Washington, D.C. between Beltsville, MD and Laurel, MD was selected as a test site, Fig. 1. This area is representative of developing urban fringe in the United States where planners and administrators are forced with serious decisions but have little information. A wide range of land use/land cover types occur in the study area. The major cover types and those used in the analysis are water, forest, agriculture, excavated sites, major transportation routes, commercial and industrial sites, and residential neighborhoods. The study site was chosen to include a 500 x 500, 28.5m TM pixel size, yielding a 14.25km^2 size area.

DATA DESCRIPTION

A 500 x 500 array of TM pixels (28.5m) covering a 14.25km^2 area was selected for analysis. Initially, a four band July 29, 1982 TM data was obtained, Fig. 2. The two middle infrared and one thermal infrared band detectors were not yet activated. Effects from a cloud shadow are evident in the right center of Fig. 2. The cloud shadowed area was not used in any quantitative calculations. Seven band, cloud free TM data was also obtained on November 2, 1982. The
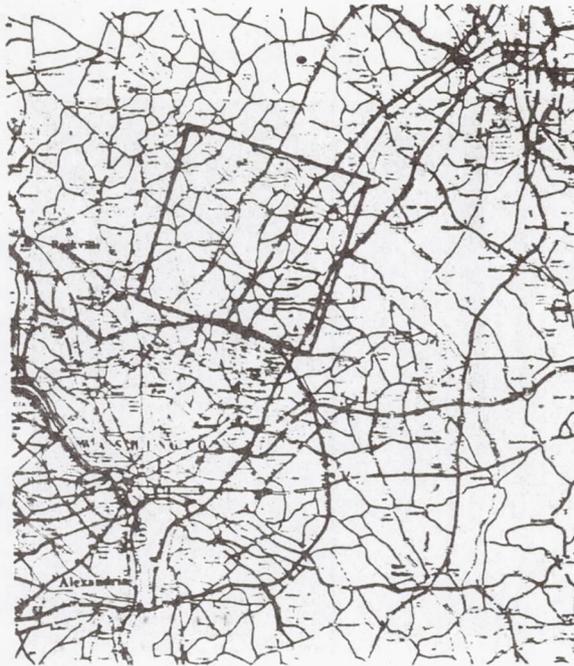
Fig 1 Beltsville-Laurel, MD Study Site Indicated by Box NE of Washington, D.C.

thermal band was determined to be systematically offset and was shifted to register with the other six bands. For selected quantitative comparisons to TM, Landsat MSS data was acquired. Since the July 29, 1982 MSS data was not recorded, a Landsat-2 MSS scene on July 11, 1981 was used (Fig. 3). The November 2, 1982 Landsat-4 MSS scene was collected and included in the data base. To assist all evaluations, color infrared (CIR) photography of 1:40,000 scale flown on July 13, was used. A comparison of MSS and TM spectral, spatial, and quantization characteristics is given in Table 1.
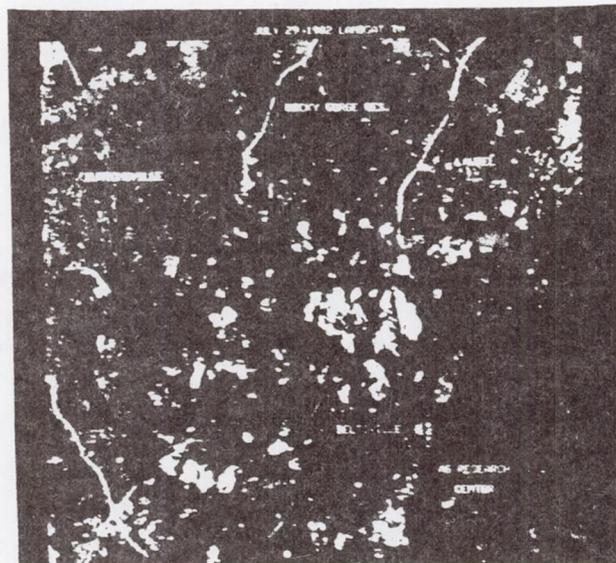
Fig 2   Landsat-4 TM of Laurel-Beltsville, MD Study Area
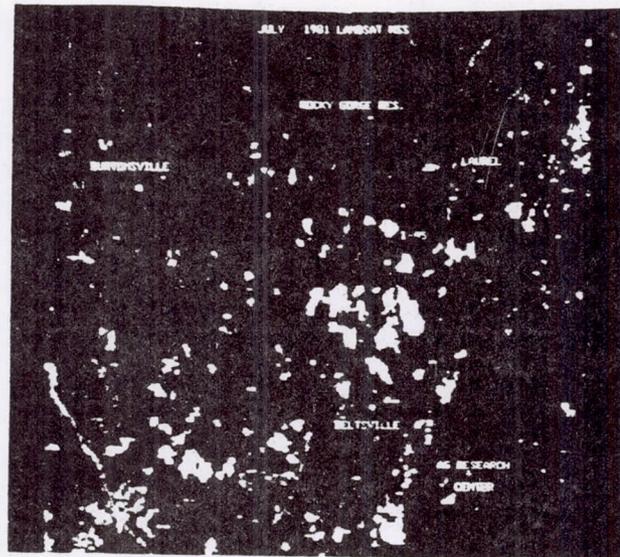
Fig 3   Landsat-2 MSS of Laurel-Beltsville, MD Study Area

Table 1
Landsat IV Sensor Characteristics

Thematic Mapper (TM)

Spectral Region	Band	(μm)	Ground IFOV	Pixel Size	Quantization
Blue	1	0.45-0.52	30m	28.5m	8 bits
Green	2	0.52-0.60	30m	28.5m	8 bits
Red	3	0.63-0.69	30m	28.5m	8 bits
Near Infrared	4	0.76-0.90	30m	28.5m	8 bits
Middle Infrared	5	1.55-1.75	30m	28.5m	8 bits
Middle Infrared	7	2.08-2.35	30m	28.5m	8 bits
Thermal Infrared	6	10.4-12.5	120m	28.5m	8 bits

Multispectral Scanner (MSS)

Spectral Region	Band	(μm)	Ground IFOV	Pixel Size	Quantization
Green	4	0.50-0.60	83m	57m	6 bits
Red	5	0.60-0.70	83m	57m	6 bits
Near Infrared	6	0.70-0.80	83m	57m	6 bits
Near Infrared	7	0.80-1.10	83m	57m	6 bits

METHODOLOGY

Photointerpretation

The initial procedure was to photointerpret the test site from the CIR. The seven major classes listed previously were delineated for the entire test site. A 250m^2 minimum mapping unit size was used. The photointerpreted work was used as reference data for quantitative comparisons with processed TM and MSS data.

Registration

To facilitate comparisons between MSS and TM and to reduce sampling costs, TM and MSS data were registered to one another using a quadratic linear transformation. Approximately 10-15 tie-points were selected for each of the four TM and MSS scenes and three of the scenes were independently registered to the July 29, 1982, Landsat-4 TM master scene. Average control point residual accuracy was less than one TM pixel cell size for each of the three registrations. In order to reduce possible spectral biases in the digital analysis through resampling, a nearest neighbor resampling scheme was implemented in which spectral data was not spectrally transformed, but was instead replicated. The resultant TM and MSS images all had a 500 x 500 28.5m pixel size.

Sensor Parameter Manipulation

In order to study effects of the "improved" TM sensor parameters, spatial resolution, spectral region and quantization level on cover class discrimination of digital spectral data, a design was implemented in which all possible sensor parameter combinations were considered. Sensor parameter specifications for both the MSS and TM were assessed, which yielded a 3 factor (i.e., 3 sensor parameter), 2 level (i.e., TM and MSS) design that provided 8 total combinations. Given next are the eight possible data arrangements.

	Spatial Resolution	Quantization	Spectral Bands*
1.	30m	8 bits	6(4) bands
2.	30m	8 bits	3 bands
3.	30m	6 bits	6(4) bands
4.	30m	6 bits	3 bands
5.	90m	8 bits	6(4) bands
6.	90m	8 bits	3 bands
7.	90m	6 bits	6(4) bands
8.	90m	6 bits	3 bands

At the top of the listing is the untransformed TM data. The following six sensor parameter arrangements are partial simulations between TM and MSS sensor parameters, in order to assess each possible combination. The last parameter combination is a simulation of MSS parameters. Because of the 120m^2 spatial resolution of TM6, the thermal infrared band (TM6) was excluded from this portion of the analysis. To preprocess the TM data, three MSS data simulations were required:

    1.   Thirty meter TM spatial resolution to 83m MSS spatial resolution;

---

*Only 4 TM bands are available for the July 29, 1982 data set.

2.   Eight bit TM quantization to 6 bit MSS quantization;

3.   Six TM band spectral regions to 3 MSS bands spectral regions.

In order to approximate the spatial characteristics of MSS data from TM data, an equally weighted 3 x 3 digital filter was convolved with the TM data (28.5m pixel size). This produced data with each pixel influenced by radiation from an area approximately equal to the MSS ground IFOV. The MSS pixel size was obtained by skipping every other line and sample of the digital image when performing the convolution. Six bit quantization was approximated by simply dividing TM data by 4. The TM spectral bands TM2, TM3 and TM4 were subset in order to simulate the MSS bands MSS4, MSS5 and MSS7 (see Table 1). MSS band 6 was not related to any of the TM bands. In further investigations, other TM spectral band combinations for use in land cover discriminations were assessed. Last, selected MSS data band combinations were also analyzed.

Sampling Procedure

Sampled pixels from the TM (and MSS) data sets were used to derive statistics for inferences on data information content and sensor parameter importance. For each of the 7 classes (or strata), 75 pixels were selected using a stratified-systematic procedure. Seventy five test pixels was determined to be adequate after inspecting various confidence levels as a function of sample size.[1,2] Since the same pixels were also used as training statistics the number of pixels necessary for computation of class signatures (e.g., computation of a covariance matrix) was also considered. The actual number of samples is a function, for example, of the number of variables, the number of classes, and the a priori probabilities.[3] The reduction in the probability of error for the classifier by increasing the sample size from 75 to a higher number was considered too costly to merit a sample size increase. Possible bias from using the same pixels for both defining the training statistics and test sites was reduced by selecting noncontiguous or widely distributed pixels. Further, if the classification accuracy was inflated it is reasonable to assume the increase would be similar between the eight sensor parameter data arrangements.

In order to determine an estimate of the grid spacing between sample selections the total number of pixels for each class was estimated and this total class area number was divided by 75. Pixels were selected through use of a CRT console in a triangular network in which pixels are located at the vertices of equilateral triangles. Noncontiguous or sampled pixels were chosen in order to increase the independence of the observations, thereby reducing probable statistical bias from using dependent (i.e., adjacent) pixels.[4,5]

Measurement Criteria

When assessing TM and MSS data, both classification accuracy and transformed divergence statistics were evaluated. For this paper, results from overall classification accuracy are presented. Overall classification accuracy is the total correct designations of the sampled pixels divided by the total number of samples (525 total pixels). Transformed divergence is a normalized measure of the separability or dissimilarity of the spectral classes. As recommended by Swain,[6] the average pair-wise divergences between all classes may be used, as

in this study, to obtain an indication of overall class discrimination performance. In the classification accuracy assessment, a standard Gaussian quadratic maximum likelihood classifier on a per-pixel basis was used.

Sub-Class Clustering for Training Statistic Generation

Each class in each data set was independently clustered to obtain training statistics. The parameter specification in the clustering algorithm was modified according to the spectral variability associated with the quantization level and spatial resolution of the data set. Previous experience indicated additional spectral information is associated with higher spatial resolution data for land cover classes as evidenced in increased variability and multimodal frequency distributions. The increased variability and modes indicates subclass information (or noise) for a given cover class. Clustering was implemented in an attempt to capture this added variability and also to provide normal or unimodal frequency distributions for the classifier.

Principal Component Analysis

To assess the information content in the TM data, principal components or linear combinations of the data were also assessed. A Karhunen-Loéve transformation was used. Through comparisons to MSS principal components, a quantification of the difference in information content could be assessed. The comparisons comprised an assessment of output images and both classification performance and transformed divergence estimates. Classification accuracy and transformed divergence statistics were computed from use of pixel coordinates selected through the sampling procedure discussed previously.

RESULTS AND DISCUSSION

Correlation Analysis

Correlations from the 4 and 7 band TM and 4 band MSS data sets are given in Table 2 (A-D). Typically, the highest correlations occur within each of the major spectral regions--visible, near infrared, and middle infrared--for both TM (Table 2A: TM1, TM2 and TM3; Table 2B: TM1, TM2 and TM3; and TM5 and TM7) and MSS (Table 2C and 2D: MSS4 and MSS5; and MSS6 and MSS7). Typically, most of the varition may be explained by one band from each of the spectral regions.

Sensor Parameter Study

Results from the sensor parameter investigation for the November 2 TM data are given in Table 3. Results of classification accuracy and transformed divergence assessments clearly indicate that adding the three new TM spectral band s(TM1, TM5 and TM7) (e.g., ~5-10% increase in accuracy and ~100-300 increase in transformed divergence) and/or increasing the quantization to approximately 8 bits (e.g., ~3-8% increase in accuracy and ~25-100 increase in transformed divergence), improved land use/land cover spectral discriminations are possible. Of the two parameters, the added spectral regions is of more importance.

Table 2
Landsat TM and MSS Band Correlations

A (7/29/82)

	TM1	TM2	TM3	TM4
TM1	1			
TM2	.96	1		
TM3	.96	.98	1	
TM4	.10	.18	-.16	1

B (7/11/81)

	MSS4	MSS5	MSS6	MSS7
MSS4	1			
MSS5	.98	1		
MSS6	.61	.68	1	
MSS7	-.02	.06	.74	1

C (11/2/82)

	TM1	TM2	TM3	TM4	TM5	TM7	TM6
TM1	1						
TM2	.98	1					
TM3	.83	.89	1				
TM4	.57	.62	.65	1			
TM5	.76	.81	.79	.20	1		
TM7	.84	.87	.84	.65	.95	1	
TM6	-.05	-.10	-.16	.05	.09	.07	1

D (11/2/82)

	MSS4	MSS5	MSS6	MSS7
MSS4	1			
MSS5	.88	1		
MSS6	.74	.70	1	
MSS7	.43	.39	.84	1

On the other side, when degrading the spatial resolution from 30m to 90m there is a substantial increase in digital classification accuracy and transformed divergence, Table 3 (e.g., ~3-9% increase in accuracy and ~75-100 increase in transformed divergence). This is attributed to the reduced within class variability as a result of averaging the spectral heterogeneity at the simulated enlarged field of view. The class mean spectral values will remain essentially unchanged and hence the between class variation will remain the same. The overall result is an increase in class separability and subsequently an increase in classification accuracy and transformed divergence.

The increase in classification accuracy at the degraded spatial resolution occurred even though the classes for all data sets were subcategorized through data clustering. As a result of the added spectral variability in the 30m · data, it was expected the higher resolution data would exhibit improved class discriminations in contrast to lower resolution data. However, results

TABLE 3

TM SENSOR PARAMETER INVESTIGATION[*]
LANDSAT TM NOV. 2, 1982
BELTSVILLE-LAUREL, MD.

SPATIAL RESOLUTION

		30m	80m
6 BANDS	8 BITS	78.7% 1876 T.D.	85.1% 1952 T.D.
	6 BITS	73.7% 1781 T.D.	77.9% 1882 T.D.
3 BANDS	8 BITS	69.3% 1576 T.D.	74.7% 1729 T.D.
	6 BITS	66.5% 1544 T.D.	69.1% 1648 T.D.

*Results are given by overall classification accuracy (%) and average pair-wise transformed divergence (T.D.)

Table 4

TM SENSOR PARAMETER INVESTIGATION [*]
LANDSAT TM JULY 29, 1982
BELTSVILLE-LAUREL, MD.

SPATIAL RESOLUTION

		30m	80m
4 BANDS	8 BITS	81.7% 1876 T.D.	85.3% 1889 T.D.
	6 BITS	81.1% 1730 T.D.	84.2% 1739 T.D.
3 BANDS	8 BITS	74.5% 1761 T.D.	80.0% 1797 T.D.
	6 BITS	74.8% 1730 T.D.	78.9% 1739 T.D.

*Results are given by overall classification accuracy (%) and average pair-wise transformed divergence (T.D.)

indicated classification accuracy improved approximately by 5-7% for both 30m and 90m data clustering over nonclustering. From these findings, then, the increase in classification accuracy and transformed divergence at the sensor parameter specification of TM (upper left box in Table 3) over MSS (lower right box in Table 3) is from the added spectral bands and finer quantization level improvements and _not_ from improved spatial resolution.

In Table 4 sensor parameters results are given for the July 29, 1982 Landsat 4 band TM scene. In contrast to Table 3, there is only a negligible decrease in overall accuracy (0-1%) and modest decline in transformed divergence (30-100) when changing from 8 bits to 6 bits. The decreased importance of quantization in July relative to November is partially associated with a difference in spectral class contrasts from phenology changes. On July 29 vegetation growth is at a near peak and is providing useful spectral information when discriminating land cover in comparison to the foliage loss and spectral changes (i.e., green to red and orange leaf changes) that is occurring on November 2. Further, the reduced solar elevation on November 2 also reduces spectral contrasts between classes. This hypothesis may be substantiated by comparing the lower four cells in Table 3 with Table 4. For these cells the sensor parameter settings between dates and sample locations are similar. However, in the November TM scene, Table 3, the classification accuracies and transformed divergences are all lower (~5-10% accuracy and ~70-190 transformed divergence) as compared in a cell-by-cell basis with the July TM data in Table 4. Hence, the expanded spectral range or quantization may facilitate class discrimination on November 2, but may be not as important or necessary on July 29. Similar to the November findings, the removal of a spectral region (the blue-green TM band 1) resulted in a decrease in accuracy and divergence. However, the decreases are not as large in Table 3, when the middle infrared bands were also included.

Similar to the findings given in Table 3, when decreasing the spatial resolution to that approximating MSS, there is an increase in overall classification accuracy (~3-6%) and transformed divergence (~10-40) as indicated in Table 4. Again, this is a function of the within class variation that is larger than in comparison to the "smoothed" 90m data. One important factor not assessed in this study is the effect of boundary pixels as a function of varying spatial resolution. The higher the spatial resolution (i.e., the smaller the cell size) the smaller is the number of mixed pixels proprotional to the total pixels. Mixed class pixels, of course, typically results in increased spectral class confusion.

Table 5 includes a list of overall accuracies for selected band combinations to the November 2, 1982 TM and MSS scene. First, when adding the thermal infrared band, TM6, the overall accuracy increased by 4.5%. This increase is a significant increase over 6 bands excluding TM 6 and may be partially attributed to additional spectral information. Fig. 4 indicates the water area appearing dark or cool, with the forests, agriculture, residential neighborhoods and commerical/industrial complexes appearing consecutively brighter or warmer. The overall spectral contrast is lower for the thermal infrared when compared to the other spectral bands. The reduced contrast was also indicated by the narrow dynamic range of the thermal data and may be partially a result of the degraded 120m spatial resolution and the reduced sensitivity of the detectors. However, even with collection during a sub-

optimal time of day (9:30 local time) and the limited dynamic range, results indicated the thermal data contributed significantly to spectral discrimination between water, vegetative cover, and impervious surfaces comprising ground cover classes.

Table 5
Classification Accuracy Summary for November 2, 1982
TM and MSS Data

7 Band TM	83.2%
6 Band TM, Excluding TM6	78.7%
4 Band MSS	74.8%
3 Band MSS, Excluding MSS6	70.2%
Simulated MSS (90m, 3 band, and 6 bits) from TM	69.1%
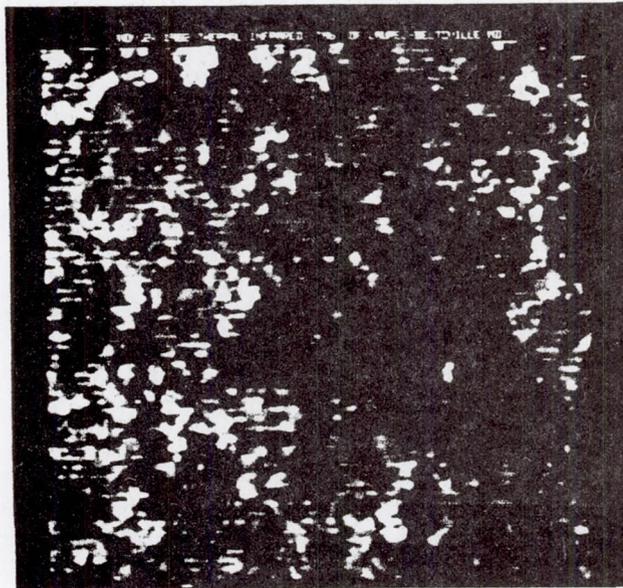
Fig. 4.   Thermal Infrared (TM6) of Laurel-Beltsville, MD Study Site

Comparison of both 6 and 7 band TM classified data indicates a substantial improvement over 4 band MSS data, Table 5. Previous results indicate the increase in accuracy may be attributed to spectral bands and quantization improvements in TM and not the higher TM spatial resolution. Further, when deleting band MSS 6, to obtain 3 band MSS data, the overall accuracy, 70.2%, is very similar to that obtained with the preprocessed TM data when simulating the MSS parameters, 69.1%. The similar accuracies indicate the procedures implemented to modify the sensor parameters of the TM data were indicative of the MSS sensor parameters.

Information Assessment through Principal Component Transformation

Images of the four principal components to the 4-band July 29, 1982 TM and July 3, 1981 MSS scene are given in Figs. 5 and 6, respectively. The first component for both TM and MSS is analogous to the "brightness" component in the Tasselled Cap Transformation.[7] For example, excavated or bare soil sites appear bright and vegetative surfaces appear dark. In the second principal component for both TM and MSS results indicate bright response for green vegetation and a darker tone for unvegatated areas. However, in the third and fourth principal components significantly more spectral contrast or land cover information may be observed in TM, Fig. 5, versus MSS, Fig. 6. The difference in useful land cover information is even though the 4 band TM has spectral information in only one additional spectral band, TM1 (.45-.52 µm) (MSS has MSS6, 0.6-0.7 µm that is not represented in TM). Further, the amount of variation in the third and fourth components as indicated by the eigen values is approximately equivalent, Table 6. In Fig. 6, for MSS, there is predominantely banding noise in the third and fourth principal components in comparison to the distinct boundaries between land cover features observable in Fig. 5 for TM. Specifically, the TM third and fourth components discriminate residential neighborhoods, forest sites, water and agriculture from one another. The added "useful" information is likely a function of the blue band, TM1 and increased spectral variability from both quantization and spatial resolution of TM. Further, other TM improvements such as an improved S/N may have increased the "useful" spectral information. Table 6 also includes a set of tabular results for the principal components for the July MSS and TM data sets. Of significant importance is that although the TM bands have slightly less variation in the third and fourth principal components in comparison to MSS the overall accuracy and transformed divergence is substantially higher. Hence, the added variation in principal components three and four of the MSS is random variation from banding and contributing little land cover discrimination information relative to TM.

Table 6
MSS and TM Principal Component Summary

		Principal Components	Percent Variation	Overall Classification Accuracy (%)	Overall Transformed Divergence (0-2000)
MSS	July 11 1981	1	54.8	49.9	1198
		2	43.9	50.1	879
		3	.8	21.7	634
		4	.5	30.3	816
		1 through 4	100.0	71.8	1793
TM	July 29 1982	1	62.7	55.0	1235
		2	36.4	49.9	1072
		3	.5	26.7	914
		4	.3	39.4	1003
		1 through 4	100.0	77.5	1894
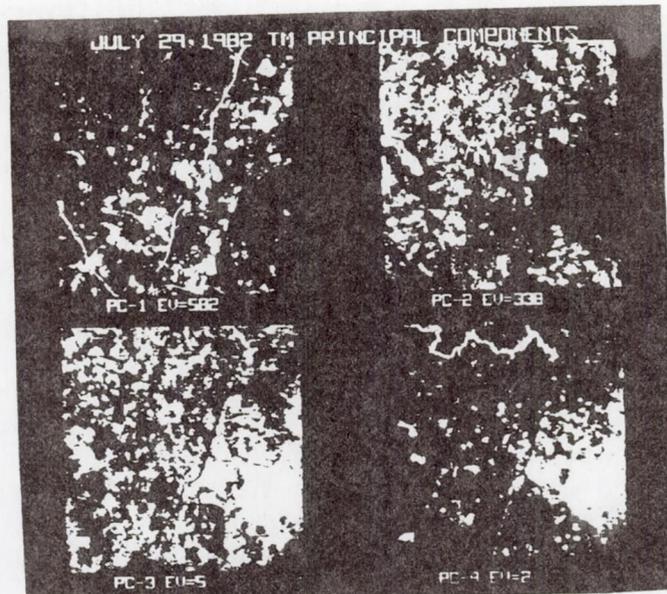
Fig. 5.   July 29, 1982 Landsat TM 4 Band Principal Components
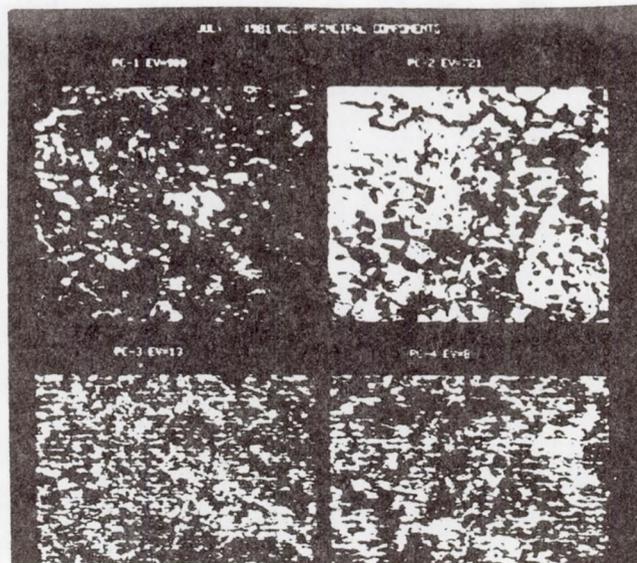
Fig. 6.   July 11, 1981 Landsat MSS 4 Band Principal Components

Figs. 7 and 8 depicts the 7 band TM November 2, 1982 and 4 band MSS November 2, 1982 principal component transformed data. Similar to the July findings the first principal component is analagous to the "brightness" component in the Tasseled Cap Transformation. However, in the second principal component, the correspondence with green vegetation reported for the July data is not apparent. This is likely a result of foliage changes (i.e., leaf spectral change and leaf loss) occurring in the November 2 data that is producing different eigen vector loadings for the bands in comparison to the July data sets.

Of special interest is the increased land cover information observed in the third through fifth principal component of the TM in comparison to the third and fourth MSS principal components. The MSS third and fourth principal component are approximate in noise (and variation) to the sixth and seventh principal component of TM. Hence, there are approximately three more principal components of useful information in TM versus MSS. As reported for the July TM and MSS data sets, this is a result of the improved sensor parameters (i.e., spectral region, spatial resolution, quantization, detector dwell time, etc.) of TM over MSS.

Table 7 provides a summary of percent variation, classification accuracy and transformed divergence for the TM and MSS November 2 principal components. Of special importance, however, is the increase in transformed divergence and classification accuracy in the third, fourth and fifth principal components of the TM versus the third and fourth principal components of the MSS. The sixth and seventh principal components provide a similar level of land cover discrimination information to the third and fourth MSS principal components, as indicated by the classification accuracy and transformed divergence. Similar to the findings in the July data analysis, the TM is providing additional overall land cover discrimination information over the MSS.

Table 7
TM and MSS Principal Component Summary for November

		Principal Components	Percent Variation	Overall Classification Accuracy %)	Overall Transformed Divergence (0-2000)
MSS	Nov. 2 1982	1	77.1	46.4	1122
		2	19.8	41.5	869
		3	2.1	24.6	251
		4	1.0	27.2	324
		1 through 4	100.0	69.9	1624
TM	Nov. 2 1982	1	70.9	57.1	1084
		2	12.5	38.1	652
		3	9.8	43.2	790
		4	4.5	37.1	578
		5	1.8	37.7	588
		6	.5	26.3	287
		7	0.0	30.1	423
		1 through 7	100.0	83.2	1912
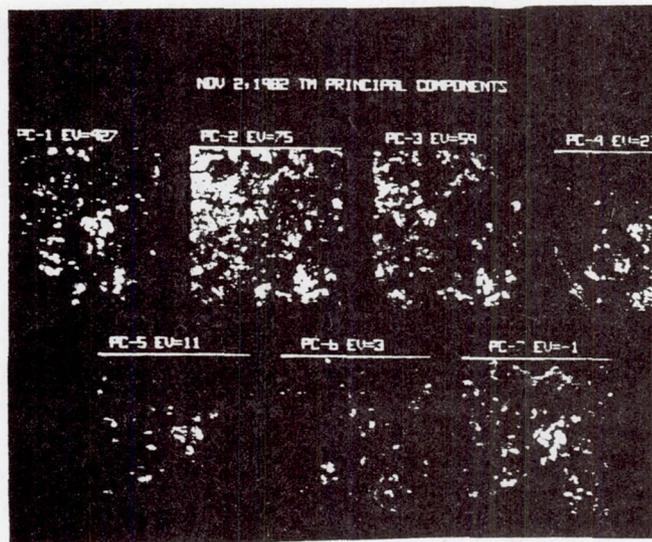
Fig. 7. November 2, 1982 Landsat 4 TM 7 Band Principal Components
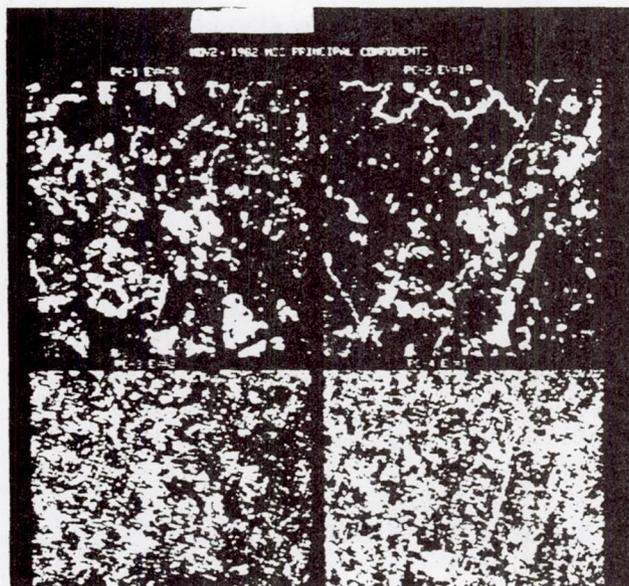
Fig. 8. November 2, 1982 Landsat MSS 4 Band Principal Components

SUMMARY AND CONCLUSIONS

Analysis of TM and MSS data provided several interesting findings. Preliminary inspection of TM in comparison to MSS indicates the substantial amount of spectral information available from TM over MSS. Of immediate utility is the detail or spectral contrast for use in image interpetation of surface features. For example, large buildings and street pattern that are resolved in TM imagery but not in MSS, should significantly improve image interpretation accuracy. Results from the digital analysis of TM with reference to MSS and/or MSS sensor parameters clearly indicates the added information content in TM over MSS when discriminating suburban/regional cover. However, there are characteristics of MSS that will improve land cover discrimination over TM when using conventional classification procedures on digital data.

Of the three improved TM sensor parameters evaluated, spectral region, spatial resolution, and quantization, the additional spectral regions of the TM (TM1, TM5, TM6 and TM7) clearly add useful information when discriminating the land cover classes for this study. During the November 2 data in which there was reduced spectral contrast between classes due to time of year, the increased 8 bit quantization of TM facilitated the discrimination of land cover. However, the July 29 data set in which vegetation growth enhanced land cover spectral separability results indicated increased quantization from 6 bit to 8 bit was insignificant. Hence, improved quantization of TM is likely valuable in situtations where there are spectral similarities between classes.

On the other side, the spatial resolution increase in TM decreased land cover discrimination as a result of increased within class variability. The added within class variability is subclass information or variation that is creating confusion or spectral overlap between classes. Subcategorizing data through clustering did not improve results as expected for the higher resolution TM data. Hence much of the variability within classes is likely spectrally similar, resulting in a poor land cover classification. Effects from boundary or mixed class pixels as a function of spatial resolution was not evaluated in this study. Clearly, the proportion of mixed pixels to the total pixels decreases with the increased spatial resolution of the TM. Since mixed class pixels confounds class discriminations, it is reasonable to assume improved TM spatial resolution will increase classification performance. Therefore, there are two factors added within class variability and reduced boundary or mixed class pixels working against one another. The extent of each is a function of within class variability and class field size. Since these two factors vary from site to site and also with the level and type of classification scheme, results as a function of spatial resolution from various investigators will continue to be muddled. More likely, new pattern recognition approaches will have to be adapted for high resolution data such as TM that are technique and site specific in order to more fully use the additional spectral/spatial information.

Spectral bands from each of the spectral regions--visible, near infrared, middle infrared and thermal infrared--all provide unique and useful information. In other words, for many general digital TM evaluations inclusion of four bands representing the four spectral regions will typically provide as much useful land cover discrimination information as when using all seven bands.

Results from inclusion of the thermal band, TM6, indicated an improvement in spectral class discrimination. Of primary spectral importance was discrimination between water, vegetative surfaces, and impervious surfaces due to differences in thermal properties. The differences in thermal properties are complex but are related to differences in the radiative, conductive, and convective processes of the materials. Further, although the time of day is not optimum for discrimination and the surface thermal properties change rapidly as a function of time, the thermal infrared band is nonetheless a random variable providing spectral contrasts between surfaces comprising land use/land cover classes.

Results from the principal component transformed data clearly indicates additional information content in TM over MSS. For both the July and November data sets, the TM had two and three additional principal components of land cover discrimination information, respectively, in comparison to MSS. The added land cover information in the TM is likely attributed to increased spatial resolution, added spectral regions, and quantization and possibly other TM sensor parameter improvements such as an increased S/N. Last, by deleting the final principal component(s), the principal component transformed data may be used as a data reduction technique. For example, TM principal components six and seven for November provided insufficient land cover discrimination information to warrant inclusion of all seven principal components in a classification procedure.

ACKNOWLEDGEMENT

REFERENCES

1. R.M. Hord and W. Brooner, 1976, "Land Use Mapping Accuracy Criteria," Photogrammetric Engineering and Remote Sensing, 42(5), pp. 671-678.

2. A.M. Hay, 1979, "Sampling Designs to Test Land-Use Map Accuracy," Photogrammetric Engineering and Remote Sensing, 45(4), pp. 529-533.

3. R.O. Duda, and P.E. Hart, 1973, Pattern Classification and Scene Analysis, John Wiley and Sons, 482 p.

4. J.B. Campbell, 1981, "Spatial Correlation Effects Upon Accuracy of Supervised Classification of Land Cover," Photogrammetric Engineering and Remote Sensing, 47(3) pp. 355-364.

5. M.L. Labovitz, D.L. Toll and R. Kennard, 1980, "Preliminary Evidence for the Influence of Physiographic Province and Scale Upon the Autocorrelation of Remote Sensing," International Journal of Remote Sensing, 3(1), pp. 13-30.

6. P.H. Swain, 1978, "Fundamentals of Pattern Recognition in Remote Sensing," in Remote Sensing the Quantitative Approach, P.H. Swain and S.M. Davis, eds, McGraw-Hill, New York, pp. 136-187.

7. R.J. Kauth and G.S. Thomas, 1976, "The Tasselled Cap--A Graphic Description of the Spectral-Temporal Development of Agriculture Crops as Seen by Landsat", Machine Processing of Remote Sensing Data Symposium, Purdue University, W. Lafayette, IN, pp. 4B41-4B51.

COMPARATIVE TECHNIQUES USED TO EVALUATE

THEMATIC MAPPER DATA FOR LAND COVER

CLASSIFICATION IN LOGAN COUNTY, WEST VIRGINIA

J. O. Brumfield
Marshall University
Huntington, WV 25701

R. G. Witt
NASA/Goddard Space Flight Center
Greenbelt, MD 20771

H. W. Blodget
NASA/Goddard Space Flight Center
Greenbelt, MD 20771

R. F. Marcell
Computer Sciences Corporation
Silver Spring, MD 20910

Page intentionally left blank

COMPARATIVE TECHNIQUES USED TO EVALUATE
THEMATIC MAPPER DATA FOR LAND COVER
CLASSIFICATION IN LOGAN COUNTY, WEST VIRGINIA

INTRODUCTION

The Eastern Regional Remote Sensing Applications Center (ERRSAC) of NASA/ Goddard Space Flight Center and Marshall University (W. Va.) conducted a joint evaluation of Landsat 4 Thematic Mapper (TM) data for mapping abandoned mine lands and reclamation progress in conjunction with the West Virginia Department of Natural Resources (WVDNR). The co-investigators proposed the research after being contacted by personnel from the WVDNR/ Abandoned Mine Lands division, who were interested in determining whether or not the improved spatial, spectral and radiometric resolution of the TM could be used to detect and assess abandoned surface mines, and delineate stages of revegetation. Thus, the objectives of the research were to identify and map active/abandoned, partially reclaimed, and fully revegetated surface mine areas, testing several digital data processing techniques for this purpose.

Changes in state and federal laws over the past decade have made the monitoring of active and abandoned surface mines a necessity. In 1973, legislative changes in surface mining and reclamation laws in West Virginia mandated back-filling practices and the basic elimination of talus slopes as well as some reduction in the vertical highwall structure in relation to surface mine reclamation. By 1977, new federal legislation with mandatory state compliance required a reclamation practice that restored the original contour with elimination of highwall and talus slopes in any form. Additional laws concerning reclamation of abandoned mine lands were also established resulting in severance tax revenue from the extracted coal being applied to reclaiming those areas that had not been properly reclaimed prior to the Surface Mining and Reclamation Act of 1977. The Logan County study area, with a large number of active and abandoned mines, was an ideal location to apply and evaluate the TM data with these considerations in mind.

PROCEDURES

All digital processing of the 4 September 1982 TM scene (path/row 18 34) was accomplished on the Hewlett-Packard 3000 computer at ERRSAC, using the Interactive Digital Image Manipulation System (IDIMS) software package, and accompanying Geographic Entry System (GES). The TM data for the central portion of Logan County were extracted to include most of the barren and disturbed areas. This subset image also contained one of the three U. S. Geological Survey (USGS) 7.5-minute topographic quadrangles for which ground verification data were obtained by WVDNR. These data were first subjected to various enhancement procedures, including a linear contrast stretch, principal components and canonical analysis transformations. At the same time, four general procedures were followed to produce six classifications as a means of comparing the techniques involved.

The general procedures were as follows:

- analysis of the full seven-band TM data subset;
- principal components analysis;
- canonical analysis; and
- analysis of four bands selected by canonical analysis.

The six classifications all were generated using an iterative unsupervised clustering algorithm on the seven bands, the four selected bands, three and four principal components, and three and four canonical axes. Each was then labelled with the aid of ground truth information, and digitally compared with the GES-encoded verification data for accuracy assessment. The following section describes these procedures in greater detail.

Digitization of Ground Verification Data (GVD)

The GVD collected by the WVDNR/Abandoned Mine Lands Div. personnel for the Holden 7.5' quad sheet was entered into the computer using the IDIMS' GES. The GVD was digitized on a Talos digitizing table with the data stored as polygons, in vector format. For the GVD to be used in parallel with the classified TM data, two transformations were applied to the data first. Both data sets had to contain the same picture element size, and the GVD had to be converted from vector to raster format before entry as an IDIMS (computer) image. A grid with specified origin and cell size was created, and the two (GVD and TM) data sets were then transformed to fit this GES grid, assuring that they were identical in areal extent. The vector to raster format conversion was done with another GES program, and the GVD could then be entered as an IDIMS image. Once coverted to image form, the GVD was compared with the classified TM data by cross-tabulation (see ESL, 1978).

Image Enhancement

A linear contrast stretch based on histograms of the data for each of the seven TM bands was done by saturating the data values from the two tails of the modal distribution and stretching the modal range of data values from 0 to 255, thereby increasing contrast. The first three axes from principal components analysis, a feature extraction technique, were used to develop a transformed image of the TM data subset (Podwysocki, 1977). The principal components transformation developed a grand mean by clustering all of the data, with the first three (orthogonal) components located so as to account for over 95% of the variance in the data. A second feature extraction technique, canonical analysis, was used to generate a canonically transformed data set. Again, the first three axes containing over 97% of the data variability were used to develop a third enhanced image (Bloemer et al,, 1981). These three enhancement procedures were then compared for highlighted information content and interpretability.

Iterative Clustering (Unsupervised) Classification

An iterative clustering algorithm (ISOCLS; see E.S.L,, 1978) was applied to the full seven-band TM data subset with control parameters set for 30 clusters, eight iterations, deviation of means at 0.5 and chaining distance of 1.0. These settings resulted in very tight grouping of clusters (i.e., very well defined relative to one another). The clusters were identified in terms of informational categories such as urban, grass, forest, active/inactive mines,

partially reclaimed, fully revegetated, cloud and shadow, then grouped and lastly subjected to accuracy assessment (see Witt et al., 1982).

Principal Components Analysis Classification(s)

Statistics involving the grand means and covariance matrix for the seven bands of TM data were developed using an iterative clustering algorithm, set for one cluster and a maximum standard deviation of 0.5 with one iteration. The resulting grand means and covariance matrix were used to develop the transformation coefficients, which were then multiplied times the raw seven-band TM data subset to develop the transformed data set (principal components axes). Most of the variability was loaded into the first three axes (95%), with an additional four per cent in the fourth component. The first three and four principal components were clustered into 30 classes and labelled as above for accuracy assessment.

Canonical Analysis Classification(s)

The iterative clustering algorithm (ISOCLS) was applied to develop statistics for 60 clusters in the raw seven-band TM data subset. These statistics of cluster means and covariance matrices were input into a canonical analysis routine developed by the Office for Remote Sensing of Earth Resources (ORSER) at Pennsylvania State University, as modified and installed by ERRSAC at NASA/ Goddard Space Flight Center. Canonical analysis is used to develop coefficients of the transformation matrix using pooled within cluster and pooled among cluster covariance matrices to bring about a rotation, translation and rescaling of data in the transformation process (Merembeck, 1977). Matrix multiplication of the raw seven-band TM data subset by the transformation matrix was done with another IDIMS function (KLTRANS), and the first three and four axes containing 97% and 99% of data variability (see Table I) were used in iterative clustering and accuracy assessment as above (Brumfield, 1981; Boyd, 1982).

Band Selection by Canonical Analysis for Classification

Canonical analysis as described above also develops a correlation coefficient matrix showing the correlation of the input data set and the canonically transformed data axes. Based on visual inspection for feature definition and variability loadings in the first four axes, the first three axes and their correlations with the raw data bands were used in band selection (Eppler, 1975). The criterion established was to evaluate the correlation coefficients for each of the bands of raw data so that the sum of the absolute values of any two of the first three axes was equal to or greater that 1.1 (see Table II). For example:

$$\text{equation 1} \quad |TC1| + |TC2| = 1.1$$

$$\text{equation 2} \quad |TC1| + |TC3| = 1.1$$

$$\text{equation 3} \quad |TC2| + |TC3| = 1.1$$

where TC1, TC2, TC3 are the correlation coefficients in transformations 1, 2, 3, for TM data bands one through seven. The only bands to meet this criterion were bands 3, 4, 5, 7 which were thereby selected for clustering as in the above procedures (Turner et al., 1978).

Accuracy Assessment

All six 30-cluster classifications were thus labelled and the classes grouped into one of the desired categories (urban, grass, forest, and mines) to correspond with the GVD. The accuracy assessment consisted of digitally comparing each of the six classifications with the GVD on a point-by-point basis by means of an IDIMS program (CONTABLE), which produced contingency tables indicating the level of agreement between the significant categories. All percentage figures in the following tables were derived from these matrices.

RESULTS

Visual Analysis of Enhanced Imagery

The images resulting from linear contrast stretching, principal components and canonical analysis transformations of the raw TM data clearly offer a high quality product for interpretability of active/abandoned surface mine areas. For example, the first three canonical axes all contain information pertaining to the mines. The first axis is positively correlated with active and abandoned surface mine areas, while the second and third axes show a negative relationship. When displayed in the form of a color composite, the transformed data sets allow interpretation of active and abandoned mines, even along narrow hillside contours or steep slopes. The tailing piles associated with underground mine sites are also easily visible. The fact that all of these mine features are quire apparent suggests that Abandoned Mine Lands personnel could use manual methods to locate active/abandoned mines, at least to update maps of the total extent of such areas. Further identification of stages of surface mining could then take place using machine processing methods.

Digital Analyses (Statistical) Results

The results of the various techniques are summarized in the following tables. Table III shows the number of pixels and the per cent correct for six classifications and the four general categories. Table IV presents a more comprehensive version of the accuracy assessment results, taking into account both commission errors and omission errors. The percentages for all classifications/categories represent an average of pixels correctly classified over row, and over column, totals.

The clustered, four-axis canonically transformed data set gave the best overall accuracy at 84.9% correct, followed by the three-axis canonical and band selected classifications at 83.3% correct. The seven bands clustered image had a slightly lower accuracy of 83.1% correct, while the poorest overall results were given by clustering four (81.8%) and three (81.1%) principal components.

For active mines, the category of greatest interest, Table IV illustrates that the two classifications of canonically transformed data had virtually the same accuracy as the seven-band clustering, 35.4% and 35.3% respectively. The band-selected classification was slightly lower at 33% correct, and the principal components images did the poorest (30.5% and 27.2%) in classifying actively mined areas.

The low absolute percentages for categories other than forest are due to the generalized nature of the ground verification data. For example, the areas delineated on the Holden quadrangle by WVDNR as active mines were instead the full extent of areas currently licensed for mining. Most of these areas have not been exposed to mine operations in their entirety, and thus are correctly classified as forest, the pre-mining land cover.

In reality, each mine is worked a portion at a time, so that within one permitted area several stages of mining or no mining at all may exist. Actual land covers within the bonded areas include forest, grass and scrub (revegetation), and barren land. In order to provide better results and a more realistic comparison between the classifications, a true field survey of the mines will be done to provide ground truth information that delineates active/inactive, partially reclaimed, and fully revegetated mine areas.

CONCLUSIONS

It is apparent from these preliminary results that various feature extraction/ data reduction techniques provide classification results equal or superior to the more straightforward unsupervised clustering technique. Also, as Figures I and II for three principal components and three canonical axes illustrates, the overall separability of classes offers greater information content relative to a variety of land cover categories than the more generalized ground verification data indicate. The data transformations that are involved initially take slightly more computer (cpu) time, but once developed using a representative subset of the data, they can be applied to the larger data set. Furthermore, analyst interaction time for labelling clusters is reduced using the canonical analysis and principal components procedures, though the canonical technique has clearly produced better results to date. Once the ground truth data are revised, it will be possible to offer a more detailed assessment of the TM data as used for mapping surface mines.

REFERENCES

Bloemer, H. L, Brumfield, J. O., Campbell, W. J., Witt, R. G., and B. G. Bly. 1981. Application of Landsat data to monitor land reclamation in Belmont County, Ohio. The Second Eastern Regional Remote Sensing Applications Conference, Danvers, Mass., March 9-11, 1981, Proceedings: pp. 167-190.

Boyd, R. K., Brumfield, J. O., and W. J. Campbell. 1983. Optimization of a non-traditional unsupervised classification approach for land cover analysis. National Conference on Energy Resource Management, Baltimore, Maryland, September 9-12, 1982, Proceedings: pp. 32-44.

Brumfield, J. O., Bloemer, H. L., and W. J. Campbell. 1981. An unsupervised approach for analysis of Landsat data to monitor land reclamation in Belmont County, Ohio. Seventh International Symposium on Machine Processing of Remotely Sensed Data, West Lafayette, Ind., June 23-26, 1981, Proceedings: pp. 428-438.

Electromagnetic Systems Laboratory. 1981. IDIMS functional guide. Sunnyvale, Calif., two volumes.

Eppler, W. G. 1975. Canonical analysis for increased classification speed and channel selection. Symposium on Machine Classification of Remotely Sensed Data, West Lafayette, Ind., June 3-5, 1975, Proceedings: pp. 1A-9-1A-22.

Merembeck, F., Borden, F. Y., Podwysocki, M. H., and D. N. Applegate. 1977. Application of canonical analysis to multispectral scanner data. Fourteenth Annual Symposium on the Application of Computers in Mine and Industry, University Park, Pa., Proceedings.

Podwysocki, M. H., Gunther, F. J., and H. W. Blodget. 1977. Discrimination of rock and soil types by digital analysis of Landsat data. NASA Technical Report X-923-77-17, NASA/Goddard Space Flight Center, Greenbelt, MD, 37 p.

Turner, Brian, et al. 1978. Satellite and Aircraft Multispectral Scanner Digital Data Users Manual, Office for Remote Sensing of Earth Resources, The Pennsylvania State University, University Park, Pa.

Witt, R. G., Bloemer, H. L., Bly, B. G., Brumfield, J. O., and W. J. Campbell. 1982. Comparing digital data processing techniques for surface mine and reclamation monitoring. American Congress on Surveying and Mapping – American Society of Photogrammetry Annual Meeting, Denver, CO, March 14-20, 1982, Proceedings: American Society of Photogrammetry, Falls Church, Va., pp. 11-16.

TABLE I

Percent Variance Loading for Canonical Analysis

Axis variance	1	2	3	4	5	6	7
Percent of total	53.73	32.41	10.08	3.24	0.38	0.11	0.05

TABLE II

Correlations Between Channels and Axes

Axis \ Channel	1	2	3	4	5	6	7
1	.45	.54	.58	.48	.70	-.06	.58
2	-.45	-.43	-.59	.70	.18	.04	-.25
3	.35	.15	.01	.24	-.52	-.63	-.49
4	-.03	-.24	-.45	-.34	.43	-.33	-.07
5	-.64	-.47	-.19	-.33	-.14	-.68	.20
6	.17	-.05	-.27	.06	-.07	.16	.56
7	-.19	.46	-.08	-.03	-.07	-.05	.02

TABLE III

CLASSIFICATION RESULTS BY LAND COVER
CATEGORY (PIXELS AND PERCENT CORRECT)

Land Cover Categories

Classification	Urban	Grass	Forest	Mines	totals
7-band	1055	711	119186	1382	122334
	28.9	8.6	89.6	61.1	83.1%
4-band	1675	319	119305	1290	122589
	27.5	7.6	88.6	56.9	83.3%
PC I	1245	825	115376	2010	119456
	32.5	8.0	90.0	40.4	81.1%
PC II	1684	797	115880	2179	120540
	38.3	8.7	89.8	45.7	83.3%
KL I	2202	629	117746	2371	122948
	40.7	9.0	89.9	54.1	83.3%
KL II	2197	377	120615	2382	125571
	41.2	10.9	89.5	54.0	84.9%
Average	34.9%	8.8%	89.6%	52.0%	82.9%

TABLE IV: AVERAGED ACCURACIES

Land Cover Categories

Classification	Urban	Grass	Forest	Mines	Overall
7-band	23.4	18.4	92.7	35.3	83.1%
4-band	27.9	10.1	92.3	33.0	83.3%
PC I	26.8	20.1	91.3	27.2	81.1%
PC II	33.4	19.9	91.4	30.5	81.8%
KL I	39.0	16.8	92.1	35.4	83.3%
KL II	39.2	12.8	93.0	35.4	84.9%
Average	31.6	16.4	92.1	32.8	82.9%
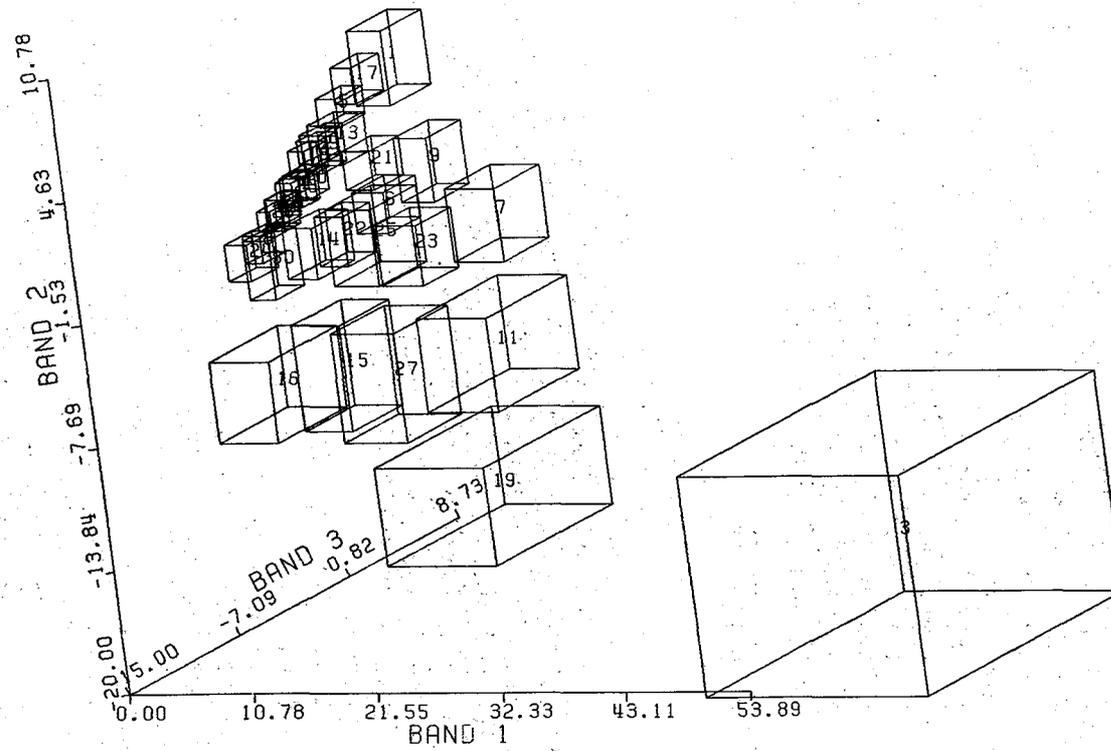
FIGURE 1. Canonical Axes 1, 2, 3

Multiple Pages Missing from Available Version

INTRODUCTION

As part of its cooperative program with the U.S. Army Corps of Engineers, NASA is assessing the most cost-effective and informative uses for Landsat data in environmental and hydrologic applications. In particular, MSS and TM data were examined to identify the relative contributions of each instrument's spatial and spectral characteristics to land cover classification accuracy. Of special interest in the Chesapeake Bay area are wetland mapping and change detection, and turbidity assessment for harbor maintenance.

Site Description

The Chesapeake Bay is a large (200 mile long) brackish estuary linking Baltimore Harbor with the Atlantic Ocean. Past dredging has allowed larger ships to use this channel while current maintenance keeps the passage open for commerce. Like the Bay itself, the wetland areas on its Eastern Shore support both a thriving fishing industry and recreational activities. In addition, some of the surrounding wetlands include wildlife preserves and major winter feeding grounds for large numbers of migratory birds (Maryland Chesapeake Bay Fisheries, Bundy, N. M., 1978).[1] Additional information on wetland vegetation, submerged aquatic vegetation, turbidity, sediment transport and general land cover would aid the Baltimore Corps District in its program planning efforts.

Data Acquisition

Data sources for this project included the following: a Landsat MSS scene acquired October 31, 1980, and a Landsat TM scene acquired November 2, 1982. Color infrared aerial photography taken October 13, 1981 was used for photointerpretation of ground cover. The digitized Level I land cover data used for ground verification was developed from photointerpretation of 1977 color infrared photography of the Taylor's Island area flown by the State of Maryland.

Spatial Registration

The Landsat MSS and TM data covering this study site were spatially registered to a digitized ground verification map using ground control points. Control points common to all data sets and uniformly distributed throughout the study area were recorded and marked on a USGS 7.5 minute topographic map. The control points were digitized from the map using a digitizing table. To produce an image data base representative of the Universal Transverse Mercator (UTM) projection, the digitized coordinates were rescaled to image coordinates representing 30-meter square pixels for TM data and 60-meter square pixels for MSS.

Two third-order polynominal equations were used to model (in a least squares fit) the relationship between image coordinates and the transformed UTM coordinates. Control points with large residuals were

iteratively deleted until the final residuals ranged from 0 to $\pm$ 1.6 pixels. The MSS and TM data were then resampled using nearest neighbor interpolation to 60 and 30 meter projections, respectively.

Band Selection

Using a transformed divergence test to measure statistical separability between class pairs, Gervin et al (1983) identified TM bands 3, 4, 5 and thermal,$_2$as a particularly promising band combination at another study site. A combination of TM bands 2, 3 and 4, (comparable to the bands of the MSS) was also examined to test the improvement provided by TM spatial resolution.

Land Cover Classification Procedure

The same classification procedures were followed with both the MSS and TM data sets. Training statistics were generated on a mosaicked image of eight subsections representative of ground cover types in the entire Chesapeake Bay area. A clustering algorithm which divided each data set (for each band combination) into spectrally homogeneous clusters was applied to this mosaicked image to produce the training statistics.

A second mosaicked image containing two large subsections of land showing an agricultural and a wetland area typical of the test site was then classified based on training statistics from the eight-part mosaics using a maximum likelihood algorithm. Each cluster was individually displayed on an interactive video display device and manually assigned a land cover type based on topographic maps, aerial photographs and two-band spectral plots of the cluster means.

Approximately 60 spectral clusters were obtained for each band combination for the Eastern Shore sites. These clusters then were assigned to the five land cover categories. The Taylor's Island test site was then classified in the above manner, and its categorized images were registered to the ground verification data for accuracy assessment. The categories identified for the purpose of accuracy assessment were water, wetland, agriculture, forest and developed/residential. The majority of the area covered by the USGS topographic map was in water or woodland.

RESULTS AND DISCUSSION

For the Taylor's Island map, comparing the MSS and TM three band (2 3 4) classifications, the increased resolution of TM produced a small improvement in overall accuracy of 1% correct due primarily to a small improvement, 1% and 3%, in areas such as water and woodland (Table 1). This was expected as the MSS data typically produce high accuracies for categories which cover large contiguous areas. However, in the categories covering smaller areas within the map there was generally an improvement of at least 10%. Classification of the important residential category improved 12%, and wetlands were mapped with 11% greater accuracy.

Accuracy decreased 8% in agriculture, possibly due to the discrepancy in the ground verification data which had been acquired three years prior to the TM data.

When the classification was expanded to include four TM bands (3 4 5 and thermal) and then to all seven bands, little or no improvement occurred in the water and woodland categories but larger improvements were observed in the other categories. The four band showed improved discrimination for agriculture over the three band combination, but showed less discrimination in the residential areas, suggesting that a trade-off had occurred.

Classification using the TM four bands was nearly as accurate as that of the seven band combination in several categories and in overall accuracy. The seven band combination produced much better results in the residential category, however. The combined benefits of increased spatial and spectral resolution of the TM seven band combination yielded greater accuracies than MSS in all categories.

These preliminary findings indicate that improvement in classification accuracy can be traced to both the improved spectral and spatial resolution of TM. These results will be verified using two additional randomly selected USGS maps, which are primarily agricultural and forested. Additional TM band combinations will also be applied to these maps. Detailed observation of wetlands and possibly (depending on data availability) multitemporal classification will also be attempted.

LANDCOVER CATEGORIES (PERCENT CORRECT)

BAND COMBINATIONS	WATER	WETLAND	AGRICUL-TURE/ GRASS	WOOD-LAND	RESIDEN-TIAL	OVERALL
MSS	95	42	52	73	14	81
TM BANDS 2, 3, 4	96	53	44	76	26	82
BANDS 3, 4, 5, 6	97	55	51	76	11	84
ALL BANDS	97	51	54	79	33	84
PERCENT COVER	60	14	8	18	0.2	100

Table 1. Taylors Island Map Accuracy Assessment

REFERENCES

1. Bundy, N. M. and John B. Williams, Maryland's Chesapeake Bay
    Commercial Fisheries, Energy and Coastal Zone Administration,
    Maryland Department of Natural Resources, Annapolis, Maryland,
    November 1978.

2. Gervin, J. C., Y. C. Lu, W. A. Hallada, R. F. Marcell, "Compari-
    son of Land Cover Information from Landsat MSS and Airborne TMS
    for Hydrological Applications", Proceedings of the National
    Conference on Energy Resource Management, September 1982,
    pp. 289-302.

Page intentionally left blank

COMPARISON OF LAND COVER INFORMATION FROM LANDSAT MULTISPECTRAL SCANNER (MSS) AND AIRBORNE THEMATIC MAPPER SIMULATOR (TMS) DATA FOR HYDROLOGIC APPLICATIONS

J. C. Gervin
NASA/Goddard Space Flight Center
Greenbelt, Maryland

Y. C. Lu
Computer Sciences Corporation
NASA/Goddard Space Flight Center
Greenbelt, Maryland

R. F. Marcell
Computer Sciences Corporation
NASA/Goddard Space Flight Center
Greenbelt, Maryland

INTRODUCTION

In a cooperative program with the US Army Corps of Engineers (Corps), NASA is evaluating the capabilities of Landsat-4 Thematic Mapper (TM) data for environmental and hydrologic applications. The spectral and spatial characteristics of the TM considerably exceed those of the MSS carried by all Landsat satellites (Table 1), but the complexity and cost of analyzing TM data may make MSS data an attractive alternative for certain applications. Both NASA and the Corps are interested in assessing the relative effectiveness of TM, MSS and conventional data for land cover classification, particularly in urban/suburban areas, and for developing parameters for input to hydrologic (flood forecasting) and economic (flood damage) models (Davis, 1979). In addition, it would be particularly desirable to establish a set of optimal TM band combinations for land cover classification and related data analysis which could reduce processing time and cost while preserving accuracy and reliability.

Several sites already under study by the Corps were selected for this program. This paper will report results for one of these sites, the Clinton River Basin in Michigan. Moreover, the data examined here were gathered by the TMS, an airborne sensor designed to simulate TM spatial and spectral resolution prior to launch.

SITE DESCRIPTION

The Clinton River Basin flows into Lake St. Clair, draining an area of approximately 760 square miles in southeastern Michigan just north of Detroit. A detailed description of its topography, geology and climate may be found in Revised Plan of Study, Clinton River Basin (Corps, 1980). The basin has experienced an increasing number of floods in recent years accompanied by rapid growth and development, particularly within the floodplain. For these reasons, the Corps has developed and revised a plan for flood control

measures. The Detroit District has established a data base and comprehensive watershed model using spatial analysis methods (SAM) developed by the Corps Hydrologic Engineering Center (Davis, 1980) as a basinwide management tool to satisfy a wide range of planning needs.

APPROACH

Detailed land cover classifications were performed on TMS and MSS data of the Clinton River Basin using supervised classification techniques. Differences in interclass separability were compared to select several promising TMS band combinations. Supervised classifications for those band combinations were completed for three US Geological Survey (USGS) topographic maps, Mt. Clemens West, Utica and Waldenburg. MSS and TMS land cover information for the basin derived from these classifications will be provided to the Corps for use in flood forecasting and damage calculation models to evaluate differences in model performance, particularly in terms of accuracy and sensitivity.

Data Acquisition

Relatively cloud-free, high quality Landsat MSS data from early summer (June 28, 1981) were obtained for the study site. TMS data were acquired by NASA on August 19, 1981, in a single 60-mile long flight line stretching from the mouth of the Clinton River at Lake St. Clair through the town of Pontiac to Ortonville. These data at a spatial resolution of 31 meters were cloud-free and of good to excellent quality in most bands. Color infrared aerial photography was flown simultaneously with the TMS aboard the NASA Earth Resources Laboratory's Lear Jet for use in visual interpretation.

Three photointerpreted USGS 7.5 minute (1:24,000 scale) topographic maps, selected from the 27 covering the Clinton River Basin, were used in verification and accuracy assessment of the classifications. Prepared by the Southeast Michigan Council of Governments (SEMCOG) using 1978 aerial photography, conventional land cover maps at a scale of 1:24,000 for Mt. Clemens West, Utica and Waldenburg were digitized and converted to raster images for comparison with TMS and MSS classifications.

Preprocessing and Spatial Registration

Preprocessing. The Landsat MSS data were reformatted to remove Earth-rotational skew and synthetic pixels. Then the data were computer enhanced to facilitate the selection of ground control points and training areas.

NASA's Goddard Institute for Space Studies (GISS) radiometrically corrected the TMS data for changes in illumination across the scan line and resampled along each scan line to correct for the aircraft scanner's variable viewing angle. The 31-meter TMS thermal band was degraded to 124 meters by simple averaging to simulate the spatial resolution of the Landsat-4 TM thermal band. No weights were used in the averaging process, as would be required to simulate the sensor point spread function resulting from the optical properties of the scanner system (Sadowski and Sarno, 1976). No attempt was made to simulate the thermal sensor signal-to-noise ratio that would characterize lower spatial resolution data or the distortion introduced by the forward and reverse scanning of the TM. This image was then expanded back to 31-meter pixels, where each block of 16 pixels had the same value, and merged with the other six bands of 31-meter spectral data.

The other TMS bands had much lower dynamic ranges than are expected from the actual TM bands (NASA, 1982). Table 2 presents the means and variances of all bands. Since variance can be related to the signal-to-noise ratio, TMS bands 1, 5 and 6 had the lowest relative noise as confirmed by visual examination. TM data are expected to provide a full radiometric range of 256 levels compared with as few as 54 levels from TMS (Band 6).

Spatial Registration. The TMS and Landsat MSS data covering the study areas were spatially registered to the digital ground verification maps using ground control points. Sixty control points common to both sets and uniformly distributed throughout the study area were recorded and marked on USGS 7.5 minute topographic maps. Ground control points were digitized from the map using a digitizing table. To produce an image data base representative of the UTM projection, the digitized coordinates were rescaled to image coordinates representing 30-meter square pixels for TMS data and 60-meter square pixels for MSS data. Two third-order polynomial equations were used to model (in a least squares fit) the relationship between image coordinates and the transformed UTM coordinates. Control points with large residuals were iteratively deleted until the final residuals ranged from 0 to ± 1.6 pixels. The MSS and TMS data were resampled using nearest neighbor interpolation to 30- and 60-meter resolution.

When the registration of the MSS and TMS data to the digital ground truth was checked on a display device, portions of the TMS data were found to be more than a pixel off, indicating that the third order polynomial used was not adequate to produce precise registration of the entire flight line. Since satellite platforms are more stable, actual TM data should not present as much of a misregistration problem.

Supervised Classifications

Forty training sites were initially located in the TMS data using ground survey data provided by the Corps Detroit District Office and simultaneous color infrared aerial photography acquired by NASA. Statistics were generated for each site and saved in a special statistics file which could be easily edited. These sites represented the following land use categories used by the Detroit District:

1. Low-, medium-, and high-density residential

2. Institutional, industrial, and commercial

3. Active cropland

4. Woodland

5. Extractive and barren

6. Brushland

7. Grassland

8. Wooded wetland

9. Open wetland

10. Water

A maximum likelihood algorithm was used to classify the whole TMS data set
based on statistics from 40 training sites. This classification image was
thresholded using a chi square confidence of 99 percent to form a second
classification image. Both classification images, the thresholded and
unthresholded, were displayed on an interactive display device. Ten colors
were assigned to the classes to represent the land use categories listed above.
By flagging the same class in each image plane and flickering between the two
classified images, it was possible to determine which classes needed to be
thresholded or further refined. Major errors of omission and commission were
found in the grassland, agricultural, and brushland categories. Moreover,
much of the TMS scene remained unclassified at the 99 percent confidence level.
Additional training sites were located in the image to minimize these errors,
bringing the total number of training sites to 67. Once the entire TMS scene
was classified, the same statistics were used to classify the registered TMS
data for the Mt. Clemens West, Utica and Waldenburg maps using the maximum
likelihood algorithm.

The same 67 training site statistics were also used to classify several data
sets using other TMS band combinations. The first was composed of TMS
Bands 2, 3 and 4, making it spectrally similar to MSS but with greater spatial
discrimination. Transformed divergence, which measures the statistical sepa-
rability between each class pair for all band combinations, was applied to
the first 40 training sites to select optimal TMS band combinations from the
127 possible permutations. An optimal band selection would reduce processing
time while preserving most of the information content in the scene. The trans-
formed divergence test identified Bands 3, 4 and 7 and 3, 4, 5 and 7 as the
optimum 3 and 4 band combinations, respectively. These three TMS data sets,
composed of Bands 2, 3 and 4; 3, 4 and 7; and 3, 4, 5 and 7 were then classified
using 67 training site statistics and a maximum likelihood algorithm.

The classifications were cross-tabulated with the digital ground truth. Using
a simple plurality decision rule, each training site signature was relabeled
based upon the most predominant land cover present. Using this method, dis-
crepancies were quickly found between the category determined by the plurality
rule and the land cover within the original training site. The majority of
confusion was between grassland (both natural and planned, such as idleland,
golf courses and parks) and agricultural areas. Using the plurality decision
rule, the 67 classes developed from the training site statistics were assigned
to one of ten categories: water, cropland, woodland, wooded wetland, open
wetland, brush, grassland, commercial/industrial, residential, and extractive.

The MSS image was classified in a similar manner using 73 different training
classes. Because of the difference in resolution between MSS and TMS data,
TMS training sites were generally too small (i.e., had too few pixels) to use
in classifying the MSS data.

Accuracy Assessment

For the accuracy assessment, the ten land cover categories were aggregated
into five because no open wetland and very little brushland or wooded wetland
were present in these study areas. Brushland, wooded wetland and woodland
were therefore combined into a single woodland category.

Grassland consisted of 1) golf courses and parks, which were easily separable, 2) idleland which merged with brushland, and 3) many fields apparently planted in hay or other grains on a multiple-year rotation schedule. Therefore, it was impossible to determine, using 1981 aerial photography, which crop had occupied a given field in 1978 when the ground verification data were gathered. Therefore, agriculture was combined with grassland for the purposes of the accuracy assessment. Finally, since the extractive/barren category included many construction sites in 1978 which by 1981 represented other land cover types, this category was removed from analysis. The resulting land cover categories were: residential, commercial/industrial, woodland, agriculture/ grass and water.

The three USGS maps used in the accuracy assessment included the primarily residential Mt. Clemens West map, the agricultural Waldenburg map and the Utica map, which represents a variety of land cover types. The watershed contains many small heterogeneous land cover areas, including industrial plants, commercial buildings along major roadways, small ponds, isolated residential developments, golf courses, narrow woodlands along streams and small agricultural fields. A pixel-by-pixel comparison was performed between the digitized ground truth maps of Mt. Clemens West, Utica and Waldenburg and each corresponding Landsat MSS and TMS classification map.

RESULTS AND DISCUSSION

The resulting accuracy comparisons, in terms of percent of pixels correctly identified in each land cover category on the ground verification data, are given in Tables 3, 4 and 5 for the Mt. Clemens West, Utica and Waldenburg maps, respectively. Table 6 summarizes the information for percent correctly classified by land cover category and MSS and TMS band combination for all three maps. The bottom row on each table indicates the percent of each map occupied by each of the land cover types examined, based on the ground verification data.

The overall accuracies for the land cover classifications of the Clinton River Basin are somewhat lower than those often reported in the literature. This can be attributed to the heterogeneity of this largely suburban area, the rigorous accuracy assessment applied, inconsistencies in the ground verification data, due in part to the passage of time between the photointerpretation and TMS data acquisition, and the separation of developed into commercial/ industrial and residential.

Although these accuracy figures could probably be improved through revised ground verification data or the use of multitemporal data, contextual classification, or other more advanced digital techniques, this might obscure the results of greatest interest: a comparison of the per point accuracy of land cover classification results between MSS and TMS and between various TMS band combinations.

For all three maps, the spectral band combination comparable to the MSS (Bands 2, 3 and 4) produced an overall accuracy of 57 percent, an increase of 9 percent over the MSS. The optimum 3-band combination selected by the transformed divergence technique provided similar results. This is largely attributable to the substantially (approximately 20 percent) higher accuracies for residential, water and agriculture/grass.

The selected 4-band combination provided nearly as good a discrimination of land cover as all seven TMS bands. The 4- and 7-band classifications did show considerable improvement in accuracy over the 3-band combinations (63 percent versus 57 and 56 percent), particularly in residential (80 and 83 percent versus 72 and 69 percent) and agriculture/grass (64 and 61 percent versus 58 and 55 percent).

The observation that using 7 bands instead of 4 bands did not improve the classification accuracy noticeably is supported by previous theoretical results of pattern-classifier systems. Swain and Davis (1978) suggest that for a fixed number of training samples there is an optimal number of spectral bands or brightness levels per band. Increasing the number of spectral bands results in a higher and higher dimensional set of statistics to be estimated with a fixed number of samples. Theoretically, increasing the dimensionality requires more training samples to characterize the added variability, but with a fixed sample, classification accuracy can actually decrease. In this case, the most optimal combination of features contained four bands, with each band from a major region of the spectrum: visible, near infrared, middle infrared, and thermal infrared.

CONCLUSIONS

TMS data produced a more accurate and spatially contiguous classification than MSS for this study site. While the accuracy of the 4-band TMS data set was as good as the 7-band, the 3-band TMS data sets were also better than the MSS. This confirms preliminary findings reported for the Mt. Clemens West map in Gervin et al. (1982). These results indicate that both the increased spectral discrimination and spatial resolution contribute to improved classification accuracy. The possibility of reducing the data analysis burden associated with large TM data volumes through effective band selection therefore appears promising.

The combination of bands selected based on the transformed divergence technique provided one band in each of the major regions of the spectrum: visible (Band 3), near IR (Band 4), middle IR (Band 5) and thermal IR (Band 7). This selection agrees reasonably well with results obtained by Dottavio and Williams (1982) using linear discriminant analysis and Latty and Hoffer (1982) using divergence measures for forest types. This would be expected in light of the intercorrelation studies of Staenz et al. (1980). Additional related studies are summarized in Irons (1982).

These results should be viewed with some caution, however. The data are from a TMS rather than the actual TM. Moreover, the MSS data were obtained in early summer while the TMS was flown in late summer; therefore some of the differences noted could be due to seasonal, atmospheric and sun angle effects rather than sensor differences.

The implications of the improved classification accuracy of TMS data are important for Corps hydrologic and economic modeling. In particular, the higher accuracies for the developed categories (residential and commercial) should improve the predictions of runoff in flood forecasting models and of flood damage for damage calculation models appreciably. Moreover, the promising results with band selection will permit users of the data to benefit from the improved classification capability without having to deal with the entire data volume.

REFERENCES

1. Corps, "Revised Plan of Study, Clinton River Basin, Michigan," US Army Engineer District, Detroit, Michigan, February 1980

2. D. W. Davis, "Flood Mitigation Planning Using HEC-SAM," Technical Paper No. 73, US Army Corps of Engineers, 1980

3. D. W. Davis, "Comprehensive Floodplain Studies Using Spatial Data Management Techniques," Paper No. 27100, Water Resources Bulletin, Water Resources Association, 1979

4. C. L. Dottavio and D. L. Williams, "Mapping a Southern Pine Plantation with Satellite and Aircraft Scanner Data: A Comparison of Present and Future Landsat Sensors," J. of Applied Photographic Engineering, Vol. 8, No. 2, 1982, pp. 58-62

5. J. C. Gervin, Y. C. Lu, W. A. Hallada, and R. F. Marcell, "Comparison of Land Cover Information from Landsat MSS and Airborne TMS for Hydrological Applications: Preliminary Results," National Conference of Energy Resource Management, September, 1982, pp. 289-302

6. J. R. Irons, "Summary of Research Addressing the Potential Utility of Thematic Mapper Data for Renewable Resource Applications," NASA Technical Memorandum TM 83965, July 1982, 39 p.

7. R. S. Latty and R. M. Hoffer, "Waveband Evaluation of Proposed Thematic Mapper in Forest Cover Classification," Proceedings of the American Society of Photogrammetry Fall Technical Meeting, Niagara Falls, New York, 1980, pp. 25-2-D-1 to 25-2-D-12

8. NASA, "Landsat-D Investigations Workshop," Goddard Space Flight Center, May 13-14, 1982

9. F. G. Sadowski and J. Sarno, "Forest Classification Accuracy as Influenced by Multispectral Scanner Spatial Resolution," NASA Contract No. NAS9-14123, May 1976

10. K. F. Staenz, J. Ahern and R. J. Brown, "Evaluation of Thematic Mapper Bands: A First Step in Feature Selection," Proceedings of the Sixth Canadian Symposium on Remote Sensing, Halifax, Nova Scotia, 1980, pp. 625-634

11. P. H. Swain and S. M. Davis, eds., Remote Sensing: The Quantitative Approach, McGraw Hill Book Co., New York, 1978

Table 1

TM AND MSS SENSOR CHARACTERISTICS

	TM	MSS
Spectral Bands (μm)	0.45-0.52	
	0.52-0.60	0.5-0.6
	0.63-0.69	0.6-0.7
	0.76-0.90	0.7-0.8
	1.55-1.75	0.8-1.1
	2.08-2.35	
	10.40-12.50	
Spatial Resolution (m)	30	80
	120 (thermal)	
Radiometric Resolution (bits)	8	6

Table 2

SUMMARY STATISTICS FOR TMS FLIGHT LINE OF CLINTON RIVER, MICHIGAN

Date: 8/19/81   Time: 9:59 a.m. Local Time

Band	Minimum	Maximum	Mean	Standard Deviation
1	31	255	56	10
2	43	255	81	18
3	2	255	72	25
4	2	234	103	19
5	0	148	49	10
6	0	185	29	9
7	0	255	101	30

Note: The thermal band on the Thematic Mapper is Band 6, not Band 7 as on the Thematic Mapper Simulator.

Table 3. Mt. Clemens West Classification Accuracy Assessment

PERCENT CORRECT

Sensor	Water	Agriculture and Grass	Woodland	Commercial/ Industrial	Residential	Total
MSS	23	35	59	49	71	54
TMS						
(2, 3, 4)	28	56	42	46	75	61
(3, 4, 7)	30	56	47	48	68	59
(3, 4, 5, 7)	32	64	47	52	81	68
All Bands	33	60	46	51	84	68
Percent Cover	1	38	9	11	41	

PERCENT CORRECT

Sensor	Water	Agriculture and Grass	Woodland	Commercial/ Industrial	Residential	Total
MSS	22	55	51	35	36	47
TMS						
(2, 3, 4)	45	52	41	54	63	51
(3, 4, 7)	46	45	46	50	69	51
(3, 4, 5, 7)	48	59	45	50	78	58
All Bands	47	57	47	51	79	58
Percent Cover	3	35	30	10	22	

Table 4. Utica Classification Accuracy Assessment

PERCENT CORRECT

Sensor	Water	Agriculture and Grass	Woodland	Commercial/ Industrial	Residential	Total
MSS	0	38	33	26	65	41
TMS						
(2, 3, 4)	18	63	21	35	81	60
(3, 4, 7)	8	62	23	41	78	51
(3, 4, 5, 7)	13	68	21	38	80	64
All Bands	18	65	22	38	82	62
Percent Cover	.1	73	12	1	14	

Table 5. Waldenburg Classification Accuracy Assessment

PERCENT CORRECT

Sensor	Water	Agriculture and Grass	Woodland	Commercial/ Industrial	Residential	Total
MSS	19	43	50	41	59	48
TMS						
(2, 3, 4)	42	58	38	49	72	57
(3, 4, 7)	42	55	42	49	69	56
(3, 4, 5, 7)	45	64	41	50	80	63
All Bands	44	61	43	51	83	63
Percent Cover	1	45	18	8	28	

Table 6. Classification Accuracy Summary for Mt. Clemens West, Utica, and Waldenburg

Page intentionally left blank

RELATIVE ACCURACY ASSESSMENT OF LANDSAT-4 MSS AND TM DATA

FOR LEVEL I LAND COVER INVENTORY

E. M. Middleton
NASA/Goddard Space Flight Center
Greenbelt, MD   20771

Y. C. Lu
Computer Sciences Corporation
Silver Spring, MD   20910

R. G. Witt
NASA/Goddard Space Flight Center
Greenbelt, MD   20771

R. S. Sekhon
Computer Sciences Corporation
Silver Spring, MD   20910

Page intentionally left blank

RELATIVE ACCURACY ASSESSMENT OF LANDSAT-4 MSS AND TM DATA

FOR LEVEL I LAND COVER INVENTORY

ABSTRACT

A study was undertaken to compare digital data for the Washington, DC scene
from the Landsat-4 Multispectral Scanner (MSS) and the Landsat-4 Thematic
Mapper (TM), simultaneously acquired on November 2, 1982 (Scene IDs: 40109-
15140). Classification success for the TM and MSS data sets was determined
by a per pixel comparison with digitized ground verification data (GVD).
These GVD were comprised of Level I land cover (developed, agriculture, forest,
water, wetlands, and barren) for four USGS 7.5-minute topographic quadrangle
maps. The relative improvement in classification success for TM was between
11 and 14%, or about a factor of 1.3, for these data. This represents a
meaningful improvement in accuracy for Level I land cover categorization for
TM relative to MSS, particularly when both errors of omission and commission
were considered.

INTRODUCTION

Due to improved radiometric, spectral and spatial characteristics, the Landsat-4
Thematic Mapper (TM) is expected to provide considerable enhancement over
its companion, the Multispectral Scanner (MSS), in the capacity to discriminate
among and correctly designate land cover categories. Quantification of this
capability is essential to determine its utility for practical inventorial
applications as well as for basic research relating to terrestrial systems.

Prior to the launch of Landsat-4, extensive research had been performed with
Thematic Mapper Simulator (TMS) data to quantify the anticipated performance of
Thematic Mapper (TM) data for delineating renewable earth resources. A compre-
hensive literature review for TMS studies can be found in Iron's report (1982).
The majority of these investigations have focused primarily on agriculture,
forestry, and general land cover mapping. For example, specific crop types
identification was improved, ranging from a factor of 3 for corn to 1.4 for
soybean (Sigman and Craig, 1981). A 21% improvement in TMS over MSS was
found for specific forest types, in contrast to only 6% for broad cover types
by Dottavio and Williams (1982). Others have observed a relative overall
improvement of approximately 12% for general land cover mapping (Gervin,
et al, 1982; Robinson, et al, 1982).

This investigation was sponsored by the Test and Evaluation Program under the
auspices of the Eastern Regional Remote Sensing Applications Center (ERRSAC).
TM and MSS data were evaluated separately by comparing the classified thematic
results with the Level I (Anderson, 1976) ground verification data (GVD).
Understanding relative classification success at the top of the land cover
hierarchy is of particular interest since some form of general land cover cate-
gorization will provide the foundation for future investigations of regional
and global dynamics. Although not expected to be optimal for TM data, this
relative assessment of MSS and TM for general classification accuracy using
standard classification techniques and standard categories should provide at
least a minimal estimate of the relative improvement afforded by TM.

METHODOLOGY

In order to ensure comparability of results, the same analysis procedures
were used for both MSS and TM data sets. These consist of procedures to
establish digital ground verification data (GVD), to process the sensor
digital image data, and to compare the classified image data acquired from
the Landsat sensors and the GVD.

Ground Verification Data (GVD)

The four USGS 7.5-minute topographic quadrangle maps (1:24,000 scale) used
for accuracy assessment in this study were a subset of 12 randomly selected
quads from a related project for which ground truth data were available within
the Washington, D.C. MSS scene area. The four 7.5' quads - Catoctin Furnace,
Woodbine, Baltimore East, and Galena - were chosen to provide a representa-
tive progression of different landforms and cover types, ranging from the
coastal plain and agricultural region of Maryland's Eastern Shore to the
forested slopes of the Catoctin Mountains.

Color infrared (CIR) aerial photographs taken on 12 April 1977 (scale approxi-
mately 1:60,000) were used to photointerpret Level I land cover categories
for each of the quads. Polygons representing unique land cover areas were
traced on mylar acetate overlaid on each of the USGS maps and assigned to
one of six Level I categories: developed, agriculture (ag)/grass, forest,
water, wetland, or barren. After each map was photointerpreted and a quality
check completed, a windshield survey was conducted to assess and update the
photointerpreted data. The field visits were necessary to account for land
cover changes which took place between the April 1977 date of the aerial
photography and the November 1982 TM and MSS image date.

Computer Processing

After the photointerpreted data were field-checked, the land cover overlays
were digitized and labelled by Level I land cover category using the Geographic
Entry System (GES). These polygonal vector data were later rasterized to image
format. These steps were accomplished with the GES and the Interactive Digital
Image Manipulation System (IDIMS) software on the ERRSAC HP-3000 minicomputer.

Once in image format, the GVD could be compared with the MSS and TM classifi-
cation results. The proportion of each Level I cover type is given for each
of these study areas in Appendix A.

Registration. For the registration process, the areas corresponding to the
four USGS 7.5-minute topographic quadrangles chosen for the accuracy assessment
were subset from the MSS and TM data sets. Separate sets of control points
(30-40 per quad) were selected on each map/image pair in order to relate the
data sets to Universal Transverse Mercator (UTM) coordinates. Once the control
points were digitized using the Geographic Entry System (GES) software, three
programs were run to geometrically correct and rescale the TM and MSS image
data. The functions are ALLCOORD; which accesses the map points from a GES
file and locates them on a UTM grid with specified cell size (in this case
30-meter square for TM and 60-meter square for MSS); TRNSFORM, which generates
transformation equations relating map points to image points up to a third-order
polynominal fitting; and REGISTER, which performs the actual image-to-map regis-
tration with a nearest neighbor interpolation according to the transformation
equations. Both data sets for each of the quads (eight total operations) were
registered in this manner. Typical error residuals associated with the
registration were $\pm$ 1.5 pixel for MSS and $\pm$ 1.0 pixel for TM data.

Classification Procedures. A conventional, well-documented unsupervised methodology (see Imhoff, Witt, Kugelmann, 1981) was used for image classification of the MSS and TM data. The parameter settings were identical for the TM and MSS processing. This approach does not explore improvements in accuracy which might be gained from TM with innovative classifiers (i.e., contextual) but does allow a determination of the minimum gain in accuracy, relative to MSS with a classification procedure optimal for classifying MSS data.

A 7.5' quadrangle adjacent to each of the four randomly selected accuracy quadrangles was selected for signature extraction and training purposes. This was done to assure that signatures were developed from one data subset and evaluated in another. The raw data from these four training quadrangles were extracted and mosaicked together, producing a single seven band image. The thermal data (band 6) were resampled to 30m. This image was then input to the unsupervised clustering algorithm (IDIMS' function ISOCLS) set to identify a maximum of 64 spectral clusters. Each resulting cluster was assigned to one of six land cover categories in an interactive mode on a color CRT using the 1977 CIR aerial photography as ground truth information. The 4 accuracy assessment images were then processed using a maximum likelihood classifier which assigned each pixel to one of the 64 spectral clusters. Clusters/ land cover assignments were made according to the labelling scheme previously determined.

Contingency Tables. Both the MSS and TM classification results were compared with the ground verification data on a pixel-by-pixel basis using the IDIMS' program CONTABLE. This program creates a contingency table showing agreement/ disagreement between all categories or classes from two different images. The matrix diagonal shows the number and percentage of Landsat classification pixels which are assigned to the same category as the GVD and therefore correspond. All of the statistical results presented in the following section are derived either directly or indirectly from these matrices. The original eight contingency tables (four MSS & four TM), have been combined into one contingency table each for TM/GVD and MSS/GVD. These aggregated four quad results are presented in Appendices B and C.

Accuracy Assessment

Since accuracy is reported many different ways in the literature, for clari- fication the computations for accuracy utilized here are defined. Accuracy or rather classification success, is considered here to be the proportional correspondence of the sensor classification to the GVD. This distinction is made because the GVD and sensor classifications may represent different measures of the same thing.

The accumulated four quadrangle results presented in the contingency tables (Appendices B and C) were analyzed to determine the relative correspondence of TM and MSS data with the GVD, and the associated errors of omission and commission per category. For this purpose the contingency tables were tabulated according to the general form illustrated in Table 1.

The computations for accuracy (computed here using 2 different approaches) and for errors are described below. The symbols in the equations refer to those

presented in Table 1 where for category n,

G_n = GVD subtotal,

L_n = Landsat subtotal,

A_n = portion of L corresponding to G,

O_n = portion of L omitted from G,

C_n = portion of G incorrectly classified by L,

and, $\sum_{1}^{n} G = \sum_{1}^{n} L$ are the grand totals summed over all rows and columns.

Table 1

GENERAL FORM OF CONTINGENCY TABLES
FOR COMPUTATIONAL PURPOSES

GVD PIXEL COUNT

CATEGORY	1 ———————→ N		TOTAL LANDSAT
1	A ACCURATELY CLASSIFIED	C COMMITTED PIXELS	L_1
N	O OMITTED PIXELS	OTHER	SUM L FOR OTHER CATEGORIES
TOTAL GVD	G_1	SUM G FOR OTHER CATEGORIES	$\sum_{1}^{N} G = \sum_{1}^{N} L$ AREA TOTAL

(LANDSAT PIXEL COUNT — vertical axis label, running 1 to N)

Accuracy - Approach 1. Accuracy is computed as the percent of the sensor classification which agrees with the GVD. This is commonly referred to as the "percent correct". Errors of omission in the assignment of GVD by a sensor classification can be derived as 100% - % correct, and comprise 100% of the categorization error associated with this approach.

o For each category, the % correspondence, $A1_n = \dfrac{A_n}{G_n} \times 100$. (1)

o The comprehensive accuracy over all
   categories, or the % correspondence, $A1 = \dfrac{\sum\limits_{1}^{n} A_n}{\sum\limits_{1}^{n} G_n} \times 100$ (2)

These statistics were computed for each individual quad and for the four quad data set, and are given in Table 2.

Accuracy - Approach 2. Accuracy here, referred to as percent mapping capability, is conceived as the intersection of two sets where the first is the GVD categorization and the second is the sensor classification. The overlap in these two sets represents the correspondence (or correctly classified) portion and equals the % correct computed in approach 1. However, the accuracy computed also includes that portion of the sensor classification that does not correspond to the GVD; this is the portion that was incorrectly assigned by the sensor to a category.

o For each category, the % mapping capability,

$$A2 = \frac{A_n}{(A + 0 + C)_n} \times 100.$$ (3)

{For each category (n), $A2_n$ is equivalent to:

$$\frac{A_n}{(L - A)_n + (G - A)_n + A_n} \times 100.\}$$

o The comprehensive accuracy over all categories, or the % mapping capability,

$$A2 = \frac{\sum\limits_{1}^{n} A_n}{\sum\limits_{1}^{n} (A + 0 + C)_n} \times 100.$$ (4)

These statistics were computed for the four quadrangle data set only (Appendices B and C).

Errors

Errors in the GVD coding process (i.e., photointerpretation and digitization), errors related to misregistration; and errors in the sensor classification process (i.e., cluster assignment) were not addressed in this analysis. Errors of interest here were the errors of omission, those GVD pixels not included in the appropriate category by the sensor classification; errors of commission, those GVD pixels incorrectly assigned to a category by the sensor classification; and total error for both omission and commission.

o The % error of omission, $E1 = \dfrac{O_n}{G_n} \times 100$, where $O_n = G_n - A_n$.   (5)

o The % error of commission, $E2 = \dfrac{C_n}{L_n} \times 100$, where $C_n = L_n - A_n$.   (6)

Total error for approach 1 is wholly due to errors of omission and can easily be computed as 100% - % "correct" from either equations (1) over an individual category, or (2) over all categories.

Total error for approach 2 is determined similarly for all categories taken together as 100% - % mapping capability from equation (4). Total error per category is the sum of the error of omission and commission.

RESULTS

The analysis demonstrates that for the TM/MSS data pair studied, the Level I land cover categorization derived from the TM was superior to that derived from its companion MSS. The TM produced higher comprehensive accuracies than did the MSS and higher accuracies for the individual cover types as well, and in general lower category assignment errors (as measured by correspondence to the GVD).

Considering the relative accuracies and both types of errors together, two categories (water and wetlands) are similar for the TM and MSS classifications. Forest, ag/grass, and developed are all improved with TM: forest benefits from a decrease in omission errors; ag/grass from large decreases in errors of omission, which together with commission errors are 21% lower than with MSS; while developed benefits from large decreases of commission, which together with omission errors are 38% lower than corresponding MSS errors.

The barren/extractive and wetland categories, which represented only 1.8% and 0.1% respectively of the four quadrangle area (See Appendix A), produced unacceptable accuracies for both TM and MSS. The classification success of these two categories was zero for barren/extractive and 53.6/50.9% (TM/MSS) for wetlands. This compares with 47.4% and 4.8% respectively for these categories with July 1981 MSS data for these same areas (Gervin, et al, 1983). November may be a better time than summer to observe wetlands, although the correspondence rates with the GVD are still not good. At that time of year it is not possible to spectrally distinguish the true barren/extractive category from seasonally bare fields under agricultural use.

Accuracy Assessment - Approach 1

The comprehensive accuracy computed over four quads and six cover types as the percent correspondence, or % "correct" with the GVD (approach 1), was 79.2% for TM versus 68.2% for MSS (Table 2). For both TM and MSS, the lowest accuracy among the major categories was recorded for developed (65.5/60.6%), the highest for forest (87.5/80.0%). Although higher for TM, accuracies for all but one category are not markedly different between TM and MSS for the individual cover types when computed this way. This is especially apparent in the TM/MSS ratios which are close to 1.0, with the exception of ag/grass. A 16.4% or factor of 1.25 improvement for that category with TM brings its accuracy into the acceptable 80% range.

Table 2

TM VS. MSS: ACCURACY AS PERCENT CORRECT (APPROACH 1)

(PERCENT CORRESPONDENCE WITH GROUND VERIFICATION DATA)

USGS 7 1/2' QUADRANGLE	SENSOR	Level I Land Cover Category* (%)						OVERALL CORRESPONDENCE
		D	A/G	F	W	Wt	B	
Baltimore East	L-4 MSS	62.6	45.6	32.4	78.7	----	0	61.0
	L-4 TM	67.9	48.0	45.5	76.7	----	0	65.8
Woodbine	L-4 MSS	13.2	63.5	80.7	2.6	----	----	68.1
	L-4 TM	8.5	74.0	86.5	33.7	----	----	76.8
Catoctin Furnace	L-4 MSS	16.1	61.8	88.7	1.8	----	----	75.4
	L-4 MSS	16.6	77.6	95.0	12.8	----	----	85.7
Galena	L-4 MSS	46.9	68.8	62.6	81.5	50.9	0	68.4
	L-4 TM	27.2	92.5	73.7	88.2	53.6	0	88.6
Over All 4 Quads		60.6	64.4	80.0	75.9	50.9	0	68.2
		65.5	80.8	87.5	79.1	53.6	0	79.2
Difference (TM - MSS)		+4.9	+16.4	+7.5	+3.2	+2.7	0	+11.0
Ratio TM/MSS		1.08	1.25	1.09	1.04	1.05	0	1.16

*KEY

    D = Developed; A/G = Agriculture/Grasslands; F = Forest; W = Water;
    Wt = Wetlands; B = Extractive/Barren

Accuracy Assessment - Approach 2

When accuracy is computed as the overlap in the GVD and Landsat categorizations
(approach 2), which considers errors of commission in the sensor classification
in addition to the errors of omission of GVD, considerably lower comprehensive
accuracies of 65.5% for TM and 51.8% for MSS result (Table 3). A larger
discrepancy between the TM/MSS results with Approach 2, 13.8% versus 11.0%
using approach 1 above, is due to lower TM rates of commission for a single
category, developed. Again, the lowest accuracy among the major categories
was recorded for developed with both sensors (59.2% TM; 39.0% MSS), but the
highest accuracies now were in the ag/grass category (72.7%) with TM and water
(70.9%) with MSS.

Table 3

TM VS. MSS: ACCURACY AS PERCENT MAPPING CAPABILITY (APPROACH 2)

(PERCENT CORRESPONDENCE IN SENSOR AND GVD CLASSIFICATIONS)

| | Level I Land Cover Category (%) | | | | | | Overall |
Relative Value	D	A/G	F	W	Wt	B	Correspondence
MSS	39.04	56.60	58.98	70.86	1.78	0	51.78
TM	59.22	72.73	62.31	71.78	2.87	0	65.62
Difference (TM - MSS)	+20.18	+16.13	+3.33	+0.92	+1.09	0	+13.84
Ratio TM/MSS	1.52	1.28	1.06	1.01	1.61	0	1.27

As with approach 1 above, the accuracies for most categories are all slightly higher with TM. Approach 2 yields similar results for three categories and reproduces the 16% improvement for the ag/grass category observed with approach 1. This is apparent from the ratios which are near 1.0 for forest and water and equal to 1.28 for ag/grass. (The computed value for wetlands is not meaningful due to sample size). In addition, a striking 20.18% improvement in the developed category versus 4.9% with the correct GVD approach, or a 4:1 increase in the TM-MSS difference, is revealed. This translates into a TM accuracy 1.52 times that of the MSS for the developed category. Errors of commission are therefore especially important in evaluating the classification success of this category.

Errors of Omission and Commission

An analysis of the errors of omission and commission by cover type is given in Table 4. Omission rates are lower for all categories with TM and especially notable for ag/grass (-16.4%) and forest (-7.6%). The commission rates are relatively similar with TM and MSS for forest, water, and wetlands, although slightly (1-3%) higher with TM. However, the commission rate is noticeably lower for ag/grass (-5.6%) and substantially lower for developed (-33.7%). In the latter category, this represents a factor of 3.43 reduction. Note that small reductions with TM in errors of omission for water and wetlands are essentially offset by small increases in errors of commission.

Table 4

TM VS. MSS: ERRORS OF OMISSION AND COMMISSION

Type	Relative Value	D	A/G	F	W	Wt	B
Omission Error	MSS	39.43	35.62	20.02	24.10	49.13	----
	TM	34.51	19.25	12.47	20.90	46.43	----
	Difference (TM - MSS)	-4.92	-16.37	-7.55	-3.20	-2.70	----
	Ratio MSS/TM	1.14	1.85	1.61	1.20	1.06	----
Commission Error	MSS	47.65	17.59	30.80	8.56	98.19	----
	TM	13.91	12.00	31.62	11.42	97.05	----
	Difference (TM - MSS)	-33.74	-5.59	+0.82	+2.86	+1.14	----
	Ratio MSS/TM	3.43	1.47	0.97	0.75	1.01	----

Total Errors Over All Categories
  (Omission and Commission)

MSS	31.77	Difference (TM - MSS):	- 11.03
TM	20.74	Ratio MSS/TM:	1.53

DISCUSSION/SUMMARY

The relative classification results are summarized in Table 5, which highlights
the comparative accuracies and errors for TM and MSS. The most important
overall finding from this study is that TM data do provide a considerable
improvement over MSS in classification success for Level I categorization of
land cover. Characterization of this difference was best accomplished
using an accuracy computation which included errors of omission and commission
(Approach 2). In that case, a relative accuracy increase of almost 14% was
observed with TM. The 11% improvement shown using the more commonly reported
approach 1 boosted the overall accuracy from 68% (MSS) to 79% (TM), despite
the less than optimal November data and the use of broad cover categories. Growing
season dates are mandatory to evaluate whether this differential between TM and MSS
remains or even is enhanced under more favorable seasonal data acquisition. However,
the results are consistent with those expected from previous TMS studies (Dottavio

and Williams, 1982; Gervin, et al, 1982; Robinson, et al; Sigman and Craig, 1981) and other TM investigations for specific Level II cover categories reported at these Landsat-4 Early Results Symposium (Bizzell and Prior, 1983; Markham 1983; Pitts, 1983; Toll, 1983). This paper is one of the few presented at the Symposium to directly address general land cover mapping success.

The very large sample size used here should provide further support of the validity of the results. The results were found to be statistically significant, but these and other related analyses will be reported elsewhere.

Table 5

TM VS. MSS: COMPARATIVE CLASSIFICATION SUCCESS

	Classification Accuracy (Correspondence to GVD)				Classification Error (Noncorrespondence to GVD)			
Land Cover Types	%Diff. TM − MSS	Ratio TM/MSS	%Diff. TM − MSS	Ratio TM/MSS	%Diff. TM − MSS	Ratio MSS/TM	%Diff. TM − MSS	Ratio MSS/TM
D	+4.92	1.08	+20.28	1.52	−4.92	1.14	−33.74	3.43
A/G	+16.37	1.25	+16.13	1.28	−16.37	1.85	−5.59	1.47
F	+7.55	1.09	+3.33	1.06	−7.55	1.61	+0.82	0.97
W	+3.20	1.04	+0.92	1.01	−3.20	1.20	+2.86	0.75
Wt	+2.70	1.05	+1.09	1.61	−2.70	1.06	−1.14	1.01
B	0	0	0	0	0	0	0	0
Over All Categories	+11.03	1.16	+13.84	1.27	RATIO (MSS/TM) TOTAL ERROR = $\frac{31.77}{20.74}$ = 1.53			

The measured improvement in TM over MSS for this November date was almost entirely due to improvements in three categories--developed, ag/grass, and forest, for which the net reductions in error from omission and commission with TM were 38.7%, 22.0%, and 6.7% respectively. The reduction in the errors of commission for the developed category are particularly impressive at 33.7%. This gain in accuracy for the developed category can probably be attributed as much to the spectral as to the spatial domain. This is shown in the two quads with localized urban areas for which relatively small improvements were made; in the 2 rural quads, where developed areas were represented primarily by low density residential, the accuracies for TM were considerably less. This is because vegetation was correctly classified in the TM data in these rural situations, but the thematic results showed low correspondence to the general GVD. Here, the GVD were not a good measure of TM classification success.

It should be realized that GVD of any kind have inherent limitations. The GVD here were originally defined at approximately a 20m spatial resolution; finer spatial resolution features were not identified. The Level I land use/cover scheme traditionally used by land use planners and employed here produces categories based primarily on land use and secondarily on cover. By definition, these categories are heterogenous in terms of spectral (and spatial) characteristics of the actual cover. This problem is especially severe in the developed and ag/grass categories. For the developed category, for example, whole subdivisions, with the exception of contigous forested land and open space, were given this general designation, a practice consistent with the Level I use/cover scheme. Further categorization of the subdivision into its cover components - yards, housing, roads and driveways, etc. was not attempted due to pragmatic considerations. These included the considerable additional burden of photointerpretation, ground verification, digitization, and problems with image misregistration at that level of detail.

The results for the barren/extractive category highlight the limitations of a categorization scheme based primarily on land use. It is more meaningful to scientists interested in biophysical relationships of terrestrial systems to call lands without vegetative cover "bare" than to designate them as agriculture. Cover designations which change seasonally are disconcerting to planners, but highly relevant for describing dynamics (i.e., energy balance).

CONCLUSIONS

For these data:

o TM outperformed MSS overall by an 11-14% margin in terms of Level I classification success. This represents a factor of 1.27 improvement in overall accuracy based on 1.53 reduction in total classification error.

o Both errors of omission and commission were found to be important for the characterization of this success.

o The developed category, though still exhibiting the lowest overall accuracy for a major land cover type, benefited the most from the improvements associated with TM.

REFERENCES

Dottavio, C. L. and D. L. Williams, 1982. Mapping a Southern Pine Plantation with Satellite and Aircraft Scanner Data: A Comparison of Present and Future Landsat Sensors. Journal of Applied Photographic Engineering, Vol. 8, No. 1, pp. 58-62, February 1982.

Bizzell, R. M. and H. L. Prior, 1983. Thematic Mapper Data Quality and Performance Assessment in Renewable Resources/Agriculture Remote Sensing. Abstract, Landsat-4 Scientific Characterization Early Results Symposium, NASA/Goddard Space Flight Center, (February 1983), Greenbelt, MD.

Gervin, J. C., Y. C. Lu, W. A. Hallada, and R. F. Marcell, 1982. Comparison of
   Land Cover Information from Landsat MSS and Airborne TMS for Hydrological
   Applications: Preliminary Results. National Conference of Energy Resource
   Management. pp. 289-302, Sept. 1982. Baltimore, MD.

Gervin, J. C. , Y. C. Lu, and P. D. Soyke, 1982. Floodplain Management
   Applications of Landsat Data for the Upper Mississippi River Basin. Pro-
   ceedings of the ASP-ACSM Fall Convention, Hollywood, Florida. pp. 159-169.
   1982.

Imhoff, M. L., R. G. Witt, and D. Kugelmann, ed., 1981. Second Eastern Regional
   Remote Sensing Applications Conference, NASA Publication 2198. 422 pp.

Irons, J. R., 1982. Summary of Research Addressing the Potential Utility of
   Thematic Mapper Data for Renewable Resource Applications. NASA Technical
   Memorandum TM 83965. 39 p., July 1982.

Markham, B. L., 1983. Preliminary Comparisons of the Information Content and
   Utility of TM Versus MSS Data. Abstract, Landsat-4 Scientific Characterization
   Early Results Symposium, NASA/Goddard S. F. C., February 1983.

Pitts, D. E., 1983. Preliminary Evaluation of Thematic Mapper Data for
   Renewable Resources. Abstract, Landsat-4 Scientific Characterization Early
   Results Symposium. NASA/Goddard S. F. C. February 1983.

Robinson, J. W., F. J. Gunther, and W. J. Campbell, 1982. Ground Truth
   Sampling and Landsat Accuracy Assessment. National Conference on Energy
   Resource Management, pp. 69-82, September 1982. Baltimore, MD.

Sigman, R. and M Craig, 1981. Potential Utility of Thematic Mapper Data in
   Estimating Crop Areas. Proceedings of Fifteenth International Symposium
   on Remote Sensing of Environment, Ann Arbor, Michigan, May 1981.

Toll, D. L., 1983. Preliminary Study of Information Extraction of Landsat
   TM Data for a Suburban/Regional Test Site. Abstract, Landsat-4 Scientific
   Characterization Early Results Symposium, February 1983. NASA/GSFC.

Appendix A

GROUND VERIFICATION DATA: PHOTOINTERPRETED LEVEL I LAND COVER

USGS 7 1/2' QUADRANGLE	% LAND COVER IN LEVEL I CATEGORY					Extrac-tive
	Developed	Ag/Grass	Forest	Water	Wetlands	
1) Baltimore East	77.3	9.4	4.4	8.8	-----	0.1
2) Woodbine	0.8	64.4	27.4	0.1	-----	7.2
3) Catoctin Furnace	2.5	40.0	56.7	0.8	-----	---
4) Galena	0.7	74.4	17.1	7.3	0.6	0.0
Over All 4 Quads	20.4	47.1	26.3	4.3	0.1	1.8

Appendix B

CONTINGENCY TABLE: (GVD VS. TM CLASSIFICATIONS)

	Category	GVD Pixel Count						Total	% Error Commission
		D	A/G	F	W	Wt	B		
TM Pixel Count	D	88790	8822	2951	2413	14	144	103134	13.91
	A/G	20073	258863	14328	824	84	54	294226	12.00
	F	20764	47245	149345	861	184	11	218410	31.62
	W	1634	292	837	22218	102	0	25083	11.42
	Wt	4322	5332	3153	1773	443	14	15037	97.05
	B	0	0	0	0	0	0	0	0
	Total	135583	320554	170614	28089	827	223	655890	
	% Error Omission	34.51	19.25	12.47	20.90	46.43	100.0		20.74% Total Error
	% Mapping Capability	59.22	72.73	62.31	71.78	2.87	0		65.7% Overall

Appendix C

CONTINGENCY TABLE: (GVD VS. MSS CLASSIFICATION)

		GVD Pixel Count						% Error
CATEGORY	D	A/G	F	W	Wt	B	Total	Commission
D	20558	15121	2983	570	18	22	39272	47.65
A/G	6587	50423	3961	181	6	30	61188	17.59
F	4074	11147	35035	284	83	5	50628	30.80
W	359	32	106	5375	6	0	5878	8.56
Wt	2361	1597	1721	672	117	0	6468	98.19
B	0	0	0	0	0	0	0	0
Total	33939	78320	43896	7082	230	57	163434	
% Error Omission	39.43	35.62	20.02	24.10	49.13	100.0		31.77 % Total Error
% Mapping Capability	39.04	56.60	58.98	70.86	1.78	0		51.78 % Overall

(Left margin labels for rows: MSS Pixel Count)

Index of Authors

Authors	Summary* Volume	Page	Proceedings** Volume	Page
Abrams, R.	I	90	II	47
	I	116	II	147
			II	373
Abrams, M.			IV	127
Ackleson, S.	II	137	IV	325
Aepli, T.	I	15		
Alford, W.	II	69	I	1
	II	85	I	9
			I	143
Amis, M.	II	60	III	571
Anderson, J.	II	82	I	119
Anderson, W.	II	129	IV	281
Anuta, P.	II	1	III	321
	II	53	III	527
Baker, J.	II	149	IV	369
Ball, D.	I	90	I	25
	I	116		
	I	130	II	47
			II	147
			II	277
			II	373
Balick, L.	II	129	IV	281
Barker, J.	I	90	I	23
	I	116		
	I	127	II	1
	I	130	II	47
	I	140	II	147
	I	186	II	235
	II	73	II	277
			II	373
			III	1
			III	233
Bartolucci, L.	II	1	III	321
Batson, R.	II	59	III	565
Bender, L.	II	35	III	497
Bennett, D.	II	81	I	77
Bernstein, R.	I	108	IV	25
Beyer, E.	I	92	II	87
Bizzell, R.	II	113	IV	153
	II	133	IV	299
Blodget, H.	II	160	IV	403
Boatwright	II	141	IV	337
Borgeson, W.	II	59	III	565
Brooks, J.	I	101	I	177
	II	91		
Brumfield			IV	403
Bryant, N.	II	46		
Butlin, T.	I	190		
Card, D.	II	55	III	553
Carnes, J.	II	113	IV	153
Castle, K.	II	15	III	389

Authors	Summary* Volume	Page	Proceedings** Volume	Page
Chavez, P.	II	33	III	471
Cicone, R.	II	28	III	443
Collins, A.			II	221
Colwell, R.	II	98	IV	91
Conel, J.	II	109	IV	127
Crist, E.	II	28	III	443
Dean, E.	II	1	III	321
DeGloria, S.	II	98	IV	91
Deschamps, P.	II	21		
DeVries, D.	II	62	I	133
			III	581
Dickinson, K.	I	189	III	257
Dinguirard, M.	II	15	III	389
Dozier, J.	II	142	IV	349
Duff, P.	I	190		
Duggin, M.	II	64		
Dykstra, J.	II	103	IV	119
Eliason, E.	II	33	III	471
Engel, J.	I	41		
	I	65		
Everett, J.	II	103	IV	119
Ezra, C.	II	15	III	389
Falcone, N.			III	497
Feuquay, J.	II	129	IV	281
Fischel, D.	I	106		
Fitzerald, A.	I	190	II	275
Fleming, E.	I	189	III	257
Friedman, S.	II	46		
Fusco, L.	I	199	III	309
	II	7	III	359
	II	40		
Gayler, J.	II	149	IV	369
Gervin, J.	II	167	IV	415
			IV	421
Gillespie, A.			IV	127
Gokhman, B.	II	46		
Goodenough, D	I	189	II	221
			III	257
Guertin, F.	II	81	I	77
			II	221
Gunther, F.	I	116	II	147
Gurney, C.	II	50	III	513
Haas, R.	II	129		
Hall, J.	II	55	III	553
	II	113	IV	153
Hardisky, M.	II	121	IV	251
Hardy, J.	II	149	IV	369
Haydn, R.	II	116	IV	217
Henderson, K.	II	148	IV	359
Holm, R.	II	15	III	389
Houston, A.	II	148	IV	359

Index of Authors

Authors	Summary* Volume	Page	Proceedings** Volume	Page	Authors	Summary* Volume	Page	Proceedings** Volume	Page
Hovis, W.	II	20	III	411	Mertz, F.	II	55	III	553
Imhoff, M.	II	69	I	1	Metzler, M.	II	23	III	421
			I	9	Middleton, E.	II	171	IV	431
			I	143	Mimms, D.	II	35		
Irons, J.	I	62	II	15		II	85	I	9
	II	93	IV	7				I	143
	II	116	IV	237	Mulligan, P.			IV	415
Jackson, M.	II	149	IV	369	Murphy, J.	I	190	I	77
Jackson, R.	II	15	III	389		II	81	III	275
Jones, O.	II	35	III	497	Nelson, R.	II	93	IV	7
Justice, C.	I	199	III	309		II	116	IV	237
Kahle, A.			IV	127	Palmer, J.	II	15	III	389
Kastner, C.	II	15	III	389	Park, W.			III	275
Kieffer, H.	II	33	III	471	Paylor, E.	II	109		
Kimmer, E.	II	91	I	177	Pitts, D.	II	113	IV	153
Klemas, V.			IV	251		II	148	IV	359
	II	137	IV	325	Price, J.	II	128	IV	271
Kogut, J.	II	54	III	537	Prior, H.	II	133	IV	299
Lang, H.	II	109	IV	127	Podwysocki, M.	II	35	III	497
Lansing, J.	I	186	III	233	Quattrochi, D.	II	111	IV	131
Larduinat, E.	II	54	III	537	Rasool, S.	II	21		
Latty, R.	II	93	IV	7	Reyna, E.	II	113	IV	153
	II	116	IV	237	Rice, D.	II	76	I	57
Lauer, D.	II	129	IV	281	Ritchie, J.	II	141	IV	337
Leung, K.	I	90	II	47	Sadowski, F.	II	129	IV	281
	I	130	II	277	Salisbury, J.	II	35		
			II	373	Savage, R.	II	15	III	389
Likens, W.	II	87	I	159	Schiebe, F.	II	141	IV	337
Logan,	II	46			Schoch, L.	II	64		
Lotspiech, J.	I	108	IV	25	Schott, J.	I	181	III	221
Lozano, F.	II	1			Schowengerdt, R.	II	32	III	467
Lu, Y.	II	167	IV	415	Seevers, P.	II	129	IV	281
			IV	421	Sekhon, R.	II	171	IV	431
			IV	431	Sheffield, C.	II	103	IV	119
Lyon, J.	I	106			Short, N.	II	114	IV	163
Malaret, E.	II	1	III	527	Slater, P.	II	15	III	389
	II	53			Sorensen, C.	II	113	IV	153
Malila, W.	II	23	I	57	Stauffer, M.	II	93	IV	7
	II	76	III	421		II	116	IV	237
Marcell, R.	II	160	IV	403	Strome, W.	I	120	II	221
	II	167	IV	421	Sturdevant, J.	II	129	IV	281
Markham, B.	I	127			Su, J.	II	91	I	177
	II	73	I	23	Thompson, D.			IV	359
	II	93	II	1	Thormodsgard, J	II	62	I	133
	II	116	II	235				III	581
	II	135	IV	7	Toll, D.	I	93	IV	7
			IV	237		I	116	IV	237
			IV	313		I	153	IV	387
MacDonald, R.	II	113	IV	153	Townshend, J.	II	149	IV	369
McGillem, C.	II	1	III	527	Trevese, D.	II	7		
	II	53			Usery, E.	II	83	I	123
Mehl, W.	I	199	III	309	Valdes, J.	II	1		
			III	359					

IV-448

Index of Authors

BIBLIOGRAPHIC DATA SHEET

1. Report No. NASA CP-2355	2. Government Accession No.	3. Recipient's Catalog No.
4. Title and Subtitle LANDSAT-4 SCIENCE CHARACTERIZATION EARLY RESULTS VOLUME IV - APPLICATIONS		5. Report Date January 1985
		6. Performing Organization Code 620/623
7. Author(s) John L. Barker, Editor		8. Performing Organization Report No. 85B0115
9. Performing Organization Name and Address NASA/Goddard Space Flight Center Greenbelt, Maryland 20771		10. Work Unit No.
		11. Contract or Grant No.
12. Sponsoring Agency Name and Address National Aeronautics and Space Administration Washington, DC 20546		13. Type of Report and Period Covered Conference Publication
		14. Sponsoring Agency Code

15. Supplementary Notes   4 Volumes
Volume I - Multispectral Scanner (MSS)
Volumes II and III - Thematic Mapper (TM)
Volume IV - Applications

16. Abstract

These four volumes of proceedings contain the collected papers of presentors at the Landsat-4 Science Characterization Early Results Symposium, which was attended by over 400 investigators on February 22-24, 1983 at NASA/Goddard Space Flight Center, Greenbelt, Maryland 20771. There is one volume on the Multispectral Scanner (MSS) sensor, two on the new Thematic Mapper (TM) sensor, and one on Applications for Earth Science of the digital imagery from these satellite remote sensors. There is one up-dated paper that includes initial characterization of the TM sensor on Landsat-5, which was launched on March 1, 1984.

These four volumes compliment the two volume set of Landsat-4 Science Investigation Summary (NASA CP-2326; NTIS Accession Numbers N84-30359 and N84-30380).

17. Key Words (Selected by Author(s)) Satellite Remote Sensing, Thematic Mapper, Landsat, Multispectral Scanner, Radiometric and Geometric characterization of Imagery from satellites, Radiometry, Earth Science Applications		18. Distribution Statement Unclassified-Unlimited STAR Category 42		
19. Security Classif. (of this report) Unclassified	20. Security Classif. (of this page) Unclassified		21. No. of Pages 458	22. Price* A20

GSFC 25-44 (10/77)